NONLINEAR ANALYSIS OF REINFORCED CONCRETE STRUCTURAL SLABS

BY

AHSANUL KABIR

BSc, MSc, MIE(B)

A thesis submitted to the Department of Civil Engineering

for the degree of Doctor of Philosophy

University of Strathclyde

Glasgow, U.K.

February, 1986

In the name of God, the most Gracious, the most Merciful

TO My Parents

and

TO the memory of
Late Sheikh Mujibur Rahman
the most beloved leader of our people

ACKNOWLEDGEMENTS

The author wishes to express his sincere gratitude and indebtedness to Dr. William Duncan for his thorough and unfailing supervision throughout the period of this research. His critical examination of the manuscript and the resulting suggestions certainly added to the clarity of the overall presentation.

The author is also grateful to Professor Ian MacLeod, Head of the Department of Civil Engineering for providing all the necessary facilities to bring this work to completion. His personal encouragement and help will be cherished evermore.

The valuable service and assistance of Messrs. Jack Morrin, John Harper and all the technical staffs of the Structure and Concrete Laboratory is gratefully acknowledged. Thanks to all of them for their help during the experimental phase.

The author is grateful to:

Dr. Rankin Kennedy, Department of Metallurgy, Mr. Roy Cairns, Department of Civil Engineering, Mr. Andrew Crockett, Department of Mechanics of Materials, Mr. Don Evans and other advisors in the Computer Service for the help and assistance they provided enthusiastically at the time of need.

The financial support of the Commonwealth Scholarship Commission is gratefully recognised, without which this study could not have been materialised.

The author is thankful to some of his old colleagues and their family, particularly Dr. Monowar and Mr. Abedin for their help and support during his stay in Glasgow.

Last but by no means the least, sincere appreciation are due to the members of author's family for their patience and considerate attitude at a very critical time of the family.

Abstract

Nonlinear response of a structure to progressive loading may originate from two different sources viz, geometric nonlinearity and material nonlinear behaviour. For a rationally proportioned concrete structure, the material nonlinear responses are believed to contribute the major part of its total nonlinear behaviour. Geometric nonlinearities become significant only when the structure is relatively slender. It is the material nonlinearities of reinforced concrete structures that are of interest in this investigation.

Two plate bending finite elements have been generalised to include coupling of inplane actions with the bending effects. This was achieved through layering concept. One of these elements had been employed by some previous researchers. But the present formulation is different from theirs in that a numerical integration scheme is introduced to evaluate the stiffnesses and internal equivalent forces.

A number of schemes for solving the nonlinear equations have been included in the present formulation. Suitability and effectiveness of these schemes in tracing the material nonlinear responses of concrete slabs have been examined.

The numerical material model behaviour is based on the experimental observation reported by various authors. Readily available material characteristic properties are used in the description of the model. The overall response of reinforced concrete slabs is found to be significantly influenced by the cracking and post cracking treatment of concrete. Some form of tension stiffening scheme seems necessary to represent the structural response realistically. A number of conventional tension stiffening schemes have been incorporated, including a simple alternative formulation. The effect of different tension stiffening schemes and some other numerical parameters on the numerical solution of concrete structures have been investigated.

Laboratory tests were carried out on a number of square and rectangular model slabs. The supporting arrangement and the applied loading systems were the main variables. These experimental records were later compared with the numerical predictions. Some other test results from literature have been included also.

CONTENTS

LIST OF FIGURES

Chapter 7

Page

List of Plates

List of Tables

Notations Used

Notations	Brief Explanation
a, b	Measurement of length, width, etc.
A	Differential operator matrix relating strains to displacement
B	Strain matrix relating strains to element nodal displacement
c	Cosine of an angle
C_l	Layer elasticity matrix
D.O.F, DOF	Degrees of freedom per node
$\Delta d, d, d_e, d_i, d_s$	Appropriate displacement vectors
D, D_l	Total, layer constitutive matrix relating stress resultants to generalised strains
e_d, e_r	Tolerance for norms of displacements and residual forces
E, E_c, E_d, E_s	Modulii of Elasticity
f_c	Allowable concrete stress
f_{cu}	Cube crushing strength
f'_c	Cylinder strength/ultimate compressive strength of concrete in flexure
f'_t	Split cylinder strength/tensile strength of concrete
f(x,y)	Polynomial functions representing displacement variation
F, F_{eq}, F_i	Appropriate equivalent nodal force vectors
G, G_o, G_t	Respective shear modulus
H	Co-ordinate function strain matrix
k	A constant; principal stress ratio σ_2/σ_1
k	Element stiffness matrix
K, K_o, K_t	Respective bulk modulus

K, K_s, K_T	Structural stiffness matrices
M, M_x, M_y M_{xy}	Bending moments per unit length
N	Shape function matrix
N, N_x, N_y, N_{xy}	Inplane forces per unit length
n_d, n_r	Norms of displacements and residual forces
p, p_w	Intensity of distributed load per unit area
P	Coordinate function matrix relating displacement to the undetermined coefficients
Q, Q^{-1}	Coordinate function matrix relating nodal displacements to the undetermined coefficients, and its inverse
Q_X, Q_y	Transverse shear forces per unit length
R, R_e, R_s, R_T	Respective applied nodal force vectors
R_i, R_i^{ex}	Nodal force or excess nodal force vectors equivalent to the relevant internal stress state
s	Sine of an angle
t	Slab thickness
T, T_ξ	Transpose; Transformation matrices
u, v, w	Displacement variables in xyz coordinate directions
x, y, z	Local coordinate system
X, Y, Z	Global coordinate system
α	Vector of undetermined coefficients
β	Shear retention coefficient
$\epsilon, \epsilon, \epsilon_1, \Delta\epsilon$	Strain or strain vectors
ϵ_{cr}	Strain at tensile cracking of concrete
ϵ_{or}, χ_{or}	Generalised reference surface inplane and bending strains (i.e. axial strains and curvatures)
ϵ_o, σ_o	Initial strain and stress vector
ϵx, ϵy, γxy	Cartesian strain triad

λ	Plasticity proportionality constant
ν	Poisson's ratio
θ_x, θ_y	Rotations about x and y axes respectively
θ, φ	Angular measurements
Ψ	Residual force vector
σ, σ_1, $\Delta\sigma$	Stress vectors
σ_1, σ_2	Principal stresses
σ_x, σ_y, τ_{xy}	Cartesian stress triad
$\bar{\sigma}_e$, $\bar{\sigma}_c$	Effective stress index (scaler function of stresses at a point)

Chapter 1

INTRODUCTION

1.1 General

The behaviour of reinforced concrete structural members has been the focus of the activity of several engineers for many years. Both experimental and analytical studies have been extensively pursued to improve our knowledge in understanding the response of the concrete structures subjected to load and other external actions. Yet the success in developing a general basis for analytical design procedure has been less spectacular. This is due to the various inherent complexities of concrete behaviour which are perhaps not yet fully understood and they act as a formidable barrier in the development of rational analytical methods for reinforced concrete. This is why the present day codes of practice, in many respects, continue to be based on empirical approach, using the results of large amounts of experimental data. The design for shear in ordinary and deep reinforced concrete beams and the design for torsion in reinforced concrete members are two such instances.

Simplified empirical approach has been necessary and still continue to be the most convenient method for ordinary design. For example, the ultimate strength of reinforced concrete slabs based on assumed yield line patterns may be suitably employed to estimate the ultimate load carrying capacity of such structures. But the recent demand for estimating the serviceable limit state makes it necessary to seek for some other comprehensive approach. The finite element method contends with its versatility to provide one such approach. It offers a powerful and general analytical tool for study of reinforced concrete behaviour throughout the loading history.

The response of reinforced concrete structures, subjected to relatively higher intensity of loads, extends beyond the elastic range. Moreover, the formation of tensile cracks in concrete at an early stage makes the computation of deflection for a cracked concrete section more difficult. The complexity arises from the uncertainties in the assumed value of instantaneous rigidity of the cracked section. The estimation of the deformation under varying sectional stiffness under progressive loading is the nonlinear analysis problem that is of interest in this study. Nonlinearities may also result from the large displacement considerations, known as geometric nonlinearity. But, this is not considered in the formulation here in view of the fact that standard concrete structures usually fail, long before a significantly higher displaced configuration is reached.

1.2 Brief Review of Finite Element Analysis of Reinforced Concrete

Soon after its introduction, the finite element method was recognised as one of the most potential and powerful tools for structural analysis of various forms. However, its wide application and popularity is principally due to the availability of fast electronic computers. During its embryonic stage, the finite element method was applied to study the elastic responses of different structural components, commonly used in aircraft construction. Its application to reinforced concrete structures was relatively slow and gradual. Absence of any reference to concrete application of the method in the classic text book by Zienkiewicz[98] clearly demonstrates its delayed inception into the field of reinforced concrete.

The earliest reported application of the finite element method to reinforced concrete structure was by Ngo and Scordelis in 1967[67]. They have used the method to analyse reinforced concrete simple beams. The

main constituents, concrete and reinforcing steel were idealised by two dimensional constant stress triangular elements. Special spring elements were devised to model the bond-slip interaction between steel and concrete. Basically, a linear elastic analysis was performed and predetermined discrete cracks were introduced along the mesh boundaries by separating and doubling the relevant nodes. For a given set of external loads, the displacements, strains and stresses were calculated. Both concrete and steel were treated as linearly elastic material and the stiffness of bond-spring elements were arbitrarily assigned. The model was used to obtain the displacement, strain and stress patterns in a reinforced concrete beam for which the location of predetermined cracks and the stiffness properties of bond-spring elements were varied.

In the following year, Nilson[68] introduced the first nonlinear model to account for the nonlinear material response of concrete and that of bond-slip relationships. He included an incremental-iterative loading scheme to facilitate the tracing of structural nonlinear response. A set of unbalanced nodal forces were derived from resulting material nonlinearities and were fed back to obtain the new iterative displacements. The effect of cracking was accounted for by stopping the solution whenever two adjacent elements indicated a tensile failure. The new cracked structure was redefined manually and the changed configuration was again fed into the computer and reloaded incrementally. Both of these two early efforts had severe limitations. In the former, the crack patterns were predetermined, while the latter required mannual alteration of the element topology to allow for the propagation of cracks. However restrictive these models may appear now, it should be recognised that they have paved the way for finite element analysis of reinforced concrete with due attention to the main sources of nonlinearity.

In the meantime, Zienkiewicz et al[99] have developed a formulation for representing generalised elasto-plastic material behaviour. They have demonstrated the application of this formulation in the case of concrete type material using the initial stress approach. The released stresses due to elasto-plastic behaviour of the materials were converted into an equivalent set of excess nodal forces and reimposed on the structure to find a new equilibrium situation. Cervenka and Gerstle[15] followed a somewhat similar approach. In addition, their effort also attempted to account for the cracking of concrete. They used constant strain triangular elements for structural discretisation. The effect of reinforcing steel in shifting the crack direction from usual principal stress direction was considered in their model.

Valliapan and Doolan[90] also used the triangular elements for representing concrete. But they made use of bar elements for reinforcing steel and assumed perfect bond between steel-concrete interface. The constitutive relationship for steel and concrete in compression were idealised as linear elastic-perfectly plastic. A von Mises yield criterion was used to determine the onset of the plastic condition. The effect of cracking was modelled by changing the material constitutive matrix in a way which later gained the reputation of the smeared cracking approach. A number of experimental results were compared with the respective analytical predictions demonstrating the effectiveness of the model.

A fairly refined and versatile isoparametric element was brought to use by Philips and Zienkiewicz[74] for discretisation of concrete in planer and axi-symmetric structures. Steel was represented by special line elements and perfect bond was assumed to exist between steel and concrete. The smeared cracking approach was followed to account for

cracking in concrete. The choice between two cracking criteria, one based on principal stress and the other on principal strain were allowed for. They observed better performance with the stress criterion. Two constitutive models, one applicable to biaxial plane stress condition and the other for axi-symmetric situations, were proposed. The provision for prestressing cables were also included in their formulation. The adopted solution techniques were either a variable stiffness method or a constant stiffness method like that of initial stress method. Numerical examples provided include reinforced concrete deep beams, prestressed concrete pressure vessels subjected to internal pressure and other flat slab cases.

Nonlinear reinforced concrete models described so far were restricted to plane stress or plane strain cases or structures which could be idealised as such. In the analytical study of reinforced concrete plates, two distinctly different approaches have been followed in modelling the necessary constitutive relations. In the first approach, sometimes known as the modified 'EI' method, a macroscopic view point is taken. An overall moment curvature relationship is employed to represent the various stages of material behaviour. This approach was applied to reinforced concrete plates by Jofriet and McNeice[47] and Bell and Elms[6]. The second approach is based on separately idealised stress-strain relations for concrete and steel. The assumption of compatibility of deformation synthesises the two constituent materials. This second approach can be materialised for flexural situations, if the material property variations across the thickness is properly accounted for. This is accomplished in a discretised fashion through the layering concept in which each layer may be allowed to have different properties. Several researchers[27,28,33,34,36,37,92-94] have used this concept for the analysis of reinforced concrete and composite steel concrete structures.

Hand et al[36] used a rectangular ACM plate bending element to which a bilinear inplane displacement function has been coupled. They have used explicit integration to evaluate the element stiffness matrix and consequently had to rely upon some averaging scheme to approximate the strains representative of the whole element. Thus, when a crack appeared, the whole layer over the element was assumed to have fissured. On the solution side, they have employed some form of Newton-Raphson scheme to achieve convergence within a load increment. The residual forces were obtained in a way like that of the initial stress method. A particular feature of their model was that the inplane and bending constitutive matrices were coupled. The effect of this coupling was demonstrated through a numerical example.

Dotreppe et al[27] followed similar analytical procedure as those just described. But instead of using a fully coupled constitutive relations, they have utilised the reduced bending stiffness concept with a view to minimise computational efforts. This was achieved by assuming the inplane stress resultants to be zero. Thus, if the incremental total constitutive relation is given as

$$\begin{Bmatrix} \Delta N \\ \Delta M \end{Bmatrix} = \begin{bmatrix} D_{11} & D_{12} \\ D_{21} & D_{22} \end{bmatrix} \begin{Bmatrix} \Delta \epsilon_o \\ \Delta \chi_o \end{Bmatrix} \qquad (1.1)$$

Then,

$$\Delta N = O \qquad \text{leads to}$$

$$\{\Delta \epsilon_o\} = - D_{11}^{-1} D_{12} \{\Delta \chi_o\} \qquad (1.2)$$

The incremental moments may be given by

$$\{\Delta M\} = D^* \{\Delta \chi_o\} \qquad (1.3)$$

where,

$$D^* = D_{22} - D_{21} D_{11}^{-1} D_{12} \qquad (1.4)$$

is the reduced bending stiffness relation.

Wanchoo and May[92] have employed exactly the reduced bending stiffness approcah for analysis of reinforced concrete plates under cracking environment. They have used 4 noded Bogner elements for structural discretisation. Gilbert and Warner[33] used the layering concept along with reduced bending stiffness approach to study the time dependent behaviour of reinforced concrete plates caused by creep and shrinkage. Compatible Bogner elements were employed for discretisation of the slab continuum. The analytical procedure was similar to any standard nonlinear solution scheme except that instead of incrementing the load, the incremental strains were derived from assumed creep law for concrete. The new equilibrium condition was established in an iterative way to satisfy the current strain state.

Wegmuller[93] has extended the layering concept to the analysis of eccentrically stiffened plates. He used layered element models for both plates and beams that form the composite bridges. He included the inplane and out of plane displacement functions for representing the element response to load. But he evaluated the inplane and out of plane stiffness matrix separately and then added the two in appropriate fashion to form the element stiffness. In doing so, he had certainly bypassed the coupling effect that exists between the inplane and bending actions. Gradual plastification of the steel stiffeners was the main nonlinear material feature that was included in his formulation. The nonlinear response of the concrete deck was not accounted for. These effects were included later by Wegmuller and Amer[94,95]. It is apparent from their reports that an explicit integration was performed to evaluate the element stiffnesses. But what is more uncertain, is the planar location of the sampling point or points, used to estimate the representative layer strains and stresses in an element.

Cope and Rao[18] provided extensive analytical results for various reinforced concrete slab type structures. They have used an initial stress formulation to obtain the residual nodal forces resulting from material nonlinearities. The adopted solution procedure was based on incremental total strain approach, employing the constant stiffness method of solution for solving the equilibrium equations. The method of direct iteration was followed to achieve equilibrium at every loading step. The structural stiffness matrix was triangularised using the Cholesky decomposition procedure. They have employed two different elements for their analysis. One for plane stress problems and the other for plate bending situations. For the plate bending elements, they have used a 3 x 3 points integration scheme in plan along the boundary of the elements with 5 sampling stations across the thickness. The numerical integration scheme across the thickness renders their model somewhat different from the layering concept, especially in the way the equivalent nodal forces are computed. This numerical aspect of the model was made more clear by them in a later paper[19] in which the boundary integration stations on plan was replaced by the standard Gaussian locations.

Johnarry[49] on the other hand, used a layered plate element formulation with 5 degrees of freedom per element node. The adjacent orthogonal steel reinforcements were smeared into a single layer having zero Poisson's effect. This deliberate omission of Poisson's ratio has in effect restored the uniaxiality of the individual steel layers. Still an arbitrary criterion to mark the plastification of the steel layer was necessary for a combined equivalent layer of steel. On the numerical side, he has followed the initial stress concept with primarily constant stiffness solution procedure. He also studied two other variable

stiffness solution scheme, both employing some form of direct iteration method. One was based on incremental total strain while the other followed a step by step accumulative incremental-iterative strain path. With the initial stress approach, he has analysed a number of reinforced concrete structures. These include some skew and rectangular bridge slab models tested by him.

Recently Cope and Rao[21] have demonstrated the effectivness of different finite element models in predicting the shear force distribution of reinforced concrete slabs. Three elements were chosen for the comparative study. These included a linear moment triangular element based on classic thin plate theory, a heterosis quadrilateral element based on Mindlin thick plate theory and a standard isoparametric brick element. Obviously, the brick element should perform the best as it is free from any assumption bias. But it is perhaps the costliest one to use. Of the two plate elements, it is reported that the heterosis element with thick plate formulation is the better in predicting shear forces near the critical edge zones. Nevertheless, very fine meshes are necessary in the edge zones to obtain a reliable prediction and thereby increasing the cost of the analysis. On the other hand it was suggested that a thin plate formulation may be advantageously utilised if appropriate consideration is given to the reaction values which should guide to a better estimate of the shear forces in the edge zones.

Nonlinear analysis of reinforced concrete is centred around a suitable model for the description of its nonlinear material response. With the growing interest in this field, various material models have emerged. A brief review of this aspect here seems in order for completeness. More will be referred to later in Chapter 3, devoted to material modelling concepts.

Although test results on concrete specimens exhibit considerable scatter even in controlled laboratory environment, the general trend is fairly conclusive. The uniaxial strength properties are well established and are reasonably well understood by the practising engineer with some experience. The multiaxial behaviour of concrete is somewhat different from those exhibited under uniaxial state of stress. The experimental investigation of Kupfer et al[58] has outlined the behaviour of concrete under biaxial state of stress. The ultimate strength envelope obtained by them may be described in terms of the readily obtainable uniaxial properties[59]. Such a description of material behaviour is necessary and forms the essential core of any nonlinear analytical solution procedure.

Test results of Liu, Nilson and Slate[61] simply confirms the findings of Kupfer et al. The proposed mathematical description of the ultimate strength envelope for concrete by Liu et al[62] was similar to and perhaps slightly different from those of Kupfer and Gerstle[59]. The only important difference was that the former (Liu et al) postulated an orthotropic model while the latter suggested an isotropic description. The biaxial strength envelope of Kupfer and Gerstle has been widely accepted in the nonlinear analysis of concrete structures[69].

Various models for concrete differ from one another in the way of treating the crack formation and other nonlinear effects introduced before the ultimate strength is reached. A reasonable estimate of the elastic constants with varying level of stress are a prerequisite for any nonlinear analysis of concrete. Fundamentally, the problem was approached by various researchers from two different angles. In one approach, concrete is idealised as initially elastic and then elastic-perfectly-plastic or elasto-plastic strain hardening material under biaxial compression. Wanchoo and May[92], Wegmuller[95], Johnarry[49]

and Huq[45] are some of the many researchers who have used some form of elasto-plastic models. Chen and Chen[16] went further and proposed a generalised elasto-plastic strain hardening model based on Kupfer and Gerstle's strength envelope. They hoped perhaps, that the marriage between the plasticity concept and the experimental findings for concrete should bring about a realistic and permanent settlement for these mutually conflicting cohabitants.

The second approach is based on fitting curves to the observed experimental behaviour of concrete. This has resulted in many different forms of simplified curves from which the elastic constants for concrete are derived. Darwin and Pecknold[24] developed an equivalent unaxial stress-strain relation in order to obtain the elasticity constants in the two principal stress directions. Thus, a family of equivalent curves were necessary for different combinations of the principal stresses. Bashur and Darwin[2] have in fact employed this model for reinforced concrete slab analysis. On the other hand, Cope et al[20] proposed the use of uniaxial stress-strain curves directly and suggested that the strain in the maximum principal strain direction be employed in conjunction to assess the current material constants. Althouth, this simplification ignores the localised interaction of biaxial compressive field at higher load levels, the overall performance may not show any appreciable change.

While uniaxial relations or its equivalents are conceptually simple, some researchers have noted a good correlation between octahedral stress-strain quantities of concrete. Gerstle, Kotsovos and Newman are perhaps the leading exponents in exploring such possibilities. Gerstle[31] in his effort for simple formulation of biaxial concrete behaviour, has shown a definitive trend in the octahedral stress-strain

relationship. On the basis of accumulated test results, he proposed two simple expressions for instantaneous shear and bulk modulus of concrete. Thus, with these two material modulii defined at any instant of loading, the basic elasticity modulus and Poisson's ratio may be obtained through standard elasticity relations.

Kotsovos and Newman followed a similar approach. But in their derivation, they tried to outline the observed physical crack formation process in the context of increasing octahedral stress and strain[54,55]. They have identified three levels of changes in the concrete behaviour with progressive loading to failure. In their formulation to describe deformational behaviour of concrete, they have tried to quantify the effects of such changes. Their proposed octahedral stress-strain relations were established by regressional analysis of a large number of available test data. In a later paper, Kotsovos[56] postulated an ultimate strength envelope of concrete to set the limiting boundary to the previously suggested deformational behaviour. Recently, Kotsovos[57] has proposed simplifications to some of their previous formulations and delineated a loading-unloading criterion based on individual components of octahedral stress state. The proposed description of the deformational behaviour of concrete by Kotsovos and Newman are founded upon statistical correlation and in that sense can claim generality. Moreover, these relations describe both biaxial and triaxial state of stress in concrete. However, their expressions are unit dependent and some future effort to reduce them to a nondimensional form may widen the scope of its greater application.

1.3 Complexities of Nonlinear Analysis of Reinforced Concrete

The finite element method is now a well established tool for structural analysis. But when it comes to the application of reinforced

concrete structures, a number of special problems are posed. Reinforced concrete, behaving far from being an ideal material, has always offered some resistance in revealing its behaviour under different loading conditions. Its various complexities has delayed the progress in developing a rational method for its design and analysis. So, it is no wonder that such complications are to be resolved in the analysis of reinforced concrete by finite element method. The major complexities of reinforced concrete analysis may be summarised as follows:

a) Reinforced concrete is composed of two materials, concrete and reinforcing steel, having widely different characteristic properties. While the properties of steel are possibly known within narrow limits, those of concrete are stochastic in nature and can vary greatly.

b) The deformational behaviour of concrete is perhaps not explicitly understood. The constitutive relations are therefore only a close approximation to the real behaviour.

c) Reinforced concrete is prone to tensile cracking and is infested with innumerable localised cracks from a very early stage of loading history. These cracks have a profound effect on the local stresses and on the overall performance of the structure as well.

d) The bond-slip relation between concrete and the embedded steel is highly nonlinear. Test results show wide scatter and an acceptable relations are yet to be agreed upon.

e) Although concrete exhibits brittle failure under tension in standard tests, such behaviour can not be expected in continuum problem. Moreover, presence of reinforcements obviously delays the release of tensile forces

after the formation of a crack. But the quantification of this tension stiffening effect is difficult and rather arbitrary.

f) Shear transfer mechanism across the crack due to aggregate interlock and dowel action may not be estimated properly. Their magnitude may differ significantly under different conditions.

g) Concrete behaviour is time dependent. Creep and shrinkage effects are known to have appreciable influence on the deformational behaviour of concrete structures subject to sustained loading.

h) Unlike isotropic situations, inplane forces are usually developed in a concrete structure. With progressive loading and sufficient boundary restraints, these forces may have significant bearing upon the structural response of concrete structures.

1.4 Scope of Present Study

The main objectives of this research are:

a) To develop a special purpose computer programme for nonlinear analysis of reinforced concrete flexural members taking into account of the coupling between inplane and bending actions.

b) To make use of the readily available material characteristic properties for the description of nonlinear material response of the numerical model.

c) To study the influence of some numerical parameters on the stability and practical usefulness of the model in the analysis of reinforced concrete plate structures.

d) To perform some experimental investigation, both, as a means of acquiring data for testing the performance of the numerical model and improving the understanding of the behaviour of reinforced concrete slabs under practical situations.

The numerical formulation of the problem was based on small displacement theory of plate within the framework of the finite element method. The contribution of the transverse shearing effects have been excluded and therefore, its application would be limited to study the behaviour of reinforced concrete structures dominated by flexural actions. The coupling of inplane and bending stiffnesses is useful in simulating the realism of the behaviour of reinforced concrete structures. The inplane forces are believed to exist in reinforced concrete members under cracking environment of such structures.

A layered element approach has been adopted in realising the coupled actions between inplane and flexural response. This technique is useful and can account for the wide differences of material properties across the thickness of the plate. Such differences may exist from the start if different constituent materials form the composite plate or may ensue later as varying state of stress or strain across the thickness causes cracking, yielding, etc. of the layers at different load levels. The inclusion of the inplane forces, also provide the means for assessing numerically the distribution of such forces mobilised in a concrete structure which would otherwise remain unknown.

The computer programme developed in this study will be broadly applied to investigate its adequacy and suitability in

i) describing the complete load deflection response of reinforced concrete structures in flexure

ii) predicting the ultimate load carrying capacity of such structures

and iii) simulating the overall crack patterns of the real structure at or near collapse.

Effects of different numerical parameters such as equation solution algorithm, number of element layers, mesh refinements, etc., will be performed also, in order to establish the stability of the overall solution process and as a basic guide for subsequent analytical problems. Obvious though, it may appear that more emphasis has been attached to the numerical aspects of this research, nevertheless, a considerable amount of time and energy was expended to realise the experimental goal of this work.

Chapter 2

FINITE ELEMENT METHOD

2.1 Introduction

The growing need for a safe and rational structural design of modern aircrafts resulted in the development of the finite element method in its present form, although sheer intuitive analogy led to its introduction[88]. However the mathematical basis of the stiffness relations for a continuum was soon recognised[65]. Since then considerable progress has been made in this field and its similarity with various classical mathematical procedures, e.g. Rayleigh-Ritz method, Collocation method, Galerkin's method etc. has been identified. Finite element method may now be viewed from all those different perspectives[3,26,100] and this has led to its application to almost all branches of applied physics, engineering and mathematics[100]. In the current context, the necessary discussions and developments will be confined to thin plate bending situations.

2.2 Basic Finite Element Procedure

The primary step in the finite element method is to replace a given continuum by a set of appropriately selected smaller elements. The process is more commonly known as element discretisation. The total continuum behaviour is in fact approximated by analysing a structure consisting of an assemblage of these (finite) elements interconnected at a finite number of joints. Obviously, the closeness of this assembled structural behaviour to that of the actual continuum depends on the closeness of the approximations by which these simple element behaviours has been idealised. In the displacement formulation, it is fundamental to select the appropriate degrees of freedom at each of the nodes of the

element. Thus, a displacement function consistent with the given element domain has to be chosen first. Usually, polynomials of suitable order with generalised co-ordinates (coefficients) are selected to represent the displacement field within the element. Thus

$$d = f(x,y) \tag{2.1}$$

$$\text{or } d = P\alpha \tag{2.2}$$

where, d is the vector of displacement variables and f(x,y) are the corresponding polynomials in x and y with generalised coefficients α.

Eq. 2.2 is an alternate way of representing Eq. 2.1 where the undetermined coefficients α are rearranged in a vector form and the elements of matrix **P** are the polynomial terms in x and y only.

Substitution of the coordinates of the element nodes in Eq. 2.2 will give the nodal displacement vector

$$d_e = Q\alpha \tag{2.3}$$

from which the undetermined coefficients can be obtained as

$$\alpha = Q^{-1}d_e \tag{2.4}$$

Substituting Eq. 2.4 back in Eq. 2,2 yields

$$d = PQ^{-1}d_e \tag{2.5a}$$

$$= Nd_e \tag{2.5b}$$

$$\text{where, } N = PQ^{-1} \tag{2.6}$$

The matrix N is commonly referred to as the shape functions[46,100].

With displacements completely describable through Eq. 2.5, the strains, which are some form of displacement derivatives, can also be determined. These strain-displacement relations can be expressed in matrix notations as

$$\varepsilon = Bd_e \tag{2.7}$$

where, the elements of matrix **B** contains the appropriate derivatives of the shape functions in matrix **N**.

Considering the first form of Eq. 2.5, Eq. 2.7 can be reproduced as

$$\varepsilon = HQ^{-1}d_e \tag{2.8}$$

where, **H** is the derivative matrix of the **P** matrix.

From the strains, the stresses can always be obtained if the constitutive relation between them is defined or can be approximated. The stresses are, therefore

$$\sigma = D\varepsilon \tag{2.9}$$

where, **D** is the constitutive matrix and is also known as the Elasticity matrix[100] or Modulus matrix[41].

Before the equilibrium relation is invoked, the term 'Equivalent Nodal Forces' need some illustration. In the finite element procedure, only an overall equilibrium condition of the structure is satisfied. Thus, the equivalent nodal forces may be defined as the forces at the nodes, corresponding to the direction of nodal displacements, which are statically equivalent to the boundary tractions and distributed loads on the element.

The governing equilibrium equation can be formulated following different approaches[3,100], e.g. minimisation of the total potential energy, principle of virtual work, etc. The virtual work formulation has been adopted here. Hence, imposing arbitrary (virtual) nodal displacements δ^*_e and equating the external work due to the applied nodal forces and other forces (e.g. body force, surface traction, etc.) acting on the element to the internal work due to internal stresses sustained during that displacement, the basic equilibrium equation can be established as follows

$$\text{External Work} = \delta^{*T}_e (F_n)_e + \int d^{*T} p dv \tag{2.10}$$

where, F_n is the vector of directly applied nodal forces.

and p is the vector of generalised body forces per unit volume corresponding to the degrees of freedom.

Using Eq. 2.5b to replace d^* in Eq. 2.10, the latter takes the form

$$\text{External Work} = \delta^{*T}_e [(F_n)_e + (\int N^T p dv)] \tag{2.11a}$$

$$= \delta^{*T}_e [(F_n)_e + F_e] \tag{2.11b}$$

$$= \delta^{*T}_e R_e \tag{2.11c}$$

$$\text{Internal Work} = \int \varepsilon^{*T} \sigma dv \tag{2.12}$$

Using Eq. 2.7 in Eq. 2.12 results

$$\text{Internal Work} = \delta^{*T}_e \int B^T \sigma dv \tag{2.13}$$

Equating the work quantities in Eq. 2.11 and Eq. 2.13 and noting their validity for any arbitrary imposed displacement, the term δ^{*T} can be omitted from either side resulting

$$\int B^T \sigma dv = R_e \tag{2.14}$$

Now replacing σ using Eq. 2.9 and recalling Eq. 2.7, the expression of Eq. 2.14 changes to

$$(\int B^T D B dv) d_e = R_e \tag{2.15a}$$

$$\text{or } k d_e = R_e \tag{2.15b}$$

where, k is the element stiffness matrix and is given as

$$k = \int B^T D B dv \tag{2.16}$$

considering the strain matrix form given by Eq. 2.8. The element stiffness matrix becomes

$$k = Q^{-1T} (\int H^T D H dv) Q^{-1} \tag{2.17}$$

Now if the element of the structure have initial strains (ε_o) and initial stresses (σ_o), then the constitutive relation of Eq. 2.9 may be restated as

$$\sigma = D(\varepsilon - \varepsilon_o) + \sigma_o \tag{2.18}$$

And this would result in two additional terms at the left hand side of Eq. 2.15 which would take a more general form now

$$Kd_e - \int B^T D\varepsilon_o dv + \int B^T \sigma_o dv = R_e \tag{2.19}$$

Letting, $\int B^T D \varepsilon_o dv = (F_\varepsilon)_e$ (2.20)

and $\int B^T \sigma_o dv = (F_\sigma)_e$ (2.21)

and rearranging the term of Eq. 2.19 would give

$$kd_e = R_e + (F_\varepsilon)_e - (F_\sigma)_e \tag{2.22a}$$

or $kd_e = (R_T)_e$ (2.22b)

where, $R_T = (R + F_\varepsilon - F_\sigma)$, is the total equivalent nodal forces and now, F_ε and F_σ may be thought of as the contributions to the consistent nodal forces due to initial strains and initial stresses respectively.

Eq. 2.15 or in a more general form Eq. 2.22 represents the equilibrium equations of fundamental importance. However, these equations have so far been established at the element level. To obtain the overall equilibrium relations for the whole structure, both the stiffnesses and the load contributions of each element are to be added consistently. Then, the assembled stiffness and the load vector would correspond to the structural degrees of freedom. The total structural equilibrium equations may be stated in a form similar to that of Eq. 2.15 or Eq. 2.22 as

$$K_s d_s = R_s \tag{2.23}$$

$$\text{where, } K_s = \sum_{i=1}^{n} k \tag{2.24}$$

$$R_s = \sum_{i=1}^{n} R_e \text{ or } R_s = \sum_{i=1}^{n} (R_T)_e \tag{2.25}$$

and n = number of elements.

2.3 Choosing a Suitable Plate Element

Many finite elements are now available for plate bending analysis[17,25,100]. An acceptable and efficient element should normally[17] display C_1 continuity ensuring interelement compatibility. The deformation of a thin plate is completely described by its lateral displacement of the midsurface[85]. Thus, the compatibility requires that the lateral displacement and its first derivatives be continuous across interelement boundaries. Further, the element should be capable of representing a constant strain condition and rigid body motion in the limit of mesh refinement.

An early but very useful rectangular element originally introduced by Adini, Clough and Melosh (consequently named after them as ACM rectangle) has been generalised with the inclusion of inplane displacements for this study. This element is nonconformable in nature. But it satisfies the necessary conditions for convergence[25,100]. Walz et al[91] have shown that its convergence is almost guaranteed for homogeneous plates. Higher order elements retaining some curvatures as nodal degrees of freedom may restore the compatibility. Smith and Duncan[81] examined the effect of imposing such additional continuities on several orders of higher derivatives. Many others[7,8] have used this process successfully to model homogeneous plate bending situations. One such simple conformable rectangular element which includes the twist as a nodal variable has been suggested by Bogner et al[8]. Higher order elements pose some problems of boundary condition application and physical interpretation of forces associated with the higher order degrees of freedom. However, the performance of the Bogner element including inplane degrees of freedom will also be investigated.

2.4 Plate Bending Relations

A flat plate supports the transverse loads primarily by bending action. The assumed stress distribution in a plate is well described in the classical theory of plates[85]. Certain approximations are obviously introduced to simplify the two dimensional plate behaviour. For example, in the small displacement theory of thin plates, the normal to the initial midsurface is assumed to remain normal to the deformed mid-surface. This is well known as Kirchoff's approximation.

Stresses σ_x, σ_y and τ_{xy} are assumed to vary linearly with z (i.e. in thickness direction) and the transverse stresses τ_{yz} and τ_{xz} vary quadratically with z. These stresses as shown in Fig. 2.1, produce moments and shear forces commonly known as stress resultants. These stress resultants developed in a plate are shown in Fig. 2.2 and their magnitudes may be given as follows

$$\left.\begin{aligned} N_x &= \int_{-t/2}^{+t/2} \sigma_x dz \\ N_y &= \int_{-t/2}^{t/2} \sigma_y dz \\ N_{xy} &= \int_{-t/2}^{+t/2} \tau_{xy} dz \end{aligned}\right\} \qquad (2.26)$$

$$\left.\begin{aligned} M_x &= \int_{-t/2}^{+t/2} \sigma_x . z dz \\ M_y &= \int_{-t/2}^{+t/2} \sigma_y . z dz \\ M_{xy} &= \int_{-t/2}^{+t/2} \tau_{xy} . z dz \end{aligned}\right\} \qquad (2.27)$$

$$\left.\begin{aligned} Q_x &= \int_{-t/2}^{+t/2} \tau_{zx}\, dz \\ Q_y &= \int_{-t/2}^{+t/2} \tau_{zy}\, dz \end{aligned}\right\} \qquad (2.28)$$

It should be noted that the Kirchoff's thin plate theory, which has been adopted in this study, ignores the transverse shear deformations. Consequently, Eq. 2.28 may be omitted from further consideration. Also, for homogeneous and isotropic plates, the axial forces N_x and N_y and the shear force N_{xy} are usually small compared to the moments. But for reinforced concrete slabs, the inclusion of reinforcing steel makes it nonhomogeneous and often nonisotropic. Further, the cracking of concrete at even low load level renders the behaviour of reinforced concrete slabs nonisotropic even though, initially it could have been isotropically reinforced.

As the plate midsurface (also referred to as reference surface later) is assumed to experience transverse displacements only, the translational displacement relation for any point on the plate element may be given as

$$\left.\begin{aligned} u &= -z\frac{\partial w}{\partial x} \\ v &= -z\frac{\partial w}{\partial y} \end{aligned}\right\} \qquad (2.29)$$

and hence the strains are

$$\left.\begin{aligned} \varepsilon_x &= -z\frac{\partial^2 w}{\partial x^2} \\ \varepsilon_y &= -z\frac{\partial^2 w}{\partial y^2} \\ \gamma_{xy} &= -2z\frac{\partial^2 w}{\partial x \partial y} \end{aligned}\right\} \qquad (2.30)$$

2.5 Finite Elements Used

As mentioned earlier, two rectangular four noded finite elements, with layering concept, have been used in this study for discretisation of the reinforced concrete slabs. In such models, two dimensional plate bending problems are treated by dividing the plate thickness into a finite number of layers parallel to the plate midplane (reference plane)[28,34,36]. Each layer is considered to be in a state of plane stress with its properties defined through appropriate biaxial stress-strain relations. The usual assumptions of the first order theory of thin plates have been employed here. It is therefore, conceivable to view these layered elements as a congregation of two standard elements namely - i) a four noded rectangular plane stress element and ii) a four noded rectangular standard plate bending element. The two different elements considered in this study differ only in their plate bending functions while the inplane behaviour is identically modelled for both. In the following sections, the basic equilibrium equations are derived through standard procedures set forth in the preceding articles. Detailed derivation, specially for the second type of element will be limited for brevity. The two elements hereinafter may be referred to as the ACM element with inplane displacements and Bogner element with inplane displacements or simply as 5 degrees of freedom (D.O.F.) ACM element and 6 D.O.F. Bogner element.

Fig. 2.3 illustrates the local and global node numbering scheme adopted for discretisation of a slab and Fig. 2.4 shows the layered representation of the element section across the thickness.

2.5.1 Displacement Functions

2.5.1.1 Inplane Displacement Functions

In both the elements, the inplane displacements are represented by

a bilinear function as

$$u = [1 \quad x \quad y \quad xy] \begin{Bmatrix} \alpha_1 \\ \alpha_2 \\ \alpha_3 \\ \alpha_4 \end{Bmatrix} \tag{2.31a}$$

$$v = [1 \quad x \quad y \quad xy] \begin{Bmatrix} \alpha_5 \\ \alpha_6 \\ \alpha_7 \\ \alpha_8 \end{Bmatrix} \tag{2.31b}$$

2.5.1.2 Out of Plane Displacement Functions

For the first element, the transverse displacement is modelled through a nonconformable plate bending element (ACM rectangle[100]). Here, the out of plane movement is simulated by a 12-term incomplete quartic polynomial of the form

$$w = [1 \quad x \quad y \quad x^2 \quad xy \quad y^2 \quad x^3 \quad x^2y \quad xy^2 \quad y^3 \quad x^3y \quad xy^3] \begin{Bmatrix} \alpha_9 \\ \alpha_{10} \\ \vdots \\ \alpha_{20} \end{Bmatrix} \tag{2.32}$$

On the other hand, the second element incorporates the standard Bogner[8] element to represent the plate bending action. This is a conformable element which includes the cross derivative (twist) as an additional degrees of freedom. The 16-term polynomial describing the transverse behaviour is

$$w = [1 \quad x \quad y \quad x^2 \quad xy \quad y^2 \quad x^3 \quad x^2y \quad xy^2 \quad y^3 \quad x^3y \quad x^2y^2 \quad xy^3 \quad x^3y^2 \quad x^2y^3 \quad x^3y^3] \begin{Bmatrix} \alpha_9 \\ \alpha_{10} \\ \vdots \\ \alpha_{24} \end{Bmatrix} \tag{2.33}$$

For the first element, 5 degrees of freedom has been assumed at each of the four nodes, totalling 20 degrees of freedom per element. The nodal degrees of freedom are

$$d_i = \begin{Bmatrix} u \\ v \\ w \\ \theta_x \\ \theta_y \end{Bmatrix}_i = \begin{Bmatrix} u \\ v \\ w \\ \frac{\partial w}{\partial y} \\ \frac{\partial w}{\partial x} \end{Bmatrix}_i \qquad (2.34)$$

It needs mentioning that the traditional sign convention for $\bar{\theta}_x$ (which follow right hand screw rule) has been deliberately reversed to get θ_x here in order to maintain positivity of $\frac{\partial w}{\partial y}$ instead. Fig. 2.5 outlines the sign convention adopted for the displacement variables. The general form of the displacement vector at any point of the element follows Eq. 2.2 and is

$$d = \begin{Bmatrix} u \\ v \\ w \\ \theta_x \\ \theta_y \end{Bmatrix} = \underset{5 \times 20}{P} \begin{Bmatrix} \alpha_1 \\ \alpha_2 \\ \cdot \\ \cdot \\ \alpha_{20} \end{Bmatrix} \qquad (2.35)$$

Substitution of the four sets of nodal coordinates in Eq. 2.35 successively will give the total element nodal displacement vector containing 20 elements

$$d_e = \begin{Bmatrix} d_i \\ d_j \\ d_k \\ d_l \end{Bmatrix} = \underset{20 \times 20}{Q} \begin{Bmatrix} \alpha_1 \\ \alpha_2 \\ \cdot \\ \cdot \\ \alpha_{20} \end{Bmatrix} \qquad (2.36)$$

And the twenty undetermined coefficients can be found

$$\alpha = Q^{-1} d_e \qquad (2.37)$$

The Q matrix inversion is carried out numerically in the computer using standard package software, although, an explicit inversion could be possible algebraically[101].

For the Bogner element with inplane displacement, the general displacement vector would contain six elements and may be given as

$$d = \begin{Bmatrix} u \\ v \\ w \\ \theta_x \\ \theta_y \\ \theta_{xy} \end{Bmatrix} = \begin{Bmatrix} u \\ v \\ w \\ \frac{\partial w}{\partial y} \\ \frac{\partial w}{\partial x} \\ \frac{\partial^2 w}{\partial x \partial y} \end{Bmatrix} \tag{2.38}$$

In this case, the Q matrix will consist of 24 x 24 terms and can be inverted similarly as that of Eq. 2.37.

2.5.2 Strain Displacement Relation

The six components of strains associated with plate bending are some kind of displacement derivatives and may be represented as

$$\varepsilon = \begin{Bmatrix} \frac{\partial u}{\partial x} \\ \frac{\partial v}{\partial y} \\ \frac{\partial u}{\partial y} + \frac{\partial v}{\partial x} \\ -\frac{\partial^2 w}{\partial x^2} \\ -\frac{\partial^2 w}{\partial y^2} \\ -2\frac{\partial^2 w}{\partial x \partial y} \end{Bmatrix} = \begin{Bmatrix} \varepsilon_{or} \\ \chi_{or} \end{Bmatrix} \tag{2.39}$$

where, ϵ_{or} and χ_{or} refers to the midsurface (reference surface) inplane strains and curvatures respectively.

Eq. 2.39 can be restated in matrix notations as

$$\epsilon = Ad \tag{2.40}$$

where, Matrix **A** consists of relevant differential operators and vector d contains the displacement variables (Eq. 2.35).

Substituting Eq. 2.35 in Eq. 2.40 and replacing αusing Eq. 2.37 would give

$$\epsilon = APQ^{-1}d_e \tag{2.41}$$

The explicit form of matrix **A** and matrix **P** are given in the Appendix A. Performing the matrix multiplication between **A** and **P** would result in the familiar strain displacement relation of Eqs. 2.10 or 2.11

$$\epsilon = HQ^{-1}d_e \tag{2.42a}$$

$$\text{or } \epsilon = Bd_e \tag{2.42b}$$

$$\text{Obviously, } B = HQ^{-1} \tag{2.43}$$

It should be recalled here that the strain vectors of Eqs. 2.39 through 2.42 represent the midsurface (reference surface) strains of a plate element. Layer strains can be obtained through invoking the Kirchoff's hypothesis as

$$\epsilon_l = \begin{Bmatrix} \epsilon_x \\ \epsilon_y \\ \gamma_{xy} \end{Bmatrix}_l = \epsilon_{or} + z\chi_{or} \tag{2.44}$$

This relation will be used later while evaluating the constitutive matrix.

2.5.3 Constitutive Relation

In the conventional plate bending analysis, the strain energy contribution of the inplane stress resultants (Eq. 2.26) are usually neglected. The generalised stress and strain vectors therefore, contain

the moment resultants (Eq. 2.27)) and the curvatures (χ_{or}) respectively. The constitutive matrix relating these two quantities are well established for isotropic or even orthotropic situations[87,100]. When the inplane stresses and strains are included, the constitutive relations may be stated as

$$\begin{Bmatrix} N_x \\ N_y \\ N_{xy} \\ M_x \\ M_y \\ M_{xy} \end{Bmatrix} = \begin{bmatrix} D_p \begin{bmatrix} 1 & \nu & 0 \\ \nu & 1 & 0 \\ 0 & 0 & \frac{1-\nu}{2} \end{bmatrix} & \mathbf{0} \\ \mathbf{0} & D_b \begin{bmatrix} 1 & \nu & 0 \\ \nu & 1 & 0 \\ 0 & 0 & \frac{1-\nu}{2} \end{bmatrix} \end{bmatrix} \begin{Bmatrix} \varepsilon_{or} \\ \chi_{or} \end{Bmatrix} \tag{2.45}$$

where,

$$D_p = \frac{Et}{1-\nu^2} \tag{2.45a}$$

$$D_b = \frac{Et^3}{12(1-\nu^2)} \tag{2.45b}$$

ε_{or} and χ_{or} are the vectors of reference surface inplane strains and curvatures (Eq. 2.39).

Obviously, the interaction between inplane movement and the fluxural behaviour are not modelled through Eq. 2.45. In order to incorporate these coupling effects in the constitutive relations, the layering concept[36] has been used successfully by many previous researchers[34,80,92,95]. Derivation of such a layered modulus matrix is described below.

2.5.3.1 Formulation of Constitutive Matrix for Layered Elements

In plate bending situations, the generalised stress vectors $[N_x, N_y, N_{xy}, M_x, M_y, M_{xy}]^T$ are usually obtained as a single step integrand

of the respective stresses over the plate thickness (Eq. 2.26-2.27). Considering the layering approach, the total plate thickness is divided into a number of finite layers, each lying in a state of plane stress. The contribution of each layer towards the total stress resultants are computed first. All such contributions are finally summed to get the total stress resultants. Thus, once the layer strains are computed from the plate reference surface generalised strains through Eq. 2.44, the layer stresses can be obtained as

$$\sigma_l = \begin{Bmatrix} \sigma_x \\ \sigma_y \\ \tau_{xy} \end{Bmatrix}_l = C_l \varepsilon_l \tag{2.46}$$

where, C_l is the usual elasticity matrix for plane stress representation i.e.

$$C_l = \frac{E}{1-\nu^2} \begin{bmatrix} 1 & \nu & 0 \\ \nu & 1 & 0 \\ 0 & 0 & \frac{1-\nu}{2} \end{bmatrix} \tag{2.47}$$

Contribution of a layer towards total stress resultant is

$$\begin{Bmatrix} N \\ M \end{Bmatrix}_{layer} = \begin{Bmatrix} \int_{z_b}^{z_t} \sigma_l \, dz \\ \int_{z_b}^{z_t} \sigma_l z \, dz \end{Bmatrix} \tag{2.48}$$

The limit of integration in Eq. 2.48 is from bottom to top surface of the layer concerned.

Substituting Eq. 2.46 in Eq. 2.48 and recalling Eq. 2.44 results

$$\begin{Bmatrix} N \\ M \end{Bmatrix}_l = \begin{bmatrix} \int C_l dz & \int C_l z dz \\ \int C_l z dz & \int C_l z^2 dz \end{bmatrix} \begin{Bmatrix} \varepsilon_{or} \\ \chi_{or} \end{Bmatrix} \tag{2.49}$$

After integration over layer thickness, Eq. 2.49 becomes

$$\begin{Bmatrix} N \\ M \end{Bmatrix}_l = \begin{bmatrix} C_l(z_t - z_b) & C_l\left(\frac{z_t^2 - z_b^2}{2}\right) \\ C_l\left(\frac{z_t^2 - z_b^2}{2}\right) & C_l\left(\frac{z_t^3 - z_b^3}{3}\right) \end{bmatrix} \begin{Bmatrix} \epsilon_{or} \\ \chi_{or} \end{Bmatrix} \tag{2.50a}$$

$$= D_l \begin{Bmatrix} \epsilon_{or} \\ \chi_{or} \end{Bmatrix} \tag{2.50b}$$

The total stress resultant can be obtained as

$$\begin{Bmatrix} N \\ M \end{Bmatrix} = \sum_{i=1}^{NL} \begin{Bmatrix} N \\ M \end{Bmatrix}_l \tag{2.51a}$$

$$= \sum_{i=1}^{NL} D_l \begin{Bmatrix} \epsilon_{or} \\ \chi_{or} \end{Bmatrix} \tag{2.51b}$$

$$= D \begin{Bmatrix} \epsilon_{or} \\ \chi_{or} \end{Bmatrix} \tag{2.51c}$$

$$\text{where, } D = \sum_{i=1}^{NL} D_l \tag{2.52}$$

NL = total number of layers.

The total modulus matrix D is thus obtained by adding consistently the D_l matrix for each layer. The latter can be computed if the layer elasticity matrix C_l is defined and the top and bottom distances (z_t and z_b) of each layer from the reference surface is supplied. Obviously, if the material properties are symmetric with respect to the reference plane, then the total constitutive matrix D will revert to that of Eq. 2.45.

The various forms of the layer elasticity matrix C_l for different constituent materials and at different stress levels will be discussed in the next chapter.

2.5.4 Evaluation of Element Stiffness Matrix

The stiffness matrix for these elements can be formed from first principles using Eq. 2.16 or Eq. 2.17. The H and Q^{-1} matrices are those of Eq. 2.42. Recalling the derivation of the total modulus matrix D (Eq. 2.49-2.52) where the integration has already been performed in the thickness direction, the remaining integration for stiffness has to be carried out over the element area. Hence the stiffness matrix takes the form

$$\begin{aligned} k &= Q^{-1^T}(\int H^T D H dA) Q^{-1} \\ &= Q^{-1^T}(\int H^T D H dx dy) Q^{-1} \end{aligned} \qquad (2.53)$$

The matrices within the integration sign can be multiplied out and integrated explicitly term by term if the D matrix is computed a priori[100]. Hand et al[36], Sarkar[80], Johnarry[49] and perhaps many others had in fact done so. But here in this research, the integration of Eq. 2.53 has been carried out numerically[4,41] using Gauss's quadrature[30,43]. Thus, the B matrix (i.e. HQ^{-1} here, Eq. 2.43) has to be evaluated at each of the Gaussian integration points and a weighted product of $B^T DB$ are added consistently to get the element stiffness. A 2 x 2 station integration was found to evaluate the stiffness matrix almost exactly. The element integration point numbering system is shown in Fig. 2.6. The essential significance of numerical integration will become apparent when the equivalent nodal forces due to internal stresses are derived in Art. 2.5.7.

2.5.5 Evaluation of External Nodal Load Vector

The nodal load vector due to externally applied load may be thought to be composed of forces comprising two different contributions. First, the loads directly applied to the nodes in consistent direction of the

assumed degrees of freedom. Second, the equivalent nodal forces which are statically equivalent to the applied body forces, distributed loads, etc. For the first category of loads, they are directly added to the structural load vector. But for the second type, the equivalent nodal load vector has to be formed at the element level before they can be added to structural load vector. From Eq. 2.11, these equivalent nodal forces can be evaluated as

$$(F_{eq})_e = \int N^T p dv \qquad (2.54)$$

For the frequent case of uniformly distributed transverse loading, the load vector p shall contain a single element p_w. Consequently, the corresponding rows from N matrix or rather P matrix (Eq. 2.6) can be eliminated and Eq. 2.54 may be revised to

$$(F_{eq})_e = \int (P_{red} Q^{-1})^T p_w dxdy \qquad (2.55a)$$

$$= p_w [(\int P_{red} dxdy) Q^{-1}]^T \qquad (2.55b)$$

where, P_{red} is a single row of original P matrix (Eq. 2.35) corresponding to the transverse degree of freedom.

Integration of the elements of P_{red} is quite straight forward and has been explicitly performed for both the element types. Later, they are to be multiplied by the Q^{-1} matrix to get the actual load vector.

2.5.6 Evaluation of the Stress Resultants

Once the assembled stiffness equations have been solved for the current loads to get the displacements, the midsurface strains can be computed. The total stress resultants can be evaluated then straight through Eq. 2.51c. But due to nonlinear behaviour of the constituent materials, the layer elasticity matrix may need updating depending upon the current stress level. Hence, during the internal stress resultant computations, the layer stresses are evaluated first through Eq. 2.46 and Eq. 2.44 and the appropriate adjustments, if necessary, are made to

update the layer constitutive matrix C_l. Then, the contribution of each layer to the total stress resultant is computed using Eq. 2.48 as

$$\begin{Bmatrix} N \\ M \end{Bmatrix}_l = \begin{Bmatrix} \sigma_l(z_t - z_b) \\ \sigma_l(z_t - z_b).(z_t + z_b)/2. \end{Bmatrix} \tag{2.56}$$

Finally, all such layer contributions are added to get the total.

2.5.7 Equivalent Nodal Forces Due to Internal Stresses

As can be seen from the basic equilibrium equation (Eq. 2.14), the internal equilibrating forces is given by $\int B^T \sigma dv$. Hence for plates, after obtaining the internal stress resultants, the consistent nodal forces due to these internal resultants can be found as

$$F_i = \int B^T \sigma dx dy \tag{2.57}$$

It should be emphasised here that the integration of Eq. 2.57 has to be carried out numerically. Some previous researchers[36,49,80] followed some what different technique to evaluate these internal equilibrating forces but in doing so they had to forego the basic equilibrium checking which is used to test the convergence of a solution corresponding to a particular load level[100]. Hand et al[36] used an integrated average of the B matrix to approximate the middle surface strains and curvatures. However, they recognised that this would make the "horizontal location" of this strain vector undefined. But they argued that their scheme would still be representing an overall average midsurface strains for the whole plate element. Later, they seem to have multiplied this average B matrix with the excess layer stress resultant vector to obtain the excess equivalent nodal forces. Johnarry[49] on the other hand, averaged the four nodal midsurface strains and assumed this averaged set to be representative of the entire element. Finally, he used the product of explicitly integrated B matrix and the accumulated stress resultant (or

the excess stress resultant) vector to estimate the equivalent nodal internal forces (or excess forces). It seems, that both these schemes are susceptible to some error unless the element strain distribution is a constant or nearly so. During the initial stages of this research, Johnarry's scheme was followed but it failed to satisfy the equilibrium even for a single step linear elastic analysis in the case of an arbitrary loading. Although computational numerical errors, e.g. truncation error, rounding off error, etc. during equation solution stage and at every other stage[73] would lead to some discrepancy[32] between the external and the internal load vectors, the magnitude of the differences obtained were unrealistic and unacceptable. Moreover, in the case of constant curvature, when the averaged strains are in fact the constant strains all over, equilibrium was achieved completely. This finding convincingly establishes the fact that the error is practically introduced through the averaging process in an arbitrary general loading case. Duncan and Johnarry's[28] comment, "attempts to satisfy complete equilibrium at each load level leads to expensive analysis and poor results" seem to have been partly due to this averaging error. However, it still remains an expensive analysis to satisfy strict equilibrium and the alternative scheme outlined by them is in fact the Initial Stress method of Zienkiewicz et al[99] and may be followed within the framework of numerical integration.

2.5.8 Residual Force Vector

Once again recalling the equilibrium equation (Eq. 2.14) and rearranging the terms, it can be restated as

$$\Psi_i = R - \int B^T \sigma dv = 0 \qquad (2.58)$$

In case of linear elastic analysis, Ψ should normally be zero or nearly so. But while modelling nonlinear material response, the stress vector σ

has to be continuously updated corresponding to the stress level induced due to current deflected configuration. Thus, Ψ will have nonzero elements which can be conceived of as residual nodal forces. These residual forces (sometimes referred to as transfer forces[92]) are to be reimposed on the structure in an iterative scheme until the residuals diminish to a preselected nominal value. It is then assumed that the solution has converged with respect to the current load level.

As an alternative, the difference between the assumed stress vector σ_a (following previous constitutive relations) and the true stress vector σ_t (after allowing for material nonlinear response) can be computed first

$$\sigma^{ex} = \sigma_a - \sigma_t \qquad (2.59)$$

These stress differences may be thought to have resulted because of material nonlinear response and may be termed as excess stress vector. Subsequently, the excess nodal forces could be obtained directly using Eq. 2.57, replacing σ by σ^{ex},

$$\Psi = \int B^T \sigma^{ex} dv \qquad (2.60)$$

Both these schemes for evaluating the residual forces have been described to be acceptable by the ASCE Task Committee[69].

It may be mentioned here that the second method (Eq. 2.60) had been followed by all those researchers[28,36,49] who have used an averaging technique of some fashion to represent the element strain as a whole. When numerically integrated elements are used, it remains the user's choice to follow either of the two methods or even an algorithm combining both may be incorporated. The computer programme developed during this investigation has the facility to trace either the first or the second or a various combination of these two methods for evaluating the residual or unbalanced forces. Thus, if desired, the first method

could be abandoned after first, second or third iterations at a load level and the second could then be followed for rest of the iterations. Alternatively, either the first or the second scheme could be used throughout all the iterations. But as can be expected, these apparently different schemes did not produce any appreciable variations on the final results.

Finally, it should be noted that while evaluating Ψ (Eq. 2.58), the external force vector should contain the reactions. Because, nodal reactions (although initially unknown) are actually external forces along with other imposed loads which maintain the overall equilibrium of the structure.

2.5.9 Convergence Criterion

The criterion for convergence of an iterative solution can be based on either the residual forces or on the current iterative displacements. As pointed out in the preceding subarticle, the iteration about a particular load level may be stopped when the vector of residual forces has substantially reduced to some predetermined small value. Usually this is a bit awkward and it may prove expensive to check that all the residual forces have reduced to a tolerable limit. Instead, some form of norms of the total residual force vector could advantageously be used. Here, a relative Eucleadian norm of residual forces, describing a relative measure of the total unbalanced force in an n-dimensional space, has been selected to estimate convergence. Mathematically, it can be expressed as,

$$n_r = \sqrt{\Psi^T\Psi / R^T R} \qquad (2.61)$$

where,

n_r = (relative) norm of residual forces

Ψ = residual force vector

R = total applied load vector.

Whenever the norm of residual forces falls below or equals a minimum assigned value, i.e.

$$n_r \leqslant \text{Tolerance } (e_r) \tag{2.62}$$

iterations about a load level is terminated. The tolerance value (e_r) can be fed into the programme as an input data and the choice of an appropriate value is left open to the user depending upon the required accuracy of the problem. Experience with current problems show that e_r = 0.01 or at most 0.001 would serve for common practical purposes.

Alternatively or even in combination with the former, a relative norm of the iterative displacements could also be used to terminate the iterative process. The norm of iterative displacements can be stated similarly as

$$n_d = \sqrt{\Delta d^T \Delta d / d^T d} \tag{2.63}$$

$$\text{and } n_d \leqslant e_d \text{ (tolerable value)} \tag{2.64}$$

where,

Δd = vector of iterative deformation

d = vector of total displacement.

The total deformation vector 'd' in Eq. 2.63 may refer to the total displacement vector just following the load increment (i.e. after first iteration) or the most recent vector after every iteration. When inplane effects are coupled with bending action Johnarry suggests that[49] it is better to use the most current vector of displacements. Because in such a situation, inplane movements and the corresponding actions may build up within iterations due to cracking of concrete and other nonlinear effects, although a truely inplane loading may be absent.

A tolerable value of 0.001 to 0.0001 may need to be satisfied by the displacement norms (e_d) to produce convergence in normal reinforced concrete plate bending situations. A value as low as 0.00001 has been

successfully used in connection with isotropic solids and may be used in any situation if the need for acuracy weighs more compared to the cost involved in additional computation.

Some other forms of convergence criterion have also been used successfully by many previous researchers. Wegmuller and Amer[94], terminated the iteration process when the computed effective stress in every layer of all the elements was within a specified tolerance. Hand et al[36] assumed their solution to have converged when there is no more than a tolerable amount (say ± 5%) of change in any of the displacement quantity between two successive solutions.

However, in this study the first two criterion, i.e. relative residual force norm and relative iterative displacement norm has been used in conjunction with each other. Thus, the iteration loop about a load increment is terminated if either the first or the second or both the criterion are met and or a given number of iterations has been exhausted. If the tolerance limit for both the criterion were set equal to each other, then it was observed that the residual force norm was satisfied more frequently than the other. If both these criterion are to be satisfied simultaneously, then it would be a good guess to set the residual force norm tolerance to about a tenth of the other.

2.5.10 Criterion Indicating Collapse

Theoretically, an analysis should continue up until the collapse load is reached when the stiffness matrix will become singular. It could really be possible if the set of equilibrium equations remain well conditioned throughout the solution process. In practice, it may not be possible to continue an analysis to such levels because instability conditions arising from the degradation of conditioning of the stiffness matrix would possibly break down the solution process long before the

matrix itself become singular. In fact, whenever a group of adjacent elements fail almost completely, the stiffness contribution to their common nodal degrees of freedom would reduce significantly. This would switch on the instability trigger and the iterative displacements may shoot up sharply during the subsequent iterations and the equilibrium situations may never be reached again.

An attractive proposition is to analyse the structure up to a limit maximum displacement. But it is then necessary to set a limit to this limiting displacement. Specially, for the constant stiffness method of analysis, the stiffness remains well conditioned throughout the solution processes and the analysis can go almost indefinitely. Johnarry[49] suggested that a limiting maximum deflection of magnitude $L^2/2000t$ should normally correspond to the ultimate states of any rationally proportioned reinforced concrete slab. But the author's experience during laboratory investigation shows that the maximum deflection at failure depends not only on the supporting length and thickness but also on type of loading, supporting arrangements and perhaps some other factors yet to be outlined. As an example, the failure deflection of the two identical square slabs, one supporting uniform pressure load and the other with four point loads (see Chapt. 6), may be compared. The deflection at failure for the former was found to be about 25% greater than the latter.

From the literature, it is seen that Dotreppe et al[27] analysed a corner supported slab under a central point load and has presented a load displacement curve up to a maximum deflection of about 0.18t. On the other hand Cope and Rao[18] re-analysed the same problem and presented their load-deflection drawing up to about 0.45t, while the experimental observation was perhaps discontinued at a deflection equalling 0.2t. The

probable explanation for this could be that, the constant stiffness procedure with limited number of iterations delayed the numerical instability stage as equilibrium was not possibly established during the final load increments within the prescribed number of iterations.

To conclude it may be said that a nonlinear analysis may be continued up to a predetermined maximum deflection of the structure[5] which can be fed into the programme as a percentage of the nominal thickness. The programme would stop when the maximum deflection equals or exceeds the preselected failure deflection or when a given number of load increments have been exhausted. However, even as an initial estimate, the maximum collapse deflection should be within 100% of the slab thickness considering the thin plate small displacement theory as a basis of this formulation. From the load-deflection behaviour obtained from this first computer run, one should be able to identify the deflection level at which the stiffness instability has occured and plot the necessary curve manually up to that level. If the plotting has to be done through another plotting programme, it may be necessary to rerun the programme to terminate at or near this deflection level.

2.5.11 Boundary Conditions

Boundary conditions considered here are only of the displacement type corresponding to the choosen degrees of freedom per node and they may be set either free or fixed. Like the nodal degrees of freedom, the boundary conditions are considered to be applied at the reference surface which is usually the plate midsurface for uniformly thick plate. They are supposed to be either normal or parallel to the plate surface containing the node. Thus, if an inplane displacement is prescribed to be zero, then only the reference surface is constrained to that direction. It does not restrict any other inplane movement through the depth.

If it is set free, then there is no constraint on the inplane movement of the reference surface. Similarly, when one of the slopes is specified to be zero, it requires that the corresponding inplane displacement through the plate depth remains constant but it does not constrain the reference surface displacements.

It is aparent that the inclusion of bilinear inplane displacement functions introduces some difficulty in interpreting the application of the appropriate boundary condition. For linearly elastic analysis, the inability to define the boundary conditions completely may not lead to significant errors. But when nonlinear effects become pronounced, specially due to substantial cracking, the coupling between inplane and flexural movements could enhance further cracking in the vicinity of a boundary which is supposedly free to move. The significance of this problem could become more prominent, if the structure has an assymetric supporting arrangement or if it is loaded unsymmetrically or both.

It should also be realised that the boundary conditions are applied to the corresponding nodal points while in reality the physical location of the supports are away from the nodes. This is more so when stiffened slabs are idealised using plate elements. Obviously, the nodal boundary conditions could be related to the physical conditions using standard transformational relations[17]. But the loss of accuracy caused by not going through such additional computations is not significant in usual cases[17,32].

Finally, the physical realisation of the boundary conditions can seldom be explicitly known. For example, the boundary conditions of a symmetric quadrant of a simply supported rectangular slab may be rationally idealised in a number of different ways. Fig. 2.7 shows six of the many more possible types of the probable boundary conditions for such

slabs. Each of them seem physically and computationally sound. Yet, the practical situations may be different in some way or other, from any of these six categories shown. All these facts should be brought to perspective while interpreting the results from any nonlinear analysis programmes.

2.6 Test of Convergence for the Elements Used

2.6.1 Convergence With Respect to Element Subdivision

In order to estimate the rate of convergence of the elements adopted (i.e. 5 D.O.F. ACM element and 6 D.O.F. Bogner element) with respect to increasing element subdivision, a simply supported isotropic plate, 1200 x 1200 x 60 in dimensions has been selected. The Poisson's ratio is set equal to 0.3. It has been analysed for an elastic case under both uniformly distributed load all over and a single point load at the centre span. The load has been applied in a single increment and results obtained after single iteration. The moment at the centre span has been obtained from extrapolating the Gauss point moments of the element containing the central node using smooth extrapolating technique of Hinton and Campbell[40]. Due to symmetry only a quarter of the plate has been discretised and the applied boundary conditions are those of type 1, Fig. 2.7.

The computed central deflection and moments are presented in tabular form, Table 2.1 for 5 D.O.F. ACM element and Table 2.2 for 6 D.O.F. Bogner element. The so called exact result of Timoshenko[85] has also been included for comparison. The rate of convergence for both the elements seem equally good and a 4 x 4 mesh show sufficiently good result to be acceptable. Although, the 5 D.O.F. ACM element is of non-conformable type, still the difference between the results of the two elements look trivial in an elastic analysis.

Table 2.1 Convergence of Computed Central Deflection and Moments With Respect to Element Subdivision for a Simply Supported Square Slab Using 5 DOF ACM Element.

Element Mesh	UDL All Over		Single Point Load at Centre Span	
	Deflection Coefficient α_1	Moment Coefficient β_1	Deflection Coefficient α_2	Moment Coefficient β_2
2 x 2	0.004329	0.05081	0.01236	0.02448
4 x 4	0.004129	0.04756	0.01184	0.03023
6 x 6	0.004092	0.04700	0.01172	0.03361
8 x 8	0.004079	0.04681	0.01167	0.03603
Exact[85] (Timoshenko)	0.004062	0.0479	0.01160	-
Definitions	$\alpha_1 = \delta c/(\frac{qa^4}{D})$	$\beta_1 = Mx/qa^2$	$\alpha_2 = \delta c/(Pa^2/D)$	$\beta_2 = 100Mx/Pa$

Note: No. of layers = 6, $\nu = 0.3$.

Table 2.2 Convergence of Computed Central Deflection and Moments With Respect to Element subdivision for a Simply Supported Square Slab Using 6 DOF Bogner Element.

Element Mesh	UDL All Over		Single Point Load at Centre Span	
	Deflection Coefficient α_1	Moment Coefficient β_1	Deflection Coefficient α_2	Moment Coefficient β_2
2 x 2	0.04178	0.05320	0.01205	0.02512
4 x 4	0.04084	0.04864	0.01175	0.03080
6 x 6	0.04067	0.04753	0.01167	0.03416
8 x 8	0.04063	0.04711	0.01164	0.03655
Exact[85] (Timoshenko)	0.04062	0.0479	0.01160	-
Definitions	$\alpha_1 = \delta c/(\frac{qa^4}{D})$	$\beta_1 = Mx/qa^2$	$\alpha_2 = \delta c/(\frac{Pa^2}{D})$	$\beta_2 = 100Mx/Pa$

Note: No. of layers = 6, $\nu = 0.3$.

2.6.2 Convergence With Respect to Number of Element Layers

Table 2.3 and Table 2.4 provide the computed centre span moments for the same square slab of Art. 2.6.1 with different number of layers. A 4 x 4 mesh was used for element discretisation for all the cases as the number of layers was varied from 2 to 12. As the material properties are symmetric about the mid surface, so the coupling effect unlocks and the stiffness will be evaluated exactly whether the number of layer is one or many. The computed deflection will also remain unaltered in this case, but the internal moments computed from average layer stresses would definitely vary with the number of layers. From the tables it is clear that a 2 layer idealisation is quite far from real. Just 4 layers improve the results drastically and a 6 or 8 layers is quite adequate.

In a nonlinear analysis, increasing the number of layers and element mesh should theoretically, improve the performance. But the added cost of computation may be discouraging compared to the slight improvements. Bedard[5] observed that a mesh size sufficient to monitor elastic behaviour produced equally good result in a nonlinear environment for plane stress problems.

Table 2.3 Convergence of Computed Moments at Centre Span with Respect to Increasing Number of Layers for a Simply Supported Square Slab Using 5 DOF ACM Element.

Number of Layers	UDL All Over ($q = 0.005\ N/mm^2$)		Single Point Load at Centre Span ($P = 1000N$)	
	Computed Moment, Mx	Moment Coefficient, β_1	Computed Moment, Mx	Moment Coefficient, β_2
2	264.176	0.03669	279.836	0.02332
4	330.219	0.04586	349.795	0.02915
6	342.450	0.04756	362.751	0.03023
8	346.730	0.04816	367.285	0.03061
10	348.711	0.04843	369.384	0.03078
12	349.788	0.04858	370.524	0.03088
Definition	-	$\beta_1 = Mx/qa^2$	-	$\beta_2 = 100Mx/Pa$

Note: Element Mesh 4 x 4, $\nu = 0.3$, a = 1200.

Table 2.4 Convergence of Computed Moments at Centre Span with Respect to Increasing Number of Layers for a Simply Supported Square Slab Using 6 DOF Bogner Element.

Number of Layers	UDL All Over ($q = 0.005\ N/mm^2$)		Single Point Load at Centre Span (P = 1000N)	
	Computed Moment, ,Mx	Moment Coefficient, β_1	Computed Moment, ,Mx	Moment Coefficient, β_2
2	270.154	0.03752	285.105	0.02376
4	337.692	0.04690	356.381	0.02970
6	342.229	0.04753	369.581	0.03080
8	354.576	0.04925	374.20	0.03118
10	356.60	0.04953	376.339	0.03136
12	357.70[1]	0.04968	377.500	0.03146
Definition	-	$\beta_1 = Mx/qa^2$	-	$\beta_2 = 100Mx/Pa$

Note: Element Mesh:- 4 x 4, $\nu = 0.3$, a = 1200.

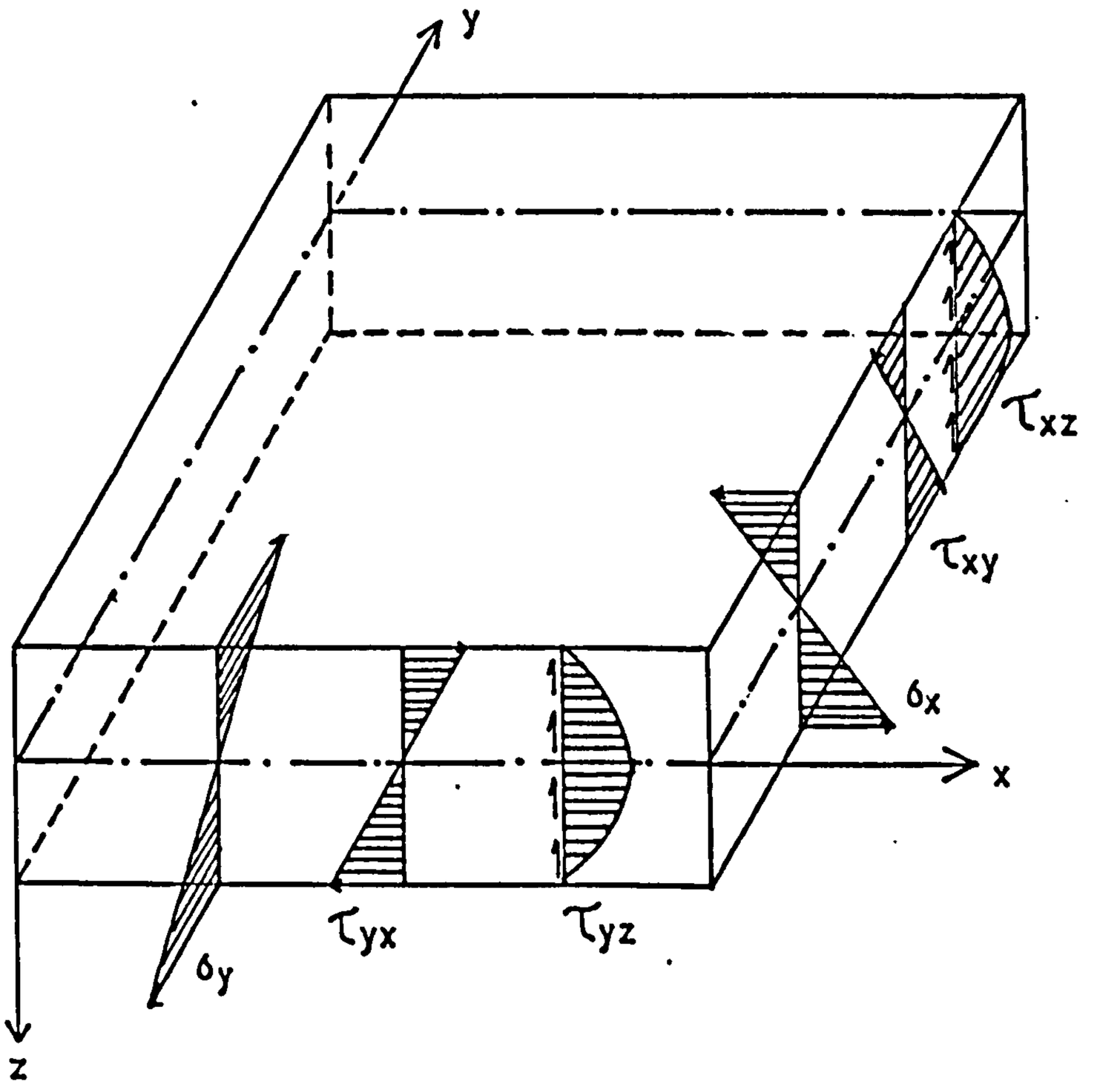

FIG. 2.1 Internal Stress Distribution across Plate Thickness

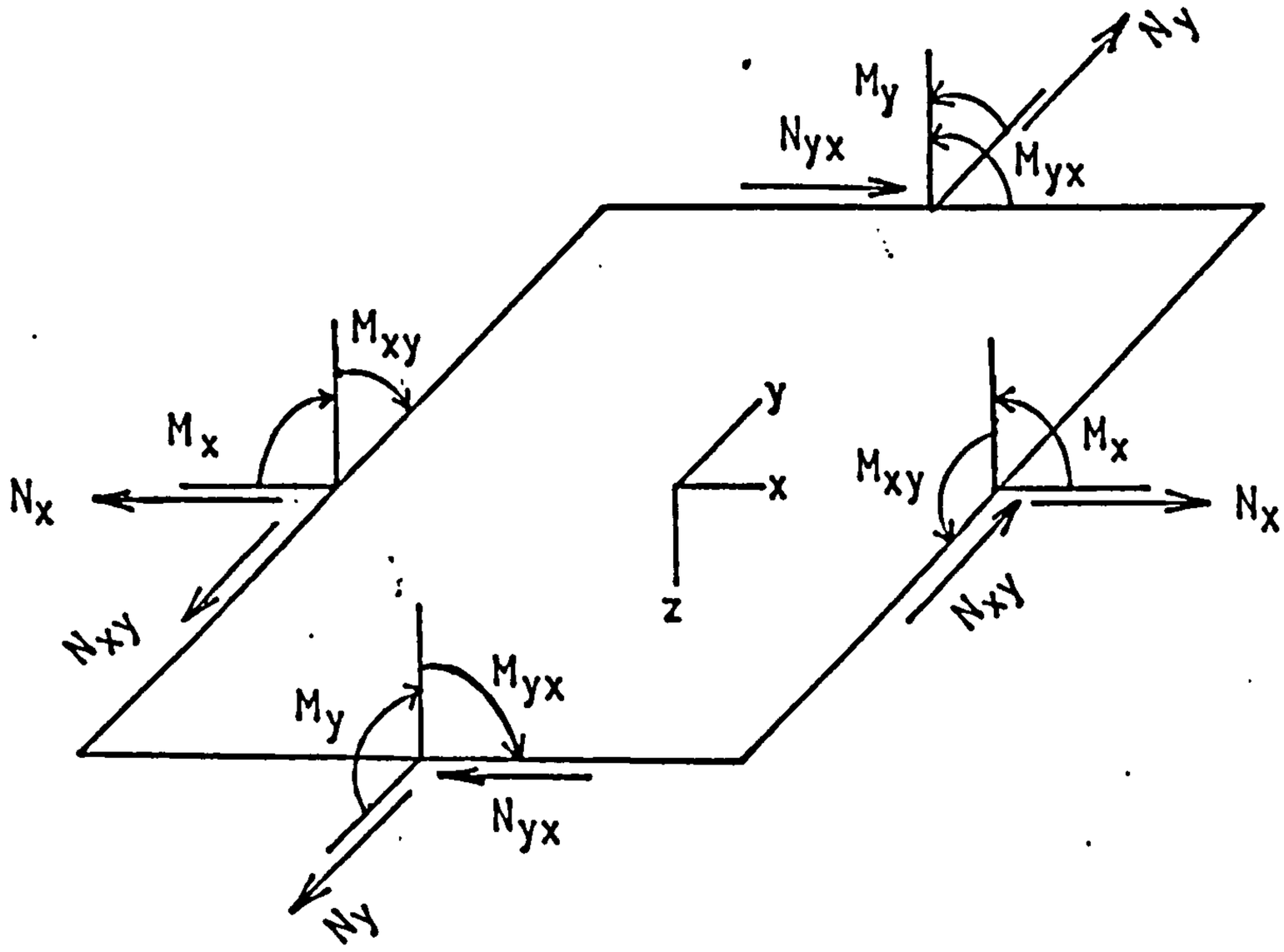

FIG. 2.2 Stress Resultants in a Plate Element

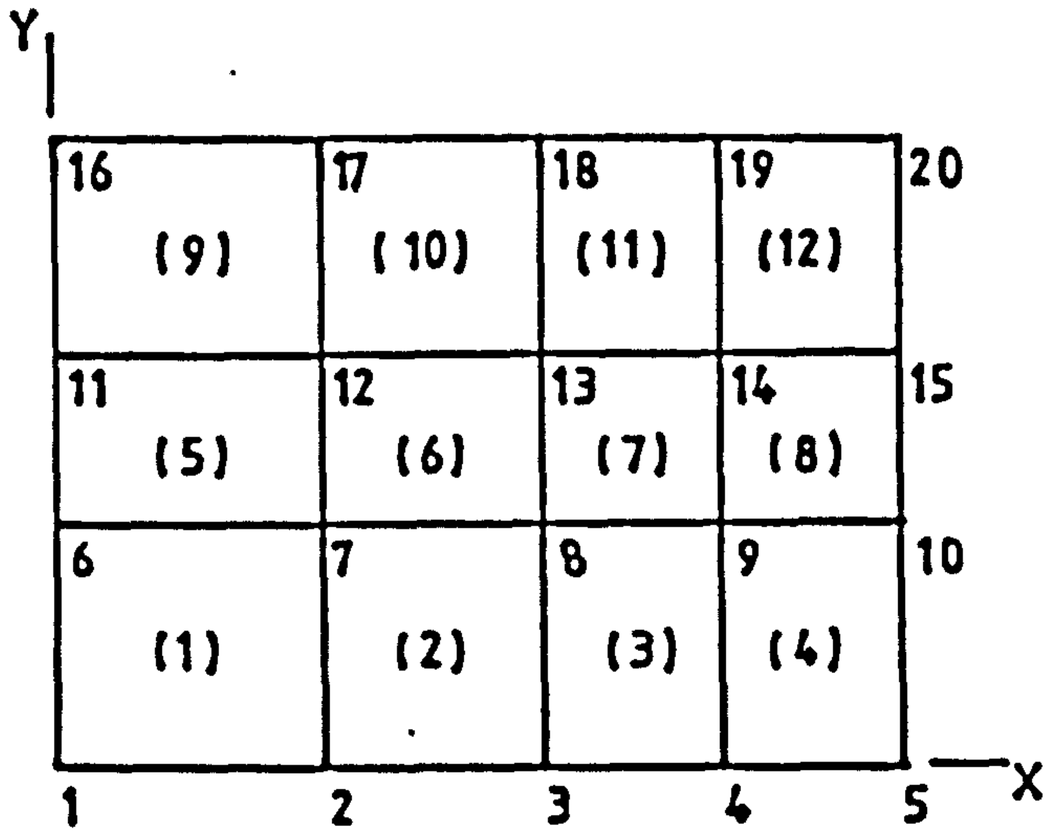

a) Global Node and Element Numbering

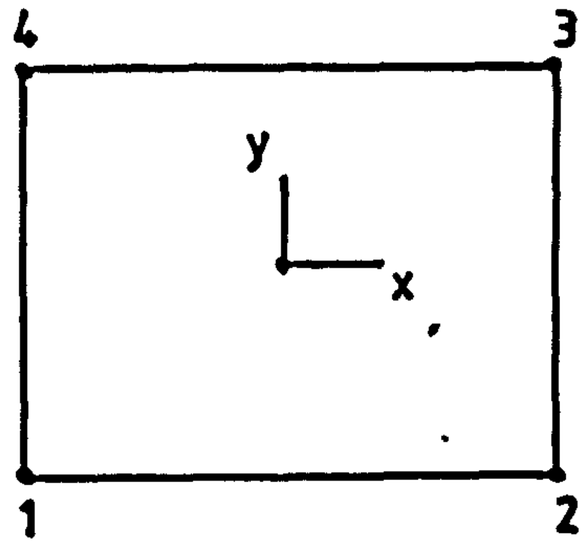

b) Element Node Numbering

FIG. 2.3 Global and Local Coordinates with Element and Node Numbering Scheme

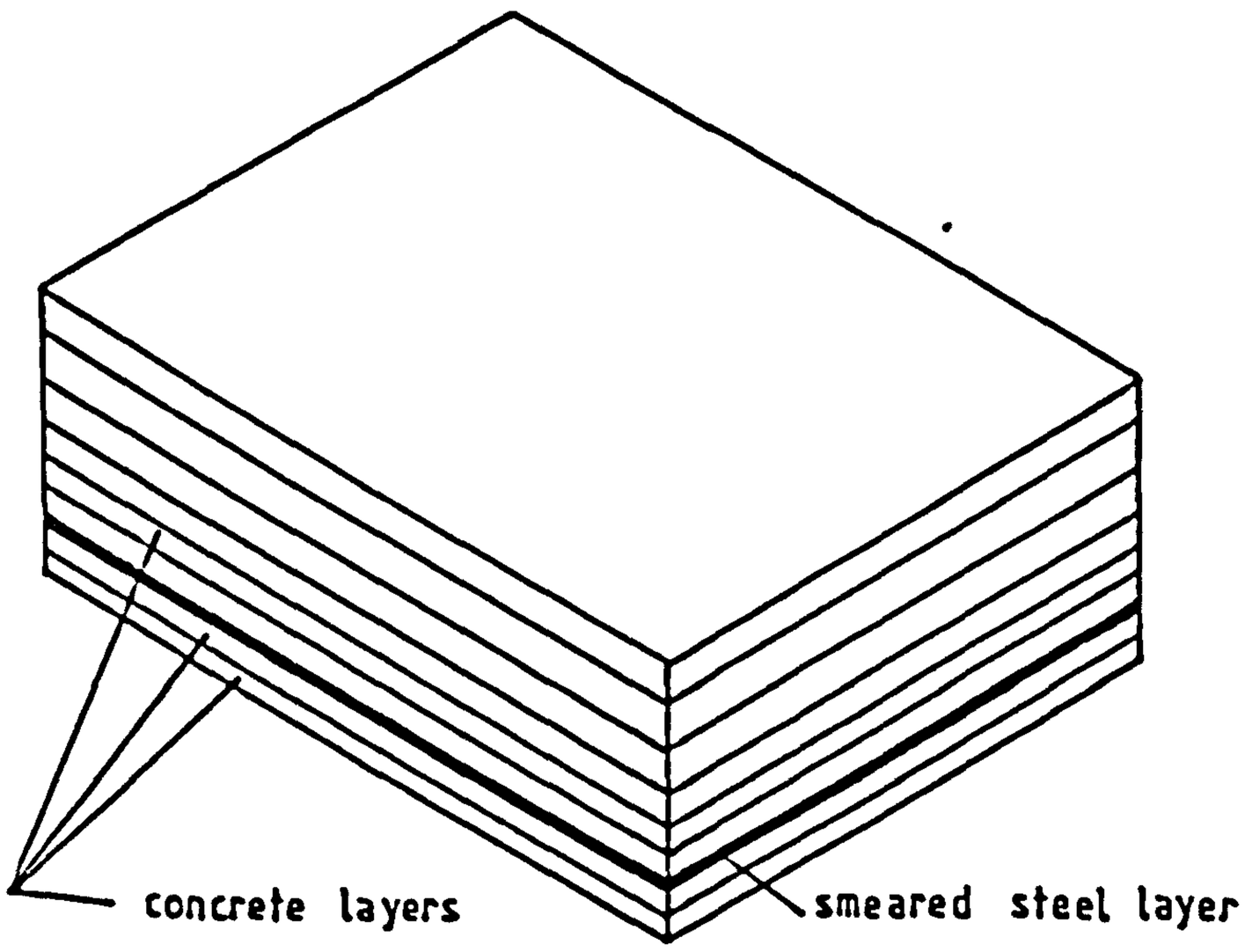

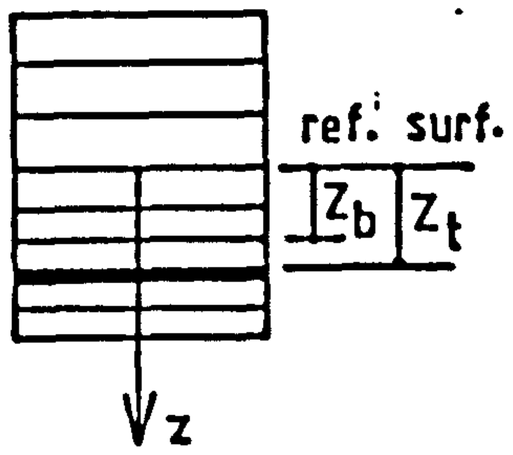

layer top & bottom distances from the reference surface

FIG. 2.4 A Layered Element Model

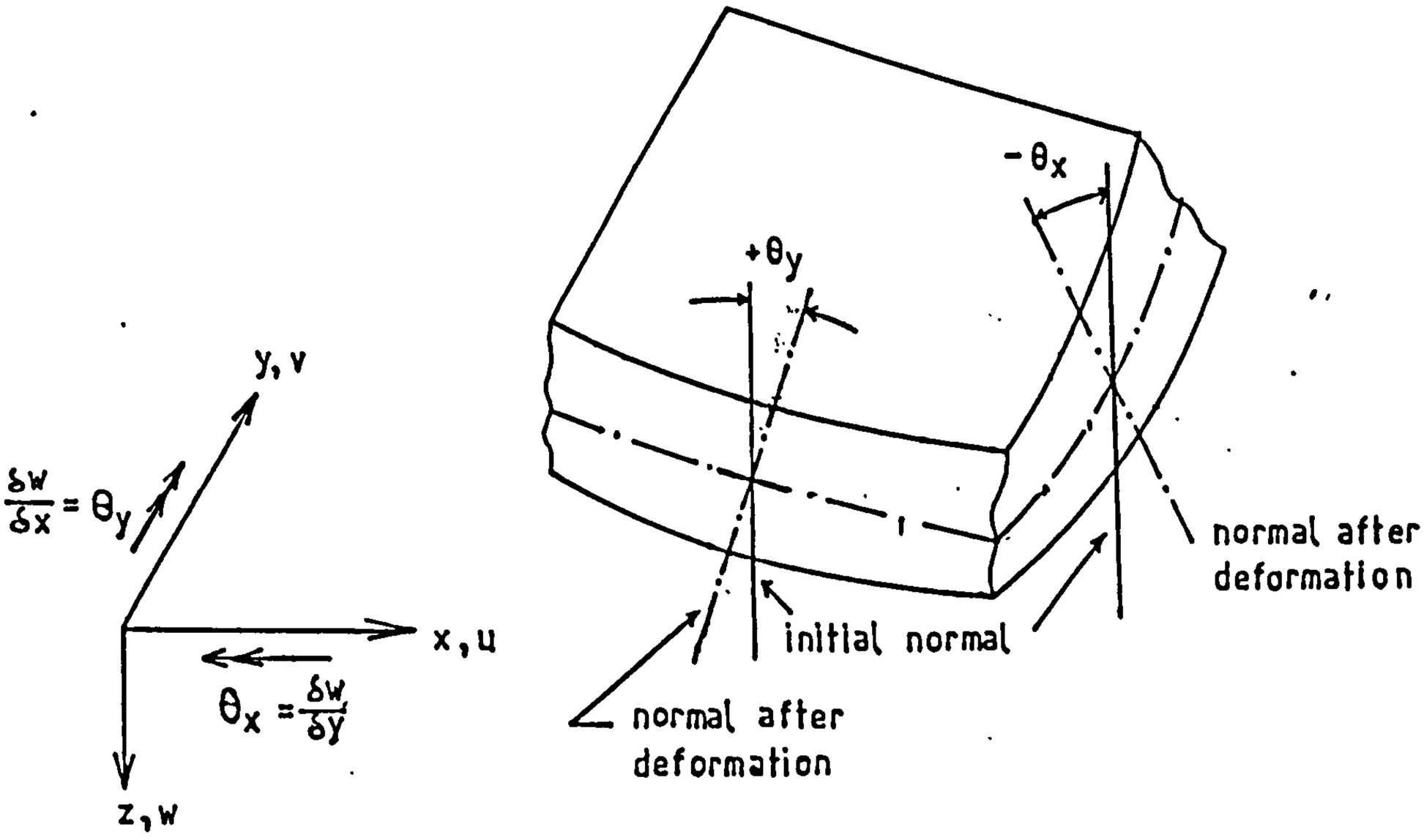

FIG. 2.5 Sign Convention for the Displacement Variables

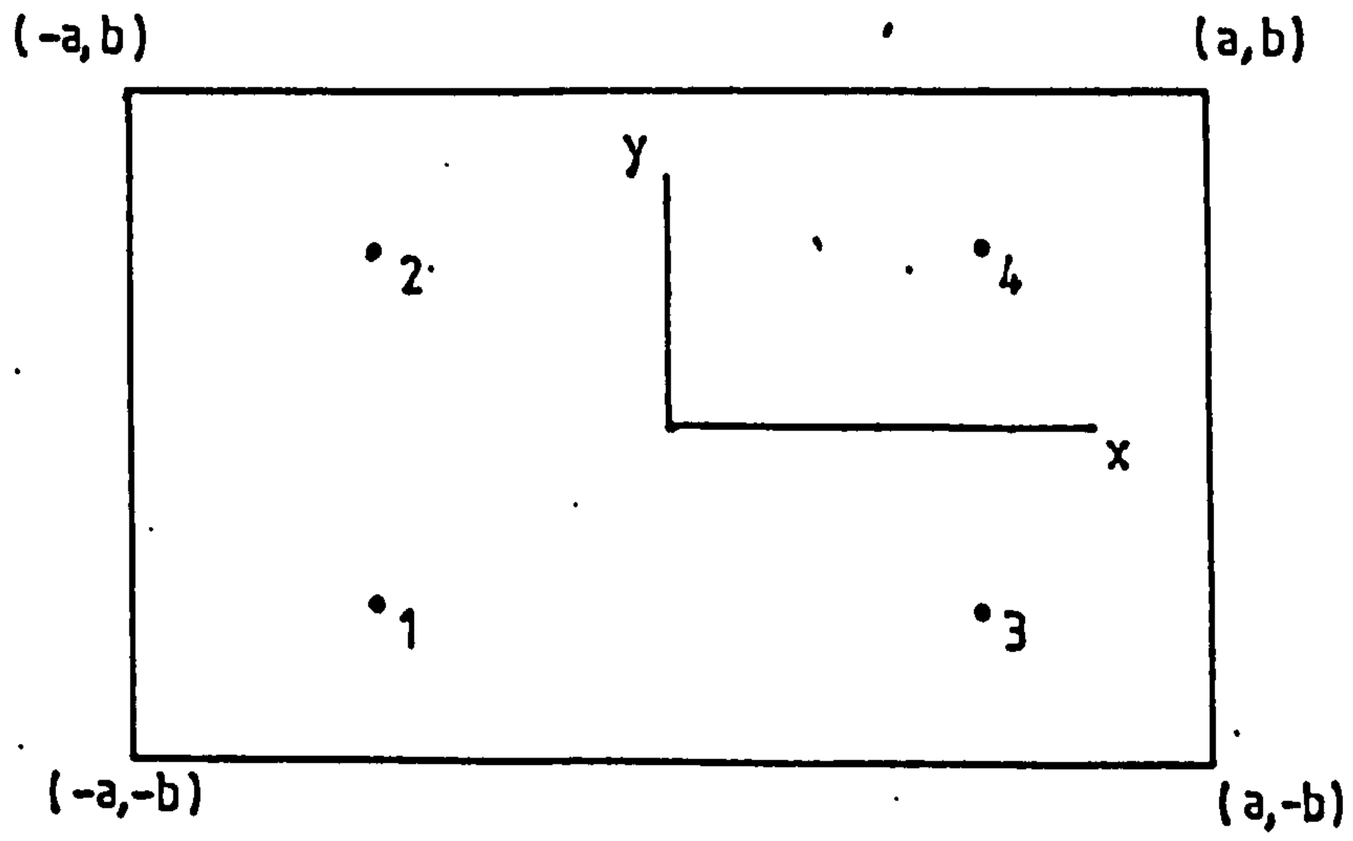

FIG. 2.6 Gauss Point Numbering Scheme at Element Level

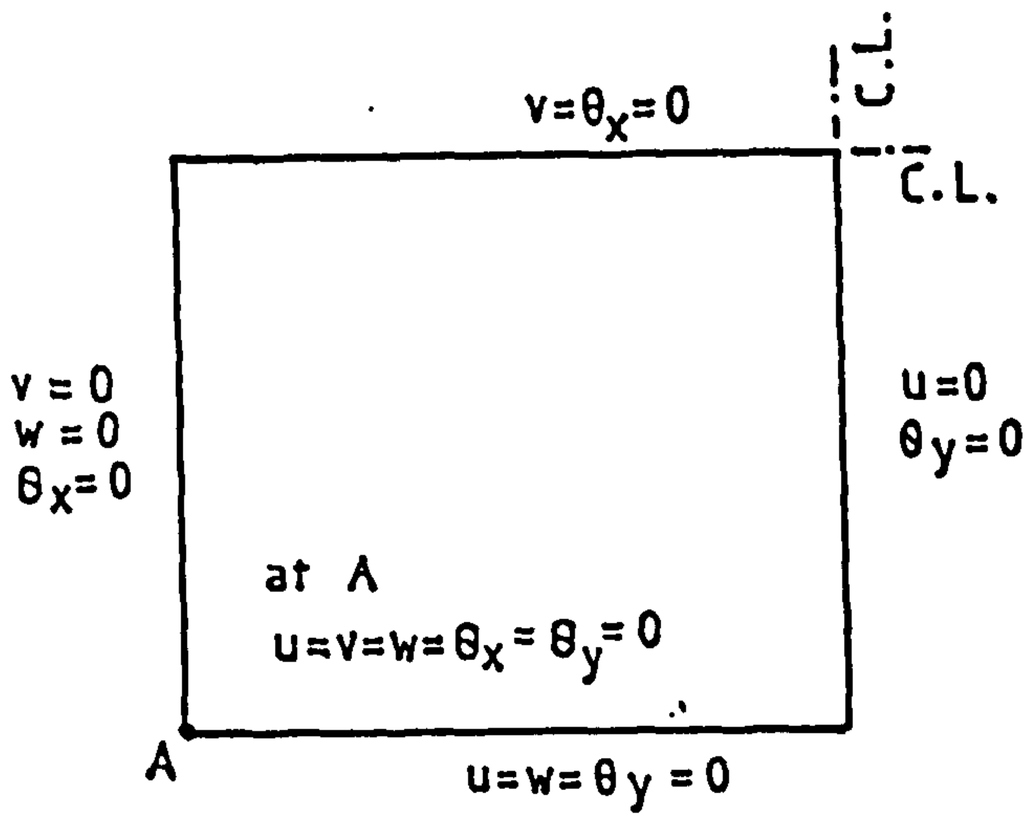

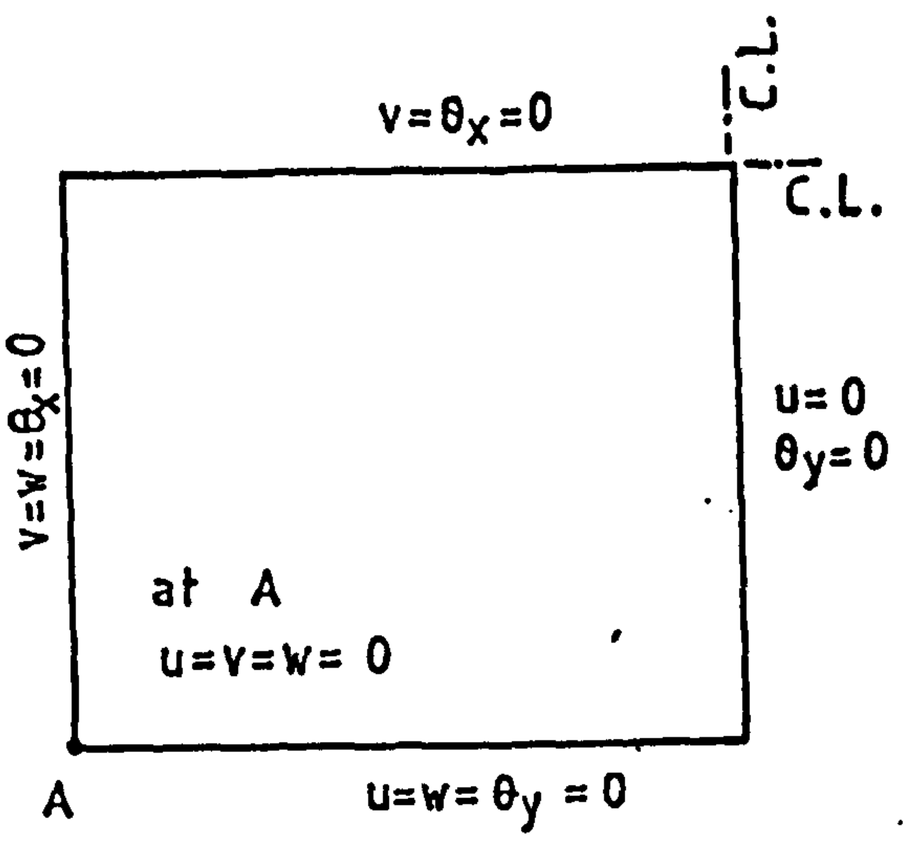

TYPE 1

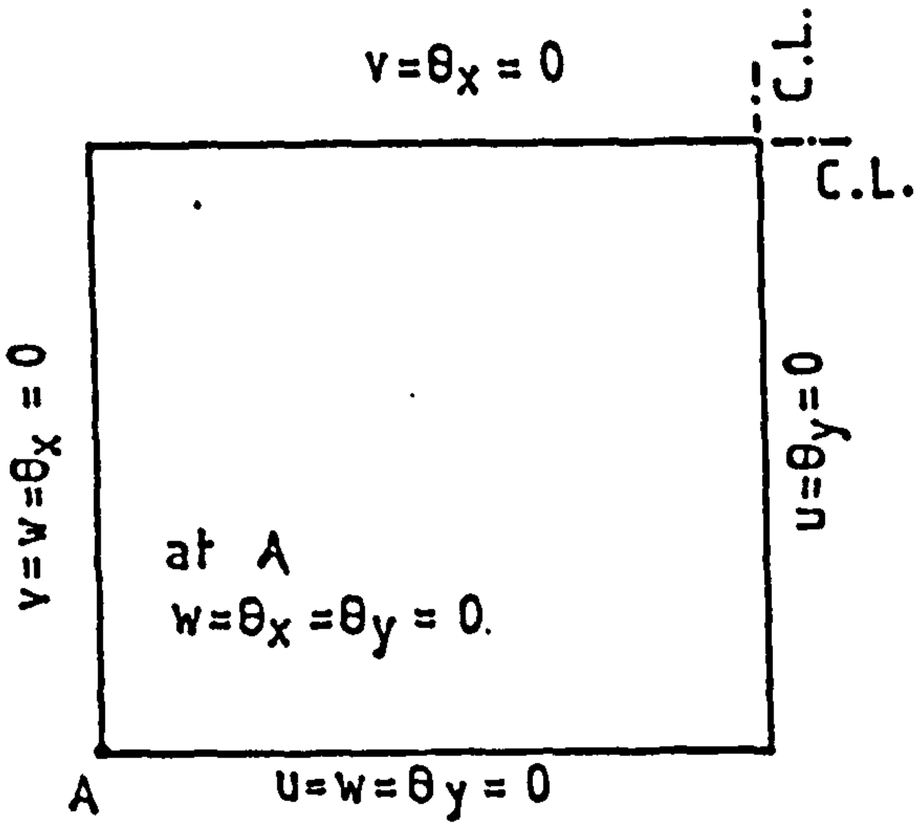

TYPE 2

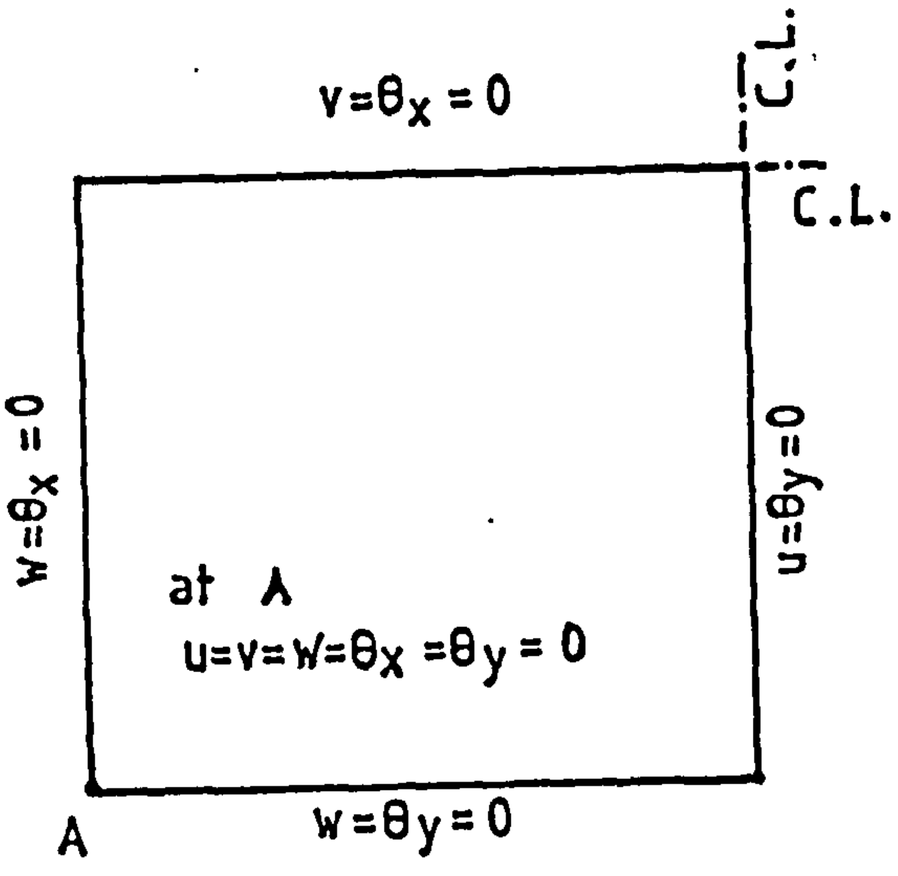

TYPE 3

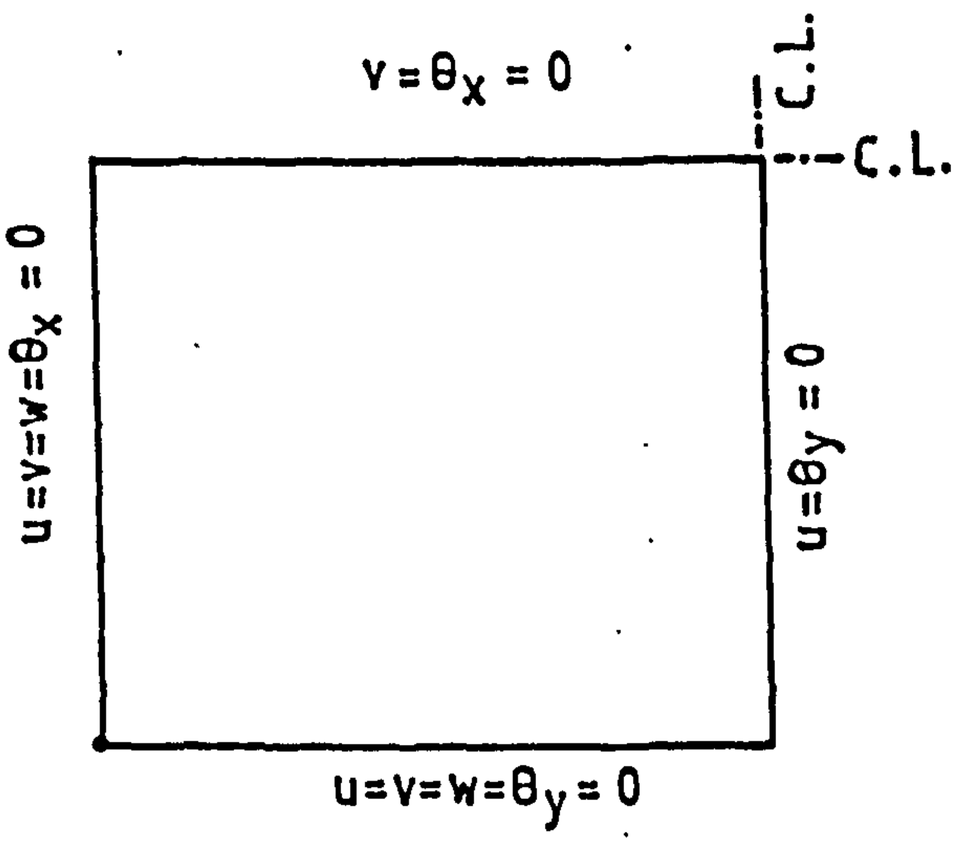

TYPE 4

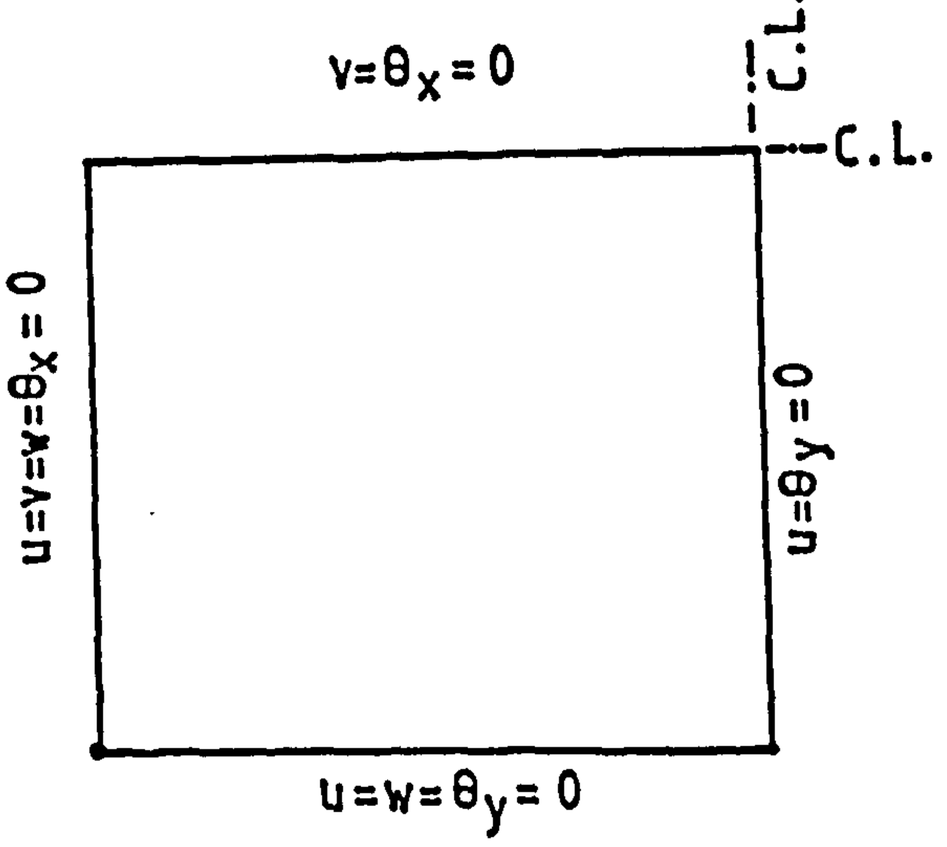

TYPE 5

TYPE 6

FIG. 2.7 Probable Types of Idealisation of the Boundary Conditions for a Symmetric Quadrant of a Simply Supported Slab

Chapter 3

MATERIAL MODELLING

3.1 Introduction

Reinforced concrete is a composite of concrete and steel. From the strength point of view, it is far from an ideal material. The concrete, itself being a composite, is subject to creep, microcracking and varying strength with age. Inclusion of reinforcement introduces the further problems of bond, anchorage and bond slip. Nevertheless, the layering concept would permit the idealisation of its constituent materials independently. The strain compatibility at the concrete-steel interface is the only link that holds them together as a composite.

In any nonlinear analysis of reinforced concrete structures, the basic information required is the multi-dimensional stress-strain relations describing adequately the characteristics of reinforced concrete materials subjected to monotonic and/or cyclic loading.These are called the constitutive relations[69] and may be viewed as the simplified mathematical description of the behaviour of the constituent materials, approximating closely to the real behaviour of reinforced concrete. In the following sections, the mathematical modelling for each of the constituent materials are described separately.

3.2 Behaviour of Concrete in Compression

Concrete can behave either elastically or inelastically depending upon the level and nature of stresses to which it is subjected. Under low stress levels, concrete behaves more or less as a linear elastic material. At higher levels of stress and under sustained loading it exhibits significant nonlinear response which have considerable effect on the behaviour of reinforced concrete structures. Besides, in a multiaxial

state of stresses, concrete displays somewhat different characteristic properties compared to those exhibited under uniaxial state[58]. These experimental observations act as the basis of the simplified models adopted for the analytical solution.

3.2.1 Uniaxial Behaviour

Under uniaxial compressive loading, concrete behaves almost linear elastically up to about 30-50% of its compressive strength. Beyond that level, concrete begins to soften gradually until it reaches the peak stress. Microcracks are believed to start forming in the mortar-aggregate interface at about the same stress level it begins to behave nonlinearly. But the macroscopic cracks indicating visual sign of damage are not usually noticeable prior to the attainment of its uniaxial compressive strength.

A typical stress-strain curve for concrete under monotonic uniaxial loading and its idealised version is given in Fig. 3.1. The uniaxial tension branch of the curves have also been included in the figure. It is obvious from Fig. 3.1 that concrete has been modelled as a bilinearly elastic, perfectly plastic material in compression and elastic-brittle material in tension. E_c and E_d are the respective modulus of elasticity for the first and second elastic regions, f_c being the transitional stress level. Concrete is assumed to go perfectly plastic when it reaches its ultimate strength f'_c and remains so until complete failure occurs at the crushing strain ϵ_u. An alternative formulation in which the modulus of elasticity becomes a function of stress level is described later (Art. 3.2.2.4) in the context of biaxial compression.

It is known that the shape of the stress-strain curves for low, normal and high strength concretes are similar[96]. The model stress-strain curve should, therefore, be able to approximate the actual behaviour for

any real concrete if the elastic modulii, transition stress, ultimate strength and crushing strains are known from a standard test. The initial modulus of elasticity for normal weight concrete may be reasonably estimated from the empirical relations provided in the codes of practice[1,23]. The second elastic modulus E_d may then be approximately taken as 30-40% of the initial value. A simple cube or cylinder crushing test would furnish the ultimate strength f'_c and 50% of this strength can be taken as the transitional value. In the alternative model, the initial modulus and the compressive strengths are the necessary data needed for the nonlinear description of constitutive relation under biaxial compression.

3.2.2 Biaxial Behaviour

Strength characteristics of concrete under different combinations of biaxial stresses are known to be different from those under uniaxial state of stress. In a state of biaxial compression, concrete displays increased compressive strength[58]. This gain in strength is dependent on the ratio of two principal compressive stresses and an increase of about 25% to that of its uniaxial compressive value has been observed[58,61]. Fig. 3.2 illustrates a typical biaxial strength envelope for concrete under various combinations of biaxial stresses.

3.2.2.1 Yielding and Failure Criteria

Yielding is a frequently used term in metal plasticity indicating the onset of plastic flow. A mathematical description of the plastic behaviour of a material is characterised by the following[39]:

a) Yield criterion - defining the elastic limit,

b) Flow Rule - relating incremental stresses to plastic strain increments, and

c) Hardening Rule - which determines the conditions for subsequent yielding after initial yield.

Thus a yield criterion may be defined as a mathematically determined critical combination of stresses which initiates the plastic flow. It is usually expressed as a scalar function of stresses and a hardening parameter. It can also be visualised as a surface in an n-dimensional space of stress components. The position of this surface at any subsequent stage of loading is determined by the initial yield surface and a hardening rule. Theoretically, a yield criterion can be expressed as

$$F(\sigma,k) = 0 \qquad (3.1)$$

where, k is a hardening parameter.

And the generally accepted flow rule relating the plastic strain increments to the yield surface may be stated as

$$d\varepsilon_p = \lambda \frac{\partial F}{\partial \sigma} \qquad (3.2)$$

where, $d\varepsilon_p$ denotes the plastic strain increments and

λ is a proportionality constant.

This rule is widely known as the normality principle because the relation in Eq. 3.2 can be interpreted as requiring the normality of the plastic strain vector to the yield surface.

3.2.2.2 Constitutive Relations After Yield

The constitutive relations in the incremental elasto-plastic formulation are based on the fact that after the onset of plasticity, the total incremental strain $d\varepsilon$ may be divided into a recoverable elastic part and an irrecoverable plastic part, so that

$$d\varepsilon = d\varepsilon_e + d\varepsilon_p \qquad (3.3)$$

The elastic strain component $d\varepsilon_e$ is related to the incremental stress $d\sigma$ by usual elasticity matrix as

$$d\varepsilon_e = D^{-1}.d\sigma \qquad (3.4)$$

The plastic strain component is obtainable from the selected yield criterion through Eq. 3.2. After some mathematical simplifications[72,100] the elasto-plastic constitutive matrix may be established. Thus,

$$d\sigma = D_{ep}.d\varepsilon \qquad (3.5)$$

where, elastoplastic matrix, D_{ep} is

$$D_{ep} = D - \frac{D\left\{\frac{\partial F}{\partial \sigma}\right\}\left\{\frac{\partial F}{\partial \sigma}\right\}^T D}{H' + \left\{\frac{\partial F}{\partial \sigma}\right\}^T D\left\{\frac{\partial F}{\partial \sigma}\right\}} \qquad (3.6)$$

The matrix D_{ep} is dependant on the chosen yield criterion, the flow rule and the hardening parameter, H'. The last one, i.e. H' actually denotes the local slope of the uniaxial stress to plastic strain diagram. This elasto-plastic matrix will remain symmetric, only if, an associated flow rule of plasticity has been invoked and shall remain defined even for an elastic-perfectly plastic material in which case H' equals zero. The explicit form of this elasto-plastic matrix for Von-Mises yield surface with an associated flow rule was introduced by Yamada et al[97] and Zienkiewicz et al[99]. Later, Nayak and Zienkiewicz[66] suggested an alternative method of expressing the yield criterion which is indeed a convenient form to generalise several classical yield conditions.

3.2.2.3 Applicability of Yielding to Concrete

Although it is evident that the incremental stress-strain relations beyond initial yielding may be mathematically modelled adequately, the choice of a suitable yield criterion describing the yield phenomenon in concrete appropriately remains debatable. The plasticity theory was

actually evolved to describe the behaviour of metals and is based on the micromechanisms of plastic slip in crystals. The nonlinear behaviour of concrete may only partly be attributed to such phenomenon. A more significant contribution to its inelastic behaviour is perhaps due to microcracking or microfracturing which is accompanied by a decrease in elastic modulii. The ASCE Task Committee[69] admits that the theory of incremental plasticity is not a very effective approach for modelling the behaviour of concrete. Nevertheless, the plasticity based models have been used successfully by many researchers[13,16,82]. In general, the plasticity based models describe concrete as an elastic-perfectly plastic material or as an elastic-plastic-hardening material. For the former case, the inelastic behaviour is in effect absent throughout the analysis because even after yielding the elastoplastic matrix (Eq.3.6) could be assigned a zero value without formal evaluation and only the stresses need to be held constant before a crushing surface is met. The strain hardening theory of plasticity has been introduced by Chen and Chen[16] to model the nonlinear behaviour of concrete under various combinations of stress. With this approach, an initial discontinuity surface is defined to mark the end of elastic behaviour. This initial surface is obtained by appropriately scaling down the assumed failure surface. On reaching the initial discontinuity surface, the subsequent stress increments are determined through an isotropic hardening rule which describes the subsequent loading surfaces, finally merging into the failure surface indicating total collapse.

3.2.2.4 Alternative Modelling of Biaxial Behaviour

In the alternative methods of formulating the behaviour of concrete under biaxial compressions two distinctive approaches may be identified. In one approach, the monotonic behaviour is of prime interest and in the

other the cyclic loading incorporating the path dependance of loading and unloading is carefully maintained. Obviously, the mathematical formulation for modelling monotonically loaded concrete is quite straight forward and simpler compared to those which strictly follow the path dependant behaviour. Both these methods have been found to be satisfactory as they can simulate the experimentally observed test results of concrete under biaxial or multiaxial state of stresses. In fact, these models are based on fitting a best-fit curve to the test data. Two such models to describe concrete behaviour under monotonic biaxial compressive stresses are illustrated below. These two have been included in the computer programme developed during this study.

In the first model, it is assumed that concrete is a bilinearly elastic material. If the representative unaxial stress-strain curve for concrete is available, then a bilinear fit to these data is easily possible. In absence of such data, the bilinear modulii of elasticities and the transitional stress may still be adequately estimated as described in Art. 3.2.1. In order to fuse this virtually uniaxial bilinear behaviour into concrete under biaxial compression, it is first necessary to assume a failure criterion under biaxial compression. The experimentally determined failure envelope (Fig. 3.2) of Kupfer et al[58] has been adopted here. The mathematical description of this surface in the biaxial principal stress space was given by Kupfer and Gerstle[59] and has been included in this study without any modification for the biaxial compressive state of stresses. Thus, the failure surface is

$$F(\sigma) = \left(\frac{\sigma_1}{f'_c} + \frac{\sigma_2}{f'_c}\right)^2 - \frac{\sigma_2}{f'_c} - 3.65\,\frac{\sigma_1}{f'_c} = 0 \qquad (3.7)$$

Noting that σ_1, σ_2 and f'_c are all negative and using absolute value for f'_c, Eq. 3.7 may be rearranged to give the major biaxial compression at failure as

$$\sigma_{2c} = -\frac{3.65 + k}{(1 + k)^2} f'_c \qquad (3.8)$$

where, $k = \frac{\sigma_2}{\sigma_1}$, the principal stress ratio.

Obviously,

$$\sigma_{1c} = k.\sigma_{2c} \qquad (3.9)$$

A second surface is then derived by appropriately scaling down the assumed failure surface. This may be taken as the initial discontinuity surface and has a similar shape to that of the assumed failure surface. It is, therefore, bounded by the transitional stress (f_c) at the two extremes instead of the ultimate strength (f'_c) in case of the failure surface. Fig. 3.3 gives a typical illustration of these two surfaces. This method of modelling was used by Hand et al[36] quite successfully. Romstad et al's[79] concept of using a number of damage regions may be regarded as an extension of this two zone concept. They proposed that the material properties be altered (but shall remain constant within each zone) as a new damage zone is reached to match the softening effect displayed by concrete.

The former model lacks the ability to represent the gradual degradation of the material properties continuously. To overcome this, a continuous uniaxial curve for concrete like that proposed by Cope et al[20] could have been used and the maximum compressive principal strains developed at any stage may be independently utilised to evaluate the current elastic constants. Alternatively, the uniaxial curve could be transformed in some way to an equivalent stress-strain curve like that of

Philips and Zienkiewicz[74] or Darwin and Pecknold[24] separating the Poisson's effect. The current material state could then be approached through these equivalent curves. While such methods remain of interest and appealing by their own virtue, a different approach proposed by Gerstle[31] has been followed to develop the second model.

This formulation is based on the observed correlation of octahedral shear stress to octahedral shear strain and octahedral normal stress to octahedral normal strain obtained from various test data. In its essence, it is presupposed that the hydrostatic and deviatoric components of responses for concrete are uncoupled. Thus, following Gerstle's approach, the tangential bulk modulus (K_t) and shear modulus (G_t) at any stage of loading, may be obtained as

$$K_t = K_o \left(1 - C_2 \frac{\sigma_o}{\sigma_{ou}}\right) \tag{3.10}$$

where, C_2 is an experimentally determined constant

K_o is the initial bulk modulus and

$$\sigma_{ou} = \frac{1}{3}\left(1 + \frac{\sigma_2}{\sigma_1}\right)\sigma_{1u} \tag{3.11}$$

σ_{1u} is the (algebraically) maximum principal stress at failure for the same principal stress ratio as the current one

and

$$G_t = G_o \left(1 - \frac{\tau_o}{\tau_{ou}}\right) \tag{3.12}$$

where, G_o is the initial shear modulus

$$\tau_{ou} = \frac{\sqrt{2}}{3}\left(\sqrt{1 - k + k^2}\right)\sigma_{1u} \tag{3.13}$$

where k is the principal stress ratio as defined in Eq. 3.8.

To evaluate σ_{1u} at any stress ratio, a failure surface under biaxial compression must be defined. Herein, also the failure surface of Kupfer and Gerstle[59] has been employed. The instantaneous values of elastic modulus (E_t) and Poisson's ratio (ν_t) may then be obtained through the standard relations of theory of elasticity[86].

From the experimental observation[58,61] it has been found that the Poisson's ratio remains almost constant throughout the loading history except, near failure it increases significantly. In view of that and due to the conflicting[31] evidence of the variations of bulk modulus in different experiments, the Poisson's ratio (ν) has been assumed to be constant throughout. This implies that the variation of elasticity modulus and hence the bulk modulus is entirely dependant on the variation of shear modulus only.

3.3 Behaviour of Concrete in Biaxial Tension and Tension-Compression State

The inherent weaknesses of concrete in tension do not seem to have any appreciable improvement under biaxial tension or in a tension compression environment. On the contrary, experimental results[58,61] show that the tensile strength falls short of unaxial value in a tension-compression situation. When both the stresses are tensile, the failure strength is only slightly greater than the uniaxial strength.

Again the strength envelope of Kupfer et al[58] has been selected for biaxial tension-tension and tension-compression state of stresses. But this time with little modification. The experimental curve (Fig. 3.2) in the biaxial tensile stress space has been idealised as an arc of a circle so that

$$F(\sigma) = \sqrt{(\sigma_1/f'_t)^2 + (\sigma_2/f'_t)^2} - 1 = 0 \qquad (3.14)$$

where, f'_t = uniaxial tensile strength.

In the tension-compression region, the observed curve has been replaced by a straight line of the form

$$F(\sigma) = \frac{\sigma_1}{f'_t} - \frac{\sigma_2}{f'_c} - 1 = 0 \qquad (3.15)$$

Thus, under either uniaxial tension or compression, Eq. 3.15 reduces to their respective unaxial strengths. Whenever concrete is subjected to tensile forces, it behaves like a linear elastic-brittle material. This indicates that the idealised strength envelopes of Eq. 3.14 and 3.15, illustrated in Fig. 3.3, may be treated as a cracking surface. Tensile strength of concrete is very low compared to its compressive strengths. It is therefore very much unlikely that the elastic constants could change under such small loads. The elastic modulus is therefore left unaltered in biaxial tension or tension-compression stress conditions.

3.4 Cracking of Concrete

The onset of cracking in concrete may be defined as a combination of stress which initiates physical disintegration of the bond that holds cement and aggregates together in a concrete matrix. Although, some microcracks may have been present even before the structure sustains any external load[61]. They are formed by differential temperature and shrinkage effects, to which any concrete structure is subjected to during the hydration and curing process. Their existence can not be altogether eliminated and they seem to have no significant contribution in the ultimate behaviour of concrete.

In an analytical treatment of a concrete structure, the physical cracking condition is of importance. In this study, a real crack in concrete is assumed to have developed when stresses at a point exceeds (or equals) the mathematically described cracking surfaces given by Eq. 3.14 and 3.15. Cracking in concrete introduces a physical discontinuity in the continuity of the structure which may be represented differently for numerical modelling. This has resulted in two different models of crack representation, namely, i) Discrete Cracking Model and ii) Smeared Cracking Model.

3.4.1 Discrete Cracking Model

The discrete crack approach introduces an actual gap in the finite element mesh. The physical separation is achieved by doubling and separating the nodal coordinates along the crack path. Ngo and Scordelis[67] introduced this approach to study the effect of cracking numerically and carried out a linear analysis of reinforced concrete beams with predefined crack patterns. Nilson[68] extended this approach to allow the finite element model to generate the location of the cracks. In any case, the physical bifurcation of the nodes necessitated renumbering of the nodes followed by changes in the element connectivity. The changing topology of the elements eventually destroys the narrow bandwidth of the structural stiffness matrix and demands additional computational efforts. The semi-automatic nature of this model restricted its wide application in the analysis of reinforced concrete structures. However, if localised behaviour of concrete structures like that of dowel action, bond, aggregate interlock, etc. are of interest, then discrete cracking model appears to be a natural choice and tool[69].

3.4.2 Smeared Cracking Model

In the smeared cracking model, the material properties are drastically changed at the location of cracking as a means to simulate the effect of discontinuity. Such a change is achieved by significant reduction of the stiffness properties in the direction normal to the crack. This does not involve any physical gap in the element mesh. Rather, it represents a crack as a finely spaced fissures at the sampling point. The introduction of this smeared cracking concept is attributed to Rashid[78] by the ASCE Committee on Finite Element Analysis of Reinforced Concrete[69].

During the stiffness computation and stress evaluation stages, material properties are evaluated at some specific points in an element called the sampling points. Alteration of the material properties at any sampling point due to cracking eventually reflects an over all material damage of the contributing region from which these properties are made up, hence smearing the effect of cracking over all that region. While this approach allows complete generality to the direction of crack, but it does not specify the extent or physical length of the crack. The exact location and the extent of penetration of a crack are not of prime importance for the study of an overall response of concrete structure. Therefore, this model seems adequate for such situations, although it fails to delineate a crack boundary. In view of the generality of application and relative ease of implementation compared to the discrete cracking method, the smeared cracking model has been adopted for crack representation.

3.4.3 Orientation of the Cracks

When the stress combination reaches one of the two cracking

criterion (Eq. 3.14 and 3.15), a crack is assumed to have formed. From the experimental evidence of Kupfer et al[58] it is known that the tensile cracking is normal to the principal tensile stress. This is true even if the second principal stress is compressive with relatively low magnitude. When the compression is quite high, the test results do not show conclusively as to the preferred direction of crack. Therefore, the crack orientation would be based on the principal tension at the time of its formation. The angle between the crack and the positive x-axis is measured counter clockwise positive as shown in Fig. 3.4 and may be deduced from

$$\tan 2\Theta = \frac{\tau_{xy}}{(\sigma_x - \sigma_y)/2} \qquad (3.16)$$

If the absolute value of the numerator and denomerator are used, the crack angle (Θ) obtained from Eq. 3.16 would be always an acute angle between 0°-45°. The actual crack direction may be determined with reference to the Mohr's circle of stress. This is illustrated in Fig. 3.5.

3.4.4 Post Cracking Behaviour

The initiation of a crack at a point in no way indicates a complete failure of that point. Rather it should be treated as the starting point of nonlinear behaviour of concrete. In the cracking environment of concrete, the overall load deflection response depends significantly on how well the post cracking behaviour is modelled in the numerical solution of such problems. A practical analysis technique should not only be capable of describing the stress-strain relations following a crack, but should also include some additional factors such as multiple cracking criterion, shear transfer across the crack, tension stiffening, etc. The numerical technique incorporating these phenomenon follows.

3.4.4.1 Constitutive Relations After First Crack

After the formation of the first crack, the concrete is assumed to lose its stiffness perpendicular to the crack direction. This implies that stress normal to the crack cannot develop henceforth. The elasticity matrix in this local crack oriented direction may be stated as

$$C_L = \begin{bmatrix} E & 0 & 0 \\ 0 & 0 & 0 \\ 0 & 0 & \beta G \end{bmatrix} \qquad (3.17)$$

where, β is a shear retension coefficient.

If the angle between the crack direction and the global X-axis is θ, then the local elasticity matrix (C_L) is transformed to Global Co-ordinate System as

$$C_G = T_\varepsilon^T C_L T_\varepsilon \qquad (3.18)$$

where, the standard strain transformation matrix[17] T_ε is

$$T_\varepsilon = \begin{bmatrix} c^2 & s^2 & cs \\ s^2 & c^2 & -cs \\ -2cs & 2cs & (c^2-s^2) \end{bmatrix} \qquad (3.19)$$

Note, $c = \cos\theta$, $s = \sin\theta$, θ = orientation of crack.

3.4.4.2 Shear Retention Coefficient

On formation of a crack, the texture of the cracked surface may play a signficant role on its subsequent behaviour. For normal concrete, the surface that results from cracking has a definite roughness. This may restrain the free movement of the separated pieces resulting in transferring some shear force along the cracked face. This phenomenon is known as aggregate interlock. Besides, some forces are transferred across a crack by dowel action which is due to the bearing of reinforcement passing a crack against uncracked concrete. To realise these facets of cracking phenomenon, a reduced shear modulus term (βG) has been included

in the post cracking constitutive relation of Eq. 3.17. This shear retention coefficient, β may be assigned any value between 0 and 1. Some early researchers[78,90,92] ignored this effect altogether, i.e. they assumed β= 0. But this has led to some numerical difficulties and brought about the use of shear retention factor β with a value greater than zero[37,82].

Thus, the shear retention coefficient has served the purpose of an escape goat to circumvent the ensued numerical difficulty. Hand et al[37] suggested that any value greater than zero should serve the purpose and the effect of varying β is not too significant. A recent study by Bedard[5] shows that too small a value (less than 0.1) for β can produce appreciable change in the predicted behaviour. Same applies for higher value near 1. But when the value of β lie between 0.1 and 0.5, a practically stable and almost identical solution is achieved. In this study, the shear retention coefficient β shall be deemed to have a value equal to 0.5 unless overruled by explicit mentioning.

3.4.4.3 Tension Stiffening

The post cracking constitutive relation of Eq. 3.17 imposes restriction on the growth of any further stresses normal to the crack. But it does not outline the way of treating the crack normal stress that initiated its formation. One way of handling this is to drop the crack normal stress to zero as soon as the crack develops. This implies that concrete is a brittle material and loses its strength and ability to transfer any stress perpendicular to crack direction. Considering the realism of crack propagation, it is known that the development of crack is a gradual process. Confining effect of the surrounding material and the presence of reinforcing steel restrains the sudden widening and full development of cracks until perhaps the yield strength of steel is

approached. The stress in concrete at a real crack is obviously zero, but it is not zero if averaged over a finite distance. With the increase in load, more cracks develop, and the tension carried by concrete is gradually reduced to zero. This observed phenomenon of gradual decay of tensile stress perpendicular to the crack is termed the Tension Stiffening effect.

The effect of tension stiffening may be included in the numerical model by asigning a descending branch to the tension portion of the stress-strain curve for concrete. This may be represented as either a gradual decay of tensile stress or as a stepwise reduction. Lin and Scordelis[60] used the former while Cope et al[20] suggested single step linear decay and Huq[45] used both. Two types of gradually decreasing model have been implemented in this programme. In the first model, the decay is linear while in the second it is given a parabolic variation. They are illustrated in Fig. 3.6 and it may be seen that the descending branch meets the strain axis at $n.\epsilon_{cr}$. Strain ϵ_{cr} represents the uniaxial tensile strain corresponding to the tensile strength f'_t and may be estimated as

$$\epsilon_{cr} = \frac{f'_t}{E_c} \qquad (3.20)$$

The value assigned to 'n' is either 10 or 20, thus resulting in four different curves of two general forms.

At any stage after cracking, the sustained stress normal to the crack becomes a function of strain in that direction. Therefore, during subsequent computation either the whole (in case of no tension stiffening) or a part of this crack normal stress is thrown back to the structure and its effect is sympathetically shared by other neighbouring regions. The stress released from a crack may be transformed to global

coordinate system as

$$\begin{Bmatrix} \sigma_x \\ \sigma_y \\ \tau_{xy} \end{Bmatrix}_{ex} = \begin{Bmatrix} s^2 \\ c^2 \\ -cs \end{Bmatrix} \Delta\sigma_1 \qquad (3.21)$$

where, $c = \cos\theta$, $s = \sin\theta$, θ = crack orientation,

$\Delta\sigma_1$ = magnitude of released stress from the crack normal direction, and left hand terms represent the excess stresses in global direction resulting from cracking.

It may be noted that the strain normal to crack would usually be different from ϵ_{cr} at the time of crack formation. This is because a stress criterion has been employed to detect the onset of cracking and under biaxial state of stress, the Poisson's effect will make the crack normal strain different from ϵ_{cr} even if the corresponding stress is f'_t. This implies that since a uniaxial tension stiffening curve has been adopted, the crack normal stress may drop suddenly on formation of a crack and would remain constant at that value until increasing strain enables it to meet the descending branch. This is what has been followed and is schematically shown by dotted lines in Fig. 3.6.

3.4.4.4 An Alternative Approach to Tension Stiffening

From what has been discussed in the preceding articles it follows that, on formation of a primary crack, the stress-strain constitutive matrix is set crack oriented and stress normal to crack is gradually withdrawn. However, this scheme does not pay appropriate attention to the actual state of stress at a cracked point. To be precise, even the strictest adherence to such a scheme may lead to a stress state which exceeds the mathematically defined cracking surface and yet the secondary cracking criteria (Art. 3.4.4.6) are not violated. To avoid such a mathe-

matically inadmissible situation, a different approach is postulated here.

This alternative approach is similar to much established method followed in plasticity relations to scale the state of stress exactly on to the yield surface[72] after the plastic work has been accounted for. This will be illustrated with the help of a schematic drawing of cracking surface in principal stress space (Fig. 3.7). Defining a term effective stress index as

$$\bar{\sigma}_e = \sqrt{(\sigma_1^2 + \sigma_2^2)}/f_t' \qquad (3.22)$$

for tension-tension condition

and $$\bar{\sigma}_e = \frac{\sigma_1}{f_t'} - \frac{\sigma_2}{f_c'} \qquad (3.23)$$

for tension-compression state.

Both the cracking surfaces (Eq. 3.14 and 3.15) may be reduced to,

$$\bar{\sigma}_e = \bar{\sigma}_c = 1.0 \qquad (3.24)$$

Therefore, if the stresses at a point results $\bar{\sigma}_e$ less than $\bar{\sigma}_c$ then it implies that the concerned point is still uncracked. This would correspond to a point say A, (see Fig. 3.7) within the crack surface. In the following iteration, the stress increment would increase $\bar{\sigma}_e$ by $\Delta\bar{\sigma}_e$ leading to point B which falls outside the crack surface. Obviously, the exact cracking state corresponds to the point C on the crack surface. The current stress increment should be reduced by an amount corresponding to BC in order to get the exact state of stresses at the initiation of primary cracking. The reduction factor RF is given by

$$RF = \frac{BC}{AB} = \frac{\bar{\sigma}_e^{\,l} - \bar{\sigma}_c}{\bar{\sigma}_e^{\,l} - \bar{\sigma}_e^{\,l-1}} \qquad (3.25)$$

where, $\bar{\sigma}_e^{\,l}$ and $\bar{\sigma}_e^{\,l-1}$ corresponds to the effective stress index for the current iteration and the previous iteration respectively.

This linear interpolation technique or a similar has been followed wherever a mathematically defined surface in stress space is exceeded for the first time.

Now, once a crack has developed, the stress state will correspond to a point on the crack surface like that of C or D. After the constitutive matrix has been adjusted for following a crack, the next iteration may lead the stress state to point E, outside the crack surface. This seems mathematically inadmissible. So, this time the stresses will be simply scaled down to point F on the crack surface. Therefore, the reduction factor by which the total current stresses have to be factored to get the excess inadmissible portion of the stresses is

$$RF = \frac{FE}{OF} = \frac{\bar{\sigma}_e^{\,l} - \bar{\sigma}_c}{\bar{\sigma}_e^{\,l}} \qquad (3.26)$$

Thus, at any stage the stresses would always remain on the crack surface. After first cracking, the crack oriented constitutive relations (Eq. 3.17) restrict the growth of any stress normal to the crack. So, whenever the subsequent total stresses are proportionally scaled down to the cracking surface, the stress normal to the crack is in effect progressively reduced. Therefore, the tension stiffening effect is automatically taken care of. However, in purely unidirectional bending situations, the post cracking constitutive relation may not produce any subsequent change in stress due to the predominantly uniaxial nature of the stress state. This scheme may then lock up the crack normal stress at the initial cracking value until a secondary failure occurs. This would certainly overestimate the effect of tension stiffening in such cases.

3.4.4.5 Crack Closure

In case of cyclic loading it is essential to include a criterion for crack closure. The effect of crack closure is to give back to the structure its lost stiffness in full or in part to retain the effect of damage already incurred upon. Even under monotonic loading, it is theoretically possible that the effect of nonlinearities may cause sufficient stress redistribution over a small region causing an existing crack to close.

Although such an unloading situation may seldom be encountered in monotonic loading, a crack closing criterion has been included to maintain generality. In the smeared cracking model, the strain normal to the crack has sometimes been used as a measure of crack width and is usually employed to follow up the tension stiffening effect. Therefore, the same can be addressed again to check crack closure. That is, when strain normal to the crack turns to be compressive the crack is deemed to have closed. But this criterion alone may give a false picture near failure condition. It has been observed[5,49] that after extensive yielding of steel, the decay in the structural stiffness coefficients introduces numerical instability to the solution. This may result in unrealistic displacement and strain quantities. To avoid such a situation, the criterion for crack closing adopted also includes the stress component normal to the crack direction. That is when both stress and strain perpendicular to the crack is found to be compressive, the crack is assumed to have closed. The layer at that Gauss point is given back the original stiffness properties with or without an arbitrarily reduced elasticity modulus.

3.4.4.6 Multiple Cracking

The direction of multiple cracking system depends on the stress-strain behaviour assumed subsequent to the initial cracking. In the smeared cracking model which does not include shear retention factor , the secondary crack is forced to develop perpendicular to the initial crack. On the other hand the model which incorporates the shear retention factor, allows the rotation of the concrete principal stress directions after primary cracking. The secondary cracks may not therefore be necessarily orthogonal to the initial crack. This demands that an admissible angle between the two sets of crack should be supplied. From the previous experiences of Bell and Elms[6] and Cope et al[20], the admissible angle has been arbitrarily taken as 50°.

In addition, the stress parallel to the crack has been subsequently checked after every iteration following the initial cracking. If this crack parallel stress exceeds the tensile strength f'_t, the secondary crack is assumed to have formed orthogonal to the primary crack. On the other hand, if this stress is compressive and exceeds the uniaxial compressive strength f'_c then a strut type compressive failure is assumed. In either case, the layer at that sampling point is assumed to loose its stiffness completely.

3.5 Local Failure

The term local failure is used to represent complete failure of a local sampling point. That is, when the total stiffness of a layer corresponding to the sampling point is completely lost. This can happen when a multiple crack has formed in the concrete or when the crack parallel stress has reached the uniaxial crushing strength of concrete. Under biaxial compression and in general a crushing surface has been defined in strain space to indicate a local failure. This has a similar

shape to that of biaxial compressive strength envelope and was employed by Rahman et al and others[45,76]. This crushing criterion is given as

$$F(\epsilon) = \sqrt{(\epsilon_x^2 + \epsilon_y^2 - \epsilon_x\epsilon_y + 0.75\gamma_{xy}^2)} - \epsilon_u \qquad (3.27)$$

When any of these local failure conditions is met at a sampling point, the constitutive relationship is reduced to

$$d\sigma = 0\epsilon \qquad (3.28)$$

3.6 Constitutive Modelling of Reinforcement

Reinforcing steel is assumed to be smeared into a thin layer of thickness equivalent to its total area. This smeared layer of steel is assumed to have unidirectional stiffness corresponding to the direction of its physical layout. The stress-strain relations for steel reinforcement in its local direction (Fig. 3.8)) is

$$\begin{Bmatrix} \sigma_{x'} \\ \sigma_{y'} \\ \tau_{x'y'} \end{Bmatrix} = C_L \begin{Bmatrix} \epsilon_{x'} \\ \epsilon_{y'} \\ \gamma_{x'y'} \end{Bmatrix} \qquad (3.29)$$

where C_L is the elasticity matrix and is given as

$$C_L = E_s \begin{bmatrix} 1 & 0 & 0 \\ 0 & 0 & 0 \\ 0 & 0 & 0 \end{bmatrix} \qquad (3.30)$$

With the steel disposed of at an angle φ counter clockwise, from the x-axis (Fig. 3.8), the local modulus matrix may be transformed to the cartesian space, thus

$$C_G = T_\epsilon^T C_L T_\epsilon \qquad (3.31)$$

where, T_ϵ is the same standard strain transformation matrix of Eq. 3.19 and now, note that $c = \cos\varphi$, $s = \sin\varphi$ and φ is the steel angle w.r.t. x-axis.

Steel reinforcement has been idealised as an elastic-perfectly

plastic material. Thus, when yielded, it is assumed to be unable to carry any increase in load and the incremental stress-strain relation reduce to that of Eq. 3.28 indicating local failure. An idealised stress-strain curve for steel is provided in Fig. 3.9.

3.7 Numerical Procedures for Material Property Changes

Fundamentally, the solution scheme is an incremental-iterative type. Following a load increment, the internal equilibrium is checked in an iterative way. It is during this internal equilibrating force computation that the material characteristic changes are exclusively searched for. When cracking occurs in concrete, or steel yields, or any changes are noticed in the constituent materials, the current characteristic material properties are updated to match the appropriate models described in the preceding articles. The current stress vector is updated after accounting for all the material characteristic changes in this current iteration and an excess stress vector comprising the inadmissible part of stresses resulting from the material nonlinearities is also computed. The equivalent internal nodal force vector corresponding to the current stress level and the internal nodal excess force vector due to the excess stresses are then computed as

$$R_i = \int B^T \sigma \, dv \tag{3.32}$$

and

$$R^{ex} = \int B^T \sigma^{ex} \, dv \tag{3.33}$$

These force vectors are initially evaluated at the element level. So, they are to be appropriately summed to get the corresponding vectors at structure level. Finally, the residual nodal force vector for the total structure can be obtained as

$$\text{either, } \Psi = R - \sum_{e=1}^{n} (R_i)_e \tag{3.34a}$$

$$\text{or } \Psi = \sum_{e=1}^{n} (R_i^{ex})_e \tag{3.34b}$$

The computational procedures for evaluating the integrals in Eq. 3.32 and 3.33 has been described in the previous Chapter (Art. 2.5.8).

For reinforced concrete structures, the analytical results may depend significantly on the magnitude of the load increments. If the load increments are too large, the initial deflected shape may not follow the realistic path and a part of the model may prematurely fail due to high strains. Only sufficiently small load increments would enable to follow highly path-dependent material like reinforced concrete. From others' [45,49] experience and the present, the preferred load increments seem to be less than 15 per cent of the load that initiates the first crack in the structure.

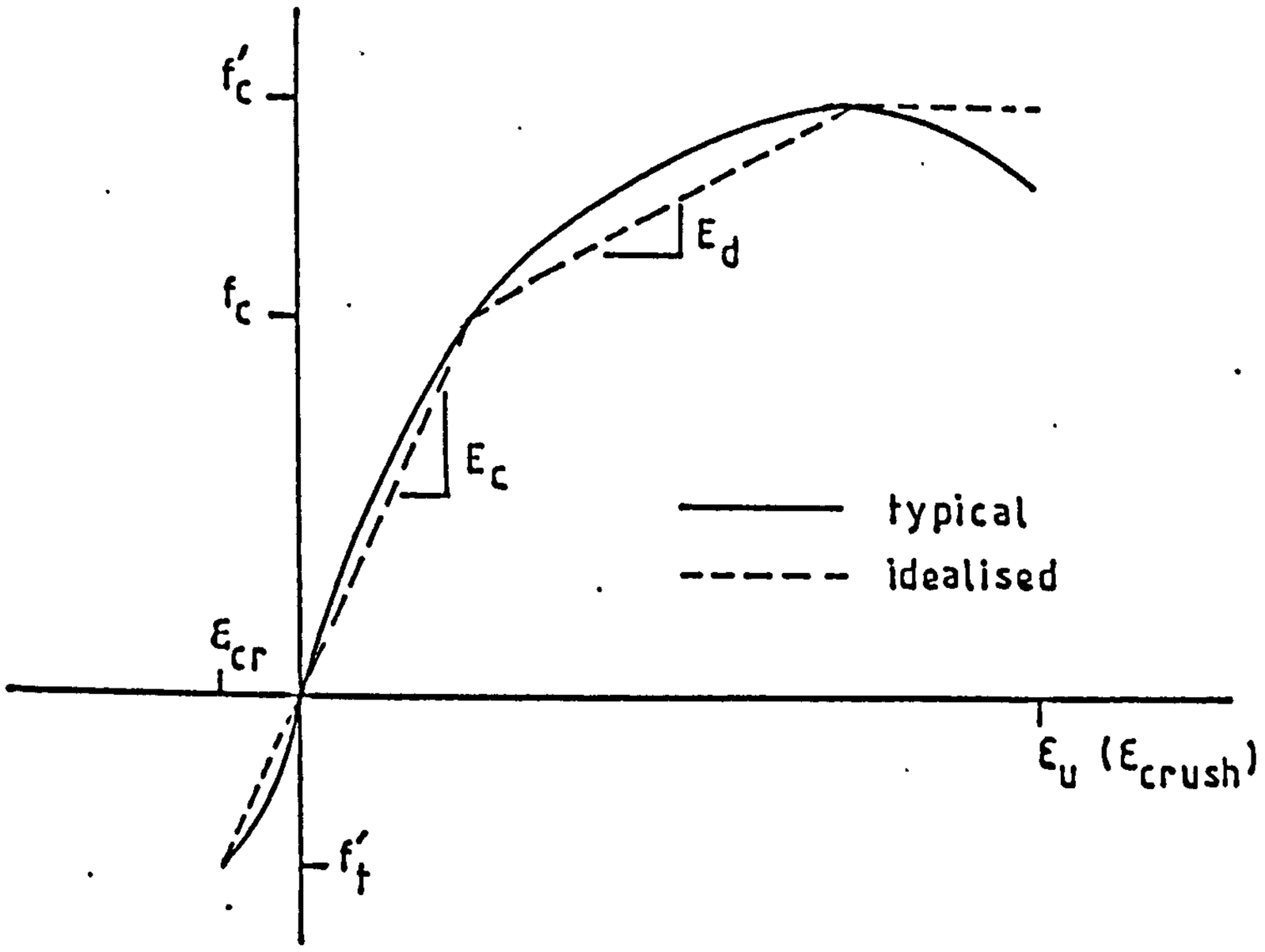

FIG. 3.1 Typical and Idealised Uniaxial Behaviour of Concrete

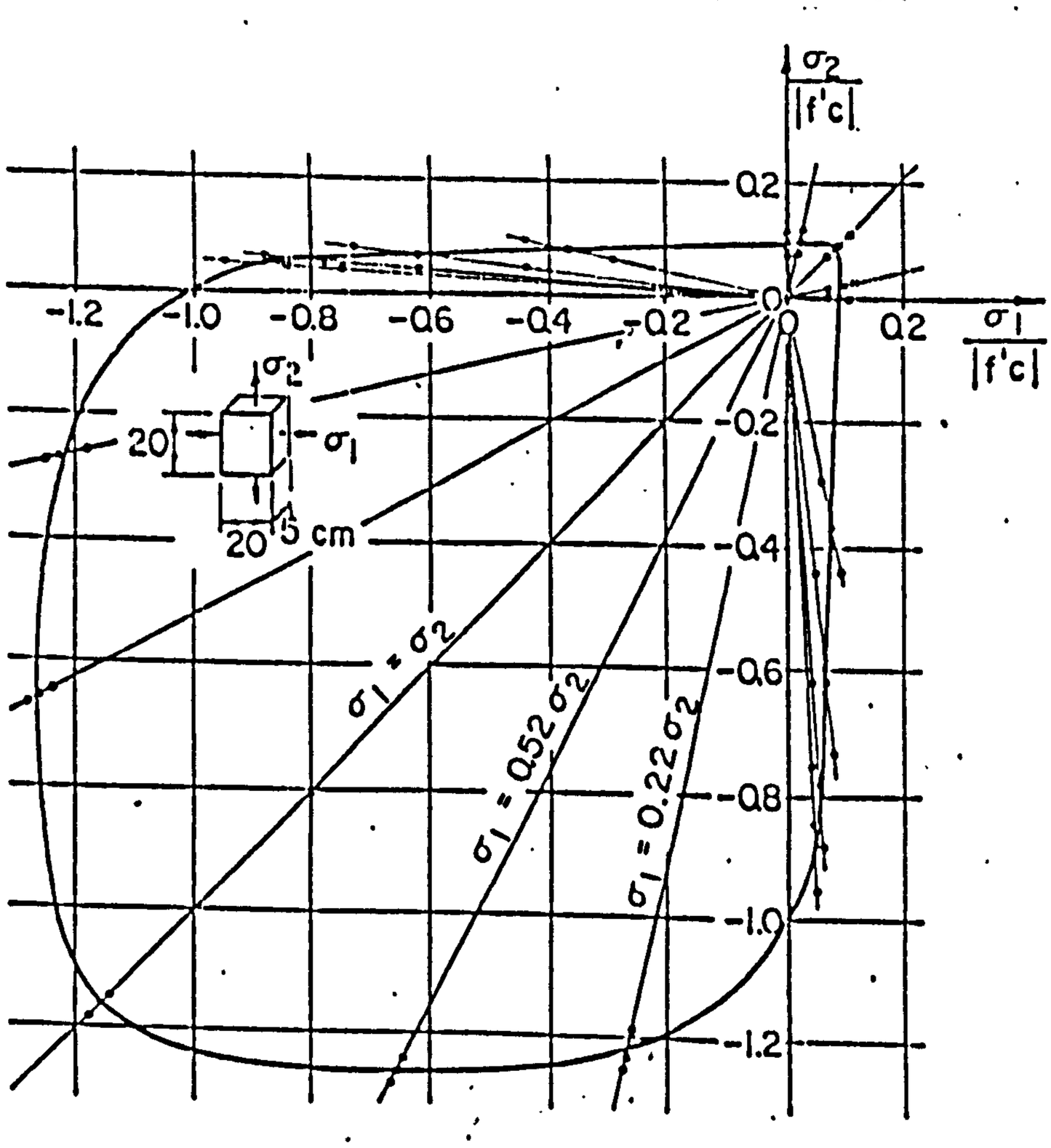

FIG. 3.2 Biaxial Strength Envelope for Concrete (ref. 58)

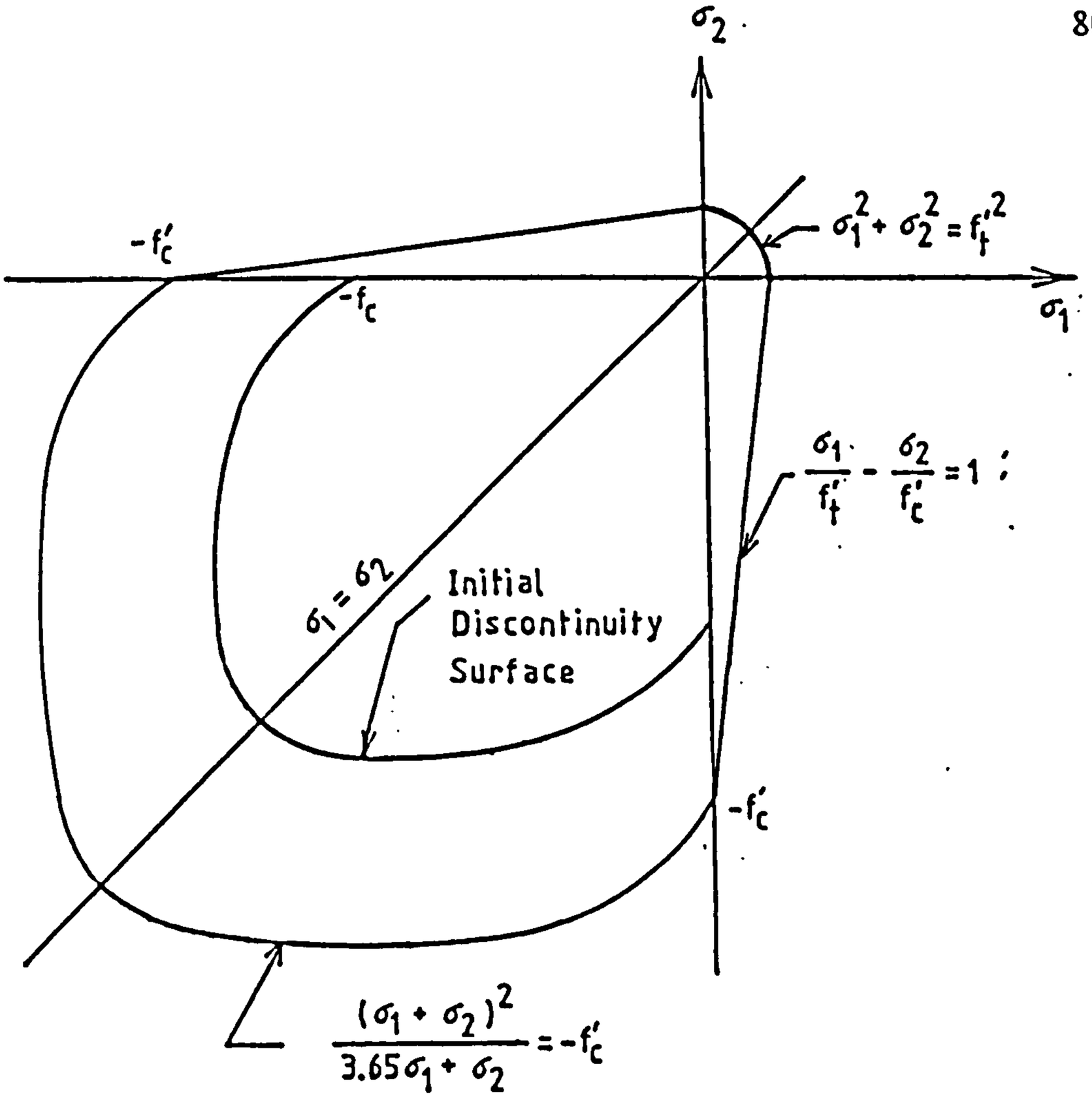

FIG. 3.3 Idealised Biaxial Strength Envelope for Concrete

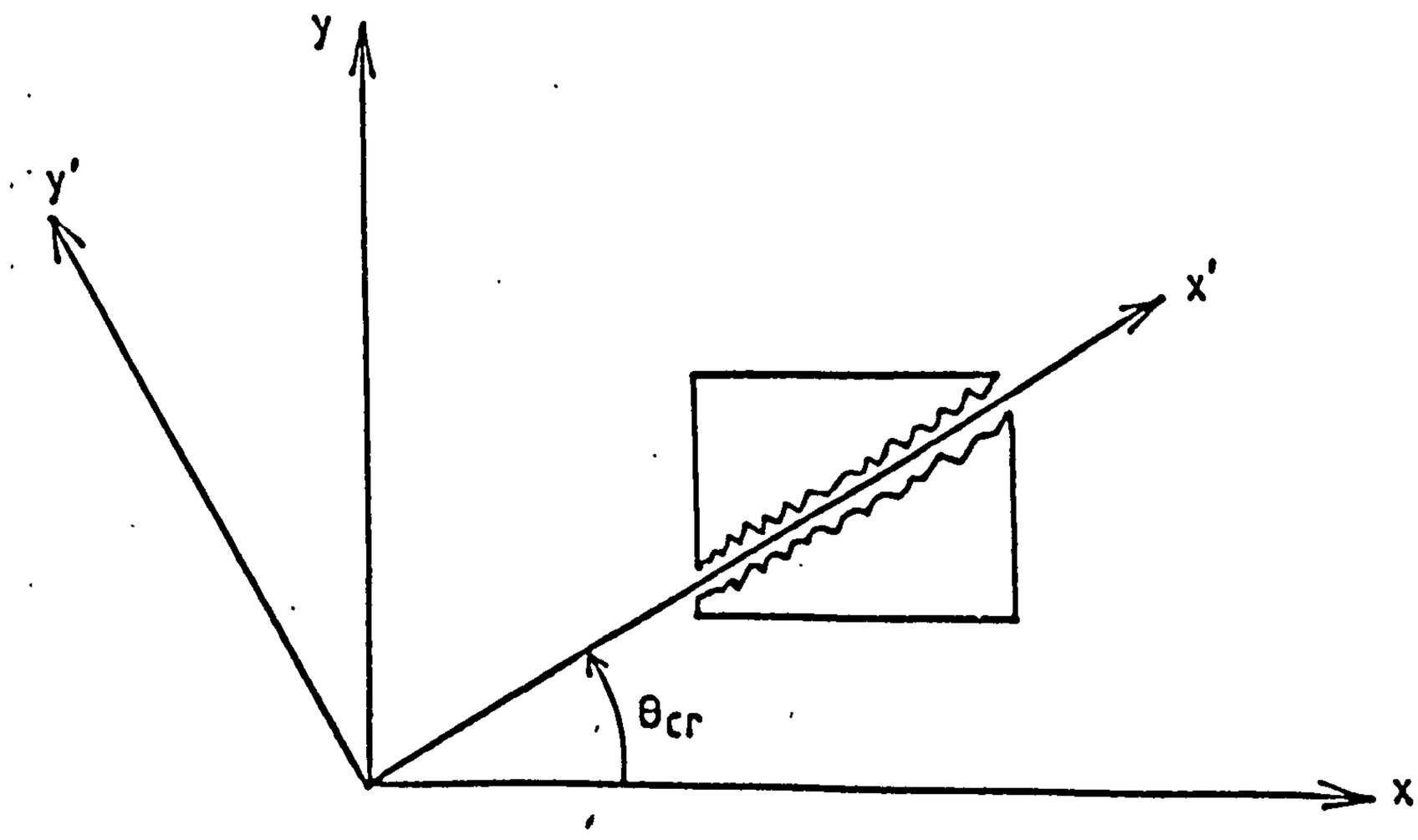

FIG. 3.4 Crack Orientation w.r.t. x-axis

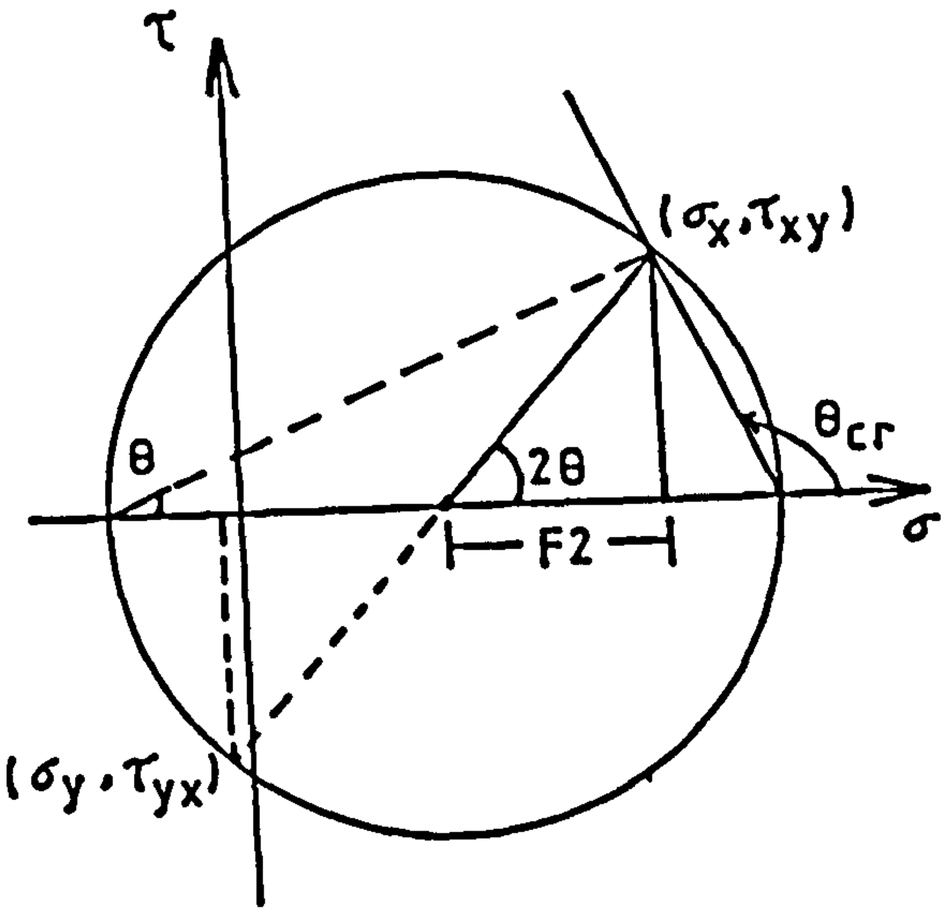

a) τ_{xy} +ve

F2 +ve

so, $\theta_{cr} = 90^\circ + \theta$

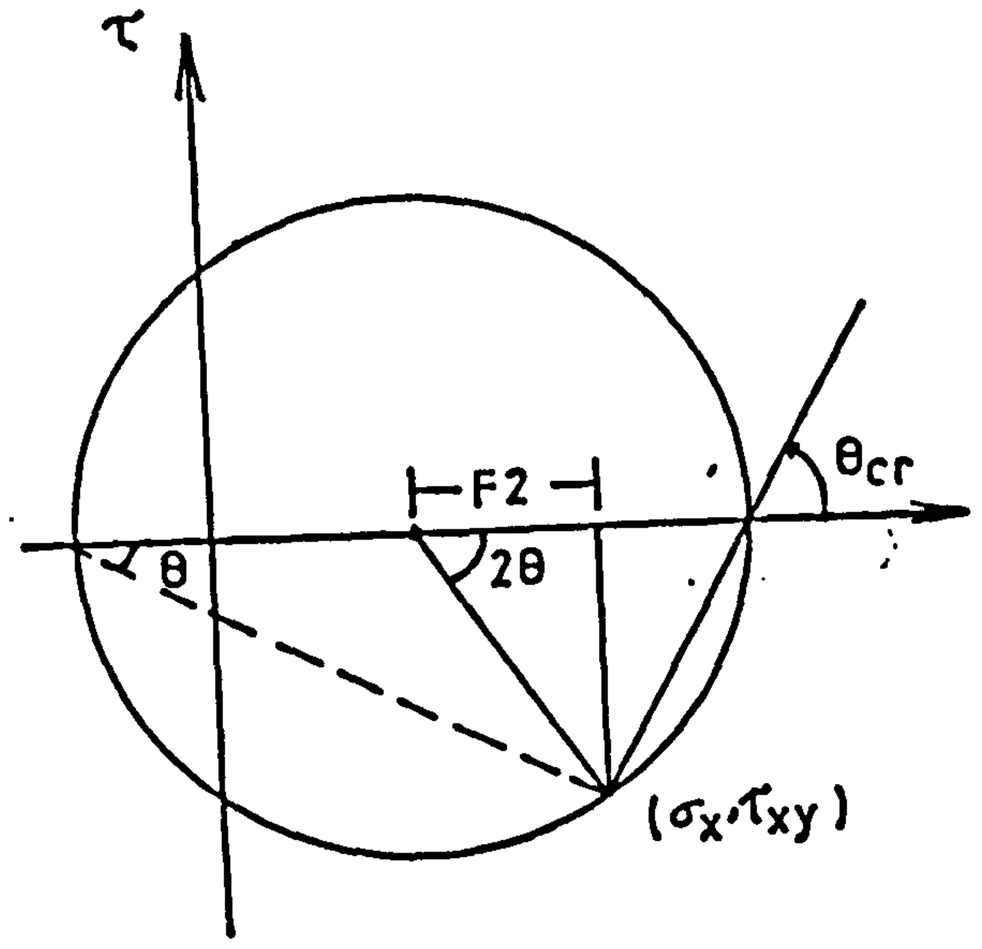

b) τ_{xy} -ve

F2 +ve

so, $\theta_{cr} = 90^\circ - \theta$

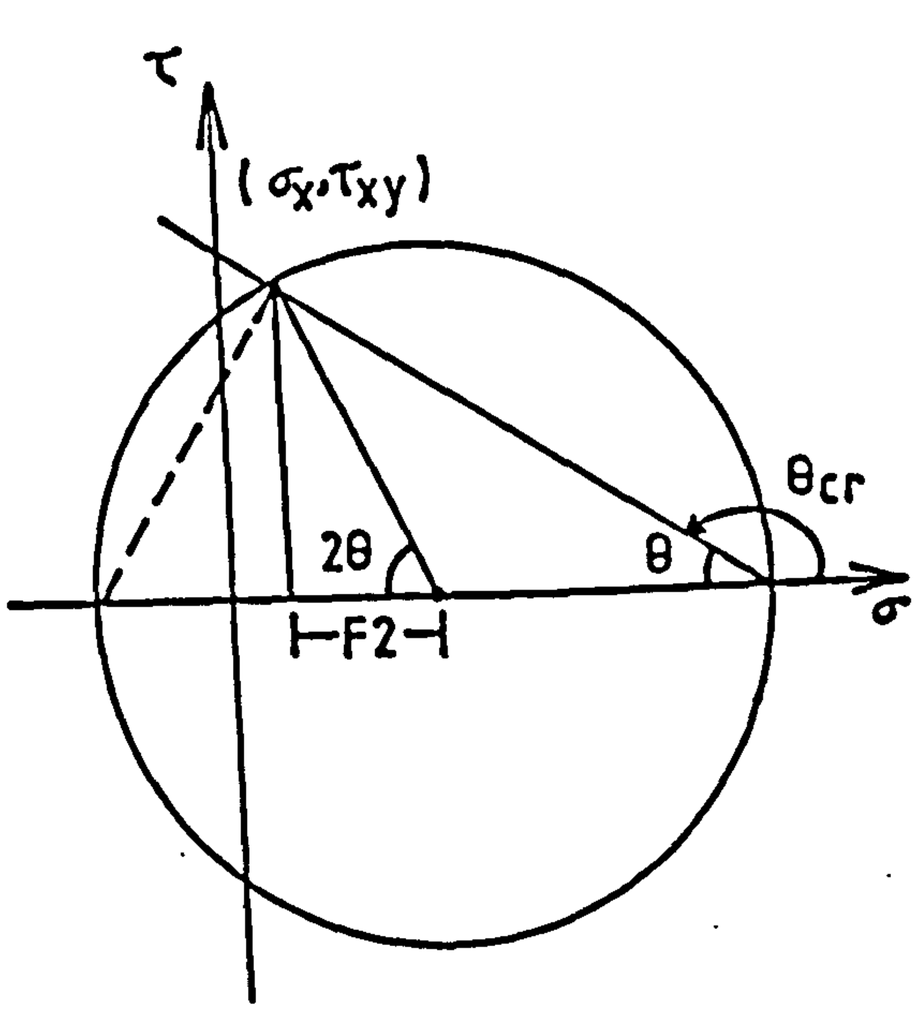

c) τ_{xy} +ve

F2 -ve

so, $\theta_{cr} = 180^\circ - \theta$

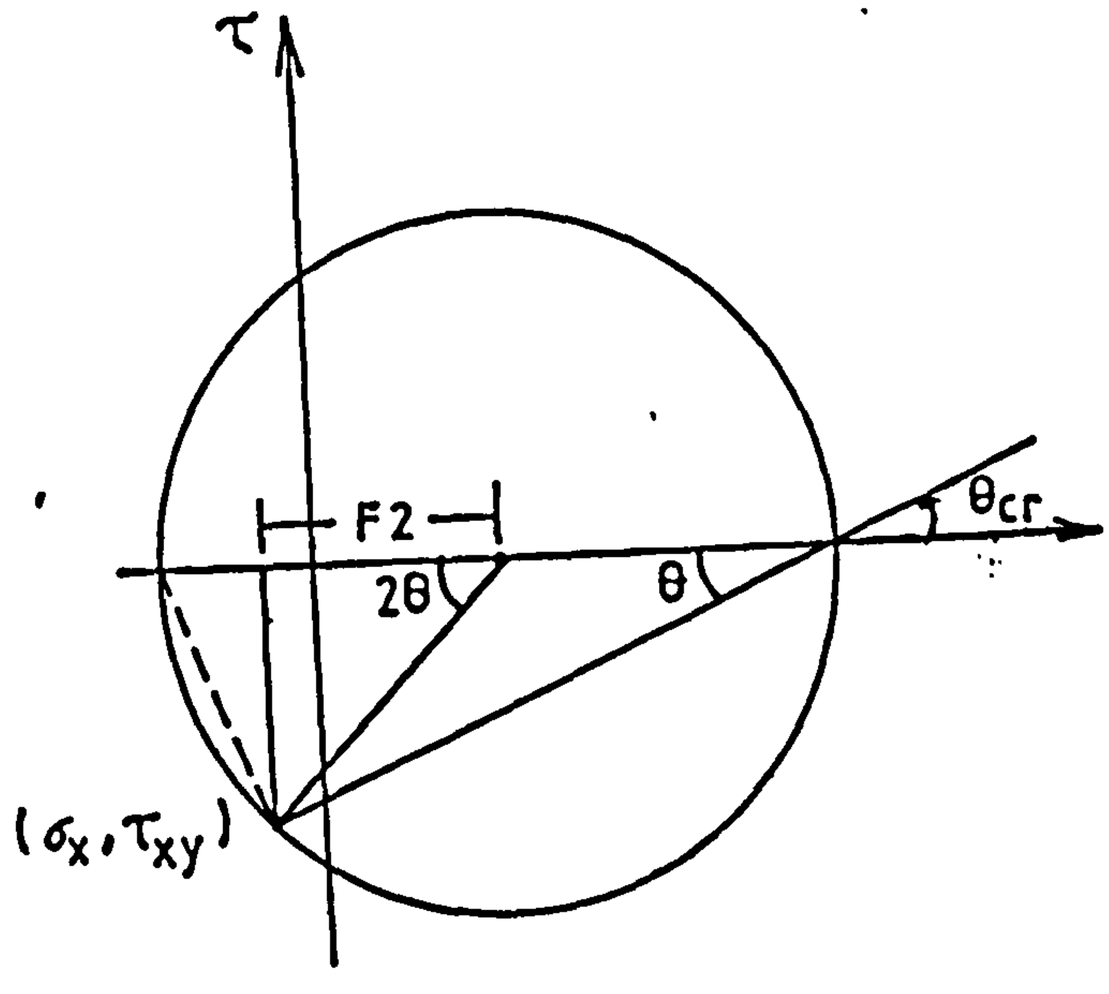

d) τ_{xy} -ve

F2 -ve

so, $\theta_{cr} = \theta$

Note: $F2 = (\sigma_x - \sigma_y)/2$

FIG. 3.5 Determination of Actual Crack Angle Using Mohr's Circle

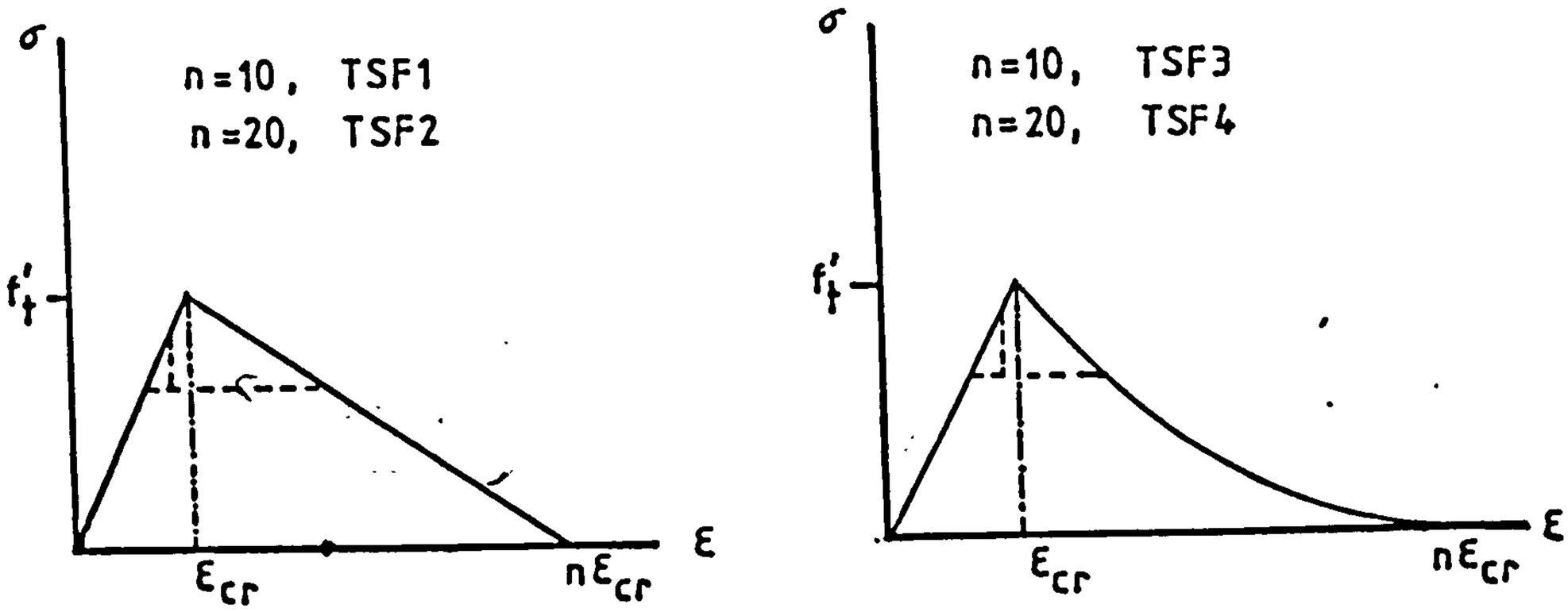

a) Linear decay b) Parabolic decay

FIG. 3.6 Typical Tension Stiffening Curves for Concrete

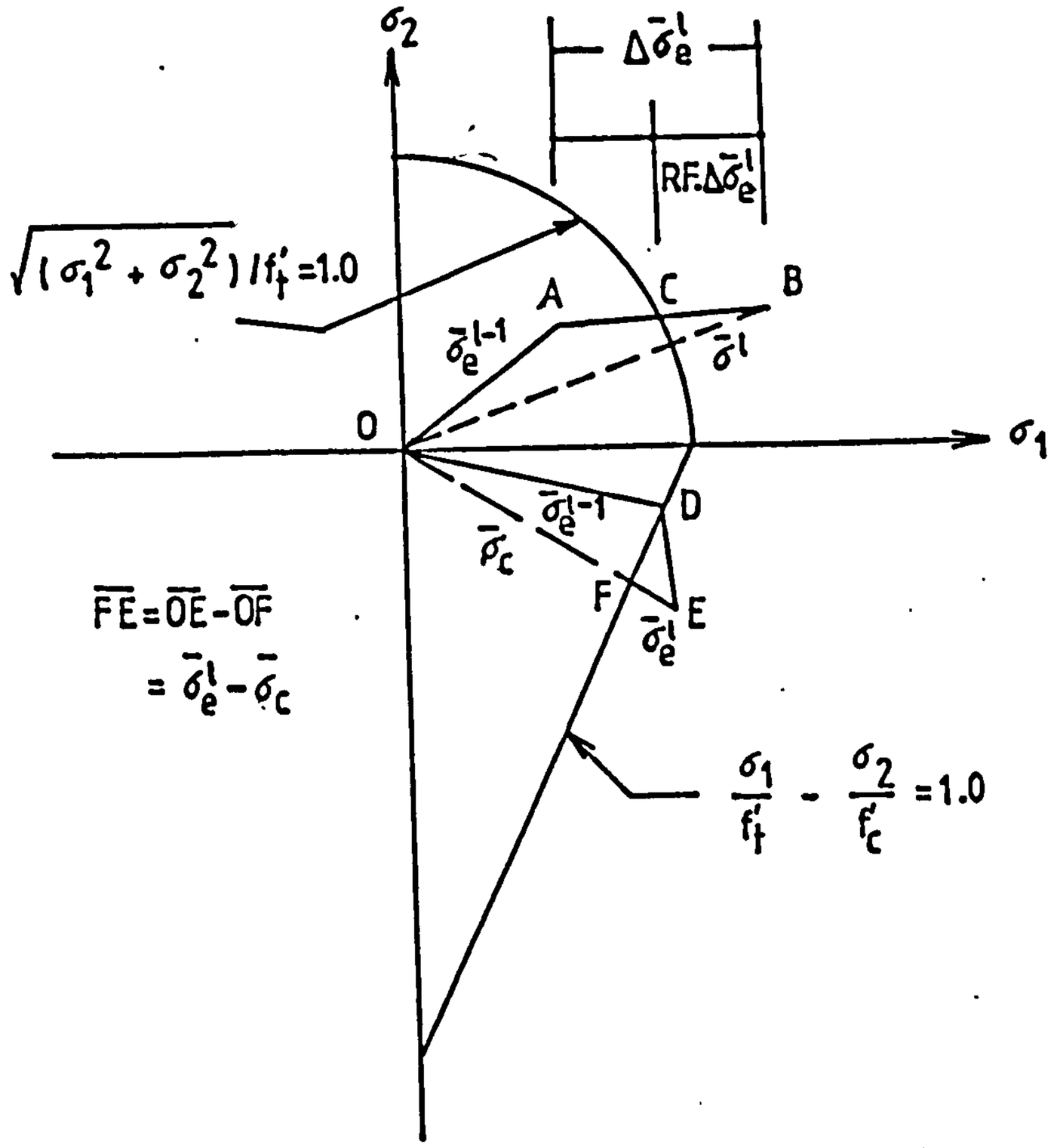

FIG. 3.7 Schematic Representation of Stress Change at or Near Cracking State.

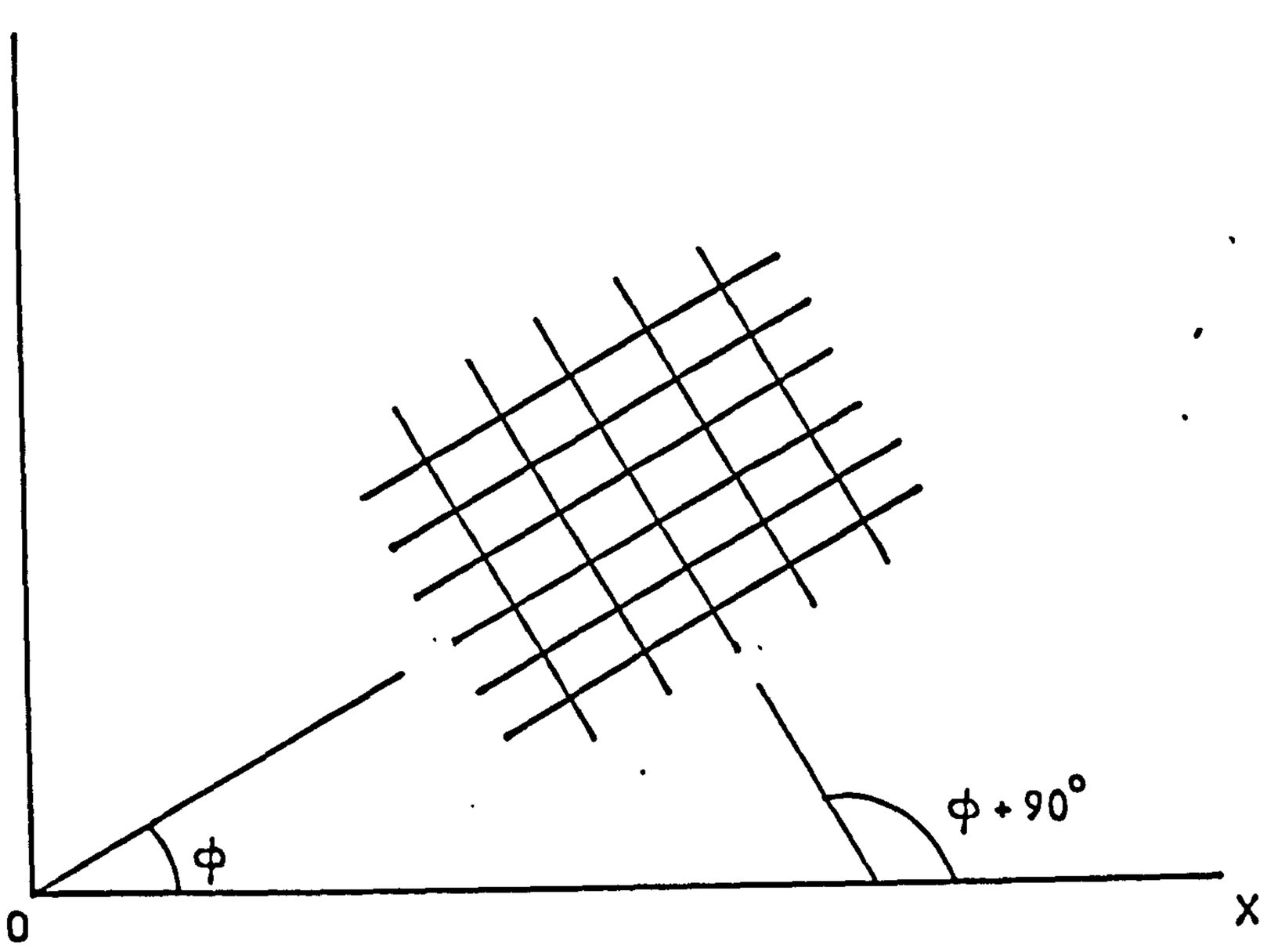

FIG. 3.8 Typical Layout of Reinforcing Steel

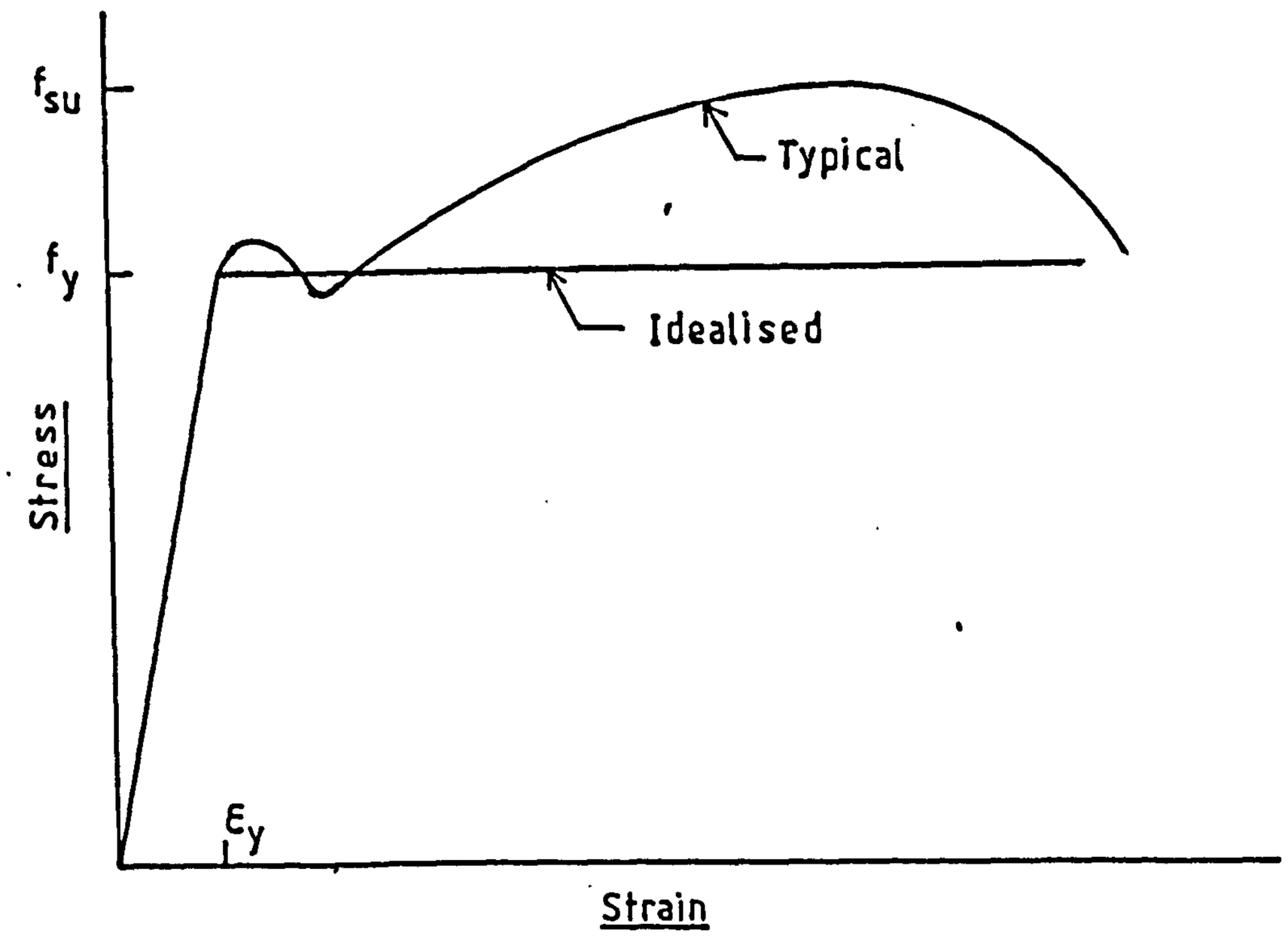

FIG. 3.9 Idealisation of Typical Steel Behaviour

Chapter 4

SOLUTION OF NONLINEAR EQUATIONS

4.1 Introduction

Finite element discretisation eventually results in a set of simultaneous equations of the form

$$\int B^T \sigma \, dv = k d_e = R_e \qquad (4.1)$$

These equations are initially formed at the element level, where, k denotes the element stiffness matrix relating the element nodal degrees of freedoms d_e to the element nodal force vector R_e. Element level stiffness relations are then transformed into the Global Structural Systems through appropriate assembling of element stiffnesses and the load vector. This would lead to the system of structural equilibrium equations which has the same format of Eq. 4.1 and is

$$Kd = R \qquad (4.2)$$

where, K is now the structural stiffness matrix and d and R corresponds to the structural displacement vector and load vector respectively.

So, before the solution of the Eq. 4.2 can proceed, the element level equations are to be assembled. In the following article only a brief overview of the assembling, storage and solution scheme of these equations will be outlined. Subsequently, the various methods of solving the nonlinear equations will be discussed, followed by the solution algorithms adopted in this study.

4.2 Equation Assembly, Storage and Solution Strategy

The element stiffness assembling process to form the global master stiffness matrix may be regarded as a housekeeping operation. A given row in the element matrix corresponds to a different row in the structural

matrix and so do their columns. The correspondence is established through the relation that the element local node number bears with the structural node number. However, because of the symmetric nature of the stiffness equations, the full structural matrix is never formed. Also, the structural stiffness matrix is banded which implies that the coefficients beyond the bandwidth are zeros. This enables to store only the symmetric half of the banded part of the stiffness matrix.

There are different schemes available to store these semi-band stiffness coefficients. All the coefficients within this semi-band width may be stored in a matrix form[17,100] or they can be stored in a one dimensional array as a vector[4,42]. Also, there are options either to keep all these coefficients[49] or only the currently active elements of continuously moving triangular matrix[80] in the active memory. There is altogether a different scheme known as the frontal solution technique where the element assembly and its reduction go hand in hand[41,46]. The suitability of one storage scheme over the other depends on the solution method adopted (e.g. Gauss elimination, Choleski decomposition), the problem size and also on the system hardware. Details may be found in the text by Irons and Ahmad[46] or elsewhere.

The stiffness assembly is therefore also dependant on the scheme adopted for the storage of the global stiffness matrix. Three addresses are necessary for any single variable to achieve the assembly of the corresponding stiffness co-efficient. They are

i) Its position in the element stiffness matrix,

ii) Its corresponding location in the actual structural matrix, and

iii) Its actual location in the storage currently in core which depends on the adopted storage scheme.

In the present context, the upper semi-band of the stiffness matrix has been stored in core and the Gauss reduction scheme employed for solving the simultaneous equations. In a nonlinear analysis, the reactions corresponding to the prescribed displacements are needed to check the overall equilibrium situations. In order to compute the reactions, the corresponding equations are written out in a disc file before zeroing all but their diagonal element, which are set to 1. After solving for the displacements, these equations are recalled from the disc and respective reactions calculated. Every time the stiffness matrix is updated, so are the equations stored in the disc. The right hand side load vector is appropriately modified corresponding to the prescribed degrees of freedom. Following a load increment, the fixed displacement is set equal to the prescribed value for the first iteration. For rest of the iterations at a particular load level, the fixed displacements are all assigned zero values.

4.3 Various Methods of Solution for Nonlinear Equations

The structural equilibrium equations expressed through Eq. 4.2 may be restated as

$$\Psi = R - K(d)d \neq 0 \qquad (4.3)$$

This indicates that by the time Eq. 4.2 is solved, the stiffness matrix K may have been changed due to the nonlinearities introduced to achieve this current configuration. Following any load increment, the external loads would not necessarily equal the internal loads developed. This lack of equilibrium would give rise to the residual forces (sometimes referred as pseudo forces) which is in fact expressed through Eq. 4.3 It is apparent that the coefficients of the stiffness matrix K depend on the basic unknown variables d (and/or their derivatives) which makes the Eq. 4.3 nonlinear.

There is no general method of solving the nonlinear equations of the form considered here because of the non-uniqueness of the solutions. In spite of these entailing difficulties, various numerical solution techniques have been suggested and applied in the field of numerical analysis. Only some of the widely used methods will be discussed here. Haisler et al[35] and Tillerson et al[84] provided more comprehensive information on different solution algorithms. The commonly used solution methods for nonlinear equations may be broadly classed into three categories, viz,

a) Incremental Methods

b) Iterative Methods

c) Combined Methods

The choice of a suitable method depends on various factors such as cost, reliability and accuracy. In addition, the physical behaviour of the structure should be well anticipated in order to select an appropriate solution method. A method suitable to trace the moderately nonlinear response may fail altogether if the nonlinearity is highly pronounced. An adequate knowledge of numerical analysis blended with an insight into the nature of the structural problem should enable an analyst to adopt a solution method efficient for the problem concerned.

4.3.1 Incremental Methods

This is one of the earliest[89] employed solution techniques for nonlinear analysis of structural problems. In this method, external load is applied as a sequence of sufficiently small increments so that the structure can be assumed to respond linearly within each increment. The structural response due to each load increment is accumulated to assess the overall behaviour at any stage of the loading process. In this way, the incremental technique seeks to solve a sequence of linear problems

wherein the stiffness matrix is recomputed for each load increment. At each load step, the incremental stiffness corresponding to the current configuration is formed and the resulting incremental equilibrium equations are then solved. The recurrence relation at any general i^{th} load increment may be given as

$$K_{Ti}\Delta d_i = \Delta R_i \tag{4.4}$$

$$d_i = d_{i-1} + \Delta d_i \tag{4.5}$$

$$R_i = R_{i-1} + \Delta R_i \tag{4.6}$$

where, K_{Ti} is the current tangent stiffness matrix or an equivalent incremental stiffness matrix. Δd_i and ΔR_i are the incremental displacements and loads respectively and d_i and R_i are the total accumulated displacements and loads respectively following the current i^{th} load step.

The incremental displacement vector Δd_i may be obtained by solving the set of simultaneous equations expressed in Eq. 4.4. The total displacements are computed using Eq. 4.5 and the corresponding increments in strains and stresses are then determined. Next, the nonlinear stiffness matrix is updated and the subsequent incremental displacements computed for the following load increment. In this manner, the succeeding points in the load-deflection curve are obtained.

It is apparent that the incremental technique seeks, without iteration, to march along the load-deflection curve. But this piecewise linearisation process introduces errors in the solution which accumulate with the increase in loads. This is evidenced by the drifting tendency of the solution from the true equilibrium curve. These truncation errors are inherent to the incremental methods since equilibrium is not satisfied exactly at any loading stage and therefore the corresponding estimate of the accuracy of the solution remains undetermined throughout. To improve

on this situation, an alternative approach incorporates a single step equilibrium correction following each load increment. That is, the residual forces after a load step is added to the next load increment. The basic incremental solution method and that with a single step correction scheme is represented schematically in Figs. 4.1 and 4.2 respectively. In either case, the drifting tendency of the solution may be reduced by making the load increment size significantly small.

4.3.2 Iterative Methods

As pointed out by Turner et al[89], a purely iterative solution scheme provides only a single point on the load-deflection curve. Thus, corresponding to a particular load level, the true solution is approached in an iterative way. There are various iterative schemes for solving the nonlinear equations. Almost invariably, all these schemes may be employed in an incremental iterative combined method of solution. In order to avoid repetition only a single scheme - method of direct iteration will be discussed here and some others will be elaborated in the context of the combined methods.

4.3.2.1 Method of Direct Iteration

In this method successive solutions are performed, in each of which the previous solution for the unknowns d is used to predict the current coefficients of the stiffness matrix K. Thus for every solution, the total deflections are recomputed using the preceeding stiffness coefficients. Rewriting the basic equilibrium equation (Eq. 4.2) as

$$d = [K(d)]^{-1}R \tag{4.7}$$

then the recursive relation for the i^{th} approximation beomes

$$d_i = [K(d_{i-1})]^{-1}R \tag{4.8}$$

It is clear from Eq. 4.8 that the stiffness matrix K has to be reformulated for each iteration. This successive solution method is also

called the method of successive approximation. The process is schematically shown in Fig. 4.3 from which it is apparent that the method employs successive secant stiffnesses to approach the true solution.

4.3.3 Combined Methods

If a complete load-displacement response of a structure is needed then an incremental method of solution must be employed. However, even with very small load increments, the solution would drift away from the true equilibrium path. In order to obtain a reliable solution, any suitable form of iterative correction scheme would be necessary to restore equilibrium after each load increment. Some of the commonly used iterative techniques are described here.

4.3.3.1 The Newton-Raphson Method

During any step of an iterative process following a load increment, the equilibrium (Eq. 4.2) will not usually be satisfied unless convergence has occurred. The lack of equilibrium would result in a system of residual forces Ψ given by Eq. 4.3. These residual forces may be interpreted as a measure of the departure from the equilibrium. Now, if an approximate solution $d = d^r$ is reached to Eq. 4.3 when the residual forces are $\Psi = \Psi(d^r)$, an improved solution can be approached using a curtailed Taylor series as

$$\Psi(d^{r+1}) = \Psi(d^r) + \left(\frac{d\Psi}{dd}\right)_r \Delta d^r = 0 \qquad (4.9)$$

$$\text{where, } \left(\frac{d\Psi}{dd}\right)^r = -J(d^r) = -K_T(d^r) \qquad (4.10)$$

in which $J(d^r)$ is the Jacobian matrix at the r^{th} solution step. In case of structural analysis problem, this Jacobian matrix may be identified as the tangent stiffness matrix K_T at that solution stage. Using Eq. 4.10 in Eq. 4.9, the general recurrence relation may be obtained as

$$\Delta d^r = [J(d^r)]^{-1}\Psi(d^r) \qquad (4.11)$$

and

$$d^{r+1} = d^r + \Delta d^r \qquad (4.12)$$

This Newton-Raphson method is also known as the tangent stiffness method because it uses the tangential stiffness matrix of the current step to reach an improved solution at the next step. Fig. 4.4 represents this solution process diagrammatically.

Now a typical term in the Jacobian matrix J is

$$J_{ij} = - \left(\frac{\partial \Psi_i}{\partial d_j}\right)^r \qquad (4.13)$$

Substituting Eq. 4.3 in Eq. 4.13, a generalised expression[72] may be obtained

$$J_{ij} = K_{ij}^r + \sum_{\substack{m=1 \\ m \neq j}}^{n} \left(\frac{\partial k_{im}}{\partial d_j}\right)^r d_k^r \qquad (4.14)$$

where K_{ij} is a general term of the stiffness matrix K at the r^{th} stage.

The last term in Eq. 4.14 may give rise to nonsymmetric terms in the Jacobian matrix. In order to preserve the symmetry of the Jacobian matrix, these nonsymmetric terms are usually excluded. This reduces the tangent stiffness method to a form of quasi-Newton procedures[70] which are a generalisation of one dimensional secant method to an n-dimensional problem. Thus, the recursive relation of Eq. 4.11 changes to

$$\Delta d^r = [K(d^r)]^{-1} \Psi(d^r) \qquad (4.15)$$

It should be recalled here that this modification to the basic Newton-Raphson method has resulted in an almost identical procedure to that of direct iteration method. Only instead of total displacements, iterative displacement increments are solved for the residual forces using the current secant stiffness matrix. The total displacements are obtained through Eq. 4.12. Although a secant stiffness is used to

approximate the tangent stiffness, this method is known as the tangent stiffness method or the generalised Newton-Raphson method in the context of structural application[72].

4.3.3.2 Modified Newton Raphson Method

The iterative solution methods described in the previous section demands reformulation and complete triangular decomposition of the structural stiffness matrix at every iteration step. For large system of equations, these operations may become very expensive. To reduce the amount of computational efforts, the use of a previously factored stiffness matrix is often advocated. The iterative solution is then achieved through the back substitution phase only. Any such method where a previously factored stiffness matrix is employed to estimate the current iterative displacements is termed a modified Newton-Raphson method. The recurrence relations may be stated in general form as

$$\Delta d^r = [K(d^i)]^{-1} \Psi(d^r) \qquad (4.16)$$

where, $K(d^i)$ is the stiffness matrix at step $i < r$.

There are two major forms of the modified Newton-Raphson method. In one of the forms, the stiffness is held constant to the initial stiffness matrix corresponding to the initial condition at the start, hence the name Constant or Initial Stiffness method. This is very simple to formulate and often may prove very economical too. But in many cases, the rate of convergence to the true solution may be very slow. To improve convergence rate, the other form, in which the stiffness matrix is updated at certain intervals, may be used. Fig. 4.5 gives a schematic outline of solution procedure for both cases. The stiffness may be reformulated once after each load increment and this updated matrix may be used to compute the rest of the iterative displacements at that load level. The updating may take place at the first iteration following a

load increment or at the second iteration. Hinton and Pica[75] reports that the latter update proves to be more efficient and economical.

Modified newton-Raphson solution technique in general, has several other versions. Initial stress and initial strain methods are two such subtypes often employed in nonlinear analysis problems. While both these methods use either a constant or an infrequently updated stiffness matrix for solving the nonlinear equations, they differ only on how the residual forces are evaluated. In the former, the residual stresses resulting from the discrepancy between stresses developed and stresses admissible are consistently transformed to get the residual forces. On the other hand, initial strain method seeks to reach the stress-strain curve horizontally and estimates the additional strains necessary to match the currently known stress level. These strains are treated as a set of initial strains which are then transformed to estimate the residual forces. Initial stress method may effectively be applied for any materially nonlinear structural problems including elasto-plasticity[99]. But as Marcal[64] pointed out initial strain method may break down in case of perfect plasticity because of nonuniqueness of strain corresponding to the yielding stress.

4.4 Solution Methods Adopted

The various methods described above, for solving nonlinear structural equations has been summarised in Fig. 4.6 Almost all the methods except constant stiffness method, need updating of the stiffness matrix at some stage in order to enhance the convergence of the solution. With this view in mind, a separate subroutine has been incorporated in the programme which triggers on or off the switch for stiffness update according to the solution algorithm selected. The different options available are 1) incremental method with single equilibrium check,

2) variable stiffness, i.e. generalised Newton-Raphson method with full equilibrium check, 3) constant stiffness method, 4) modified Newton-Raphson method with stiffness update at the first iteration or 5) stiffness update at the second iteration following a load increment.

In combination with the above algorithms, a separate parameter (value prescribed as a data) has been included. The value assigned to this parameter determines whether the residual forces are to be computed as a total discrepancy between the external and the internal loads or as a load equivalent to the initial stresses released due to material nonlinear response. The former ensures complete equilibrium check, while the latter is in fact the initial stress method. Also, an option is available to use them both in some combination (see Chapt. 2), i.e. checking equilibrium for some initial iterations and then evaluating the residuals using initial stress concept for rest of the iterations. With all these alternatives, the choice is left to the user and the suitability may then depend on the required accuracy of the solution and the cost involved. Obviously, the modified Newton-Raphson method provides the best trade off between the two factors.

4.5 An Example Problem

In order to study the effectiveness of the different solution algorithms, an experimental slab (model S63P1) has been selected. The details of this slab and its material characteristics are given in Chapters 6 and 7. Fig. 4.7 shows the element discretisation on symmetric half of the slab. The same slab has been analysed using five different solution algorithms included in the computer programme for 5 DOF ACM plate bending element. The total load displacement response for the middle point of the free edge (Node 25) are plotted in Fig. 4.8 along with the experimentally recorded values. It may be seen that all the

solution algorithms traces the load deflection response with reasonable accuracy. Other aspects of the different solution strategies are given in Table 4.1. It may be noted that the solution algorithms ALG2, ALG3 and ALG4 produced almost identical results. The remaining algorithms ALG1 (constant stiffness) and ALG5 (variable stiffness with single equilibrium check) produced curves similar to each other. But both these cuves show more stiff results near failure. For ALG5 such behaviour is obvious because strict equilibrium was not enforced. For the constant stiffness case (ALG1), the principal reasoning remains the same. But the lack of convergence cropped up from the insufficient number of permitted iterations. The maximum number of iterations were held constant to 12 for all the solution algorithms and a convergence limit of 0.001 was set for both the residual force and iterative displacement norms. As the initial stiffness coefficients were used throughout the solution process, the convergence norms were not satisfied within the specified iterations during the later stages of load increments.

Another interesting feature of the constant stiffness approach is that it appears to be the costliest of all the solution algorithms incorporated here (Table 4.1). Although the stiffness matrix was triangularised only once, but the slow convergence rate demands the solution of the iterative residual load vectors many more times compared to other algorithms. The increased number of solution processes ultimately offsets the time saved by not reformulating the stiffness matrix. Even the complete variable stiffness method (ALG4) with 81 times stiffness updates, saved about 30% of the CPU time compared to the constant stiffness method. Thus, it is believed that a trade off solution scheme like that of ALG2 or ALG3 with one stiffness update in every load increment is perhaps better suited for nonlinear analysis of concrete. These are economic considering cost and produce fairly acceptable results.

Table 4.1 Comparative Study of Various Solution Algorithms on Slab Model S63P1.

Solution Algorithm	Number of Stiffness Update	d_{max} (mm) at failure	Ultimate Load (KN)	CPU Time (secs.)
ALG1	1	34.4	5.75	1795
ALG2	34	37.27	5.02	902
ALG3	36	36.32	5.02	864
ALG4	81	35.78	5.02	1228
ALG5	42	35.88	5.75	573

Note:

ALG1: Constant stiffness method

ALG2: Stiffness update at first iteration following a load increment

ALG3: Stiffness update at second iteration following a load increment

ALG4: Variable stiffness method

ALG5: Incremental variable stiffness method with single step equilibrium correction

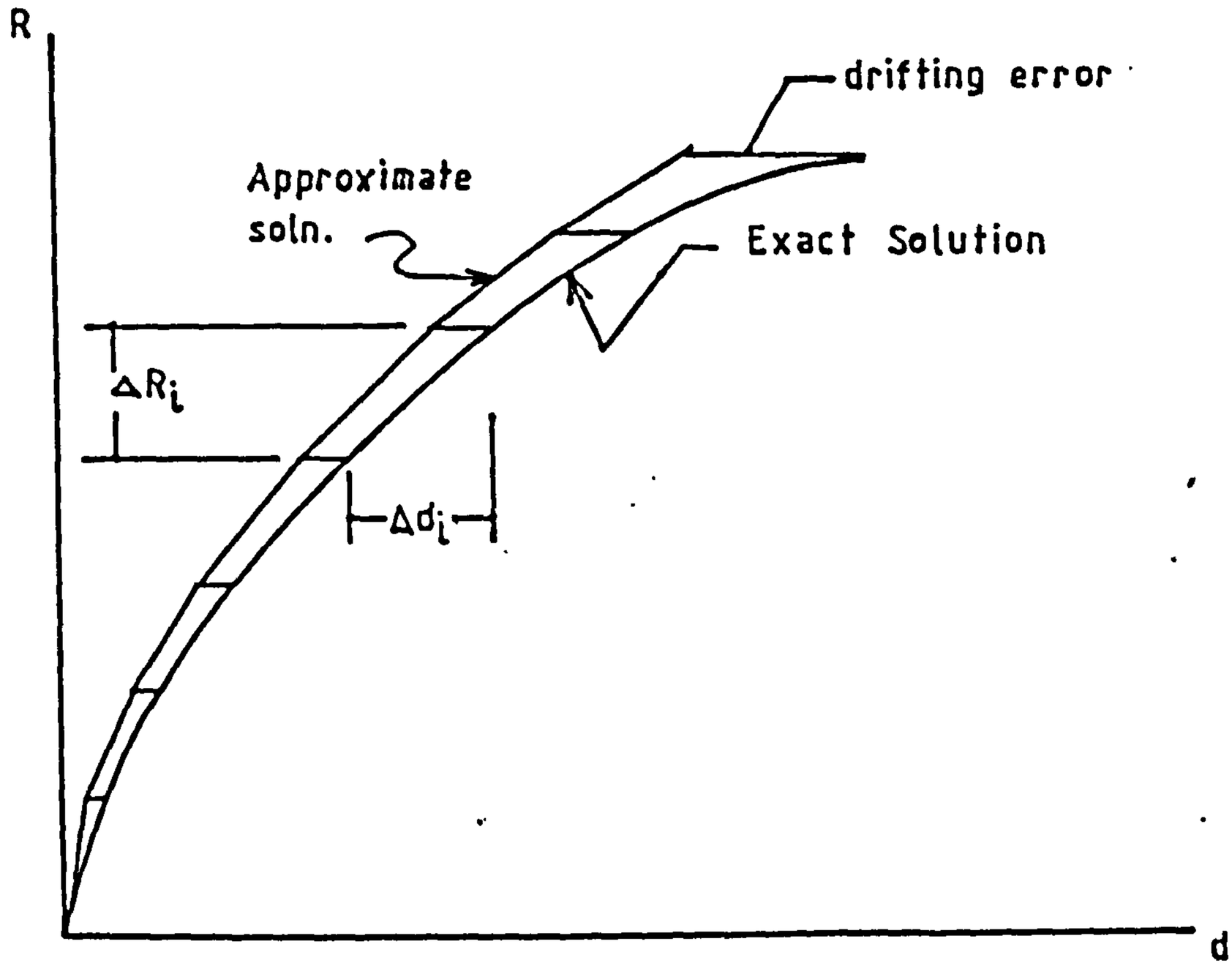

FIG. 4.1 Basic Incremental Stiffness Method of Solution

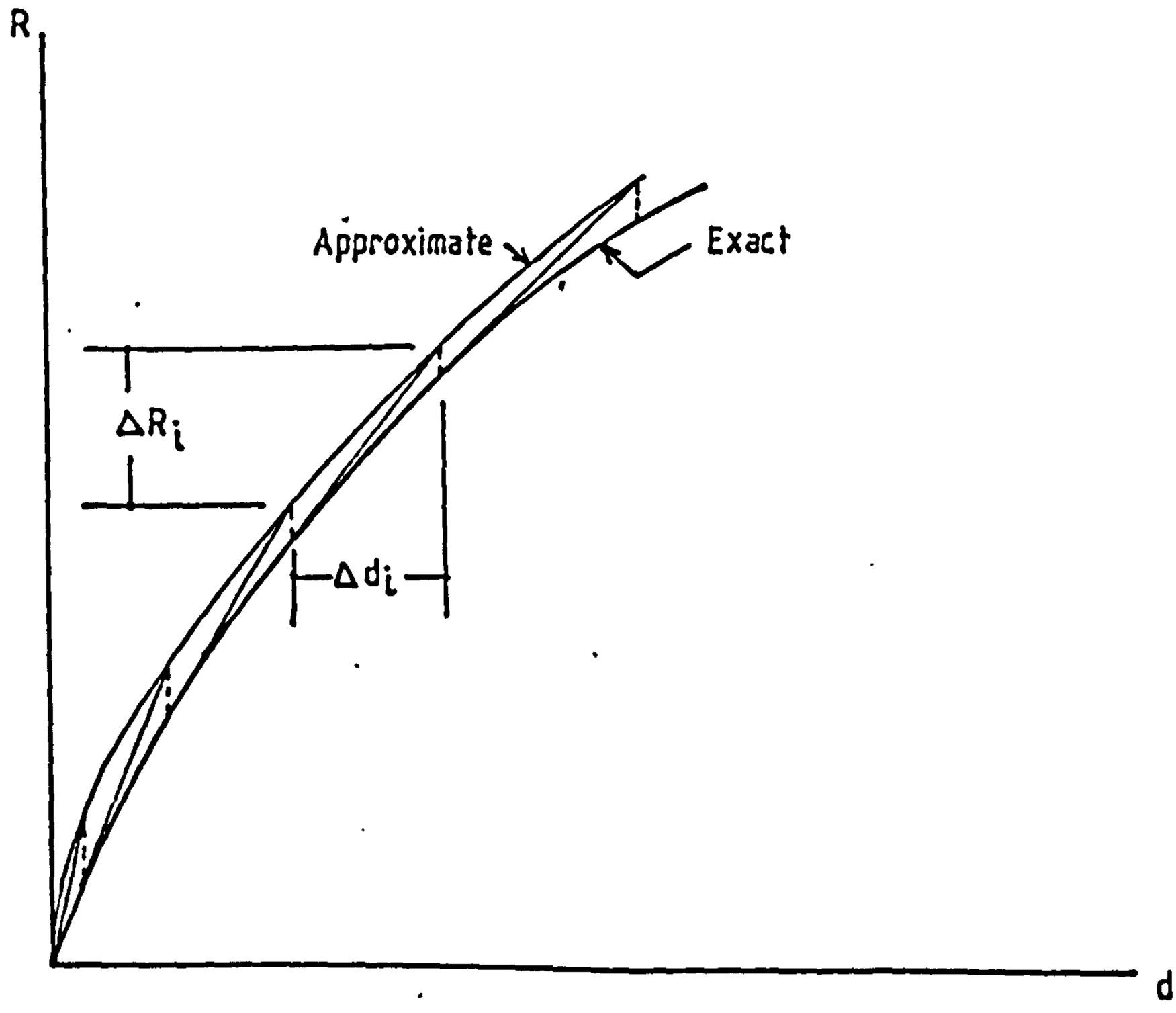

FIG. 4.2 Incremental Solution Scheme with Single Step Equilibrium Correction

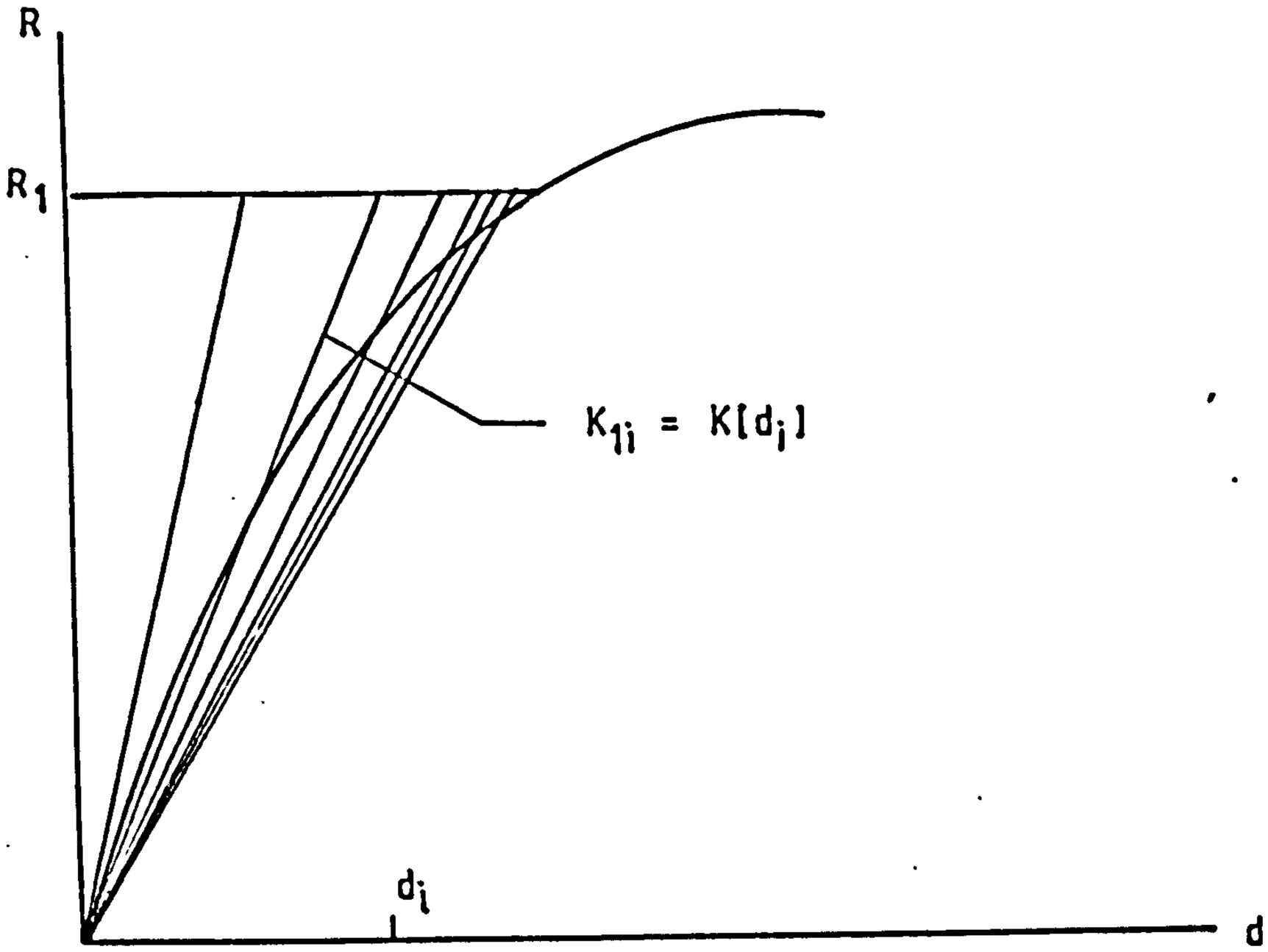

FIG.4.3 Method of Direct Iteration for a Single Step Loading

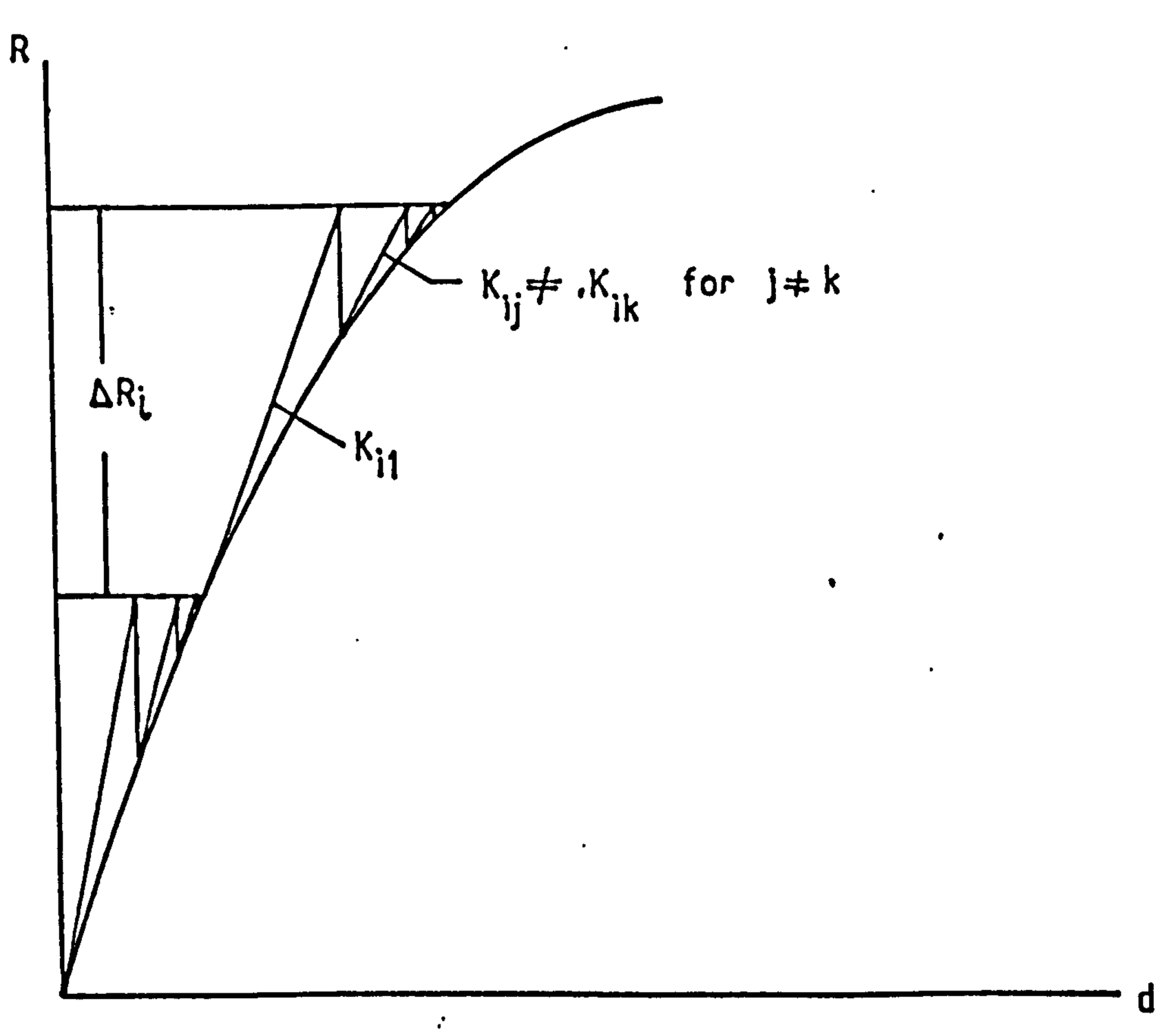

FIG. 4.4 Incremental Newton-Raphson Solution Scheme

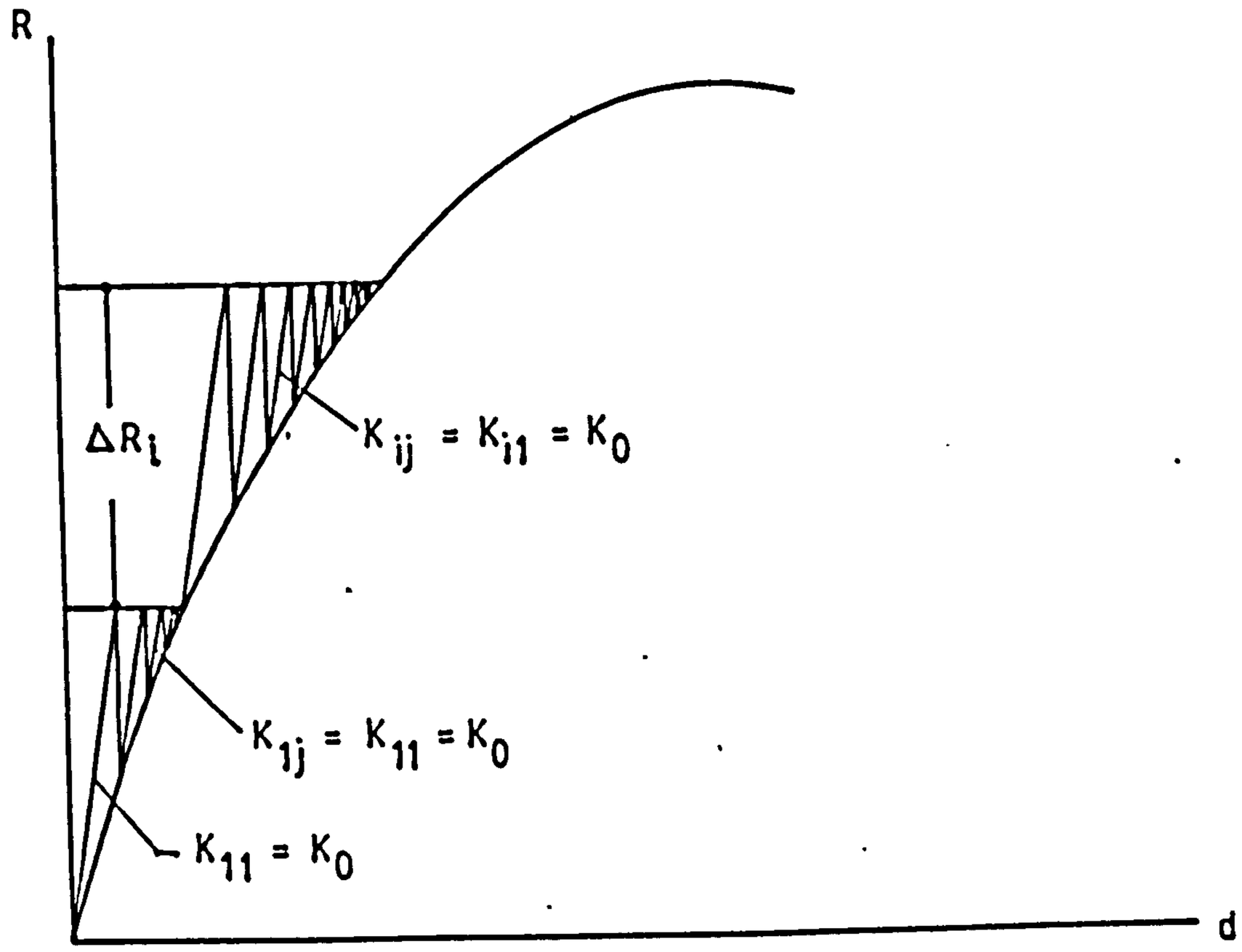

a) Constant Stiffness Solution Scheme

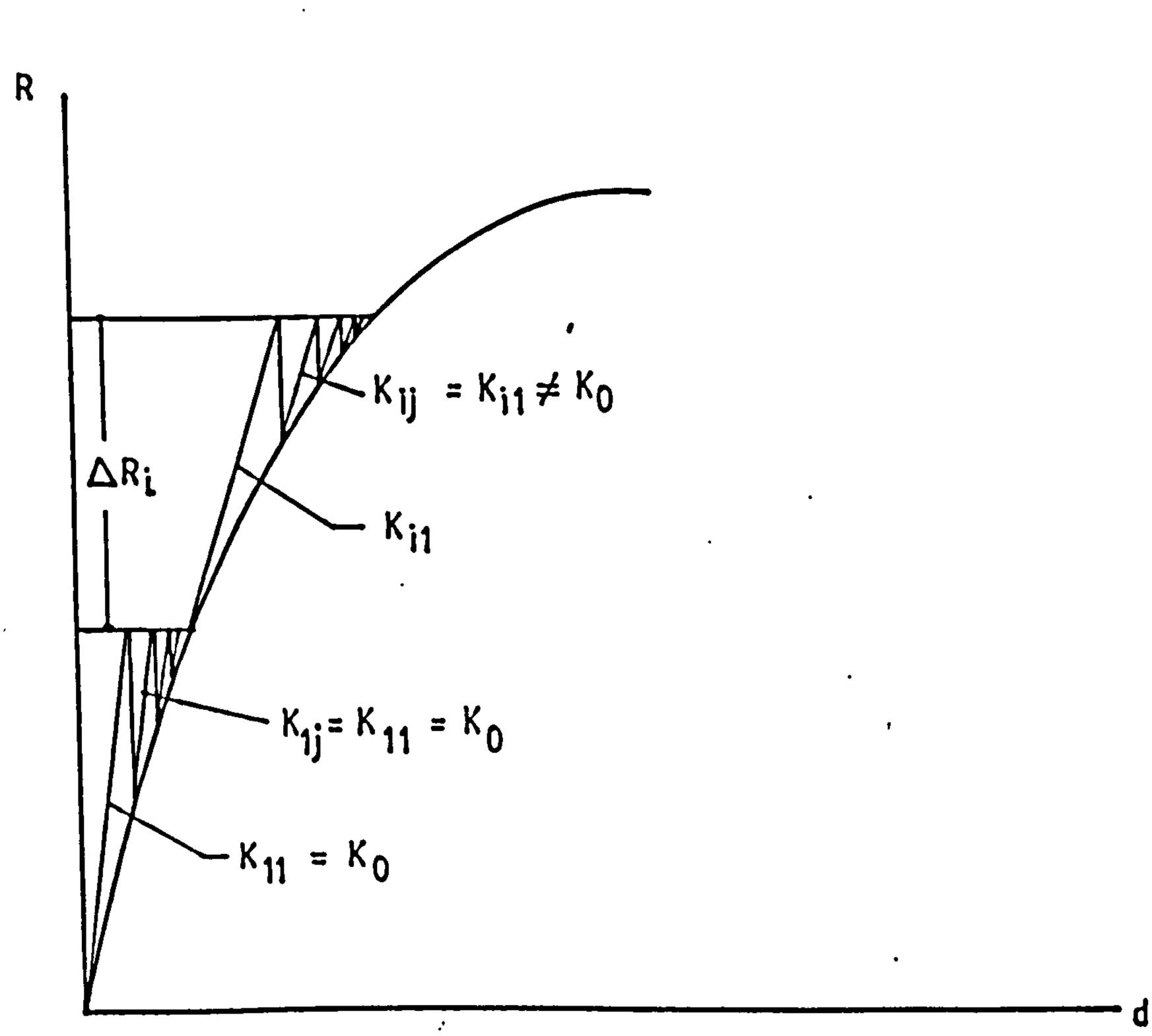

b) Solution Scheme with Infrequent Stiffness Updates

FIG. 4.5 Two Modified Newton-Raphson Solution Schemes

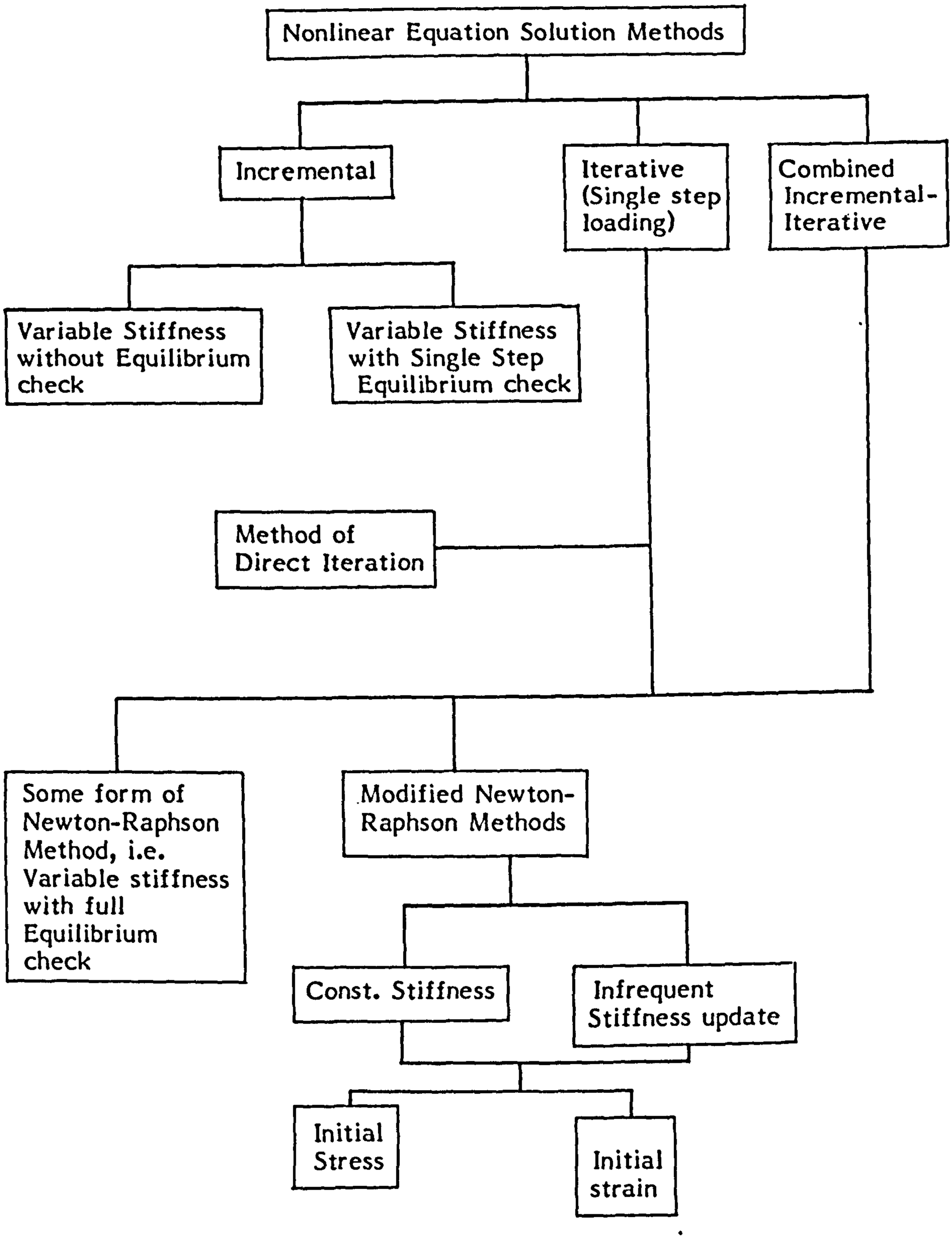

FIG. 4.6. Various Methods of Solution of Nonlinear Equations.

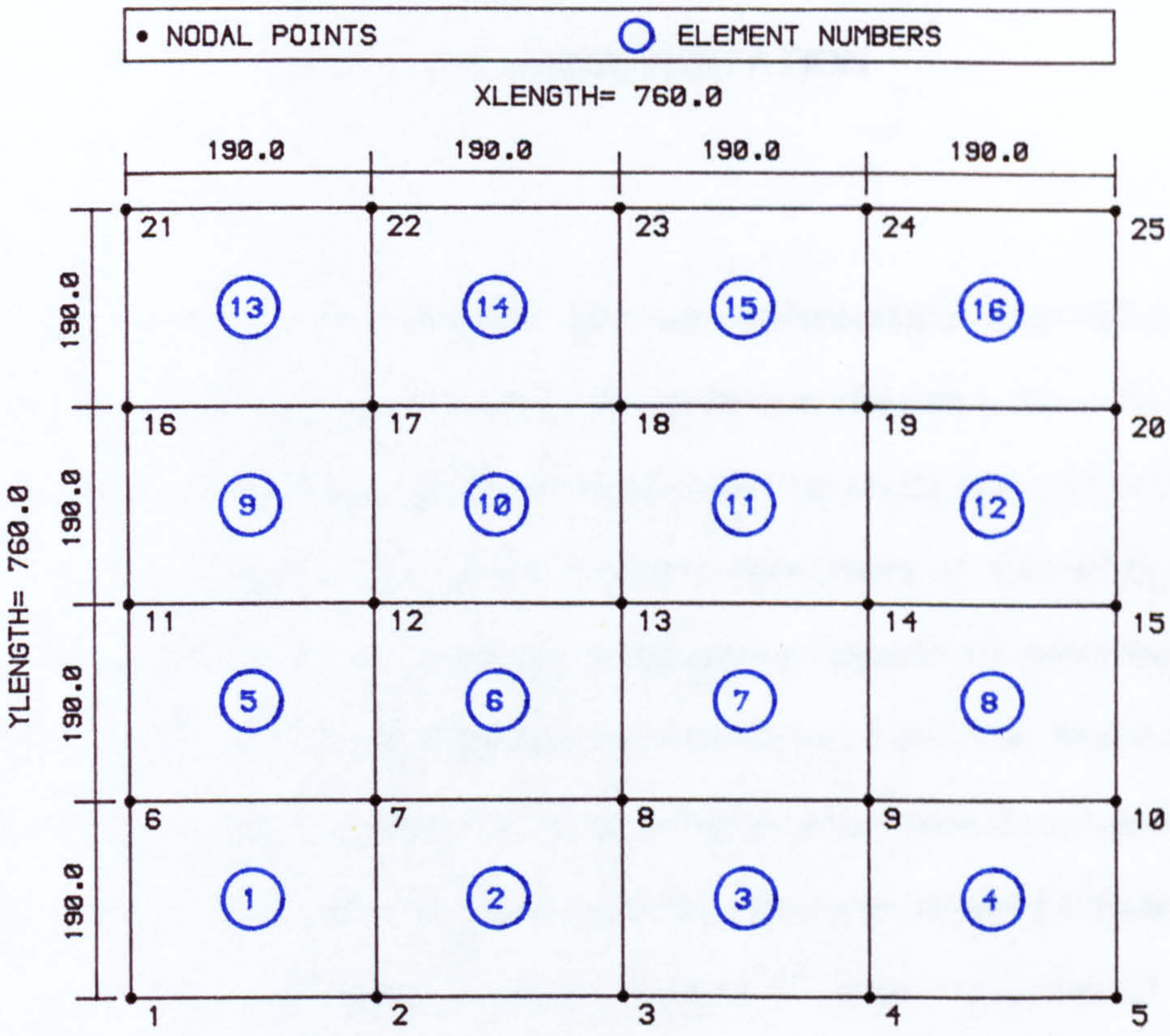

FIG. 4.7 ELEMENT DISCRETISATION FOR S63P1 EXP

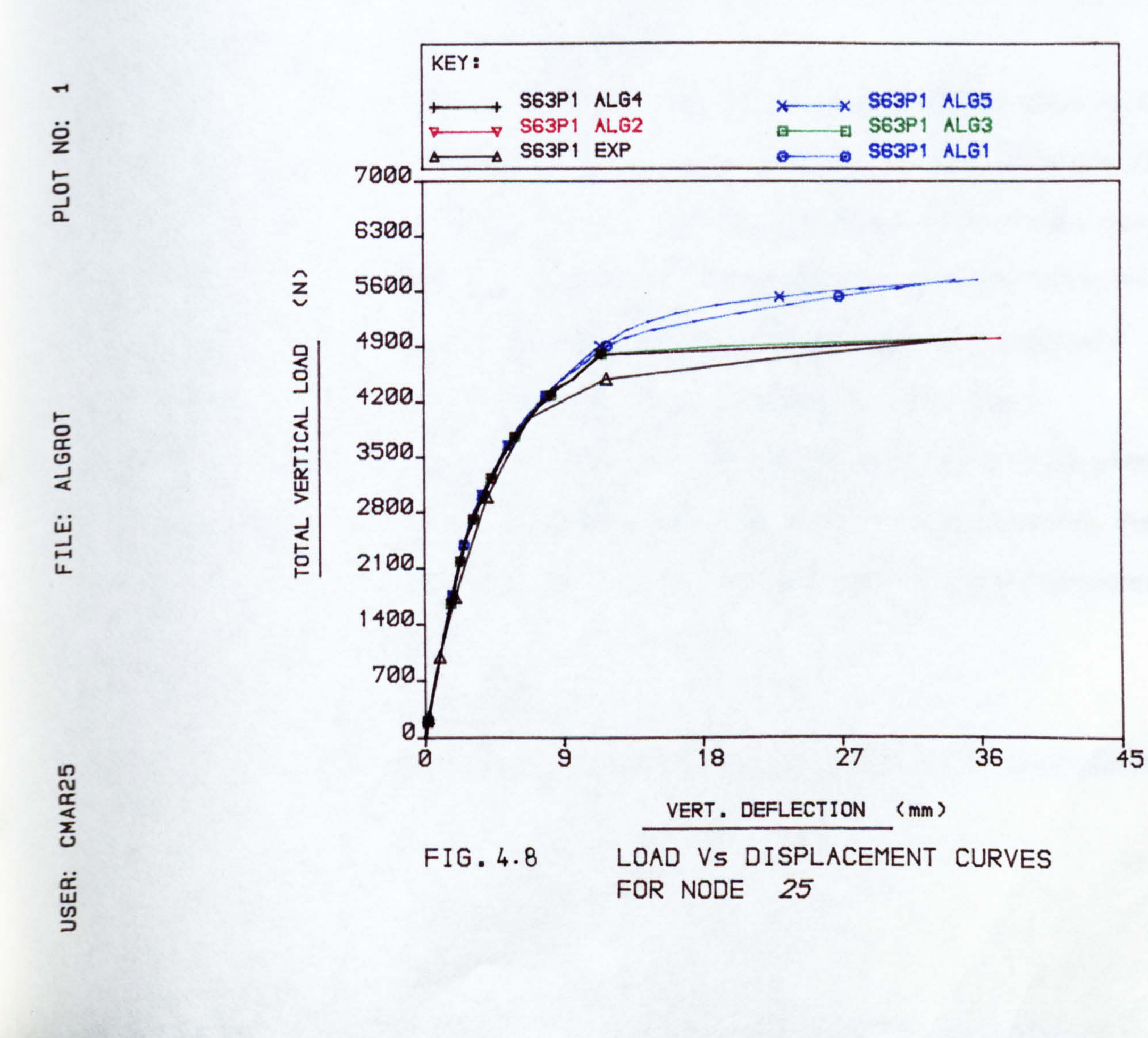

FIG. 4.8 LOAD Vs DISPLACEMENT CURVES FOR NODE *25*

Chapter 5

COMPUTER IMPLEMENTATION

5.1 General

The finite element formulations and the mathematical description of the constituent materials, described in the previous chapters, have to be transformed into a computer programme in order to study the analytical response of the structure. One of the primary objectives of this work was to develop a special purpose computer programme capable of describing the complete nonlinear structural response for reinforced concrete flexural members. As mentioned earlier, two such programmes were developed from scratch. In one of them, the element discretisation was achieved through layered ACM rectangular plate bending element[100] with 5 degrees of freedom per node. In the other, a standard Bogner element[8] was used with generalised 6 degrees of freedom per node. The material modelling options remains the same for both cases.

The element characteristic formulation was aimed at studying the predominantly flexural response of a reinforced concrete structure. Consequently, the element stiffness derivation is based on the small displacement theory of thin plates[85]. The strain energy contribution from the transverse shearing stress and strains have been excluded, their effect being considered insignificant for relatively thin plates. However, their inclusion would be realistic in considerably thick plate bending situations[17,22]. Leaving aside all the theoretical aspects, the practical computer implementation schemes adopted will be projected in the following sections of this chapter.

5.2 Programme Structure

In any finite element solution procedure, the overall programming

structure can be divided into several component modules. This modular structure of the programming lends generality and flexibility to the total computational procedures followed. The fundamental operational structuring of a computer programme for nonlinear analysis problems may be categorised as

i) Input of Pertinent Data.

ii) Evaluation of the Element Stiffnesses and their assembly to form structural stiffness.

iii) Formation of the incremental (element) nodal load vectors and assembly to get the structural load vector.

iv) Solution of assembled structural equations.

v) Evaluation of stresses and equivalent nodal forces.

vi) Check for convergence of solution.

vii) Output of results.

In nonlinear analysis of structural problems, each of the afore-mentioned steps are to be addressed in a repetitive manner following each load increment. So, separate subroutines can be employed to perform the different operations required in a nonlinear solution process. This modularity of the programme structure not only lends clarity to the overall programming effort but also add elegance and flexibility to it. Thus, each of the subroutines become a separate entity performing a distinct operational function and can be modified with ease, if necessary, by another user without upsetting rest of the modules designed for achieving other purposes. The logical sequence of the basic operational steps followed in the development of the current computer programmes is shown in Fig. 5.1 and may be elaborated in words as follows:

a) Read all the necessary data;

b) Initialise to zero the various vectors and matrices subsequently required to store accumulated variables

c) Compute the incremental external load vector ΔR_i and accumulated total external load vector as

$R_i = R_{i-1} + \Delta R_i$

d) Get the incremental load vector taking into account of the residual forces from previous solution as

$\Psi_i = \Delta R_i + \Psi_{i-1}$.

e) Compute the (structural) stiffness matrix K_i as per the specified solution algorithm

f) Solve for the incremental displacements $\Delta d_i = K_i^{-1} \Psi_i$ and compute $d_i = d_{i-1} + \Delta d_i$

g) Evaluate incremental midsurface strains, $\Delta \epsilon_{r_i} = B \Delta d_i$, hence the layer strains $\Delta \epsilon_i$

h) Evaluate incremental layer stresses $\Delta \sigma_i = D \Delta \epsilon_i$ and the total stresses $\sigma_i = \sigma_{i-1} + \Delta \sigma_i$

i) Check this current stress state against the appropriate transitional criteria such as cracking, crushing, yielding, etc. Update the stress level as per the incorporated material model and obtain the excess inadmissible part of the stress σ_i^{ex}. Keep record of the modified elastic constants of the layer

j) Calculate the contribution of each layer towards element total, actual and excess stress resultant vectors

k) Compute the contributions towards total equivalent nodal force and total excess equivalent nodal force as $f_i = \int B^T \sigma dv$ and $f_i^e = \int B^T \sigma^{ex} dv$

l) Follow steps (g) to (k) for each element, each Gaussian sampling points within an element and each layer therein

m) Obtain the residual force vector Ψ_i as either

$\Psi_i = R_i - f_i$ or $\Psi_i = f_i^e$

n) Check for convergence and total collapse

o) If the solution has not converged, start from step (e) again with a new iterative value of Ψ_i as given in (m)

p) If solution has converged, print out some selected results or draw some contour maps as per the request data. Then begin from step (c)

q) The programme finally stops, either if the total collapse criterion in (n) is met or if total number of specified load increment is depleted.

5.3 Brief Description of Modular Routines

The elementary steps of computer implementation, outlined in the previous article have to be expanded in order to formulate the various subroutines. Each of the subroutines is given a separate name for its distinctive identity. The overall computational procedure adopted here is accomplished through the various subroutines given in the general flow diagram of Fig. 5.2. A brief description of the operational functions achieved in these routines are furnished below.

ACMLAY: This is the master segment controlling the entire solution procedure for nonlinear analysis of reinforced concrete slab problems using 5 D.O.F. ACM element. It calls the various subroutines in an orderly sequence to perform the different operations like that of reading in the relevant element data, slab geometry, loading data, etc. It also calls the subprograms that computes the applied load increment, evaluates

stiffness matrices, solves for incremental displacements, compute the strains, stresses and equivalent nodal forces and checks for convergence. When convergence is achieved, it calls some other subroutines to output some specified accumulated results, draw moment contours and crack patterns for different layers if initially requested for this load increment and store some relevant data in a separate file which will be used later by a separate plotting programme for drawing load-displacement curves for the specified nodes.

INPUTP: This subroutine reads in most of the data necessary for solution of the currently discretised structural system. The control variables, the element material properties, the slab geometry, the different layer thicknesses along with their identifying codes are all fed into the programme through this subroutine. The element nodal connectivity is automatically generated within this subprogram. The node numbers with prescribed boundary conditions, the corresponding fixity codes and the prescribed value of the displacements are also read in here. From the fixity codes, the cumulative restraint list vector is formed which will be required for computing the reactions during the solution process. Finally, it calls in another subroutine CORDXY which generates the global coordinates of nodal points and all the Gaussian sampling points.

ZERO: This module is entered before any load increment is applied. Its function is to initialise to zero various vectors and matrices at the beginning of the solution process. In some machines, the unassigned variables are initialised to zero by default while on others the programme would break down if unassigned variable is encountered. If the programme is executed in the former type of machine, this module can be omitted.

STIFPL/STIFPV: These two subroutines are almost identical functionally and are employed to evaluate the element stiffness matrices. STIFPL is called only once in the programme to form the element stiffnesses corresponding to the initial material characteristics of the elements. It calls MATXFG and MATXCI to form the H matrix and the inverse of the undetermined coefficient matrix and get their product through matrix multiplication routine MATMUL to establish the B-matrix. It also asks GAUSSQ to supply the generalised Gaussian sampling point coordinates and the respective Gauss Weights. It also calls UDLRNA to form the equivalent element nodal vector for unit magnitude of the uniformly distributed loads. It then stores the B matrix, the nodal load vectors and the layer material constants in separate scratch disc files. Subroutine STIFPV differs from the former only in detail. Thus instead of forming the B-matrix, it restores them from the disc space and same applies for material constants. From both these routines ASEMPK is called to assemble the element stiffnesses to form the global master stiffness matrix.

LOADPL: This routine is called following every load increment. It restores the element equivalent nodal load vector due to unit intensity of uniform load and scales that to the current state using the presently applied intensity. It assembles these element load vectors to form the structural load vector. The directly applied concentrated nodal loads are then added consistently to the master load vector.

SETSOL: In this routine, the solution indicator is set to the appropriate value depending upon the solution algorithm adopted. This indicator, later dictates whether a reformulation of the stiffnesses have to be undertaken or not. Its value also determines whether the solution demands triangularisation of the master stiffness matrix or just a resolution of the current load vector using previously reduced coefficients is

sufficient. Stiffness reformulation dictated by the selected solution logic is overruled if a second counter indicates that nowhere in the structure any material constants has changed recently.

BANSOL: The solution of the simultaneous stiffness equations are carried out in this module. The advantage of the bandedness of the stiffness relations are taken into consideration in its development. A full triangular decomposition of the stiffness matrix is carried out first before proceeding to the reduction of the current load vector. The reactions developed corresponding to the prescribed boundary conditions are also computed here. Before exit, the incremental displacements and reactions are added to the respective accumulative vectors.

STRESP: Purposefully, this subroutine performs a number of operations. It evaluates the reference surface strains $\Delta\epsilon_r = B\Delta d_e$, computes the incremental layer strains and stresses and then obtains the layer total strains and stresses at each of the element Gauss points. It calls TENCOT and COMCOM to check if the concrete stress conditions are following the respective material description. The reinforcing steel characteristics are checked within itself. It also checks if the concrete strains have reached the definition of crushing. Accordingly, it updates the layer stresses and extracts the excess stresses. Finally, it evaluates the equivalent nodal total and excess forces due to internal stress states and assembles them to find the residual force vector in structural sense.

TENCOT: This is called from subroutine STRESP when a concrete layer principal stresses are either both tensile or one of them tensile and the other compressive. The principal stress combinations are checked against cracking and the current stress state is updated accordingly. The angle of the formed crack is recorded and the material characteristics are set to crack oriented axes. These material constants are then transformed to

the global axes using standard transformation through another routine CRAMAT.

COMCOM: This routine is also addressed from STRESP. It is called when both the principal stresses are compressive. The principal stress states are checked against the adopted transitional criterion and the material constants are updated accordingly. The stress state is also checked against the ultimate strength envelope of Kupfer et al (see Chapt. 3) and if it is exceeded, the further development of stress is totally restricted until a crushing surface is reached.

ELDISP: The subroutine is called from STRESP to extract the element nodal displacement vector from the structural displacement vector.

CONVER: The convergence of the solution is checked in this routine. Both the displacement and residual force convergence criterion are employed. The value assigned to the convergence counter (LITER) would later indicate which of the two criteria or if both were met to abandon the iterative loop. The maximum admissible vertical deflection criterion indicating total collapse is also checked in this subroutine.

OUTPUT: This subroutine outputs some of the selected results. The layer stresses and strains, the total stress resultants at each of the element Gauss points for the selected elements may be printed out. In addition the imposed total load vector, the residual force vector and the reactions at the restrained boundary nodes may be listed in any combination.

OUTP78: This is another outputing routine to print out some other results through channel 7 and 8. It employs another subroutine DISPNOD to print out the accumulated nodal displacements. During the execution of the programme, the layers are marked with different integer numbers to

identify the state of stress it had experienced. These layer markings and the orientation of the crack (if cracked) at each of the Gauss points of the selected elements may be printed from this routine if desired.

MATXCI: The undetermined coefficient matrix for each of the different types of element are formed here and then inverted through a standard matrix inversion routine of NAG Library.

UDLRNA: In this routine, the element equivalent nodal load vector is formed corresponding to unit magnitude of applied distributed loading.

ASEMPK: The element stiffness matrix is assembled in this segment to form the global stiffness matrix. Only, the upper symmetric band of the master stiffness matrix is stored.

MATMUL: This is a matrix multiplication routine. Any two matrices (including vectors) may be multiplied here to obtain their product matrix.

PRINST: This routine calculates the principal stresses or strains if the respective orthogonal coordinate quantities are supplied. It is called from STRESP, COMCOM and TENCOT.

DISFIL: This subroutine is called from the master segment. If displacement quantities of a few nodes are of interest and a load vs. displacement curve is required, then this routine is employed. This routine writes some of the relevant parameters and the total load and selected displacement quantities in a file during the execution of the programme. These stored values are fed in directly as data for another plotting programme.

CRADRA: This is a plotting routine called in from the main programme. The crack orientation at the Gaussian points of each layer is drawn through this subprogram. Thus, the discrete crack angles for the whole structure is represented separately for each of the layers. To get an overall

averaged picture of the crack direction, a second option is included in the programme. In this case, the crack angles of all the cracked layers at the same Gauss point is averaged to get a mean crack direction. This averaged crack directions are then plotted for the whole structure. But if the crack angles differ significantly through the layers at the same point, the second method may present a false picture of the crack patterns.

CONTOR: This is the second plotting routine incorporated in the programme. It is called in if the contour map of the stress resultants are required. The distribution of the membrane forces N_x, N_y, N_{xy} and the moment resultants M_x, M_y and M_{xy} can be drawn in any combination for the whole structure. The input code values determine which of the stress resultant contours are required and at which load increment. In addition, the isometric view of the deflected shape of the discretised structure may be drawn through this routine.

Some of the subroutine may have been omitted from the descriptions here. It is believed that they would be quite straight forward and self explanatory. The volume of the total programme listing deters its presentation here. Only, the input parameters are briefly provided in the Appendix C. The detail description and the programme listing is given elsewhere[52].

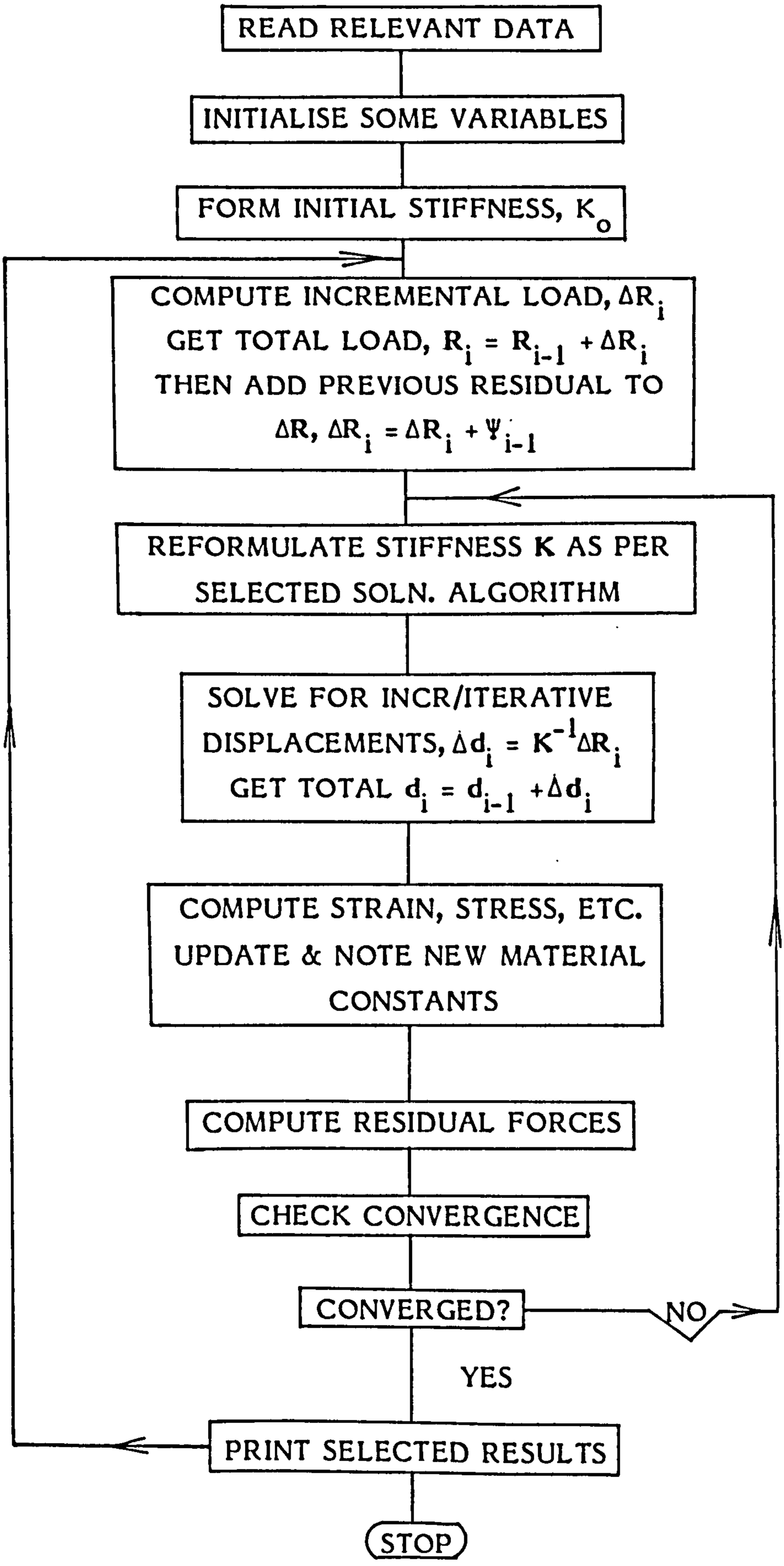

FIG. 5.1. Basic Operational Steps Describing the Adopted Computational Procedure.

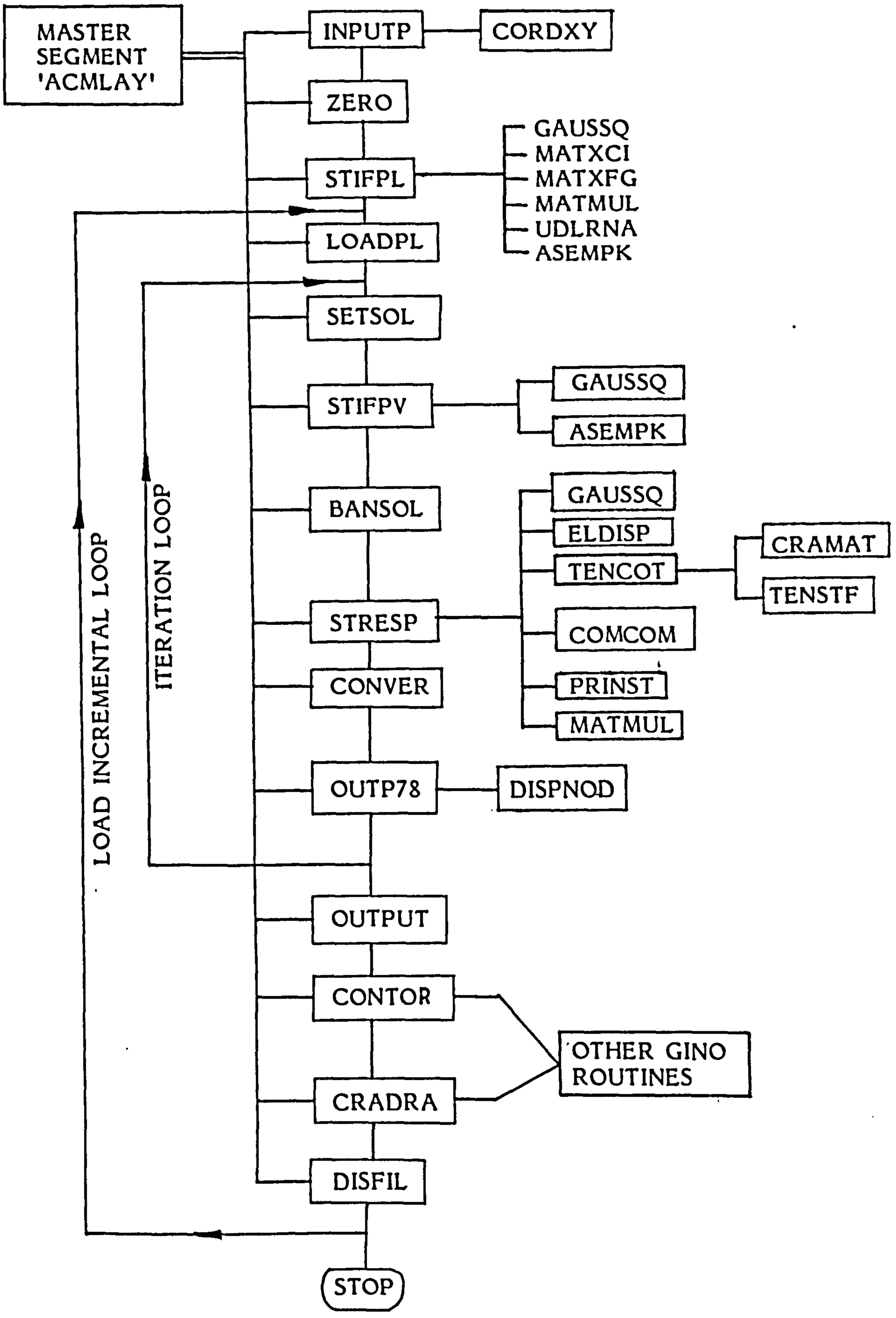

Fig. 5.2. Programme Flow Diagram for ACMLAY

(Nonlinear RC Slab Analysis Programme Using 5DOF Layered ACM Element).

Chapter 6

EXPERIMENTAL INVESTIGATION

6.1 Introduction

The mathematical modelling and material idealisation necessary for finite element analysis of nonlinear behaviour of reinforced concrete flexural members have been described in some of the previous Chapters. But the numerical predictions need to be compared with some experimental observations for validation. Published results on experimental study of reinforced concrete structures have grown steadily throughout the past three decades. Yet, the importance of further experimental investigation should not be underrated. The practical implementation and the associated difficulties inherent to the experimental study lends deeper and clearer insight to an analyst in understanding the behaviour of reinforced concrete members. The experiments carried out in this investigation are described in this Chapter.

6.2 Parameters of Study

Geometrically the experimental slabs were either rectangular or square slabs. A total of six slabs were tested. Half of them were rectangular slabs and the rest were square. The side ratio, sometimes called the aspect ratio of all the rectangular slabs was kept constant at 2.0. All the test slabs were 38 mm thick. Two different types of loading were considered namely, i) Uniformly distributed pressure loading and ii) Point loading system. The supports for all the slabs were simple supports in nature. Four of the six models had supports all around their four edges. The remaining two, both rectangular slabs had one of their longer sides completely free resembling that of a balcony type slab.

For all the tests, the following things were recorded:

i) the lateral deflection at some preselected locations.

ii) the steel strains in either direction at some predetermined locations.

iii) the cracking load/pressure at first visible crack.

iv) the failure load/pressure.

In addition, the overall crack pattern after failure on both the tension and compression faces of the models were photographed.

6.3 Slab Designation

The six experimental slabs are designated as S14UD, S24P1, S34P4, S43UD, S54UD and S63P1. The first two letters represent the slab model number, the next letter - a numeral indicates the number of simply supported edges and the last two letters represents the type of loading which are either UD for uniformly distributed pressure loading or P1 for single point load and P4 for four point loads on the slab.

Table 6.1 gives the details of slab dimension, steel percentages in either direction, type of loading and the boundary conditions associated with each of the model slabs. The location of the point loads and the edges having simple supports are shown in Fig. 6.1 for all the test slabs. Both in Table 6.1 and Fig. 6.1, the slab dimensions are the effective spans. All the slabs had an overhang of 40 mm beyond the centre line of the supports.

6.4 Materials for Microconcrete

The constituents materials of the microconcrete used were cement, sand and water. Ordinary portland cement and normal tap water were used in all the tests. The sand suply was from the Springbank quarry in Bridge of Allan.

The sand was air dried before use and sieved through a 5 mm sieve in order to screen out any unusually large particles. The particle size

Table 6.1 Details of the Experimental Slabs.

Slab Designation	Dimension (mm)		Steel percent -age (p)		Loading Types	Supporting Conditions
	Length	Width	L	W		
S14UD	760	760	0.506	0.506	UDL all over	Simple supports on all 4 edges
S24P1	760	760	0.506	0.506	1 Point Load at centre span	do
S34P4	760	760	0.506	0.506	4 Point Loads at quart. span	do
S43UD	1520	760	0.506	1.013	UDL all over	1 Long edge free, rest simple supt.
S54UD	1520	760	0.506	1.013	UDL all over	Simple supports on all 4 edges
S63P1	1520	760	0.506	1.013	1 Point Load	Same as S4 3UD

Note: For all the slabs,

Over all thickness, t = 38 mm
Effective depth, d = 31 mm
Steel percentage, $p = 100 \times A_s/bd$

where, A_s is the steel area in the direction concerned.

distribution of this sand was then performed using some representative samples and following the standard procedure set forth in BS 812 part 1:1975[10]. A typical gradation curve for this sand is shown in Fig. 6.2 and it seems to have complied with the requirements of Type S sand of BS 1200:1976[11].

6.5 Properties of Microconcrete

The characteristic properties of concrete required by an analyst are those of modulus of elasticity, compressive strength, tensile strength, strain at failure, etc. Determination of such properties is described in the following subsections.

6.5.1 Uniaxial Stress-Strain Relations

For the determination of modulus of elasticity and complete stress-strain uniaxial behaviour, a concrete prism specimen is required with a suitable means of measuring strain. In this investigation a 200 mm long and 100 mm in diameter microconcrete cylinder was used. The test procedure followed was that of BS 1881:Part 121:1983[12] for determination of static modulus of elasticity. Thus an initial conditioning load corresponding to about a third of its estimated compressive strength was applied and held constant for one minute and then reduced to about 0.5 N/mm^2. This was repeated three times and at each of these load steps strains along three vertical lines at six different locations were recorded using a 2 inch Demec strain gauge. The cylinder specimen was then steadily loaded to failure and strains were recorded at suitable load increments. The estimate of the compressive strength for initial conditioning load was made possible by prior testing of three 100 mm cubes which were cast along with the cylinder itself. Fig. 6.3 shows two representative stress-strain curves for this cocnrete - one for vibrator compacted casting and the other for hand compacted one. As seen from the

figure a bilinear curve was drawn through the recorded points. The initial modulus of elasticity obtained from the first slope of this stress-strain curve are found to be nearly equal to the secant modulus of elasticity as defined in BS 1881 Part 121:1983.

From Fig. 6.3 it is also noticeable that the initial discontinuity starts at about 50% of the compressive strength. This is well within the generally accepted elastic range of 30% and 60%. Even much conservative codes of practice ACI 318-77[1] allows linear elastic behaviour up to 0.45 f'_c.

6.5.2 Compressive Strength

American concrete Institute Building Code ACI 318-77 relies upon concrete cylinder crushing strength to estimate the compressive strength of concrete in flexure. On the other hand CP 110[23] normally suggests concrete cube strength tests and then to reduce the cube strength to 67% of its value to account for the flexural situations. It is well known that the cube strengths are usually about 25% to 33% higher than that of cylinder strengths because of its restraining effects due to smaller height to side ratios. Thus, both the codes of practice accept approximately the same strength in flexural compression.

Here in this study, the concrete cube strengths were multiplied by 0.80 to estimate the compressive stress level at failure due to flexure. During the few laboratory tests the ratio of cylinder to cube compressive strength on mortar concrete was found to lie between 0.78 and 0.89. Considering practically the ideal controlled conditions of a laboratory mix, the reduction factor of 0.8 seems realistic and not too far beyond the value of 0.67 as suggested in CP 110.

6.5.3 Tensile Strength

Concrete is much too weak in tension compared to its compressive

strength. Practical design procedures frequently ignore its tensile strength. But for numerical analysis the onset of cracking depends on the value given to its tensile strength. There are different experimental methods for estimating the tensile strength of concrete. Some of these methods are

a) Direct tension test on specially prepared specimens.

b) Modulus of rupture test on beams.

c) Cylinder splitting test.

The last method, an indirect tension testing procedure was adopted here and the tensile strength being given as

$$f'_t = \frac{2P}{\pi DL}$$

where, P = total force causing splitting

D = diameter of cylinder

L = length of cylinder.

In general, the results obtained confirm the popularly accepted tensile strength value of the order of 7-10% of compressive strength[29].

6.6 Design of Microconcrete Mix

The microconcrete for the test slabs were designed for a target mean cube strength of 21 N/mm^2 at 7 day. Aggregate (sand) to cement content ratio was chosen to be 4 by weight. A number of trial mix with different water cement ratio was tried and finally the water-cement ratio of 0.6 was selected. 7-day mean cube strength of 22 N/mm^2 was achieved on this trial mix at the selected water-cement ratio. The consistency of the mix was found to be just sufficient considering vibrator compaction of the models and the specimens.

6.7 Properties of Reinforcing Steel

Mild steel is a well behaved material compared to concrete.

Information regarding reinforcing steel needed in a numerical solution are the modulus of elasticity of steel, percentage of reinforcement and the yield strength of steel. The first two parameters are readily known but for the last bit of information a routine tension test would be necessary. Some high tensile strength steels and cold worked mild steels do not show a well defined yield phenomenon. But for all practical purposes, a simple tension test would furnish the 0.2% proof stress level which can be replaced for the yield value. The 4 mm nominal diameter (actual diameter also 4 mm after annealing and removing scales) mild steel bars used for the test slabs were annealed after purchase. The commercial bars not only lacked a well defined yield point but also failed to show any appreciable elongation prior to failure. Tension testing on the annealed bars were carried out following BS 18:Part 2:1971[9]. Instron autographic tension testing machine of the Mechanics of Materials Laboratory was used for this purpose. Fig. 6.4 shows a representative stress-strain curve for the used reinforcing bars. A number of randomly taken samples were tested and the average yield and ultimate strength are found to be 240 N/mm^2 and 330 N/mm^2 respectively.

6.8 Design of Models

Before proceeding to casting and subsequent testing of a model, one should estimate the ultimate load at failure with reasonable accuracy. A model should be as nearly equal to the prototype as is practicable[71]. But the available laboratory space, limited capacity of the loading rig, handling difficulties and costs involved are some of the many factors[63] which curtail the physical dimension and limit the steel percentage of a model reinforced concrete structure. The materials used for fabricating the test models should be carefully selected so as to simulate the actual behaviour of the prototype with close conformity[14]. When the dimension

and the reinforcement amount is agreed upon, the ultimate capacity may be estimated using some method of limit state design. The yield line theory pioneered by Johansen[48] and others[50,51] is one such ultimate load theory for slab design. It is based on assumed collapse mechanisms and plastic properties of under reinforced concrete slabs. Yield line analysis is well established for estimating the failure load of reinforced concrete flexural members. Details can be found in any standard text on reinforced concrete design[44,53].

The yield line theory has been followed here to estimate the ultimate load capacity of the test slabs. The assumed yield line patterns for the test slabs are shown in Fig. B.1 of the appendix B. A sample calculation to determine the ultimate load is also provided there.

Reinforcement detailing for the different test slabs are shown in Fig. 6.5 through Fig. 6.7. Plates 6.1 and 6.2 are two representative photographs of the actual steel mesh provided.

6.9 Loading Arrangement

Two different types of loading were applied on the test slabs. The means of achieving them are described below.

6.9.1 Point Loads

The range of point loading system considered were applied either as a single concentrated load or as a set of four concentrated loads each spread over a finite area. The distribution area for these point loads was determined following Section 3.4.5.2 of CP 110[23], so as to prevent any premature failure due to punching. Thus, for slab S24P1 the single point load was distributed over 50 mm x 50 mm square area. For slabs S34P4 and S63P1 each of the 4 point loads and the single point load respectively was dispersed over 40 mm x 40 mm square area. Accordingly, an appropriate number of 12 mm thick steel square plates of required

dimension were prepared. To each of these plates 12 mm thick hard rubber pad was glued underneath using commercial adhesives - rapid setting araldite. On the top face of the steel plate a hemispherical groove was formed right at its centre. The rubber pad side of this assembly was placed on the concrete surface of the slab at the required location and a high strength steel ball bearing was placed into the groove of the steel plate. Load was applied to the ball bearing either directly from the ram of the jack for single point load or through an intermediate cross piece placed between the ram and the ball bearings for four point loading. The cross piece was made of rectangular hollow steel sections and semi-hemispherical cup groove was also formed underneath the cross piece at appropriate location of contact points. The location of the point of application of the concentrated loads is shown in Fig.6.1. The physical arrangement of the point loading system may be seen in the photographs of Plate 6.3 through Plate 6.5. The total applied load could be directly read from the digital displaying unit of Dartec monitoring and controlling unit for the jack. It also provided a load-displacement curve for the jack.

6.9.2 Uniformly Distributed Load

Uniform pressure load was applied to the slabs through an air bag prepared from commercially available polyethelene cloth used for making shower curtains. The air bag dimensions were made equal to that of the slab under consideration. The complete closure of the bag was achieved by sealing the open edges using commercial adhesive evo-stick. The overlapping width of the joining cloths were about 60 mm on either face of the edges. Two holes were made at appropriate location on the bottom face of the bag. Two pressure valves were glued to these holes for air inlet and outlet. During a test, the pressure bag was completely enclosed

within 2" x 2" steel angles welded all around the 3 mm rectangular steel base plate. The base plate was stiffened by rectangular hollow steel sections running across its bottom at suitable close spacings. Wooden boards were placed within the enclosure in order to reduce the gap between the base for the bag and the rim of the enclosing angles. This gap was left at about 10 mm. The air bag was then laid over the wooden board and the two valves were led out through two pre-drilled holes in boards and base plate. A thin polyethelene sheet was then spread on top of the air bag passing over the angle rims. The slab was placed on top of the rims with its compression face down and the supporting frame put on top of the tension face. The whole assembly was then tied down to the floor. Fig. 6.9 and Plate 6.6 show this loading arrangement.

The inlet valve was connected to an air pressure cylinder through a pressure transducer and a controlling valve. The transducer reading was transmitted to a digital voltmeter where the output was in millivolts (mV). The transducer-DVM assembly was precalibrated and the DVM output of 1 mV was found to correspond to 1 psi of pressure. The outlet valve was connected to an extension tube with a stop valve attachment.

6.10 Supports

The simple supporting system for all the slabs was achieved by placing 12 mm diameter high strength steel bars all along the supporting edges of the slab. These bars were given a very smooth finish on their surface in order to reduce the possible friction to a minimum. The support bars were welded to steel flats of 50 mm x 12 mm in section. Subsequently the steel flat sections were tack welded to the main supporting frame. The main frame is shown in Fig. 6.8 and consisted of two long beams and two short beams. 200 mm x 133 mm x 25 Kg standard steel universal beams were used as the long beams and 150 mm x 110 mm

available steel beam sections were used for the shorter ones. The distance between the two short beams could be varied along the longer ones to give the side ratios necessary for the square and the rectangular test slabs. For the balcony type one edge free slabs, one of the longer beams was replaced by a smaller depth 100 x 100 x 8 square hollow steel section. The bottom edge of this hollow section was made level with the bottom edge of the remaining long beam. Thus ample room was left above this smaller section for the free edge of the slab to deflect. The 3-way supporting system can be better visualized from the photograph of Plate 6.5.

For the slabs tested under point loads, the supporting frame was in turn supported on four steel columns which were themselves connected to steel beam sections at their bases. On the other hand for uniformly distributed loading case, the supporting frame was placed upside down on to the slab. The support lines of these slabs were in fact squeezed between supporting bars and the angles enclosing the pressure bag. The support frame was then tied down to the structural floor of the laboratory with the help of two 100 x 100 x 8 steel hollow sections (running across the frame) and four long steel bolts passing through the holes provided in the laboratory floor. Fig. 6.9 and Plate 6.6 show this form of supporting arrangement.

The corners of a simply supported slab subjected to transverse loading only are liable to lift up and might reduce the load carrying capacity of the slab. To prevent corner lift ups, the slabs under point loads were held down at their corners using a suitable clamping device. About 100 mm x 100 mm x 3 mm thick ply wood board was placed at the corners infringing about a quarter (50 mm x 50 mm) of its own area from within the support lines. On top of these plywood boards, 12 mm thick

steel plate was placed and it was then clamped to the supporting frame. Moderate hand pressure was used to tighten these clamps. For the slabs under uniform pressure load, no such corner supports were necessary because they were actually sandwiched all along their support lines.

6.11 Deflection Measurement

Deflection of the test slabs at some preselected locations was recorded. Mechanical dial guages with a minimum subdivision corresponding to 0.01 mm were used for this purpose. Before putting the slab on to its supporting frame, a suitable grid was drawn on one of its faces. Later, the deflection dial gauges were placed at the required grid points either from the top or at the bottom face as suitable. For some of the slabs (see Plates 6.3 and 6.4) a separate frame was built around the loading frame to hold the deflectometers.

Deflections were recorded on at least two symmetric locations wherever such symmetry existed and the average of such readings were taken as the deflection of any one of those symmetric locations. The locations of the deflection recording stations and the corresponding load-deflection curves for those points are shown in Fig. 6.10 through 6.15 for all the test slabs. Each of these symmetrical locations on the slab are given identical grid point numbers in these figures.

6.12 Steel Strain Measurement

Two millimetre foil type electrical resistance strain gauges were used to measure the steel strains. Prior to casting, strain gauges were attached to the reinforcing bars at appropriately selected locations. The physical location of these gauges were so selected that they remain close to some Gaussian integration points during analytical discretisation of the slabs into finite elements. The coordinates of the actual location of the strain gauges and those of a nearby integration point are given in

Table B.3 of Appendix B.

Commercially available SHOWA strain gauges with a resistance of 120 ± 0.5 ohms and gauge factor 2.1 ± 1% were used throughout. The gauges were installed on the reinforcing steel using an M-bond 200 adhesive following the manufacturer's instructions. After soldering the lead wires to the strain gauge terminals, the whole connection was coated with an air drying M-coat to protect against humidity and temperature. Later, another vinyl mastic coat was overlapped over the entire junction to guard against any water leakage and mechanical damage during casting. Load versus steel strain diagrams are provided in Figures 6.16 through 6.19.

6.13 Casting and Curing

The reinforcing mesh was assembled on the formwork (Fig. 6.20) after the position of the bars were marked with a chalk. Details of reinforcement mesh for the test slabs are shown in Fig. 6.5 through Fig. 6.7. The steel bars with the strain gauges were placed last just before casting. The microconcrete mix was then prepared in a drum type rotating batch mixture. The amount of the constituent materials required for each of the square and rectangular slabs along with the control specimens are given in Table B.2 of the Appendix B. Each model was cast by pouring fresh concrete into the form in 3 layers and vibrating the mould after each addition. A vibrating hammer called the Kango hammer was used for this purpose. At the end of the final layer, the excess concrete was screeded off and the top surface was trowel finished. Finally the mould was given some gentle tapping to ensure overall smoothness of the top surface. The control specimens were cast in a similar way simultaneously with the model.

The test slab together with the control specimens were then covered completely with polyethelene sheets to control humidity. This cover was

removed after six days and the formwork stripped. The tension face of the slab was painted white with a solution of plaster of paris in water. On drying, other necessary preparations were carried on for the testing on the seventh day.

6.14 Test Procedure

After placing the test slab on its supports and securing the corners from lifting up, the strain gauge lead wires were connected to the strain indicator through a wheatstone bridge junction box. The strain readings were checked for any possible damage to the strain gauge connections. The strain indicator with its connection to the gauges was then given a heating up time of about 4-6 hours for stability of strain outputs during the test. In the mean time, the deflection dial guages were placed at their proper grid point locations and the verticality of these gauges were checked.

At the beginning of the test, all the test slabs were subjected to a small amount of initial conditioning load while the contact between the deflectometers and the slab surface were checked. The conditioning load was then removed completely. Later, the slab was progressively loaded to failure. The load was applied at suitable increments so as to reach the estimated ultimate load in at least ten increments. Except for model S4 3UD, the total number of load increments were actually much more than ten. For the point loading systems the load increments were usually 0.5 KN or 1.0 KN and the jacking stroke was maintained at 0.002 mm/sec until near failure when the stroke speed had to be increased considerably. In the case of pressure loading the increments were normally 0.5 psi or 0.25 psi depending upon the expected ultimate load.

At zero load and after each load increments, the deflection gauge and the strain gauge readings were read and recorded manually. As the

loading continued the tension face of the model was continuously inspected for the first visible crack. The load/pressure corresponding to the appearance of the first crack was recorded. The ultimate stage was assumed to have been reached when the deflection readings continuously moved on without any significant change in the applied load. Specially for the uniform pressure loads, a unique deflection corresponding to the ultimate load was not possible because the deflection gauges drifted on and on although the pressure was left almost stationary.

At the end of the test, the accompanying test cubes and cylinders were tested for compressive and tensile strengths respectively. Usually an average of 3 cube test results and 2 cylinder split results were taken as their representative values.

6.15 Brief Discussion of Test Results

The details of the supporting arrangement and applied loading systems are shown in Fig. 6.1 and summarised in Table 6.1. The representative cube crushing strengths and the split cylinder tensile strengths of the accompanying control specimens for different test slabs are furnished in Table 6.2. The total load on the slab at the instant of sighting the first tensile crack and that at failure are termed herein, as the cracking load and the ultimate load respectively. In case of uniform pressure loading, the total load is obtained as the product of the pressure intensity and the total loaded area of the slab. The cracking and the ultimate loads for different experimental slabs are provided in Table 6.3.

The test model S14UD was a square slab, simply supported all around the four edges and loaded with uniformly distributed load. The first crack was observed near the centre span at about 5.7 psi of pressure. This corresponds to 0.0393 N/mm^2 and totals to 22,700 N of load on the

Table 6.2. Average Concrete Strengths of the Control Specimens for the Respective Test Slabs.

Slab Model	Cube Strength f_{cu} (N/mm^2)	Sp. Cylinder Strength f'_t (N/mm^2)
S14UD	21.9	2.29
S24P1	18.0	1.62
S34P4	20.0	2.10
S43UD	19.5	2.00
S54UD	21.6	2.20
S63P1	18.3	1.69

Table 6.3. Total Load at Cracking and Ultimate Stage of the Test Slabs.

Slab Model	Cracking Load P_{cr} (KN) (Pressure, N/mm^2)	Ultimate Load P_u (KN) (Pressure, N/mm^2)
S14UD	22.70 (0.0393)	36.04 (0.0624)
S24P1	5.15	9.29
S34P4	16.00	25.20
S43UD	9.55 (0.00827)	15.93 (0.01379)
S54UD	30.27 (0.0262)	52.57 (0.04551)
S63P1	3.10	5.00

slab. The load vs steel strain diagrams are shown in Fig. 6.16. It may be observed from the figure that strain gauge 3, although only 55 mm away from gauge 2, had undergone relatively higher extension compared to the other even before the visible macro crack appeared. Gauge 3 was located very near to the centre span and it is more likely that the microcracks had developed over this location. Their gradual growth enhanced the strain increments in steel there while widening their crevices. The cracks propagated along the diagonal towards the corner and spread very quickly until they covered about two-thirds of their total journey. Relatively very low strains in gauge 1 indicates that the reinforcements towards the supporting edges remain understressed except perhaps near the corners. Subsequently, the slab failed at a pressure intensity of 0.0624 N/mm^2. Plates 6.7 and 6.8 show the crack patterns of the tension and compression faces respectively for this slab after failure.

The test slab S24P1 was identical to the first model except that it was loaded with a single point load at the centre span. The first visible crack was observed underneath the load when it reached a magnitude of 5150 N. But this time the cracks propagated slowly towards the corners and instead of a single crack approaching the corners, the crack bifurcated near its origin. Thus a pair of branched cracks gradually moved on increasing the distance between them and finally crossed the supporting edges near the corners. Plates 6.9 and 6.10 show the crack patterns on both faces after failure. Although the photographs show a clear punching effect around the point load, the failure was primarily in flexural mode. The flexural cracks were developed fully and the slab sustained hardly any extra load during the formation of punching cracks. The ultimate load sustained by this slab was 9290 N. Steel strain recording for this slab and the following one (S34P4) were not possible

because of strain gauge installation error.

The third slab S34P4 was also a square slab identical to the former two in dimension and supporting arrangements. But this slab was loaded with four point loads placed at the quarter spans. The first crack appeared at the centre span when the total load (sum of 4 loads) reached about 16 KN. The central cracks progressed along the diagonal but soon new cracks along lines joining the point loads and parallel to the supports were formed. On further loading these edge parallel cracks originating from under the loading points moved inwards to meet each other and the former diagonal cracks eventually split into two as they proceeded outwards to the corners. Photographs of Plates 6.11 and 6.12 give details of the cracking patterns for this slab. The slab failed completely at a total load of 25.2 KN.

Model S43UD was a rectangular balcony type slab which was supported on three sides and the fourth side was completely free. It was loaded with uniformly distributed pressure loading system. The first crack was observed near the centre of the free edge. It slowly progressed inwards, remaining parallel to the short edges. Soon afterwards, inclined cracks were sighted near the free edge which extended towards the supported corners. The pressure intensity at the time of first cracking was recorded as 0.00827 N/mm^2. Fig. 6.17 shows the load-steel strain diagrams for this slab and Plates 6.13 and 6.14 furnish the crack patterns.

Strains in the longer steel near the centre span (Gauge 2 and 3) is relatively very low while that in gauge 1 are considerably higher. This is because gauge 1 lies right across the potential inclined cracks. Strains in the central short bar (gauges 4, 5 and 6) is relatively low as well. The recorded steel strains and the observed crack patterns suggest that the principal effect of bending is more prominent elsewhere away

from the centre of the slab. The slab failed at a pressure of 0.01379 N/mm^2 which amounts to 15.93 KN of total load on the slab.

Slab S54UD was a two way rectangular slab, loaded with uniform pressure loads. Because of its higher aspect ratio, the principal bending action should be along the shorter direction. The first crack had formed at the centre span when the pressure reached about 0.0262 N/mm^2. The crack gradually extended towards the shorter edges moving parallel to the longer sides. As can be expected, these primary cracks bifurcated on reaching the quarter spans and the two branches gradually crept towards the corners. The overall crack patterns are shown in the photographs of Plates 6.15 and 6.16. It may be noticed that, instead of a single crack moving along, a system of evenly spaced cracks were developed along with the prominent cracks. This was more so for the branched inclined cracks reaching the corners. Load-steel strain diagrams are presented in Fig. 6.18 and it may be seen that the strains in shorter direction were much higher compared to those in the longer direction. Specially, strain gauge 4 had shown appreciable extension soon after the long edge parallel crack appeared at the centre. The ultimate pressure at failure reached 0.04551 N/mm^2.

Test slab S63P1 was the second balcony type rectangular slab like that of S43UD. But it was loaded with a single point load located midway along the longer sides and a quarter of the shorter span inside the free edge (Fig. 6.1.f). The first visible crack was observed underneath the load extending up to the free edge at 3.1 KN load. This crack then branched out as it moved towards the supported longer edge. These branched cracks did not move towards the corner, instead they widened apart only slightly before reaching the longer support. The crack patterns at the tension face are shown in Plate 6.17. Although some

evenly spaced fine inclined cracks were formed but none of them could reach the corners. The reason for such behaviour would become clear when the compression face crack patterns of Plate 6.18 is noticed carefully. Two prominently negative yield lines had developed connecting the long supported edge with the corners of the free edge. So, the progress of the inclined cracks at the tension face was arrested by the formation of the negative yield lines and they could not proceed much beyond these. negative cracks. The load-steel strain diagrams are presented in Fig. 6.19. The slab collapsed at an ultimate load of 5 KN.

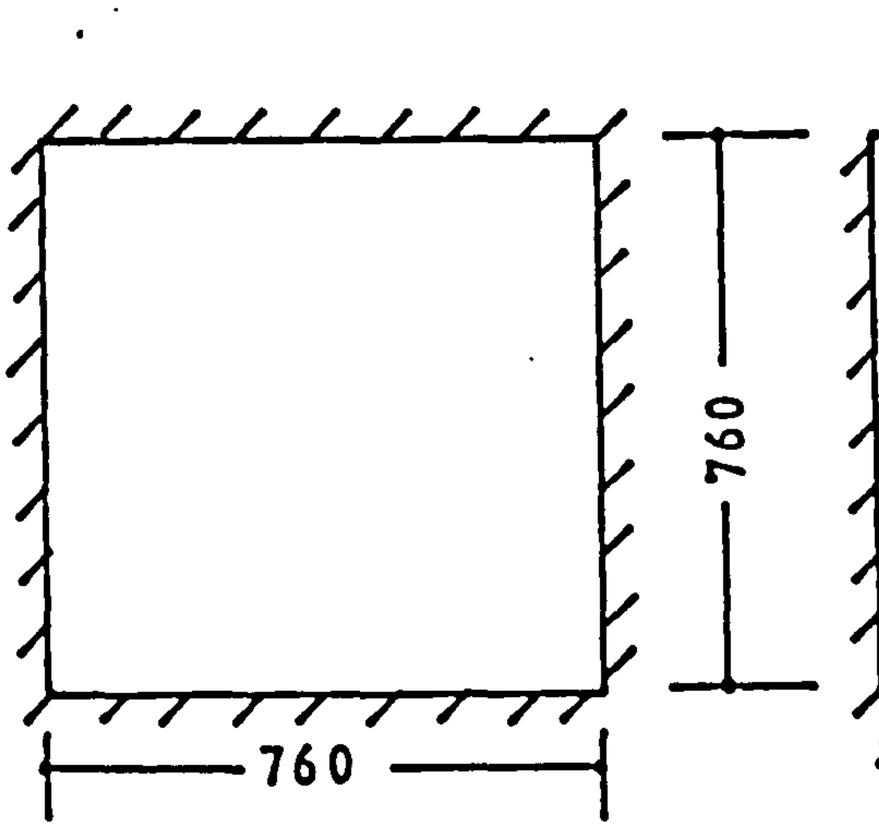

a) Model S1 4UD,
UDL all over

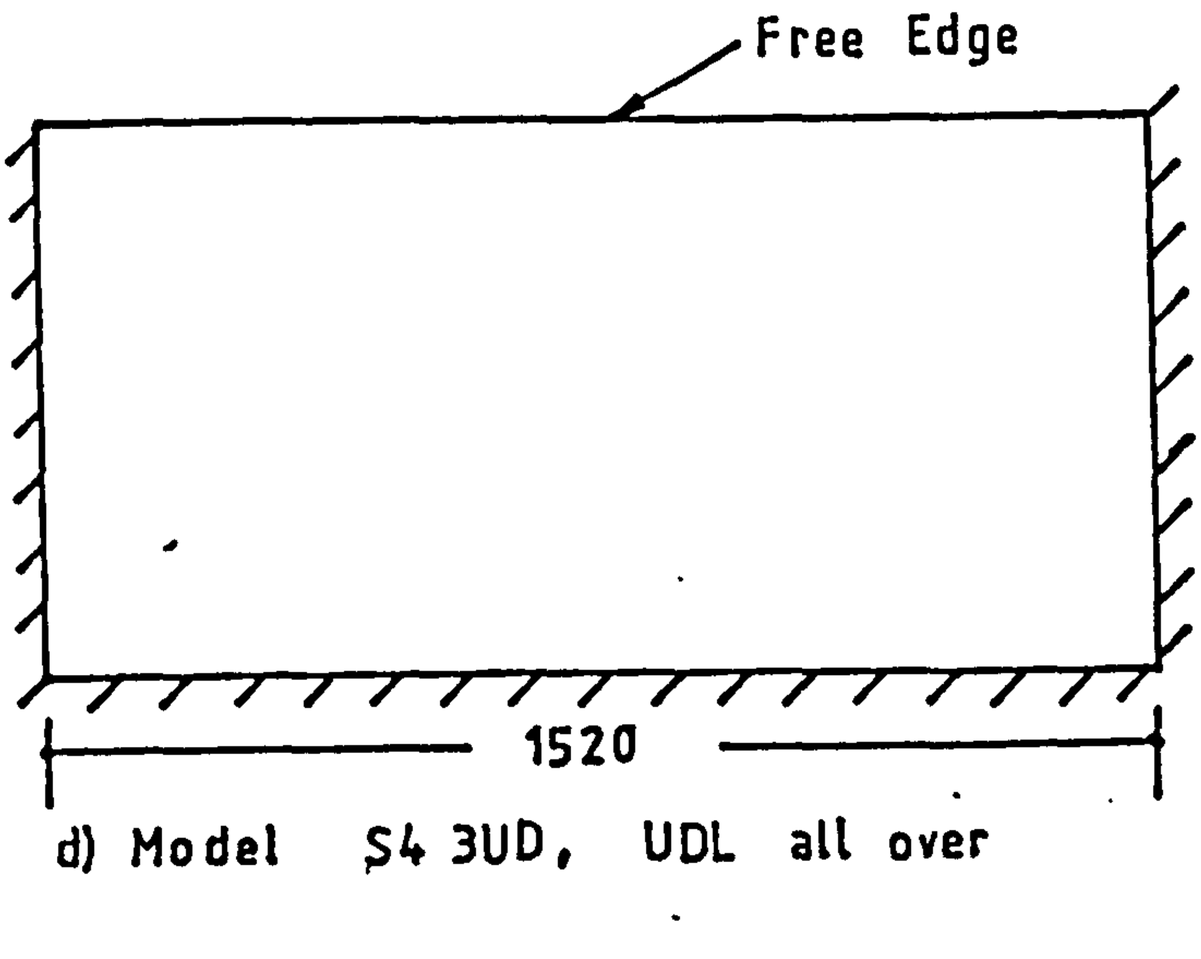

d) Model S4 3UD, UDL all over

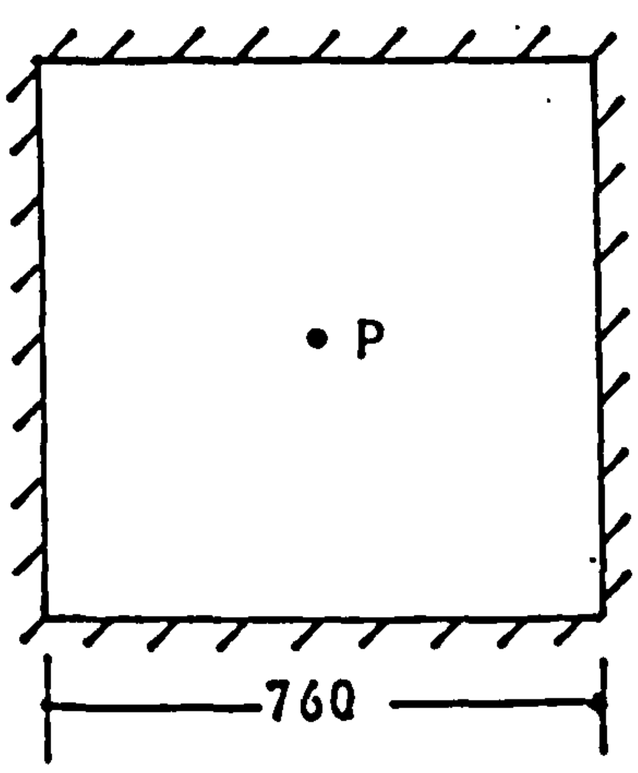

b) Model S2 4P1,
Single Point Load

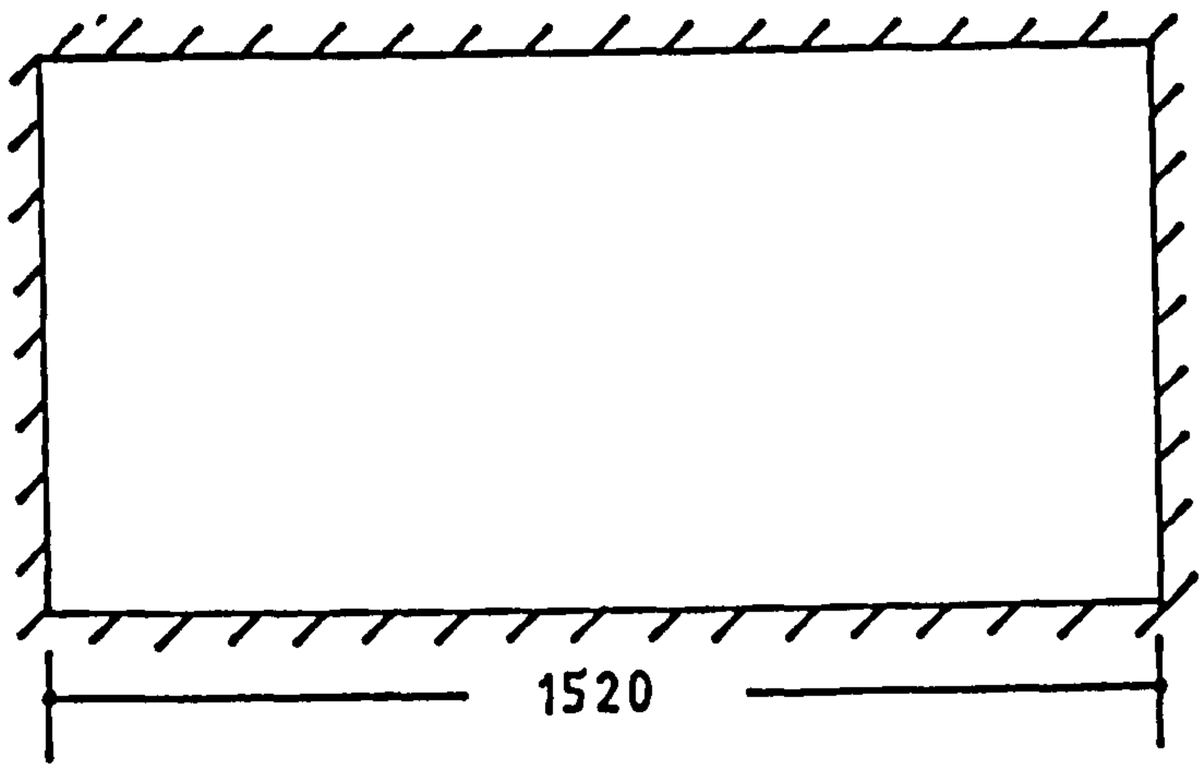

e) Model S5 4UD, UDL all over

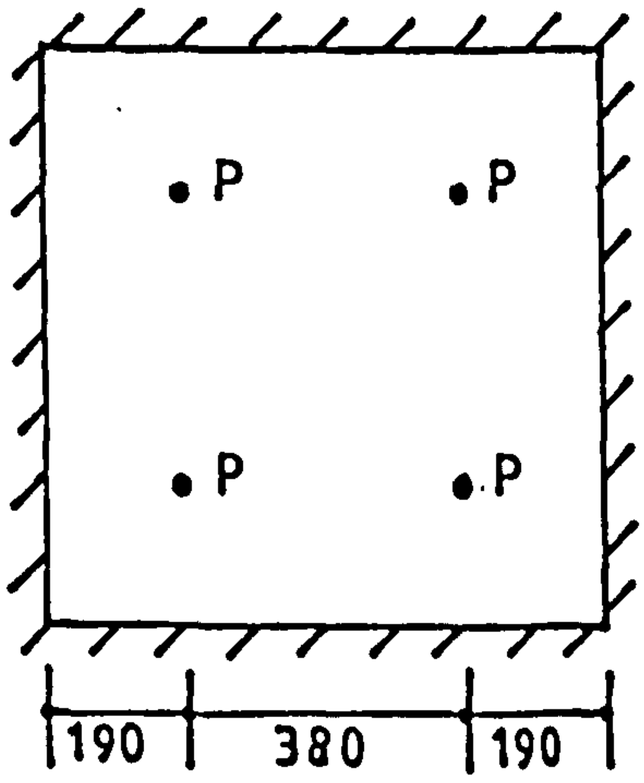

c) Model S3 4P4,
4 Point Loads

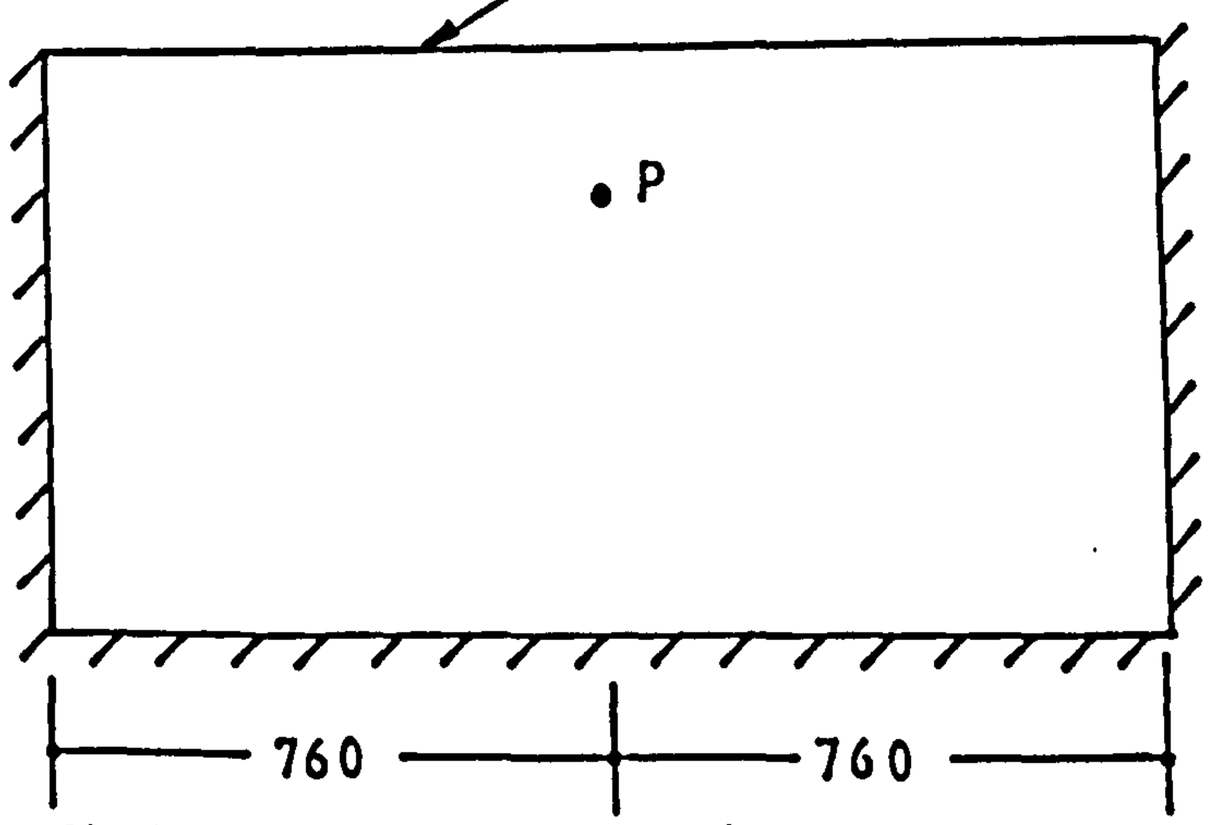

f) Model S6 3P1, Single Point Load

FIG 6.1 Support conditions and Loading arrangement for the Test Slabs.

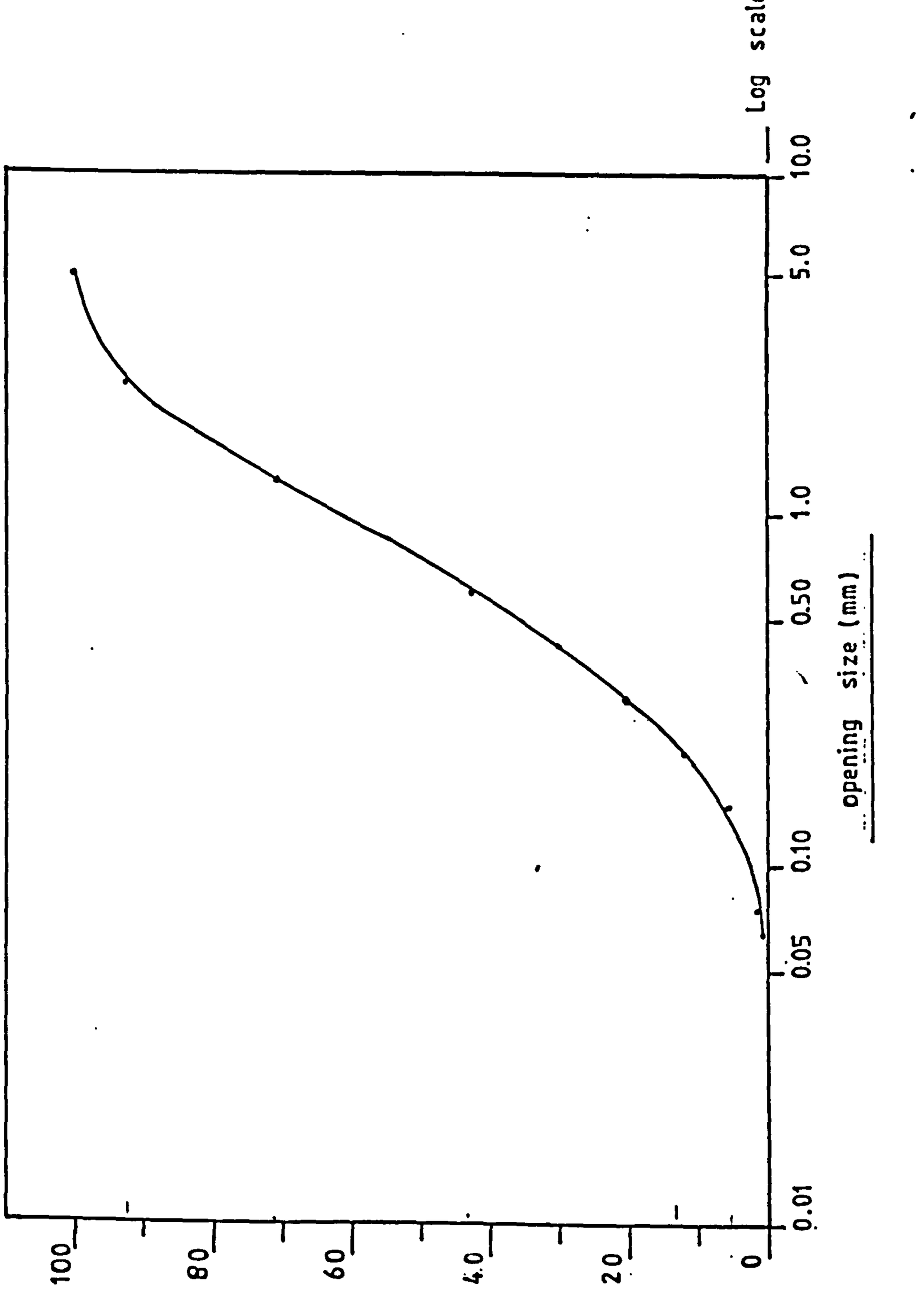

FIG. 6.2 Typical Gradation curve of the sand for microconcrete

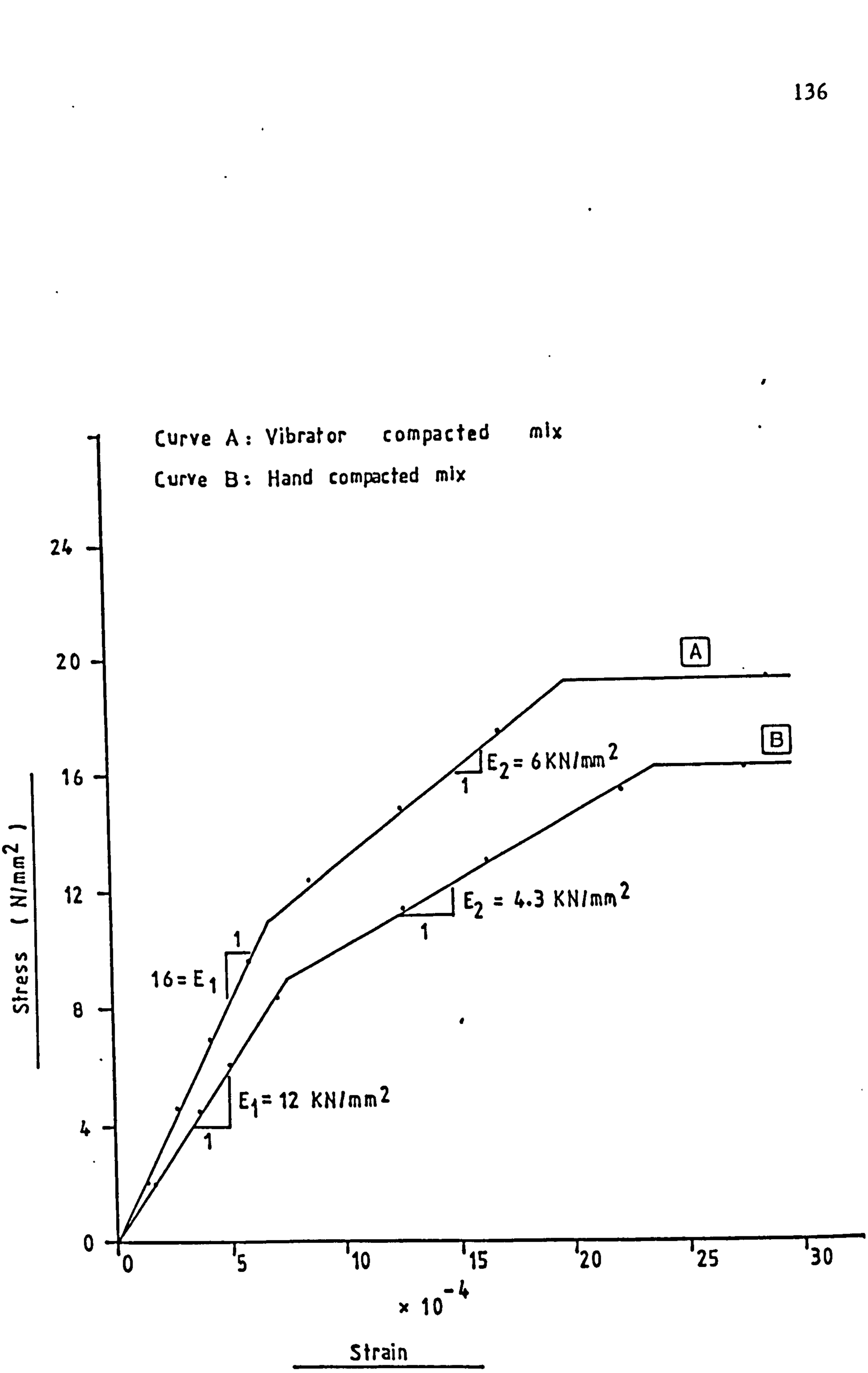

FIG. 6.3 Uniaxial Stress-Strain Curves for Microconcrete

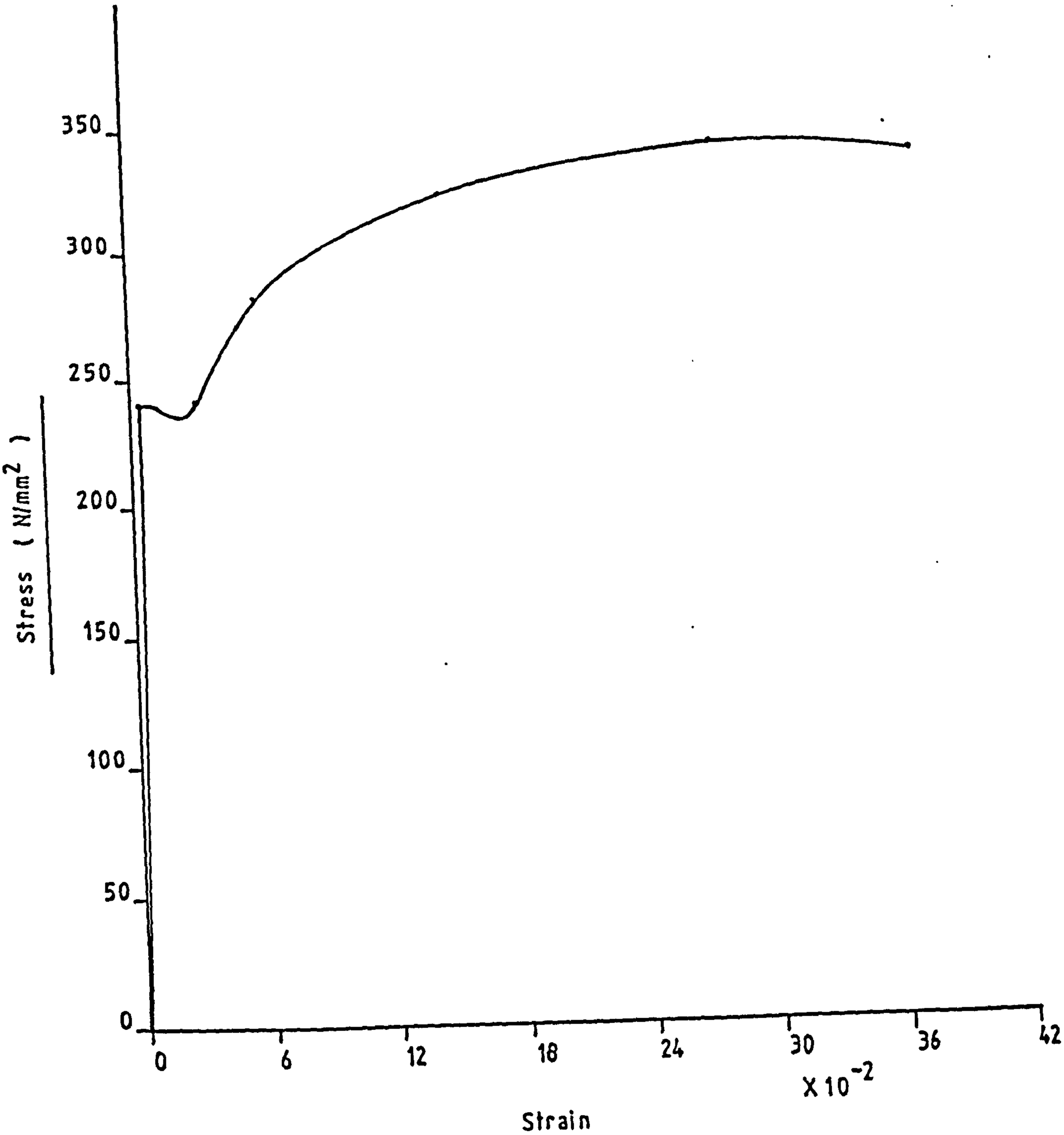

FIG. 6.4 Stress-Strain curve for (annealed) reinforcing steel

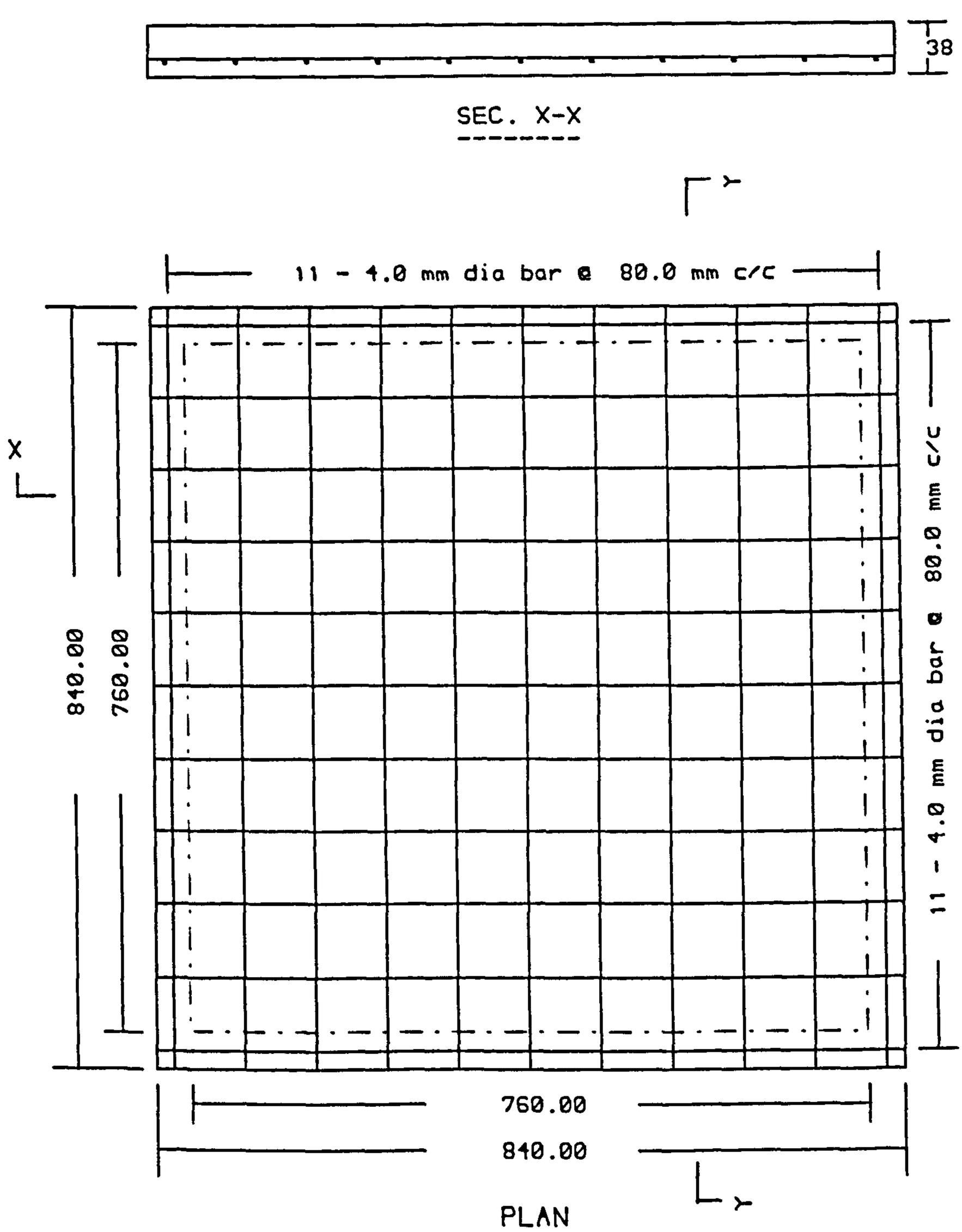

FIG. 6.5 REINFORCEMENT LAYOUT FOR SLAB S1:4UD, S2:4P1 & S3:4P4

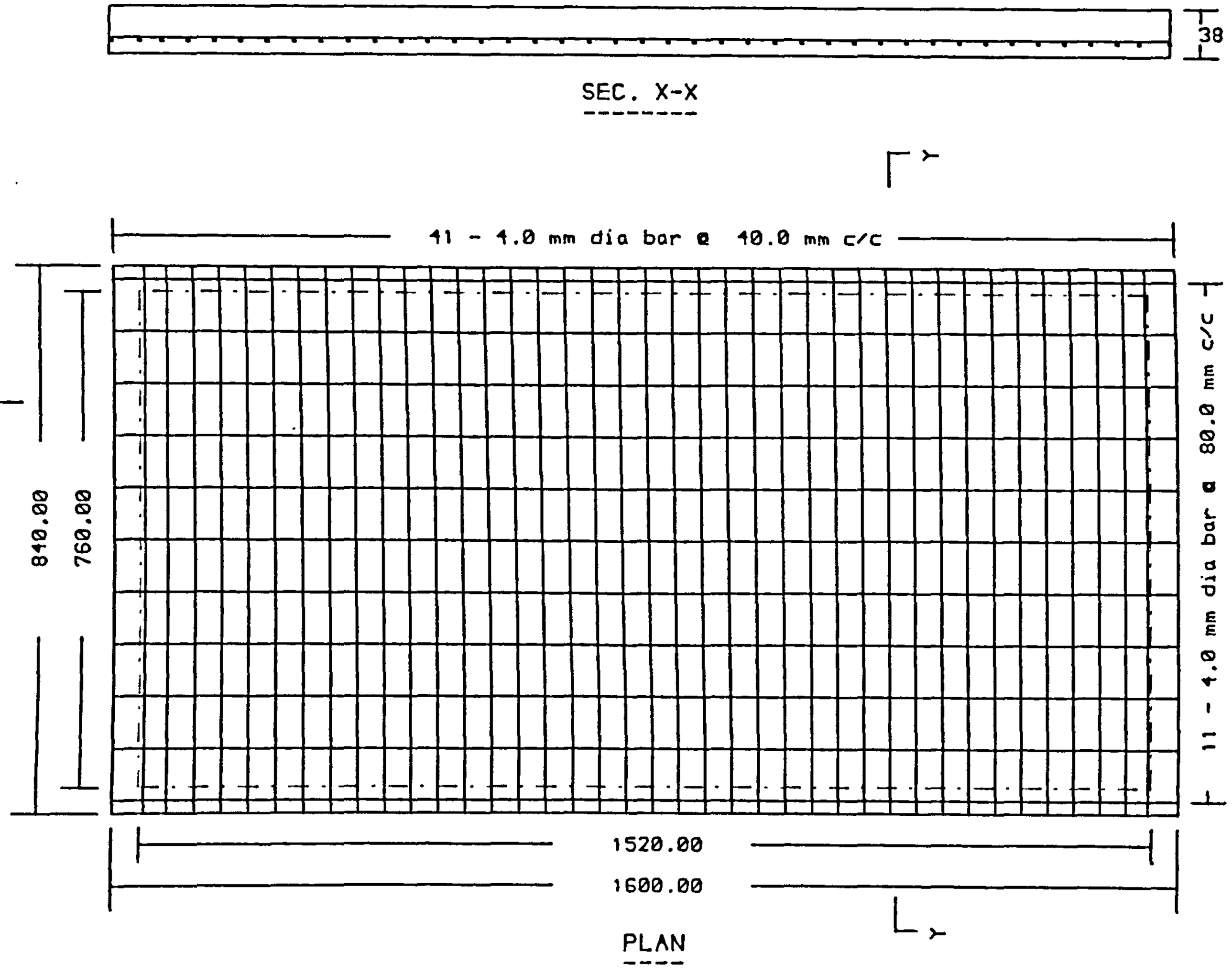

FIG. 6.6 REINFORCEMENT LAYOUT FOR SLAB S5:4UD

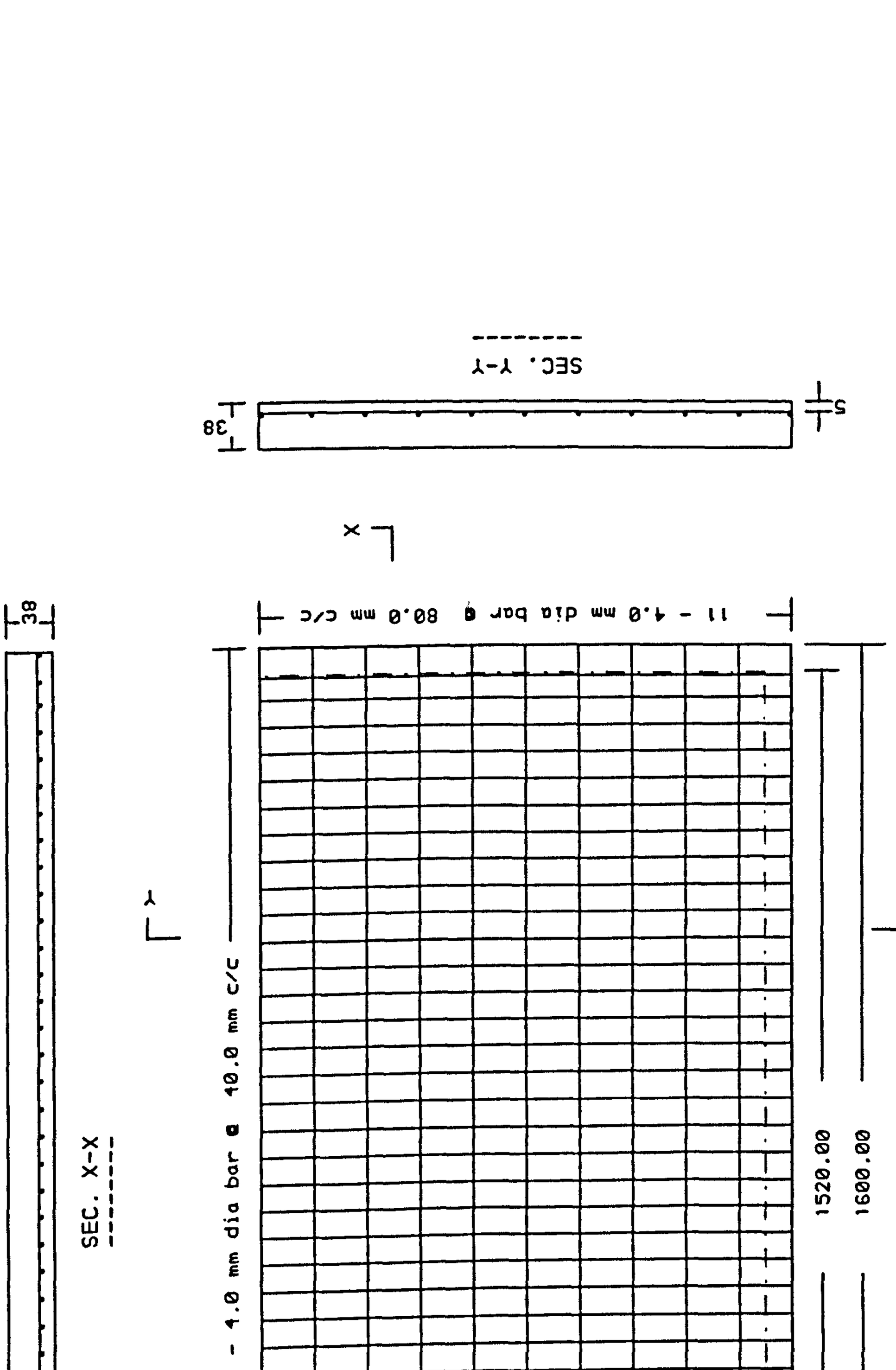

FIG. 6.7 REINFORCEMENT LAYOUT FOR SLAB S4:3UD & S6:3P1

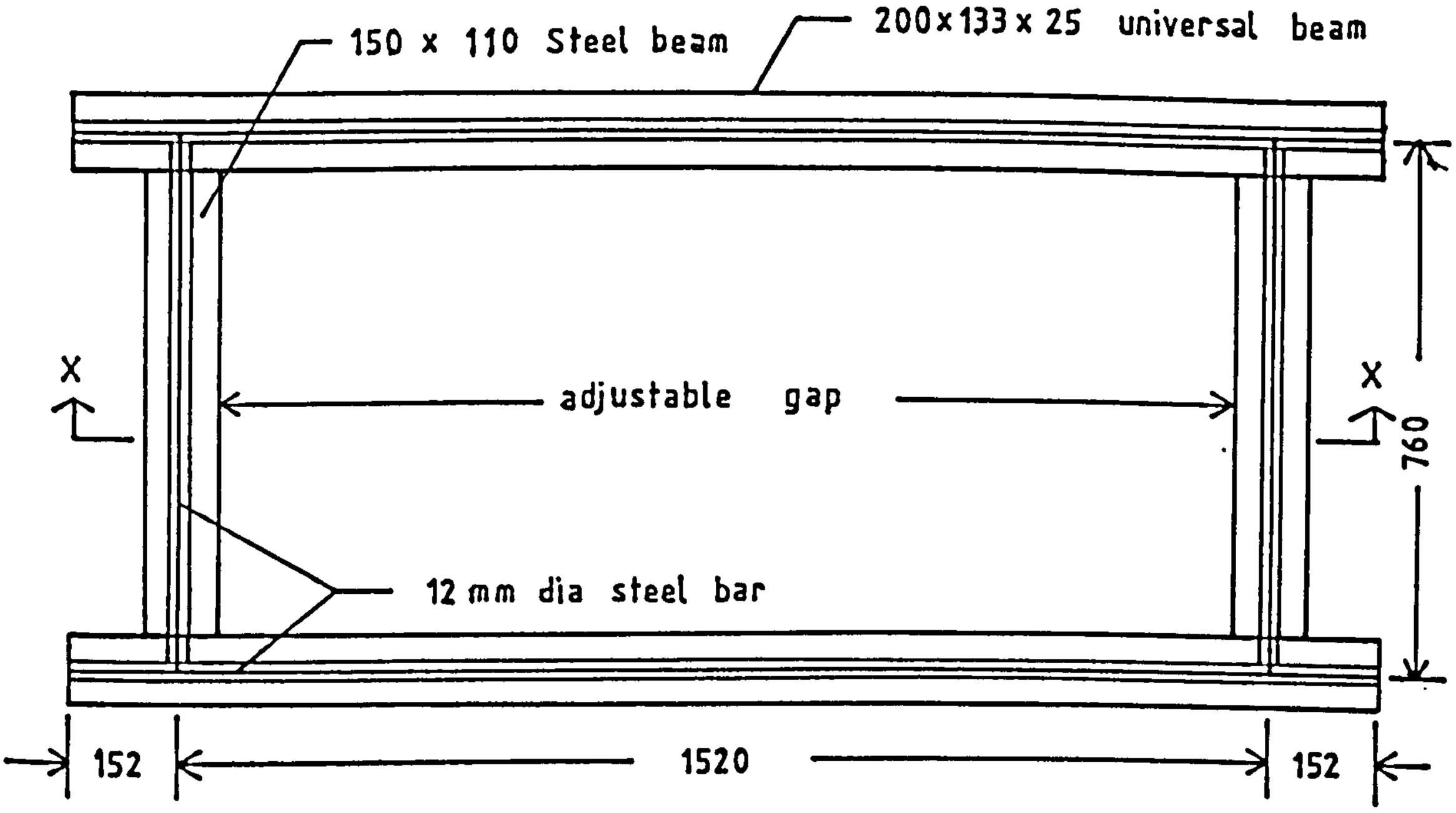

PLAN

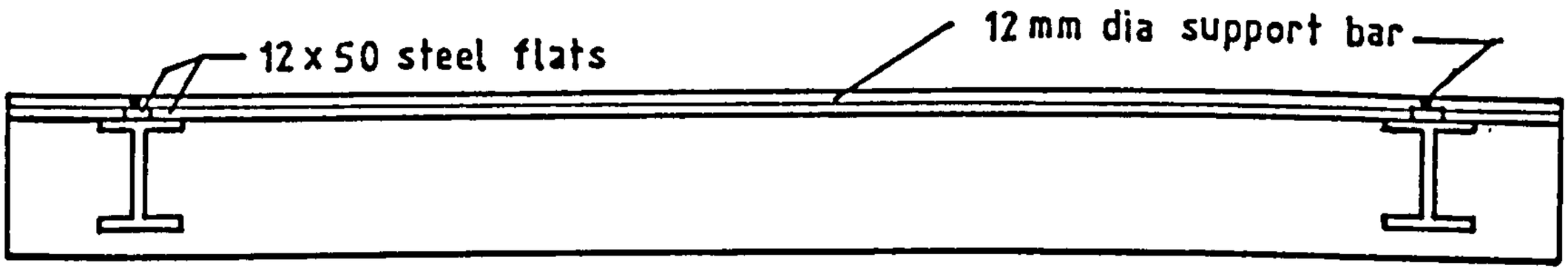

SEC. X-X

FIG. 6.8 Details of Supporting frame for the test slabs

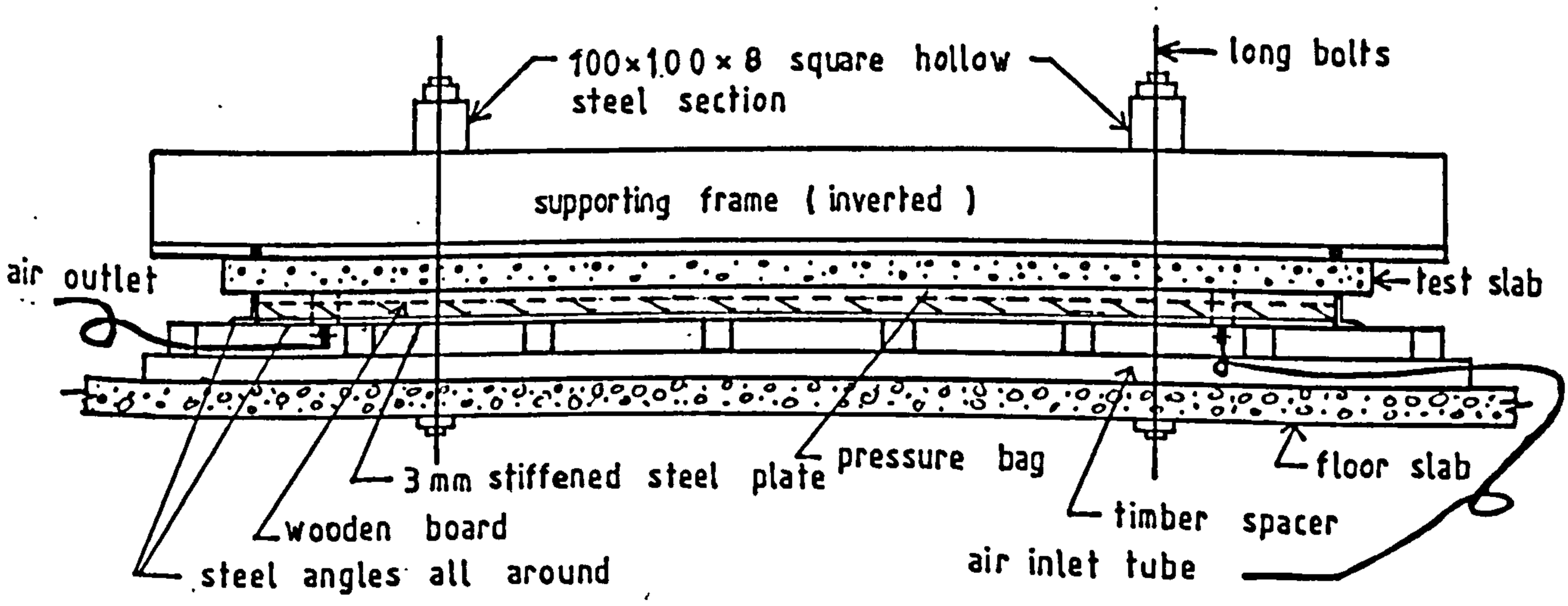

FIG. 6.9 Test Arrangement for uniformly distributed loading

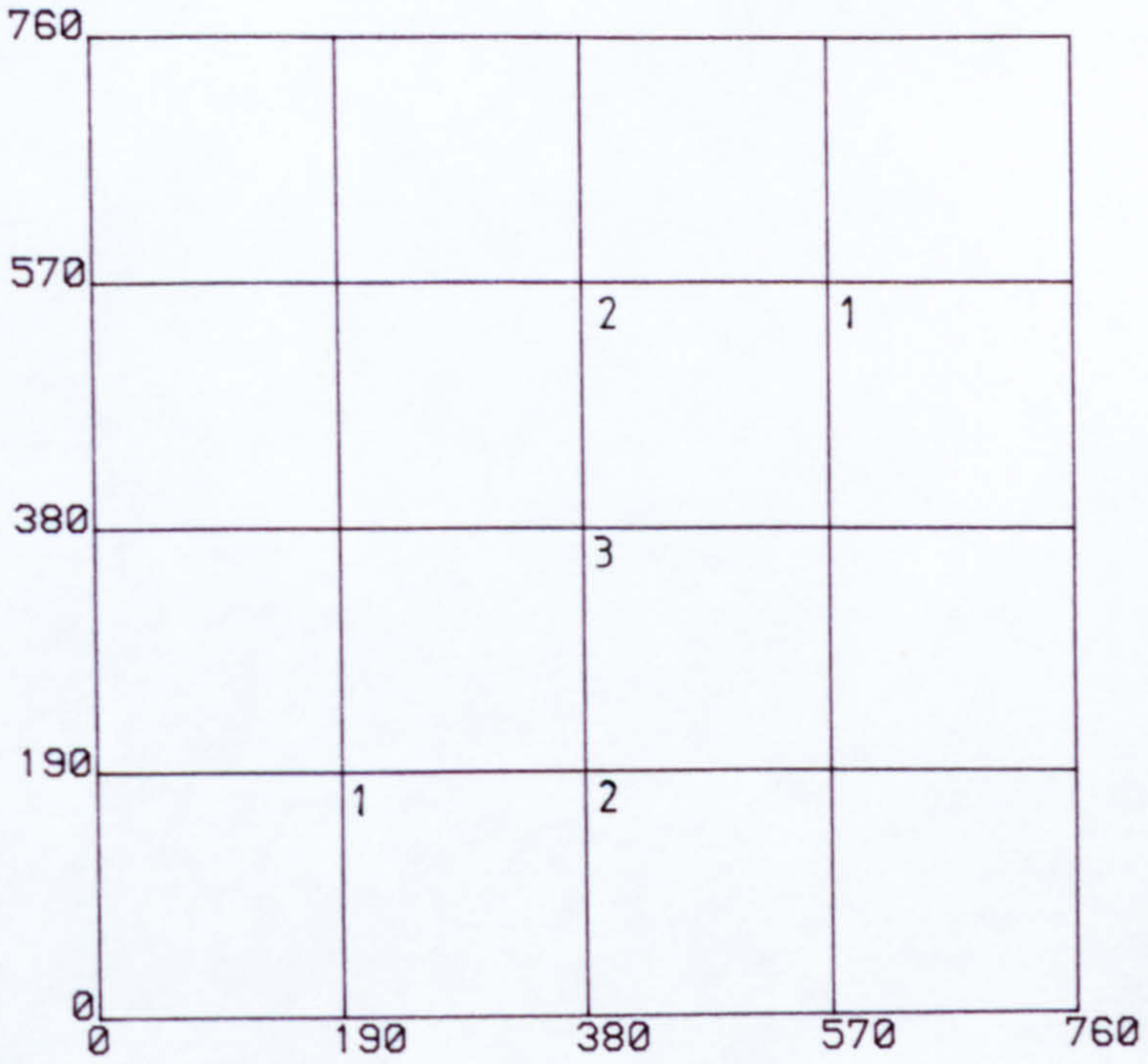

FIG.6.10a LOCATION OF DEFLECTION RECORDING STATIONS FOR TEST SLAB S1:4UD

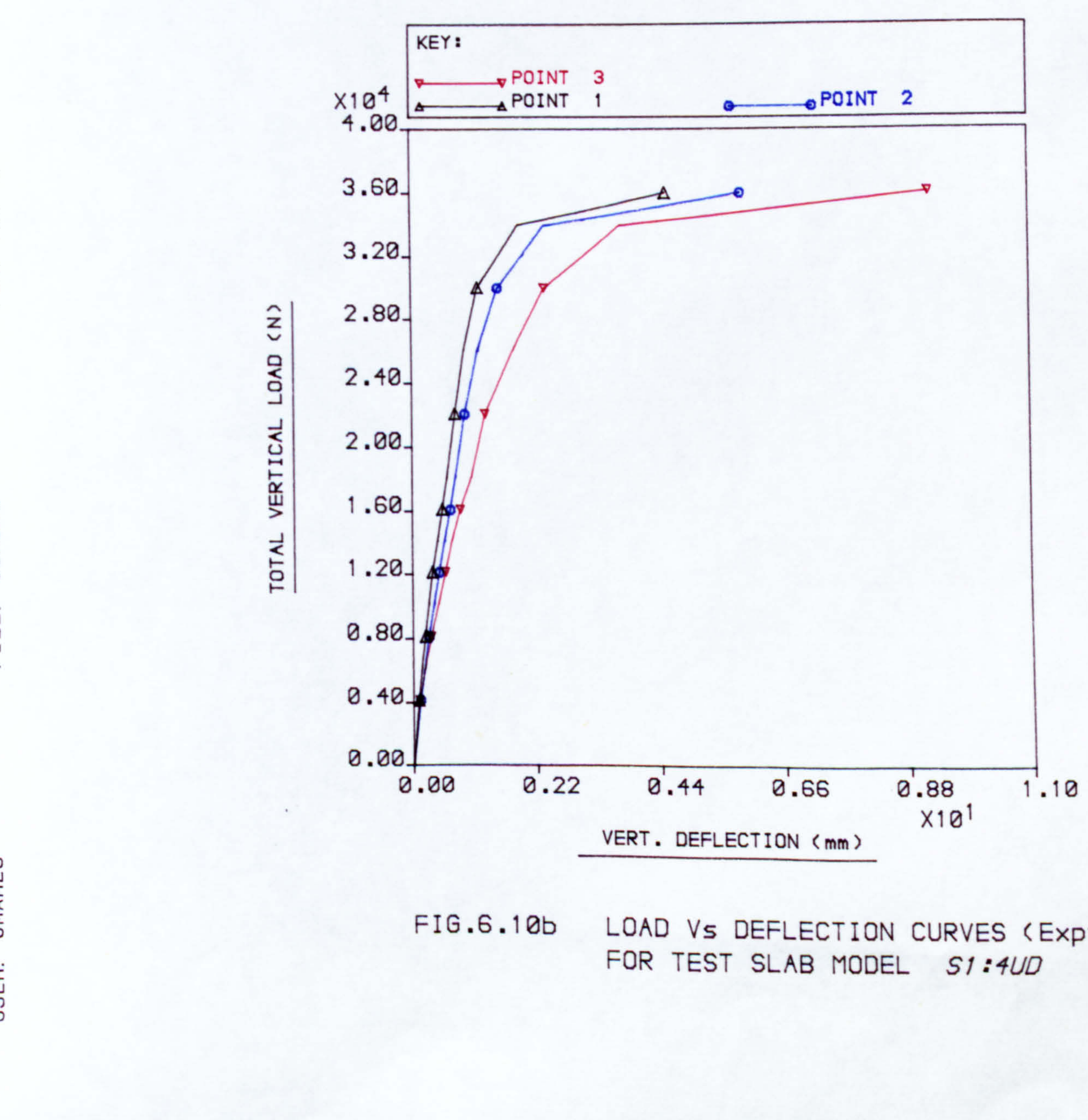

FIG.6.10b LOAD Vs DEFLECTION CURVES (Expt) FOR TEST SLAB MODEL *S1:4UD*

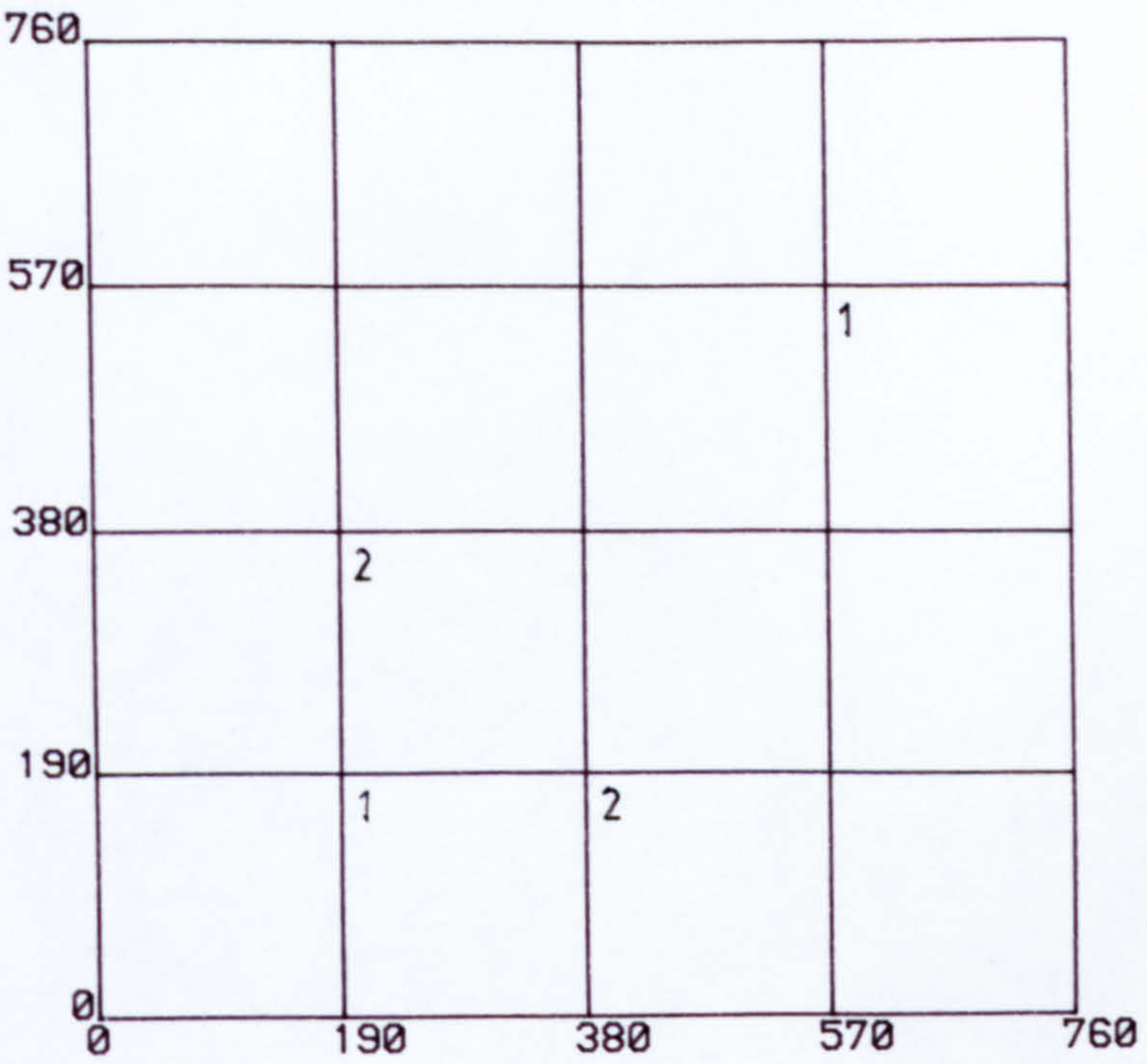

FIG.6.11a LOCATION OF DEFLECTION RECORDING STATIONS FOR TEST SLAB S2:4P1

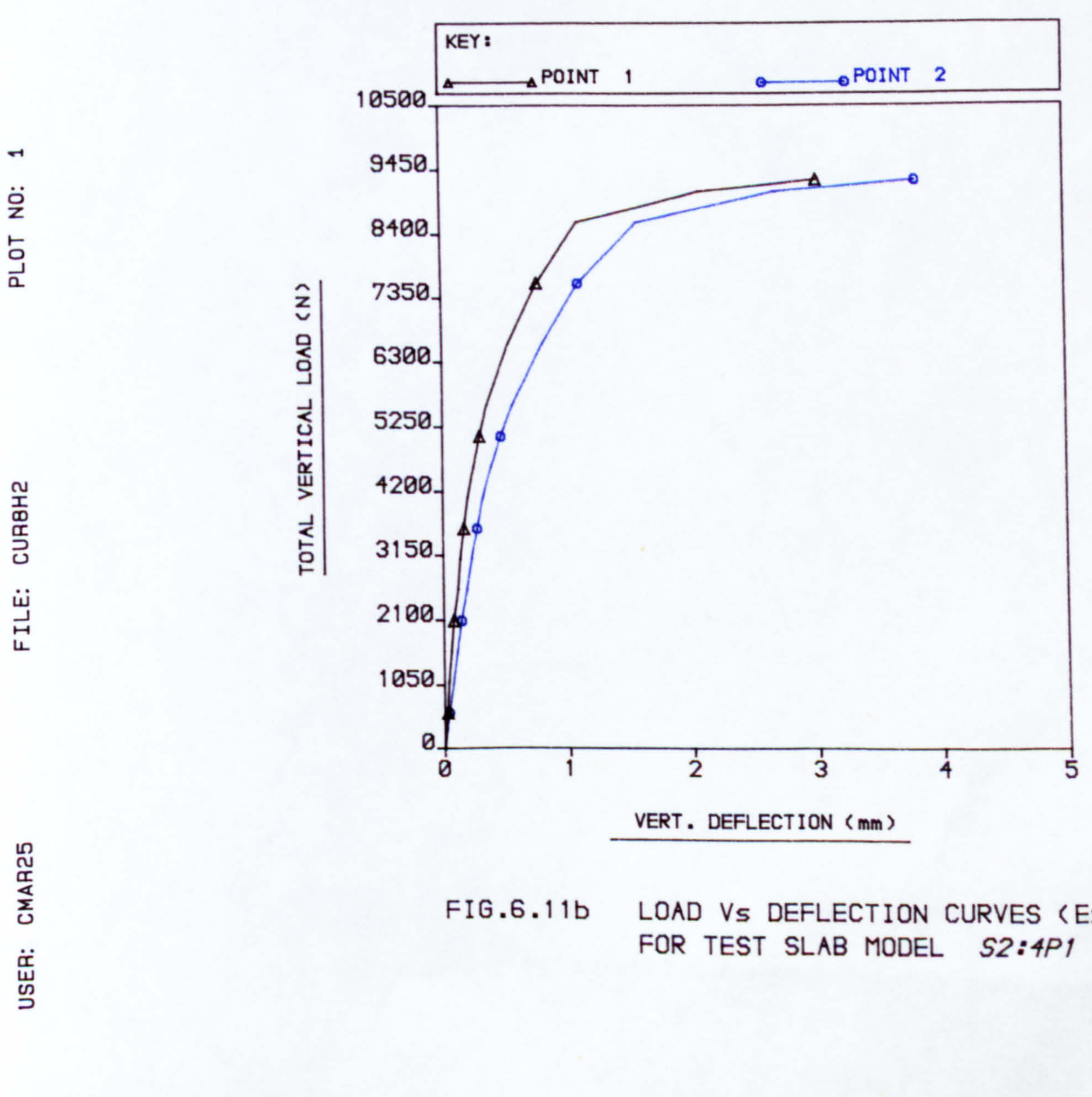

FIG.6.11b LOAD Vs DEFLECTION CURVES (Expt) FOR TEST SLAB MODEL *S2:4P1*

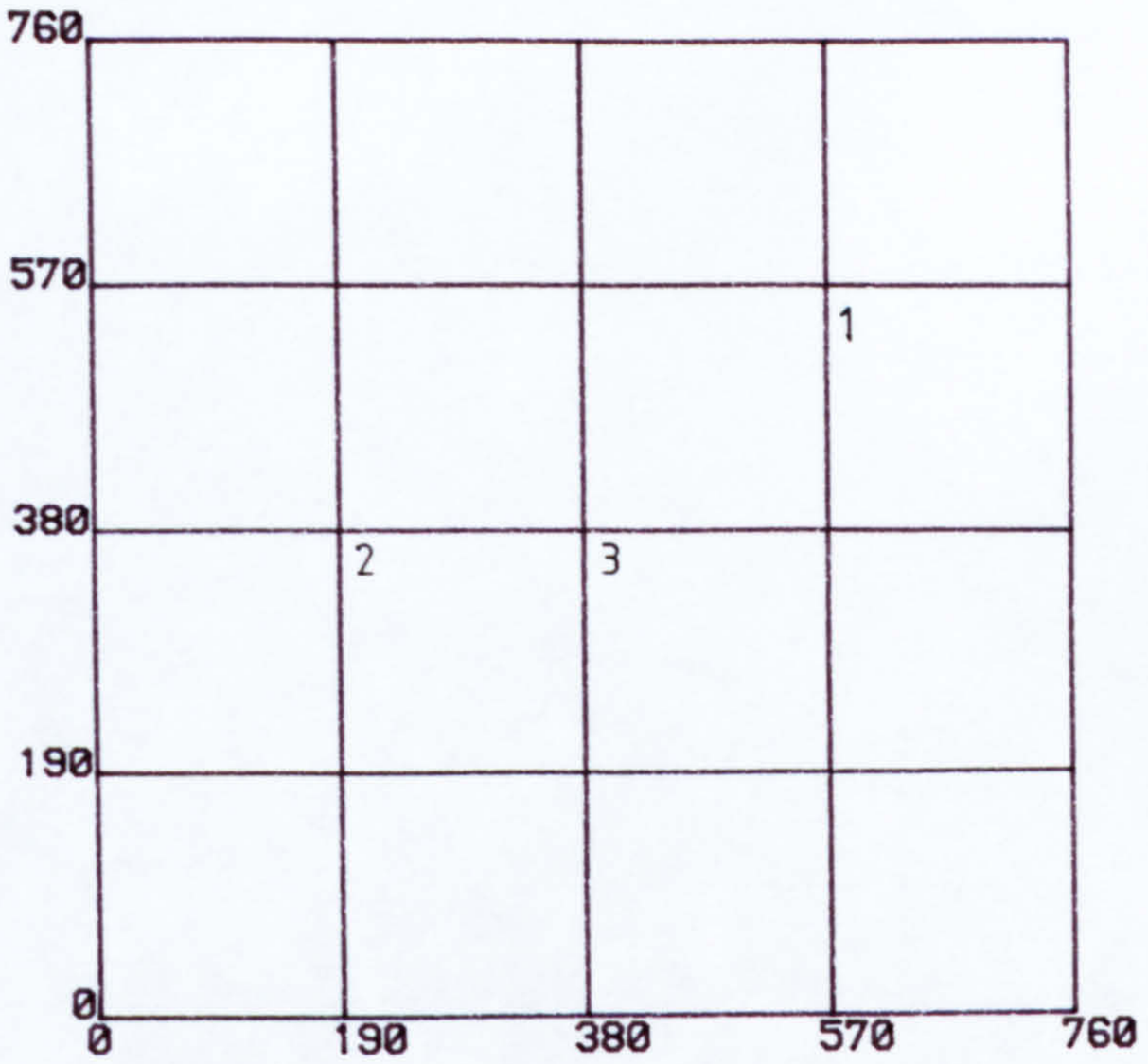

FIG.6.12a LOCATION OF DEFLECTION RECORDING STATIONS FOR TEST SLAB S3:4P4

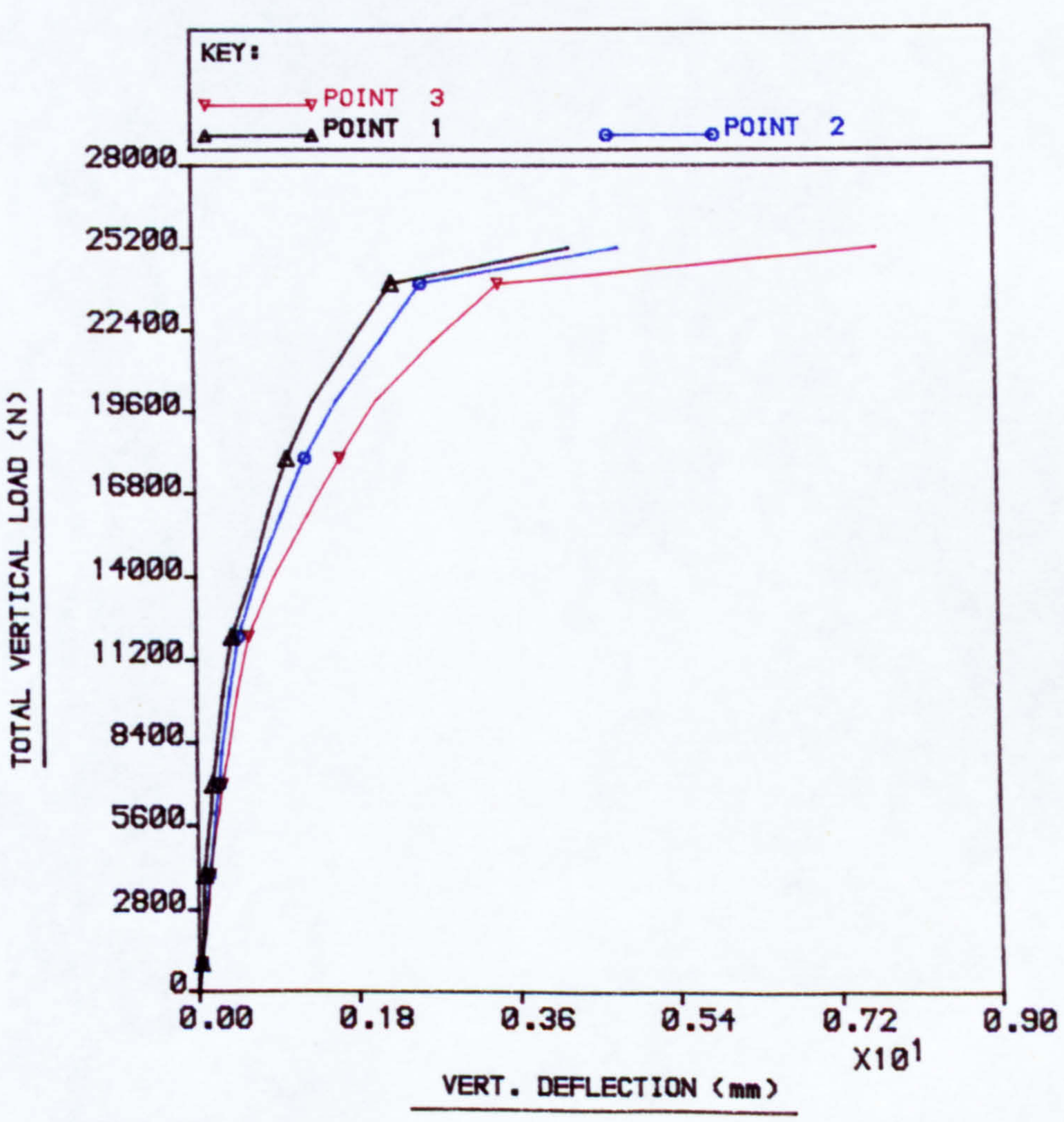

FIG.6.12b LOAD Vs DEFLECTION CURVES (Expt) FOR TEST SLAB MODEL *S3:4P4*

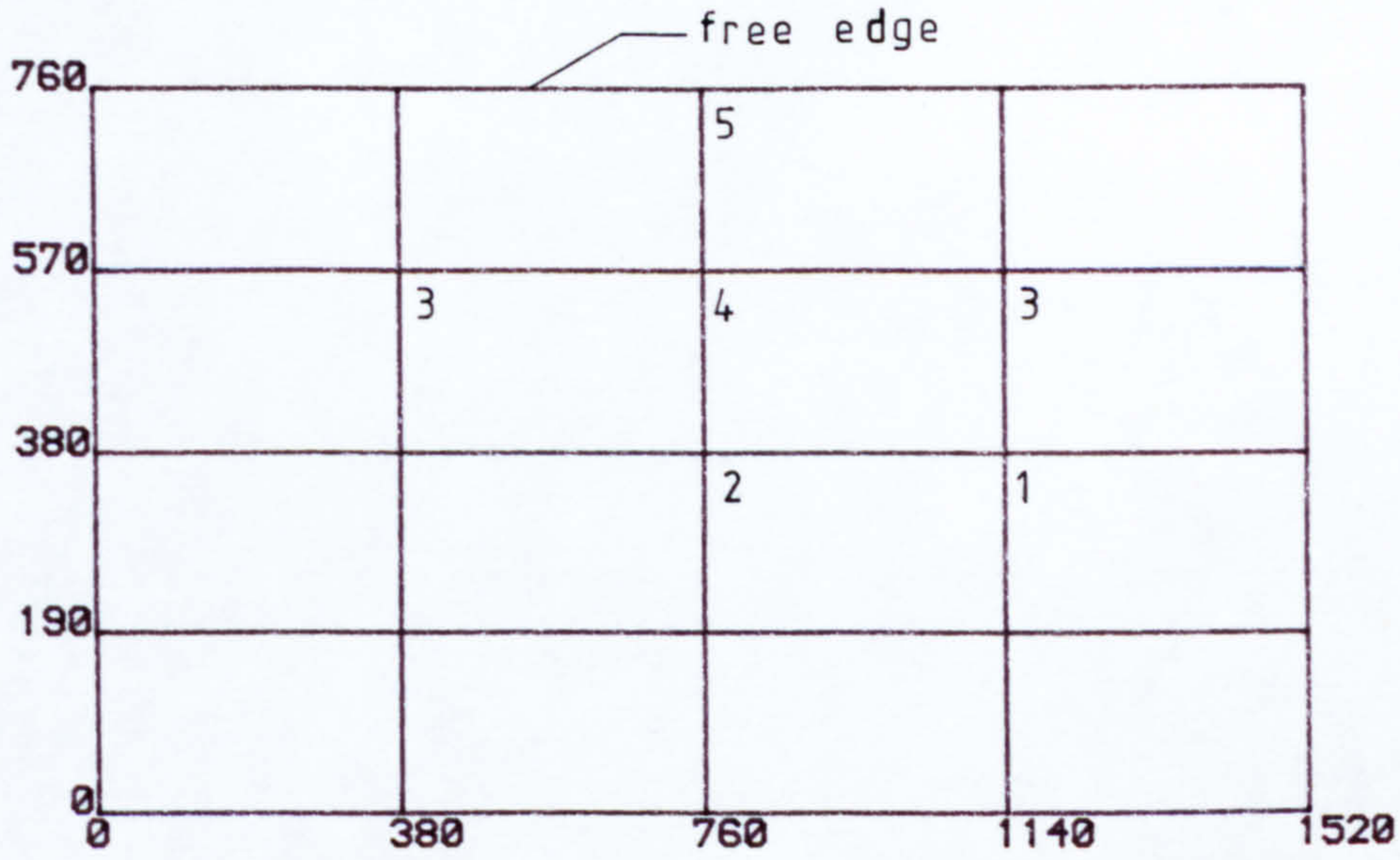

FIG.6.13a LOCATION OF DEFLECTION RECORDING STATIONS FOR TEST SLAB S4:3UD

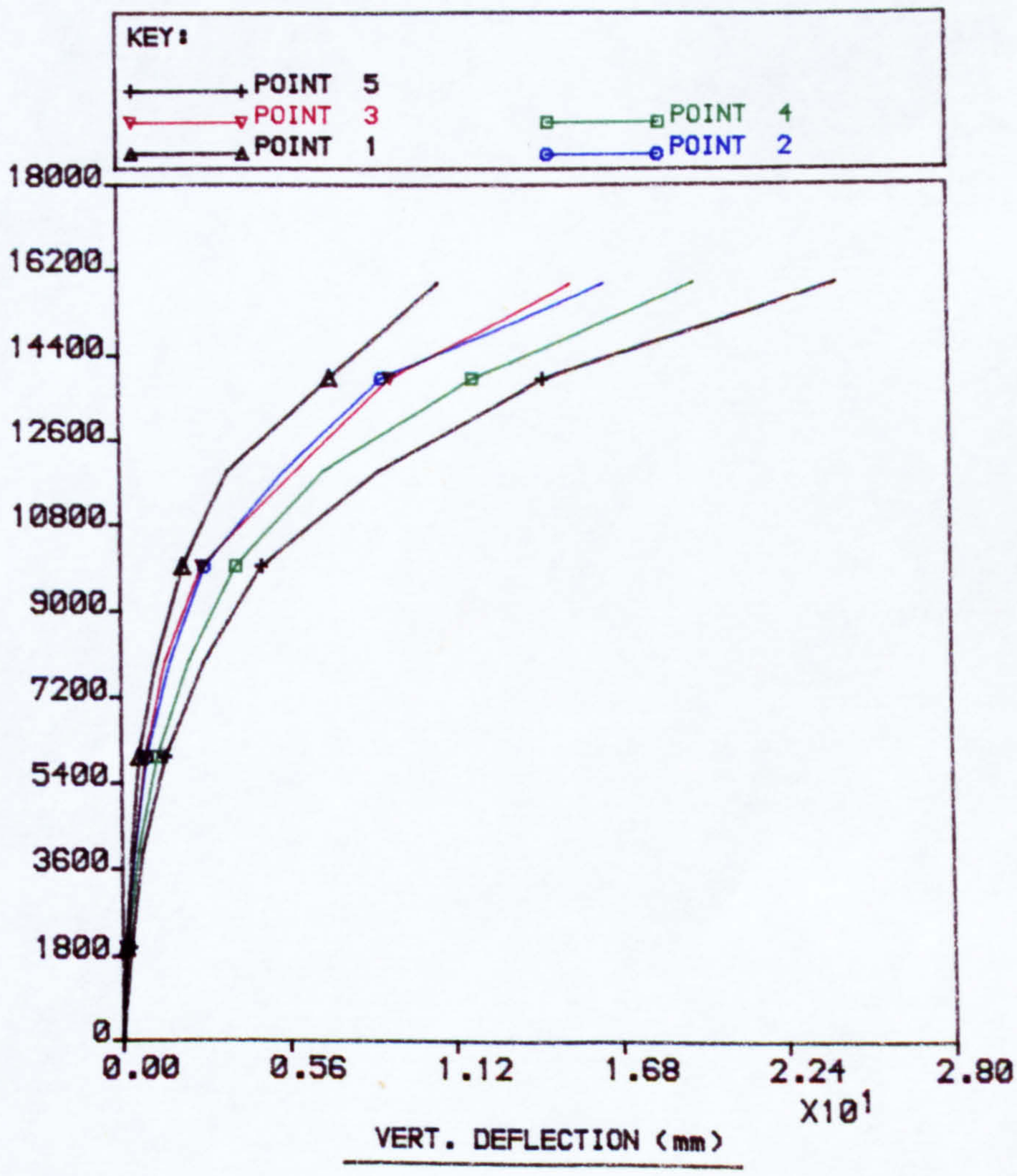

FIG.6.13b LOAD Vs DEFLECTION CURVES (Expt) FOR TEST SLAB MODEL *S4:3UD*

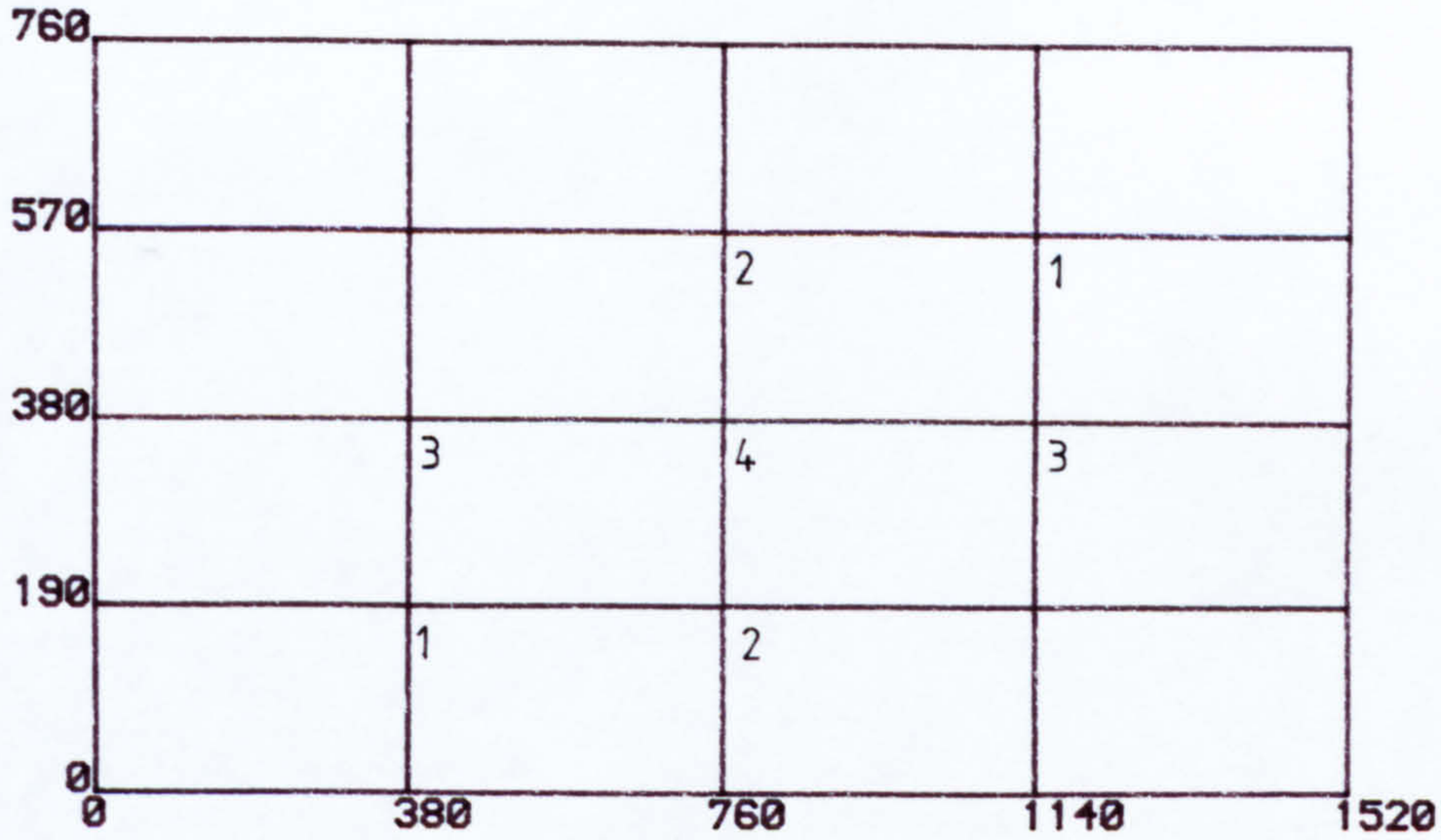

FIG.6.14a LOCATION OF DEFLECTION RECORDING STATIONS FOR TEST SLAB S5:4UD

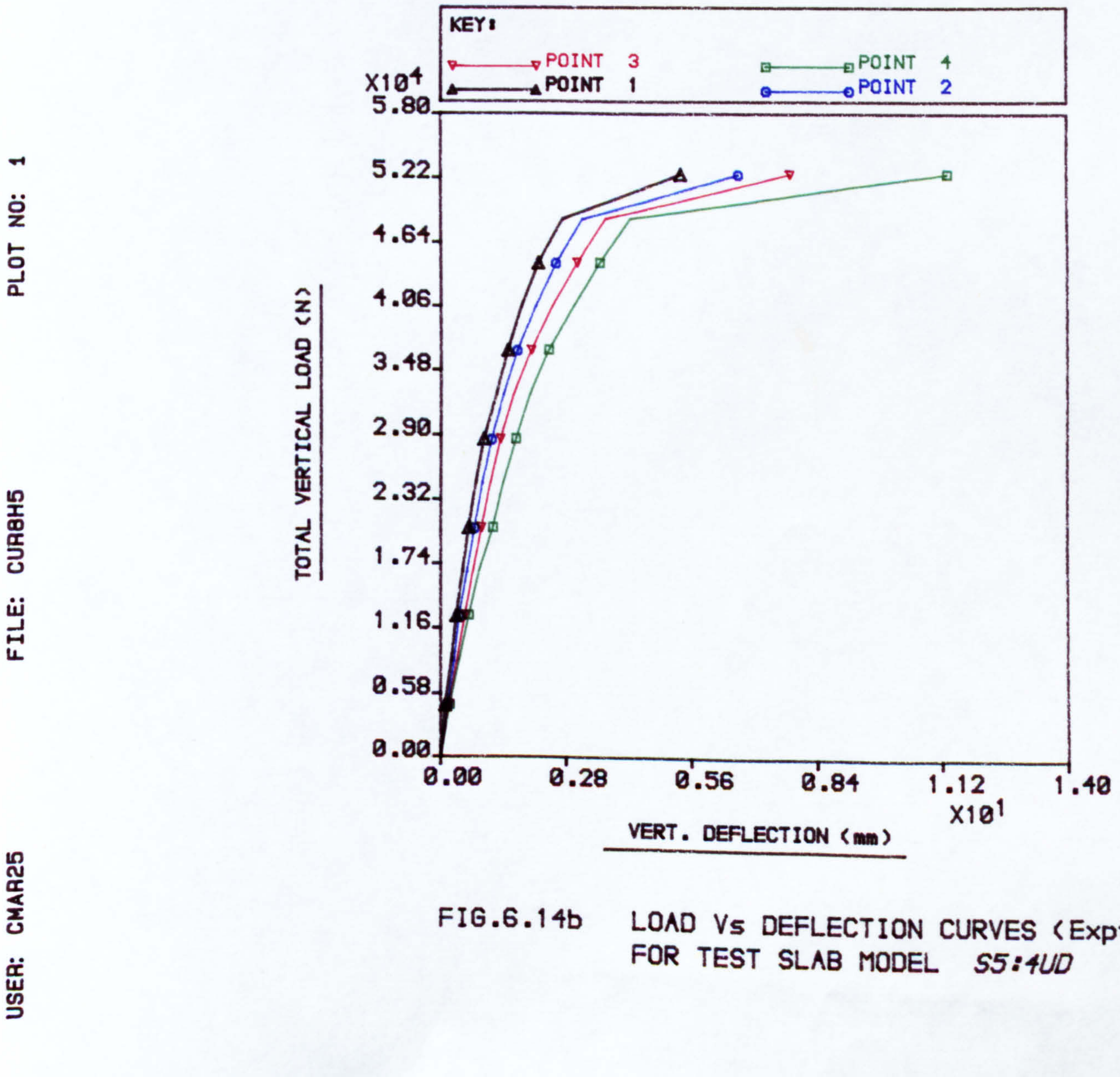

FIG.6.14b LOAD Vs DEFLECTION CURVES (Expt) FOR TEST SLAB MODEL *S5:4UD*

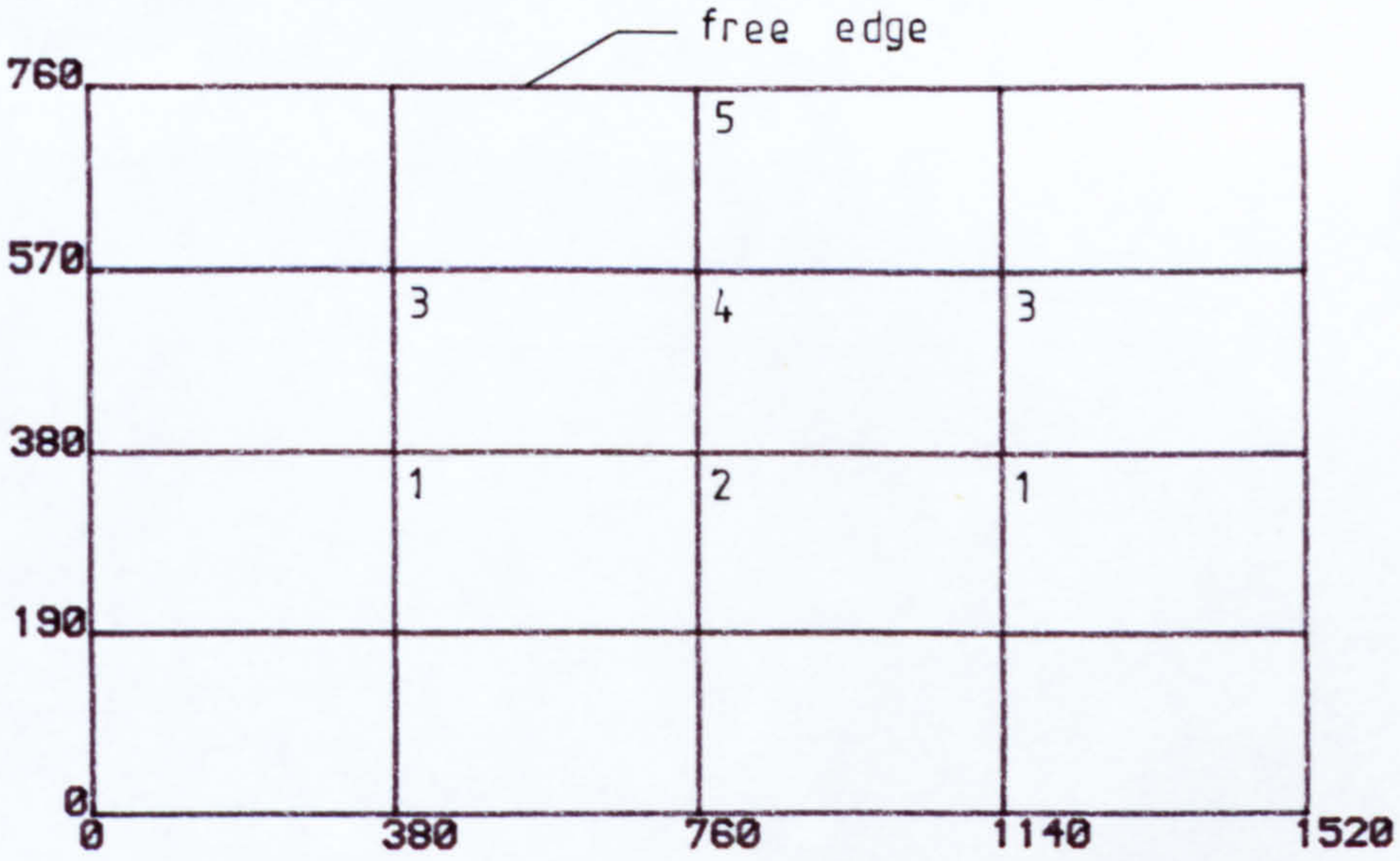

FIG.6.15a LOCATION OF DEFLECTION RECORDING STATIONS FOR TEST SLAB S6:3P1

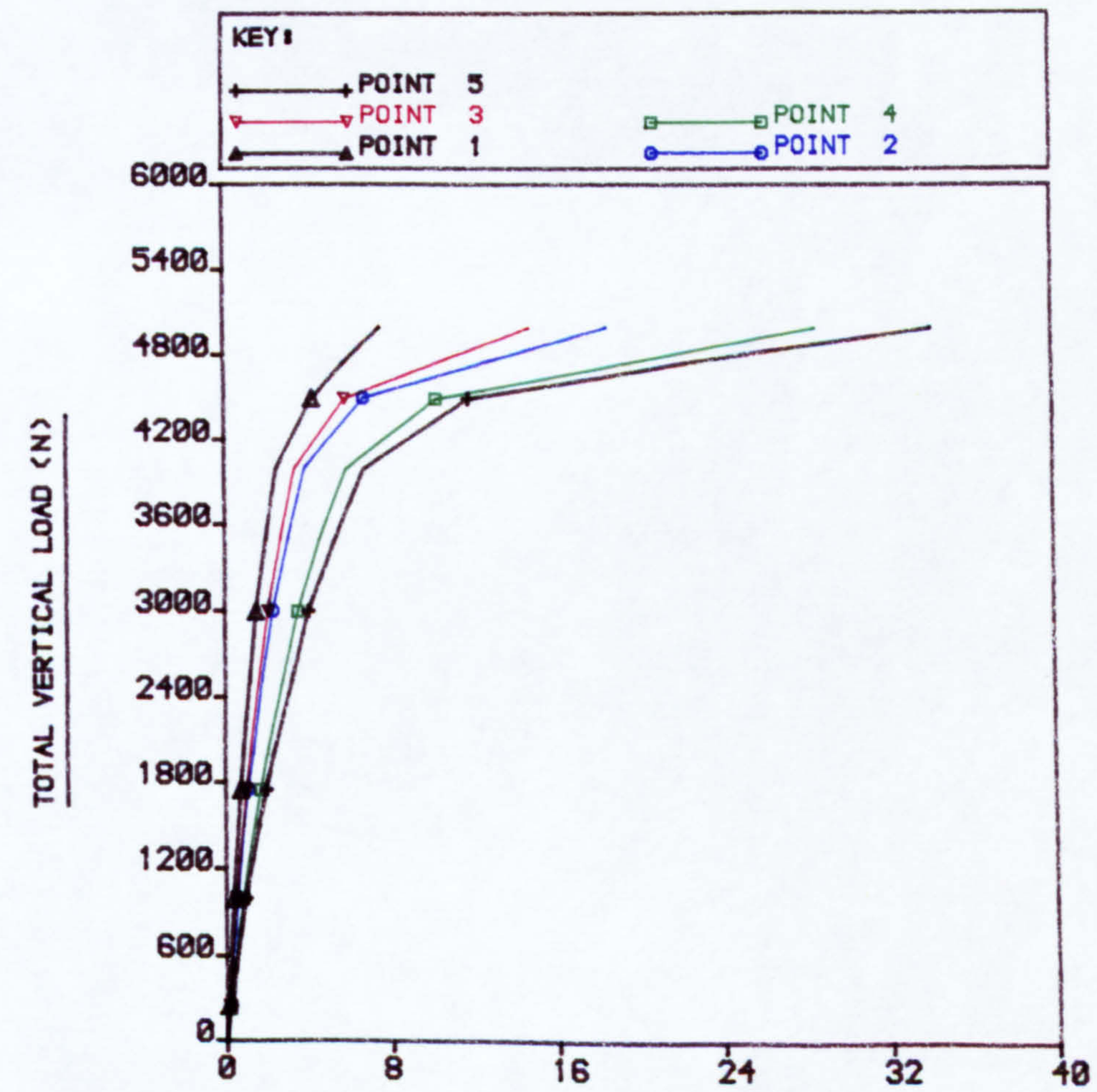

FIG.6.15b LOAD Vs DEFLECTION CURVES (Expt) FOR TEST SLAB MODEL *S6:3P1*

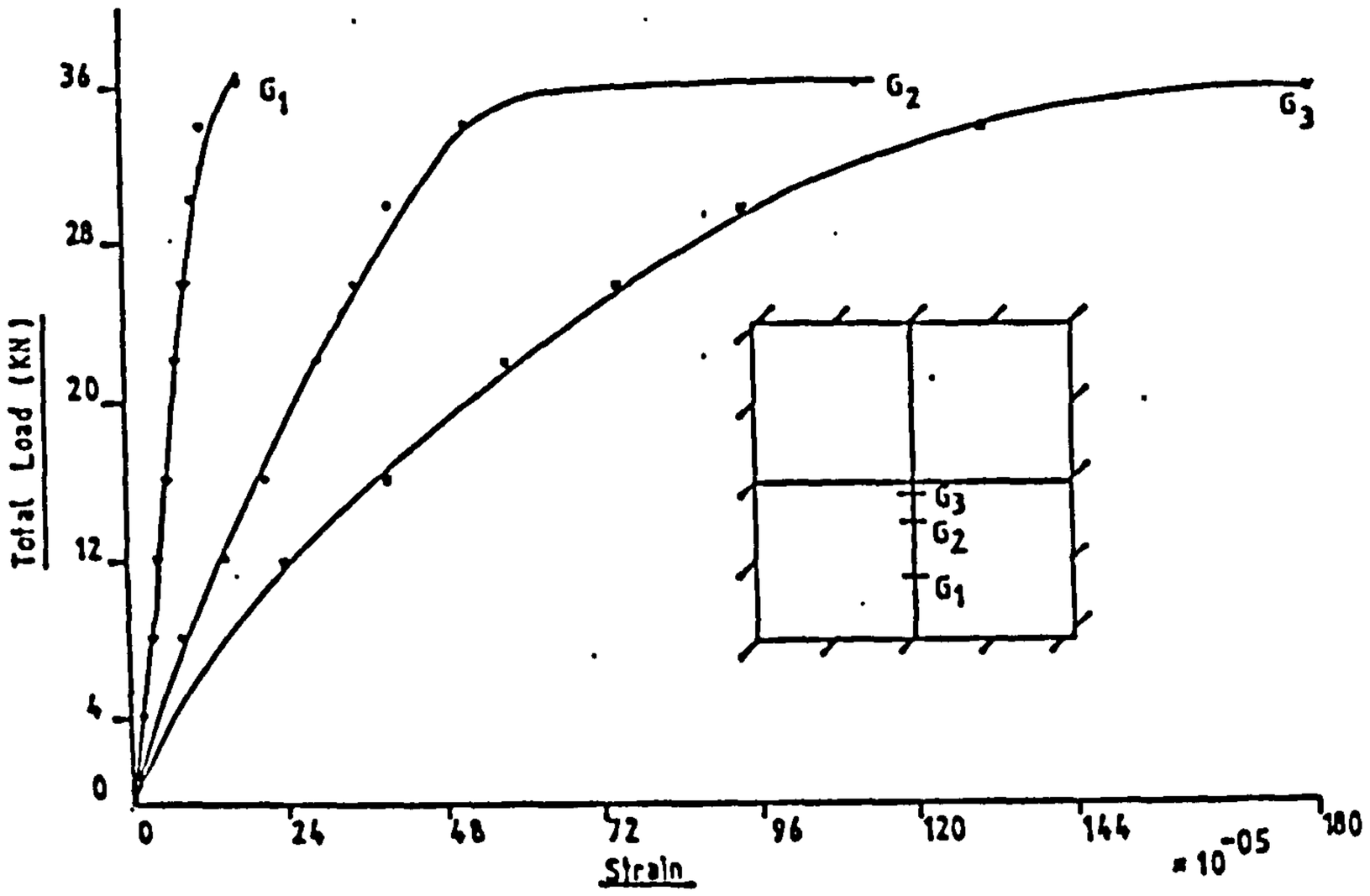

FIG. 6.16 Load vs. Steel Strain Curves for Slab S1 4UD

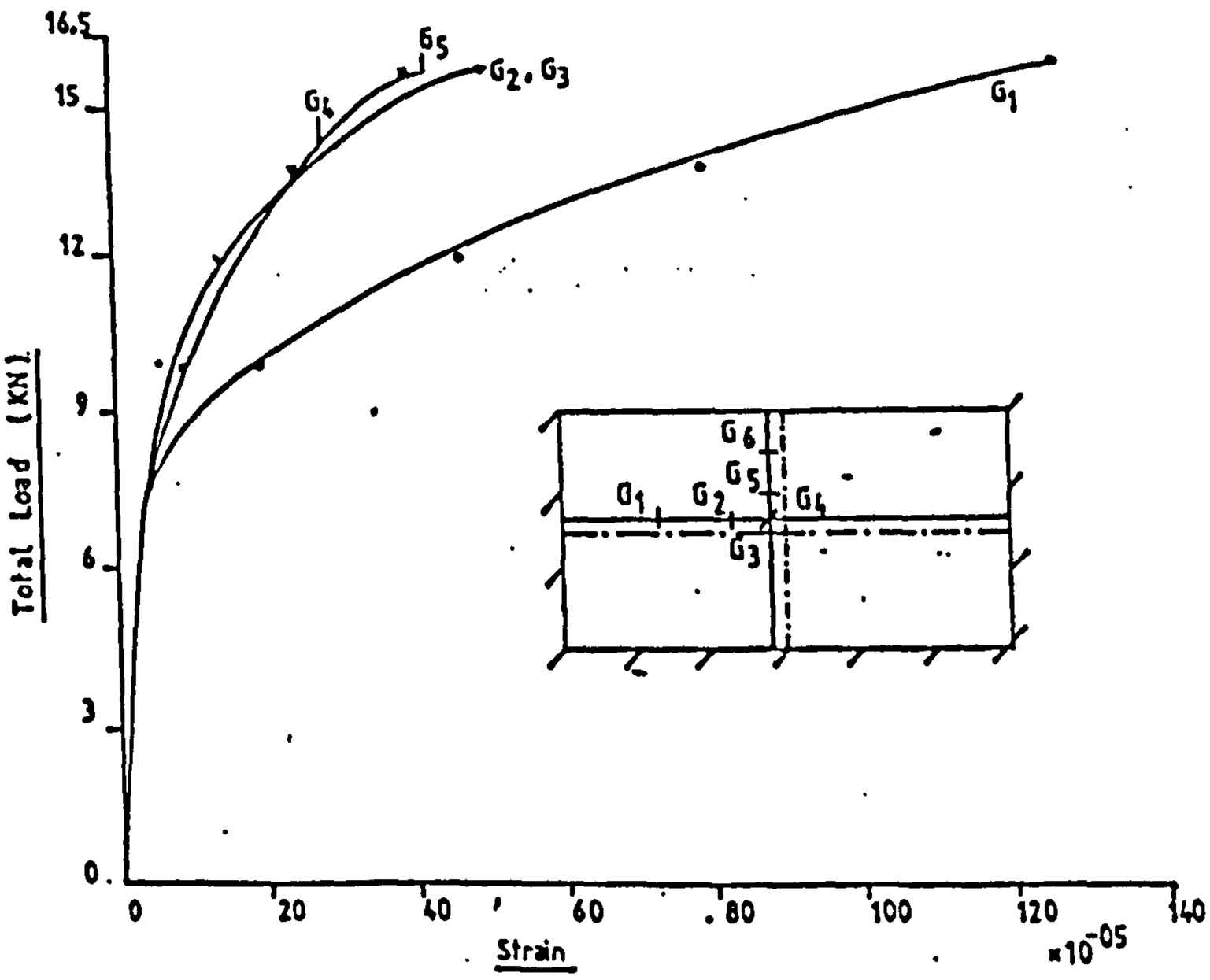

FIG. 6.17 Load vs. Steel Strain Curves for Slab S4 3UD

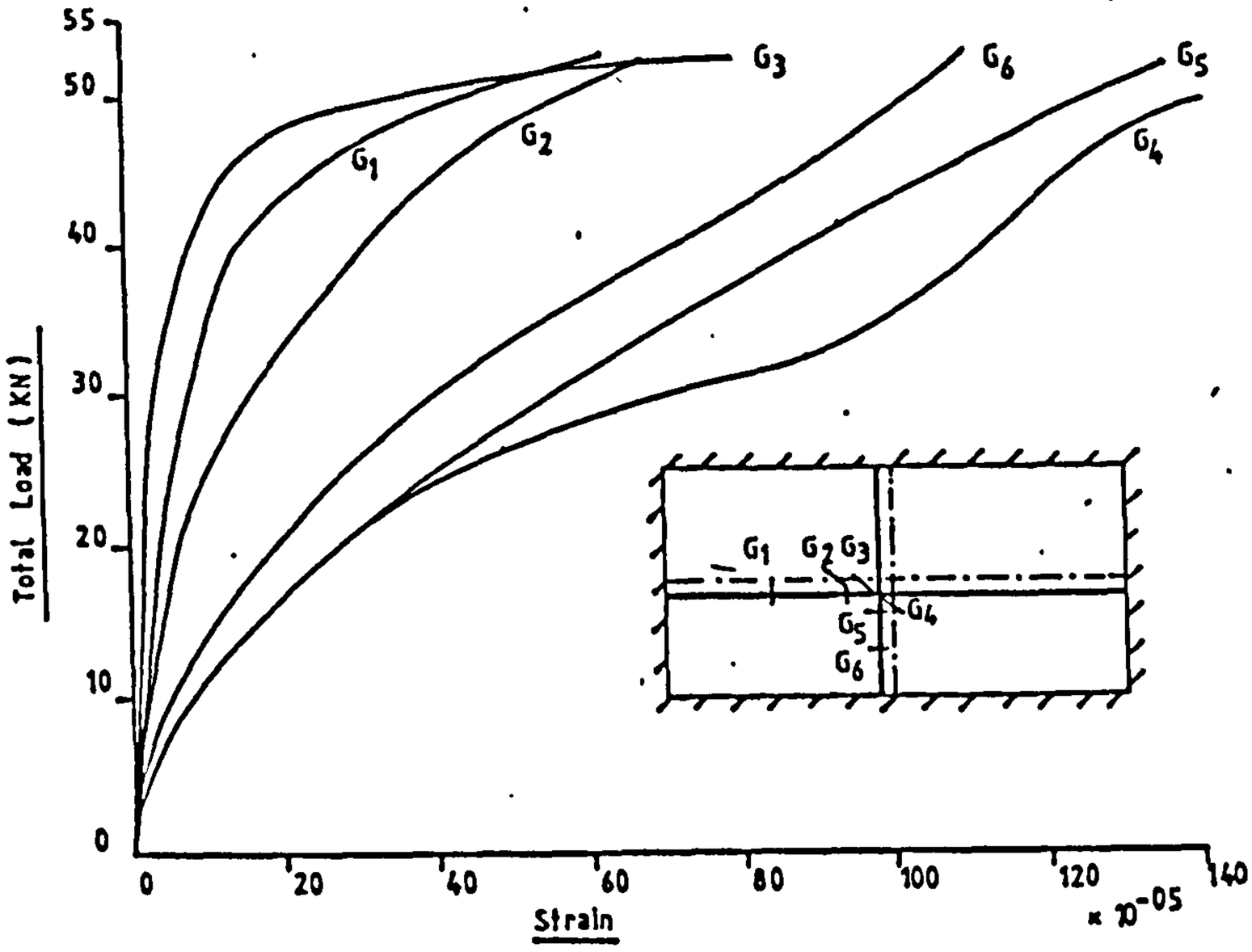

FIG. 6.18 Load vs. Steel Strain Curves for Slab S5 4UD

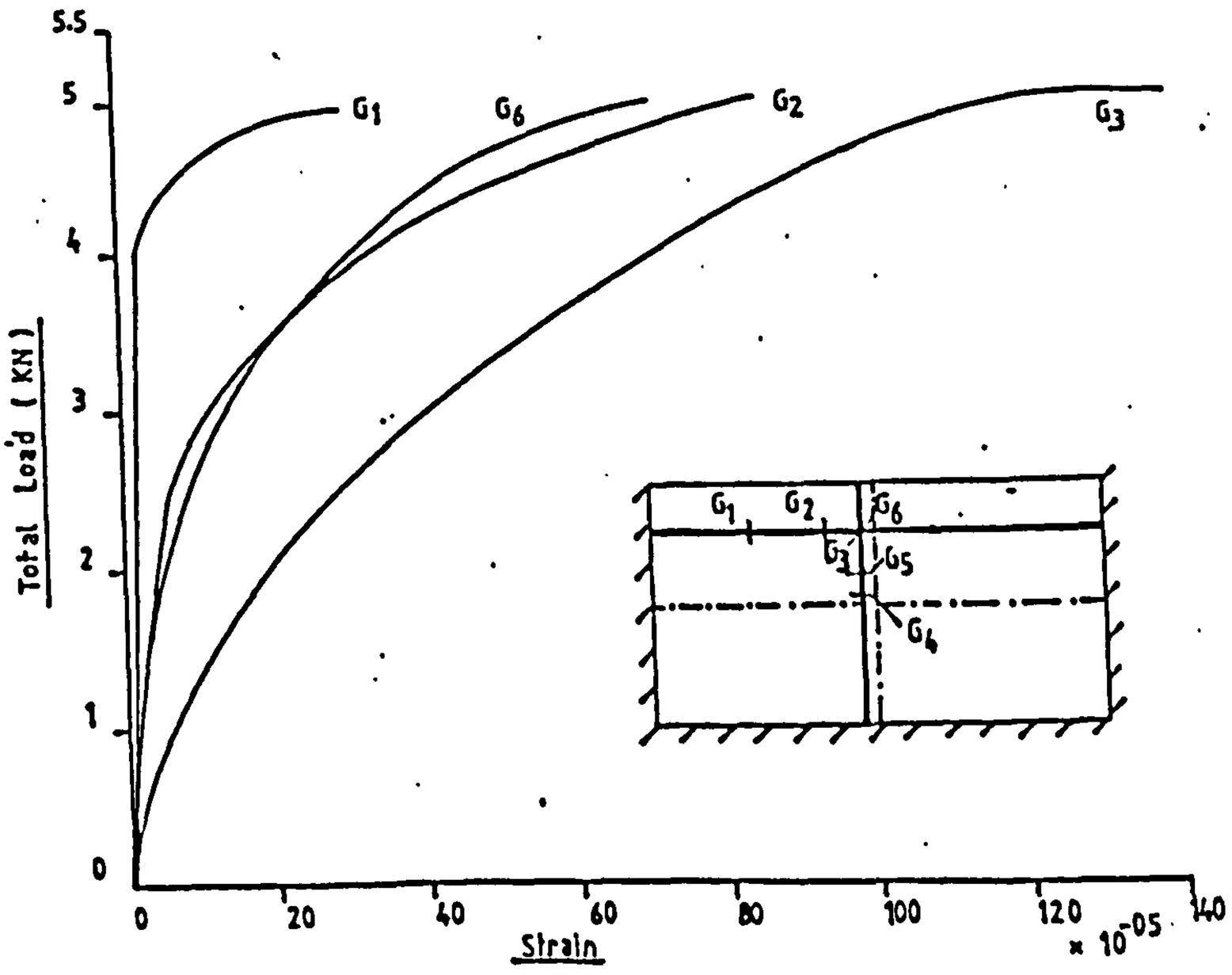

FIG. 6.19 Load vs. Steel Strain Curves for Slab S6 3P1

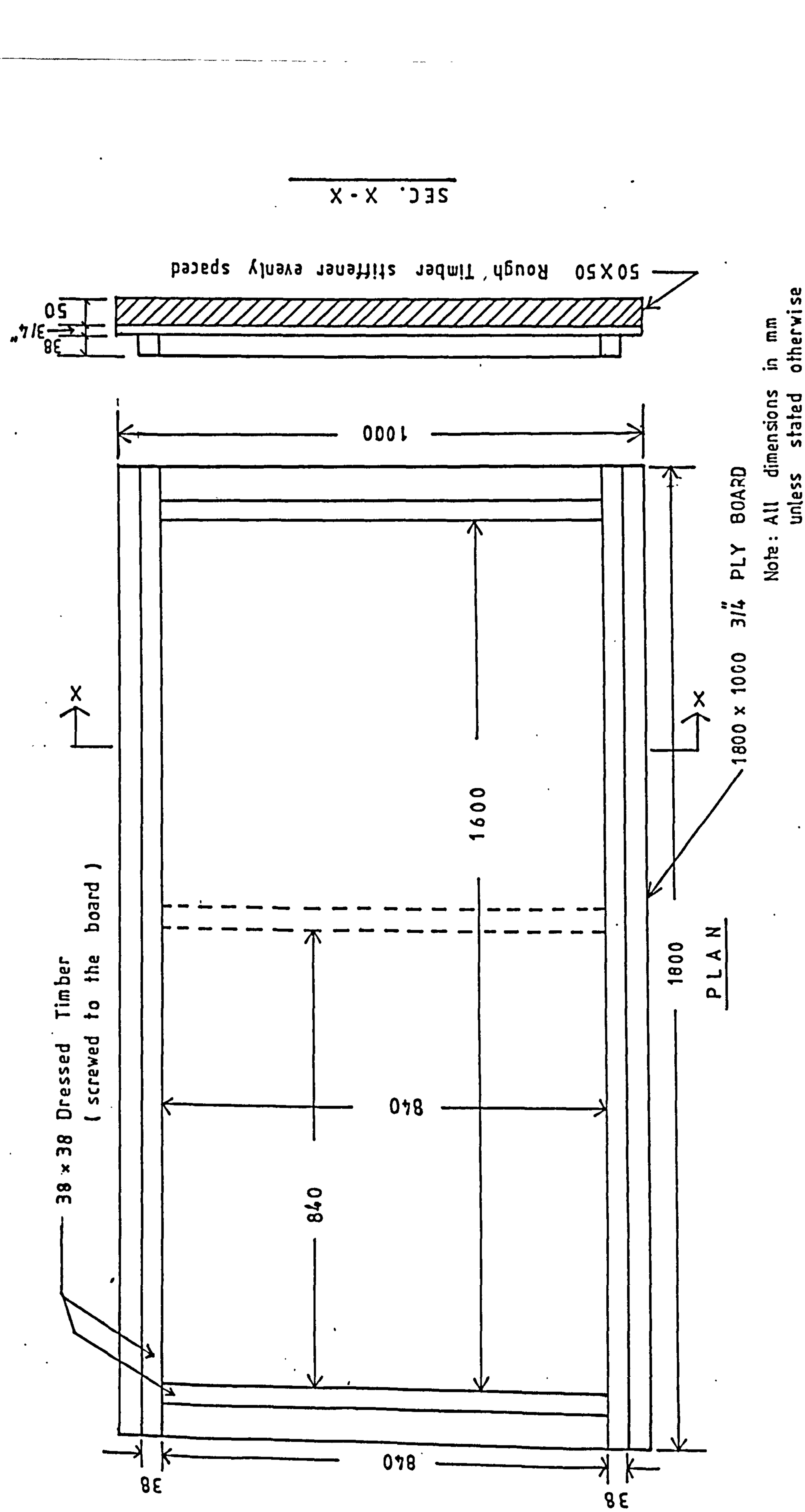

FIG. 6.20 Formwork Details for the Test Slabs

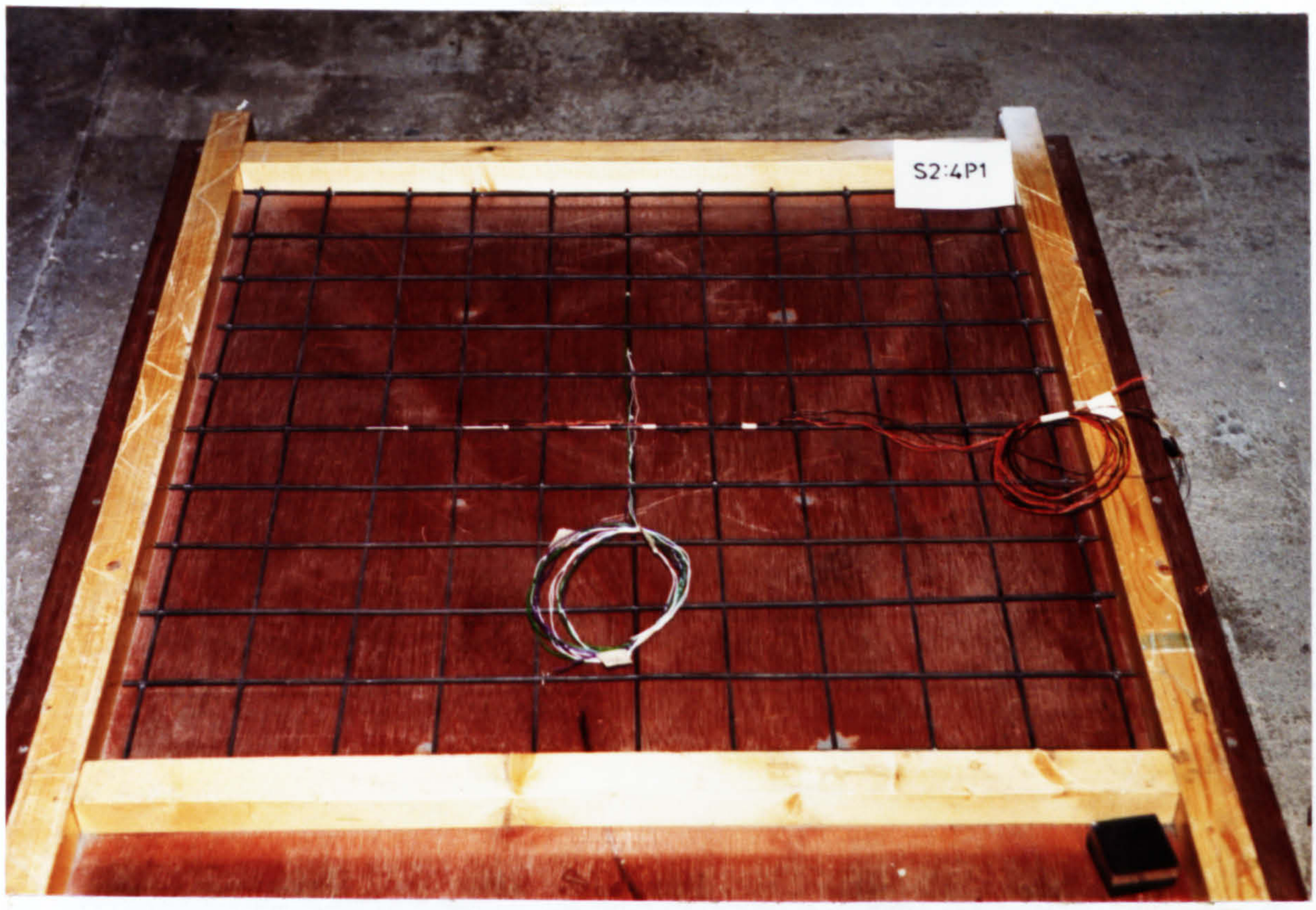

Plate 6.1 Reinforcement Mesh for the Square Slabs.

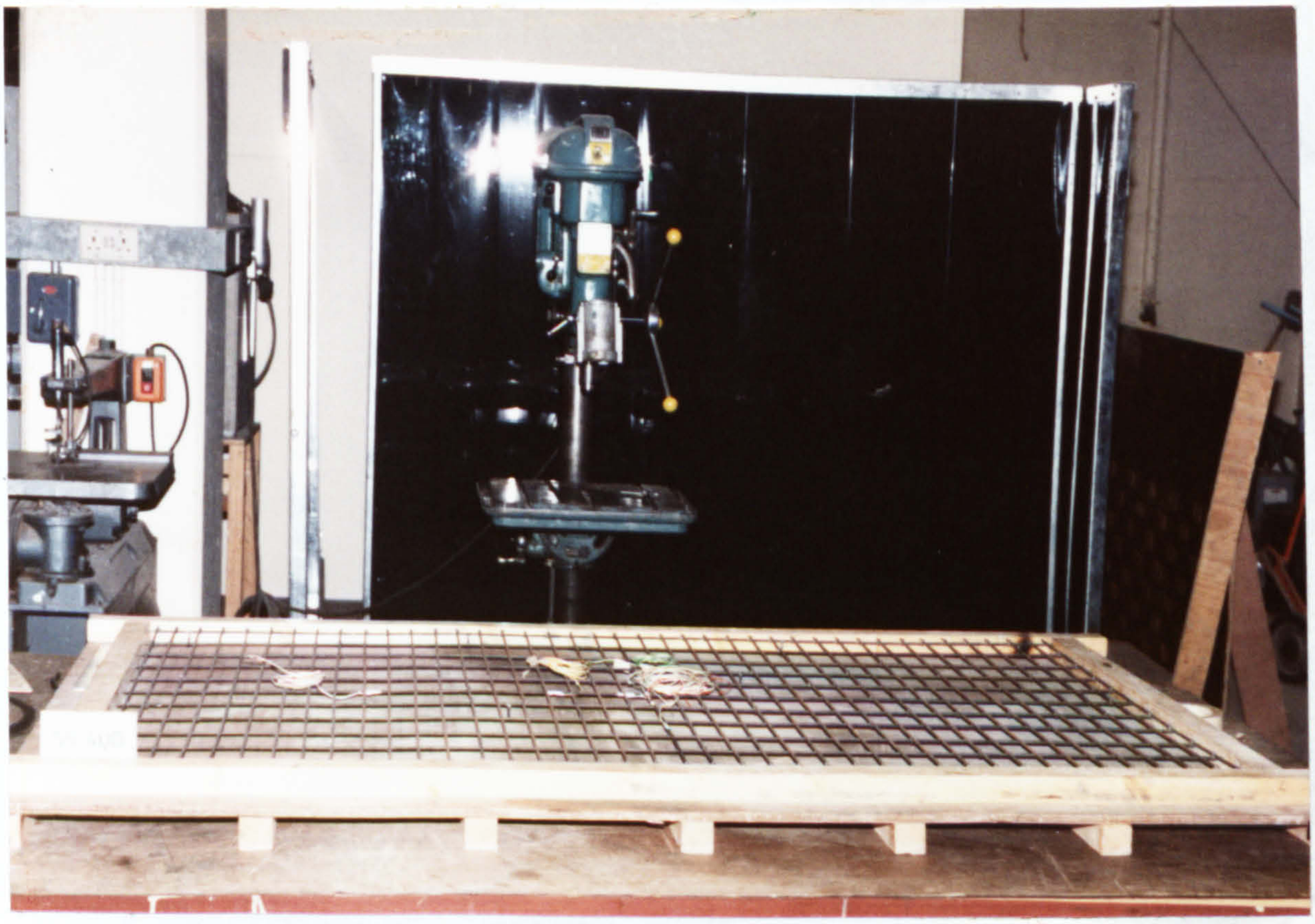

Plate 6.2 Reinforcement Mesh for the Rectangular Slabs.

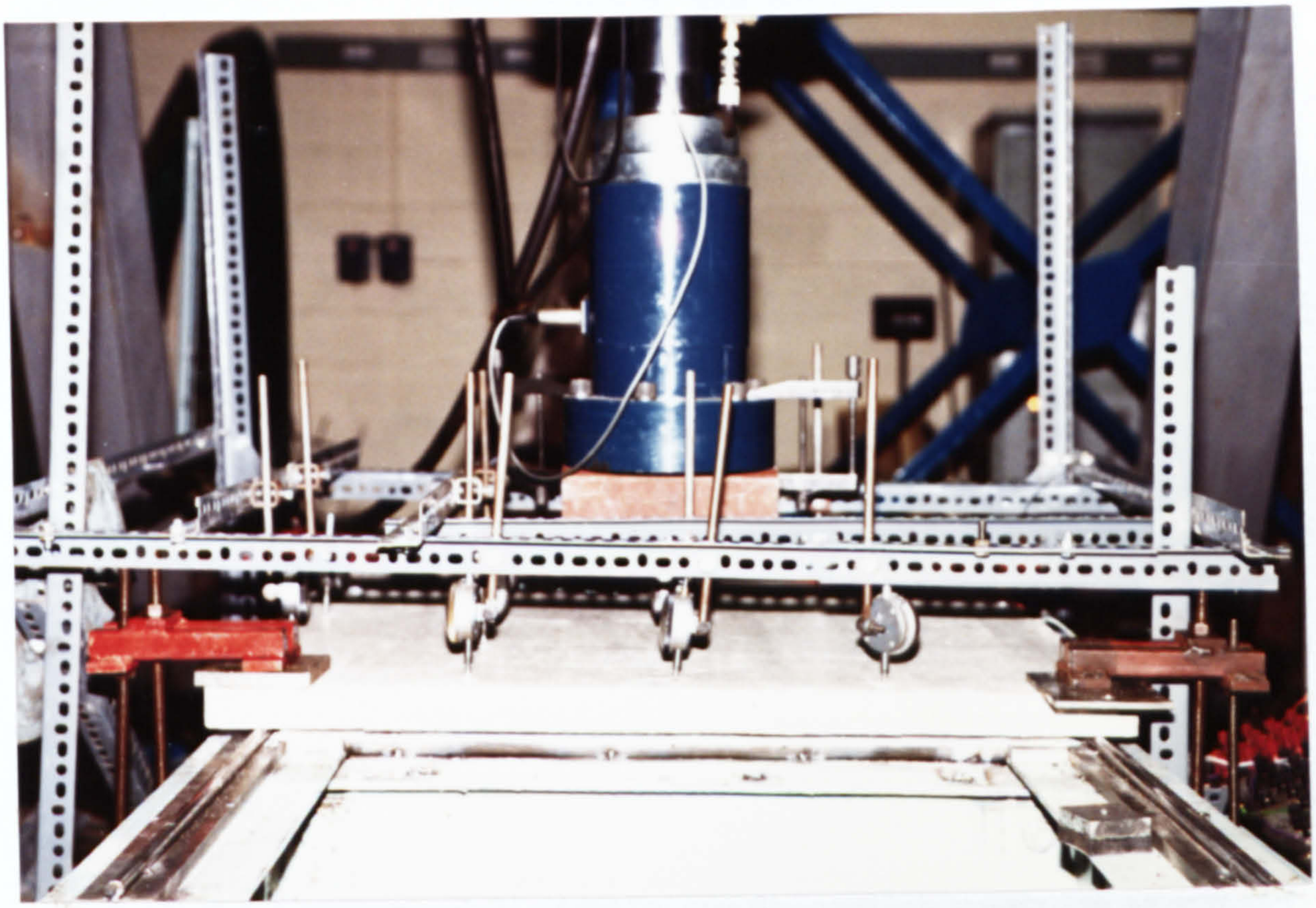

Plate 6.3 Test Set Up for Model S24P1.

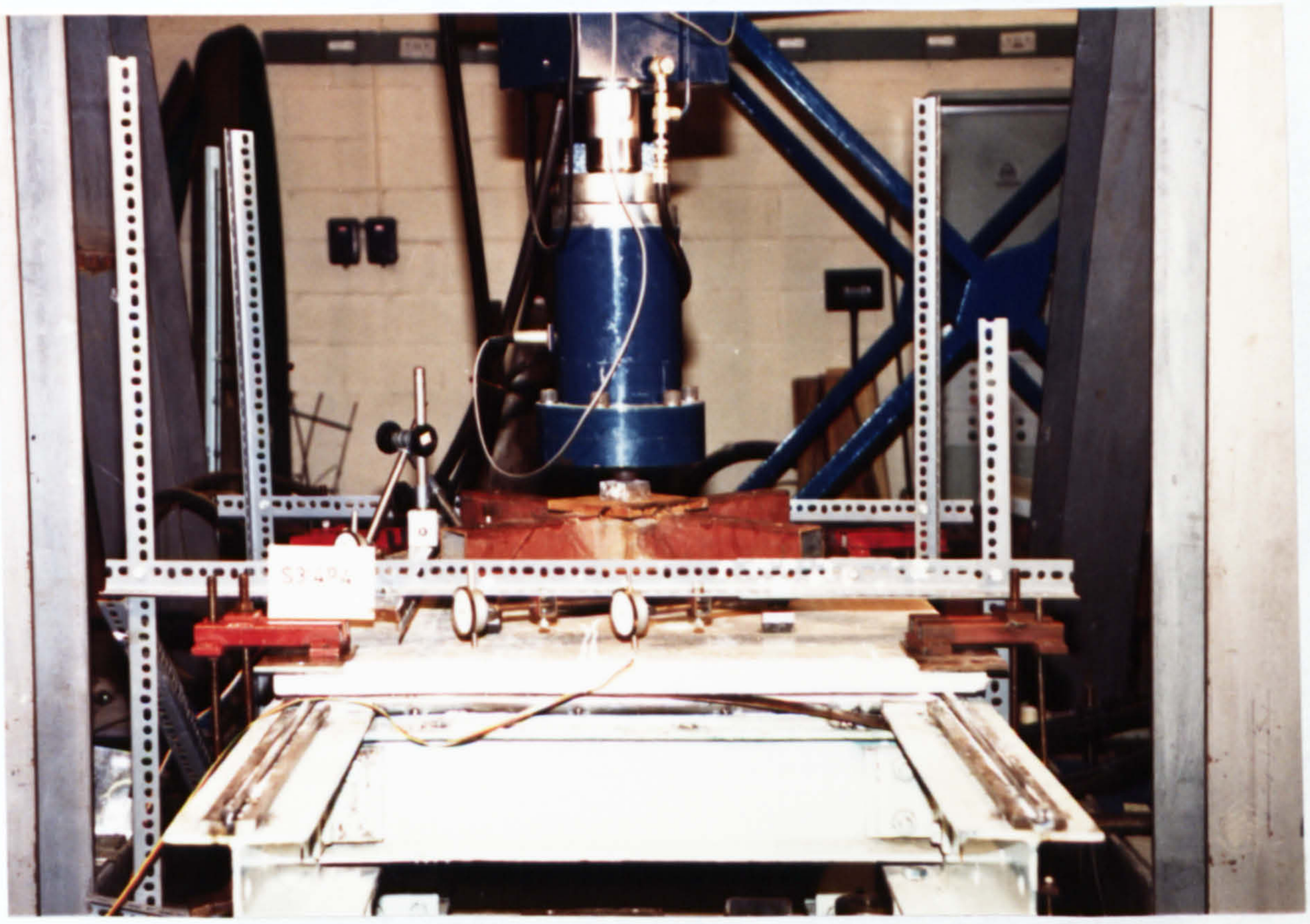

Plate 6.4 Four Point Loading Through an Intermediate Cross-piece for Slab S34P4.

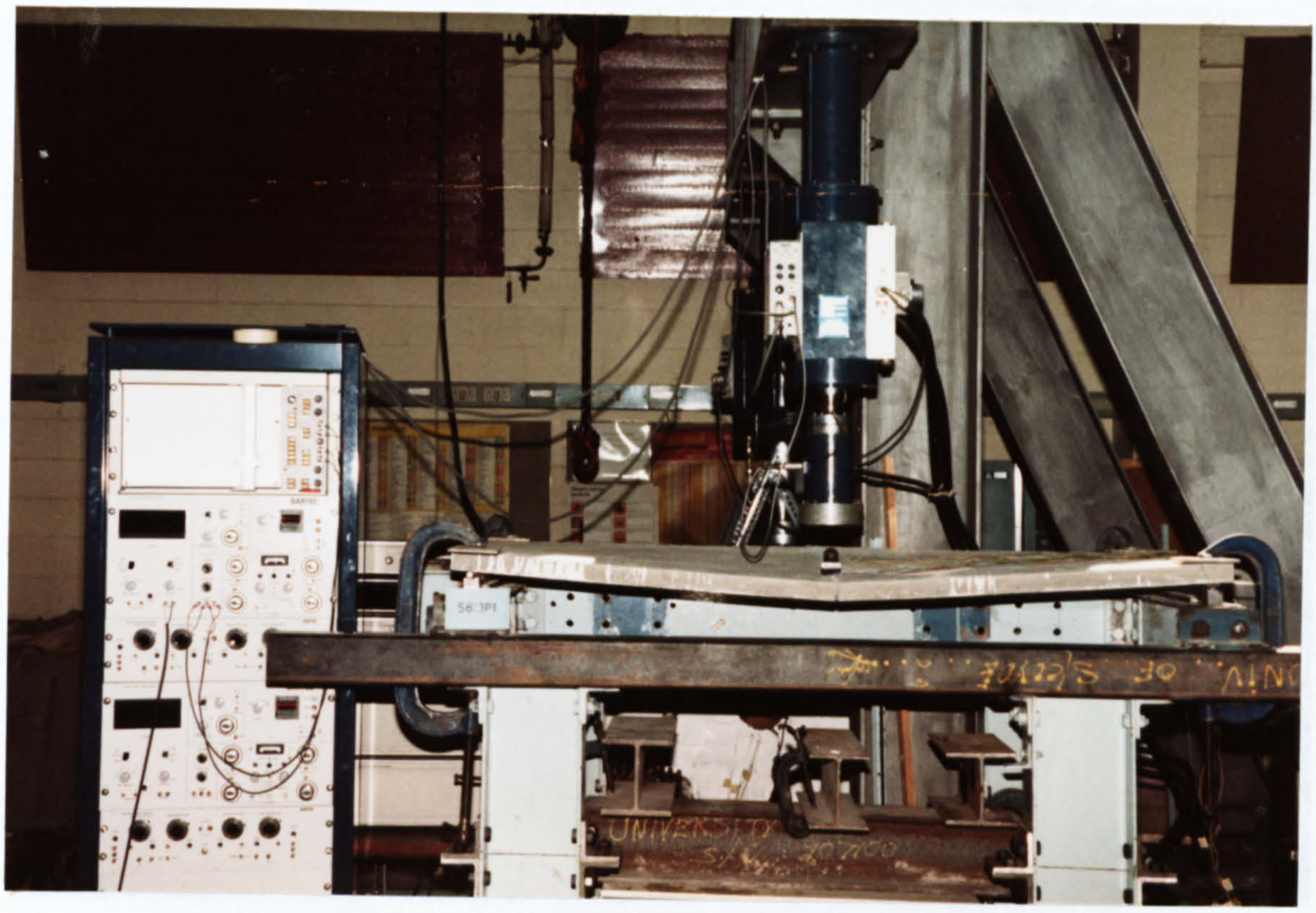

Plate 6.5 Single Point Loaded Rectangular Slab S63P1 (after failure photograph).

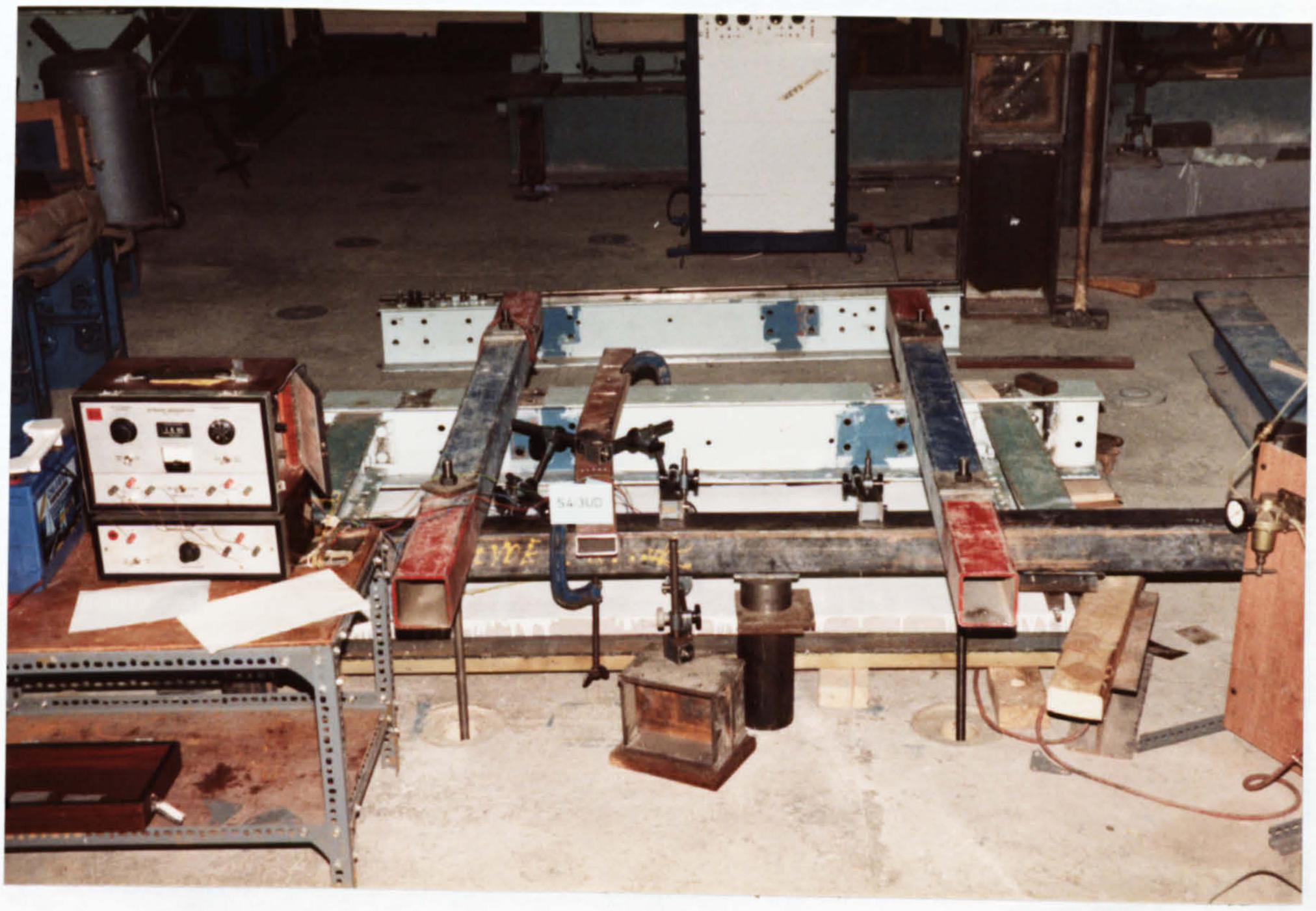

Plate 6.6 Test Set Up for Pressure Loaded Rectangular Slab With a Free Edge (S43UD).

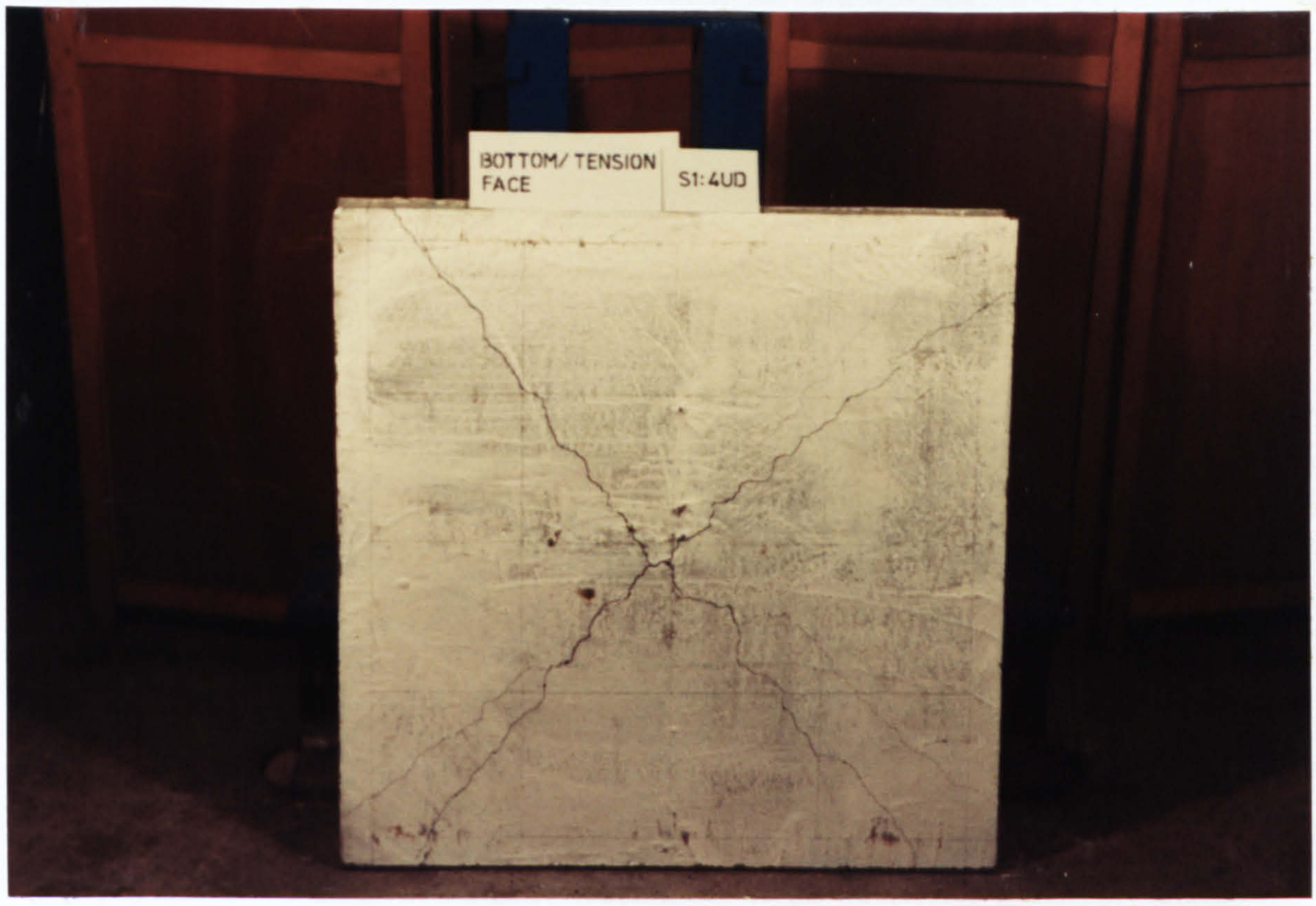

Plate 6.7 Crack Patterns at Failure on the Tension Face of Model S14UD.

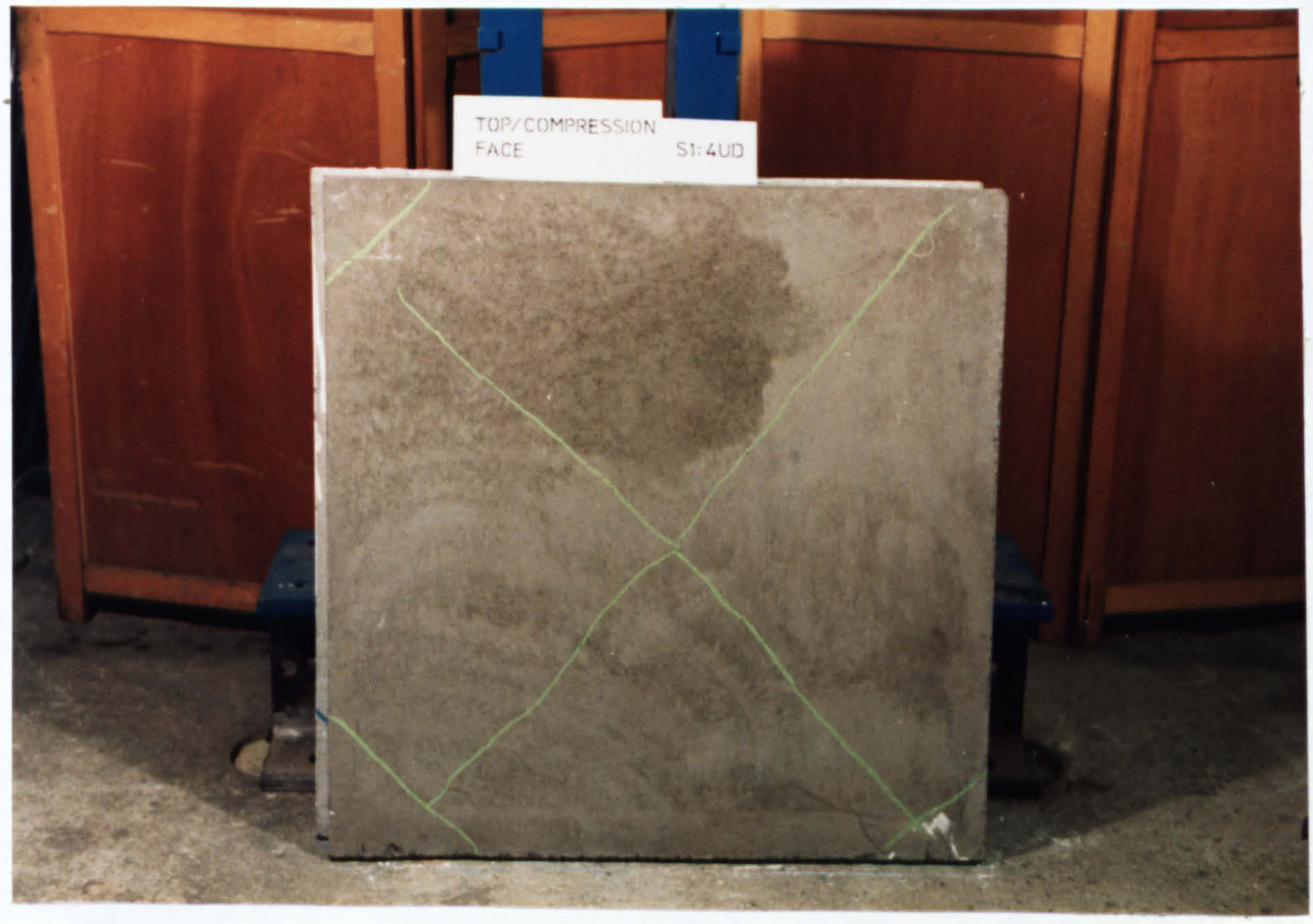

Plate 6.8 Compression Face of Model S14UD After Failure.

Plate 6.9 Crack Patterns at Failure on the Tension Face of Model S24P1.

Plate 6.10 Compression Face of Model S24P1 After Failure.

Plate 6.11 Crack Patterns at Failure on the Tension Face of Model S34P4.

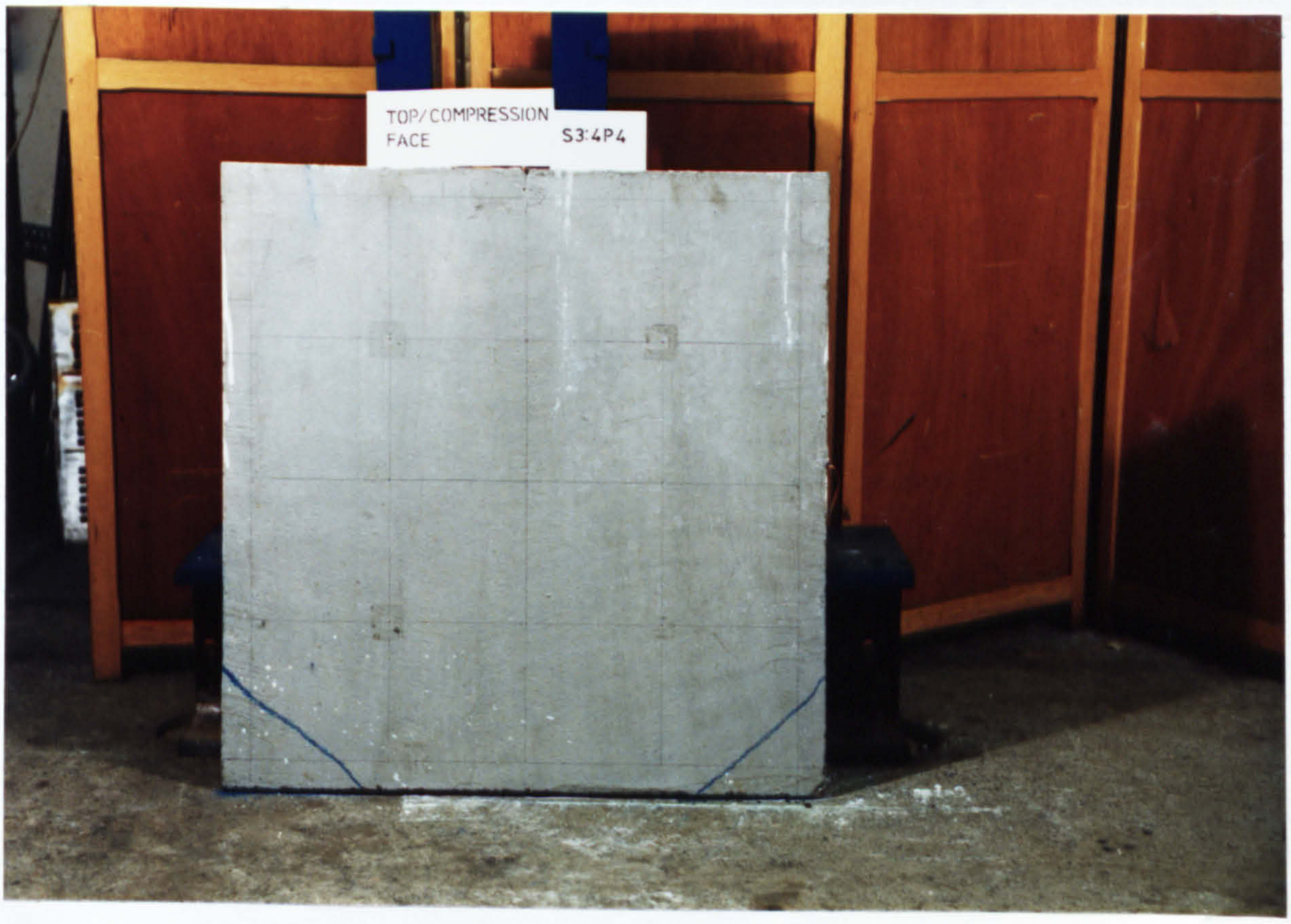

Plate 6.12 Compression Face of Model S34P4 After Failure.

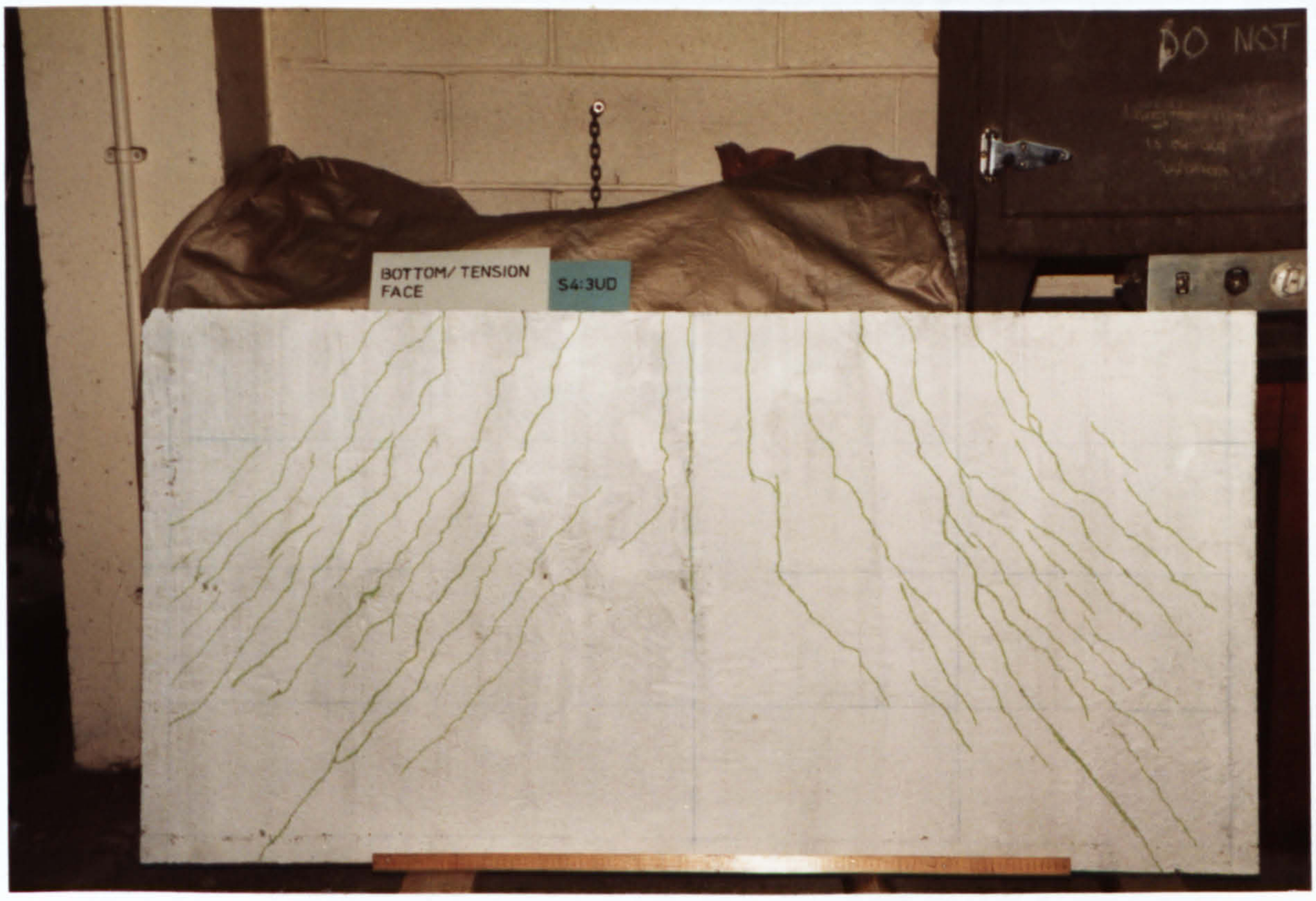

Plate 6.13 Crack Patterns at Failure on the Tension Face of Model S43UD.

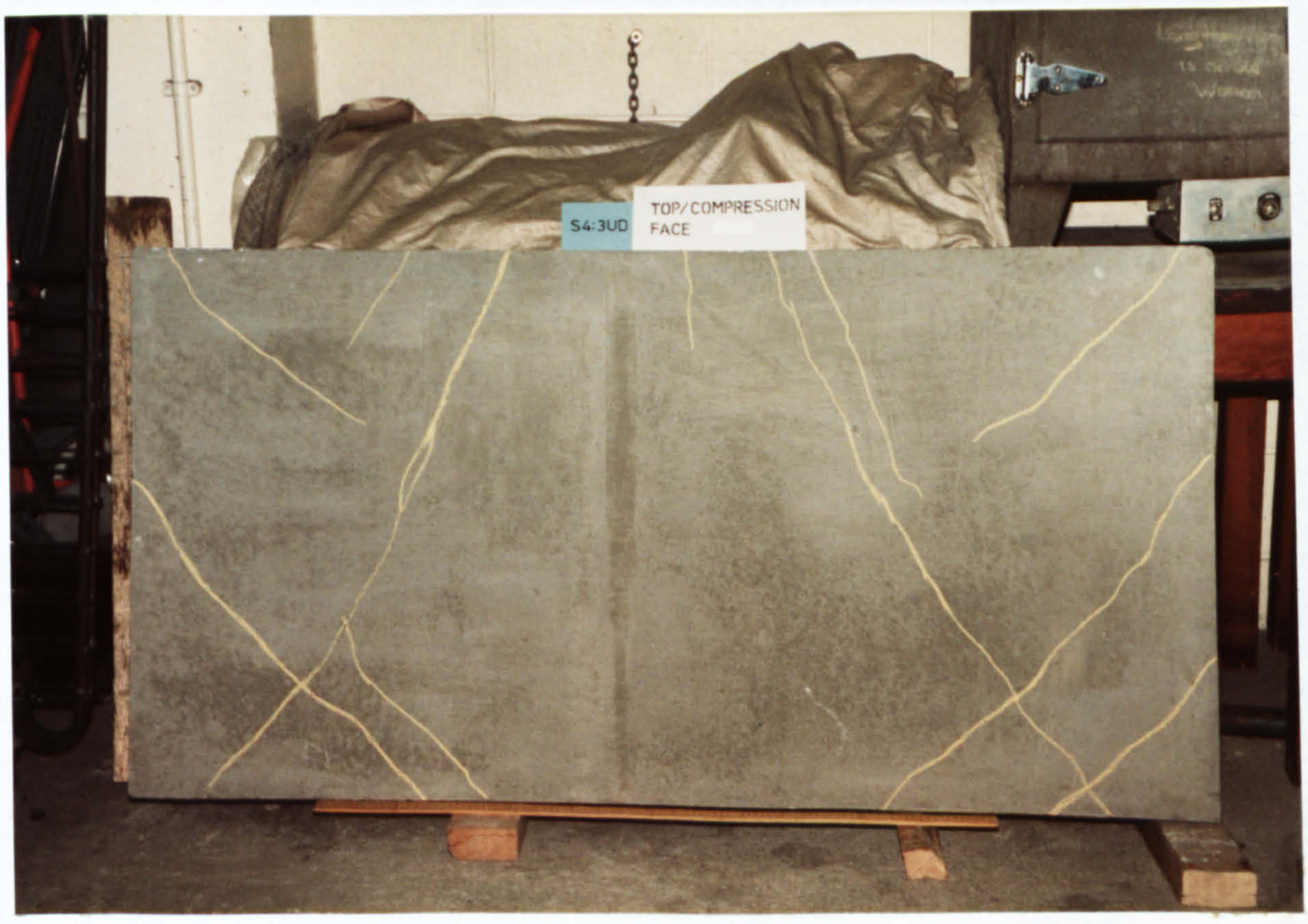

Plate 6.14 Compression Face of Model S43UD After Failure.

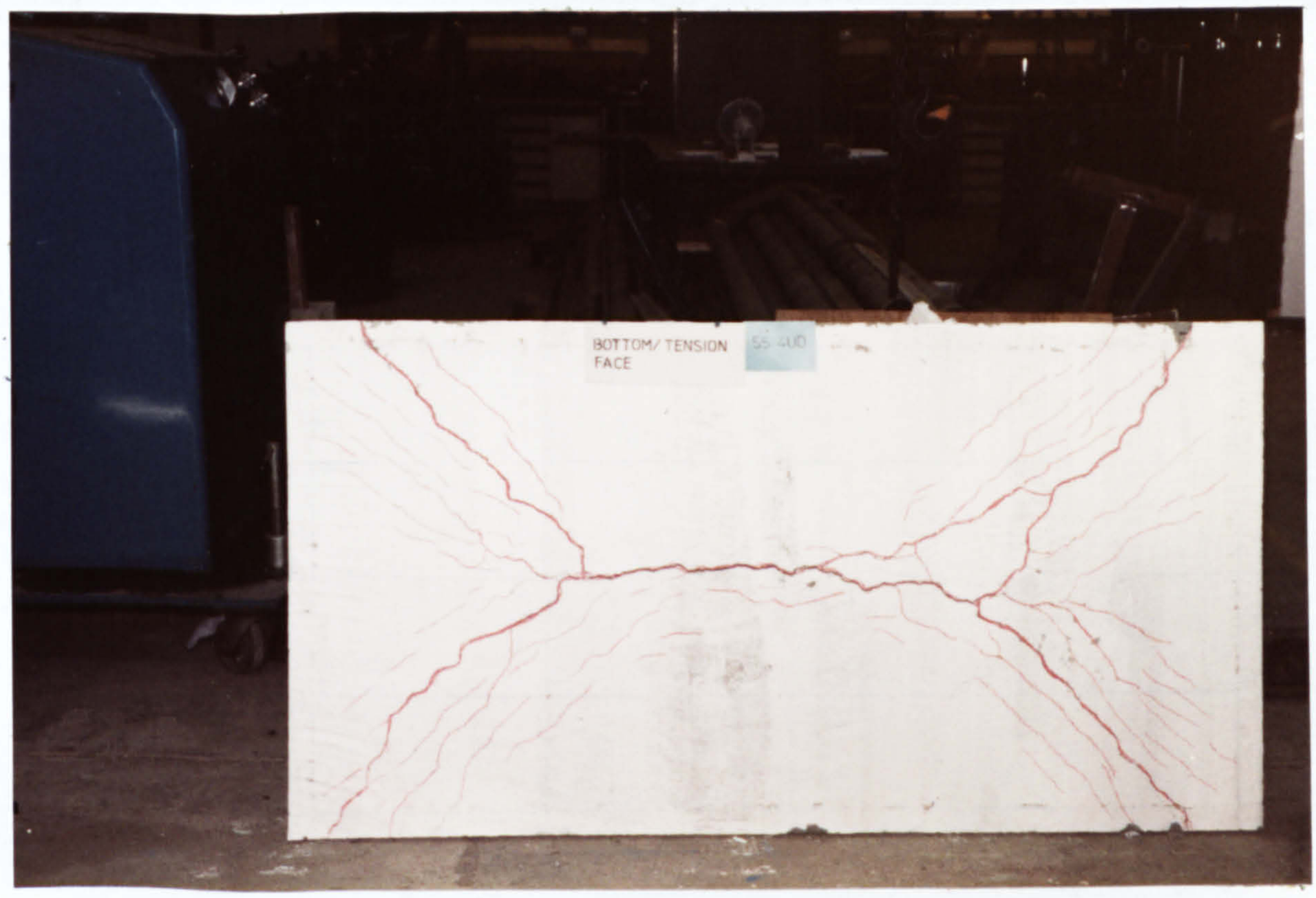

Plate 6.15 Crack Patterns at Failure on the Tension Face of Model S54UD.

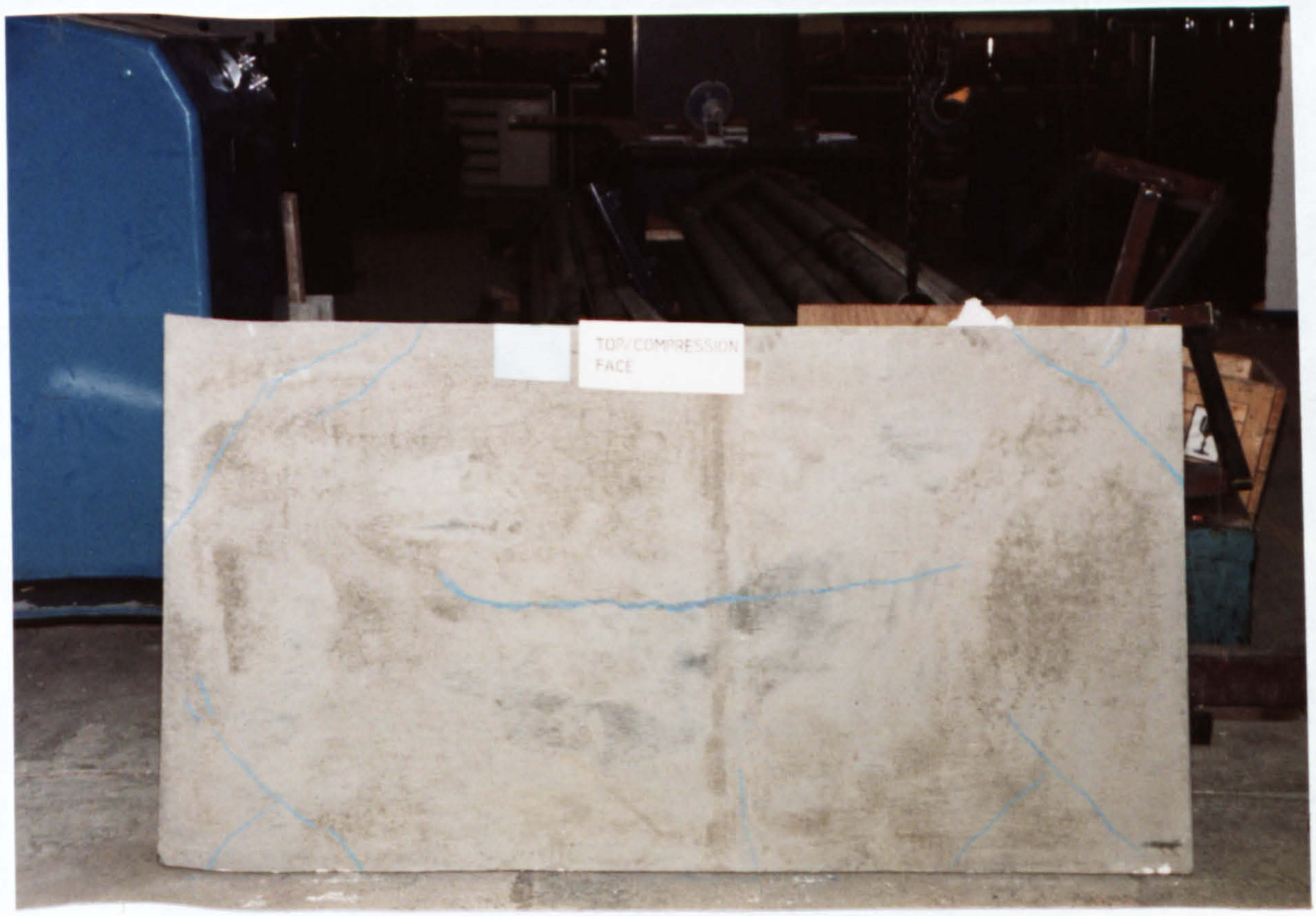

Plate 6.16 Compression Face of Model S54UD After Failure.

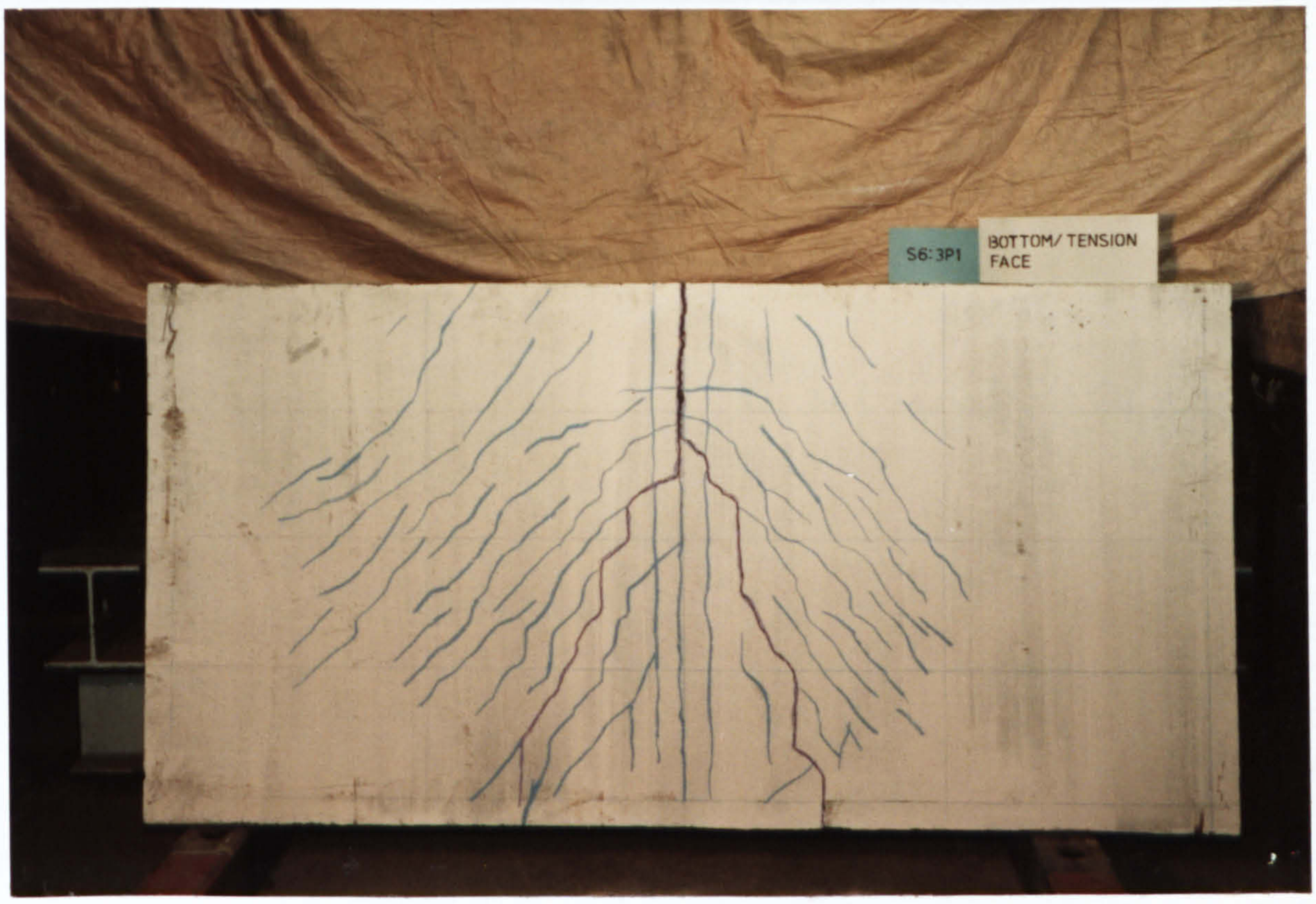

Plate 6.17 Crack Patterns at Failure on the Tension Face of Model S63P1.

Plate 6.18 Compression Face of Model S63P1 After Failure.

Chapter 7

NUMERICAL EXAMPLES AND COMPARISON OF RESULTS

7.1 Introduction

The numerical formulation of the problem and the details of the experimental investigation have been already described in the preceding chapters. The outcome of the computer model will be exemplified here. Besides testing the sensitivity of the numerical solution with respect to some of the key parameters, the overall performance of the model in predicting the behaiour of reinforced concrete slab type structures is presented. The experimental results of the test slabs provide the bases for comparing the analytical predictions. The test results of some other reinforced concrete members reported by various authors will also be used.

Graphs and figures are simple and sometimes more effective means of illustration. Hence, their presence in abundance in this chapter is not only a natural consequence but also a useful necessity. A number of figures have been transferred to the appendix D in an effort to optimise the volume of this chapter.

7.2 The Experimental Slabs

The geometric details of the test slabs and their characteristic material properties have been furnished in Chapter 6. The load-deflection records at some selected locations and the observed failure crack patterns have also been provided there. The numerical predictions for these slabs will be compared here. But before presenting the overall performance of the numerical model, the influence of some of the numerical parameters on the solution process will be outlined first. The effect of following different solution schemes has been given in Chapter 4 in

reference to the test slab S63P1. Here, the effects of some other parameters will be studied on one or the other experimental slabs. The choice of a test slab to study the effect of any particular parameter was made arbitrarily and was aimed at forming the guidelines as to their appropriate values to be used in the subsequent analyses.

7.2.1 Effect of Load Increment Size

The size of load increment is believed to have some influence on the solution of a nonlinear structural problem. The computer implementation scheme is based on the assumption that a very small amount of load will be input to initiate the solution process. The numerical cracking load will be then automatically scaled up in the subsequent load increment and all the following load increments will be made at a certain specified percentage of the cracking load (supplied as data). The effect of different load increment size was studied on test slab S14UD. A 4 x 4 element mesh was used on a symmetric quarter of the slab (Fig. 7.9) and 8 layers was allowed across the thickness. The different load increment sizes were 5, 10, 20 and 30% of the numerical cracking load. The load displacement curves are provided in Fig. 7.1 for the centre point (Node 25) of the slab along with the experimentally recorded deflection. The key provided with Fig. 7.1 includes some trailing letters such as EXP, 5%P, 10%P, etc. after the slab identifier S14UD. The word experimental deflection is abbreviated to EXP and 5%P, 10%P, etc. denote the load increment size in percent of the cracking load that has been followed to obtain the corresponding solutions. In the following figures similar convention has been pursued and the meaning of the trailing letters should become aparent from the respective discussions.

As can be expected, the load increment size up to 20% do not

exhibit any appreciable influence on the load-deflection response. Even with 30% load increment size the noticeable difference stems out only at a later stage near failure. Complete equilibrium was checked at every load level following an increment. So, if equilibrium is reached within the specified number of iterations, the size of load increment should not have any significant effect during the early stages. This is true provided the load displacement response is only mildly nonlinear. In any case, when the load increment size is very large, the number of iterations required to satisfy equilibrium may increase significantly and the final load increment may lead to an unrealistic position of instability. For most of the analysis that follow, a 10% load increment size was adopted.

7.2.2 Effect of Various Tension Stiffening Schemes

The effect of following different tension stiffening schemes has been tested on model slab S24P1. Different tension stiffening models included in the programme have already been described in Chapter 3. Fig. 7.2 provides the load displacement responses of the central node of slab S24P1. Allowing no tension stiffening, i.e. removing the principal tension completely soon after formation of a crack resulted the curve TSF0. It can be seen (Fig. 7.2) that this has considerably underestimated the actual response and the numerical failure was met at about 70% of the experimental failure load. Curve TSF1 allows for a linear descending branch which meets the strain axis at a strain level equal to 10 times the uniaxial cracking strain. This has improved the response remarkably. TSF4 performs even better where a parabolic descending branch up to 20 ϵ_{cr} has been allowed for. The automatic tension stiffening scheme (ASTF) which ensures that the stress state is always enclosed by the cracking surface, seem to have demonstrated the

best correlation with the experimental results. Similar trend of results was also observed in another test case with different tension stiffening schemes. This clearly demonstrates the need for including some form of tension stiffening scheme for concrete slabs.

7.2.3 Effect of Different Biaxial Compressive Law

Test slab S34P4 was selected to study the effect of two different biaxial law (see Chapt 3) under both compressive stress state. It is evident from Fig. 7.3 that the bilinearly elastic model (BIL) shows somewhat stiffer prediction near failure compared to simple formulation by Gerstle[31] (SFG). But both lead to a satisfactory prediction and either of the formulation may be recommended. Gerstle's simple formulation has a little edge over the other because the second modulus need not be known. For the remaining test slabs the bilinear model was adopted as the second modulus of elasticity has already been determined experimentally. For the other slabs from literature Gerstle's simple formulation has been followed.

7.2.4 Effect of Element Mesh Refinement

The effect of increasing the number of elements for structural discretisation was carried out on slab S43UD. Load deflection response of the midpoint of the free edge was chosen to bring forth the effect. For symmetry, half of the slab was discretised. The different element mesh sizes considered are 4 x 4, 4 x 8 and 8 x 8 element subdivisions. The different responses are recorded in Fig. 7.4. It is interesting to note that even quadrupling the element numbers failed to produce any significant change in the load-displacement response for this particular problem. It therefore seems sufficient to discretise the rest of these small scale model slabs into 4 x 4 mesh on either symmetric half or symmetric quadrant of the actual slab.

7.2.5 Effect of Material Strengths

Although the constituent material strengths are usually evaluated from the tests on accompanying control specimens, but these are only an estimate of the real strengths of the materials in the actual structure. Moreover, the strength of conrete is known to vary over the span of the structure. The centre span load displacement response of the model slab S54UD was replotted with slight change in the material strengths of the constituent materials. All such curves with different material strength are grouped in Fig. 7.5. Curve C0T0 is with material strengths as obtained from tests. C1T0 is for 10% greater compressive strength of concrete while tensile strength is maintained at test value. C0T1 is for other way round with tensile strength 10% higher. ST03 is the curve with steel yield strength 3% higher while the concrete strengths remain at the base value. Fig. 7.5 clearly demonstrates that the solution is more sensitive to the tensile strength of concrete and least to the compressive strength. This also indicates that the numerical analaysis of reinforced concrete structures is very much dependant on the numerical treatment of the cracking which in effect depends on the tensile strength of concrete. Yield strengths of steel are usually known within narrow limits. Here in this example, the change produced with 3% variation in steel strength is almost identical to that caused by 10% increase in compressive strength. In any case, slight uncertainties of materials strengths do not affect the overall response drastically. So, a fairly close estimate of material strengths seems acceptable.

7.2.6 Effect of Number of Layers

A 4 x 4 grid of elements was maintained on symmetric half of the test slab S63P1 while the number of layers were changed from 8 to 12 through 10. The effect of varying the number of layers is shown in Fig.

7.6. Load displacement curve for the free edge midpoint of this slab seem to remain unaffected with increased number of layers. For the elastic case it was demonstrated that a 6-8 layer proved satisfactory. In nonlinear environment also, more than 8 layers is perhaps unnecessary. Of the total number of layers, possibly two would be reserved for reinforcing steel disposed in two directions. Hence, concrete would in fact be divided into about 6 layers.

7.2.7 Effect of Shear Retention Factor (β)

Susceptibility of the overall solution to the value assigned to the shear retention factor β was studied on the test slab S14UD. As described earlier, shear retention factor was included in the crack oriented constitutive matrix in order to allow for dowel action and shear transfer across the numerical crack. Different values of β assigned for this problem varied from 0.0 to 0.9 with two intermediate values of 0.1 and 0.5. The load displacement responses of the centre span are plotted in Fig. 7.7 The observed change is really insignificant even with β equal to zero. This finding justifies the use of a constant value of shear retention factor as has been followed by some of the previous researchers[36,37]. However, theoretically a numerical problem can crop up if all the cracks formed have same inclination and the structure has freedom of movement in the crack normal direction. Such situations need further investigation, but in the present context shear retention factor can possibly be assigned any value between 0 to 1.

7.2.8 Effect of Various Schemes of Residual Force Computation

Residual forces could be evaluated either as a total discrepancy between the applied load and internal equilibrating equivalent loads or as an excess equivalent load due to stresses released from nonlinear actions (see Chapt. 2). Both these schemes have been incorporated in the

programme independently and in combination. Three different schemes were followed to obtain the load deflection curves of Fig. 7.8 for the middle point of the free edge of slab S43UD. Curve (EQA) is obtained in which complete equilibrium was checked at every iteration following a load increment. Curve (EQ∅) is just the opposite with no equilibrium check, i.e. the initial stress formulation. Finally, curve (EQ1) is with single equilibrium check following a load increment and for rest of the iteration initial stress scheme followed. Comparing these curves with the experimental response, it is found that the total initial stress formulation results somewhat stiffer prediction beyond halfway mark. Checking equilibrium once only at every load increment has significantly reduced the drifting tendency of the initial stress method of residual force computation.

7.2.9 Overall Behaviour of the Experimental Slabs

Having studied the influence of different parameters on the numerical solution procedure, the overall numerical response of the test slabs can now be pursued. Some of the important features of interest include the numerical cracking and ultimate load, the overall crack pattern and the load deflection response. The geometric details of the test slabs and the material strengths of the constituents have been furnished in the preceding chapter (Fig. 6.1 and Tables 6.1 & 6.2). Just as a recap, the flexural compressive strengths are assumed to be 80% of the respective cube strengths and yield strength of steel is 240 N/mm^2. Crushing strain and Poisson's ratio of concrete are respectively assumed to be 0.003 and 0.2 for all the test slabs.

7.2.9.1 Comparison of Cracking and Ultimate Loads

The analytical cracking loads for the test slabs are compared with the respective experimental values in Table 7.1. It may be seen that the

Table 7.1 Comparison of Cracking Loads.

Slab Designation	Experiment Cracking Load, P_{cr} (KN)	Analytical Cracking Load, P'_{cr} (KN)	Relative Ratio, P'_{cr}/P_{cr}
S14UD	22.70	15.565	0.685
S24P1	5.15	1.85	0.36
S34P4	16.0	7.453	0.466
S43UD	9.554	5.31	0.555
S54UD	30.267	14.11	0.466
S63P1	3.1	1.25	0.403

Avg = 0.489
Std.deviation = 0.117

Table 7.2 Comparison of Failure Loads

Slab Designation	Total Load at Failure		Ratio, P'_u/P_u
	Experimental P_u (KN)	Analytical P'_u (KN)	
S14UD	36.042	35.048	0.972
S24P1	9.29	9.497	1.022
S34P4	25.20	23.673	0.939
S43UD	15.93	15.698	0.985
S54UD	52.57	50.679	0.964
S63P1	5.00	5.021	1.01

Avg = 0.98

analytical model underestimates the cracking load considerably. The ratio of analytical to experimental cracking loads ranges from 0.36 for slab S24P1 to 0.685 for slab S14UD - with an average of 0.489, standard deviation of 0.117. This is perhaps due to the fact that the analytical cracking load indicates the total load at which the cracking criterion is met for the first time at a sampling station, while in reality a crack is not visible unless it has spread over a certain distance and has widened enough. However, from these limited number of observations, it may be said that doubling the numerical cracking load value should give a reasonable estimate of the physical cracking load for reinforced concrete slabs.

Table 7.2 compares the analytical loads at failure to the experimentally observed ultimate loads. The agreement appears to be fairly good in this case. It may be mentioned here that for most of the slabs complete equilibrium was not satisfied within the stipulated number of iterations at a load level just prior to the failure load. This implies that the numerical failure load can have any value between these last two load levels. Very small load increments (10% of cracking load) were applied in these analyses. So, even if the total load at the previous increment is taken to be the failure load, the figures in Table 7.2 would at most be changed by 4%.

7.2.9.2 Load Deflection Response

As mentioned earlier, deflections were recorded at some preselected locations for the experimental slabs. Fig. 7.9 gives the element discretisation on the symmetric quadrant of the slab S14UD for numerical analysis. The analytical load-deflection responses at the centre of the slab S14UD (Node 25) are compared with the experimentally recorded values in Fig. 7.10. Two analytical curves are presented, one

using 5 DOF ACM element and the other using 6 DOF Bogner element. Both the analytical curves agree fairly well with the test results. 6DOF Bogner element show slightly stiffer predictions compared to the other analytical model.

Fig. 7.11 compare the recorded deflection at Node 15 (see Fig. 7.9) of slab S24P1 and Fig. 7.12 compare that at centre span (Node 25) of slab S34P4 with the respective analytical solutions. For these and the rest of the test slabs, the analytical curves using both the element types are included. Both these slabs had identical dimensions and supporting arrangement to that of the first square slab S14UD. Hence the 4 x 4 element discretisation of Fig. 7.9 was maintained.

Test slab S43UD had only one axis of symmetry. So, half of the slab was discretised to a 4 x 4 grid as shown in Fig. 7.13. Nodes 21-25 are on the free edge of this slab and Nodes 5-25 are on the axis of symmetry. Fig. 7.14 groups the analytical load-deflection curves with the experimental one for the midpoint of the free edge. The element grid of Fig. 7.15 is on the symmetric quarter of the rectangular (all edges) simply supported slab. The experimental load-deflection records are compared with the analytical solutions in Fig. 7.16 for the central point. The element discretisation for slab S63P1 was identical to that of slab S43UD and is shown in Fig. 7.17. The load-deflection responses of the centre point of the free edge is compared in Fig. 7.18.

The experimental load-deflection curves for some other grid point locations (recorded during experiment) are shown along with their respective analytical counterparts in the figures D.1-D.16 of Appendix D. It may be seen that in every case the analytical response is in fair agreement with the experimental records. It is noticed that the 6 DOF Bogner element is in general slightly stiffer near failure, only for the

slabs supporting point loads. In case of uniformly loaded slabs the difference in response is hardly distinguishable.

7.2.9.3 Distribution of Internal Forces

Nonlinear analysis by finite element method demands evaluation of the internal stress resultants at the sampling stations. These are needed in order to obtain the internal equivalent forces which in turn checks the equilibrium state. Thus, the current distribution of the internal forces at any stage of loading could be obtained as a by-product. Such distribution of inplane forces (N_x and N_{xy}) are shown in Figs. 7.19 and 7.20 for test slab S14UD at a total load level of about 26 KN. The contour maps of inplane forces for rest of the test slabs are given in Appendix D (Figs. D.17-D.26).

The distribution of bending moments (M_x and M_y or M_{xy}) are given in Fig. 7.21-Fig. 7.32 for all the test slabs. All these contours were drawn at a total load level corresponding to about 75% of the respective ultimate loads. Standard GINO package routines were used for these drawings during the execution of the programmes.

7.2.9.4 Overall Crack Pattern

The inclination of the layer cracks at each of the Gaussian sampling points are recorded as soon as the numerical cracking condition is met. The orientation of the cracks at the discrete sampling stations are shown in Fig. 7.33 to Fig. 7.38 for all the experimental slabs. Each of these figures consist of several components representing each of the concrete layers used in element idealisation. It may be seen from these figures that the general trend in the crack direction agrees fairly well with the crack patterns obtained during the tests (Plates 6.7-6.18). The number of discrete numerical cracks may appear to be quite high compared to experimentally observed cracks. But it should also be realised that

many hairline cracks in the models would go unnoticed to the naked eye. Moreover, in real structure an already formed crack may intensify further before another crack can appear. Such a condition could possibly be included in a numerical model if they can be established from experimental investigation with sophisticated microscopic observation of crack propagation. For the present model, the direction of the cracks are based on principal stress criterion. It seems to be quite adequate in predicting the inclination of the major cracks that may develop in a reinforced concrete slab.

7.2.9.5 Load-Steel Strain Response

Steel strains were recorded at some preselected locations of the test slabs. Numerical predictions at a nearby Gaussian integration point were output during the execution of the programme. The experimental values are compared with the numerical values of steel strains in the figures 7.39 through 7.42 for 4 test slabs. In each slab a comparison is made here at the gauge with the greatest measured strains. The comparisons with some other gauges are given in Figs. D.27-D.30 of Appendix D.

The numerically computed steel strains appear to be in fair agreement with the experimentally recorded values. In general, the analytical predictions tend to underestimate the actual steel strains. It may be recalled here that perfect bond has been assumed between steel and concrete in the analytical model. In the real structure, cracking of concrete in the vicinity of reinforcing steel would always be accompanied by some bond-slipping action. Dowel action, shrinkage of concrete and some other complex internal mechanisms may also influence the steel strains locally in an indeterminate way. Such considerations are important in the assessment of any numerical results.

7.3 Other Numerical Examples

In order to study the effectivness and limitations of the present nonlinear model, test results reported by some other investigators are also analysed. Some more slabs and beam type structures are solved using the programme developed. The material properties used are mostly taken from the respective reports. But in some examples one or the other value had to be assumed because they were not reported by the respective authors. These will be duly mentioned in the ensuing discussion. The initial elasticity modulus E_c is estimated using the empirical relation of ACI-318-77 Building Code of Practice[1] as

$$E_c = 33w^{1.5}\sqrt{f'_c} \qquad (7.1)$$

where, f'_c = cylinder strength in psi

w = unit weight of concrete in lbs/ft^3.

7.3.1 Johnarry's Rectangular Slab S590

This is a simply supported rectangular one way slab tested by Johnarry[49]. The slab dimensions are 760 mm x 1080 mm. It was loaded with an unsymmetrically placed single point load. The loading point was situated halfway in the shorter direction and one-sixth of the longer span inside from the free shorter edge (Node 16, Fig. 7.43). Only the longer two sides were simply supported. The other relevant properties are

$E_c = 14$ KN/mm^2 $\qquad$ $E_d = 6.43$ KN/mm^2

$f_{cu} = 21$ N/mm^2 $\qquad$ $f'_c = 16.8$ N/mm^2 $(0.8f_{cu})$

$f'_t = 2.1$ N/mm^2 $\qquad$ $\varepsilon_u = 0.0025$

$E_s = 200$ KN/mm^2 $\qquad$ $f_y = 250$ N/mm^2

$p_x = 0.29\%$ $\qquad$ $p_y = 0.61\%$ (shorter direction)

$t = 38$ mm $\qquad$ $d = 32$ mm

The whole slab has been (deliberately) discretised into 6 x 4 mesh

as shown in Fig. 7.43. The load displacement curves for the relevant node are compared in Fig. 7.44. An isometric view of the deflected shape of the slab is shown in Fig. 7.45. The inplane force distribution N_y (shorter direction) of Fig. 7.46 shows that virtually no significant force has developed in that direction. The distribution of the moments are given in Figs. 7.47-7.48 for this slab at about 65% of the ultimate load level. The probable crack patterns are presented in Fig. 7.49. All these predictions are found to be in good agreement with the experimental results reported.

7.3.2 McNeice's Corner Supported Slab

The corner supported slab reported by Jofriet and McNeice[47] has been analysed using the present nonlinear model. The respective properties used for the analysis are

E_c = 4150 ksi, f'_c = 5500 psi,

f'_t = 550 psi, E_s = 29000 ksi, f_y = 60,000 psi (assumed)

$p_x = p_y$ = 0.85% t = 1.75 in d = 1.31 in.

This slab was loaded with a single concentrated load at centre span. A quarter of the slab was discretised from symmetry (Fig. 7.50). The effects of boundary restraints was studied on this slab. Fig. 7.51 includes three analytical curves (ROLL, UROL & HING) for each of the three different boundary conditions assigned to the corner node. The curve ROLL is for the slab having a ball roller at the corners permitting free translation in any direction. UROL is for a unidirectional roller restraining movement in the other direction and HING denotes a corner hinge support preventing translation in both directions. It may be seen that restraining both the translational movement significantly increased the load carrying capacity. The unidirectional roller support approximates the experimental load deflection response closely indicat-

ing its closeness to the actual supporting arrangement in the test. Moment contours for this slab are shown in Figs. 7.52-7.53 and Fig. 7.54 gives the numerical crack patterns.

7.3.3 Taylor, Maher and Hayes's Slabs (S4 & S6)

Two of the simply supported square plates S4 and S6 are selected from the experimental results of Taylor et al[83]. These were tested to study the effect of different reinforcement arrangements on the behaviour of slab. Both of these slabs were 6 ft. x 6 ft. square slabs, simply supported all around. The overall slab thickness was 2 inch with an effective depth of 1.875 inch for the lowermost layer of steel. The reinforcement arrangements for these two slabs are reproduced in Fig. 7.55. Closer spacings refer to the top of two bottom layers of steel. The material properties for the respective slabs are

For slab S4,

E_c = 3900 ksi f'_c = 4510 psi f'_t = 451 psi

E_s = 29000 ksi f_y = 54.5 ksi t = 2 inch

For slab S6,

E_c = 4000 ksi f'_c = 4980 psi f'_t = 498 psi

E_s = 29000 ksi f_y = 61ksi t = 2 inch

Both these slabs were loaded with sixteen point loads equally spaced over the span. Fig. 7.56 shows the element grid used for the analysis on a symmetric quarter of these slabs. The location of the four point loads on this quadrant are also shown in this figure. Load deflection responses at the centre span are compared in Figs. 7.57 and 7.58 for slabs S4 and S6 respectively. The experiments were continued up to very high deflection level (1.5t), although the authors admitted that the verticality of the applied loads could not be maintained at higher deflections. In the present numerical formulations, the failure would be encountered at a much lower level of deflection. The analytical

solutions were carried up to the experimental failure deflection deliberately. But the flatter top portion of the analytical curves indicate that it was achieved without any further load increment.

7.3.4 Ramakrishnan and Ananthanarayana's Deep Beams

Two deep beams B3 and K2 (designated here as RDBB3 and RDBK2) tested by Ramakrishnan and Ananthanarayana[77] has been analysed using the present model. The details of these beams are given in Fig. 7.59 and the analytical element grid used is shown in Fig. 7.60. The material properties for the respective beams are:

RDBB3:

E_c = 3200 ksi f'_c = 3590 psi f'_t = 335 psi

E_s = 29000 ksi f_y = 46000 psi ν = 0.0

RDBK2:

E_c = 2600 ksi f'_c = 2020 psi f'_t = 229 psi

E_s = 29000 ksi f_y = 46000 psi ν = 0.0

The first of these two beams RDBB3 was loaded with two points loads while the latter, RDBK2 supported uniformly distributed loads (Fig. 7.59). The analytical load deflection responses of the centre span are compared with the experimental records in Figs. 7.61 and 7.62 for the respective beams. It may be observed that the numerical responses were far too stiff right from the start. In deep beams, the deflections are very small and a designer is seldom concerned about their magnitude. As regards the ultimate loads, it may be seen that the numerical predictions are fairly close to the actual values. In the former case, the numerical estimation is 16% higher while for the latter it is 5% lower than the actual loads reported. The high estimation of the ultimate load for RDBB3 is perhaps due to the lack of precise knowledge of the yield strength of steel used in that beam. Only an average value

has been reported although the bar size used in that beam was different from the average bars used in most of the test beams.

7.3.5 Hayes and Taylor's Slab-Beams

Two slab-beam panels A1 and A2 of Hayes and Taylor[38] have been selected to study the performance of the present model in such situation. Fig. 7.63 provides the details of these two panels while Fig. 7.64 gives the element mesh used for discretisation. The material properties are

HSBA1:

$E_c = 25$ KN/mm^2 $f'_c = 28.3$ N/mm^2 $f'_t = 3.5$ N/mm^2

$E_s = 200$ KN/mm^2

$f_y = 414$ N/mm^2 for slab steel

$f_y = 300$ N/mm^2 for beam steel (assumed)

HSBA2:

$E_c = 22$ KN/mm^2 $f'_c = 21$ N/mm^2 $f'_t = 2.99$ N/mm^2

$E_s = 200$ KN/mm^2

$f_y = 414$ N/mm^2 for slab steel

$f_y = 320$ N/mm^2 for beam steel (assumed)

Both of these slab-beam panels were loaded to failure by uniform pressure loads. The 51 mm thick slabs were monolithically cast with the 152 mm thick edge beams running all round the four edges. Supports were placed at the four corners only under the beams. The load deflection curves for the centre of the slab of HSBA1 are compared in Fig. 7.65. Similar curves for the centre of the edge beam and the centre of the slab in case of Panel HSBA2 are provided in Figs. 7.66 and 7.67 respectively. It may be mentioned here that the first numerical cracking appeared at the centre of the beams in both cases at a total load of 21 KN and 19 KN for HSBA1 and HSBA2 respectively. The experimental values

are reported to be between 18 to 22 KN. The agreement is very good in these cases compared to those in case of the test slabs.

7.3.6 Cope and Rao's T Beam T2

A T beam reported by Cope and Rao[18] is considered here as another numerical example. The geometric details and the element grid used on symmetric quadrant are provided in Figs. 7.69 and 7.70. The relevant material properties are

$E_c = 35$ KN/mm^2 $f'_c = 38.4$ N/mm^2 $f'_t = 3.84$ N/mm^2

$E_s = 200$ KN/mm^2 $f_y = 250$ N/mm^2

$\nu = 0.0$ for beam segment

and

$\nu = 0.2$ for flange part

This beam was over reinforced and would therefore test the capability of the present formulation in coping with such problems. The numerical load displacement response at the centre span is compared with the experimental values in Fig. 7.68. The experimental deflection measurement was discontinued at 114 KN although failure was recorded at 127 KN. With the present analysis, numerical failure was encountered at a total load of about 134 KN and the analytical curve is presented up to that level. The overall response and the ultimate loads are found to be in good agreement with the experimental values.

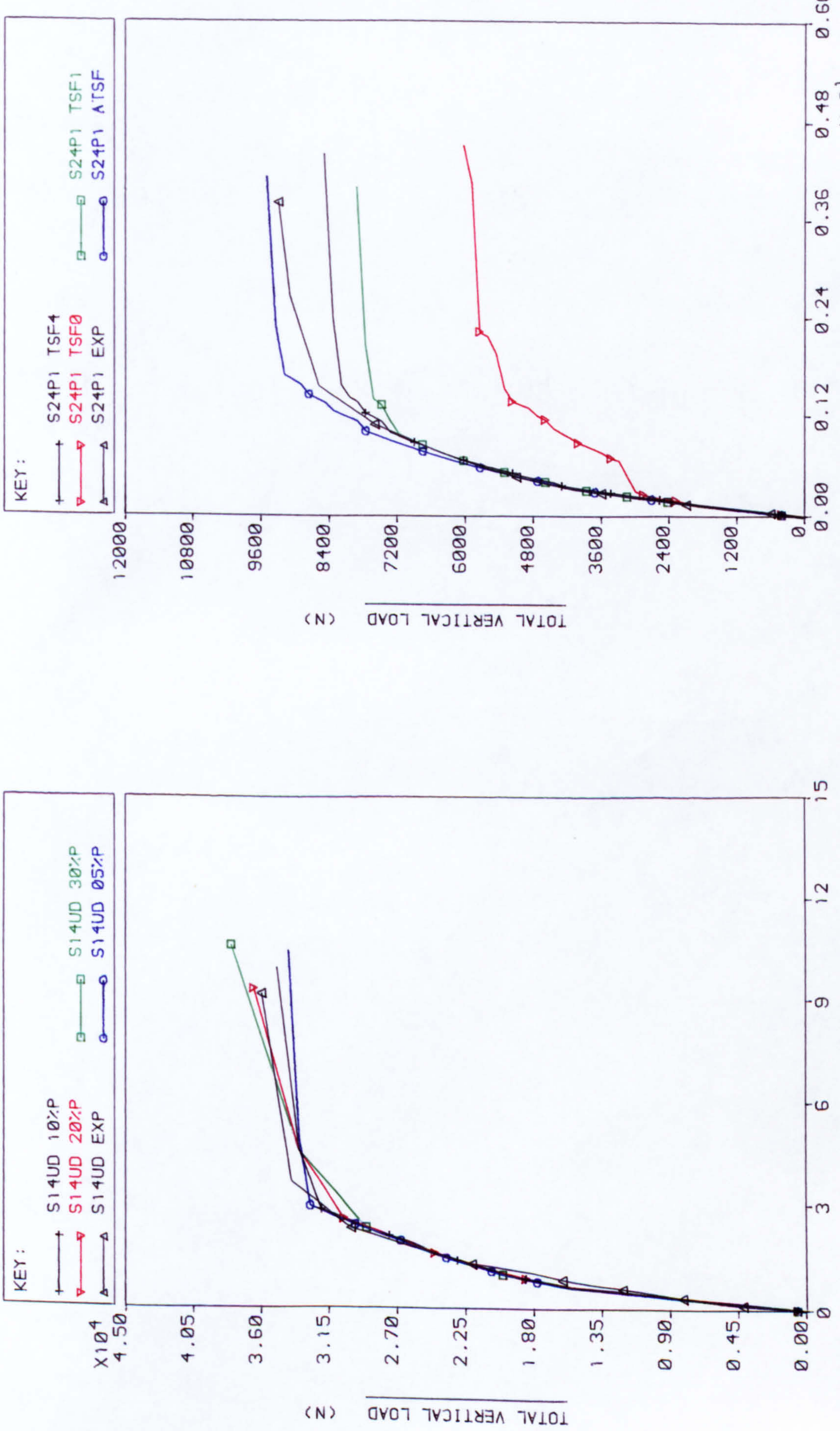

FIG.7.2 LOAD Vs DISPLACEMENT CURVES FOR NODE 15

FIG.7.1 LOAD Vs DISPLACEMENT CURVES FOR NODE 25

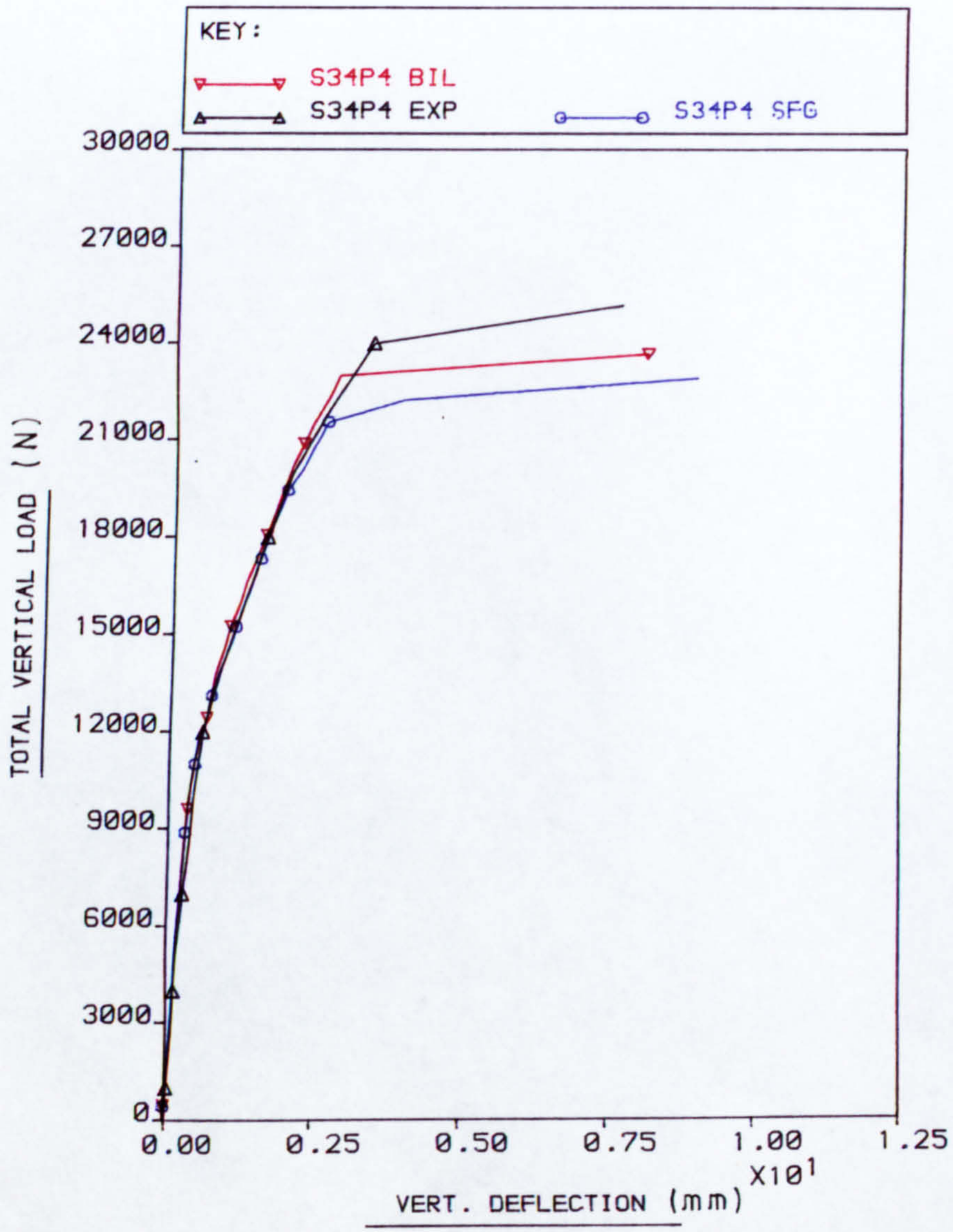

FIG. 7.3 LOAD Vs DISPLACEMENT CURVES FOR NODE *25*

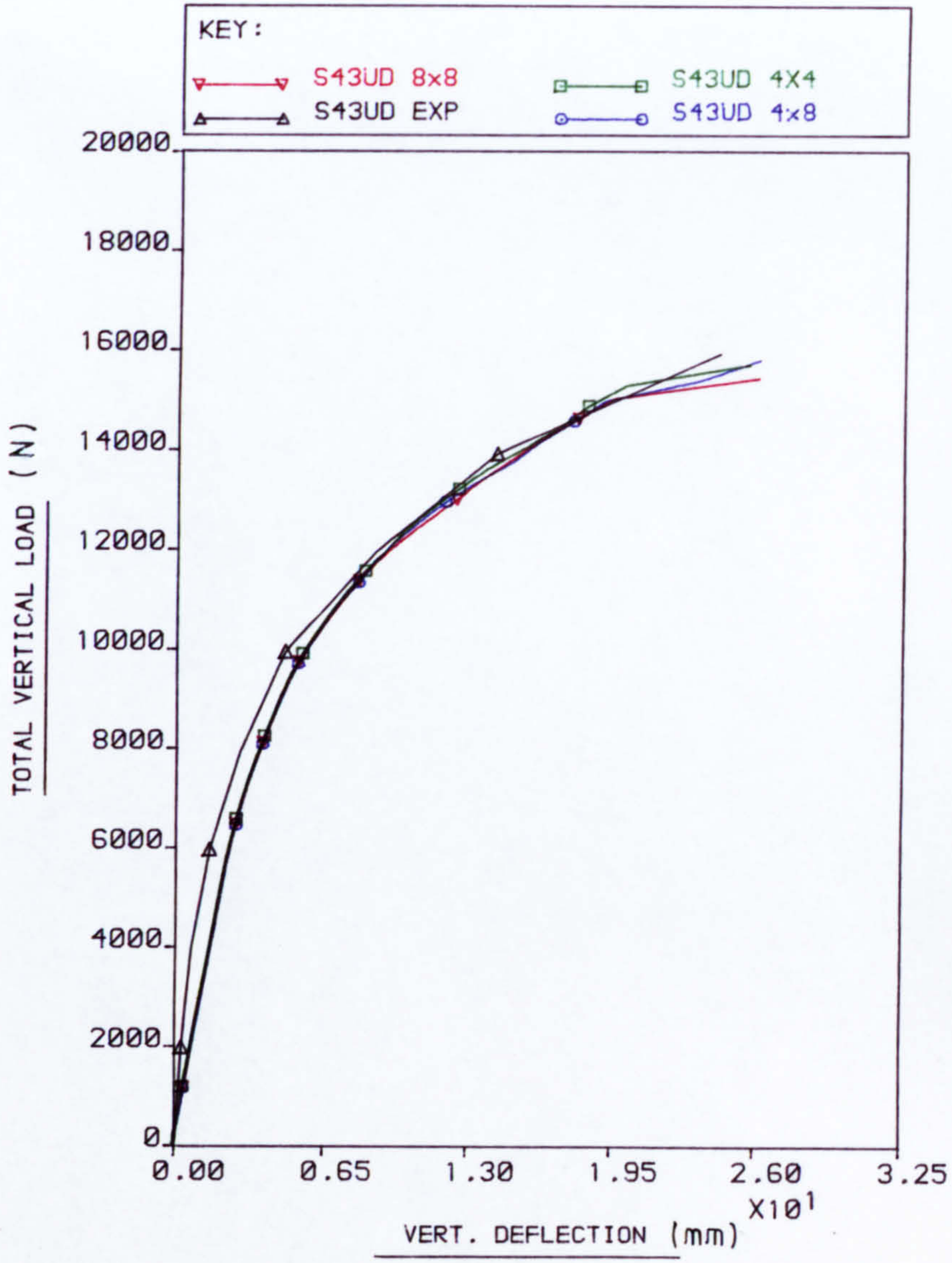

FIG. 7.4 LOAD Vs DISPLACEMENT CURVES FOR NODE *25*

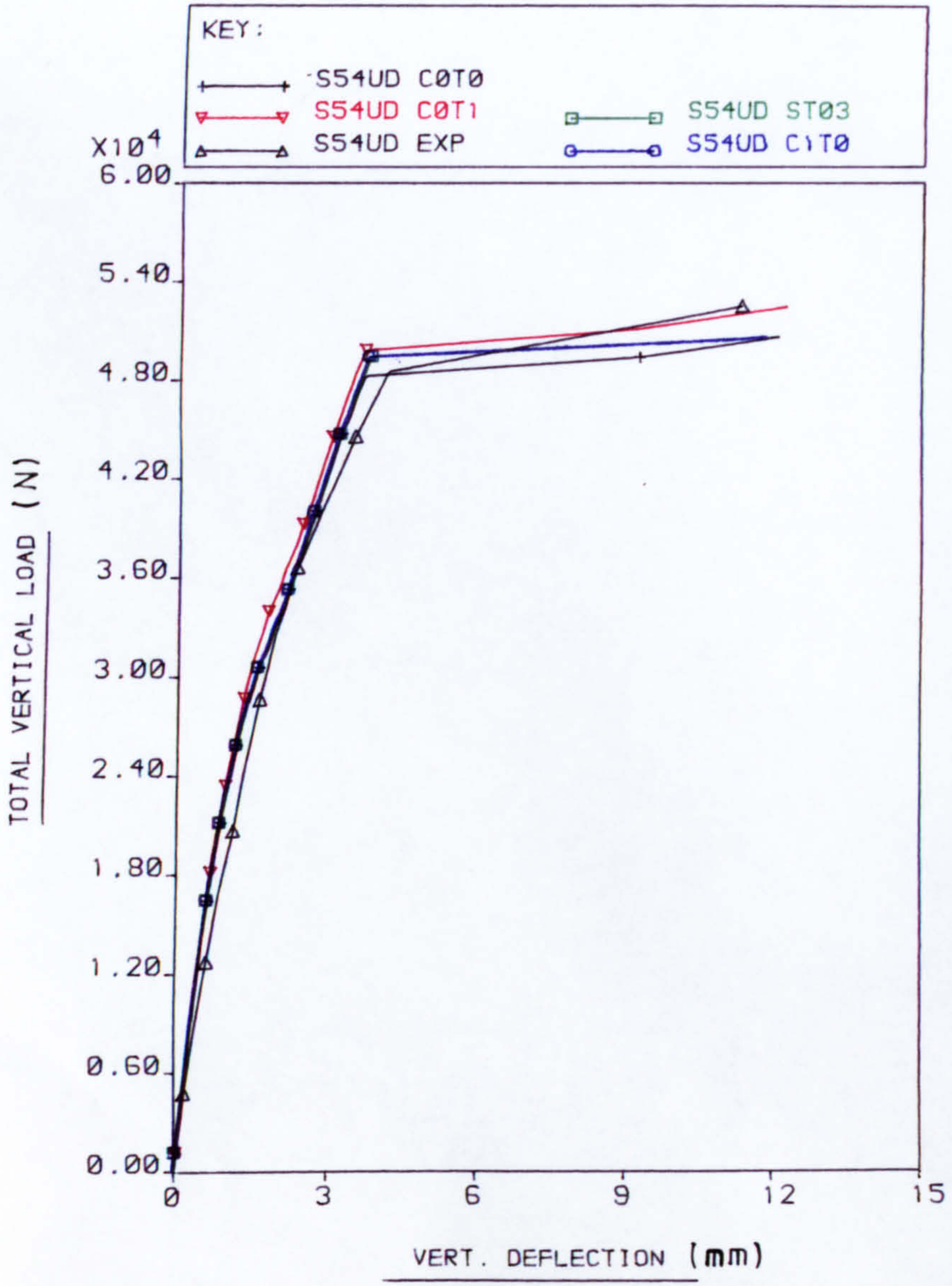

FIG. 7.5 LOAD Vs DISPLACEMENT CURVES FOR NODE *25*

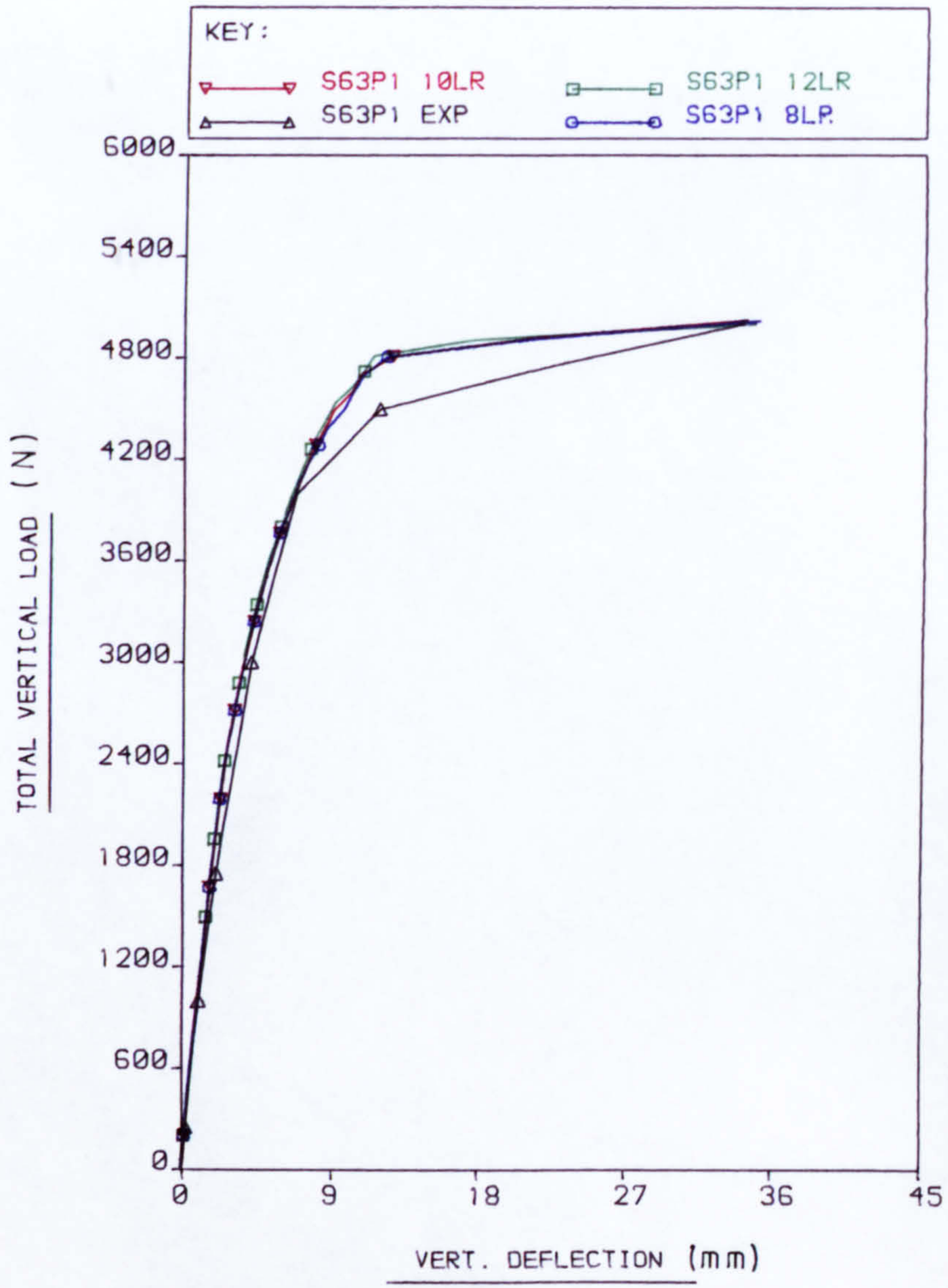

FIG. 7.6 LOAD Vs DISPLACEMENT CURVES FOR NODE *25*

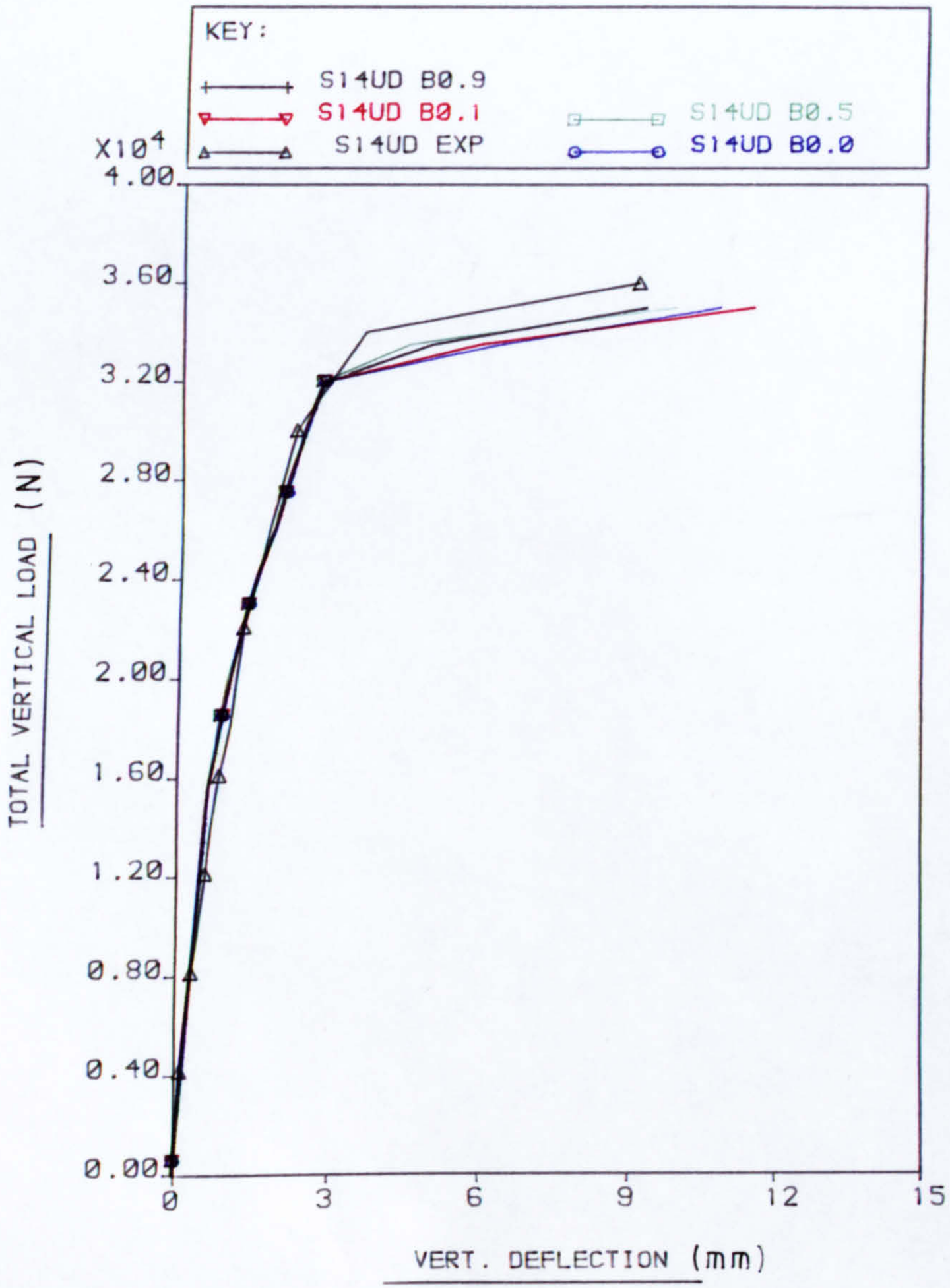

FIG. 7.7 LOAD Vs DISPLACEMENT CURVES FOR NODE *25*

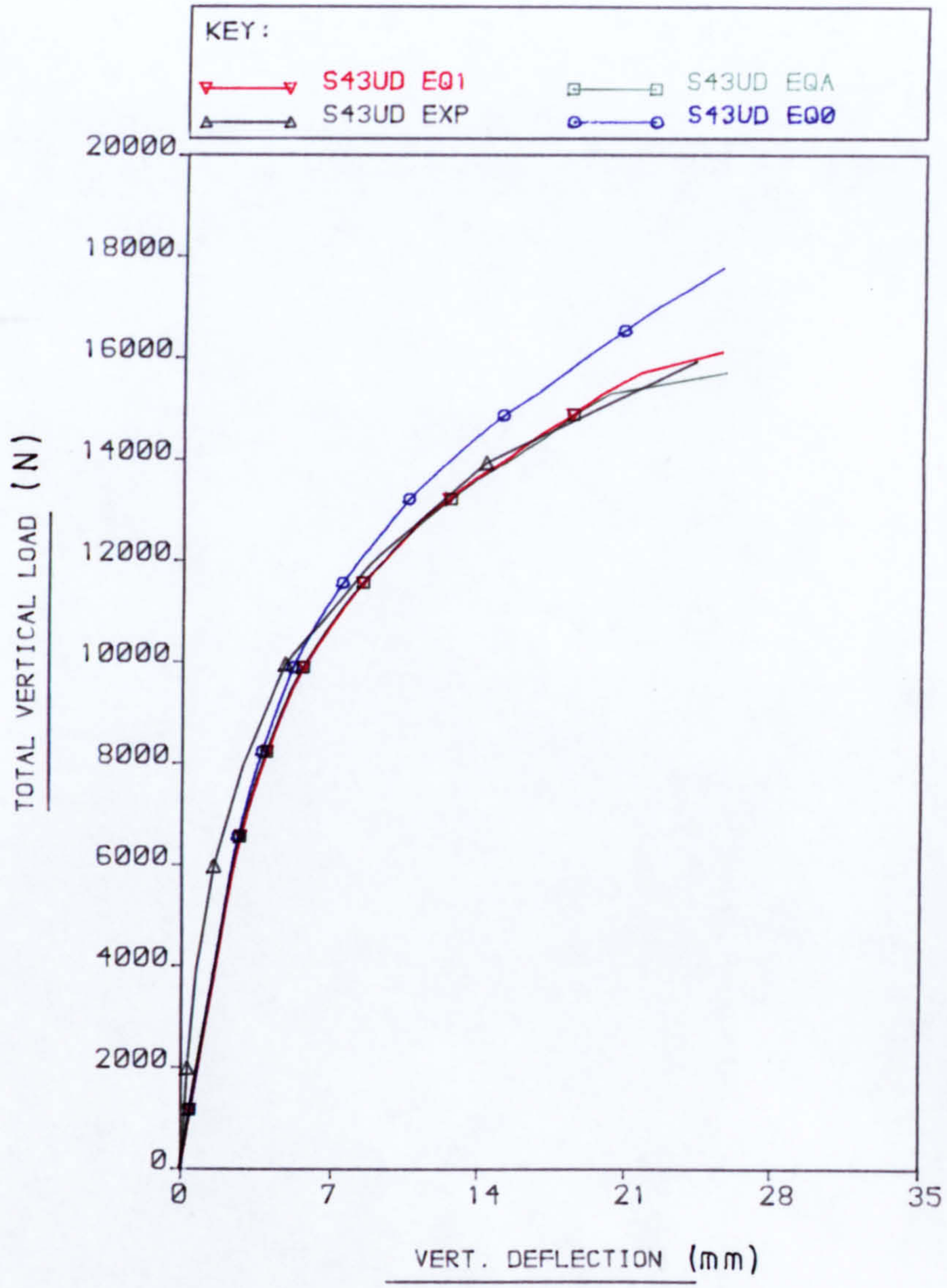

FIG. 7.8 LOAD Vs DISPLACEMENT CURVES FOR NODE *25*

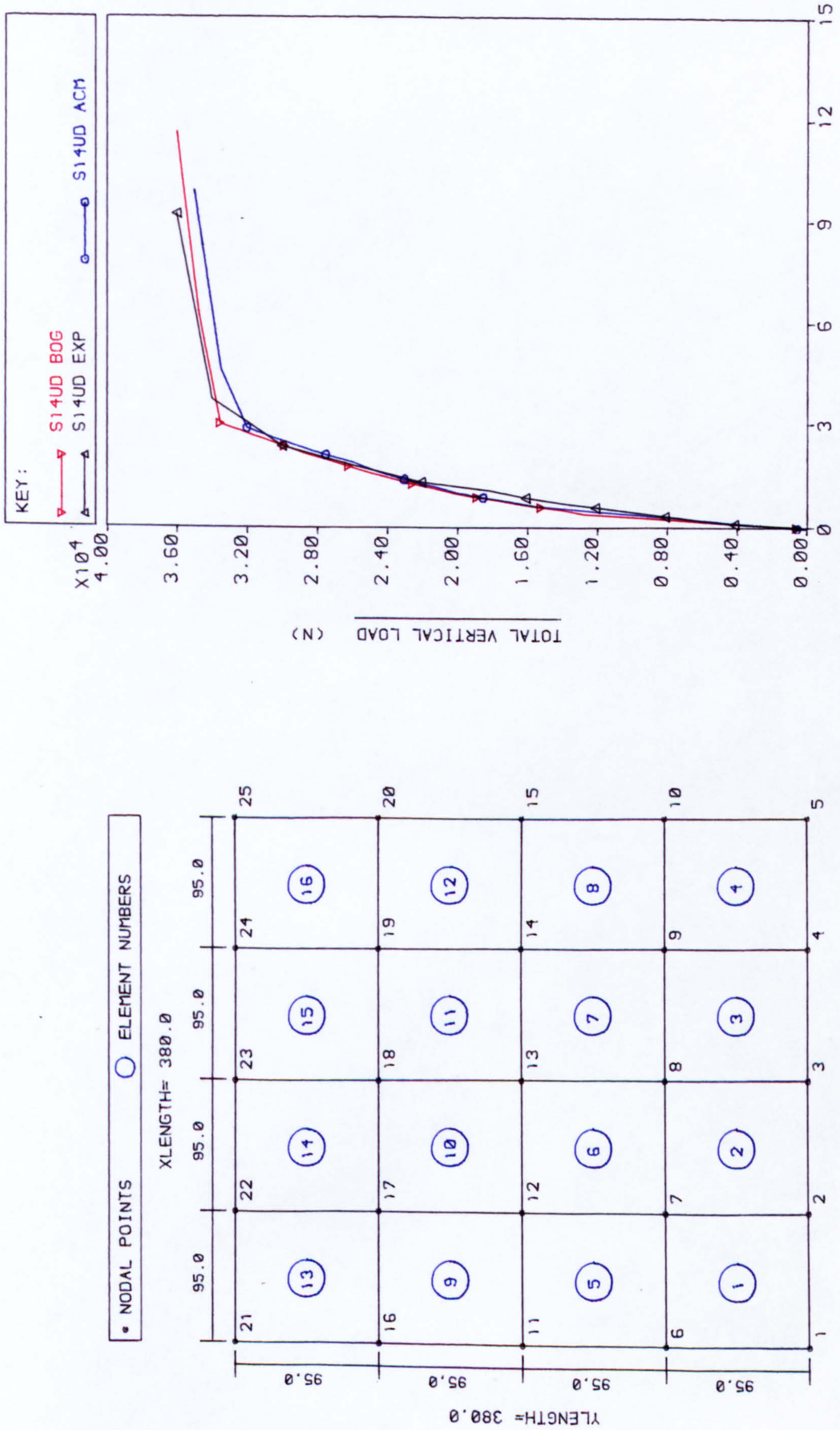

FIG. 7.10 LOAD Vs DISPLACEMENT CURVES FOR NODE 25

FIG. 7.9 ELEMENT DISCRETISATION FOR S14UD EXP

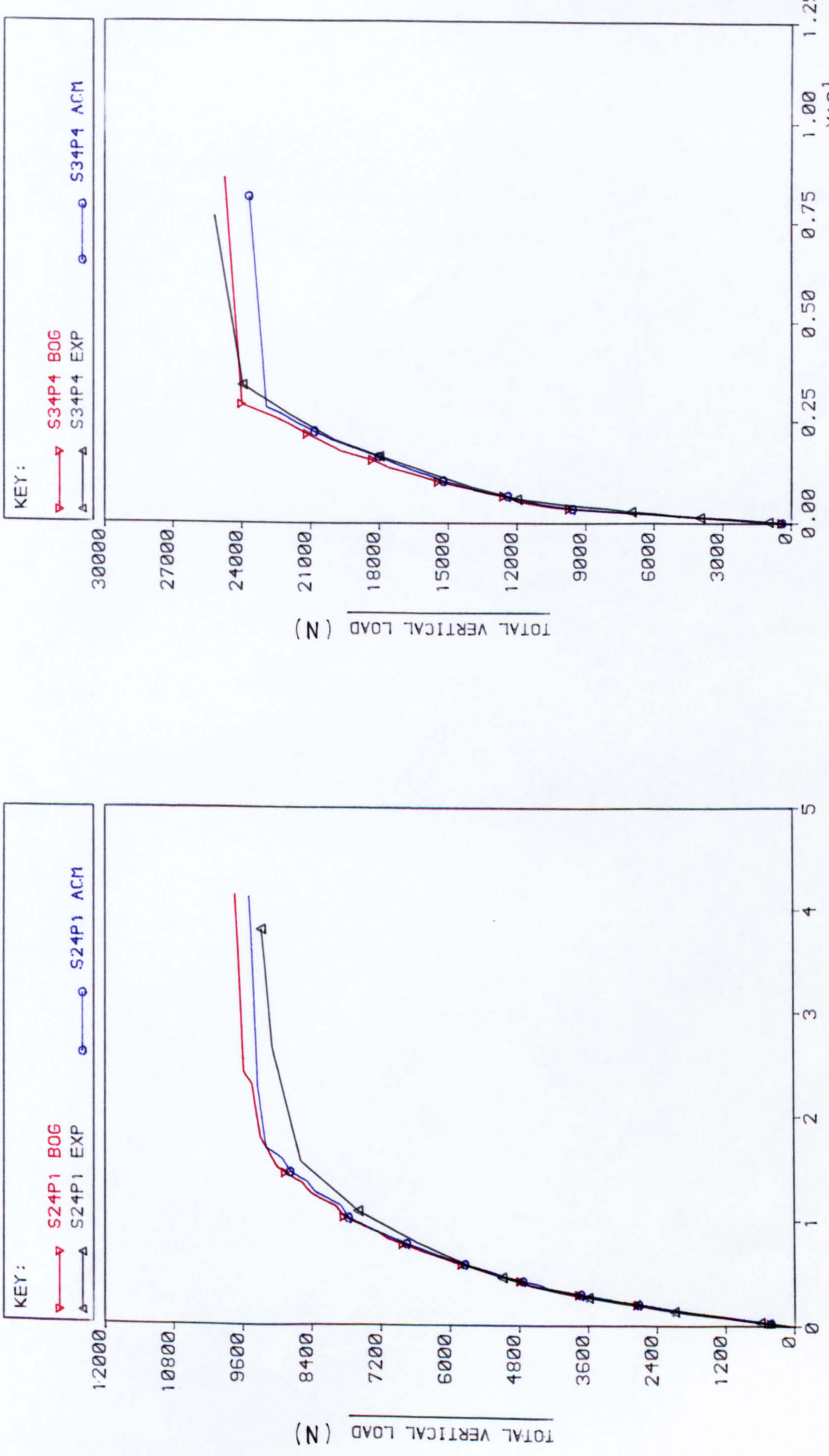

FIG. 7.12 LOAD Vs DISPLACEMENT CURVES FOR NODE *25*

FIG. 7.11 LOAD Vs DISPLACEMENT CURVES FOR NODE *15*

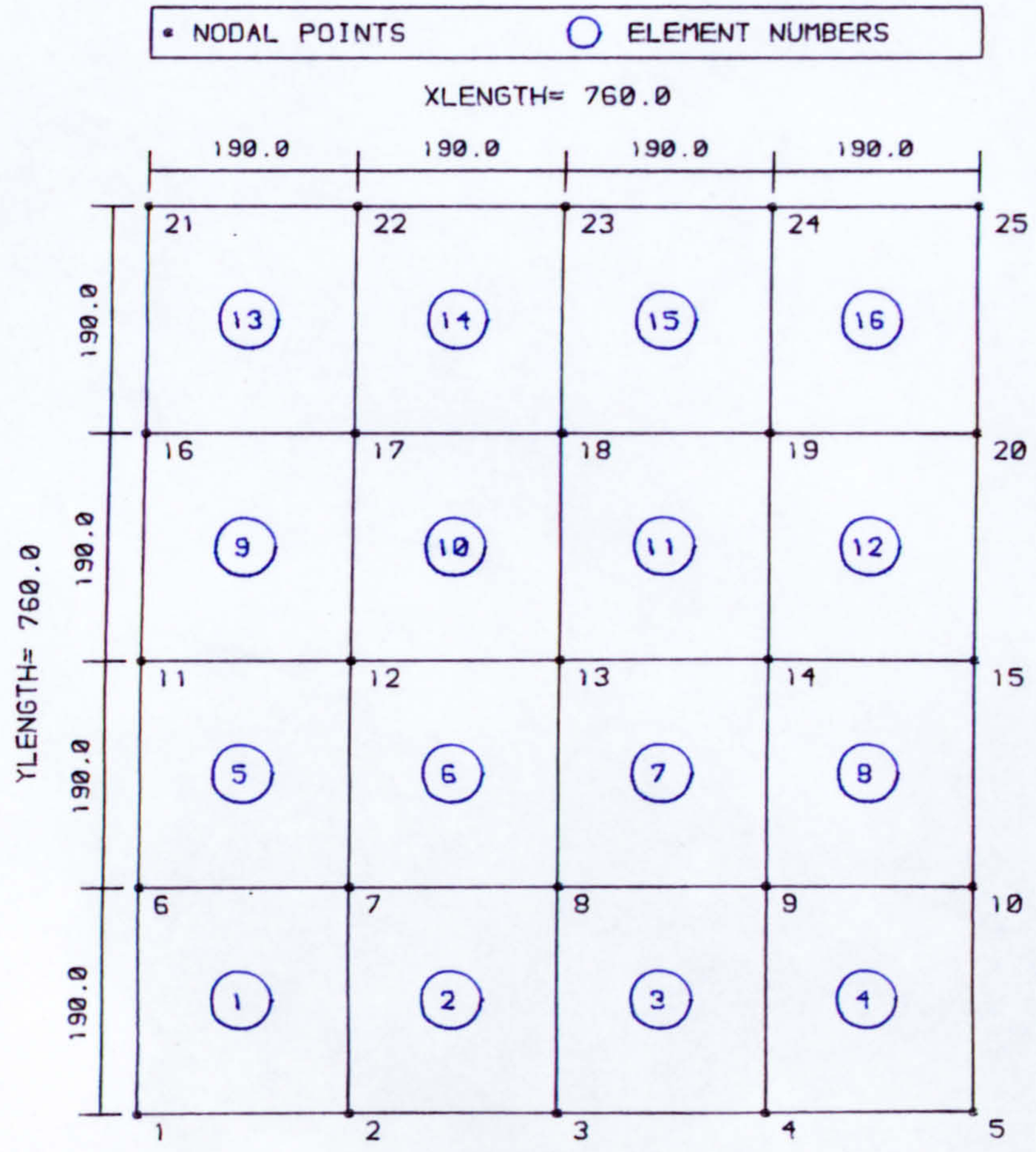

FIG. 7.13 ELEMENT DISCRETISATION FOR S43UD EXP

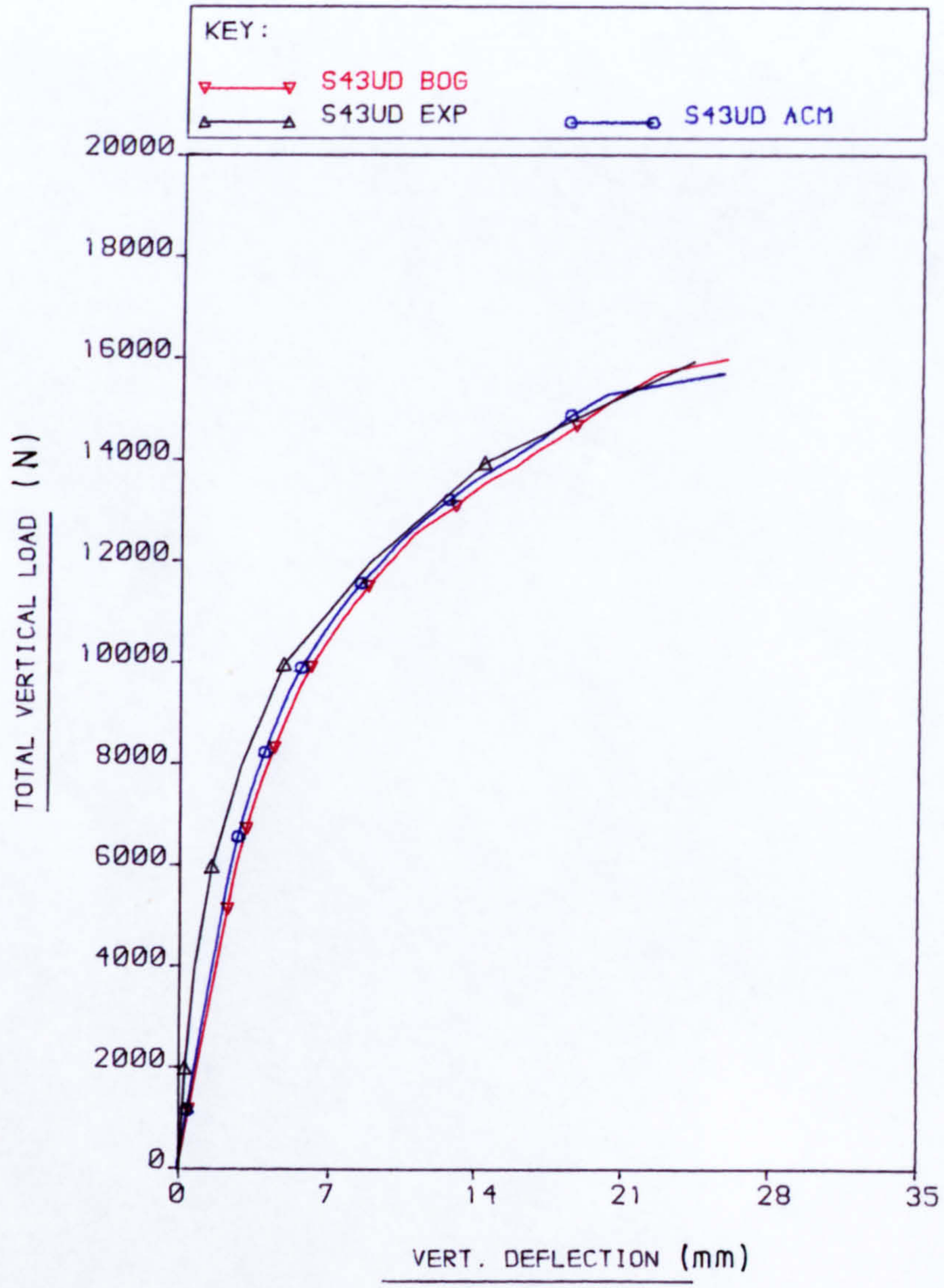

FIG. 7.14 LOAD Vs DISPLACEMENT CURVES FOR NODE *25*

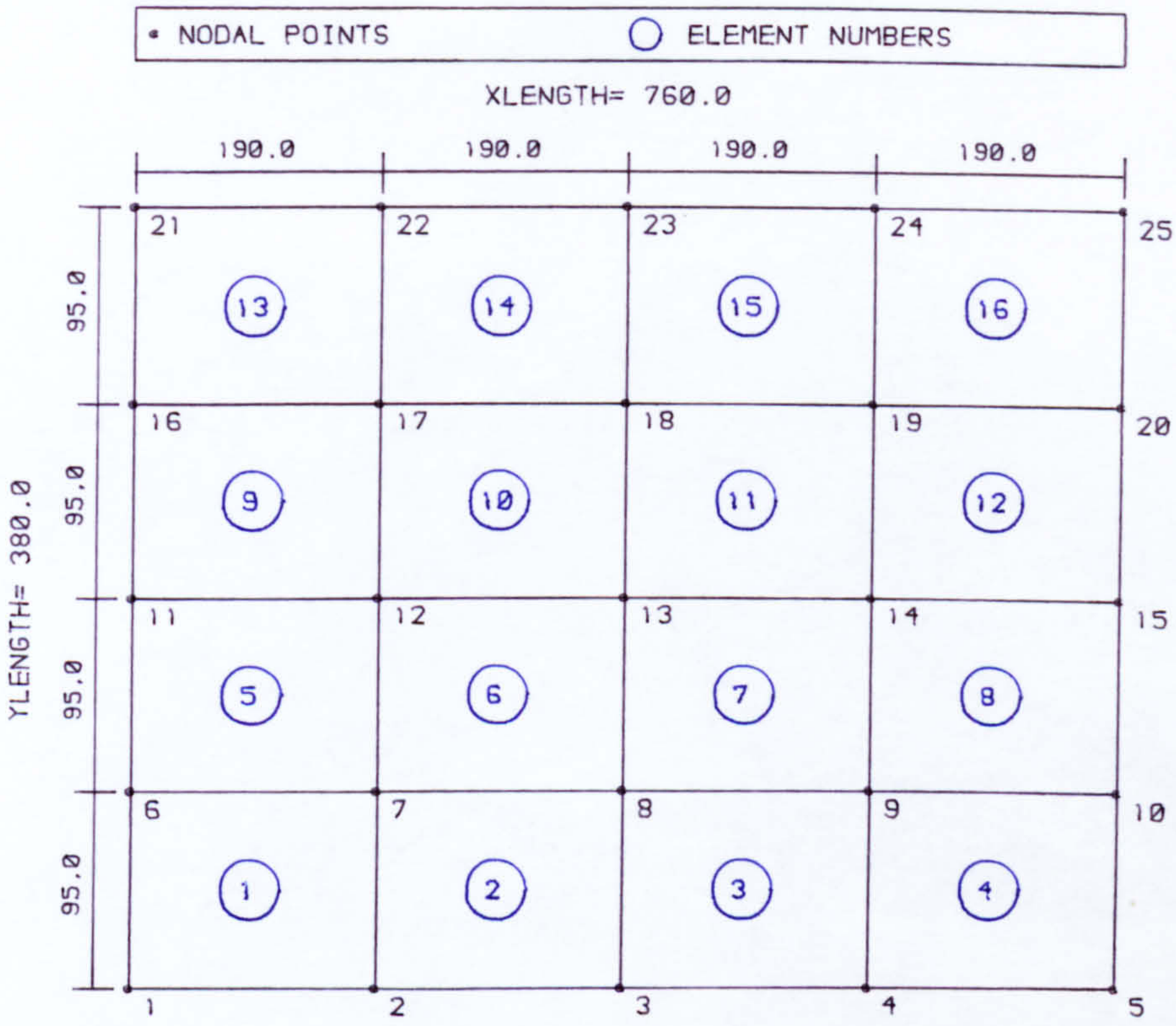

FIG. 7.15 ELEMENT DISCRETISATION FOR S54UD EXP

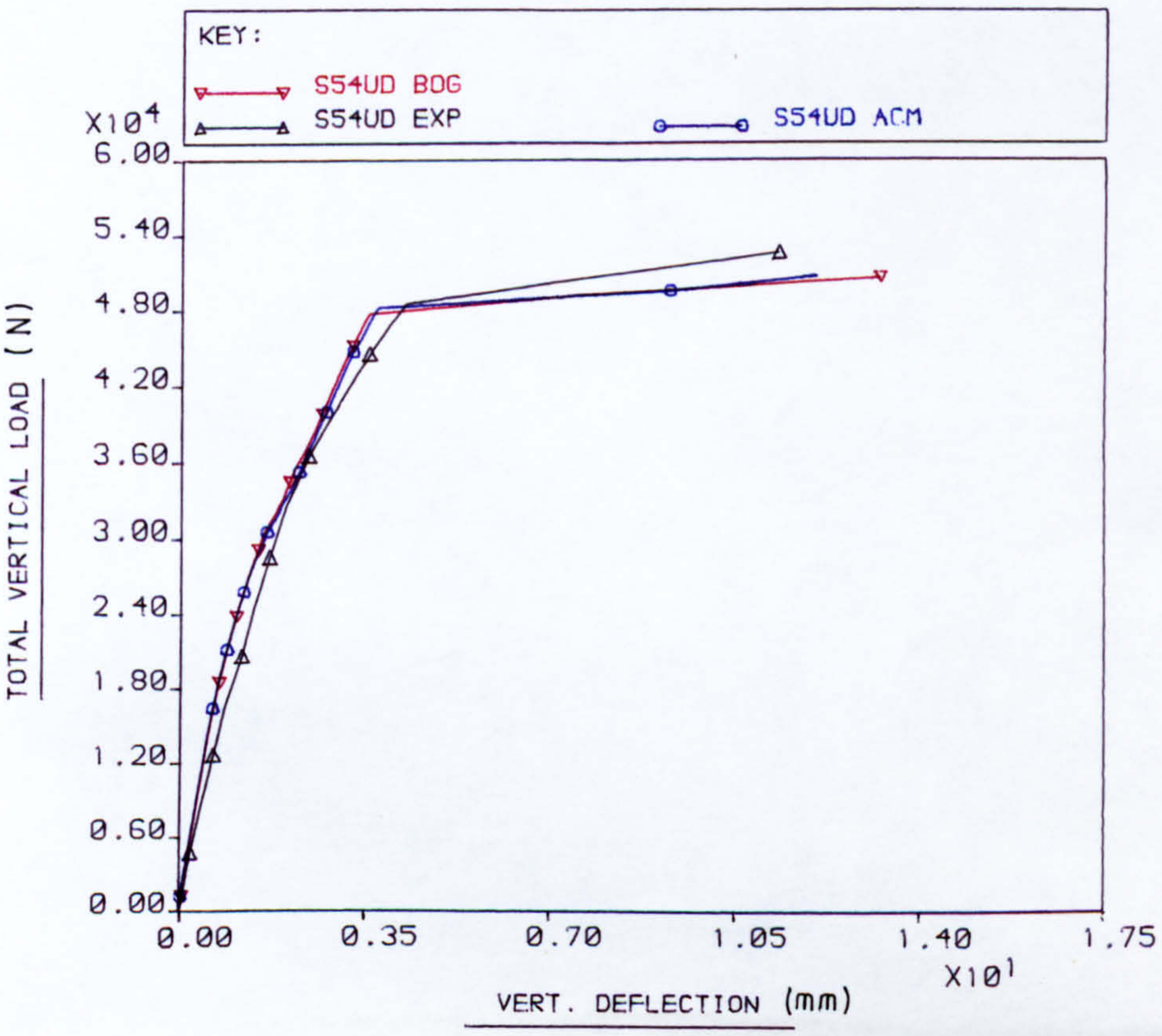

FIG. 7.16 LOAD Vs DISPLACEMENT CURVES FOR NODE 25

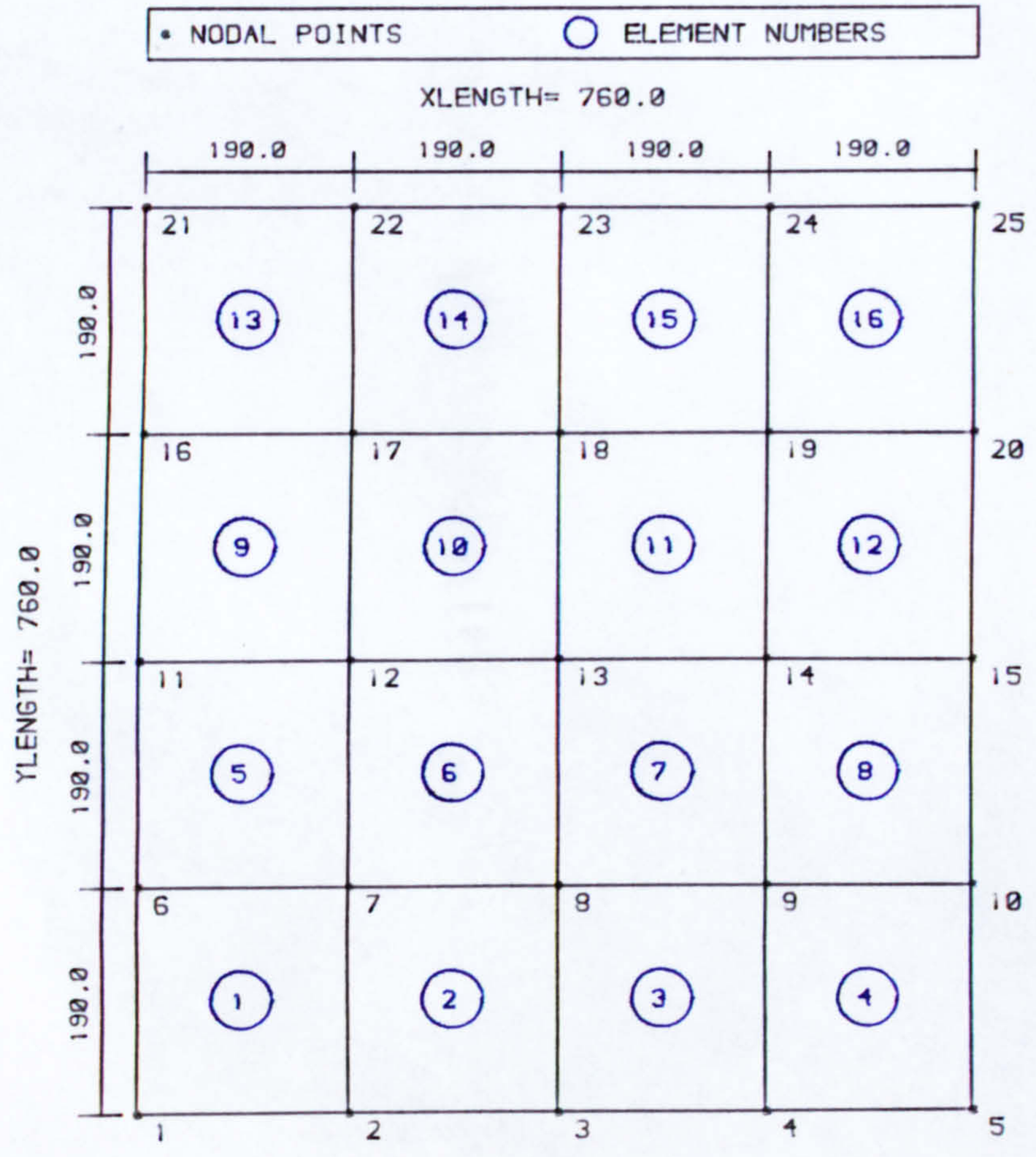

FIG. 7.17 ELEMENT DISCRETISATION FOR S63P1 EXP

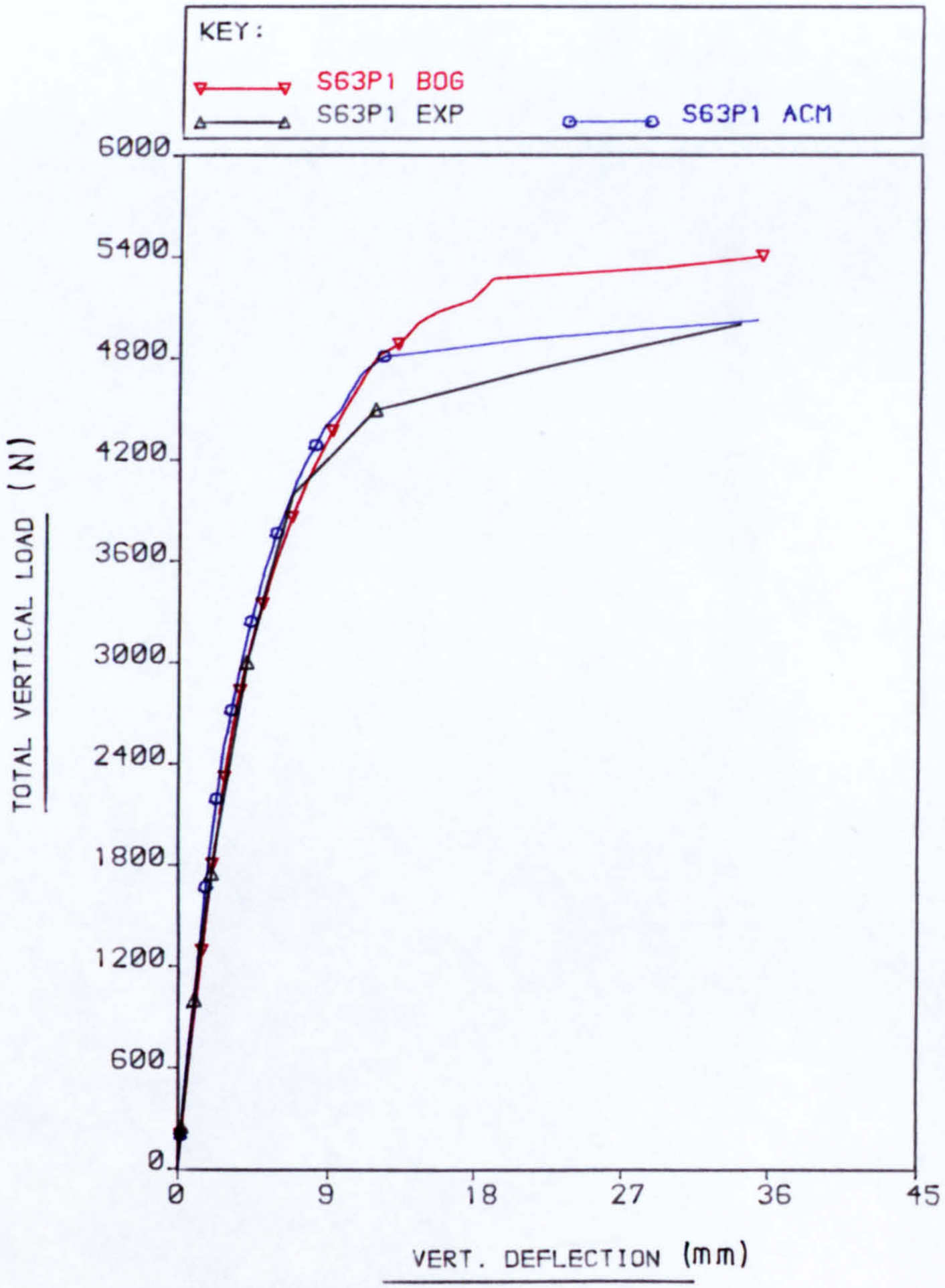

FIG. 7.18 LOAD Vs DISPLACEMENT CURVES FOR NODE *25*

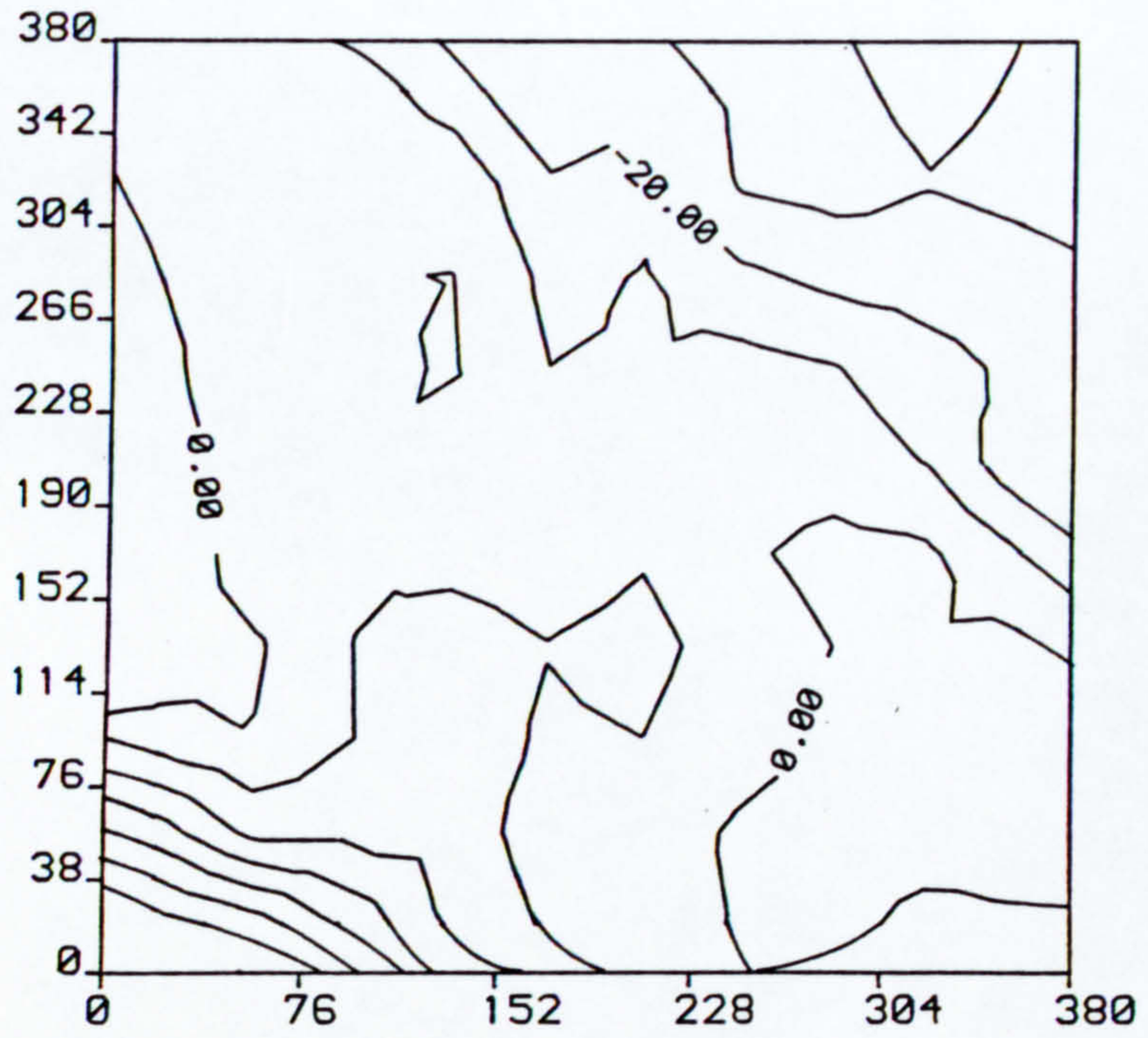

FIG. 7.19 CONTOUR OF NX FOR S14UD ACM
AT TOTAL VERTICAL LOAD= 26056.0 N
(N/mm)

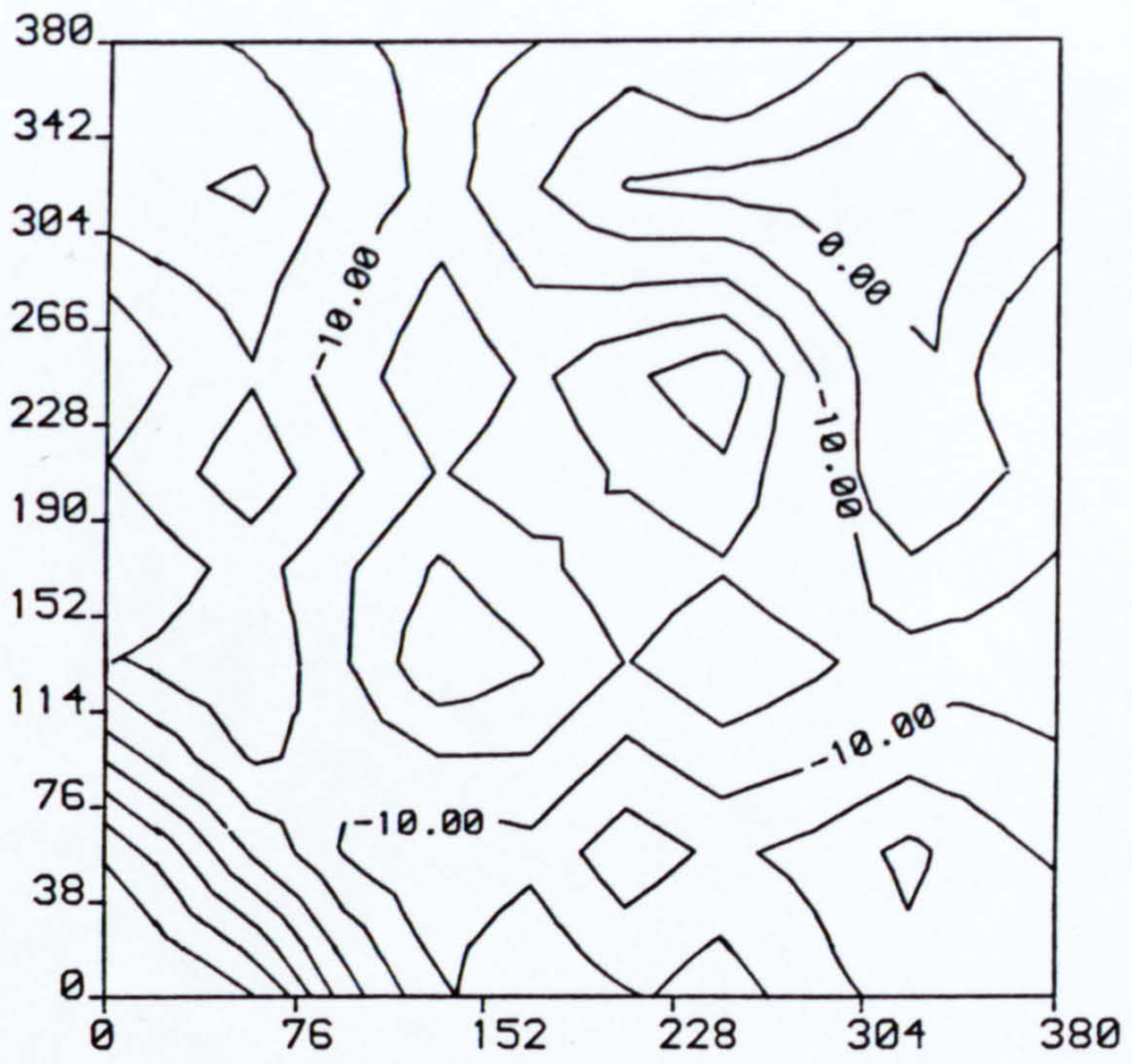

FIG. 7.20 CONTOUR OF NXY FOR S14UD ACM
AT TOTAL VERTICAL LOAD= 26056.0 N
(N/mm)

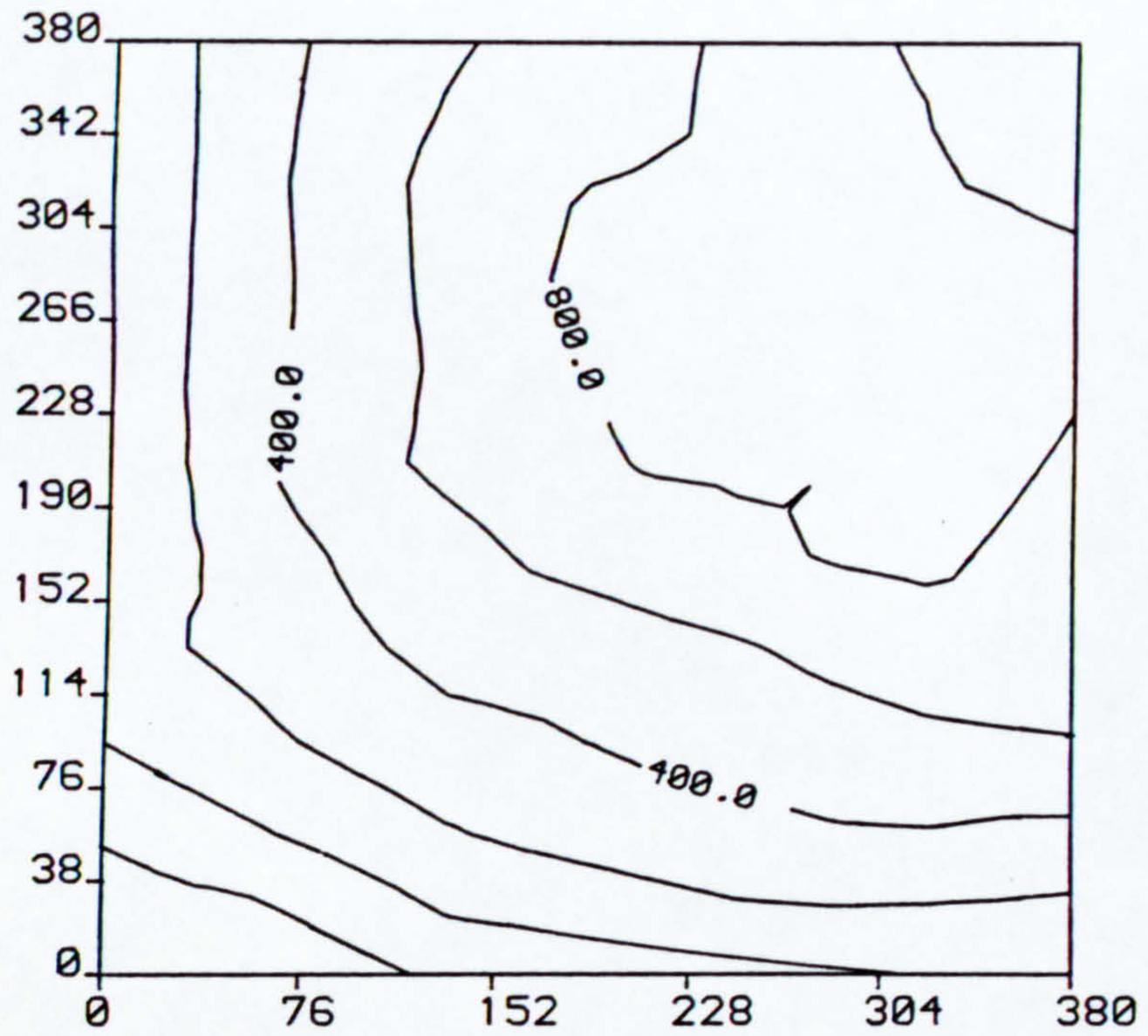

FIG. 7.21 CONTOUR OF MX FOR S14UD ACM
AT TOTAL VERTICAL LOAD= 26056.0 N
(N-mm/mm)

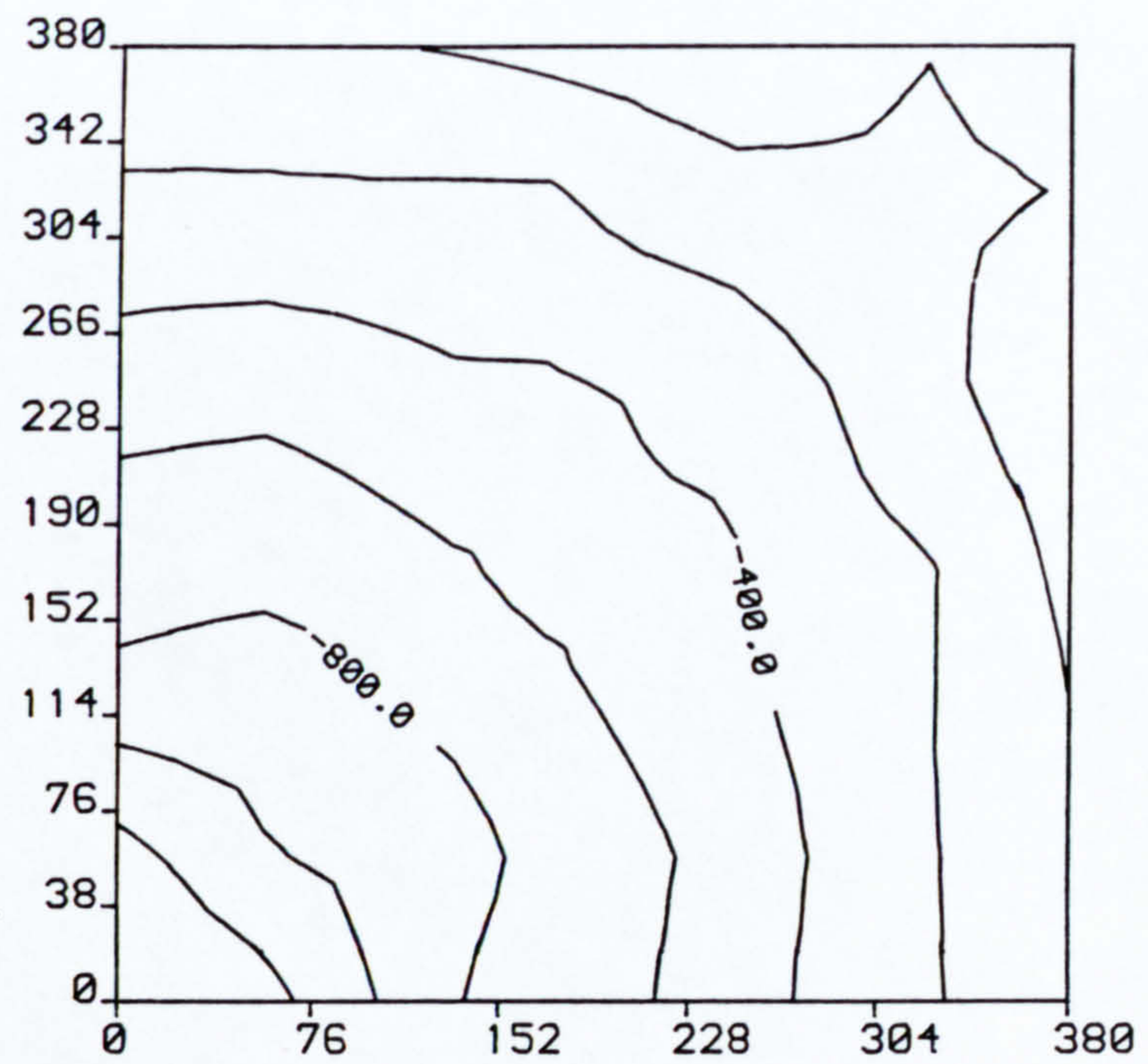

FIG. 7.22 CONTOUR OF MXY FOR S14UD ACM
AT TOTAL VERTICAL LOAD= 26056.0 N
(N-mm/mm)

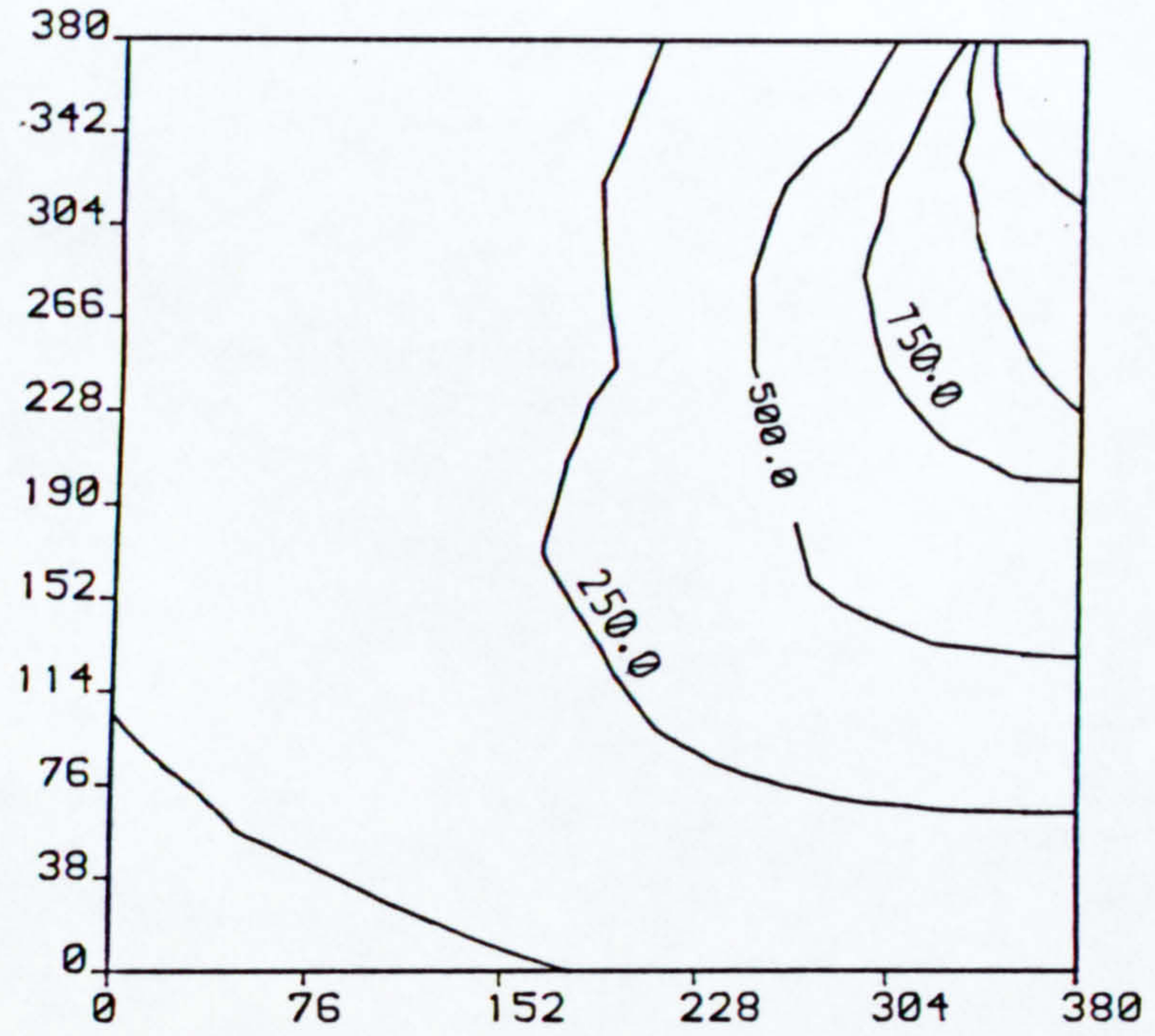

FIG.7.23 CONTOUR OF MX FOR S24P1 ACM
AT TOTAL VERTICAL LOAD= 7042.5 N
(N-mm/mm)

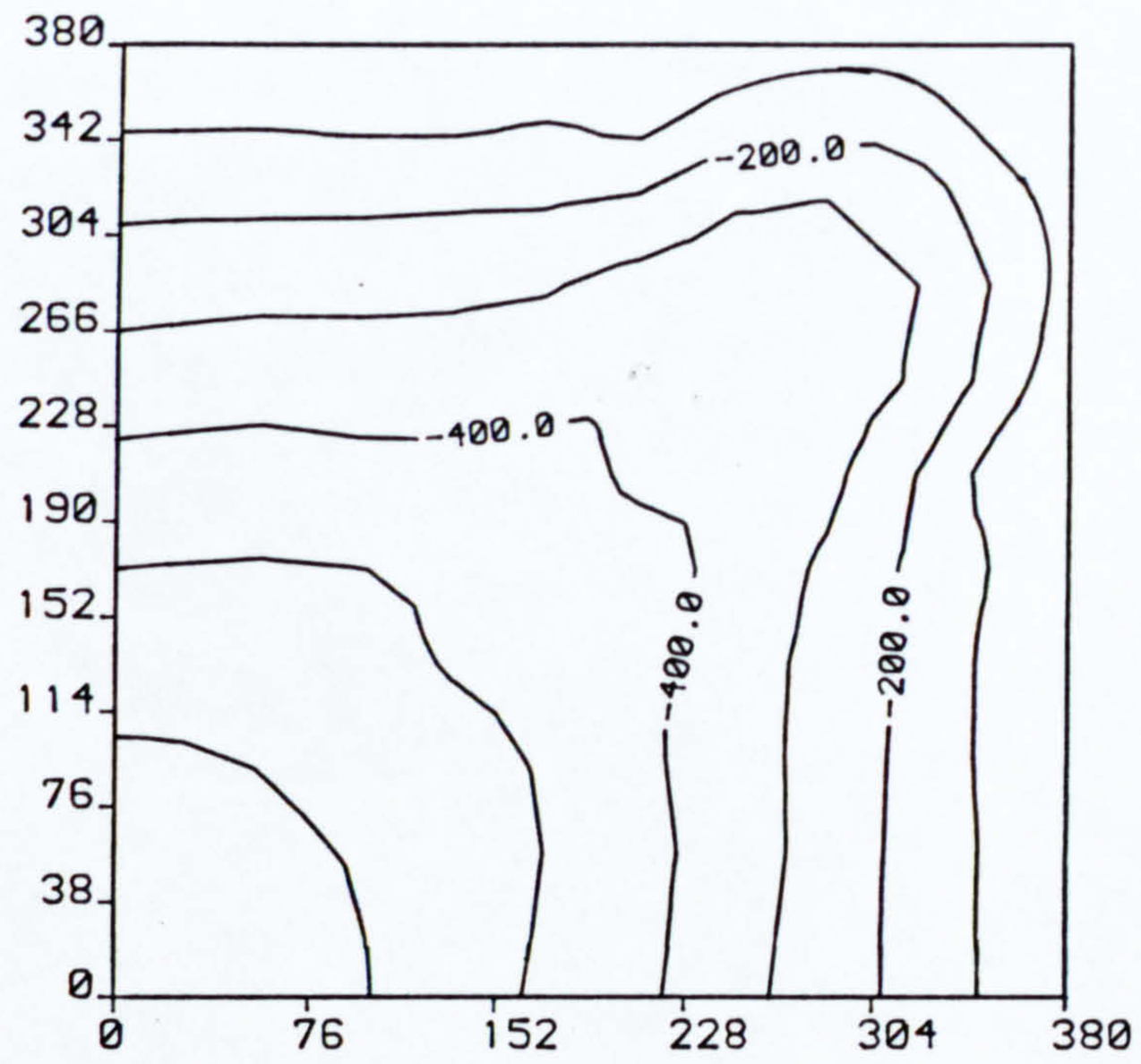

FIG.7.24 CONTOUR OF MXY FOR S24P1 ACM
AT TOTAL VERTICAL LOAD= 7042.5 N
(N-mm/mm)

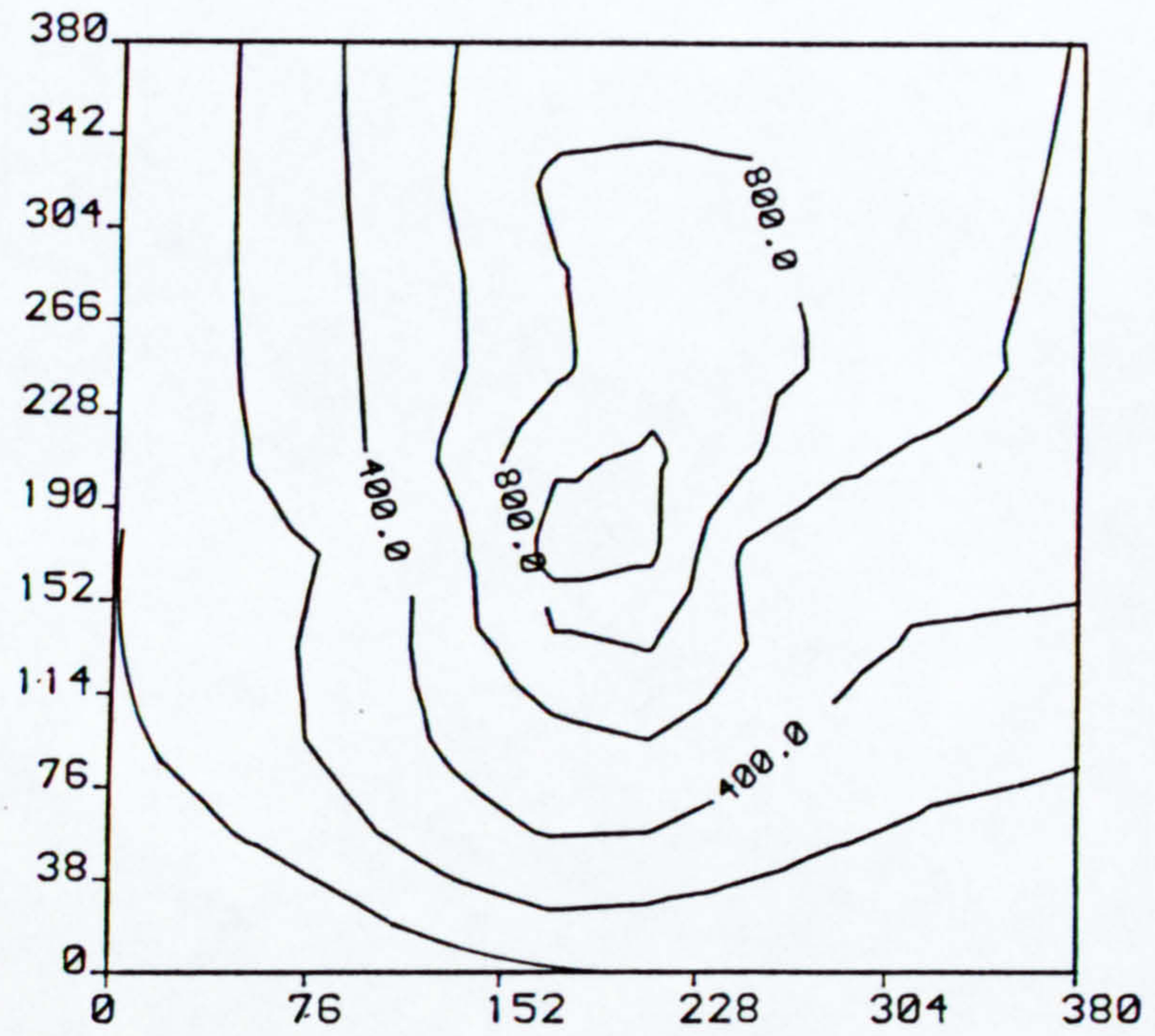

FIG. 7.25 CONTOUR OF MX FOR S34P4 ACM
AT TOTAL VERTICAL LOAD= 16620.7 N
(N-mm/mm)

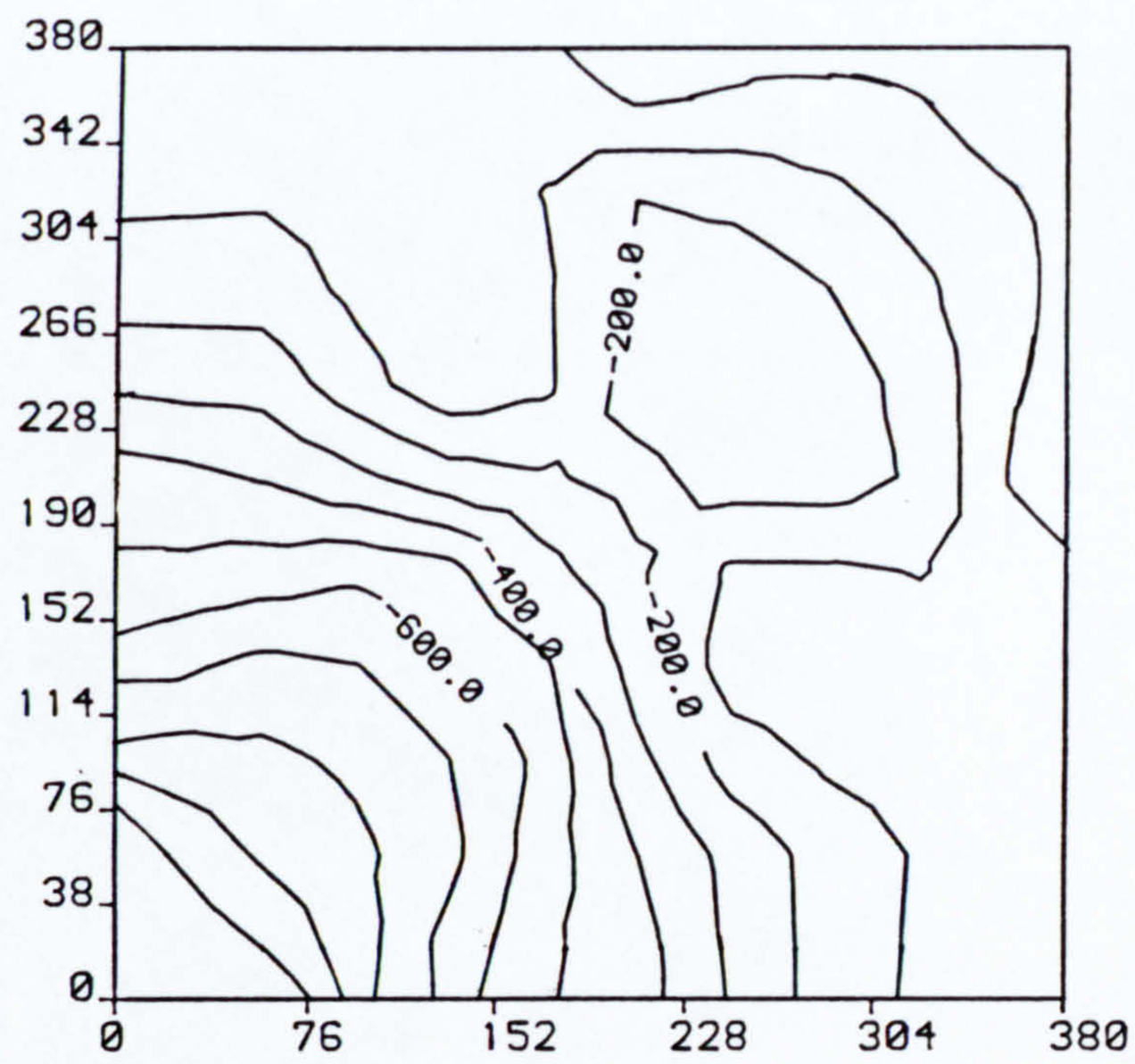

FIG. 7.26 CONTOUR OF MXY FOR S34P4 ACM
AT TOTAL VERTICAL LOAD= 16620.7 N
(N-mm/mm)

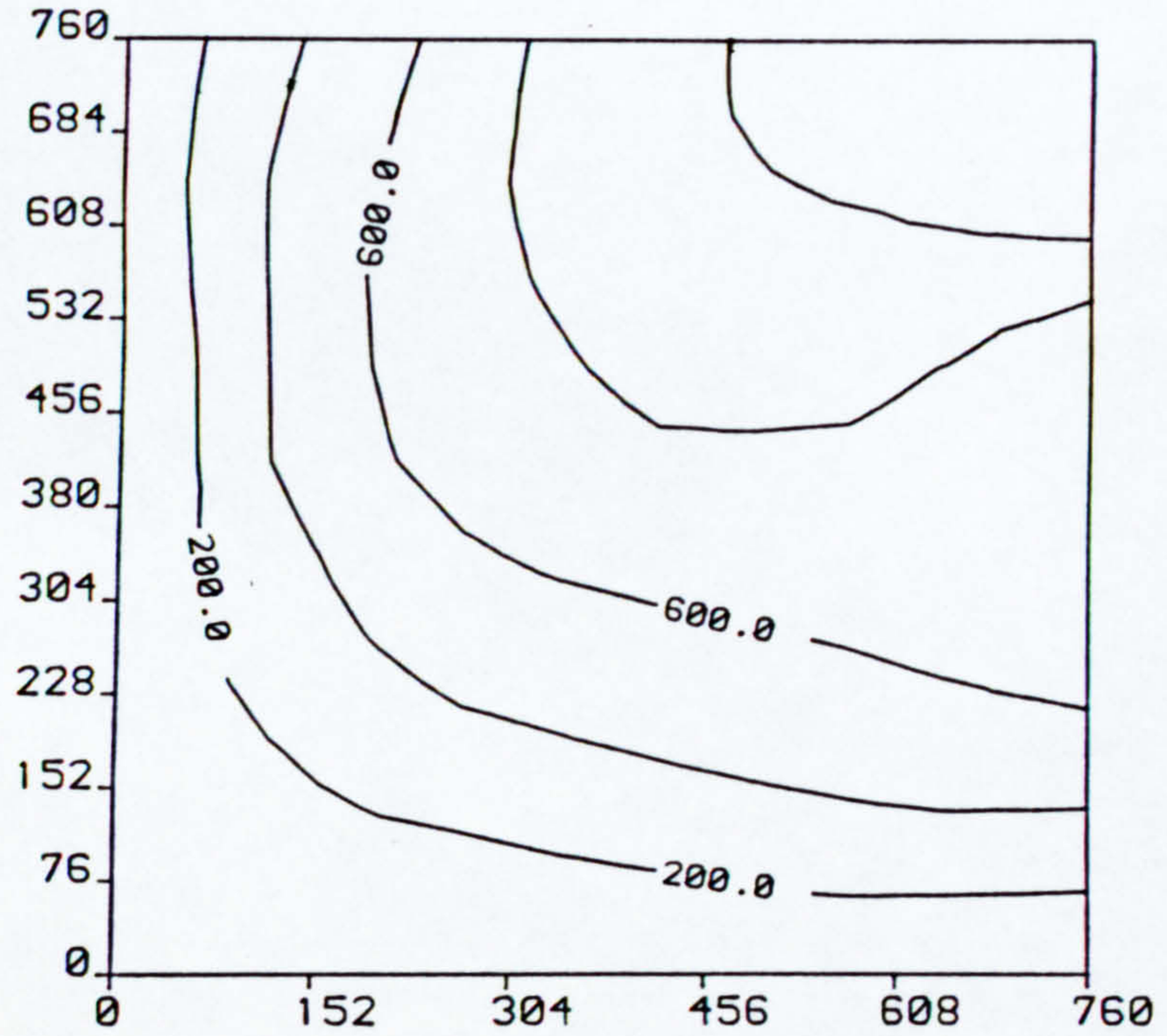

FIG.7.27 CONTOUR OF MX FOR S43UD ACM
AT TOTAL VERTICAL LOAD= 11958.2 N
(N-mm/mm)

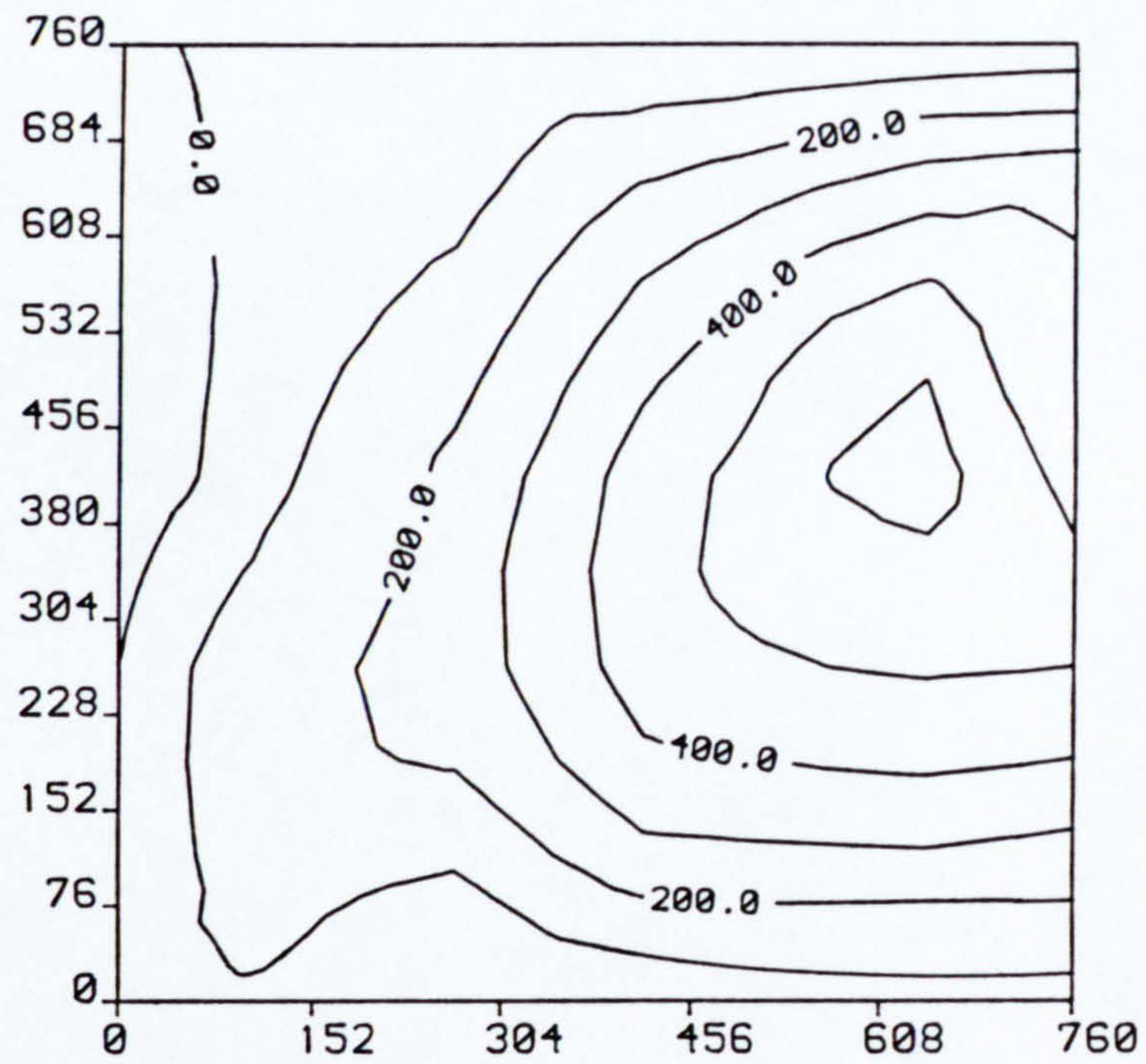

FIG.7.28 CONTOUR OF MY FOR S43UD ACM
AT TOTAL VERTICAL LOAD= 11958.2 N
(N-mm/mm)

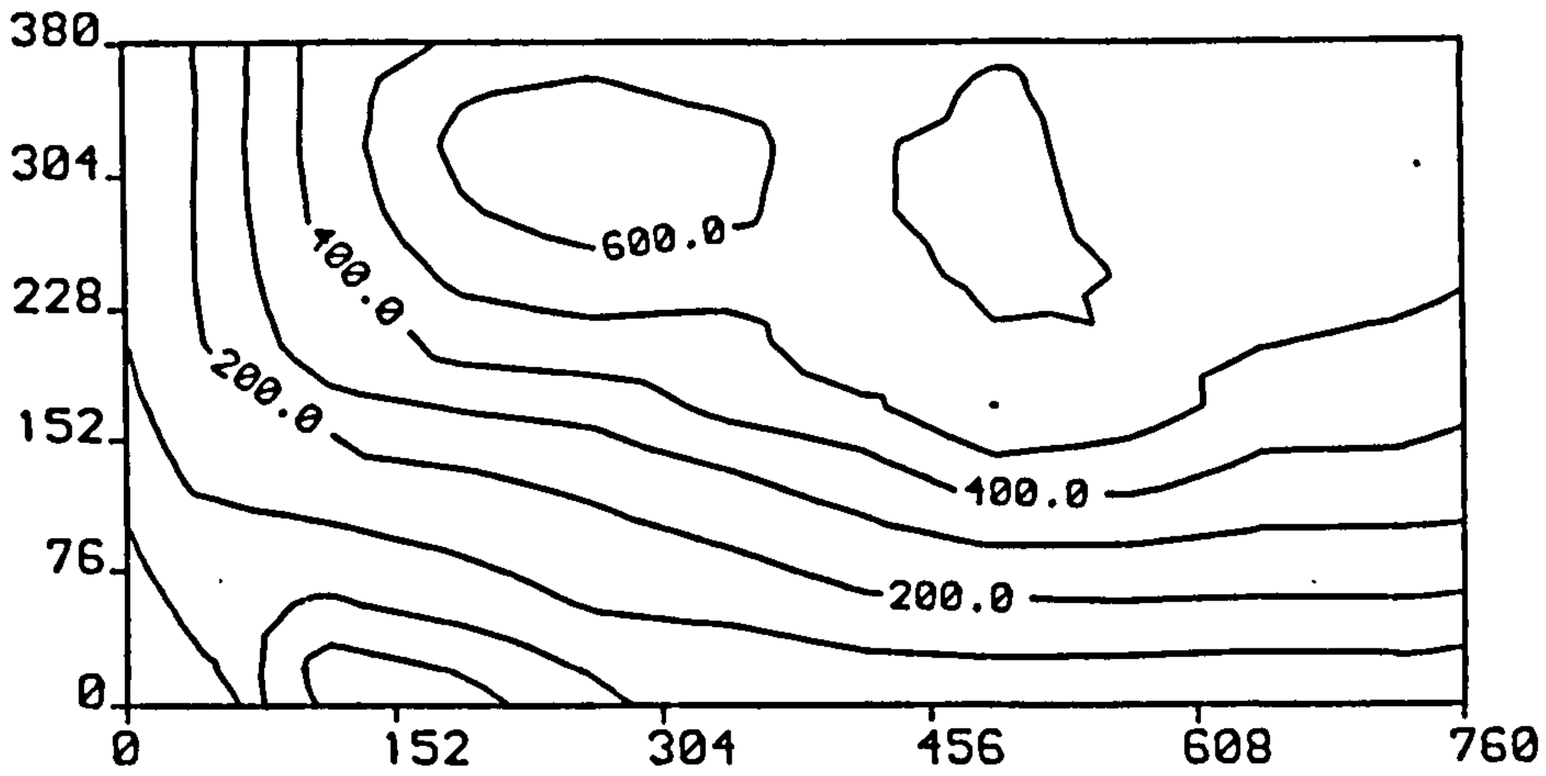

FIG. 7.29 CONTOUR OF MX FOR S54UD ACM
AT TOTAL VERTICAL LOAD = 38881.5 N
(N-mm/mm)

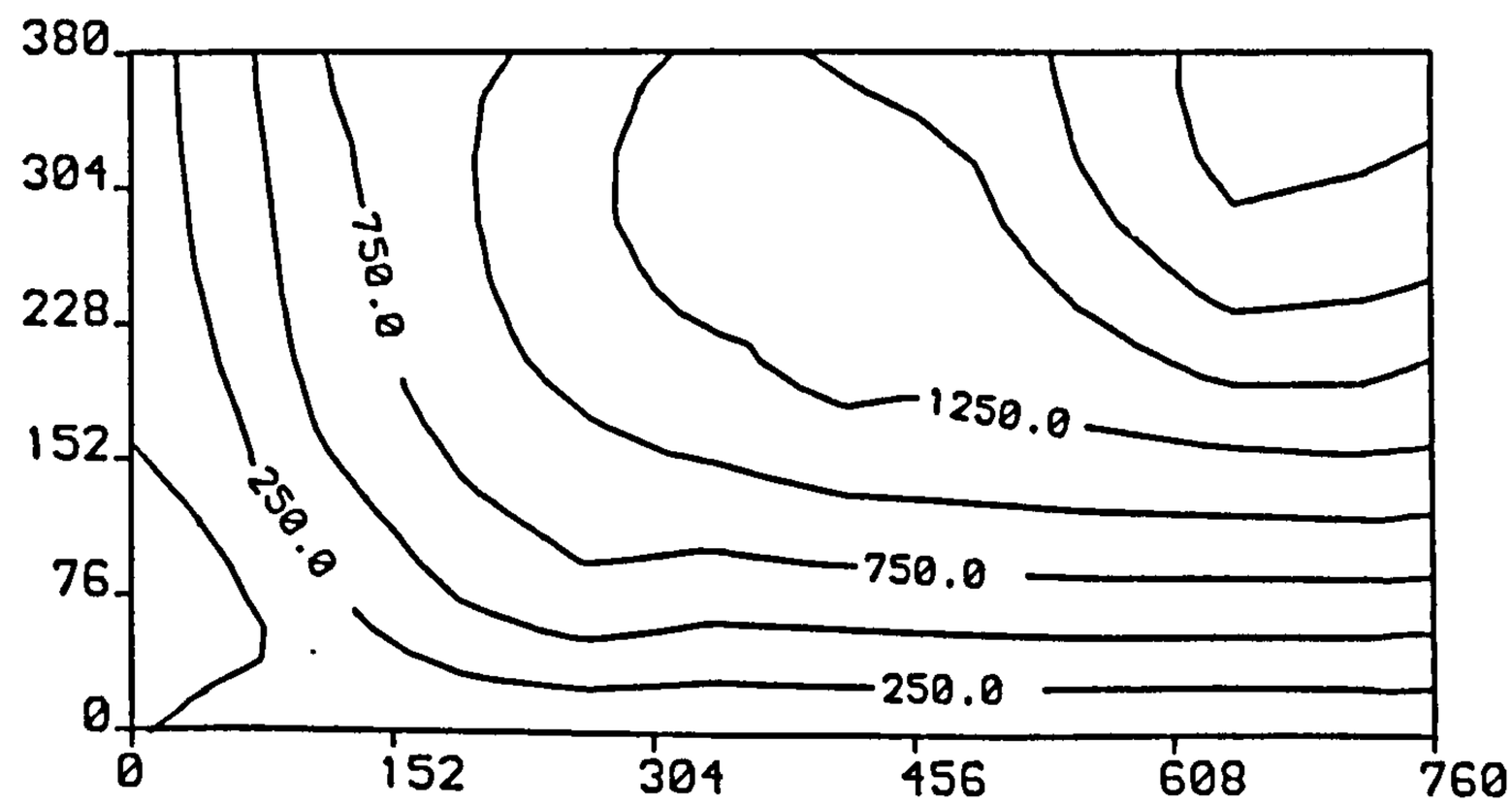

FIG. 7.30 CONTOUR OF MY FOR S54UD ACM
AT TOTAL VERTICAL LOAD = 38881.5 N
(N-mm/mm)

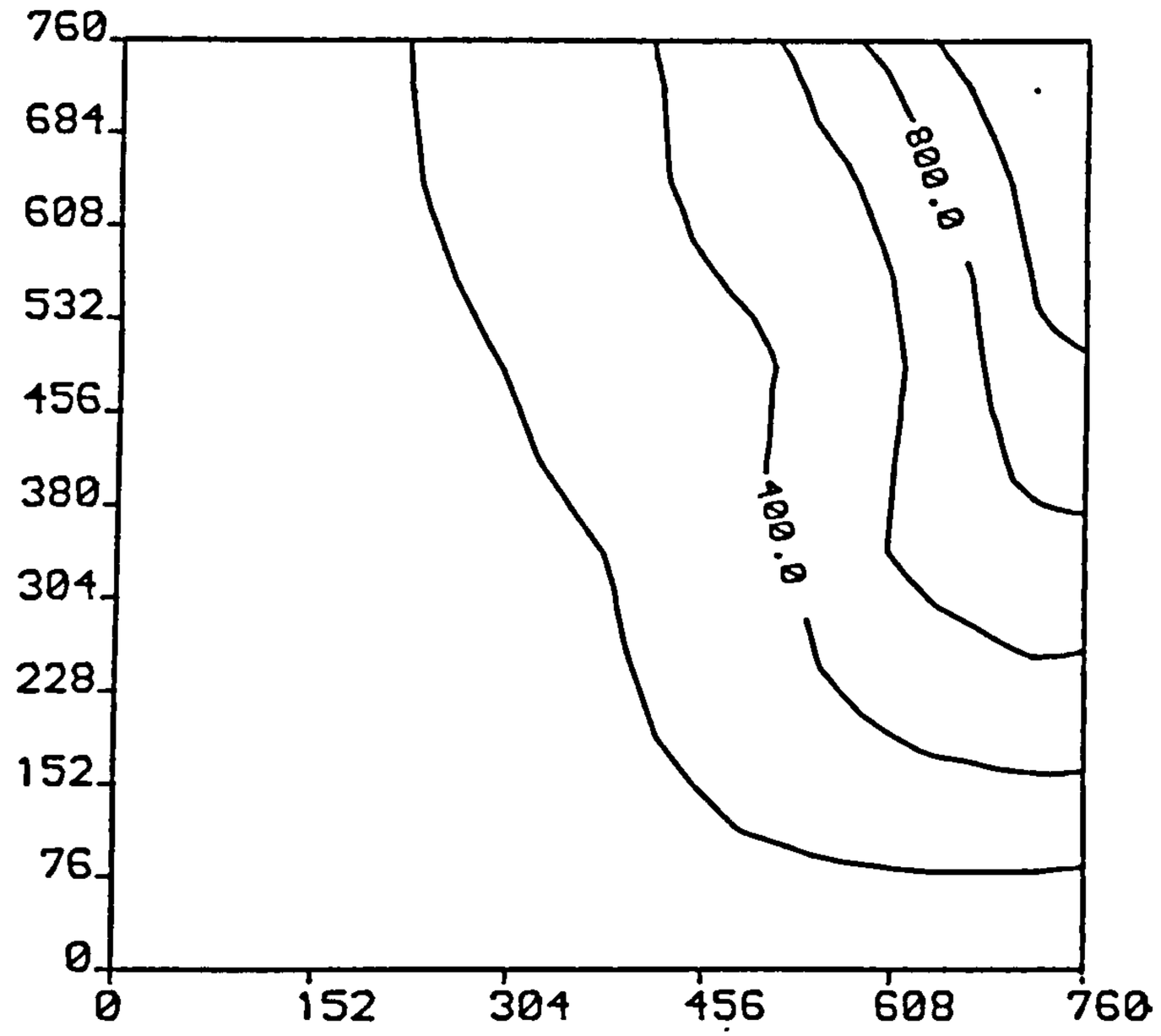

FIG.7.31 CONTOUR OF MX FOR S63P1 ACM
AT TOTAL VERTICAL LOAD= 3763.4 N
(N-mm/mm)

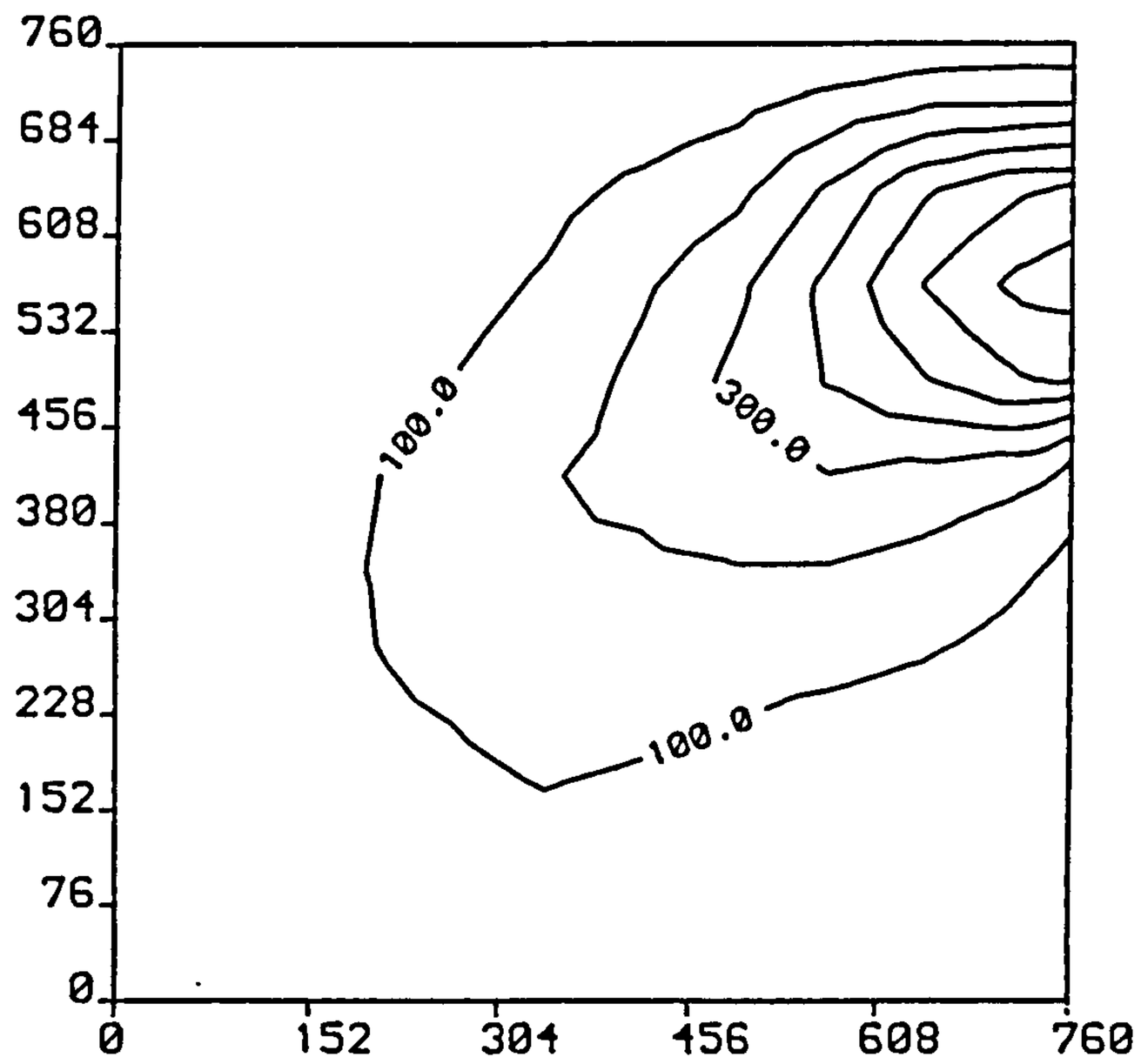

FIG.7.32 CONTOUR OF MY FOR S63P1 ACM
AT TOTAL VERTICAL LOAD= 3763.4 N
(N-mm/mm)

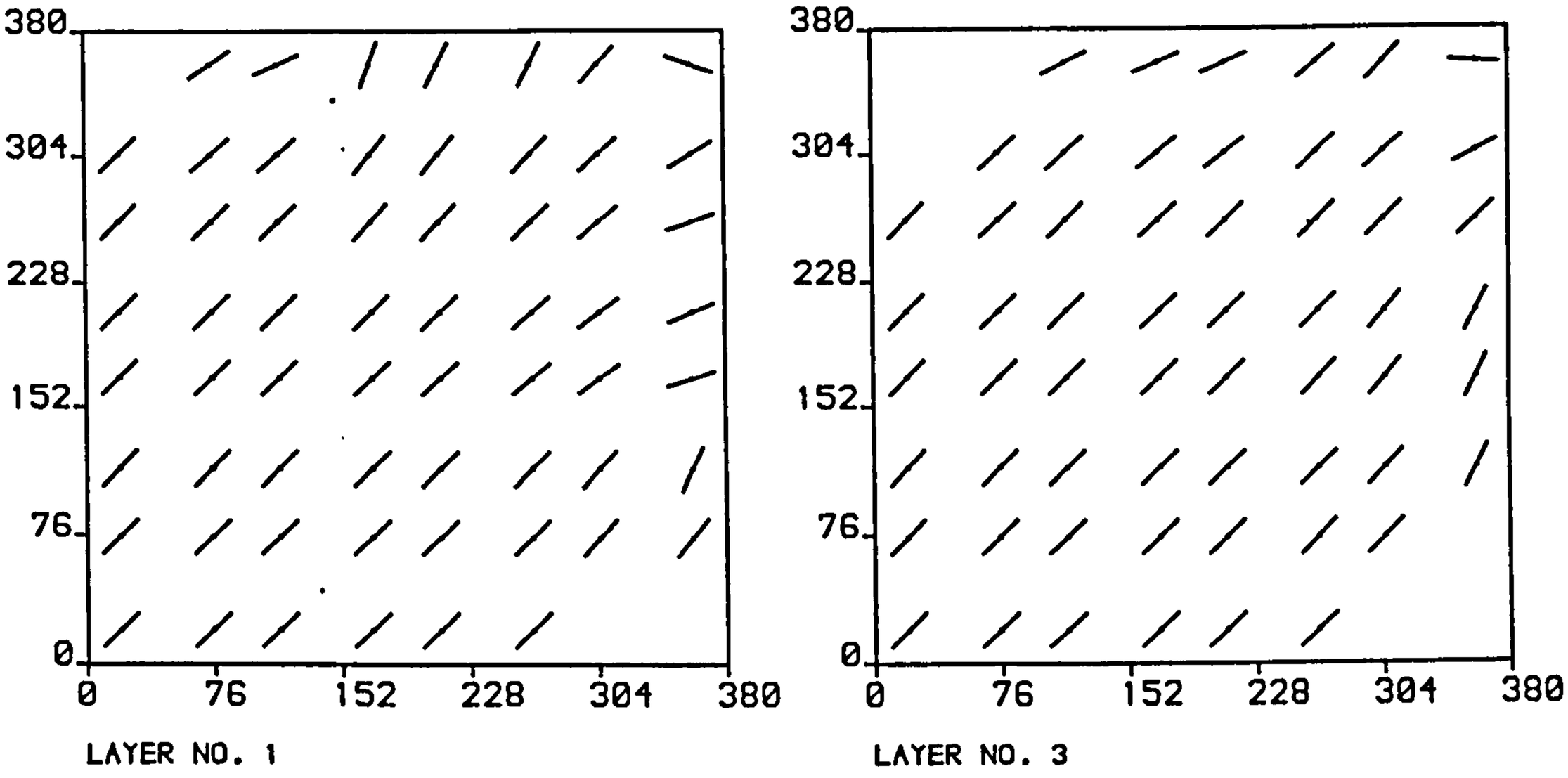

FIG.7.33a CRACK PATTERN FOR SLAB S14UD ACM
AT TOTAL LOAD = 32050.9 N

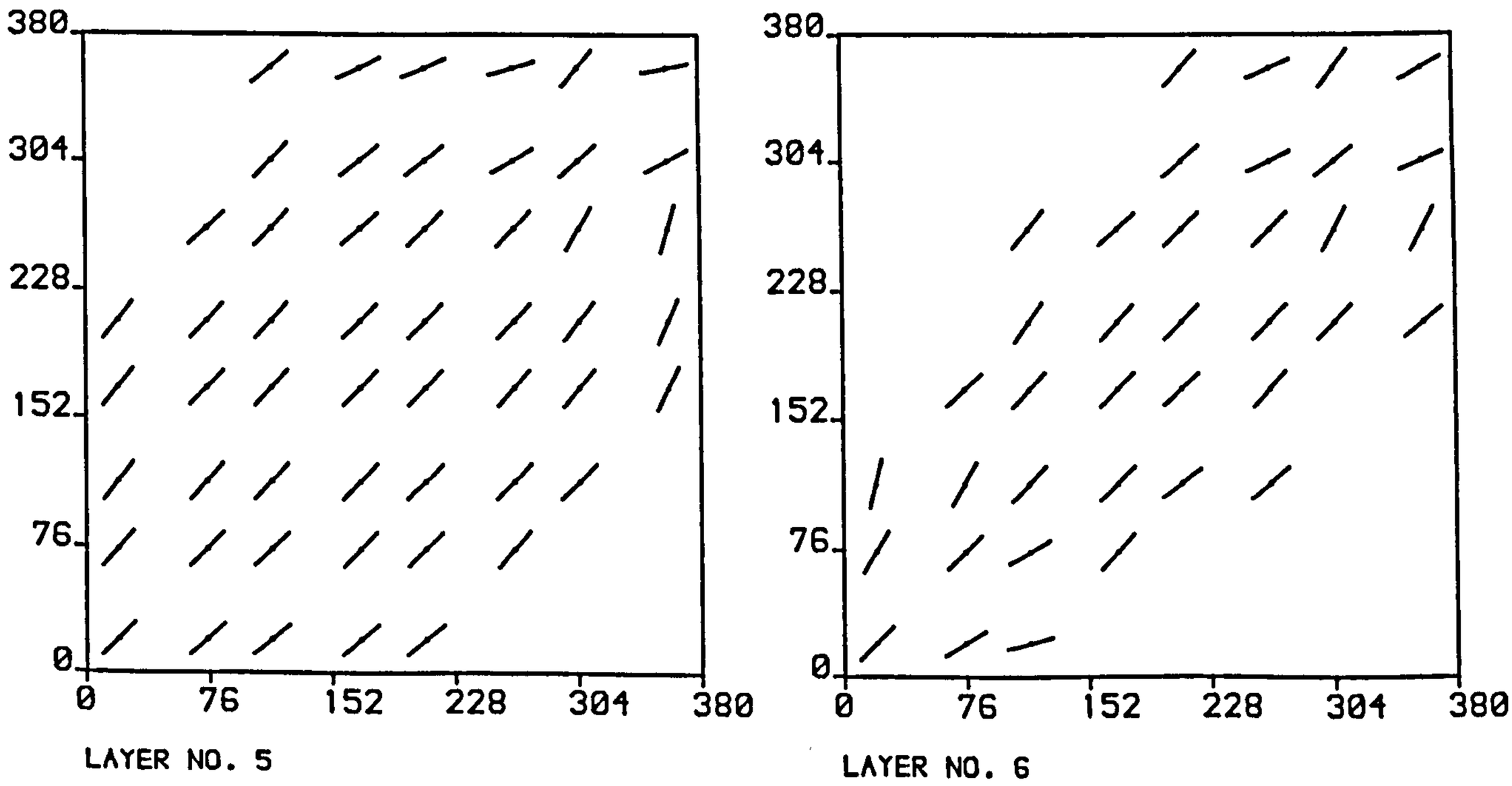

FIG.7.33b CRACK PATTERN FOR SLAB S14UD ACM
AT TOTAL LOAD = 32050.9 N

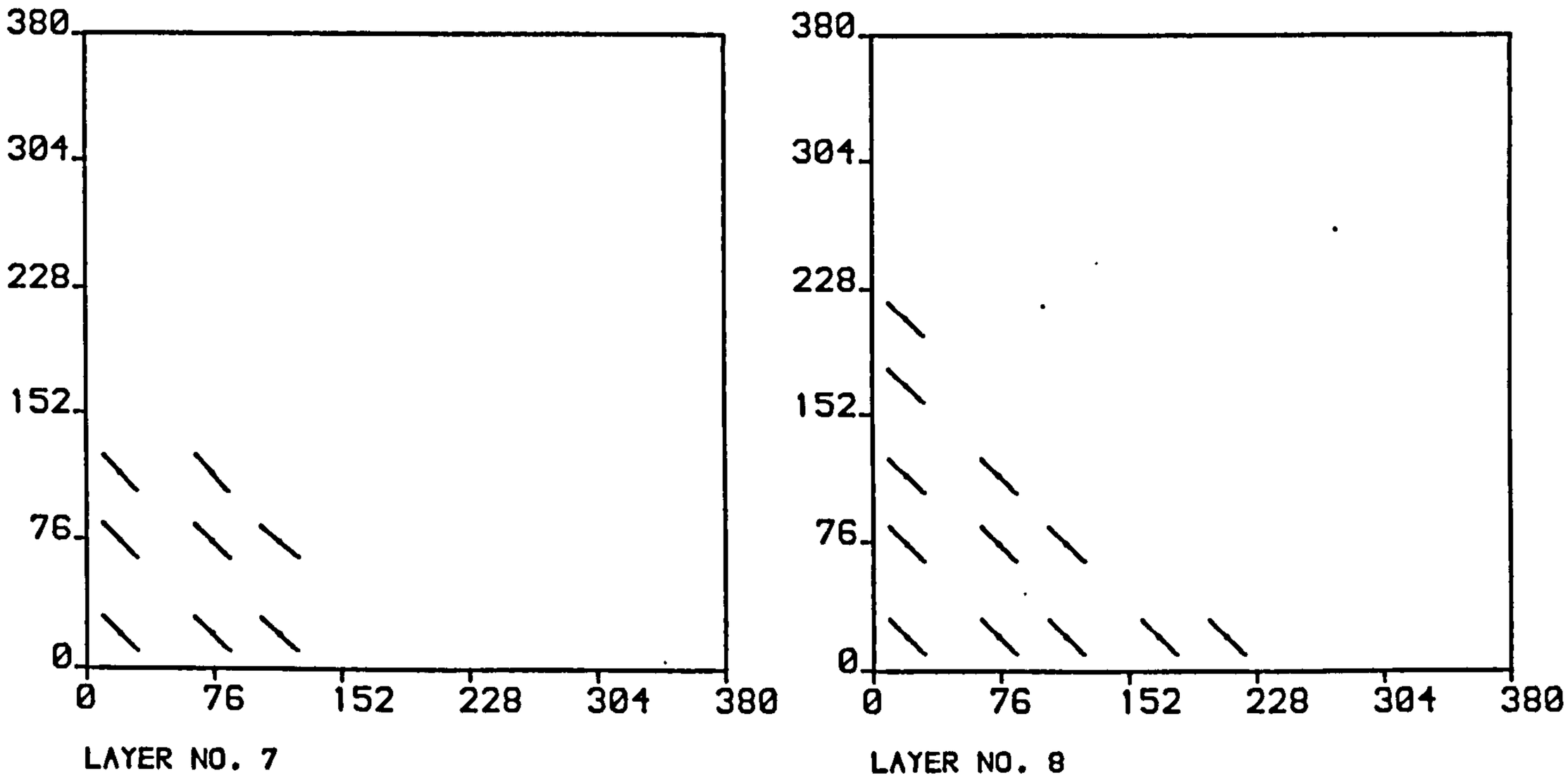

FIG. 7.33c CRACK PATTERN FOR SLAB S14UD ACM
AT TOTAL LOAD = 32050.9 N

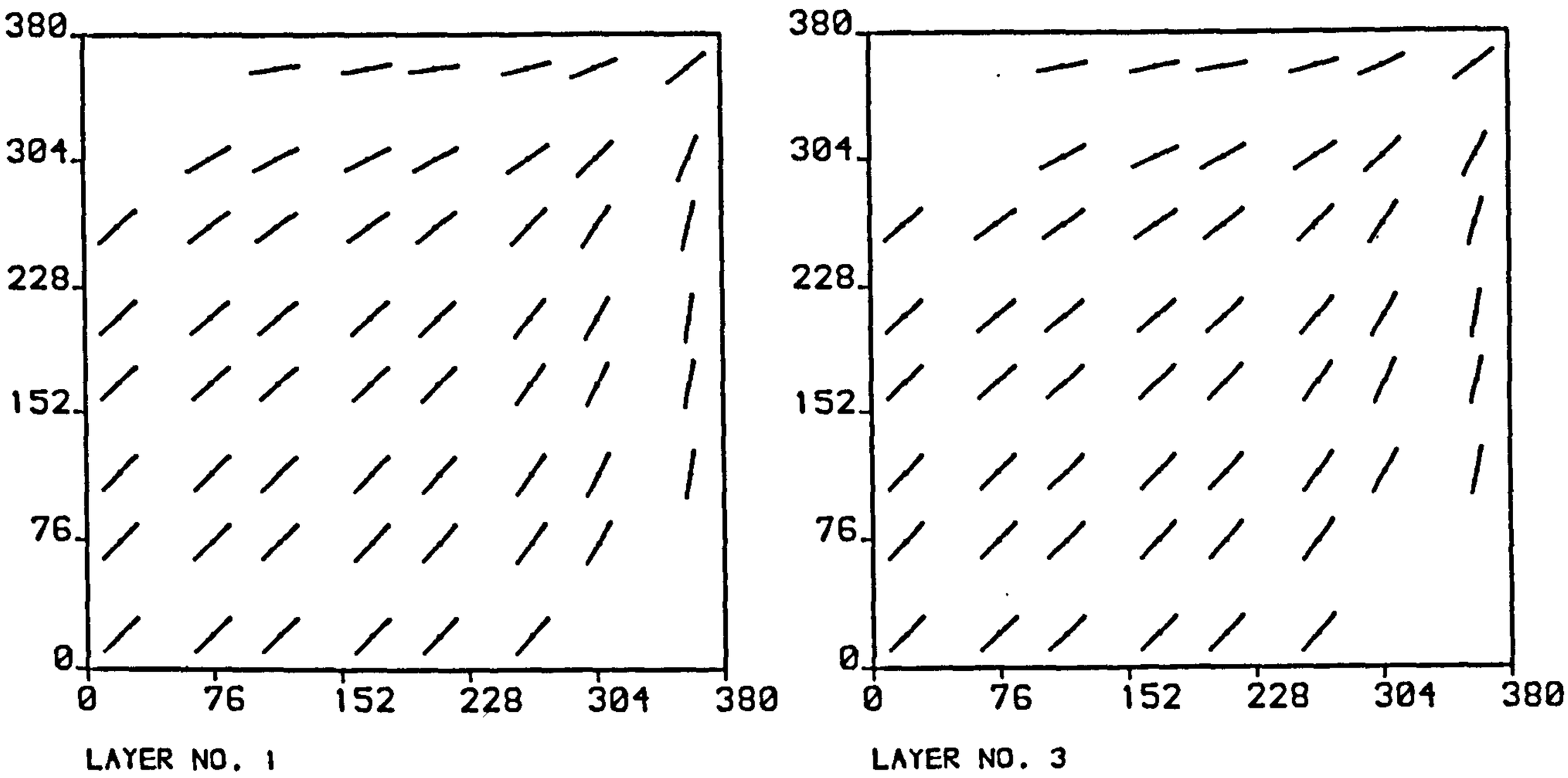

FIG. 7.34a CRACK PATTERN FOR SLAB S24P1 ACM
AT TOTAL LOAD = 9208.5 N

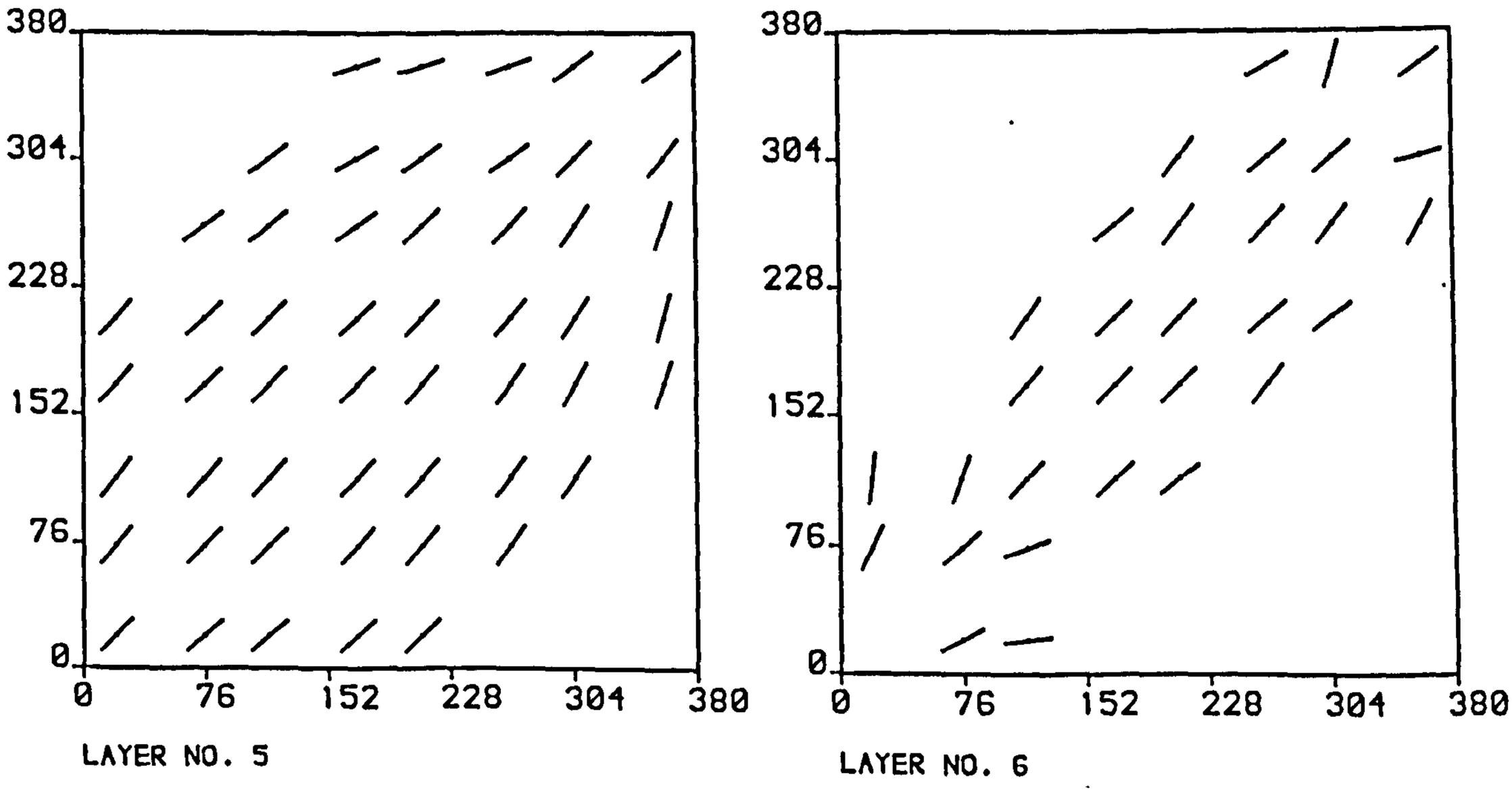

FIG. 7.34b CRACK PATTERN FOR SLAB S24P1 ACM
AT TOTAL LOAD = 9208.5 N

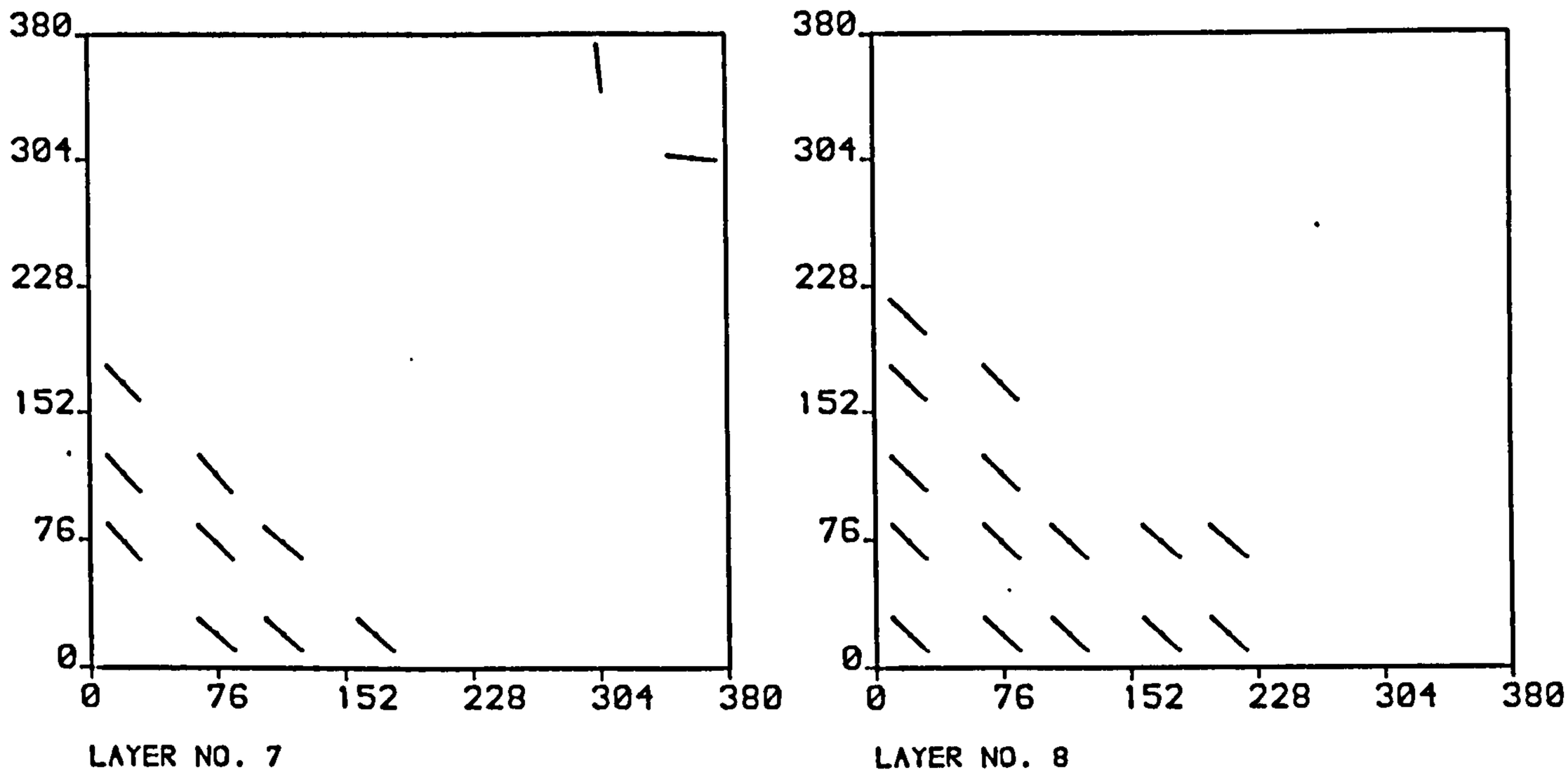

FIG. 7.34c CRACK PATTERN FOR SLAB S24P1 ACM
AT TOTAL LOAD = 9208.5 N

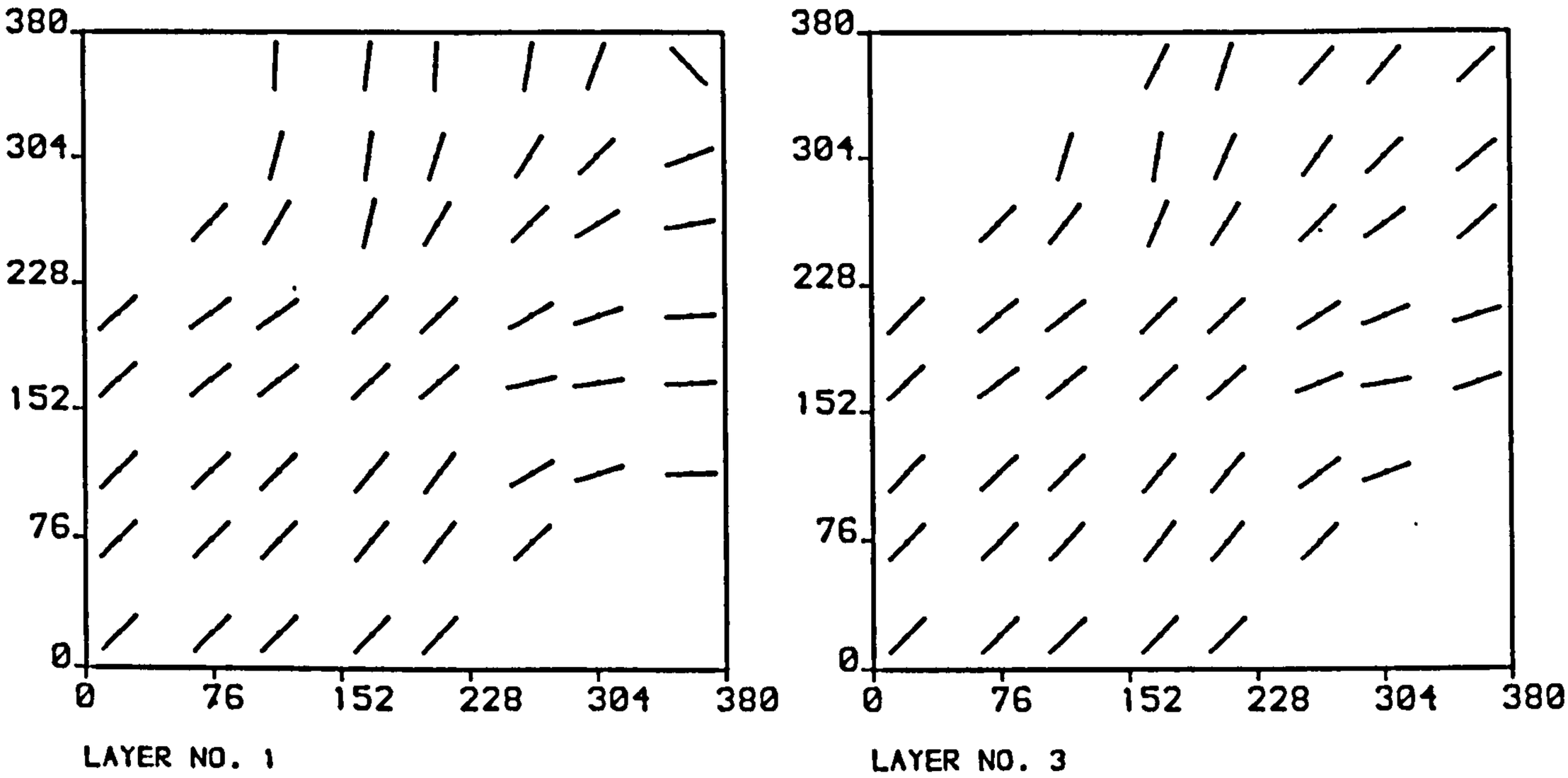

FIG. 7.35a CRACK PATTERN FOR SLAB S34P4 ACM
AT TOTAL LOAD = 22262.6 N

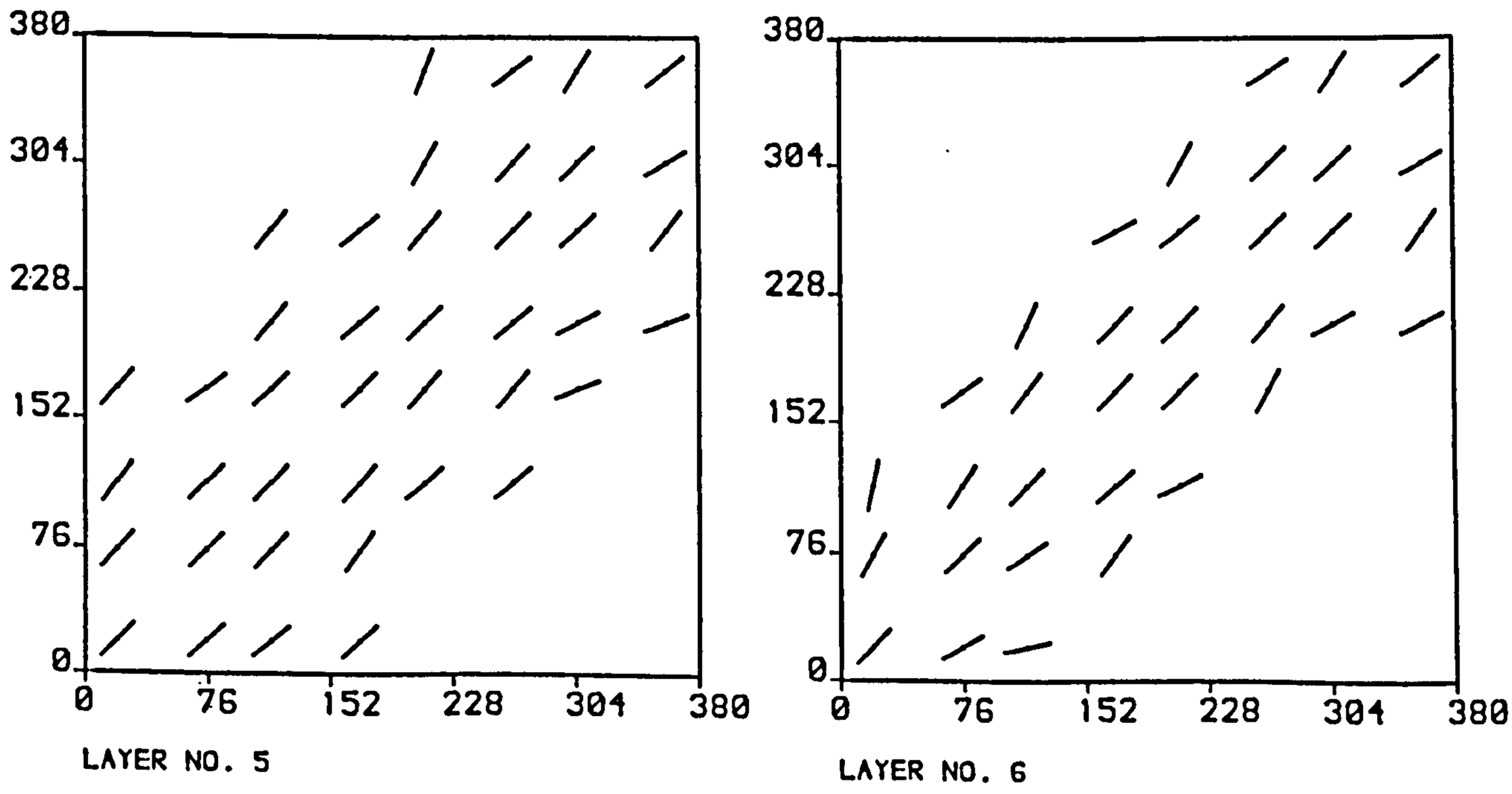

FIG. 7.35b CRACK PATTERN FOR SLAB S34P4 ACM
AT TOTAL LOAD = 22262.6 N

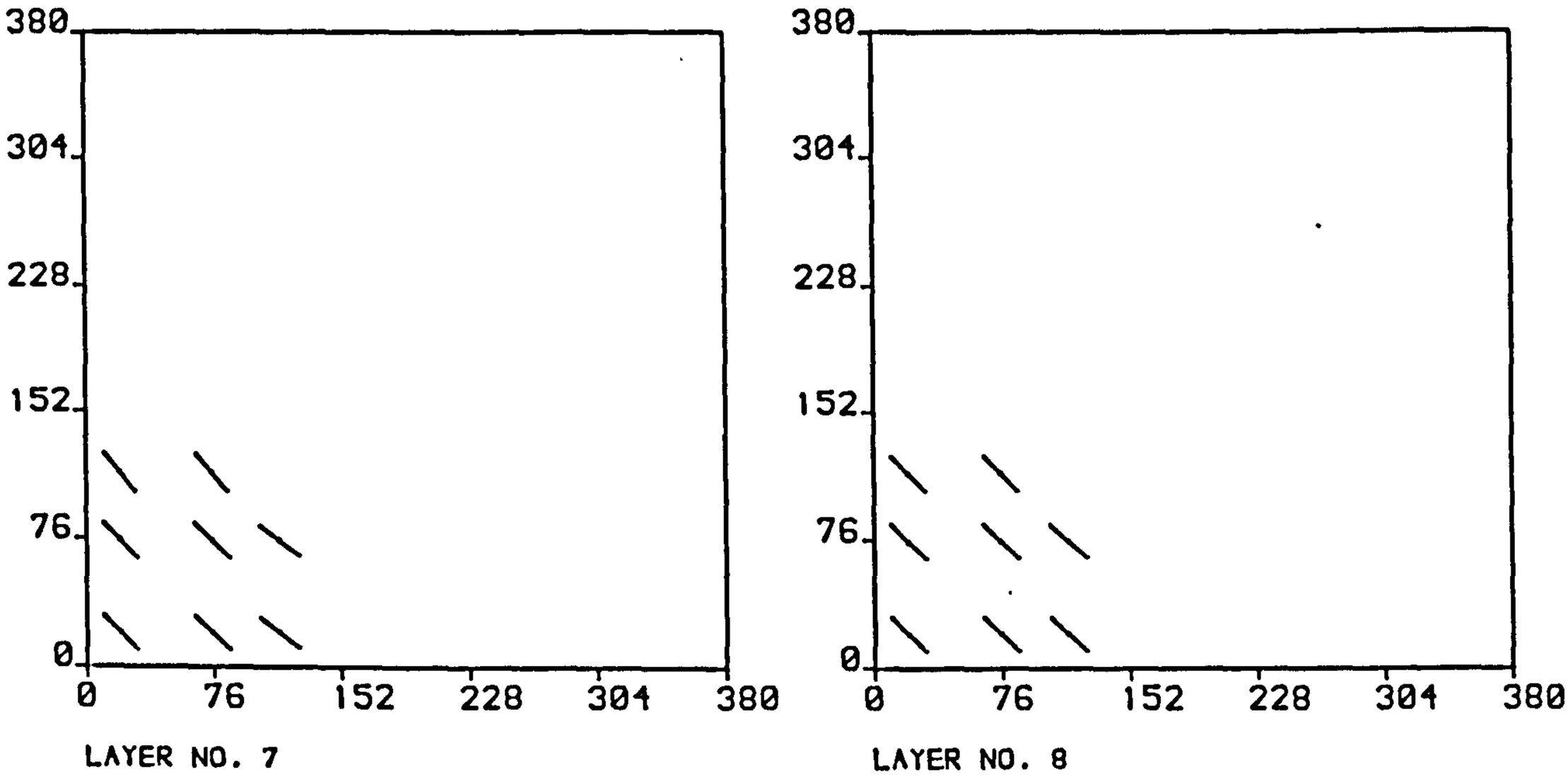

FIG.7.35c CRACK PATTERN FOR SLAB S34P4 ACM
AT TOTAL LOAD = 22262.6 N

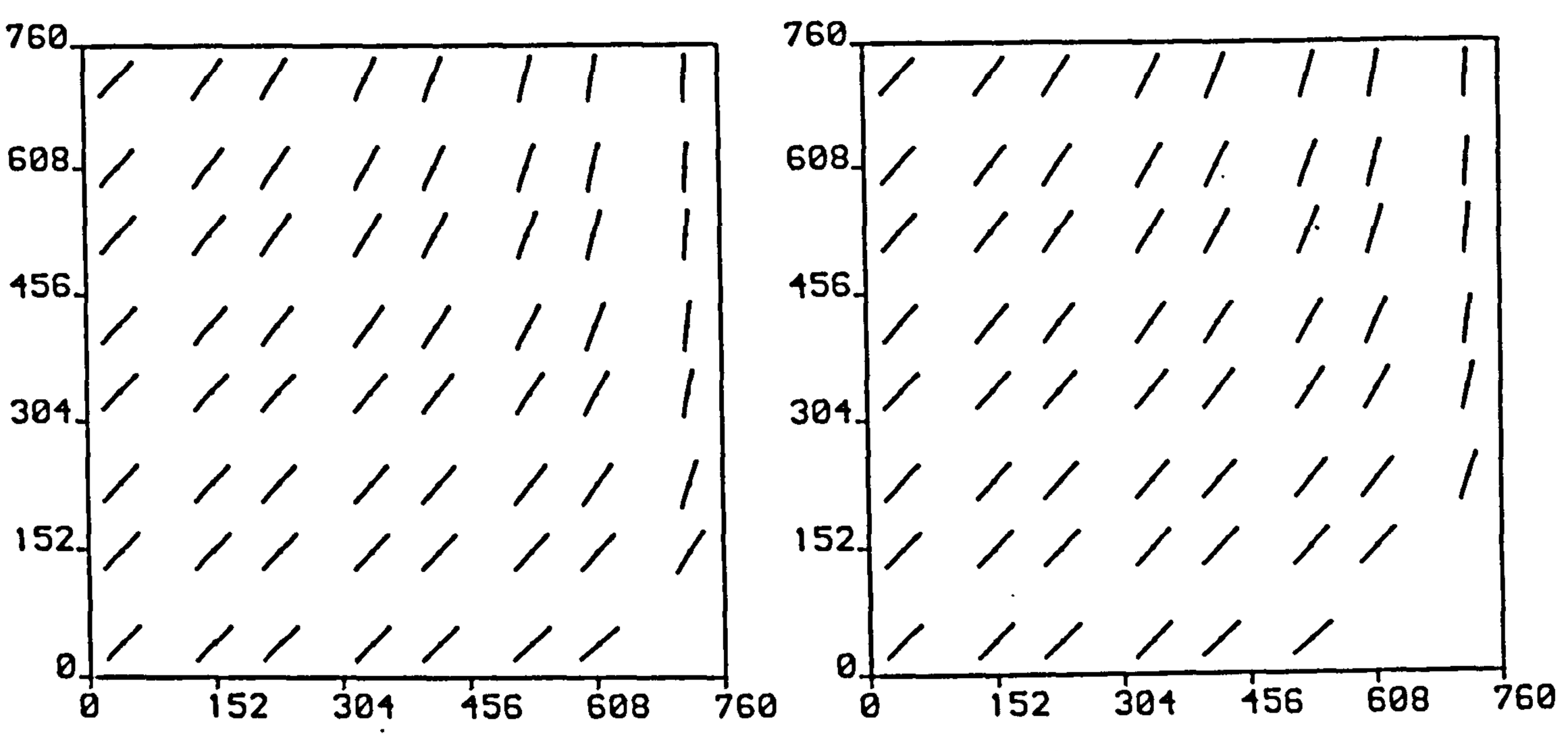

FIG. 7.36a CRACK PATTERN FOR SLAB S43UD ACM
AT TOTAL LOAD = 14866.7 N

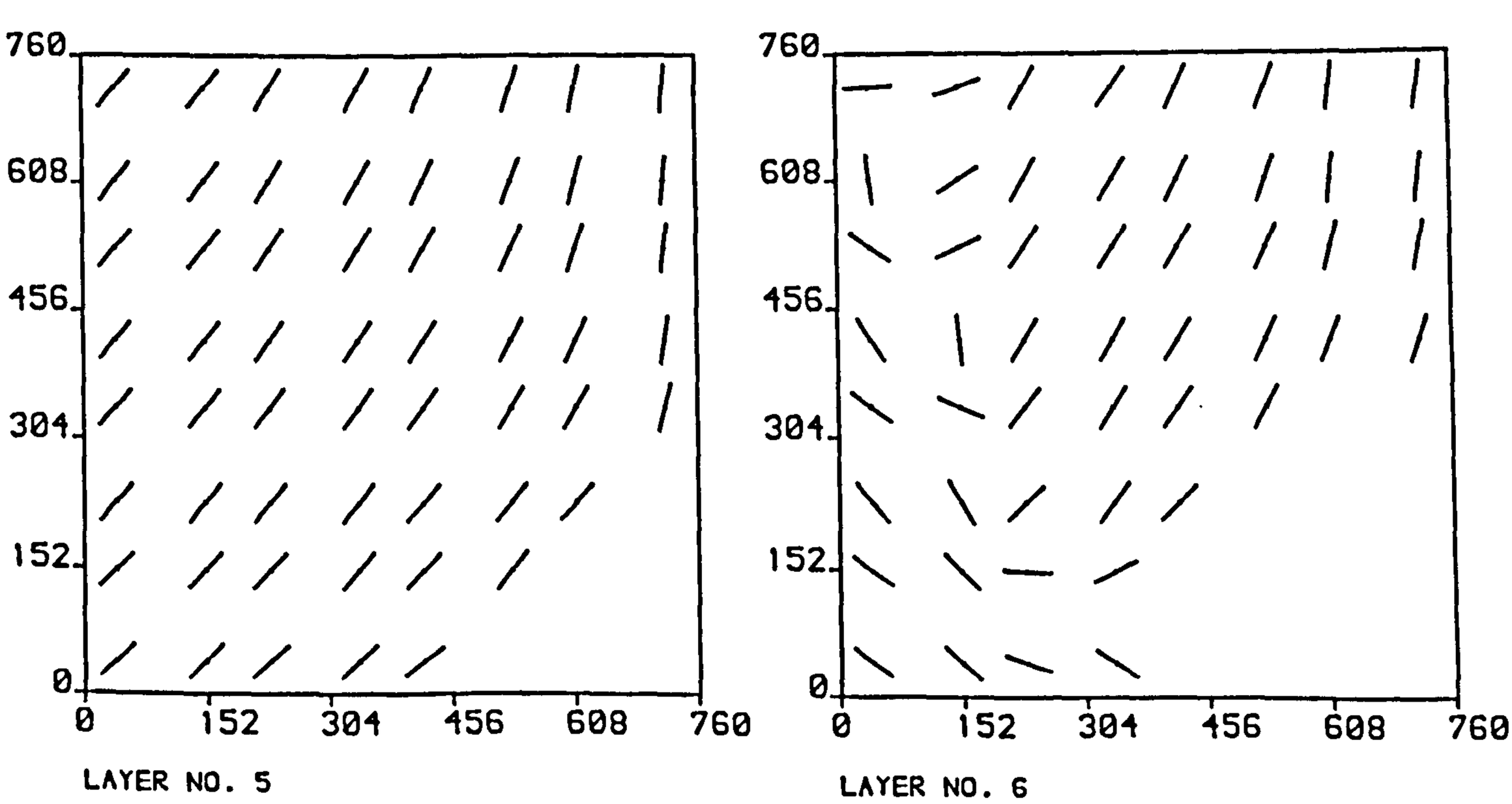

FIG. 7.36b CRACK PATTERN FOR SLAB S43UD ACM
AT TOTAL LOAD = 14866.7 N

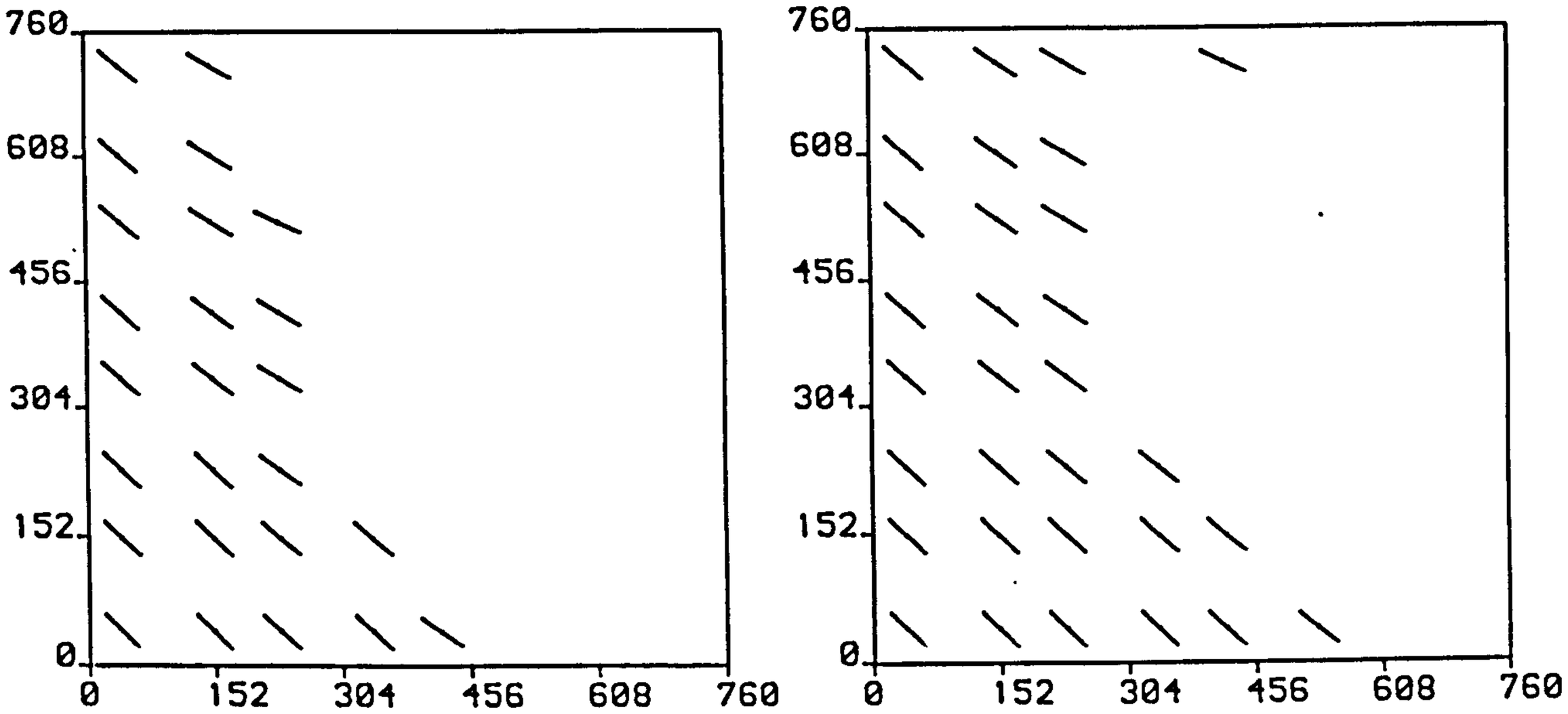

FIG. 7.36c CRACK PATTERN FOR SLAB S43UD ACM
AT TOTAL LOAD = 14866.7 N

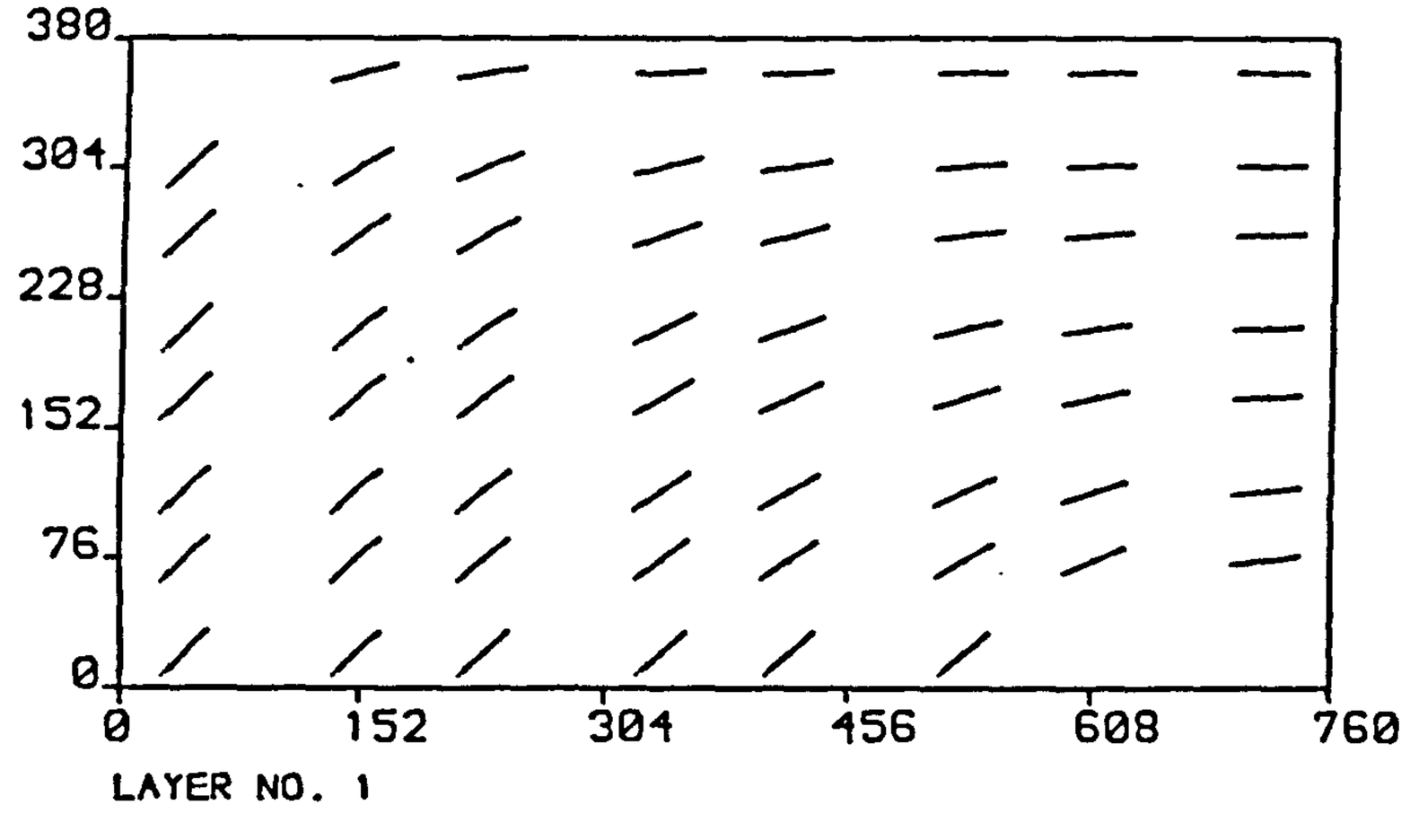

FIG.7.37a CRACK PATTERN FOR SLAB S54UD ACM AT TOTAL VERT. LOAD = 48319.3 N

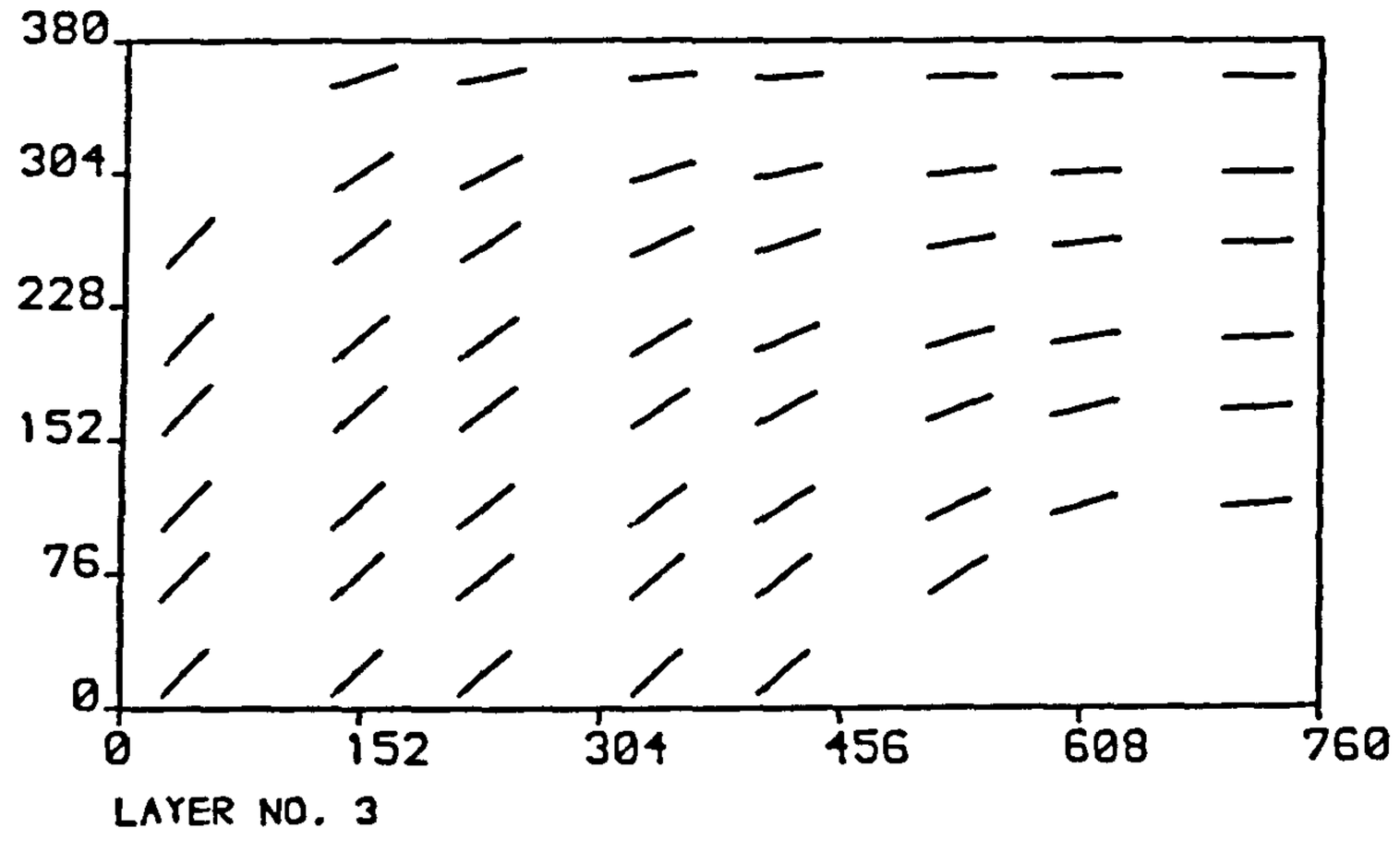

FIG.7.37b CRACK PATTERN FOR SLAB S54UD ACM AT TOTAL VERT. LOAD = 48319.3 N

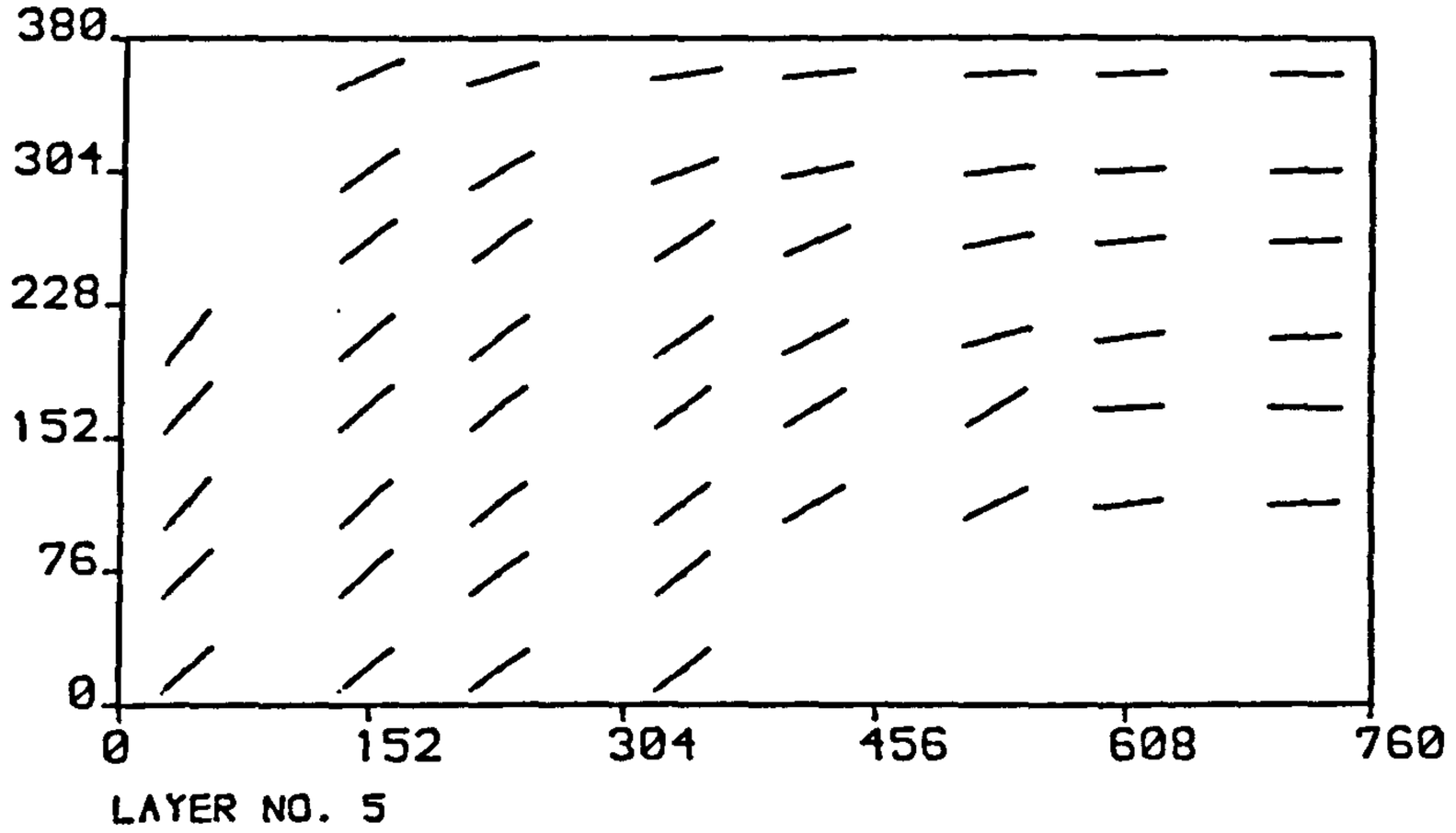

FIG.7.37c CRACK PATTERN FOR SLAB S54UD ACM AT TOTAL VERT. LOAD = 48319.3 N

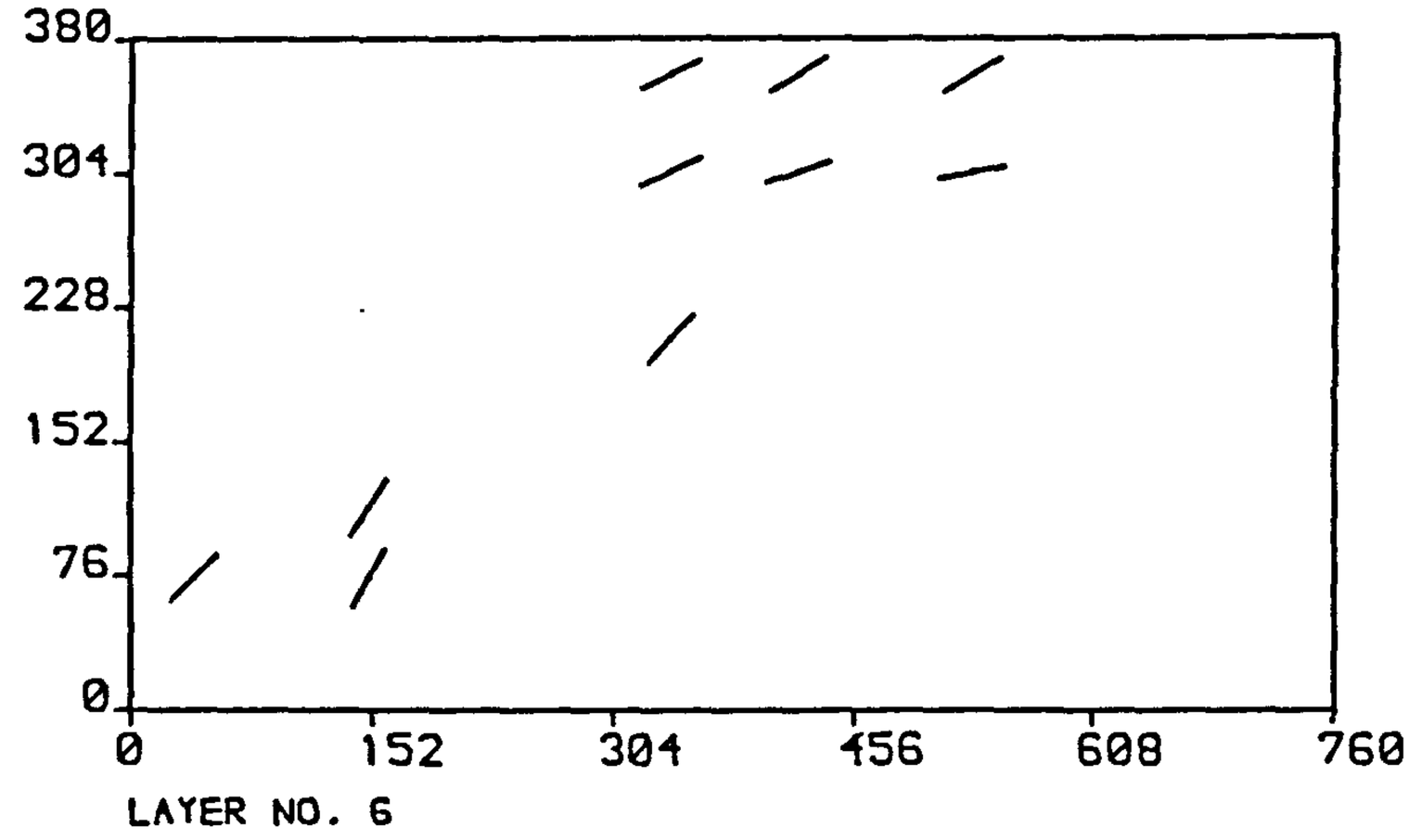

FIG.7.37d CRACK PATTERN FOR SLAB S54UD ACM AT TOTAL VERT. LOAD = 48319.3 N

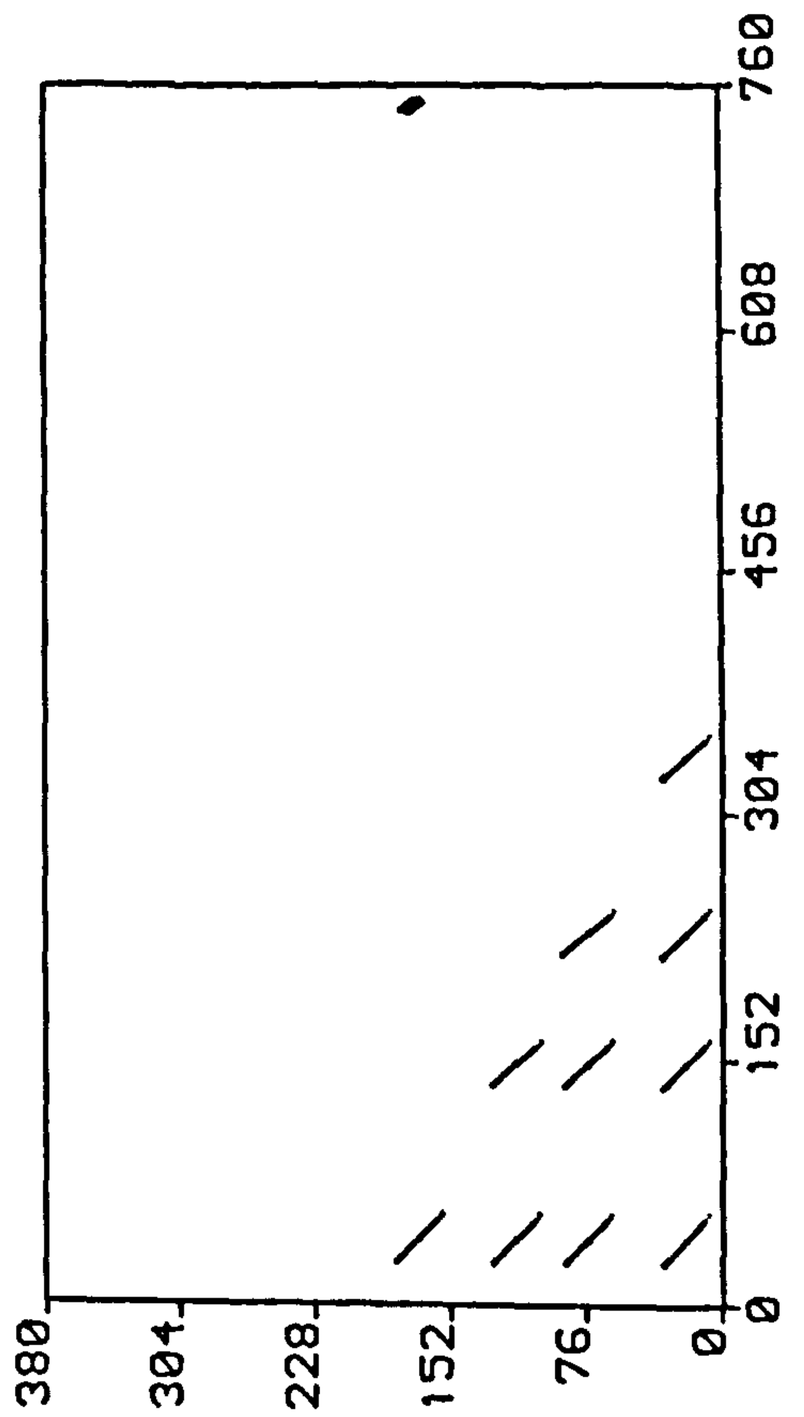

FIG. 7.37f CRACK PATTERN FOR SLAB S54UD ACM
AT TOTAL VERT. LOAD = 48319.3 N

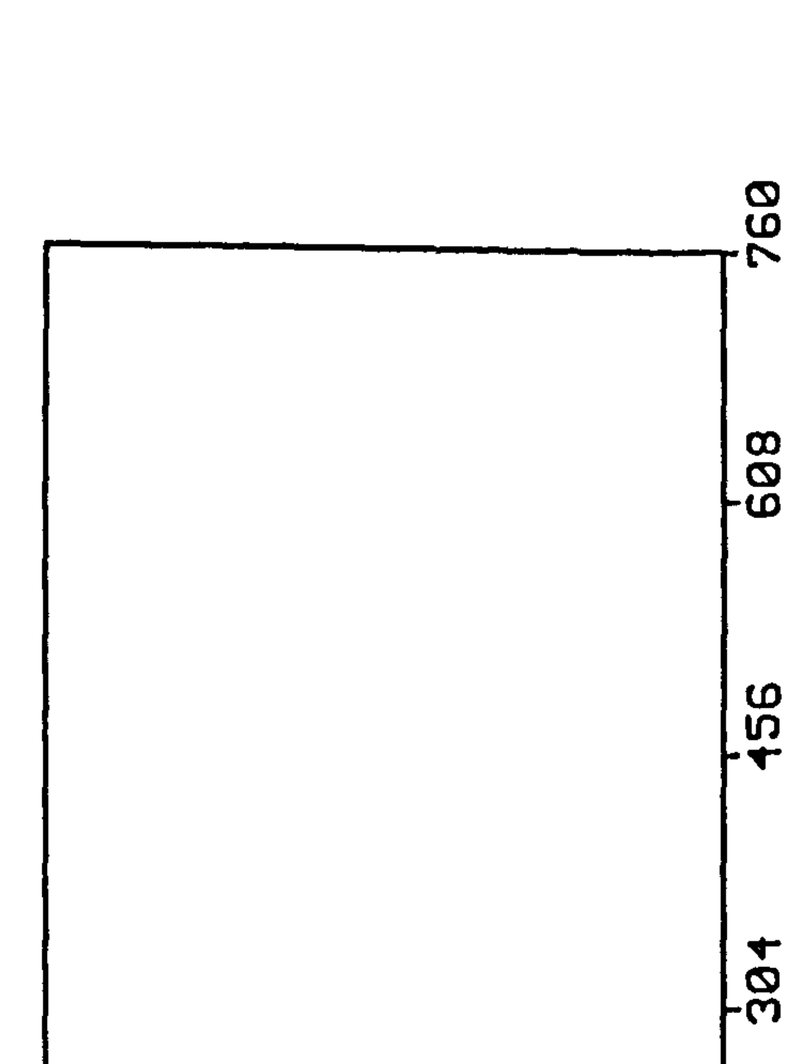

FIG. 7.37e CRACK PATTERN FOR SLAB S54UD ACM
AT TOTAL VERT. LOAD = 48319.3 N

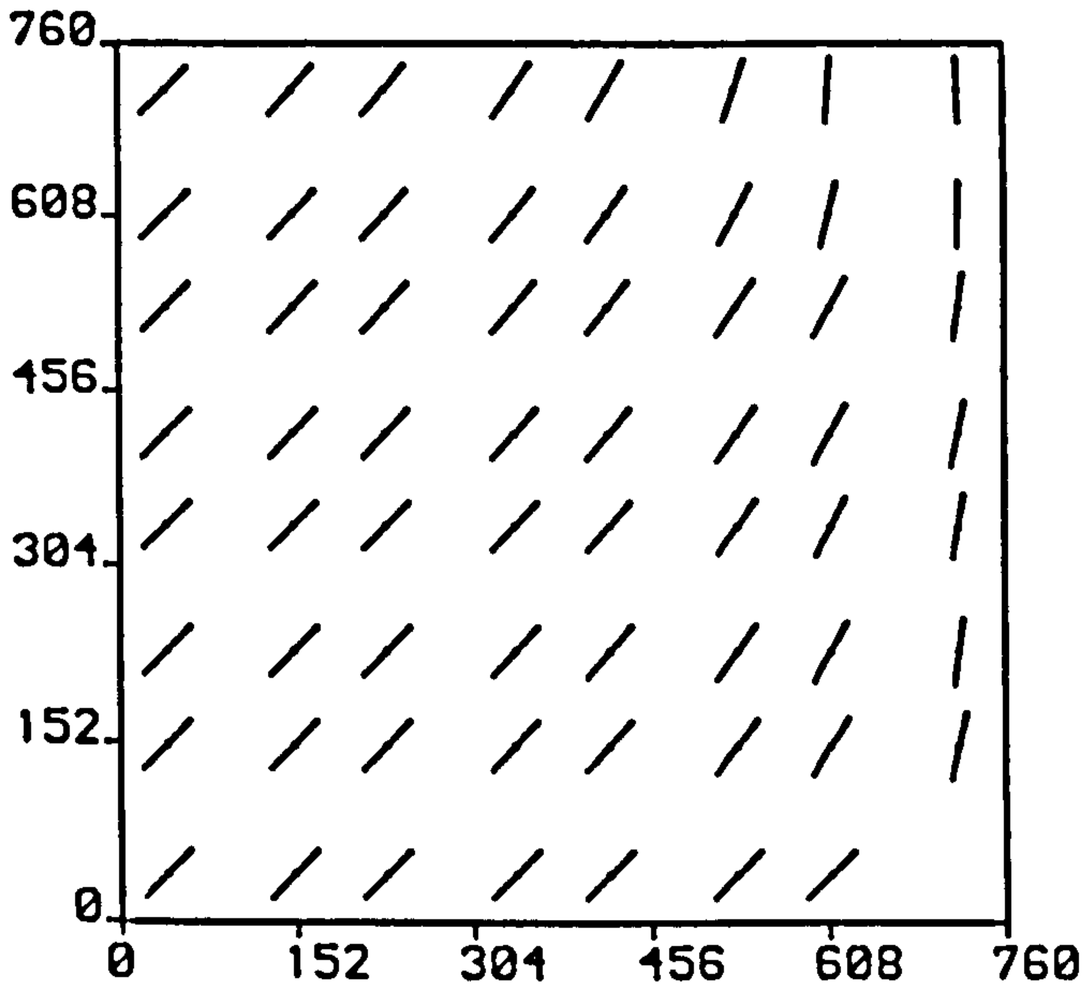

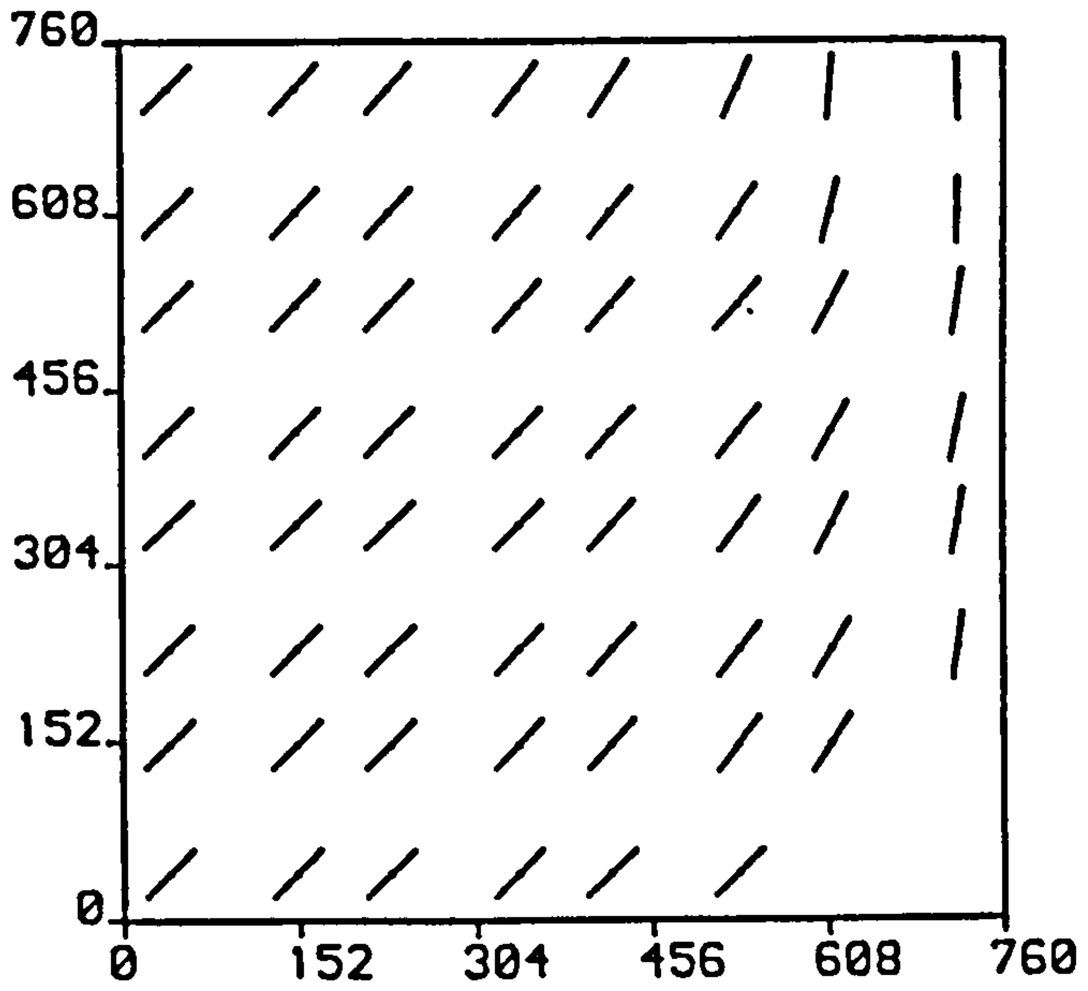

FIG.7.38a CRACK PATTERN FOR SLAB S63P1 ACM AT TOTAL LOAD = 4811.4 N

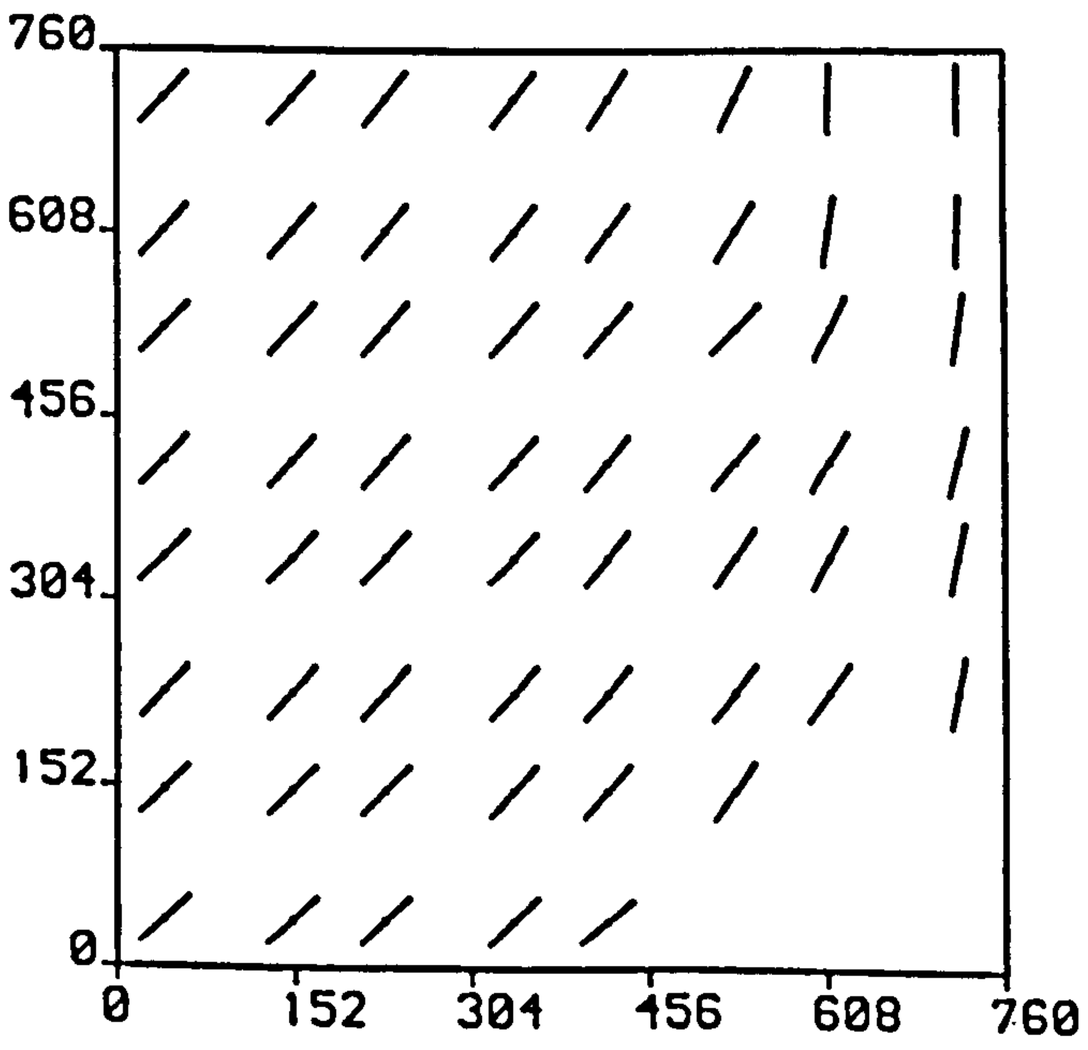

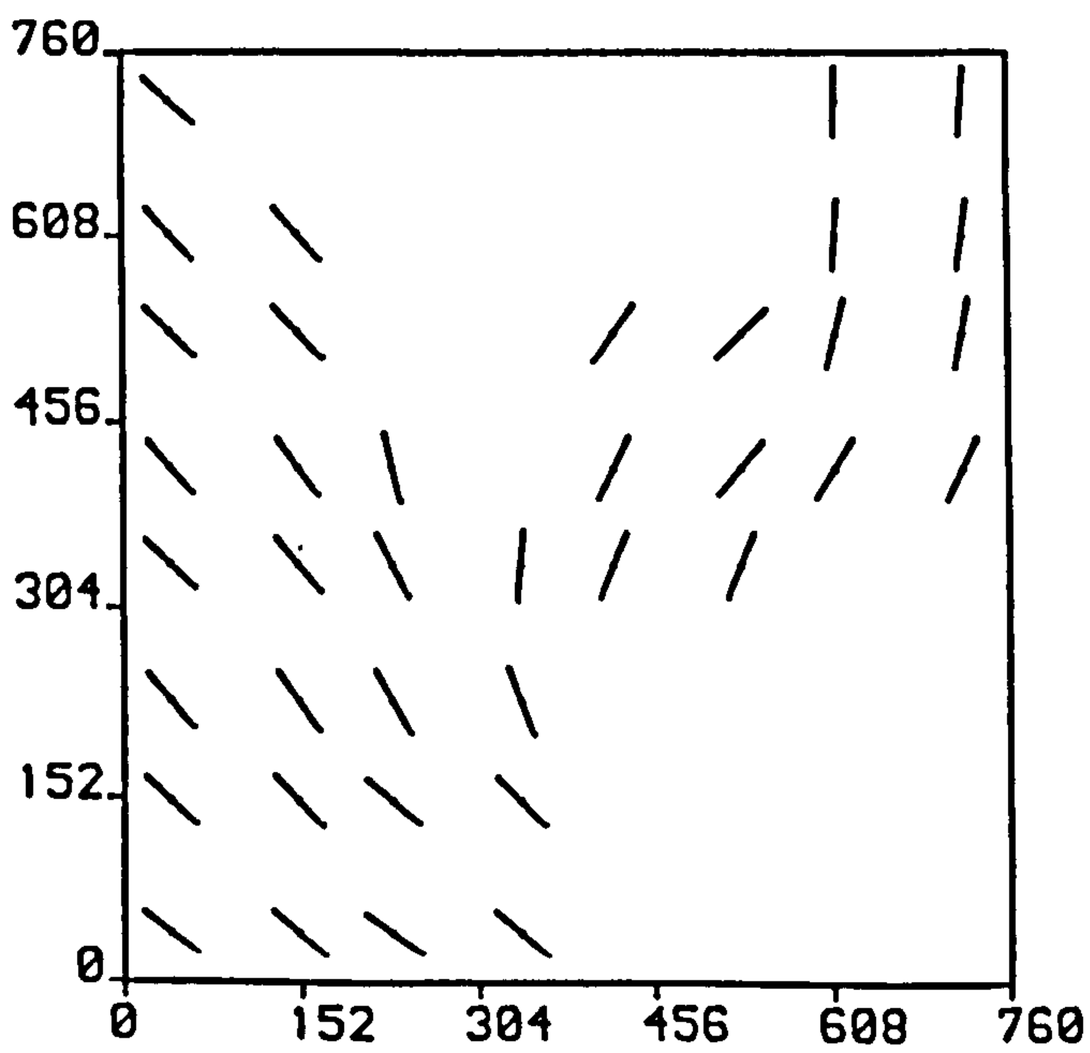

FIG.7.38b CRACK PATTERN FOR SLAB S63P1 ACM AT TOTAL LOAD = 4811.4 N

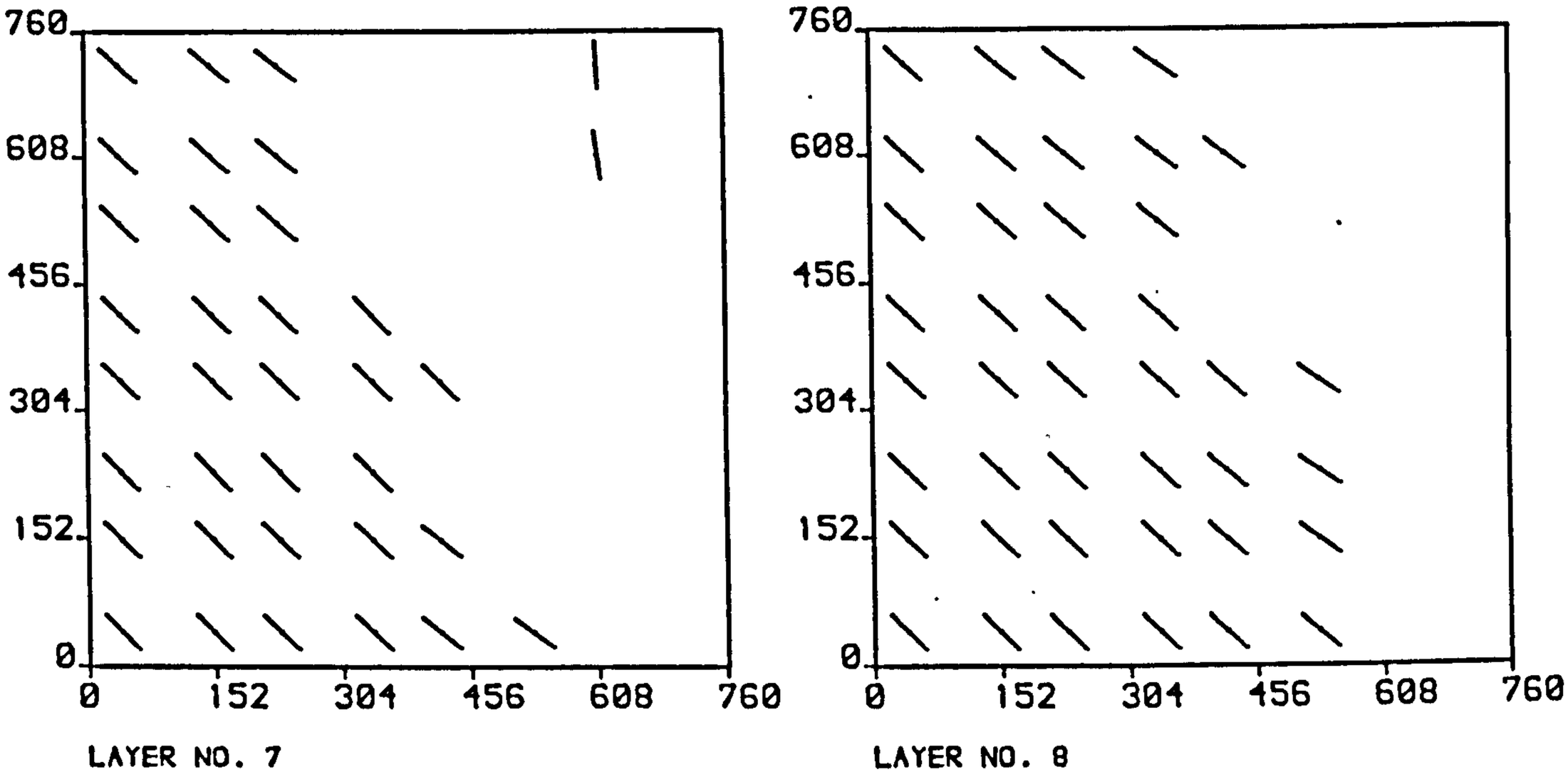

FIG.7.38c CRACK PATTERN FOR SLAB S63P1 ACM
AT TOTAL LOAD = 4811.4 N

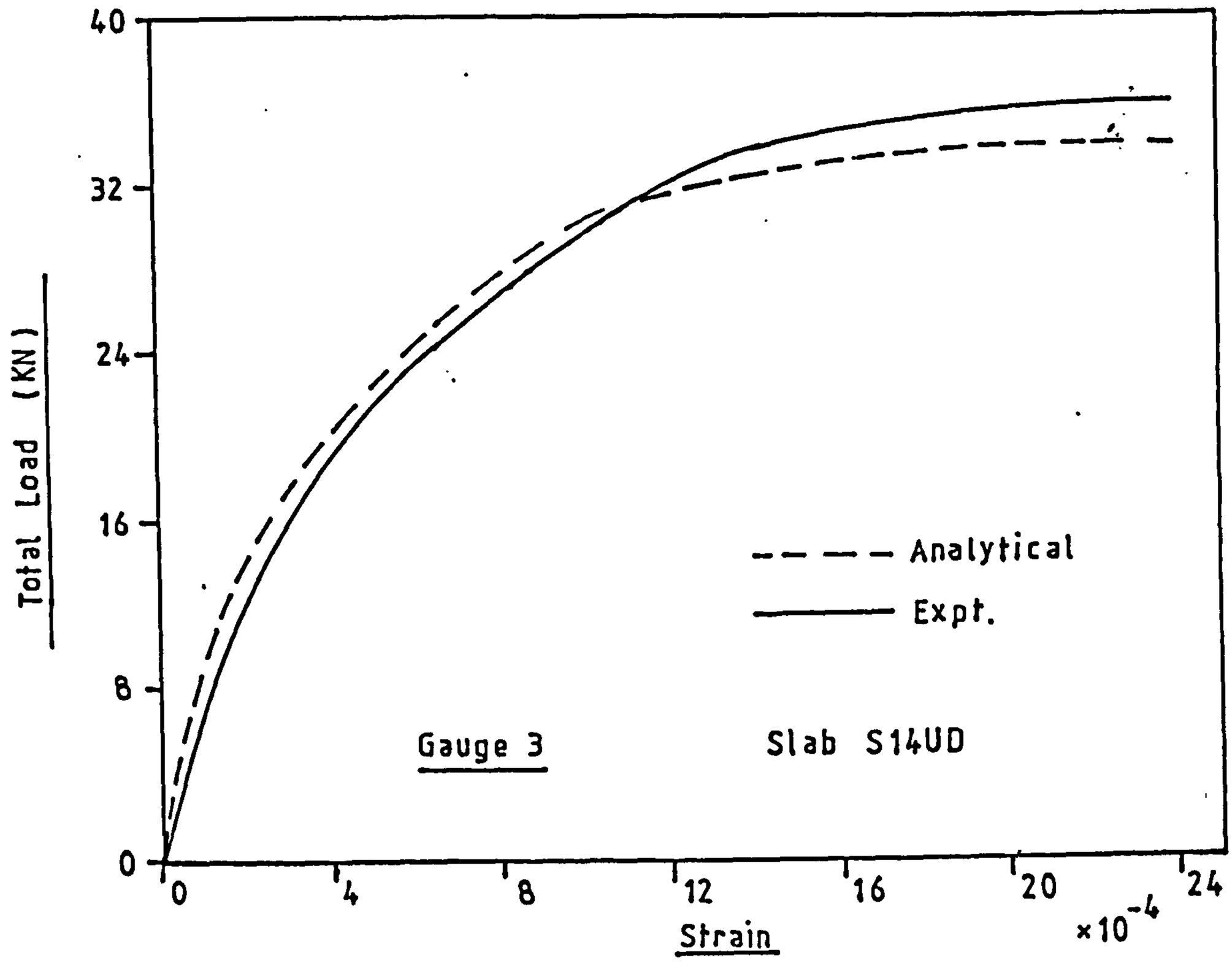

FIG. 7.39 Comparison of Load-Steel Strain Response at G3 of S14UD.

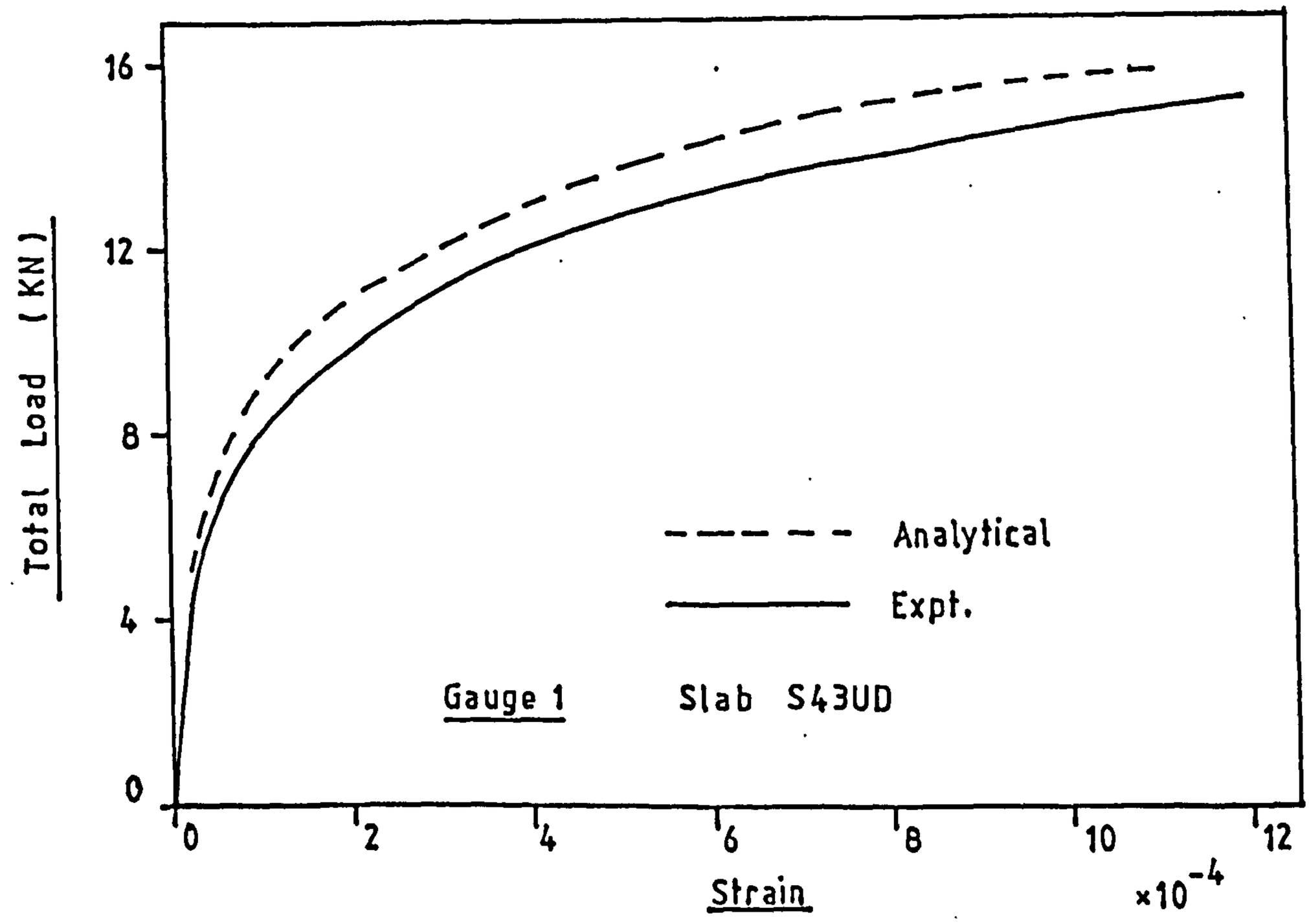

FIG.7.40 Comparison of Load-Steel Strain Response at G1 of S43UD.

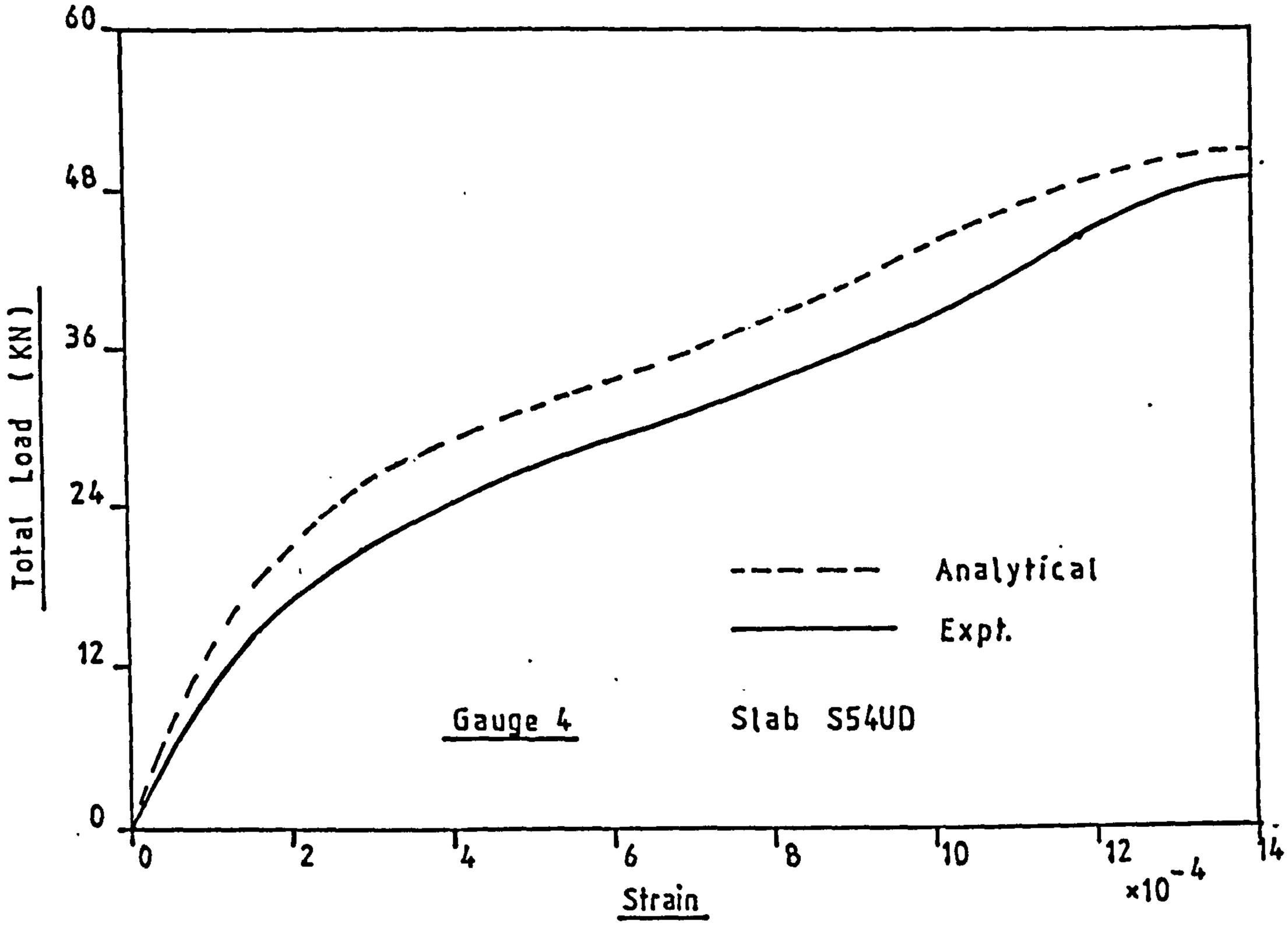

FIG. 7.41 Comparison of Load-Steel Strain Response at G4 of S54UD.

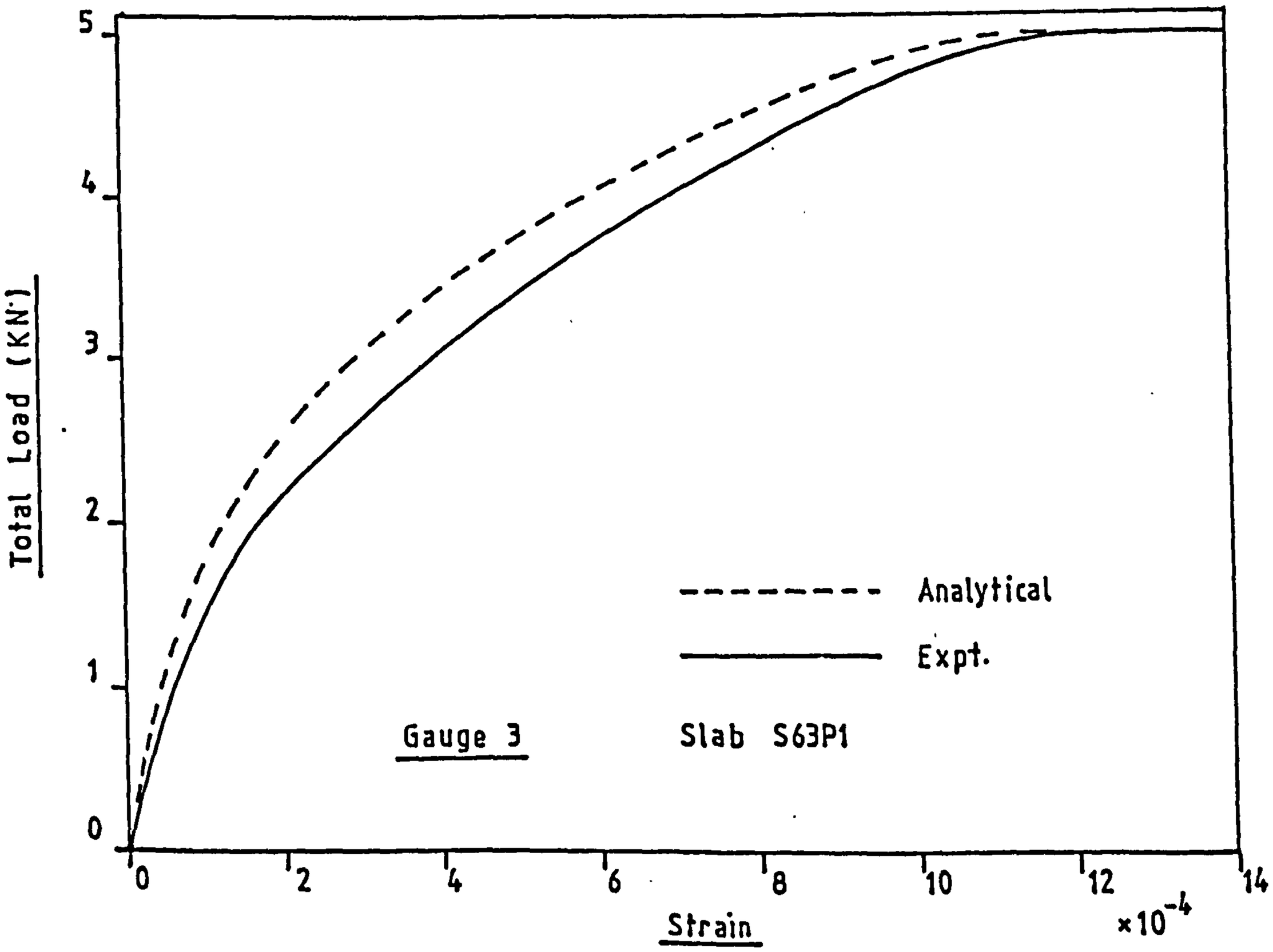

FIG. 7.42 Comparison of Load-Steel Strain Response at G3 of S63P1.

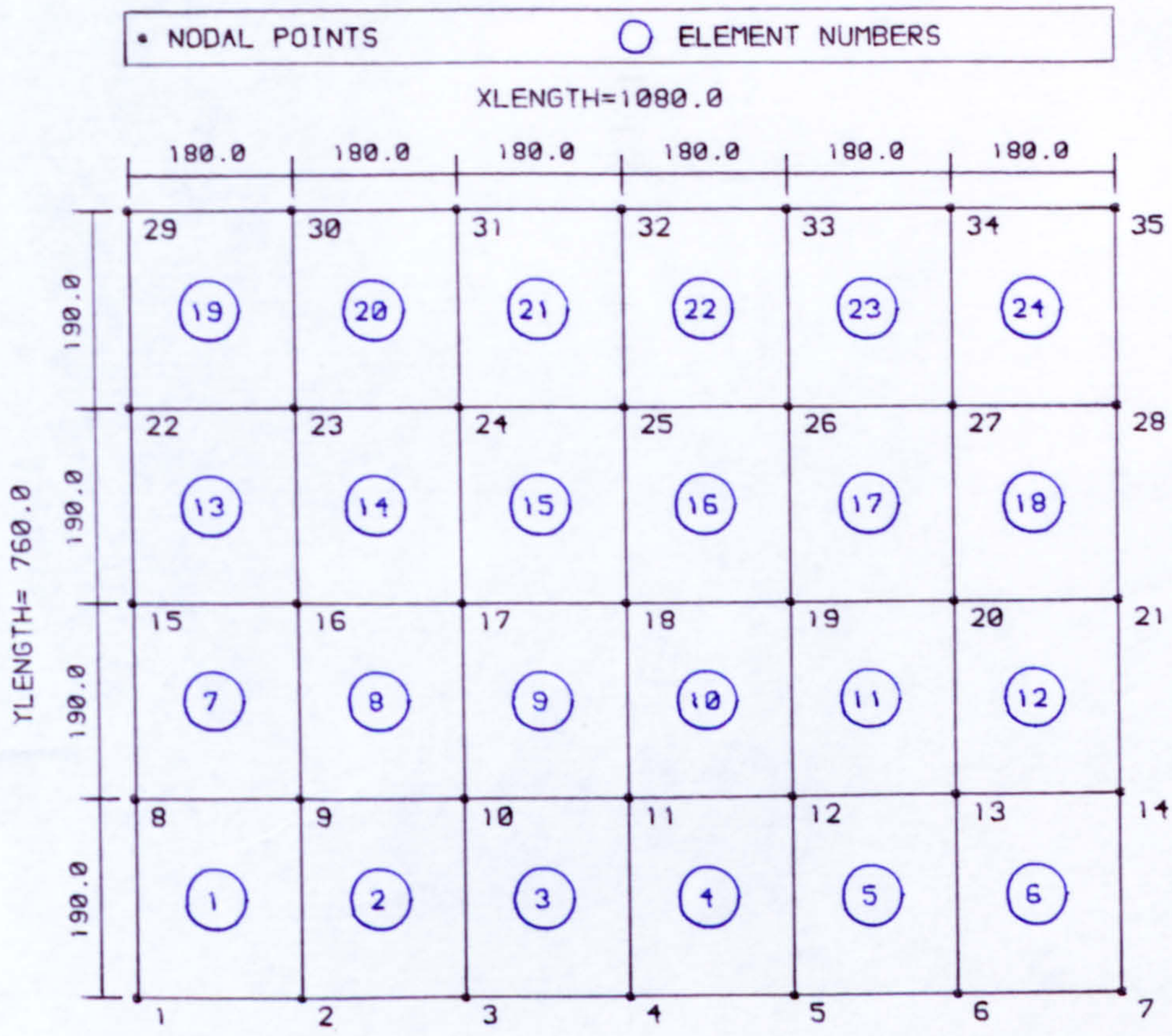

FIG.7.43 ELEMENT DISCRETISATION FOR JS590 EXP

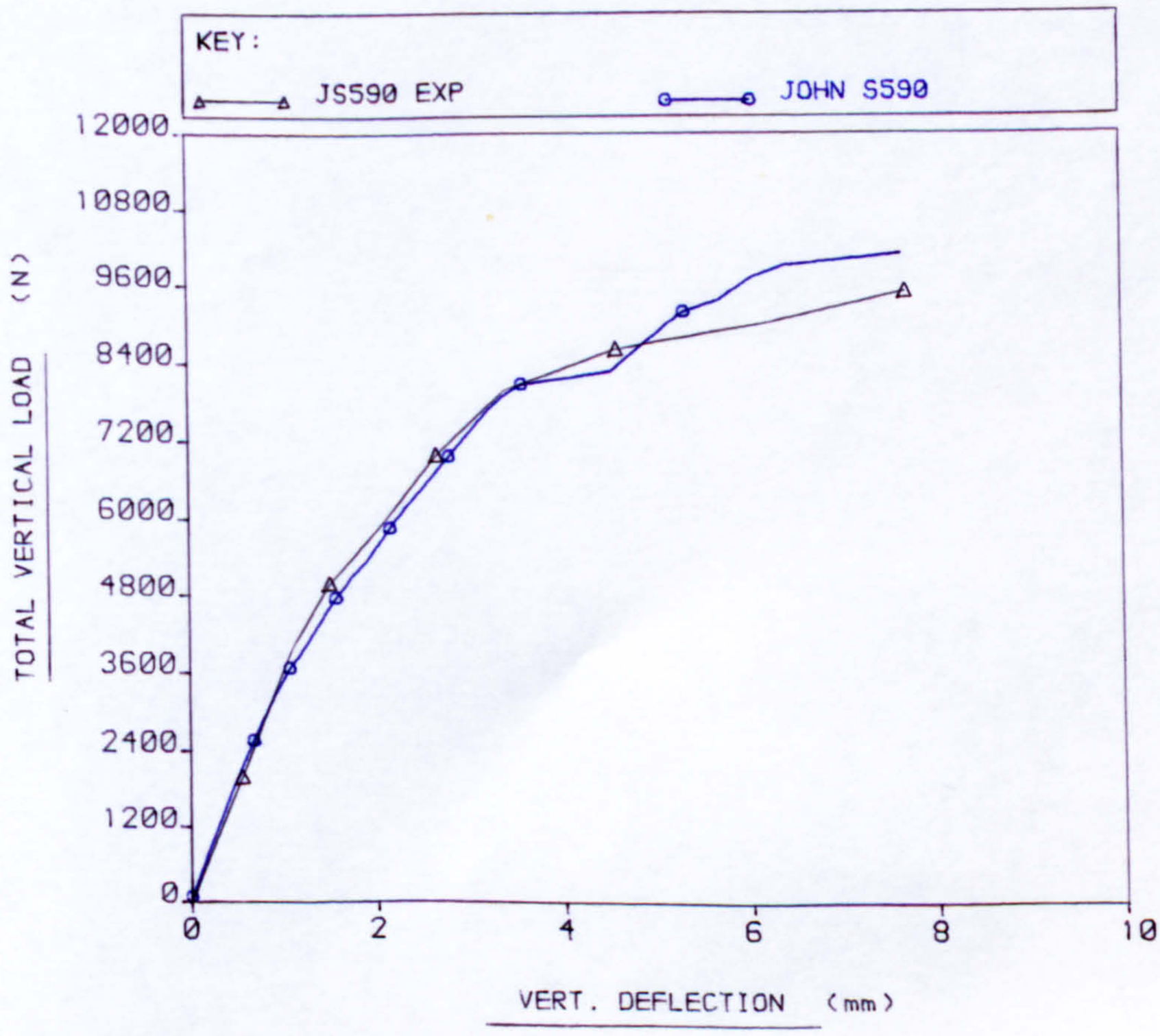

FIG.7.44 LOAD Vs DISPLACEMENT CURVES FOR NODE 15

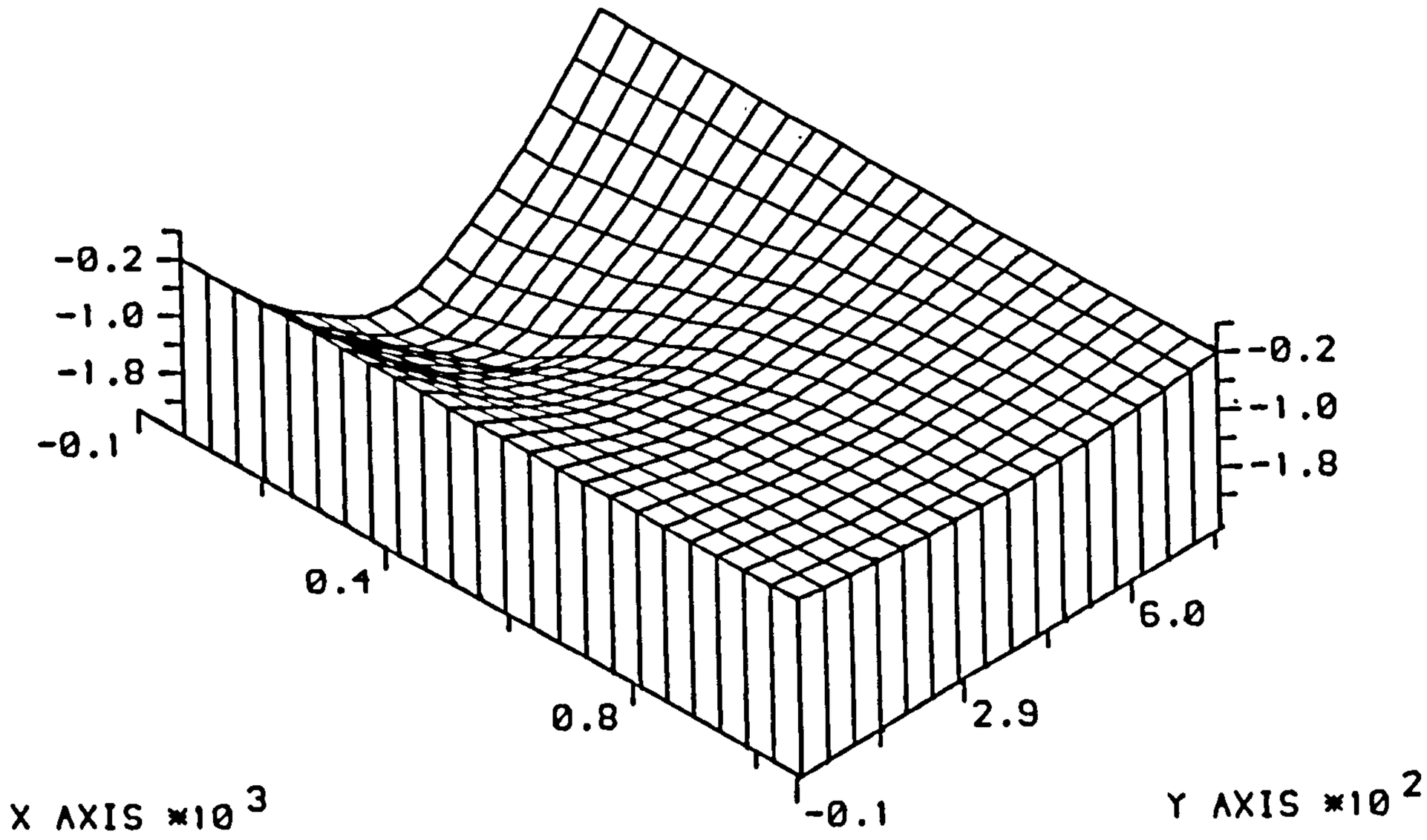

FIG.7.45 ISOMETRIC VIEW OF SLAB
DEFLECTION FOR JOHN S590
VERT LOAD: 6250.5 N

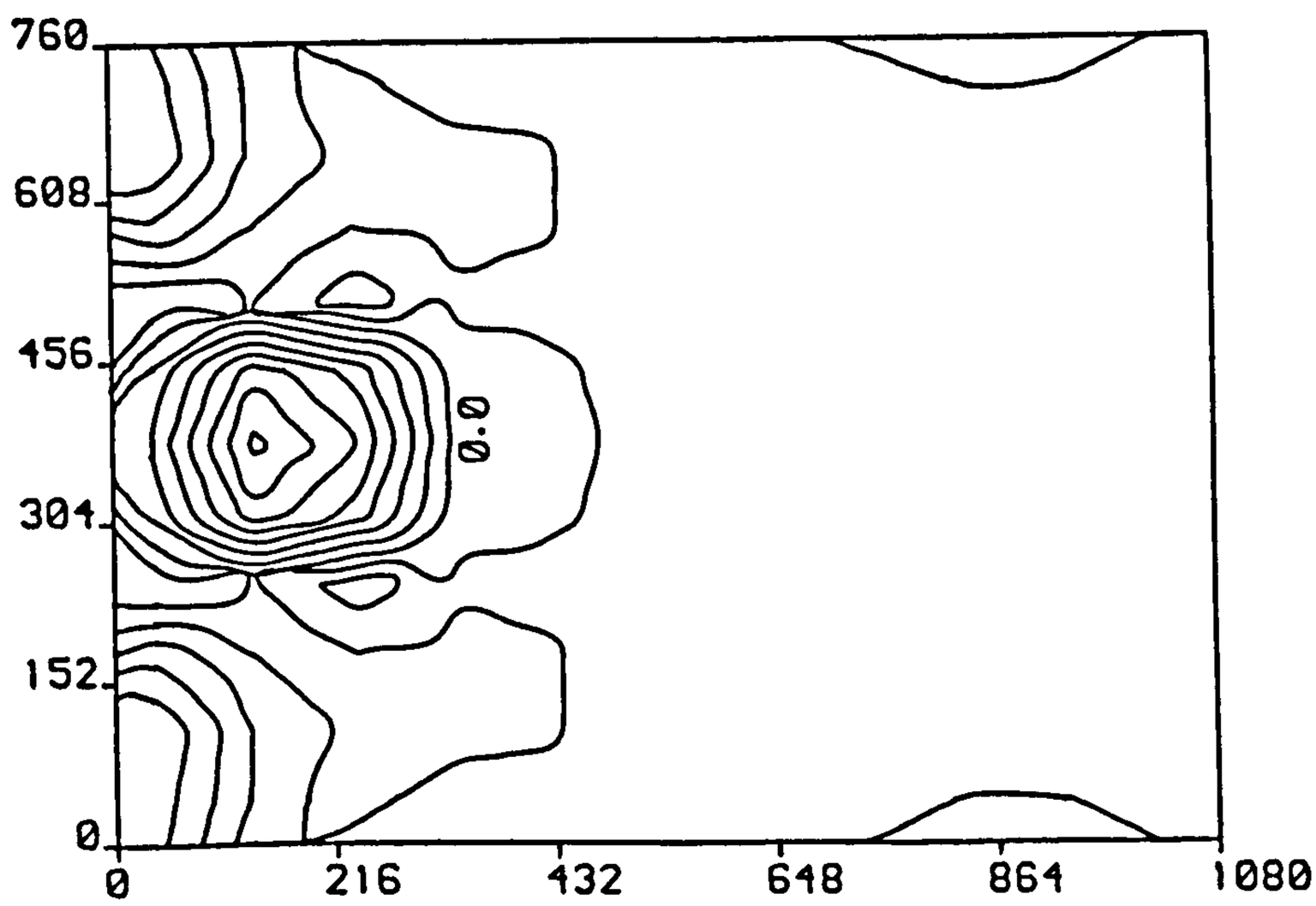

FIG.7.46 CONTOUR OF NY FOR JOHN S590
AT TOTAL VERTICAL LOAD = 6250.5 N
(N/mm)

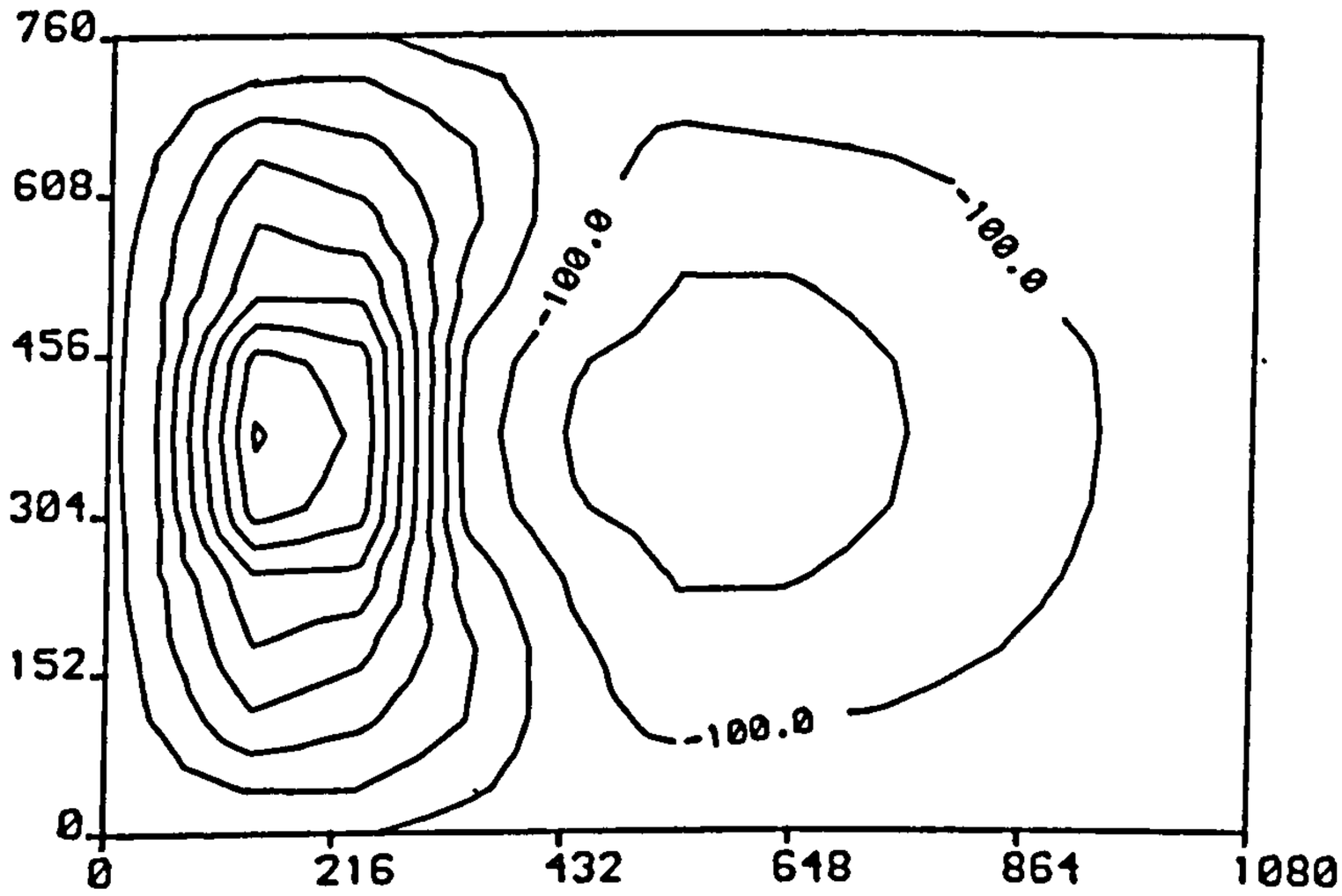

FIG. 7.47 CONTOUR OF MX FOR JOHN S590
AT TOTAL VERTICAL LOAD = 6250.5 N
(N-mm/mm)

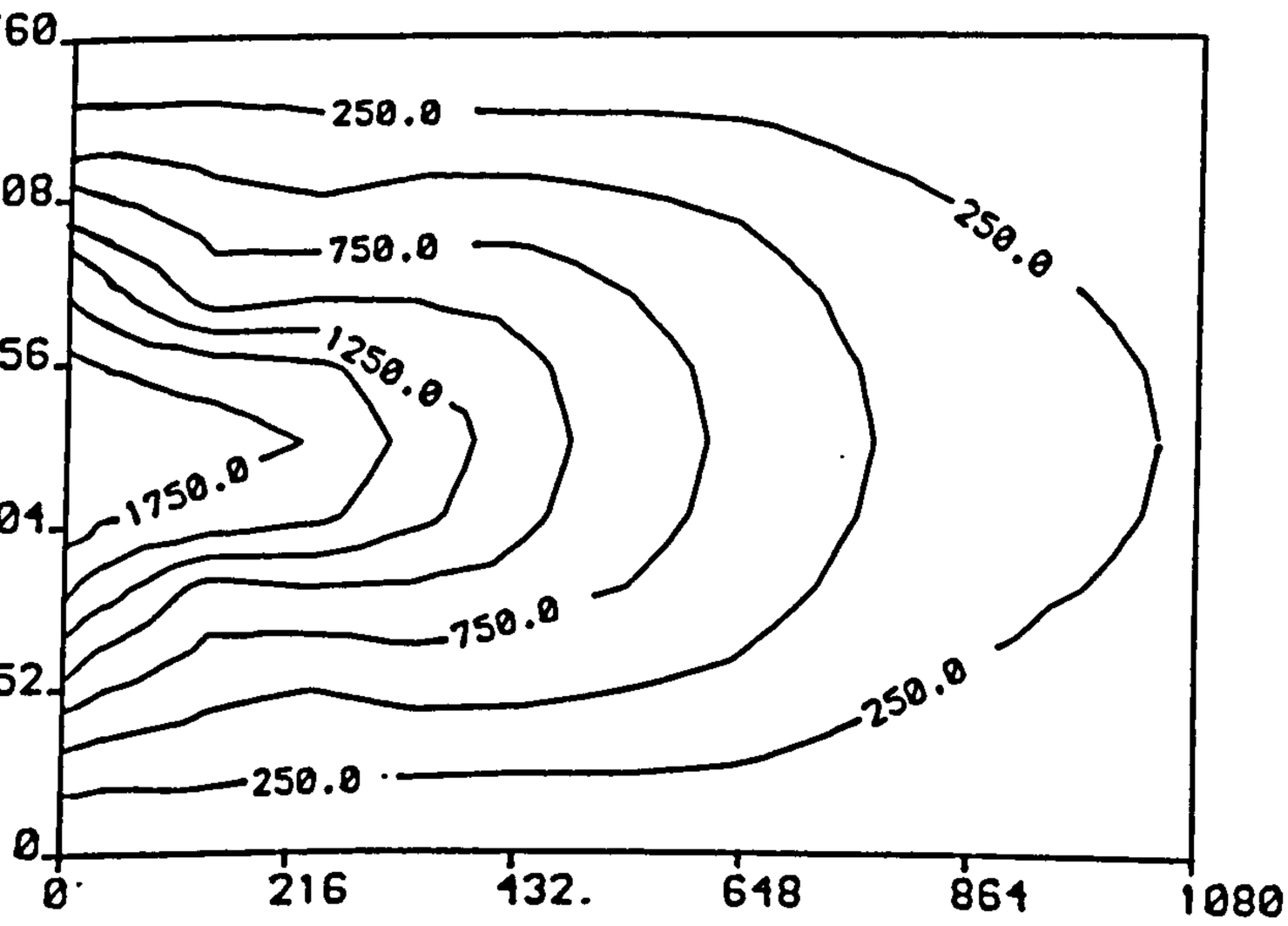

FIG. 7.48 CONTOUR OF MY FOR JOHN S590
AT TOTAL VERTICAL LOAD = 6250.5 N
(N-mm/mm)

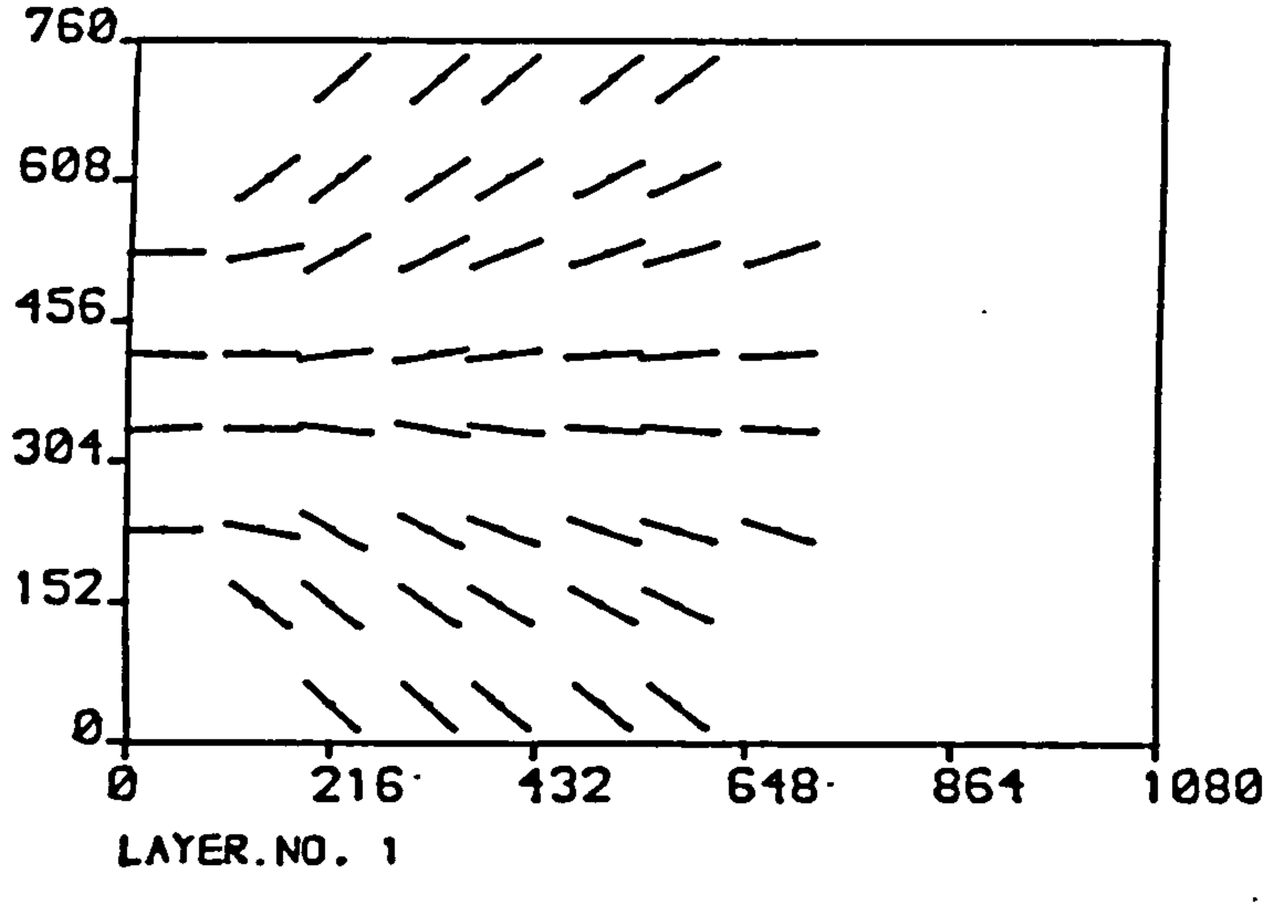

FIG.7.49a CRACK PATTERN FOR SLAB JOHN S590
AT TOTAL VERT.. LOAD = 6250.5 N

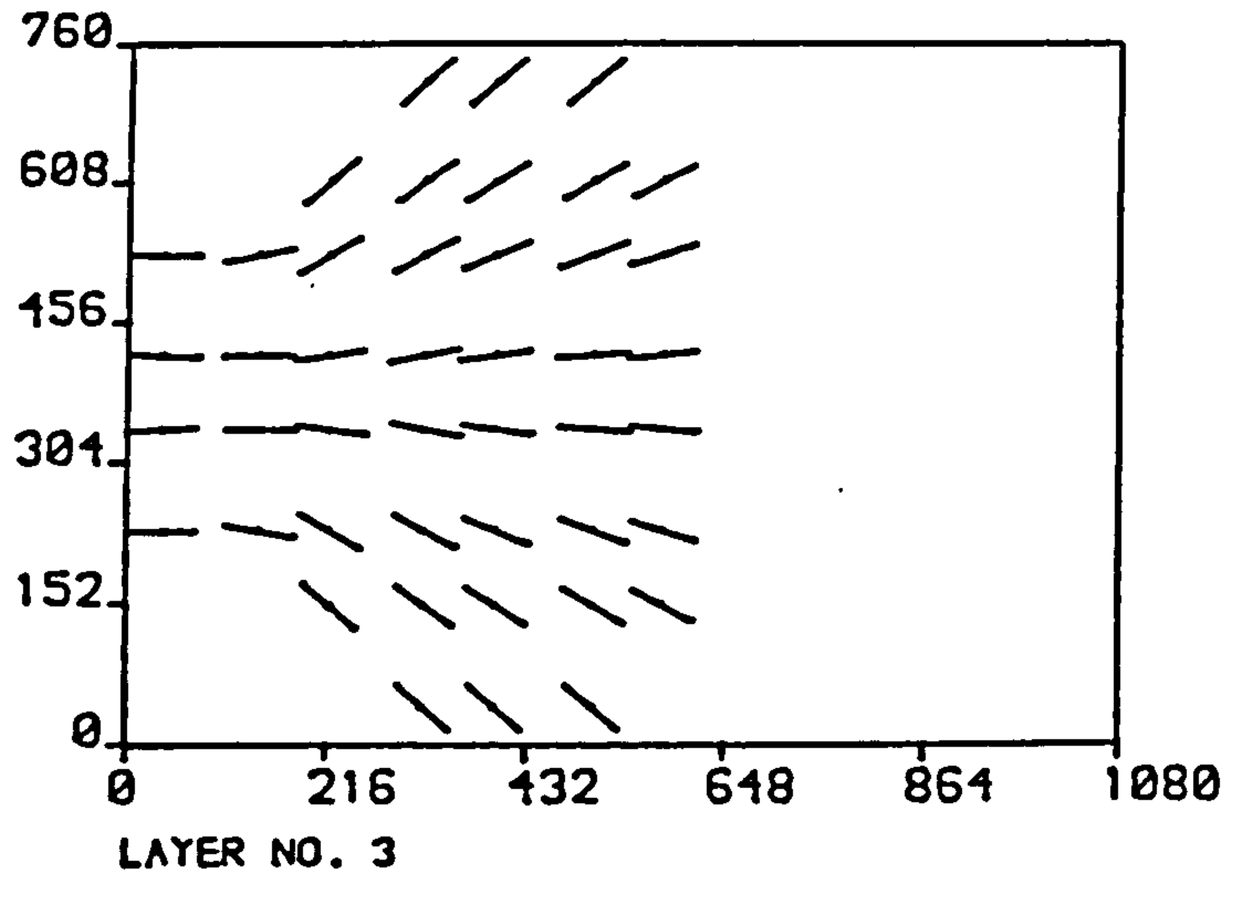

FIG.7.49b CRACK PATTERN FOR SLAB JOHN S590
AT TOTAL VERT. LOAD = 6250.5 N

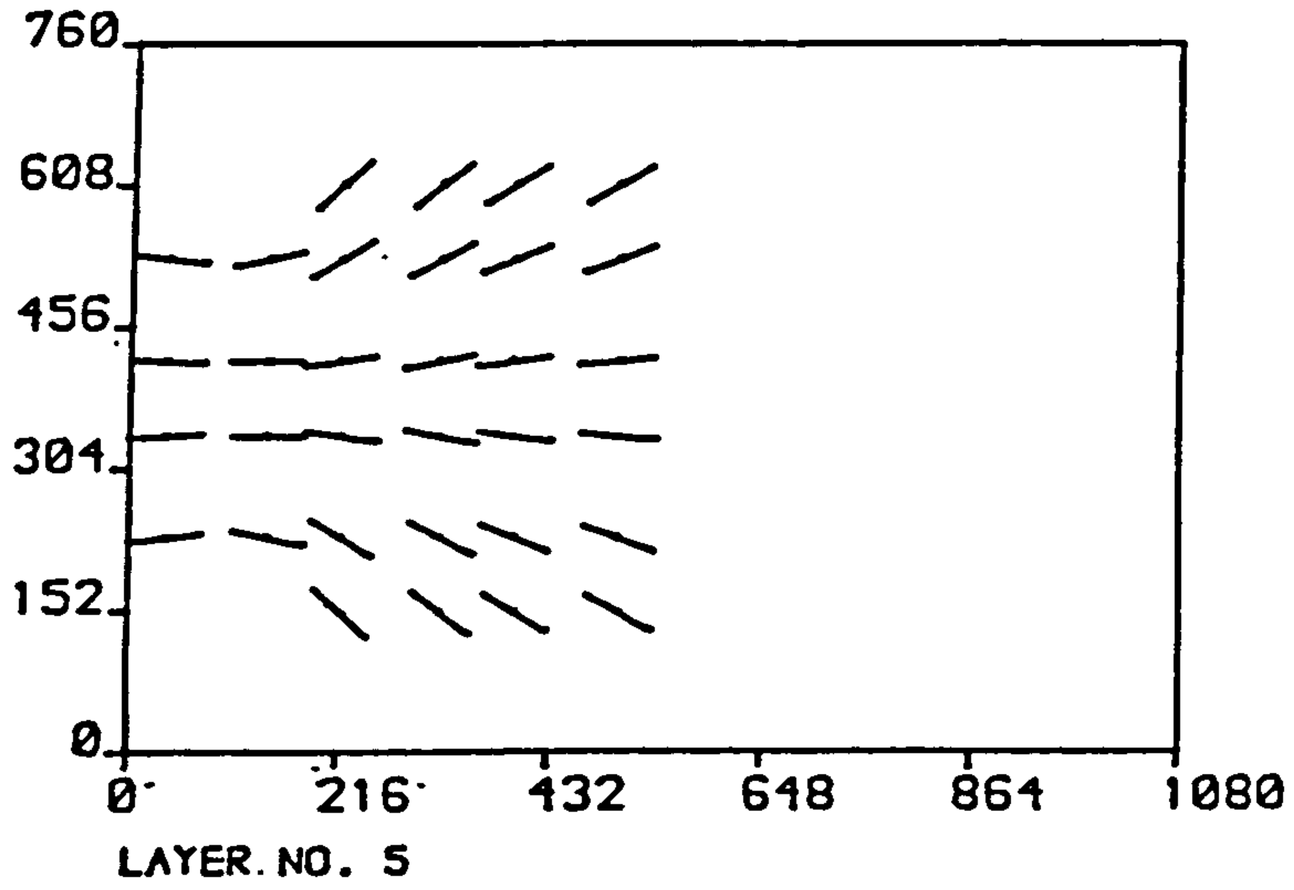

FIG.7.49c CRACK PATTERN FOR SLAB JOHN S590
AT TOTAL VERT. LOAD = 6250.5 N

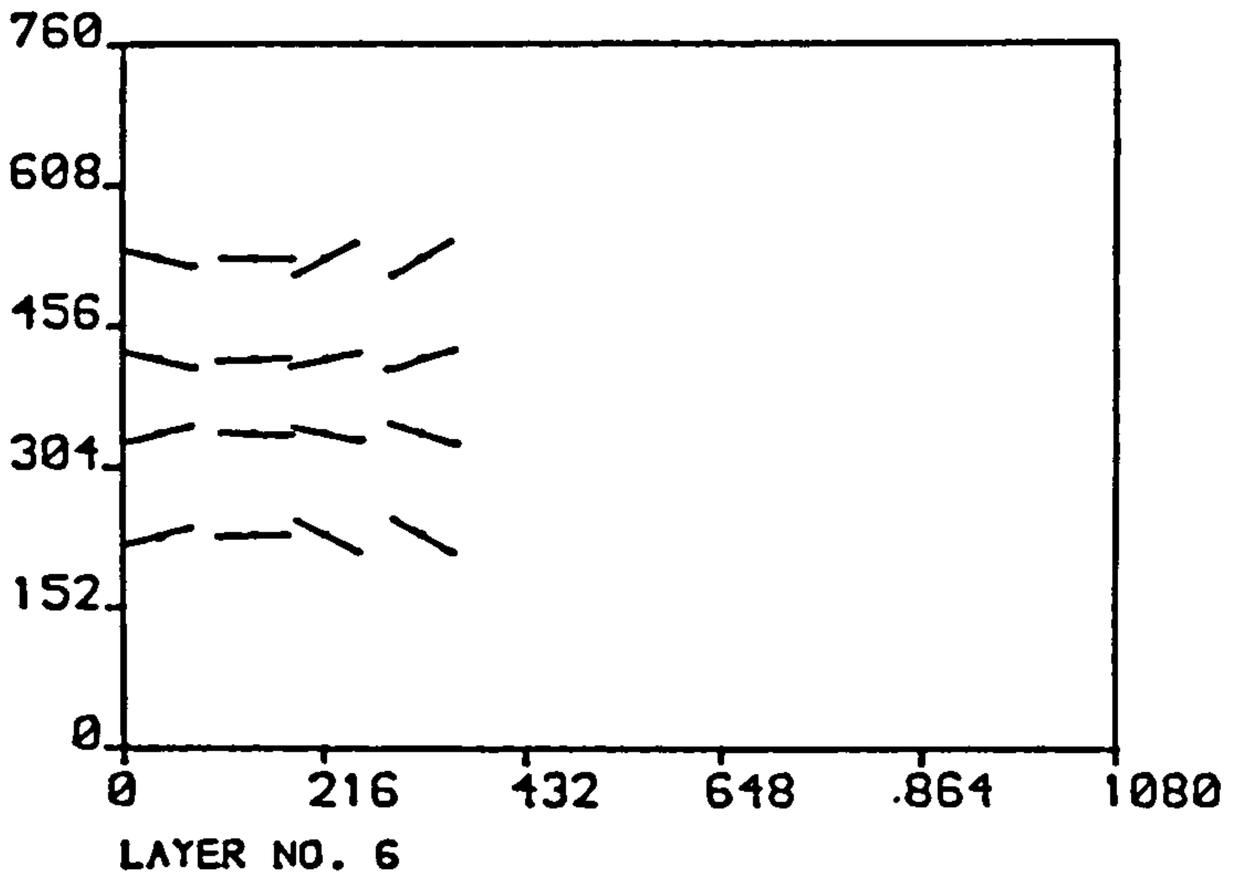

FIG.7.49d CRACK PATTERN FOR SLAB JOHN S590
AT TOTAL VERT. LOAD = 6250.5 N

USER: CMAR25 FILE: MAC1CUR PLOT NO: 1

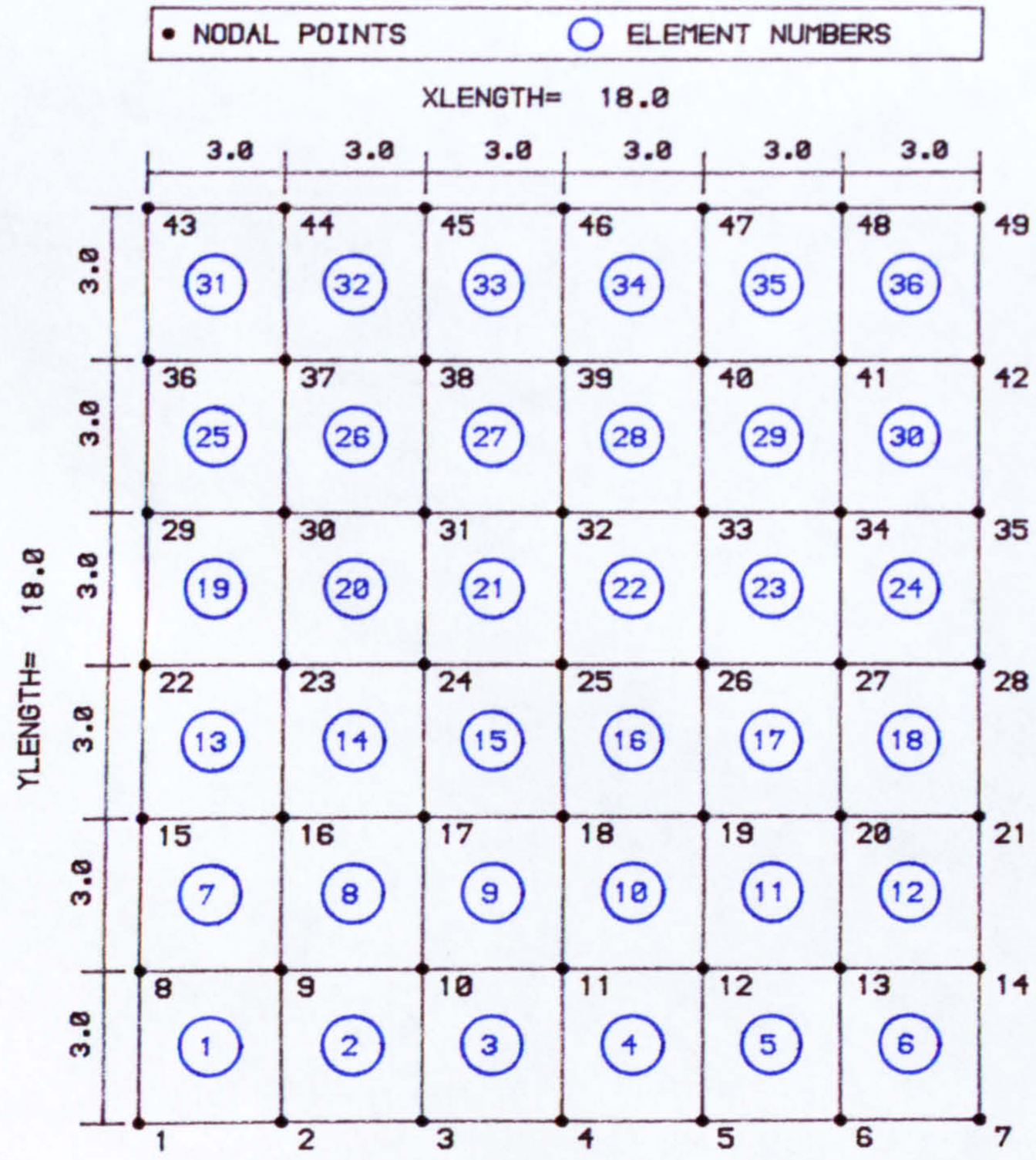

FIG.7.50 ELEMENT DISCRETISATION FOR MACSS EXP

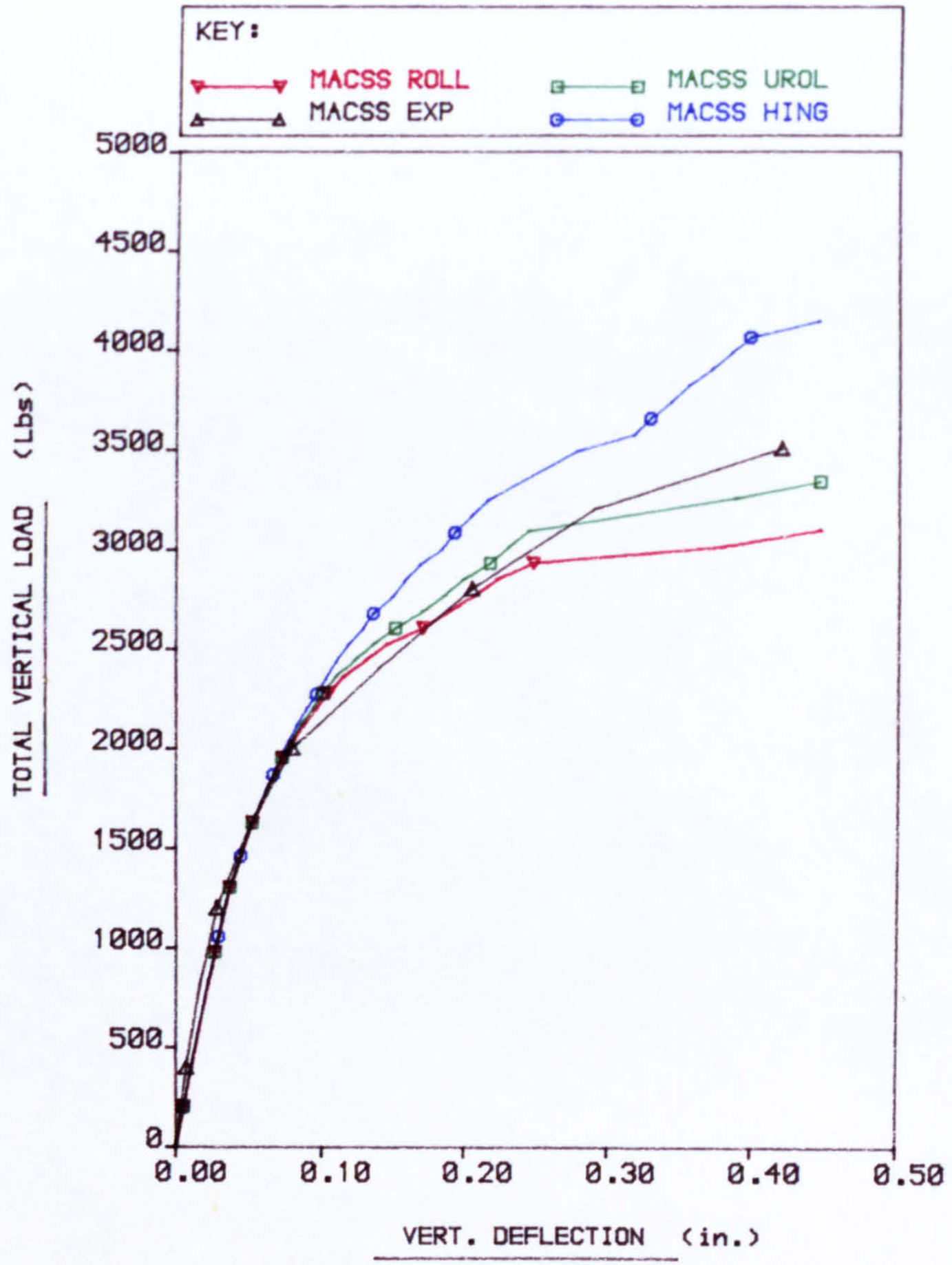

FIG.7.51 LOAD Vs DISPLACEMENT CURVES FOR NODE *48*

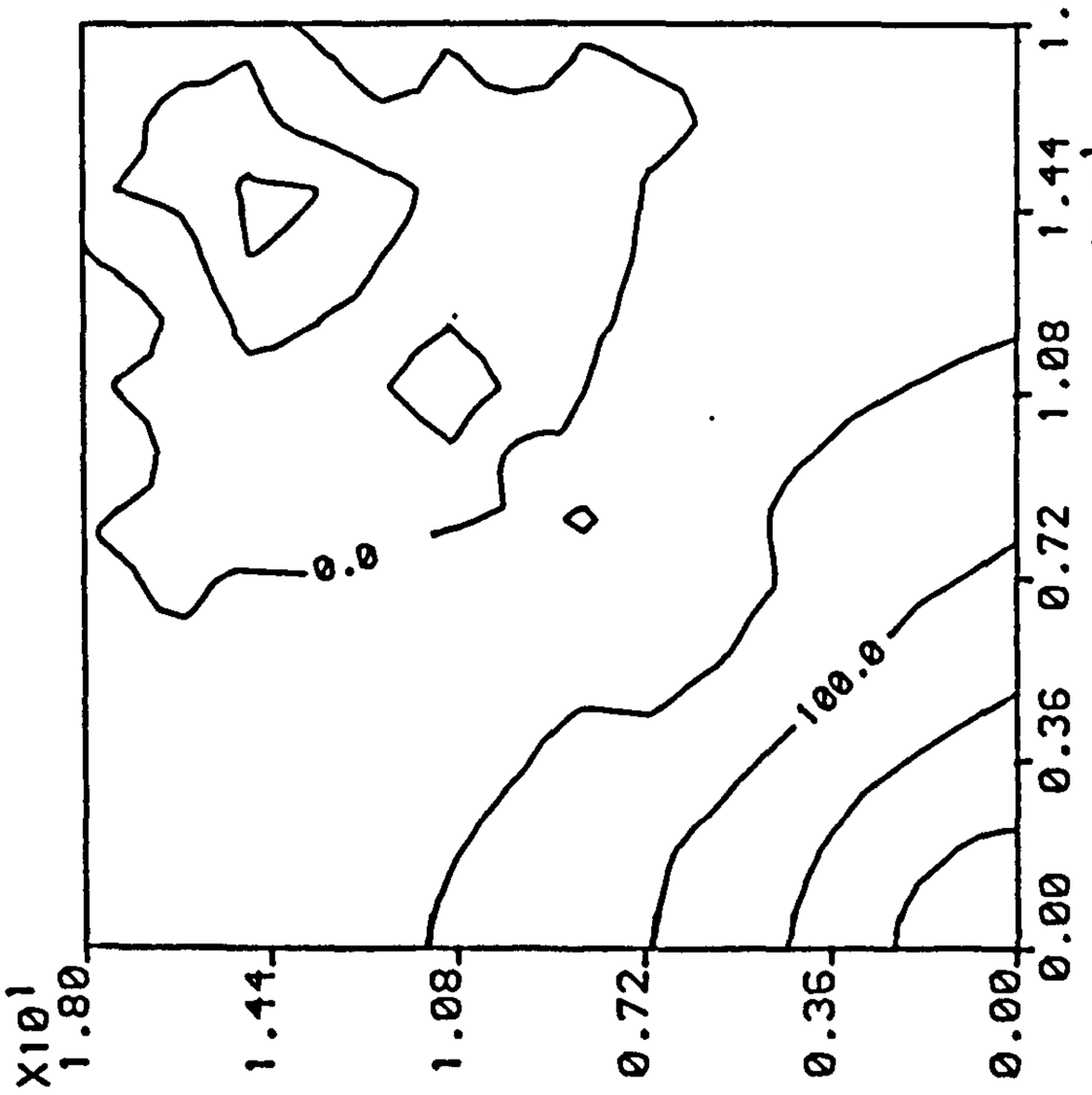

FIG. 7.53 CONTOUR OF MXY FOR MACSS UROL AT TOTAL VERTICAL LOAD = 2437.4 lbs. (lbs-in/in.)

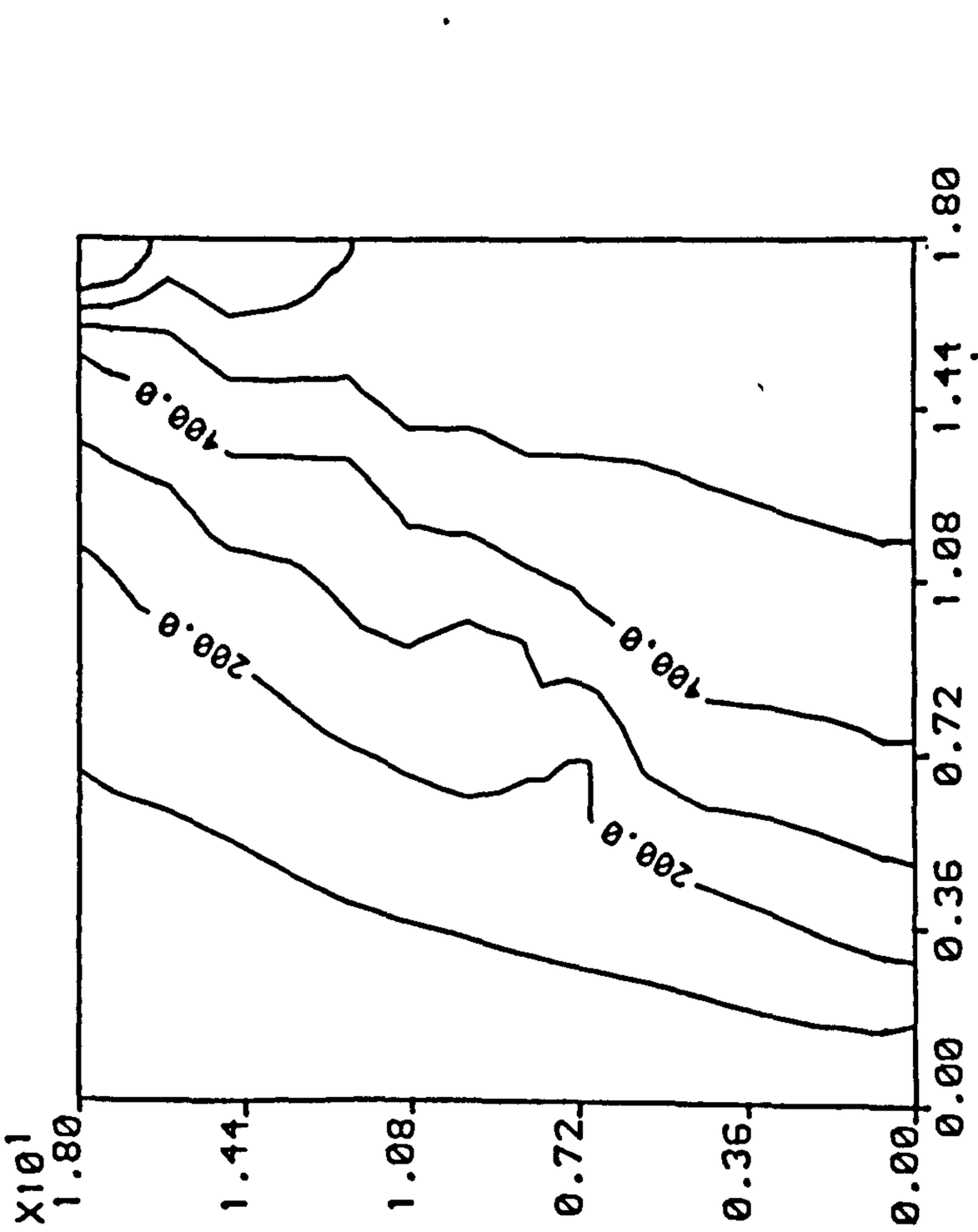

FIG. 7.52 CONTOUR OF MX FOR MACSS UROL AT TOTAL VERTICAL LOAD = 2437.4 lbs. (lbs-in./in.)

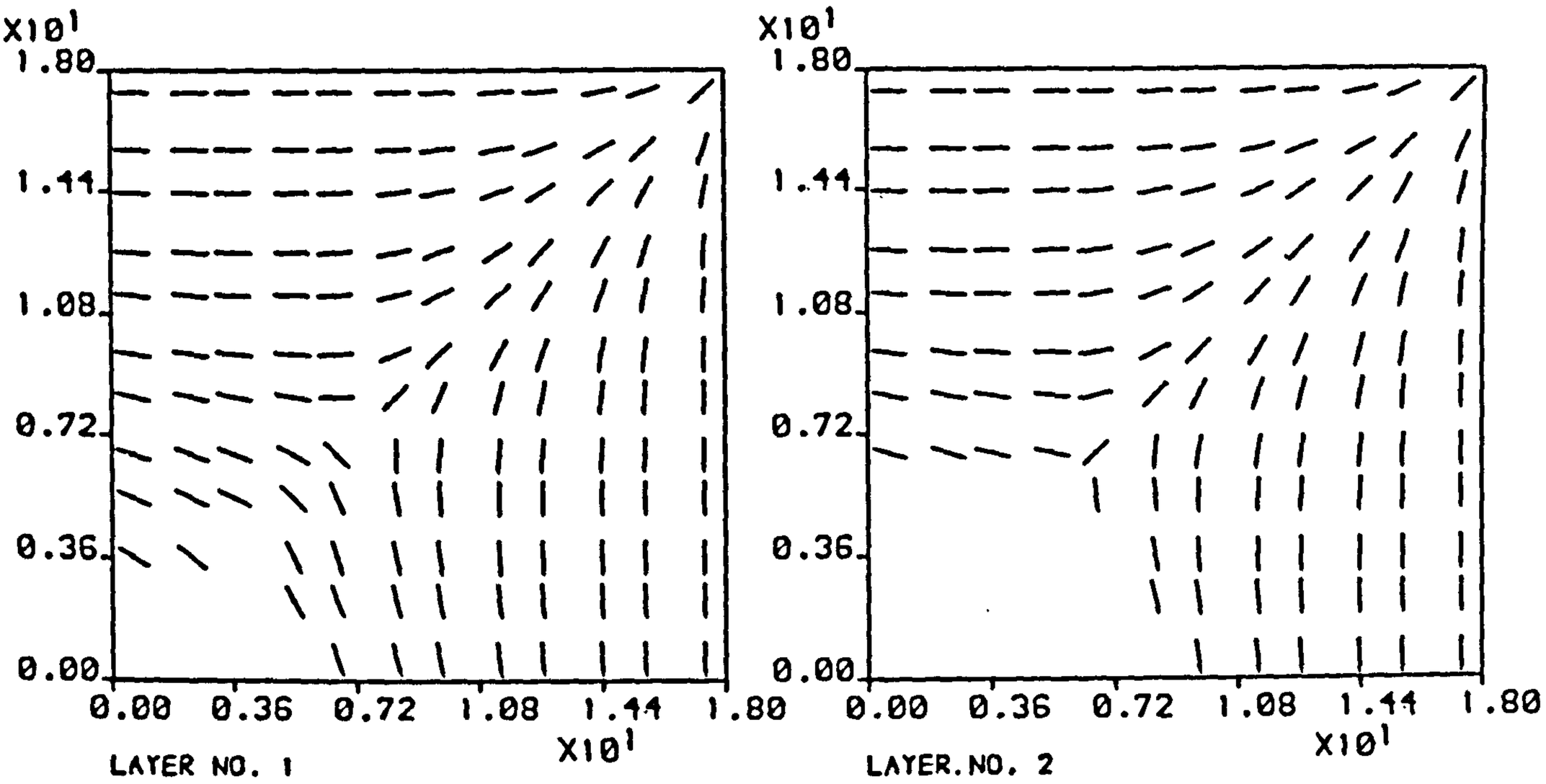

FIG.7.54a CRACK PATTERN FOR SLAB MACSS UROL
AT TOTAL VERT. LOAD = 2437.4 lbs.

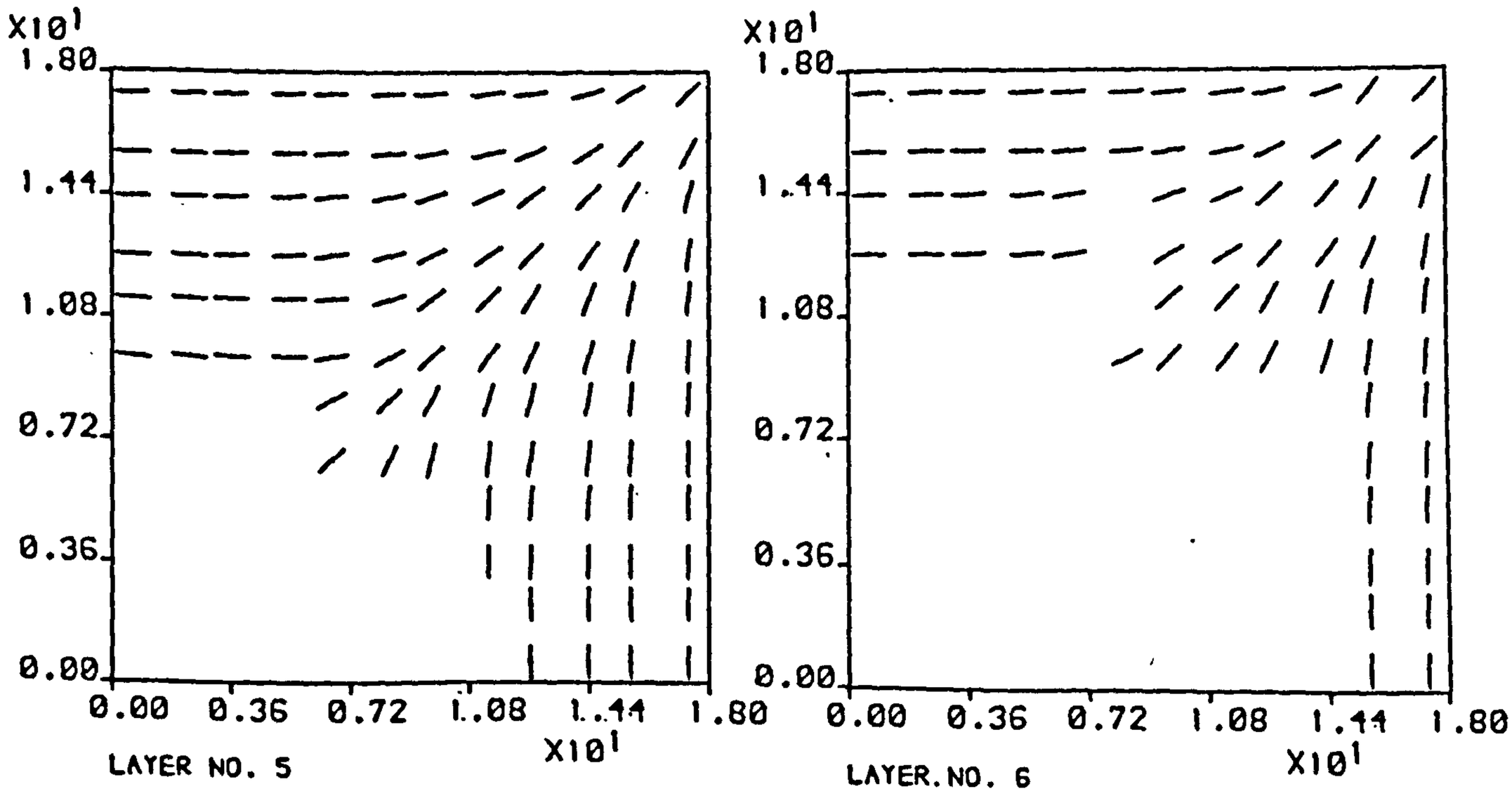

FIG.7.54b CRACK PATTERN FOR SLAB MACSS UROL
AT TOTAL VERT. LOAD = 2437.4 lbs.

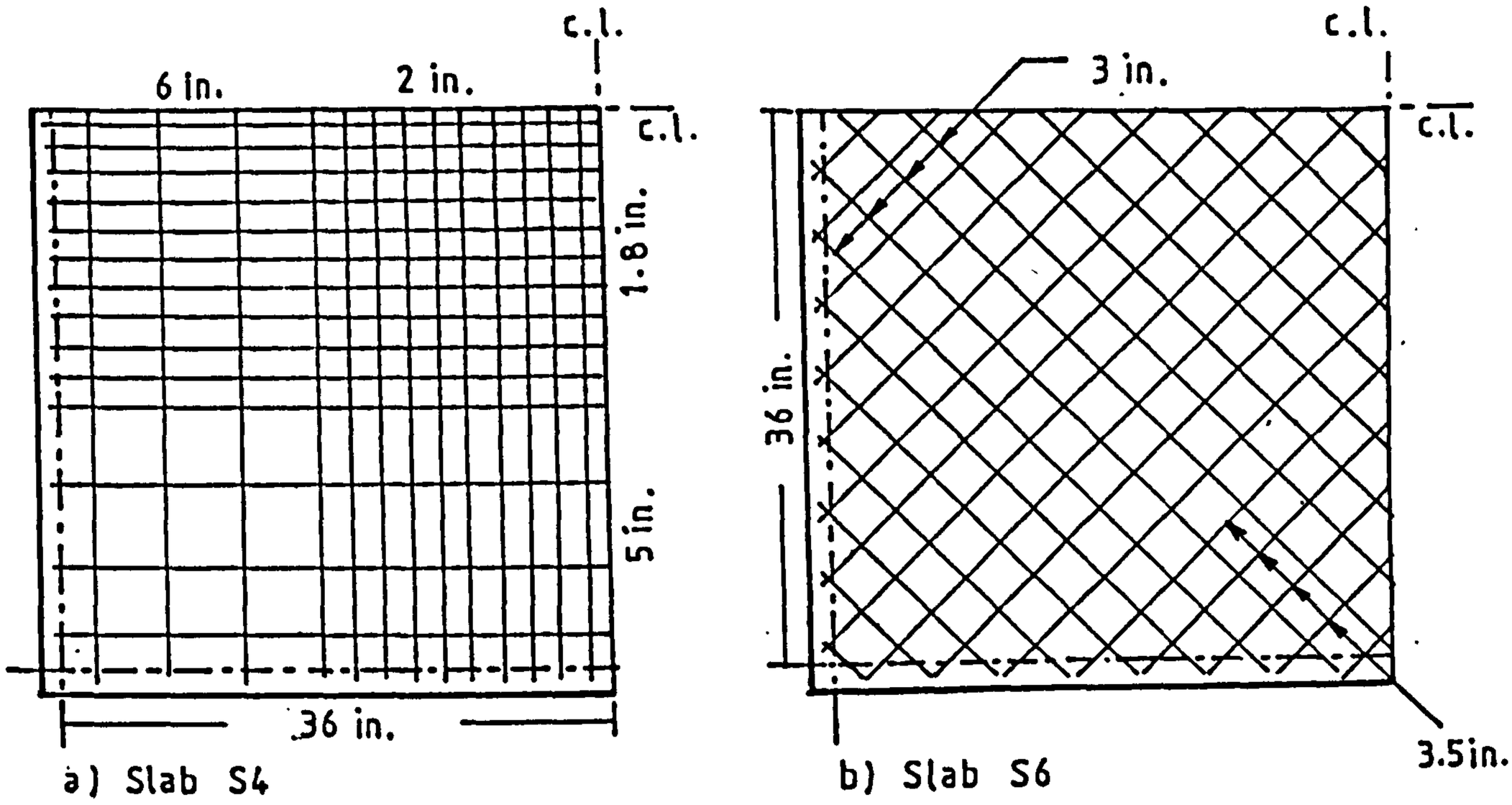

FIG. 7.55 Reinforcement Arrangements for Taylor's Slabs.

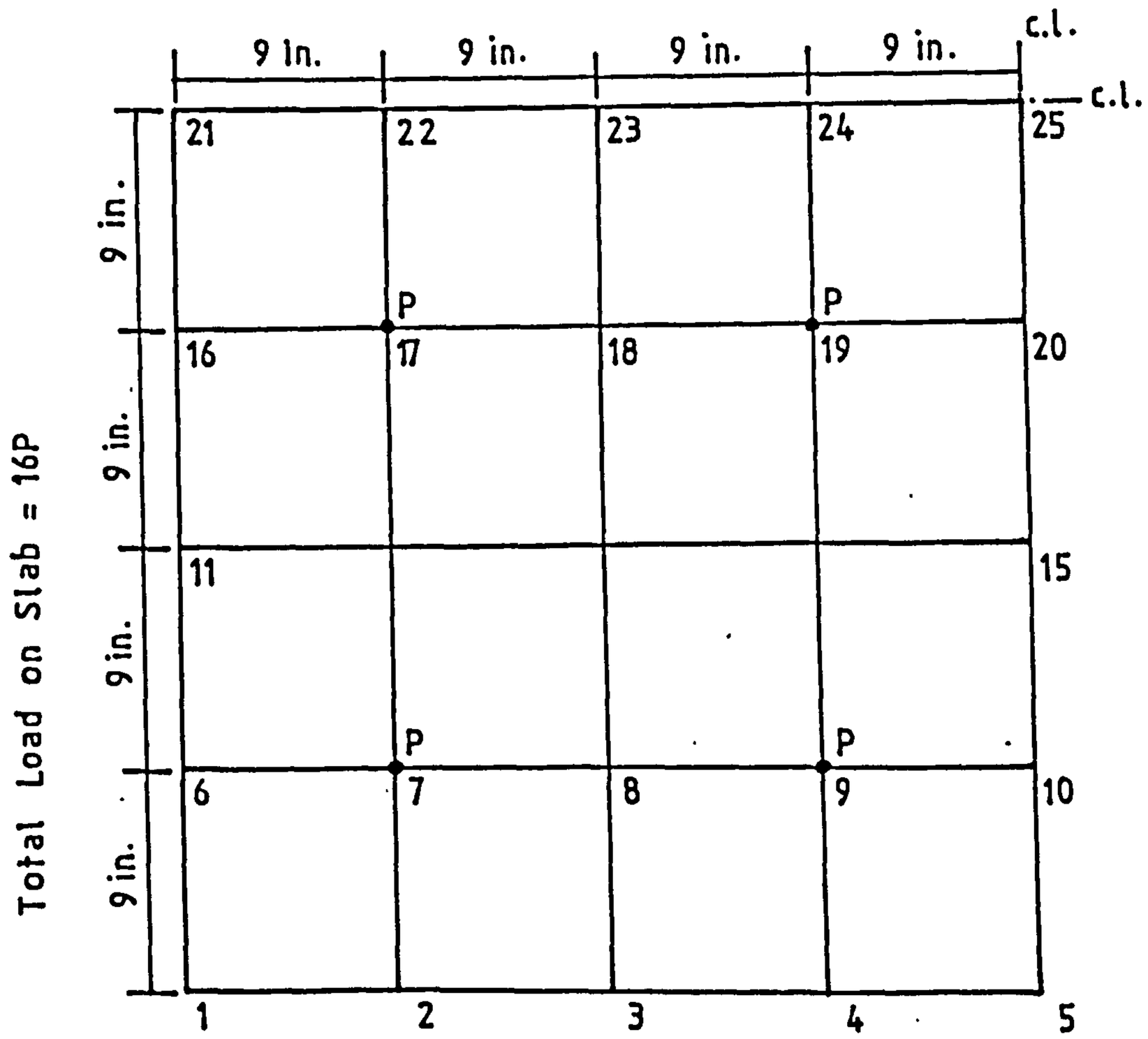

FIG. 7.56 Element Grid and Location of the Point Loads on Symmetric Quarter of the Taylor's Slabs.

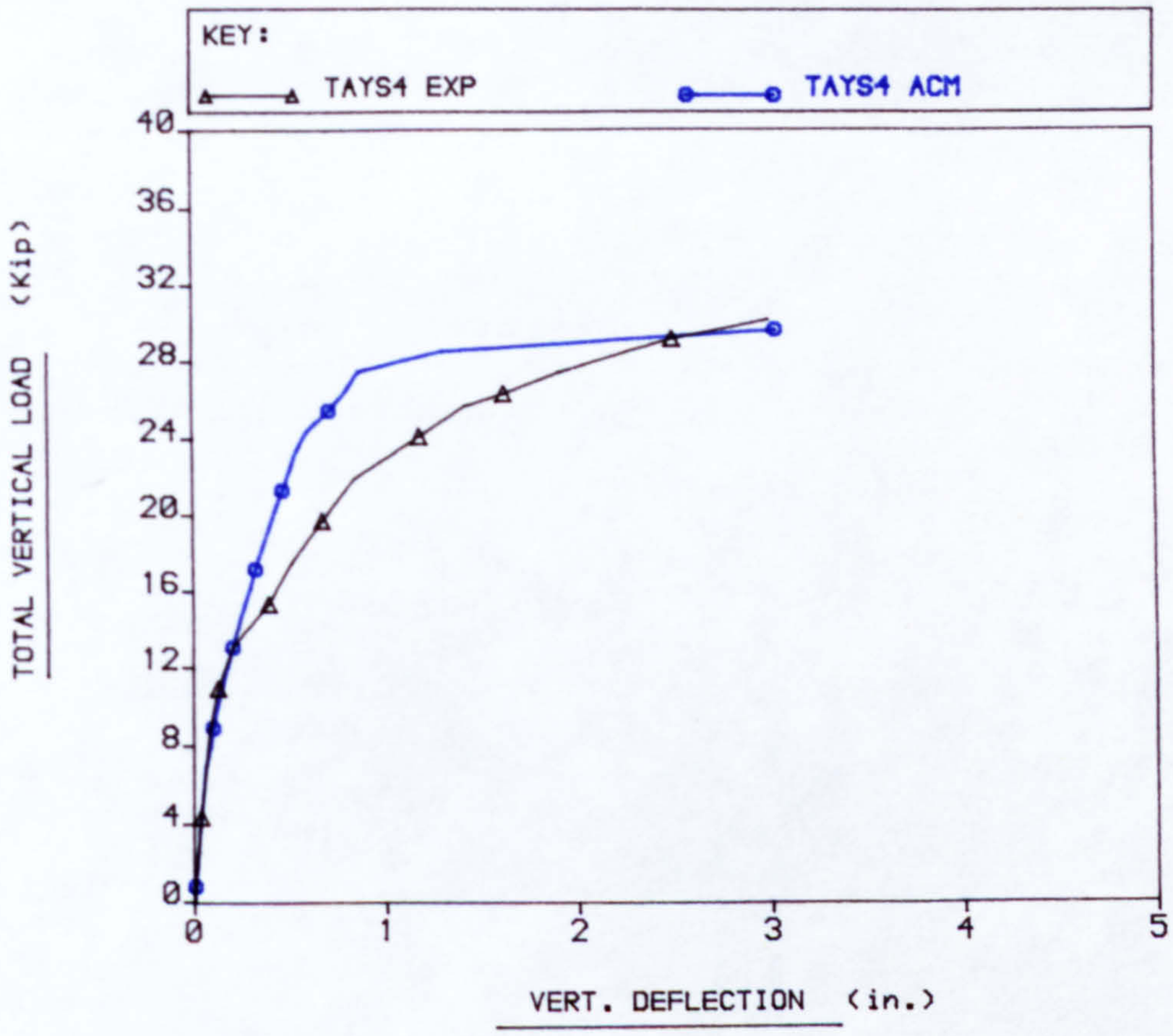

FIG.7.57 LOAD Vs DISPLACEMENT CURVES FOR NODE *25*

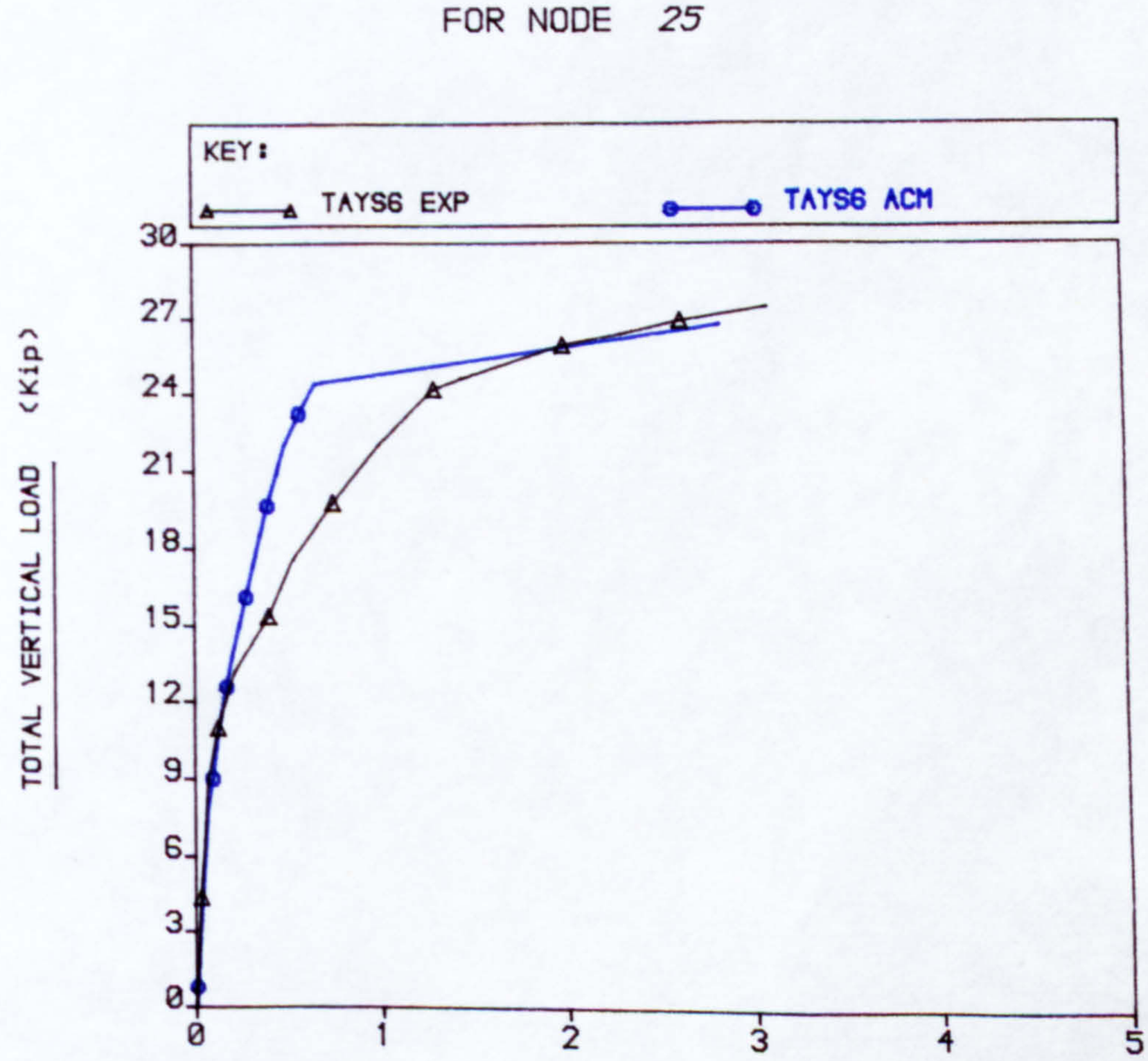

FIG.7.58 LOAD Vs DISPLACEMENT CURVES FOR NODE *25*

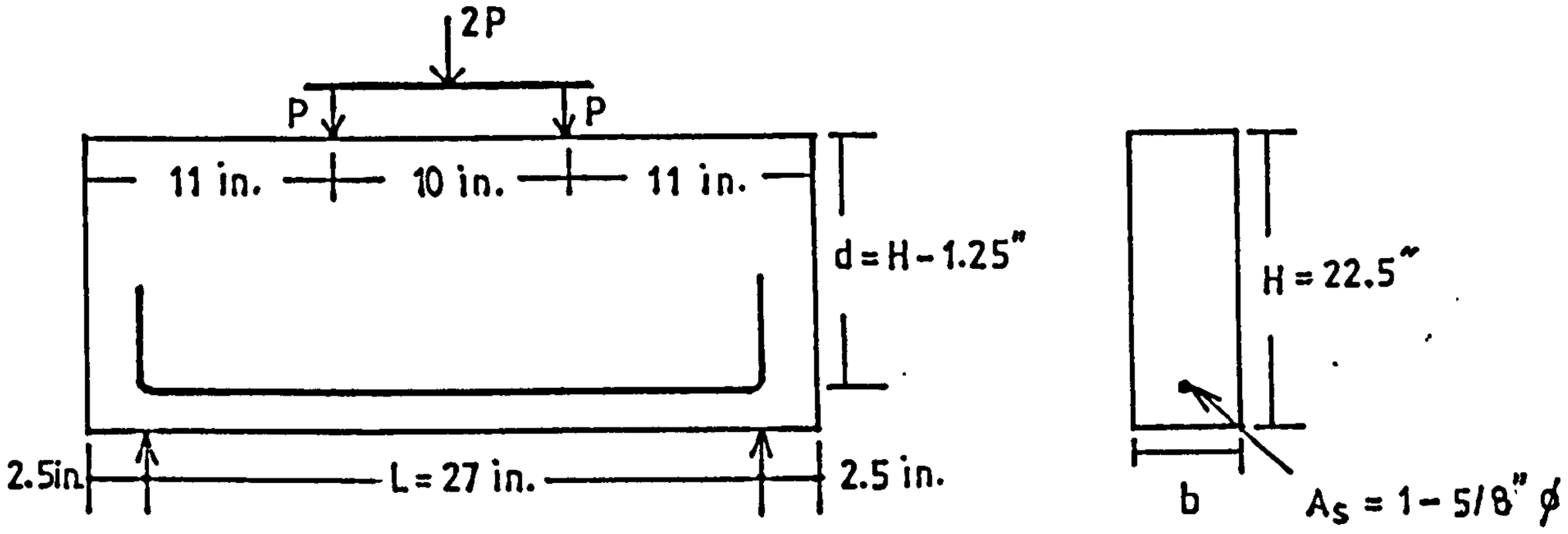

a) DB B3

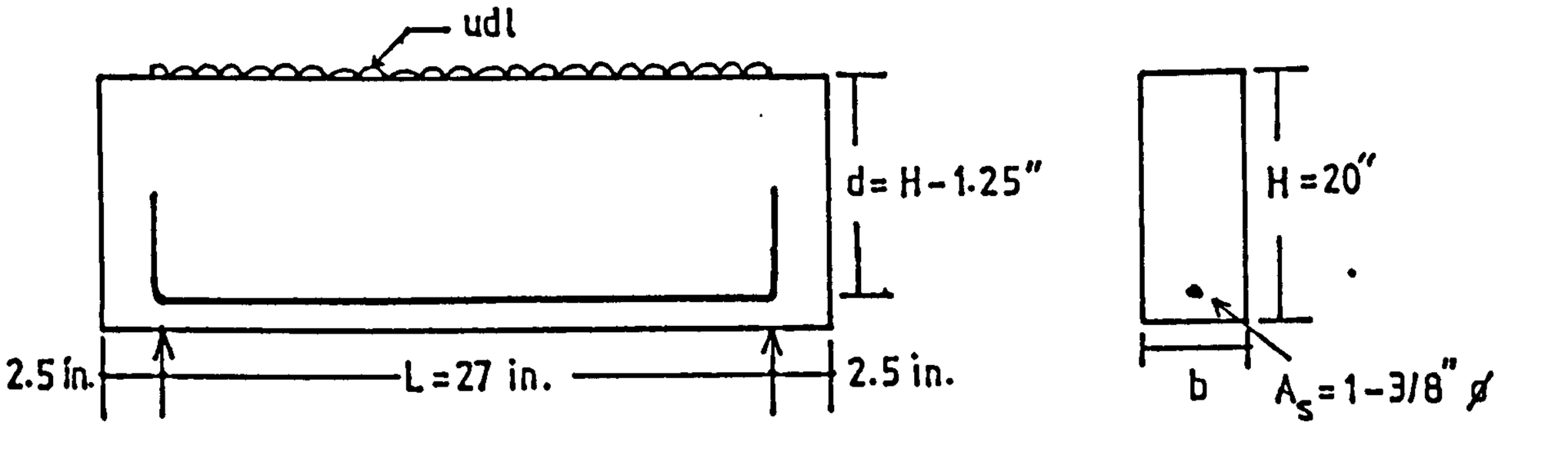

b) DB K2

FIG. 7.59 Geometric Details of the Deep Beams B3 and K2.

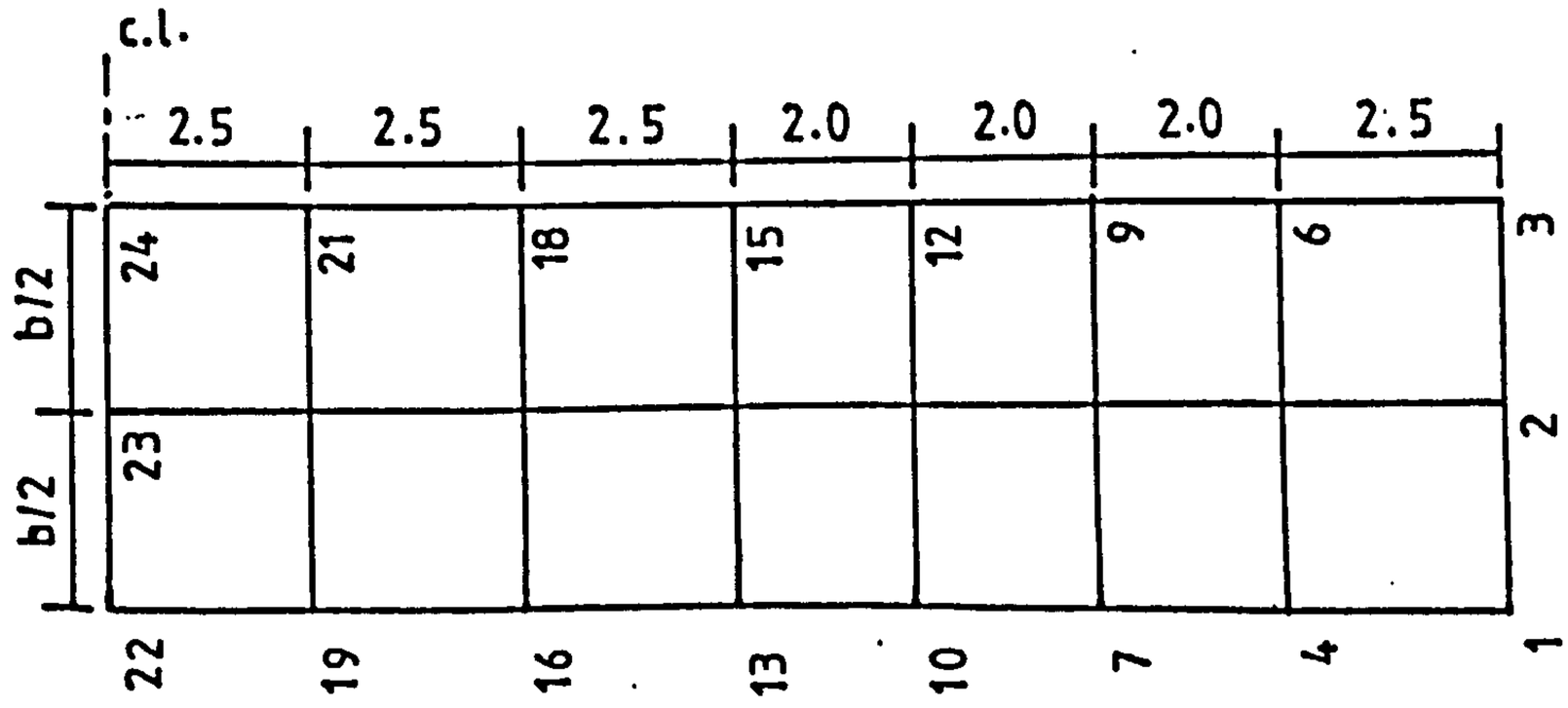

FIG. 7.60 Element Grid Used for the Deep Beams.

USER: CMAR25 FILE: RABKCUR PLOT NO: 1

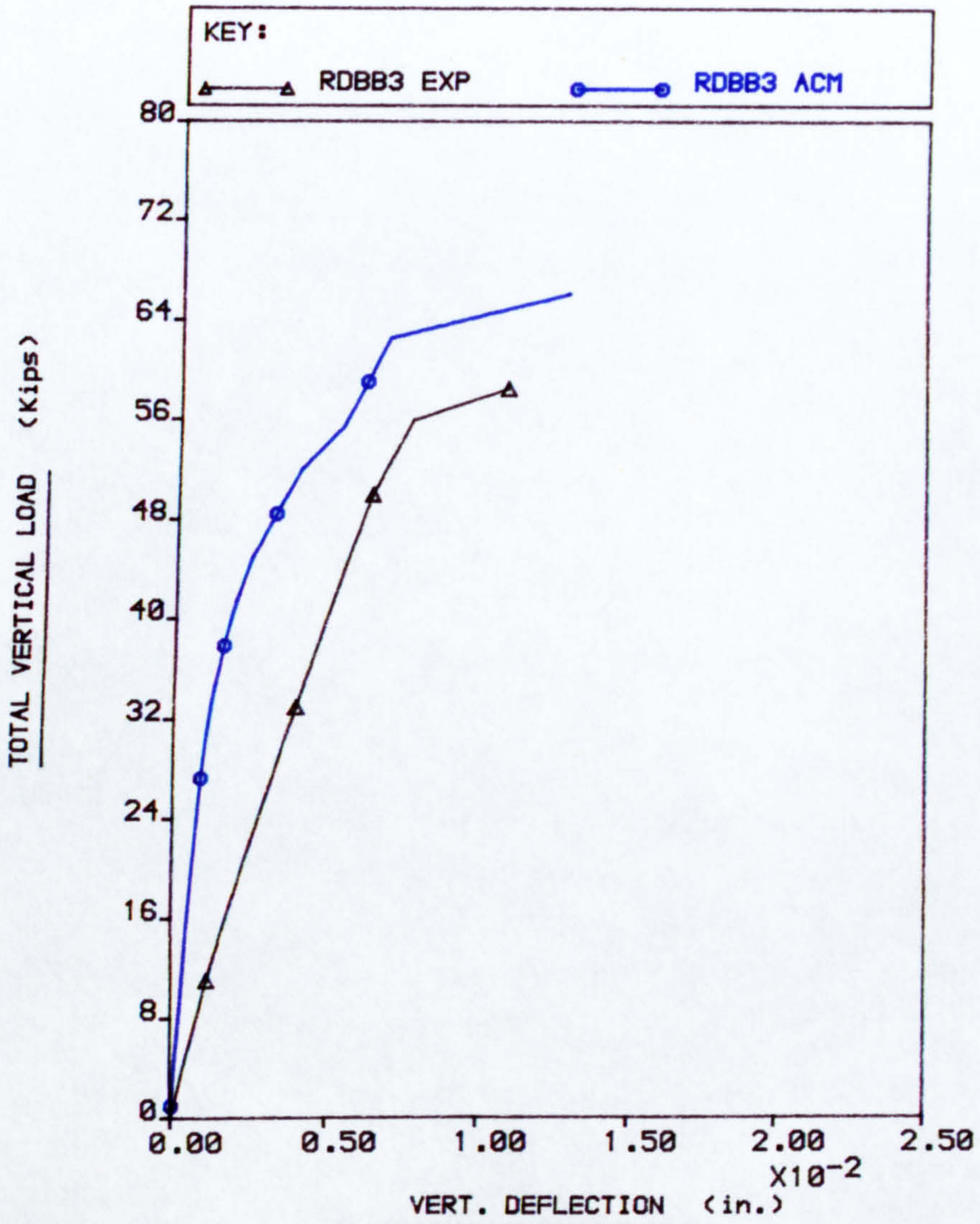

FIG. 7.61 LOAD Vs DISPLACEMENT CURVES FOR NODE *23*

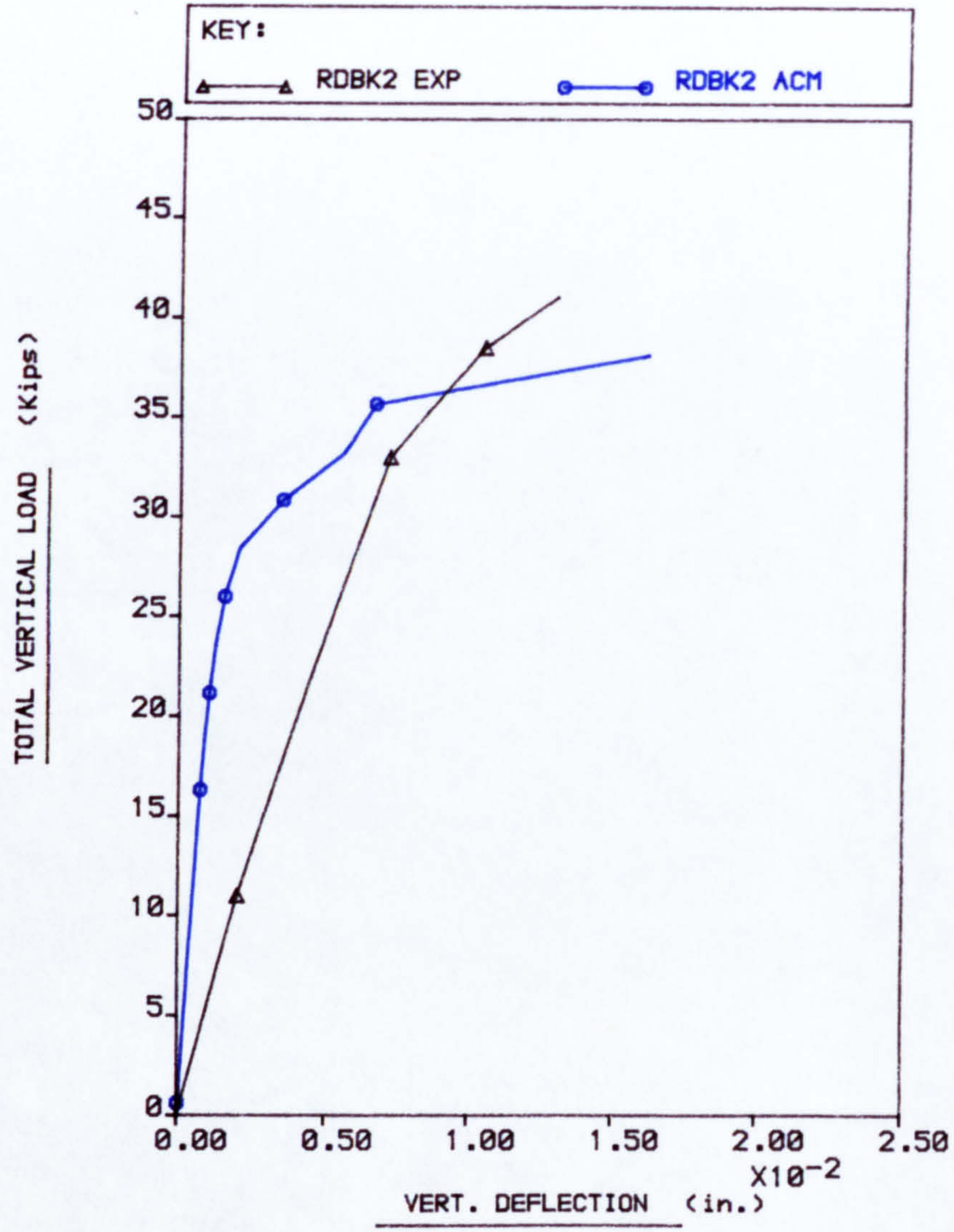

FIG. 7.62 LOAD Vs DISPLACEMENT CURVES FOR NODE *23*

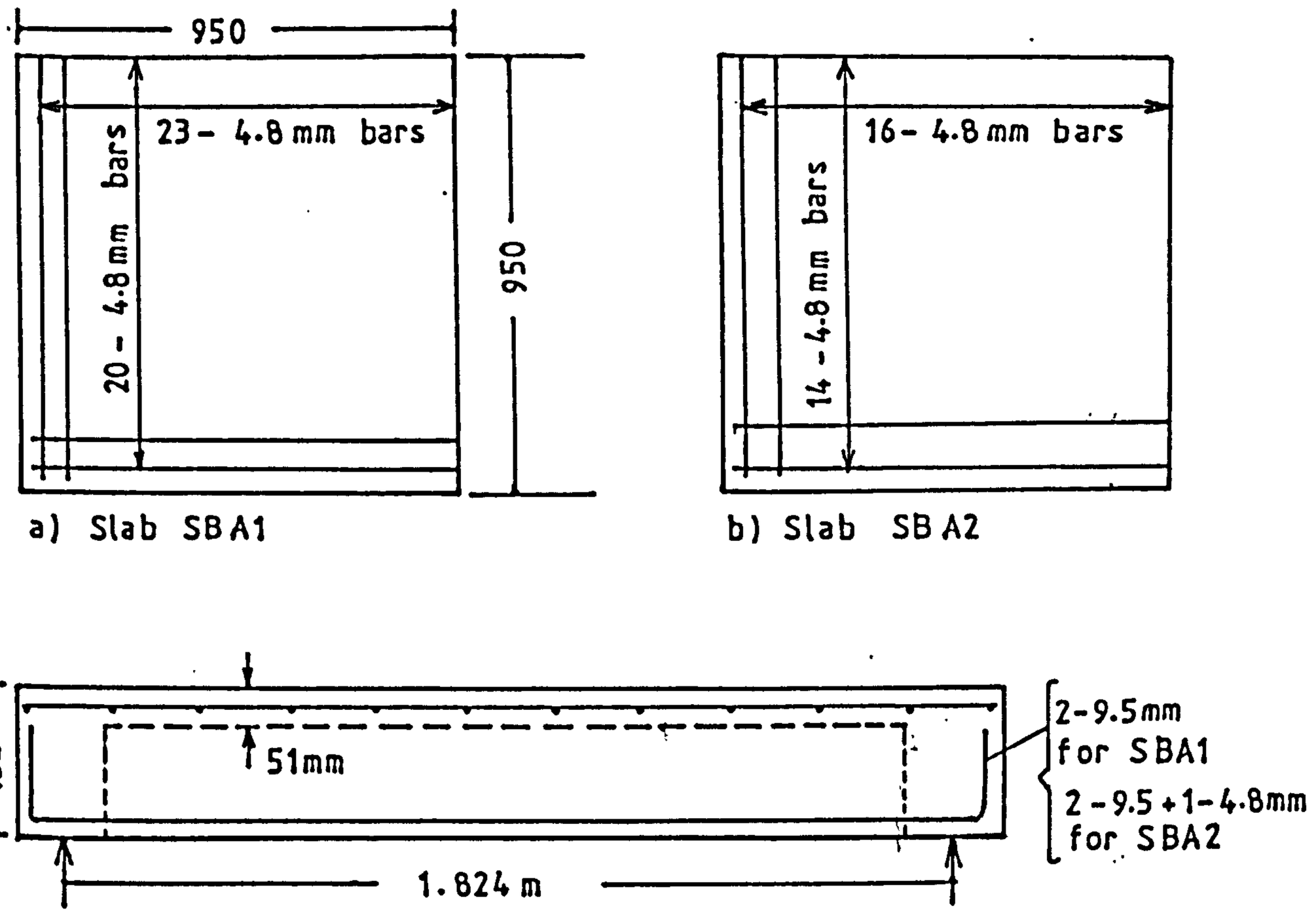

a) Slab SBA1 b) Slab SBA2

c) Beams for SBA1 and SBA2.

FIG. 7.63 Details of Slab Beam Panels SBA1 and SBA2.

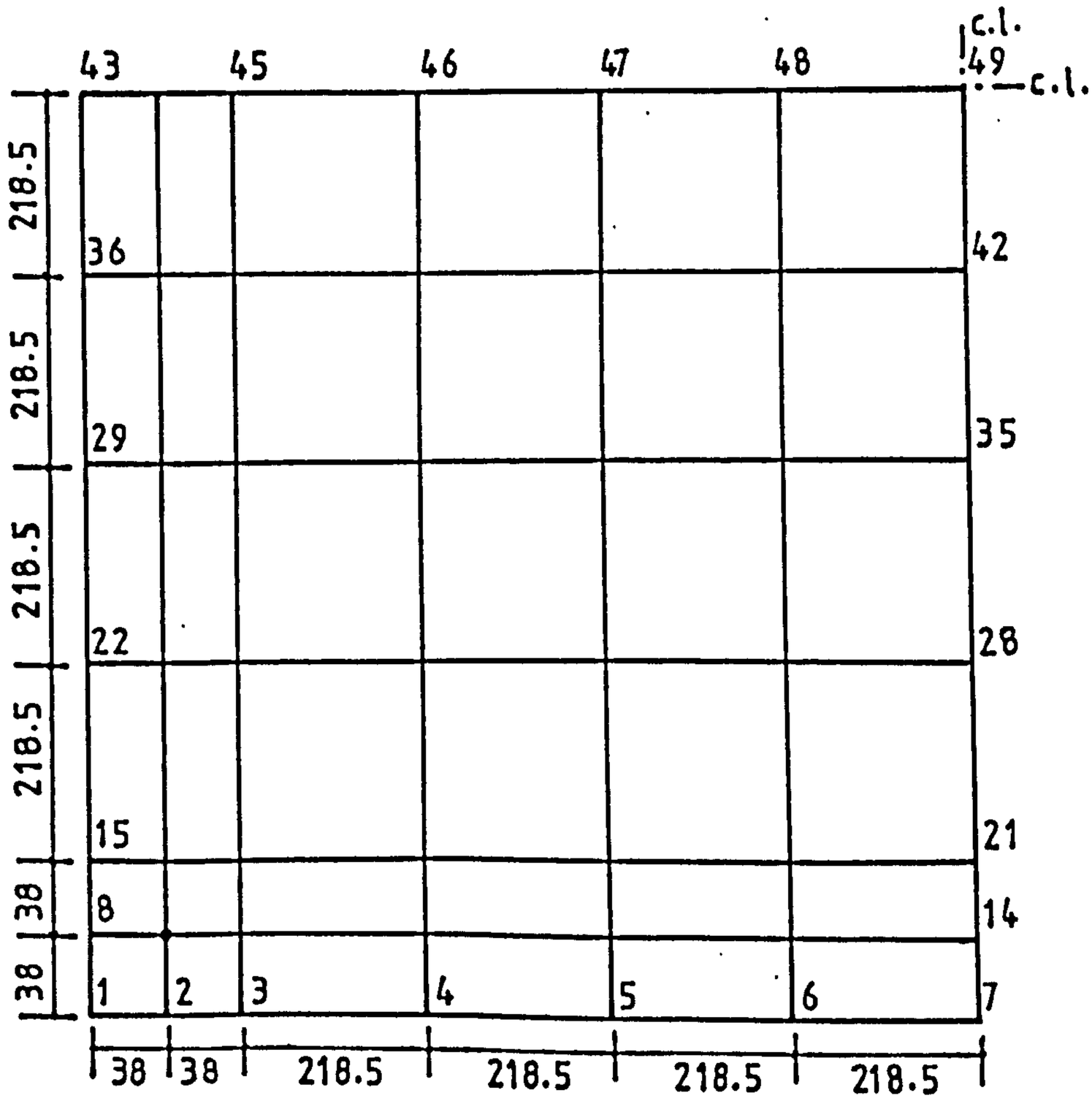

FIG. 7.64 Element Mesh on the Slab Beam Panels.

USER: CMAR25 FILE: HAYRAO PLOT NO: 1

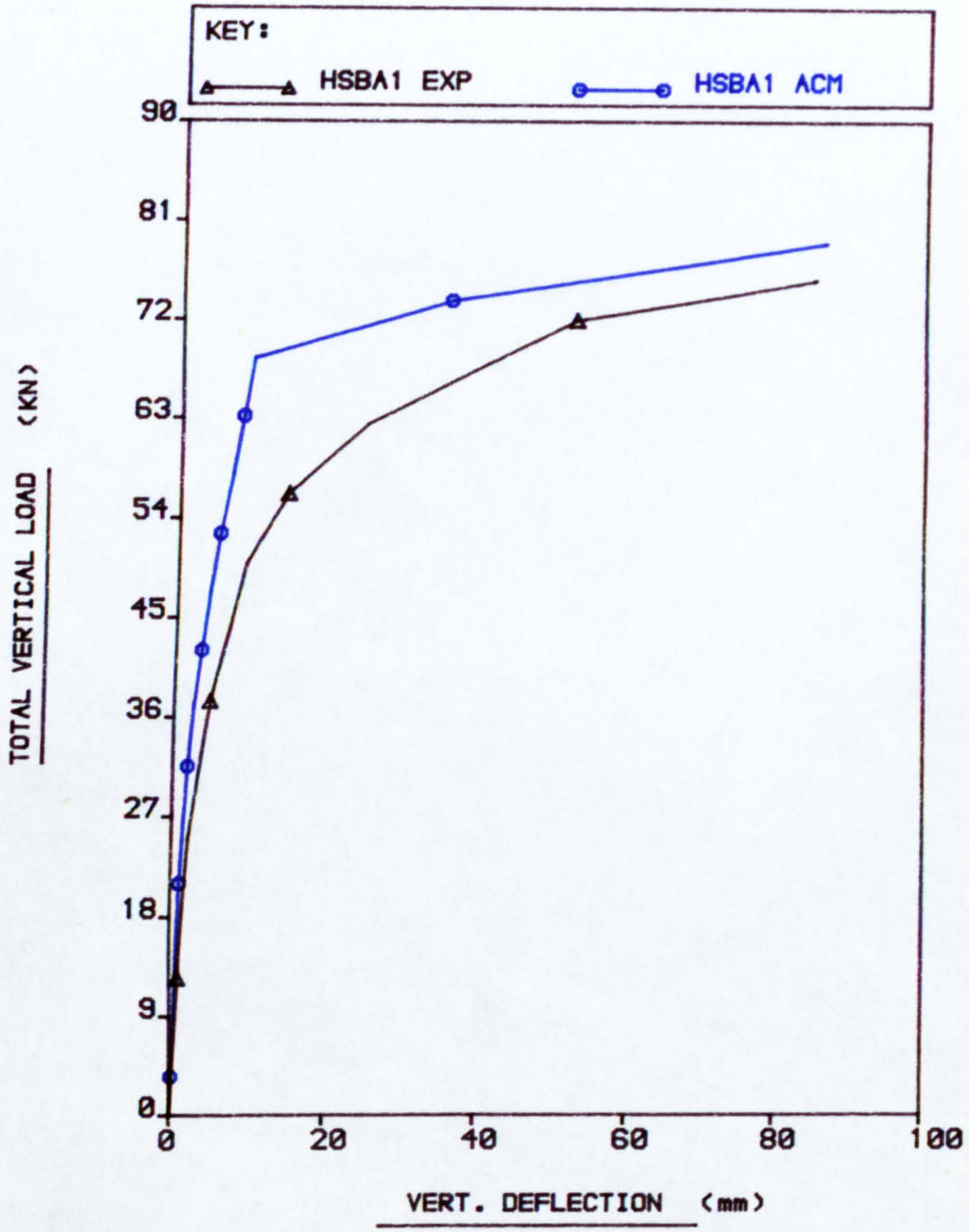

FIG.7.65 LOAD Vs DISPLACEMENT CURVES FOR NODE *49*

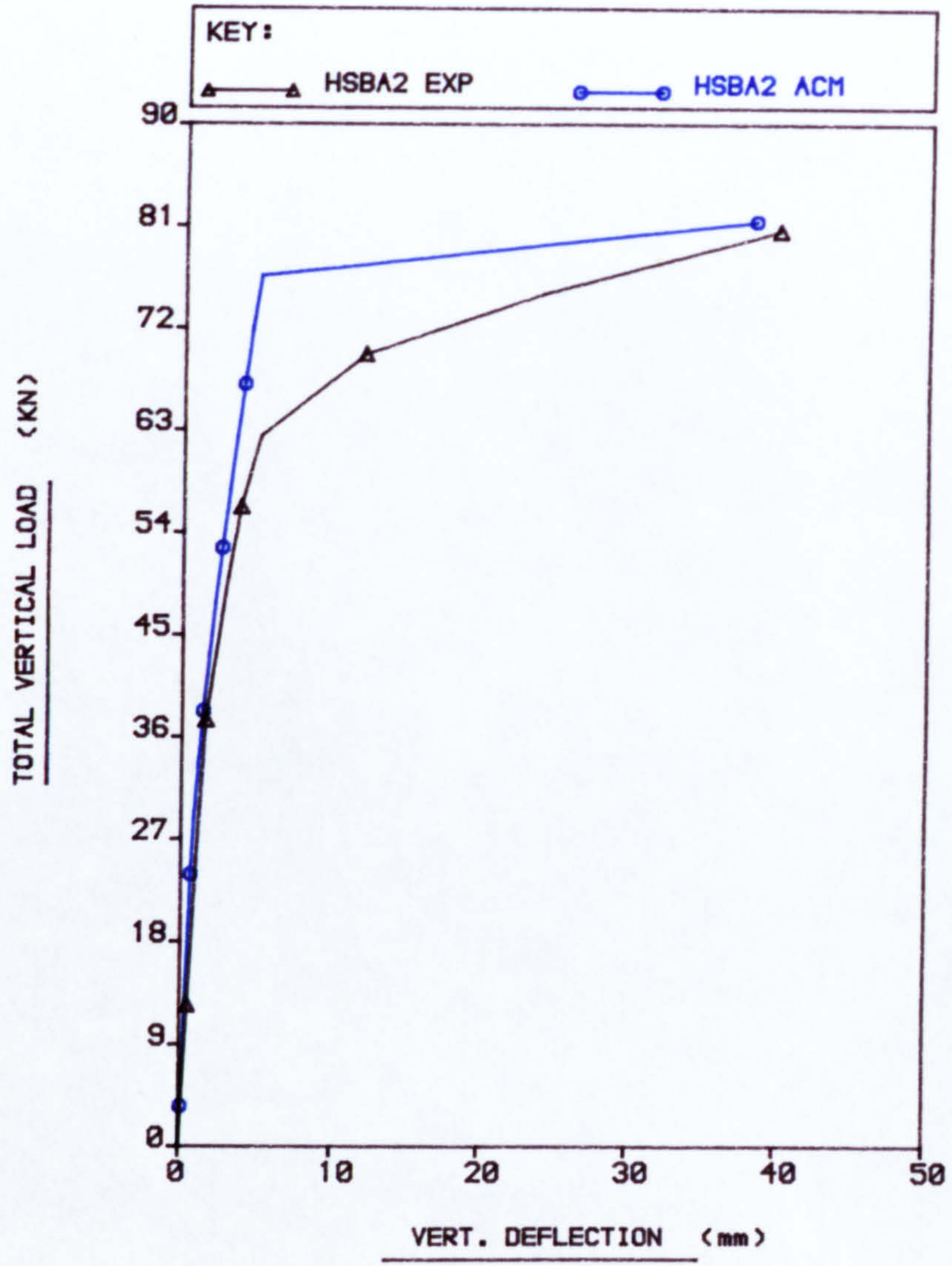

FIG.7.66 LOAD Vs DISPLACEMENT CURVES FOR NODE *14*

USER: CMAR25 FILE: HAYRA0 PLOT NO: 2

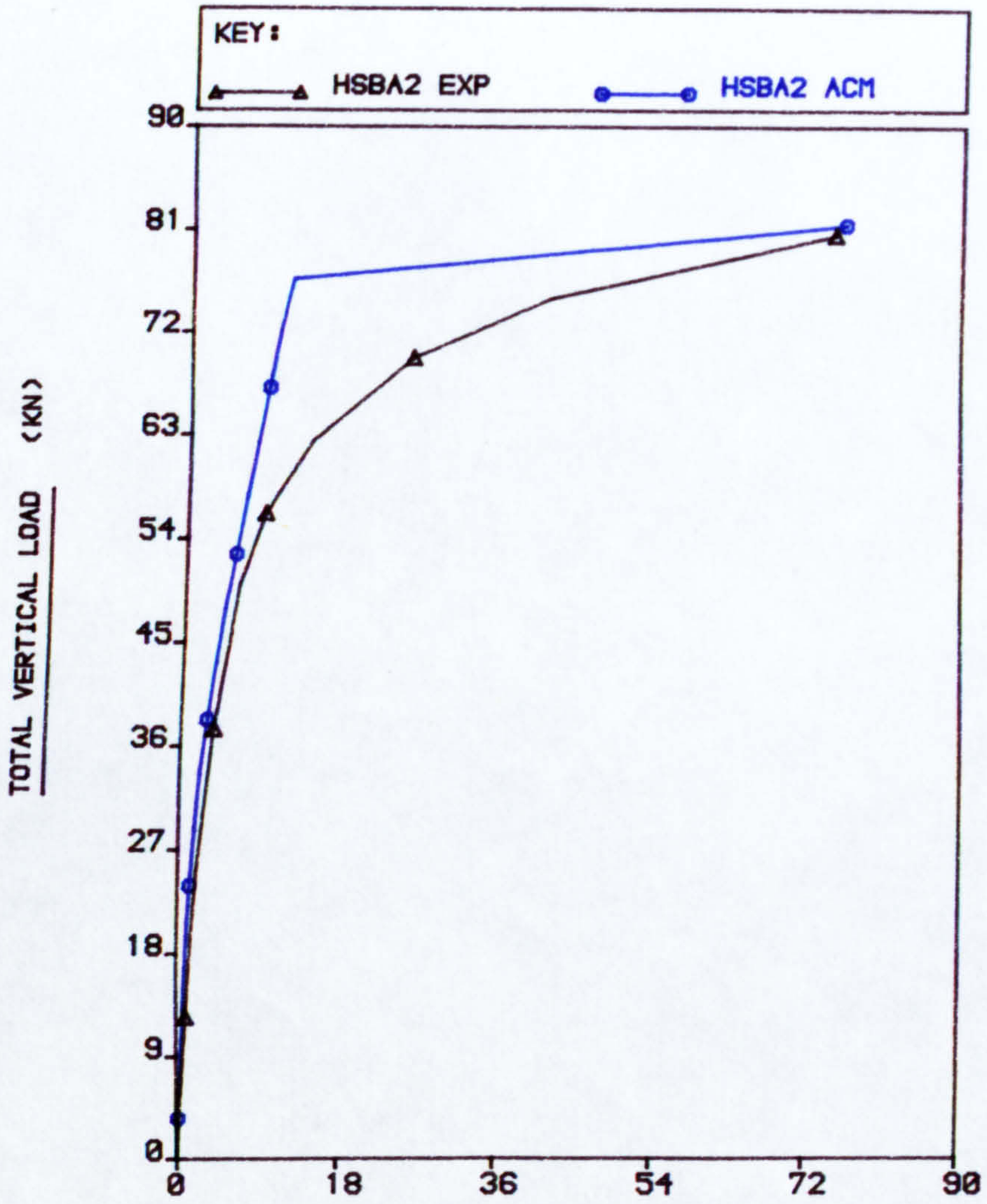

FIG.7.67 LOAD Vs DISPLACEMENT CURVES FOR NODE *19*

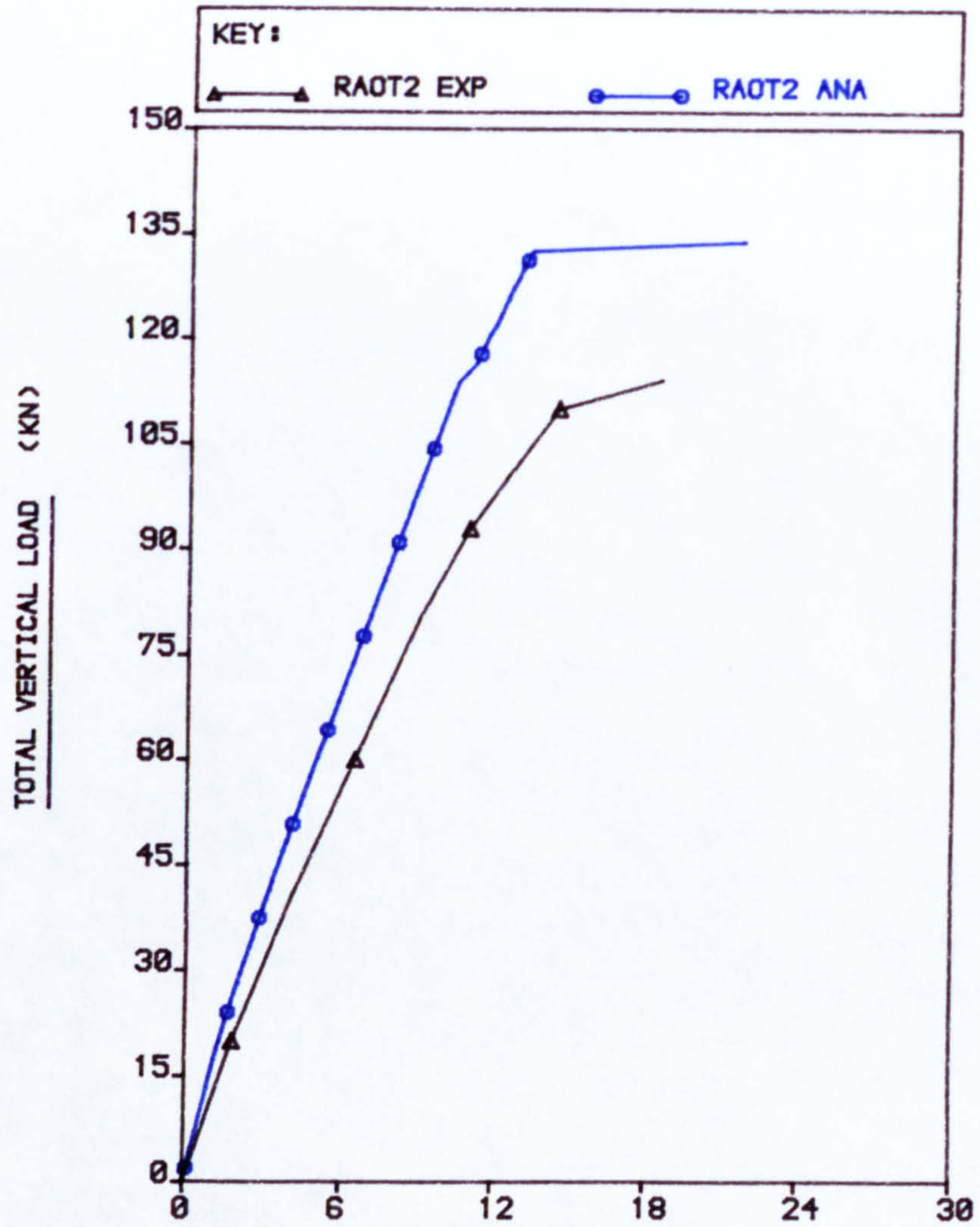

FIG.7.68 LOAD Vs DISPLACEMENT CURVES FOR NODE *27*

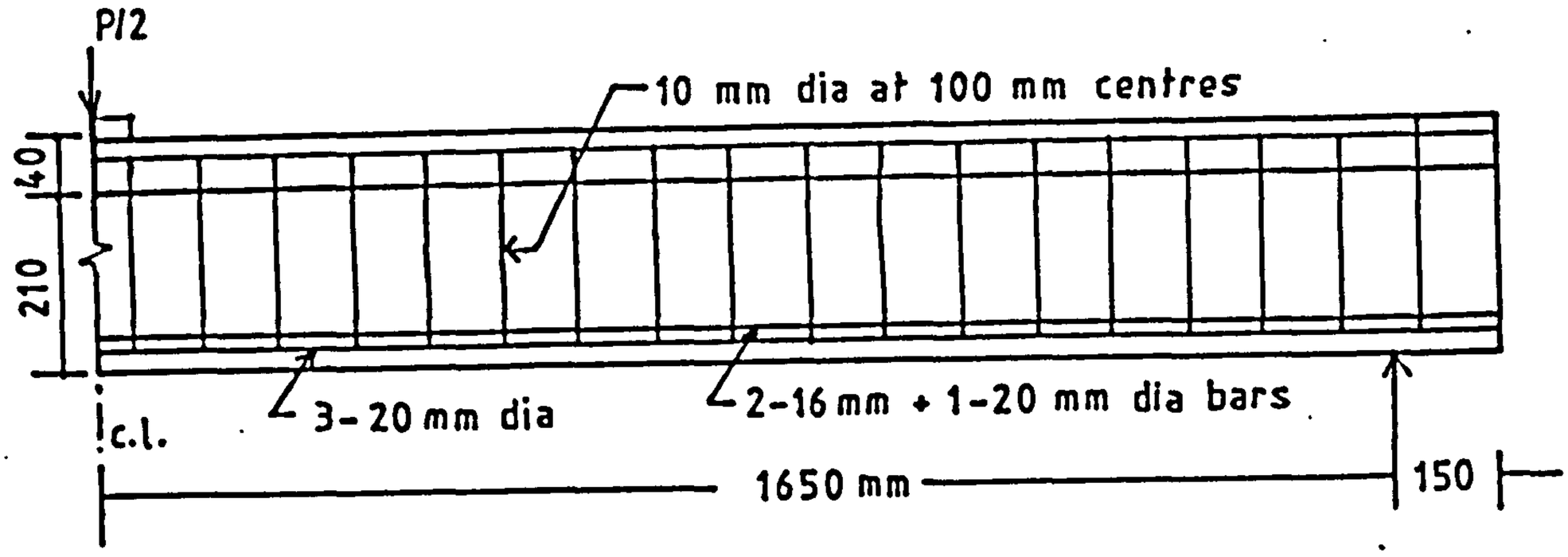

a) Half Elevation of T Beam T2

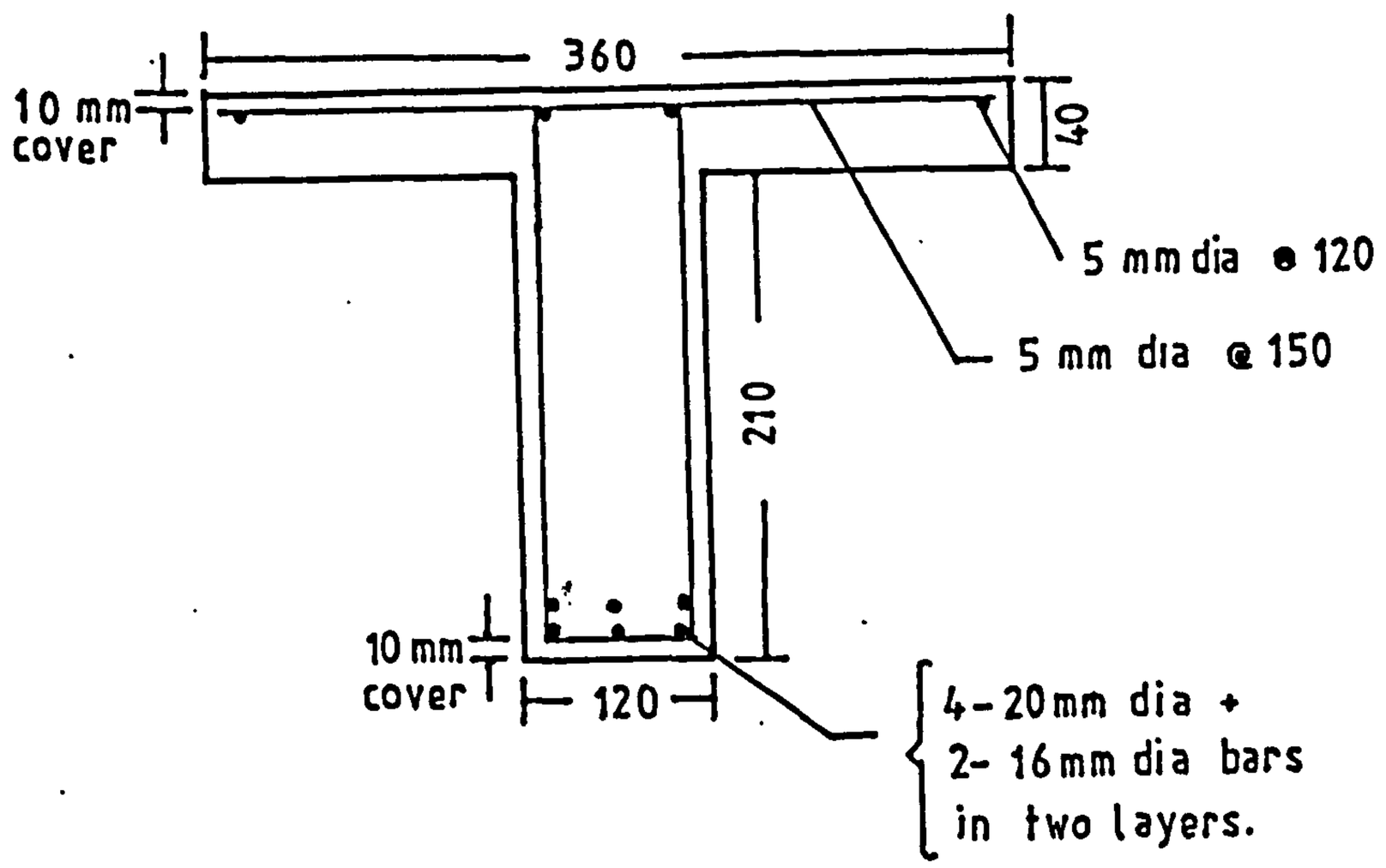

b) Section of the Beam T2

FIG. 7.69 Details of T Beam T2.

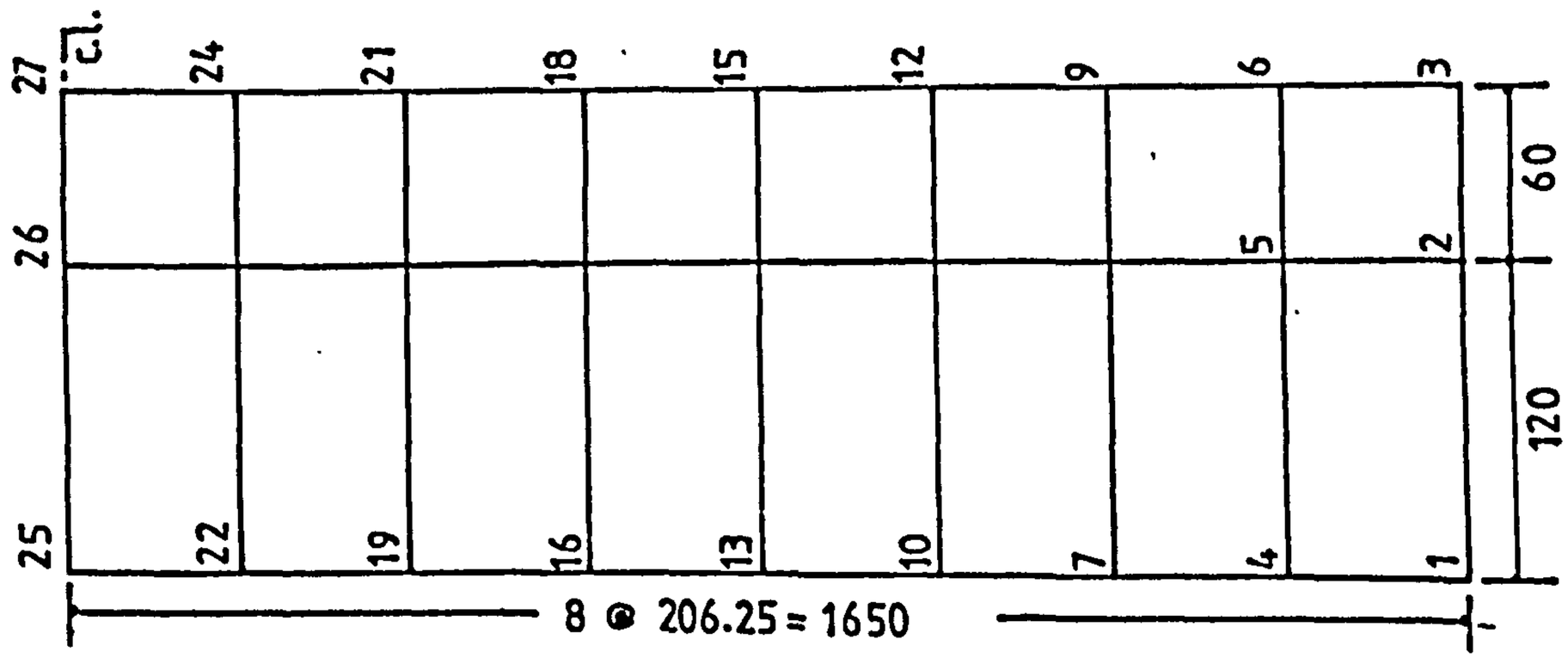

FIG. 7.70 Element Grid on Symmetric Quadrant of theT Beam T2.

Chapter 8

CONCLUSIONS AND SUGGESTIONS

8.1 Conclusions

The numerical techniques for the complete description of the nonlinear response of reinforced concrete structures may be broadly grouped into two categories. The first group comprises the purely numerical aspects such as element discretisation, evaluation of the internal and external actions, various solution strategies, etc. The second group includes the mathematical idealisation for nonlinear constitutive relationships of the constituent materials. Both of these aspects have been investigated at some detail in this study. The principal findings emerging out from the discussions of the previous chapters are summarised below.

1) The 5 DOF ACM plate bending element and the 6 DOF Bogner element are both equally efficient in describing the nonlinear response of reinforced concrete slabs provided the nonlinear material responses are adequately modelled. The 6 DOF Bogner element has shown slightly stiffer predictions in the case of slabs supporting point loads. Computationally, the former element is slightly faster compared to the latter. Hence, the use of this 5 DOF ACM element may be recommended. Although it is a noncompatible element, it has been successfully employed in all the numerical examples studied.

2) The numerical integration scheme for evaluation of the internal equivalent nodal forces seems essential because the averaging techniques followed by some previous researchers[36,37,49] are not satisfactory in a general

type of loading. Such approaches are error-prone and can not satisfy equilibrium state for any arbitrary type of external loading.

3) Any of the well established numerical solution algorithms described in Chapter 4 could be used for solution of the resulting nonlinear equations. But from this study it appears that the modified Newton-Raphson procedure with provision for at least one stiffness update at each load level is perhaps best suited. Such algorithms are efficient and economic in tracing the nonlinear response of reinforced concrete.

4) Relative norms of residual forces and/or relative norms of iterative displacements can be used for terminating the iterative processes about a load increment. Their tolerable minimum value should preferably be limited between 0.01 and 0.001. Much lower tolerable limit could be set but it may increase the cost of computation without any appreciable overall influence.

5) The number of elements for structural discretisation seem to have less pronounced effect on the overall load-displacement response of reinforced concrete members in flexure. Thus, the minimum number of element mesh size which is optimum for predicting elastic response seems to be adequate under nonlinear environment also. But if the localised stress or strain quantities are of interest then the element grid should be increased (if necessary) so that the point of interest fall as near to one of the element sampling stations as possible.

6) Six to ten layers including two steel layers are sufficient for sampling the nonlinear responses across the thickness of the element. In fact, increasing the number of layers beyond 8 are found to have no significant effect and is perhaps unnecessary. Care should be taken so that the centroid of any layer does not coincide with the reference axis. The effect is usually small but could become signifi-. cant if the particular layer happen to be of considerable thickness.

7) There are two ways of evaluating the residual forces (Chapt 2). Both can be advantageously used if the numerical integration schemes are adopted for their computation. However, if the initial stress approach is selected then a single equilibrium check after each load increment has shown better performance compared to the approach where such check has been omitted altogether. Complete equilibrium checking procedure is certainly the safer of the two.

8) The load increment size should be small. The preferred size of load increment should be limited to between 5% and 20% of the cracking load. If the cracking load is well estimated numerically then 10-15% size of increment is fairly good. Pre-anticipation of the nonlinear response is also helpful in selecting the optimum load increment size. For highly nonlinear response, smaller increment size should always be preferred. In general, if relatively higher load increment size is selected then the permitted number of iterations should also be increased. This should permit the equilibrium to be achieved at each load level. A 10% load increment size is recommended as a general rule.

9) The numerical treatment of cracking appears to be the most important source of nonlinearity in the context of overall material model. Its numerical representation greatly influences the postcracking constitutive relations. The primary features of cracking consists of i) a criterion to determine onset of cracking and ii) postcracking modelling.

10) The principal stress criterion of Kupfer and Gerstle[59] has been adopted as a citerion for the onset of cracking. The orientation of the crack is also determined on the basis of maximum principal tension at the time of formation of the crack. The crack directions predicted for the reinforced concrete example slabs are found to be in fair agreement with the respective experimental observations.

11) Of the postcracking treatments, the tension stiffening schemes have a significant influence on the numerical model. Considering concrete as a no-tension material at the discrete sampling points may lead to considerable underestimation of actual loads. For realistic representation, some form of tension stiffening scheme is necessary. The proposed alternative approach of effecting tension stiffening in concrete appears to have performed satisfactorily for all the test cases.

12) The theoretical predictions seem to be less sensitive to the value assigned to the shear retention factor. In other words, the numerical treatment of the dowel action and shear transfer across crack has insignificant influence on the overall response of the slabs considered. However, its importance in preventing the numerical instability can not be overruled. This may occur when all the layers in all

the sampling stations of some adjoining elements crack in the same directions. In view of that some fractional value greater than zero is recommended for the shear retention coefficient β.

13) The representative strengths of the constituents of reinforced concrete members are seldom known precisely. Therefore, some engineering judgement is always necessary in the interpretation of any analytical results. The present nonlinear model has been found to be relatively more influenced by tensile strength of concrete than compressive strengths. However, if the material properties are known within ±10% of the real value, the overall response could be assessed without serious error.

14) Under biaxial compressive stress, both the bilinearly elastic model and the gradually softening model of Gerstle[31] are found to perform satisfactorily. If the second elastic modulus is unknown, Gerstle's simple formulation is the obvious choice. Bilinearly elastic model may predict slightly stiffer response near failure compared to the other model.

15) The inplane boundary restraints may have significant effect on the performance of the analytical models. This has been demonstrated with the McNeice's[47] corner supported slab. The realistic use of the present model (which include in-plane degrees of freedoms) demands that the inplane boundary conditions be known with fair degree of precision. Otherwise, the analytical solution could differ considerably from the actual behaviour.

16) The generality of the present nonlinear analysis procedure has been demonstrated with the help of several numerical examples. Its capability to cope with different boundary conditions and loading systems are fairly conclusive. The numerical predictions regarding load-displacement curves, cracking patterns, load-steel strain response and ultimate load levels are found to be quite satisfactory in most cases. The present programme permits the analysis of reinforced concrete slabs where the slab thickness may discretely vary over the span. A beam slab assembly is an extreme of such cases. Some examples of this form (including a T beam) has been studied. The general agreement is fair. It is known that in deep members the transverse shear may affect the results. The present model ignores these effects. In view of that it is believed that further experimental results of these types of structures are needed to arrive at a definite conclusion. Only then the adequacy of the present model can be outlined for handling such structural forms.

8.2 Suggestions

As stated earlier, the present formulation is based on thin plate theory of flexure. This would meet the requirements of many of the reinforced concrete structural slabs. Even, relatively shallow beams may be analysed using this formulations assigning a zero value to the Poisson's ratio. The numerical aspects are based on well established procedures such as numerical integration schemes, various solution algorithms, etc. The principal areas to which the present formulation may be extended, with slight alteration and addition to the present programme, are suggested below.

i) A different material model for the description of material responses may be incorporated.

ii) Reinforcing steel response may be generalised to include the elasto-plastic strain hardening behaviour of steel.

iii) Provision for description of cyclic loading may be included.

iv) Time dependent behaviour of concrete such as creep and shrinkage can be added to the existing programme structure. They are known to have appreciable influence on the long term behaviour of reinforced concrete structures.

v) Effect of geometric nonlinearities may be included to study how it influences the behaviour of reinforced concrete slabs.

vi) The present formulation may be altered to Mindlin plate formulation which includes the effect of transverse shear forces. It should generalise the capabilities to handle relatively thick flexural structures with confidence.

vii) A separate layered beam element may be included. This would enable the discretisation of beam-slab structures with two different types of elements. The present model makes use of the plate elements to discretise the beams.

Some other aspects of future study could be directed to

a) Formulate a generalised model for concrete in order to describe its behaviour under any combination of stress state unlike the present segmental representation as both tensile, tensile-compressive, etc.

b) Study experimentally the behaviour of some slab-beam structures. Such experimental informations are necessary to test the capabilities of the present programme or any other analytical methods in predicting the behaviour of slab-beam type structures.

REFERENCES

1. ACI Standard 318-77.
Building Code Requirements for Reinforced Concrete, American Concrete Institute, Detroit, Michigan, U.S.A., 1977.

2. Bashur, F.K. and Darwin , D.
Nonlinear Models for Reinforced Concrete Slabs, J. Struct. Div., Proc. ASCE, Vol. 104, No. ST1, Jan. 1978, pp.157-170.

3. Bathe, K.J.
Finite Element Procedures in Engineering Analysis, Prentice Hall, Inc., Englewood Cliffs, New Jersey, p.735, 1982.

4. Bathe, K.J. and Wilson, E.L.
Numerical Methods in Finite Element Analysis, Prentice-hall, 1976.

5. Bedard, C.
Non-Linear Finite Element Analysis of Concrete Structures, Ph.D. thesis, Imperial College, Univ. of London, 1983, p.286.

6. Bell, J.C. and Elms, D.G.
Nonlinear Analysis of Reinforced Concrete Slabs, Mag. of Concrete Research, Vol. 24, No. 79, June, 1972, pp.63-70.

7. Bell, K.
A Refined Triangular Plate Bending Element, Int. J. Num. Meth. in Engrg., Vol. 1, 1969, pp.101-122.

8. Bogner, F.K., Fox, R.L. and Schmit, L.A.
The Generation of interelement Compatible Stiffness and Mass Matrices by Use of Interpolation Formulae, Proc. 1st Conf. Matrix Methods in Struct. Mechanics, Wright Patterson Air Force Base, Ohio, 1965, pp.111-190.

9. BS 18: Part 2:1971.
Methods for Tensile Testing of Metals, Part 2, Steel (General) British Standard Instn., 2 park St., London.

10. BS 812: Part 1:1975.
Testing Aggregates, part 1, Methods for Determination of Particle Size and Shape, British Standard Institution, London.

11. BS 1200:1976.
Sands for Mortar for Plain and Reinforced Brickwork, Block-walling and Masonry, British Standard Instn., 2 Park St., London.

12. BS 1881: Part 121:1983.
Testing Concrete, Part 121, Method for Determination of Static Modulus of Elasticity in Compression, British Standard Instn., 2 Park St., London.

13. Buyukozturk, O.
Nonlinear Analysis of Reinforced Concrete, Comp. & Struct., Vol. 7, 1977, pp.149-156.

14. Carpenter, J.E., Roll, F. and Zelman, M.I.
Techniques and Materials for Structural Models, 'Models for Concrete Structure', ACI Publication, SP-24, Detroit, 1970, pp.41-63.

15. Cervenka, V. and Gerstle, K.H.
Inelastic Analysis of Reinforced Concrete Panels: Theory, Int. Assoc. for Bridge and Struct. Engrg. (IABSE), Vol. 31, II, 1971, pp.31-45.

16. Chen, A.C.T. and Chen, W.
Constitutive Relations for Concrete, J. Engrg. Mech. Div., ASCE, Vol. 101, No. EM4, Aug. 1975, pp.465-481.

17. Cook, R.D.
Concept and Application of Finite Element Analysis, John Wiley and Sons, 1974, p.402.

18. Cope, R.J. and Rao, P.V.
Nonlinear Finite Element Analysis of Concrete Slab Structures, Proc. Instn. of Civil Engrs., part 2, Vol. 63, March, 1977, pp.159-179.

19. Cope, R.J., Rao, P.V. and Edwards, K.R.
Nonlinear Finite Element Analysis Technique for Concrete Slabs, Numerical Methods for Nonlinear Problems, Taylor, Hinton and Owen (Edts.), Vol. 1, Univ. College Swansea, Pineridge Press, 1980, pp.445-456.

20. Cope, R.J., Rao, P.V., Clark, L.A. and Norris, P.
Modelling of Reinforced Concrete Behaviour for Finite Element Analysis of Bridge Slab, Proc. Int. Conf. on Numerical Methods for Nonlinear Problems, Edtrs. Taylor, C., Hinton, E. and Owen, D.R.J., Vol. 1, Univ. College Swansea, Pineridge Press, 1980, pp.457-470.

21. Cope, R.J. and Rao, P.V.
Shear Forces in Edge Zones of Concrete Slabs. The Structural Engineer, Vol. 62A, No. 3, Mar., 1984, pp.87-92.

22. Cope, R.J. and Clark, L.A.
Concrete Slabs, Analysis and Design, Elsevier Applied Science Publishers, London, 1984, p.502.

23. CP110: Part 1: 1972.
The Structural Use of Concrete, Part 1, Design, Materials and Workmanship, British Standard Institution, London.

24. Darwin, D. and Pecknold, D.A.
Nonlinear Biaxial Stress-Strain Law for Concrete, Jnl. of Engrg. Mech. Div., ASCE, Vol. 103, No. EM2, April, 1977. pp.229-241.

25. Desai, C.S. and Abel, J.F.
Introduction to Finite Element Method, Van Nostrand Reinhold, 1972.

26. Desai, C.S.
Elementary Finite Element Methods, Englewood Cliffs, N.J., Prentice Hall, 1979, p.434.

27. Dotreppe, J.C., Schnobrich, W.C. and Pecknold, D.A.
Layered Finite Element Procedures for Inelastic Analysis of Reinforced Concrete Slabs, Int. Assoc. of Bridge and Structural Engrg., 33-II, 1973, pp.53-68.

28. Duncan, W. and Johnarry, T.
Further Studies on the Constant Stiffness Method of Nonlinear Analysis of Concrete Structures, Proc. Instn. of Civ. Engrs., Part 2, Vol. 67, Dec. 1979, pp.951-969.

29. Dunham, C.W.
The Theory and Practice of Reinforced Concrete, 4th Ed., McGraw Hill Book Co., N.Y., 1966, Chapt. 1, pp.36-37, p.629.

30. Gerald, C.F.
Applied Numerical Analysis, Addison-Wesley Publishing Co., 1970

31. Gerstle, K.H.
Simple Formulation of Biaxial Concrete Behaviour, Jnl. of ACI, V. 78, No. 1, Jan./Feb. 1981, pp.62-68.

32. Ghali, A. and Neville, A.M.
Structural Analysis, A Unified Classical and Matrix Approach, 2nd Ed., Chapman and Hall, 1978, p.779.

33. Gilbert, R.I. and Warner, R.F.
Time Dependent Behaviour of Reinforced Concrete Slabs, IABSE Proc., P-12/78, Int. Assoc. for Bridge and Struct. Engrg., Feb. 1978, p.12.

34. Grayson, R. and Stevens, L.K.
Nonlinear Analysis of Structural Systems of Steel and Concrete, Proc. of the Third Int. Conf. in Australia on Finite Element Methods, July, 1979, held at the Univ. of New South Wales, pp.179-196.

35. Haisler, W.E., Striklin, J.A. and Stebbins, F.J.
Development and Evaluation of Solution Procedures for Geometrically Nonlinear Structural Analysis, AIAA Jnl., V. 10, No. 3, Mar. 1972, pp.264-272.

36. Hand, F.R., Pecknold, D.A. and Schnobrich, W.C.
A Layered Finite Element Nonlinear Analysis of Reinforced Concrete Plates and Shells, Univ. of Illinois, Urbana, Struct. Research Series 389, 1972, p.123.

37. Hand, F.R., Pecknold, D.A. and Schnobrich, W.C.
Nonlinear Layered Analysis of RC Plates and Shells. J. Struct. Div., Proc. ASCE, Vol. 99, No. ST7, July, 1973, pp.1491-1505.

38. Hayes, B. and Taylor, R.
Some Tests on Reinforced Concrete Beam Slab Panels, Mag. of Concrete Research, Vol. 21, No. 67, June, 1969, pp.113-120.

39. Hill, R.
The Mathematical Theory of Plasticity, Oxford, Clarendon Press, 1950.

40. Hinton, E. and Campbell, J.S.
Local and Global Smoothing of Discontinuous Finite Element Function Using Least Square Method, Int. J. Num. Meth. in Engrg., Vol. 8, 1974, pp.461-480.

41. Hinton, E. and Owen, D.R.J.
Finite Element Programming, Academic Press, U.K., 1977.

42. Hinton, E. and Owen, D.R.J.
An Introduction to Finite Element Computations, Pineridge Press, Swansea, U.K., 1979, p.385.

43. Hornbeck, R.W.
Numerical Methods, Quantum Publishers, Inc., N. York, 1975, p.310.

44. Hughes, B.P.
Limit State Theory for Reinforced Concrete Design, 3rd Edition, 1980, The Pitman Press, Bath, U.K., pp.349-425, p.697.

45. Huq, M.M.
Nonlinear Finite Element Analysis of Plates and Shells, Ph.D. thesis, Univ. of Wales, Swansea, 1980.

46. Irons, B. and Ahmad, S.
Techniques of Finite Elements, Ellis Horwood Ltd., Sussex, U.K. p.529.

47. Jofriet, J.C. and McNeice, G.M.
Finite Element Analysis of Reinforced Concrete Slabs, J.Struct. Div., Proc. ASCE, V. 97, No. ST3, Mar, 1971, pp.785-806.

48. Johansen, K.W.
Yield Line Theory, Cement and Concrete Association, London, 1962, p.181.

49. Johnarry, T.
Elasto-Plastic Analysis of Cocnrete Structures Using Finite Elements, Ph.D. thesis, Univ. of Strathclyde, 1979, p.301.

50. Jones, L.L.
Ultimate Load Analysis of Reinforced and Prestressed Concrete Structures, Chatto and Windus, London, 1962, p.248, pp.109-226.

51. Jones, L.L. and Wood, R.H.
Yield Line Analysis of Slabs, Thames and Hudson, London, 1967, p.405.

52. Kabir, A. and Duncan, W.
NONARCS: Users Guide to Nonlinear Analysis Programme for Reinforced Concrete Slab Structures, Internal Report, Dept. of Civil Engrg., Univ. of Strathclyde, Glasgow (Under Preparation)

53. Kong, F.K. and Evans, R.H.
Reinforced and Prestressed Concrete, Thomas Nelson & Sons Ltd., Middlesex, U.K., 1975, Reprint 1978, p.229.

54. Kotsovos, M.D. and Newman, J.B.
Behaviour of Concrete Under Multiaxial Stress, ACI Jnl., V.74, No. 9, Sept. 1977, pp.443-446.

55. Kotsovos, M.D. and Newman, J.B.
A Mathematical Description of the Deformational Behaviour of Concrete Under Complex Loading, Mag. of Concrete Research, Vol. 31, No. 107, June, 1979, pp.77-90.

56. Kotsovos, M.D.
A Mathematical Description of Strength Properties of Concrete Under Generalised Stress, mag. of Concrete Research, Vol. 31, No. 108, Sept. 1979, pp.151-158.

57. Kotsovos, M.D.
Concrete. A Brittle Fracturing Material, Materiaux et Constructions, (Materials and Structures), Vol. 17, No. 98, Mar-April, 1984, pp.107-115.

58. Kupfer, H., Hilsdorf, H.K. and Rüsch, H.
Behaviour of Concrete Under Biaxial Stresses, Jnl. of Am. Concrete Instn., Vol. 66, No. 8, Aug. 1969, pp.656-666.

59. Kupfer, H.B. and Gerstle, K.H.
Behaviour of Concrete Under Biaxial Stresses, Jnl. of Engrg. Mech. Div., ASCE, Vol. 99, No. EM4, Aug. 1973, pp.853-866.

60. Lin, C.S. and Scordelis, A.
Nonlinear Analysis of RC Shells of General Form, Jnl. of Struct. Div., ASCE, No. ST3, Mar. 1975, pp.523-538.

61. Liu, T.C.Y., Nilson, A.H. and Slate, F.O.
Stress-Strain Response and Fracture of Concrete in Uniaxial and Biaxial Compression, ACI Jnl., Vol. 69, No. 5, May, 1972, pp.291-295.

62. Liu, T.C.Y., Nilson, A.H. and Slate, F.O.
Biaxial Stress-Strain Relations for Concrete, Jnl. of Struct. Div., Proc. ASCE, Vol. 98, No. ST5, May, 1972, pp.1025-1034.

63. Long, A.
A Review of Recent Developments in Concrete Modelling, 'Reinforced and Prestressed Microconcrete Models', Edited by F.K. Garas and G.S.T. Armer, The Construction Press, London, 1980, pp.1-15.

64. Marcal, P.V.
A Comparative Study of Numerical Methods of Elasto-Plastic Analysis, Tech. Note, AIAA Jnl., Vol. 6, No. 1, Jan., 1968, pp.157-158.

65. Melosh, R.J.
Basis of Derivation of Matrices for the Direct Stiffness Method, Jnl. of AIAA, Vol. 1, 1963, pp.1631-1637.

66. Nayak, G.C. and Zienkiewicz, O.C.
Elasto-Plastic Stress Analysis, Generalisation for Various Constitutive Relations Including Strain Softening, Int. Jnl. Num. Meth. in Engrg., Vol. 5, 1972, pp.113-135.

67. Ngo, D. and Scordelis, A.C.
Finite Element Analysis of Reinforced Concrete Beams, Jnl. of Am. Concr. Inst., Vol. 64, No. 3, March, 1967, pp.152-163.

68. Nilson, A.H.
Nonlinear Analysis of Reinforced Concrete by Finite Element Method, Jnl. of Am. Concr. Inst., Vol. 65, No. 9, September, 1968, pp.757-766.

69. Nilson, A.H. (Chairman)
Finite Element Analysis of Reinforced Concrete, State-of-the Art Report on Finite Element Analysis of Reinforced Concrete/ Prepared by Task Committee on Finite Element Analysis of Reinforced Concrete Structures of the Structural Division Committee on Concrete and Masonry Structures, ASCE, New York, 1982, p.560.

70. Nour-Omid, B., Parlett, B. and Taylor, L.
A Newton-Lanczos Method for Solution of Nonlinear Finite Element Equations, Comp. and Struct., Vol. 16, No. 4, 1983, pp.241-252.

71. Oberti, G. and Fumagalli, E.
Criterion for the Choice and Use of Model Materials for Reinforced Concrete Structures, 'Reinforced and Prestressed Microconcrete Models', Edited by F.K. Garas and G.S.T. Armer, The Construction Press, London, 1980, pp.205-213.

72. Owen, D.R.J. and Hinton, E.
Finite Elements in Plasticity: Theory and Practice, pineridge press, Swansea, U.K., 1980.

73. Parett, B.
Round Off Errors in Solution of Finite Element Systems, U.S.-Germany Symposium on Formulations and Computational Algorithms in Finite Element Analysis, Edt. Bathe, K.J., Oden, J.T. and Wunderlich, The Massachussets Inst. of Techn., U.S.A., 1978, pp.632-654.

74. Philips, D.V. and Zienkiewicz, O.C.
Nonlinear Analysis of Concrete Structures, Proc. Instn. of Civil Engrs., Part 2, Vol. 61, Mar., 1976, pp.59-88.

75. Pica, A. and Hinton, E.
The Quasi-Newton BFGS Method in Large Deflection Analysis of Plates, Proc. Int. Conf. on Numerical Methods for Nonlinear Problems, Edtrs. Taylor, C., Hinton, E. and Owen, D.R.J., Vol. 1, Univ. College Swansea, Pineridge Press, 1980, pp.355-365.

76. Rahman, H.H.A., Hinton, E. and Huq, M.M.
Nonlinear Finite Element Analysis of Reinforced Concrete Slab and Slab-Beam Structures, Proc. Int. Conf. on Numerical Methods for Nonlinear Problems, Edtrs. Taylor, Hinton and Owen, Vol. 1, Univ. College Swansea, Pineridge Press, 1980, pp.493-502.

77. Ramakrishnan, V. and Ananthanarayana, Y.
Ultimate Strength of Deep Beams in Shear, ACI Jnl., Vol. 65, Feb. 1968, pp.87-98.

78. Rashid, Y.R.
Analysis of Prestressed Pressure Vessels, Nuclear Engrg. and Design, Vol. 7, No. 4, April, 1968, pp.334-344.

79. Romstad, K.M., Taylor, M.A. and Herrman, L.R.
Numerical Biaxial Characterization for Cocnrete, Jnl. of Engrg. Mech. Div., ASCE, Vol. 100, No. EM5, Oct. 1974, pp.935-948.

80. Sarkar, D.
Nonlinear Elasto-Plastic Finite Element Analysis of Skew Slab Bridges, M.Sc. thesis, Univ. of Strathclyde, 1975.

81. Smith, I.M. and Duncan, W.
The Effectiveness of Nodal Continuities in Finite Element Analysis of Thin Rectangular and Skew Plates in Bending, Int. J. Num. Meth. in Engrg., Vol. 2, 1970, pp.253-258.

82. Suidan, M. and Schnobrich, W.C.
Finite Element Analysis of Reinforced Concrete, Jnl. of Struct. Div., ASCE, Vol. 99, No. ST10, October, 1973, pp.2109-2122.

83. Taylor, R., Maher, D.R.H. and Hayes, B.
Effect of the Arrangement of Reinforcement on the Behaviour of Reinforced Concrete Slabs, Magazine of Concrete Research, Vol. 18, No. 55, June, 1966, pp.85-94.

84. Tillerson, J.R., Striklin, J.A. and Haisler, W.E.
Numerical Methods for the Solution of Nonlinear Problems in Structural Analysis, Edt. Hartung, R.F., Numerical Solution of Nonlinear Structural Problems, ASME, New York, 1973, pp.67-101.

85. Timoshenko, S.P. and Woinowsky-Krieger, S.
Theory of Plates and Shells, 2nd Ed., McGraw Hill Book Company, 1959.

86. Timoshenko, S. and Goodier, J.N.
Theory of Elasticity, 3rd Ed., McGraw Hill Book Company, 1970.

87. Troitsky, M.S.
Stiffened Plates: Bending, Stability and Vibrations, Elsevier Scientific Publishing Company, Amsterdam-Oxford-New York, 1976, p.410.

88. Turner, M.J., Clough, R.W., Martin, H.C. and Topp, L.J.
Stiffness and Deflection Analysis of Complex Structure, Jnl. of Aero/space Science, Vol. 23, 1956, pp.805-823.

89. Turner, M.J., Dill, E.H., Martin, H.C. and Melosh, R.J.
Large Deflections of Structures Subjected to Heating and External Loads, Jnl. of Aero/space Science, Vol. 27, No. 2, Feb. 1960, pp.99-106.

90. Valliapan, S. and Doolan, T.F.
Nonlinear Stress Analysis of Reinforced Concrete, Jnl. of Struct. Div., ASCE, Vol. 98, No. ST4, April, 1972, pp.885-898.

91. Walz , J.E., Fulton, R.E. and Cyrus, N.J.
Accuracy and Convergence of Finite Element Approximation, Proc. 2nd Conf., Matrix Method in Struct. Mechanics, Wright Patterson Air Force Base, Ohio, 1968.

92. Wanchoo, M.K. and May, G.W.
Cracking Analysis of Reinforced Concrete Plates, J. Struct. Div., Proc. ASCE, Vol. 101, No. ST1, Jan. 1975, pp.201-215.

93. Wegmuller, A.W.
Full Range Analysis of Eccentrically Stiffened Plates, J. of Struct. Div., Proc. ASCE, Vol. 100, No. ST1, Jan. 1974, pp.143-159.

94. Wegmuller, A.W. and Amer, H.N.
Nonlinear Response of Composite Steel-Concrete Bridges, Computers & Structures, V. 7, No. 2, April, 1977, pp.161-169.

95. Wegmuller, A.W.
Overload Behaviour of Composite Steel Concrete Bridges, J. Struct. Div., Proc. ASCE, No. ST9, V. 103, Sept. 1977, pp.1799-1819.

96. Winter, G. and Nilson, A.H.
Design of Reinforced Concrete Structures, 8th Ed., McGraw Hill Book Company, 1973, p.615.

97. Yamada, Y., Kawai, T., Yoshimura, N. and Sakurai, T.
Analysis of the Elastic-Plastic Problems by Matrix Displacement Method, Proc. 2nd Conf. on Matrix Methods in Structural Mechanics, Wright Patterson Air Force Base, Ohio, 1968, pp.1271-1299.

98. Zienkiewicz, O.C. and Cheung, Y.K.
The Finite Element Method in Structural and Continuum Mechanics McGraw Hill Book Co., 1967.

99. Zienkiewicz, O.C., Valliapan, S. and King, I.P.
Elastoplastic Solutions of Engineering Problems - Initial Stress Finite Element Method, Int. Jnl. of Num. Methods in Engrg., Vol. 1, No. 1, 1969, pp.75-100.

100. Zienkiewicz, O.C.
The Finite Element Method, McGraw Hill Book Company, England, 1977, p.787.

101. Zienkiewicz, O.C. and Cheung, Y.K.
The Finite Element Method for Analysis of Elastic Isotropic and Orthotropic Slabs, Proc. Instn. of Civ. Engrs., Vol. 28, 1964, pp.471-488.

APPENDICES

Appendix-A

EXPLICIT FORM OF SOME OF THE MATRICES NEEDED IN MATHEMATICAL FORMULATIONS OF THE ELEMENTS USED

The plate strain operator Matrix, A

$$= \begin{bmatrix} \frac{\partial}{\partial x} & 0 & 0 & 0 & 0 & 0 \\ 0 & \frac{\partial}{\partial y} & 0 & 0 & 0 & 0 \\ \frac{\partial}{\partial y} & \frac{\partial}{\partial x} & 0 & 0 & 0 & 0 \\ 0 & 0 & 0 & -\frac{\partial^2}{\partial x 2} & 0 & 0 \\ 0 & 0 & 0 & 0 & -\frac{\partial}{\partial y 2} & 0 \\ 0 & 0 & 0 & 0 & 0 & -2\frac{\partial^2}{\partial x \partial y} \end{bmatrix}$$

The explicit form of the H matrix (Eq. 2.42) for 5 DOF ACM Plate Bending Element is given in the following page.

$$H \longrightarrow \left[\begin{array}{cccccccc|c|cccccccccccc} 0 & 1 & 0 & y & 0 & 0 & 0 & 0 & & & & & & & & & & & & \\ 0 & 0 & 0 & 0 & 0 & 0 & 1 & x & & & & & & & & & & & & \\ 0 & 0 & 1 & x & 0 & 1 & 0 & y & & & & & & & & & & & & \end{array}\right.$$

$$\left.\begin{array}{c|cccccccccccc} & 0 & 0 & 0 & -2 & 0 & 0 & -6x & -2y & 0 & 0 & -6xy & 0 \\ & 0 & 0 & 0 & 0 & 0 & -2 & 0 & 0 & -2x & -6y & 0 & -6xy \\ & 0 & 0 & 0 & 0 & -2 & 0 & 0 & -4x & -4y & 0 & -6x^2 & -6y^2 \end{array}\right]$$

$0_{3 \times 8}$

$0_{3 \times 12}$

Matrix H for the 6 D.O.F. Bogner Element,

$$
\begin{bmatrix}
0 & 1 & 0 & y & 0 & 0 & 0 & 0 & & & & & & & & \\
0 & 0 & 0 & 0 & 0 & 0 & 1 & x & & & & & & & & \\
0 & 0 & 1 & x & 0 & 1 & 0 & y & & & & & & & & \\
 & & & & & & & & & & & & & & & \\
 & & & & & & & & 0 & 0 & 0 & -2 & 0 & 0 & -6x & -2y \\
 & & & & & & & & 0 & 0 & 0 & 0 & 0 & -2 & 0 & 0 \\
 & & & & & & & & 0 & 0 & 0 & 0 & -2 & 0 & 0 & -4x \\
\end{bmatrix}
\quad
\begin{matrix}
\\ \\ \\ \\ \\ \\ \\
\end{matrix}
\quad
\begin{bmatrix}
0 & 0 & -6xy & -2y^2 & 0 & -6xy^2 & -2y^3 & -6xy^3 \\
-2x & -6y & 0 & -2x^2 & -6xy & -2x^3 & -6x^2y & -6x^3y \\
-4y & 0 & -6x^2 & -8xy & -6y^2 & -12x^2y & -12xy^2 & -18x^2y^2
\end{bmatrix}
$$

$0_{3 \times 16}$ $0_{3 \times 8}$

Matrix P, for 5 D.O.F. ACM Element,

$$
\begin{bmatrix}
1 & x & y & xy & 0 & 0 & 0 & 0 & & & & & & & & & & & & & & \\
0 & 0 & 0 & 0 & 1 & x & y & xy & & & & & & & & & & & & & & \\
 & & & & & & & & \multicolumn{12}{c}{\multirow{2}{*}{$\underset{2 \times 12}{0}$}} \\
 & & & & & & & & & & & & & & & & & & & & & \\
 & & & & & & & & 1 & x & y & x^2 & xy & y^2 & x^3 & x^2y & xy^2 & y^3 & x^3y & xy^3 \\
 & & & & & & & & 0 & 0 & 1 & 0 & x & 2y & 0 & x^2 & 2xy & $3y^2$ & x^3 & $3xy^2$ \\
 & & & & & & & & 0 & 1 & 0 & 2x & y & 0 & $3x^2$ & 2xy & y^2 & 0 & $3x^2y$ & y^3
\end{bmatrix}
$$

$$\underset{3 \times 8}{0}$$

Matrix P for 6 D.O.F. Bogner Element,

$$
\begin{bmatrix}
1 & x & y & xy & 0 & 0 & 0 & 0 & & & & & & & & \\
0 & 0 & 0 & 0 & 1 & x & y & xy & & & & & & & & \\
 & & & & & & & & & & & & & & & \\
 & & & & & & & & & & & & & & & \\
 & & & & & & & & & & & & & & & \\
 & & & & & & & & & & & & & & & \\
 & & & & & & & & & & & & & & & \\
 & & & & & & & & & & & & & & &
\end{bmatrix}
\quad
\begin{matrix} 0 \\ 2 \times 16 \end{matrix}
$$

$$
\begin{matrix} 0 \\ 4 \times 8 \end{matrix}
\quad
\begin{bmatrix}
1 & x & y & x^2 & xy & y^2 & x^3 & x^2y & xy^2 & y^3 & x^3y & x^2y^2 & xy^3 & x^3y^2 & x^2y^3 & x^3y^3 \\
0 & 0 & 1 & 0 & x & 2y & 0 & x^2 & 2xy & 3y^2 & x^3 & 2x^2y & 3xy^2 & 2x^3y & 3x^2y^2 & 3x^3y^2 \\
0 & 1 & 0 & 2x & y & 0 & 3x^2 & 2xy & y^2 & 0 & 3x^2y & 2xy^2 & y^3 & 3x^2y^2 & 2xy^3 & 3x^2y^3 \\
0 & 0 & 0 & 0 & 1 & 0 & 0 & 2x & 2y & 0 & 3x^2 & 4xy & 3y^2 & 6x^2y & 6xy^2 & 9x^2y^2
\end{bmatrix}
$$

The vector, $\{\int P_{red} dxdy\}$ (Eq. 2.55) for the 5 D.O.F. ACM element may be given as,

$[0, 0, 0, 0, 0, 0, 0, 0,$

$xy, x^2y/2, xy^2/2, x^3y/3, x^2y^2/4, xy^3/3, x^4y/4, x^3y^2/6,$

$x^2y^3/6, xy^4/4, x^4y^2/8, x^2y^4/8]^T$

Putting the limits for x (-a to +a) and y(-b to +b), the above vector reduces to

$[0, 0, 0, 0, 0, 0, 0, 0, 4ab, 0, 0, 4a^3b/3, 0, 4ab^3/3, 0, 0, 0, 0, 0, 0]^T$

Similarly, the vector $\{\int P_{red} dxdy\}$ for the 6 D.O.F. Bogner element, after performing the integration and putting limits is,

$[0, 0, 0, 0, 0, 0, 0, 0,$

$4ab, 0, 0, 4a^3b/3, 0, 4ab^3/3, 0, 0, 0, 0, 0, 4a^3b^3/9, 0, 0, 0, 0]^T$

Appendix B
ESTIMATION OF ULTIMATE LOADS FOR THE TEST SLABS

The assumed yield line patterns for the different test slabs are shown in Fig. B.1. The ultimate load expressions and their actual magnitudes for the test slabs are provided in Table B.1. The square slabs were assumed to be equally reinforced in either direction with a steel percentage of 0.5%. The rectangular slabs would have the same steel percentage in the longer direction while the shorter direction steel being doubled to 1%. A sample calculation for yield moment per unit length for 0.5% steel percentage and the resulting ultimate load for slab S4 3UD is given below.

A SAMPLE CALCULATION:

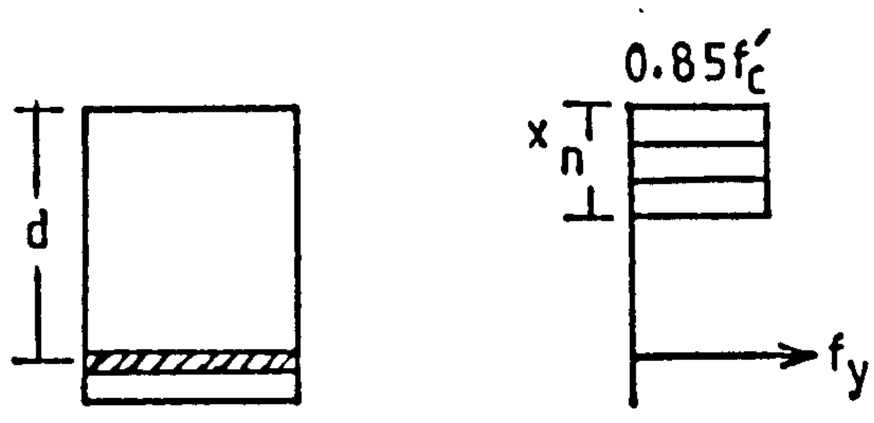

Fig. x Assumed ultimate stress block.

The assumed stress block at ultimate state is that of ACI 318-77 and is shown in Fig. x.

Given: target mean cube strength, $f_{cu} = 21\ N/mm^2$

yield strength of steel, $f_y = 250\ N/mm^2$

steel ratio , $p = \frac{A_s}{bd} = 0.005$

slab thickness, $t = 38$ mm

effective depth, $d = 38 - (5 + 2) = 31$ mm

So,

steel area per unit length, $A_s = 0.005 \times 1 \times 31 = 0.155\ mm^2$

flexural compressive strength, $f'_c = 0.8 \times f_{cu} = 16.8\ N/mm^2$

$$x_n = \frac{A_s f_y}{0.85 f'_c b} = \frac{0.155 \times 250 \times 1}{0.85 \times 16.8 \times 1} = 2.71 \text{ mm}$$

$\therefore$ the yield moment/unit length, $m = A_s f_y \left(d - \frac{x_n}{2}\right)$

$= 0.155 \times 250\ (31\text{-}1.355)$

$= 1.15$ Kn-mm

Hence, for rectangular slabs

$m_1 = m = 1.15$ KN-mm and $m_2 = 2m = 2.30$ KN-mm

Ultimate load computation for slab S43UD:

The assumed yield line is shown in Fig. B.1.d along with the probable rigid regions A, B & C. The ultimate load expression is obtained by equating the internal work to the external work at yielding

Internal Work for Rigid Region, A = $m_1 a . \frac{1}{x}$

Internal Work for Rigid Region, C = $m_1 a \frac{1}{x}$

Internal Work for Rigid Region, B = $m_2 . 2x . \frac{1}{a}$

Total Internal Work = $2 (m_1 a/x + m_2 x/a)$

Due to applied uniform loading of intensity, q per unit area and b = 2a,

External Work = $4 . \frac{1}{3} (\frac{1}{2} ax) . q + 2(a-x) . \frac{a.q}{2}$

$$= (a^2 - \frac{ax}{3}) q$$

Equating the internal work expression to external work and using $m_1 = \frac{1}{2} m_2 = m$, it can be shown that the yield condition attains a minimum energy dissipation (i.e. for m/q maxima) when x = 0.56a.

Hence, the expression for ultimate load intensity reduce to

$$q = 7.145 \, m/a^2$$

and the total ultimate load on the slab = q.a.b

= 14.29 m.

The material requirements for casting each of square and rectangular slabs are given in Table B.2. Location of the strain gauges and that of a nearby Gaussian integration point are tabulated in Table B.3 for the different test slabs.

TABLE B.1 Estimated Ultimate Load Expressions and its Magnitude for the Test Slabs.

Slab Model	Ultimate Load Expression	Computed Actual Magnitude of the Total Ultimate Load, P_u (N)
S14UD	$P_u = qa^2 = 24$ m	27,600
S24P1	$P_u = 8$ m	9,200
S34P4	$P_u = 16$ m	18,400
S43UD	$P_u = qab = 14.29$ m	16,433
S54UD	$P_u = qab = 48$ m	55,200
S63P1	$P_u = 7.33$ m	8,430

TABLE B.2 Material Quantities Required for Casting of Square and Rectangular Test Slabs Plus the Control Specimens.

Slab Type	Constituent Material	Amount (kg)
Square	Cement	15
	Sand	60
	Water	9
Rectangular	Cement	26
	Sand	104
	Water	15.6

TABLE B.3 Coordinates of Steel Strain Gauge Locations and a Nearby Gaussian Integration Point.

Slab Model	Gauge Location	Physical Location		Nearest Gauss Point Location		Corresp. Elm No.	Local Gauss Pt. No.	Comment
		X	Y	X	Y			
S14UD	G1	380	170	359.9	169.9	8	4	4 x 4 Mesh on Quarter Slab
	G2	380	305	359.9	305.1	16	3	
	G3	380	360	359.9	359.9	16	4	
S43UD	G1	340	400	339.9	400.1	18	3	4 x 8 Mesh on Half Slab
	G2	610	400	610.1	400.1	20	1	
	G3	720	400	719.9	400.1	20	3	
	G4	720	400	719.9	400.1	20	3	
	G5	720	455	719.9	454.9	20	4	
	G6	720	590	719.9	590.1	28	3	
S54UD	G1	340	360	339.9	359.9	14	4	4 x 4 Mesh on Quarter Slab
	G2	610	360	610.1	359.9	16	2	
	G3	720	360	719.9	359.9	16	4	
	G4	720	360	719.9	359.9	16	4	
	G5	720	305	719.9	305.1	16	3	
	G6	720	170	719.9	169.9	8	4	
S63P1	G1	340	600	339.9	590.1	26	3	4 x 8 Mesh on Half Slab
	G2	610	600	610.1	590.1	28	1	
	G3	720	600	719.9	590.1	28	3	
	G4	720	400	719.9	400.1	20	3	
	G5	720	455	719.9	454.9	20	4	
	G6	720	590	719.9	590.1	28	3	

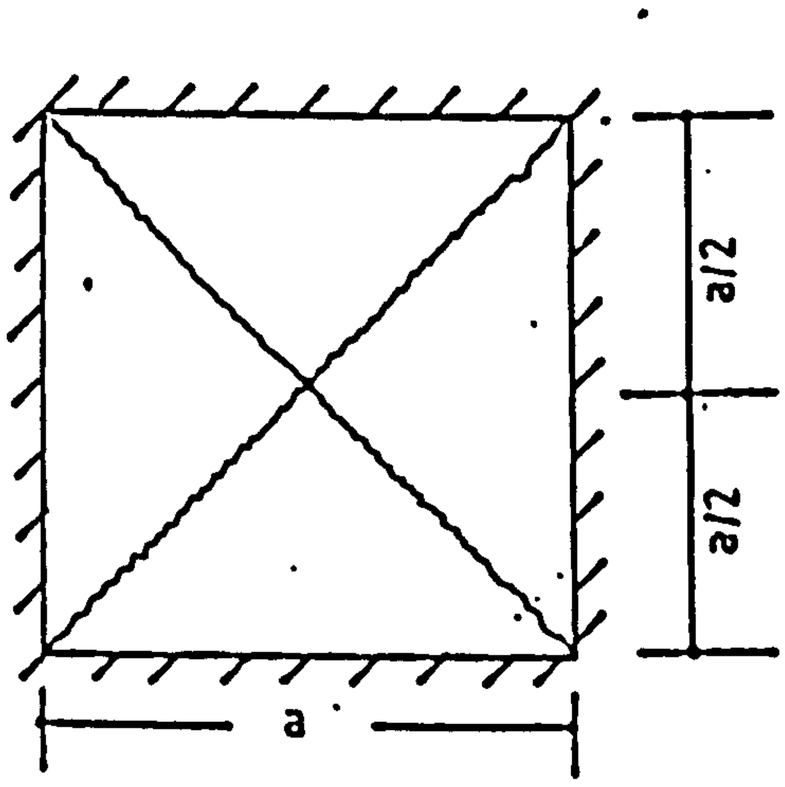

a) Model S1 4UD, UDL all over

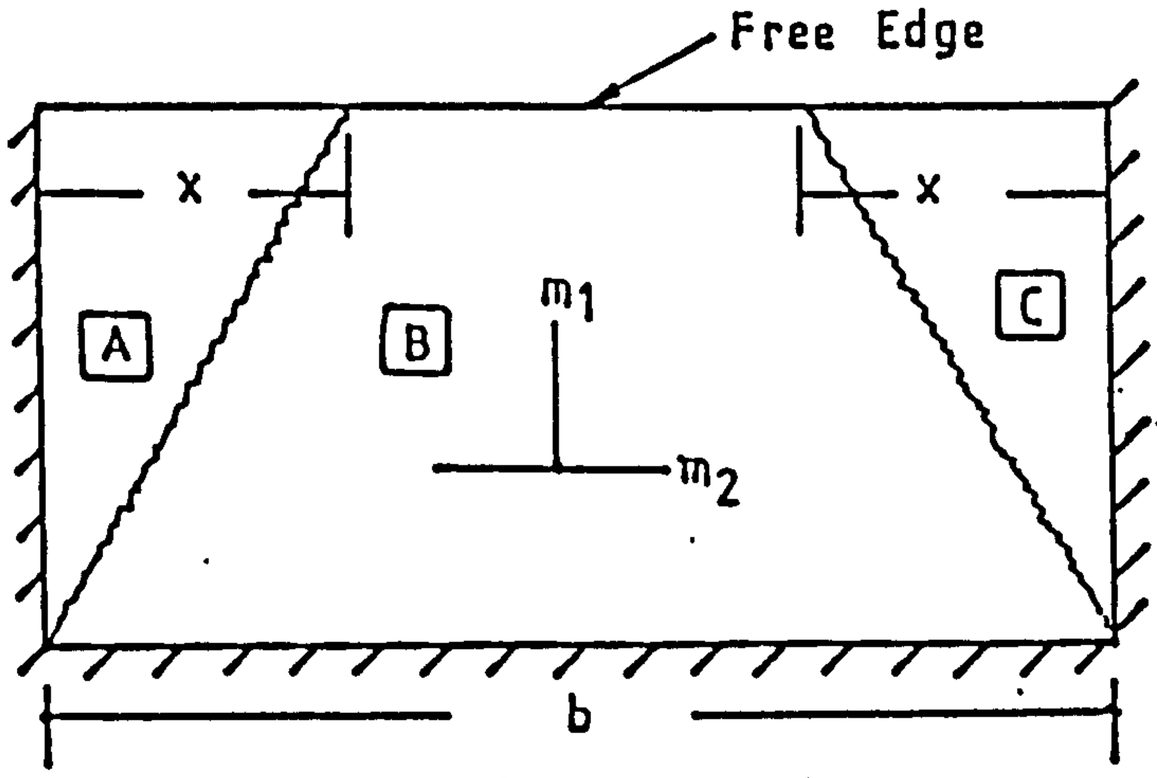

d) Model S4 3UD, UDL all over

Note: $x=0.56a$, for $b=2a$ & $m_2=2m_1=2m$.

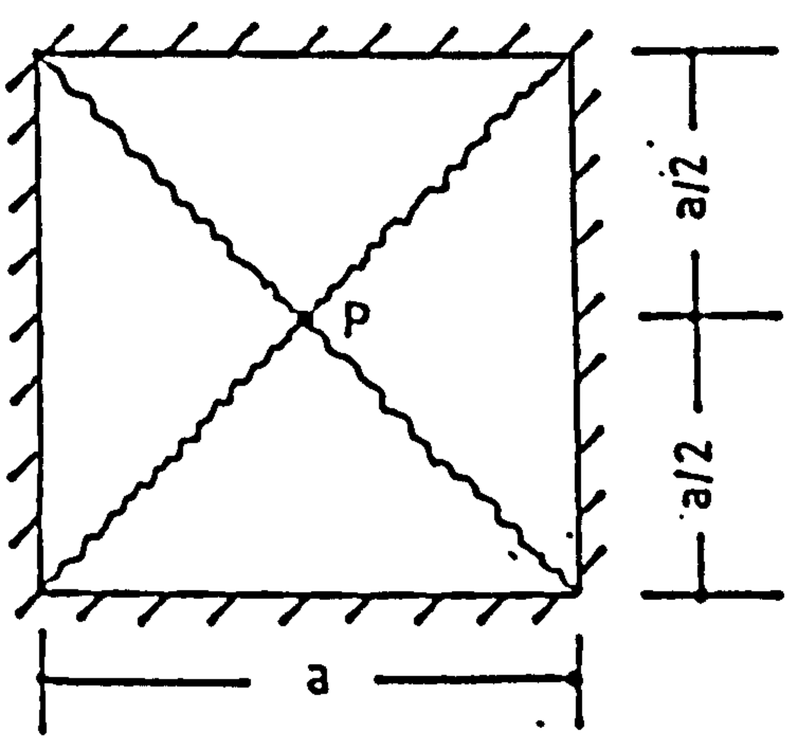

b) Model S2 4P1, Single Point Load

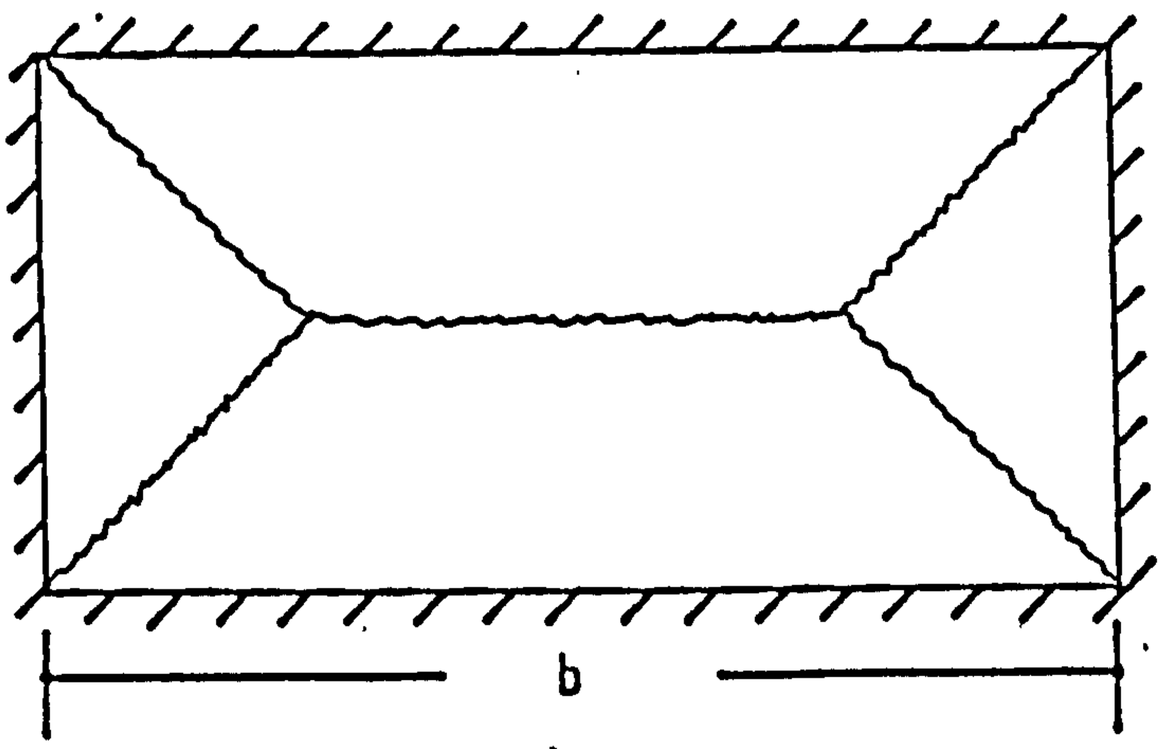

e) Model S5 4UD, UDL all over

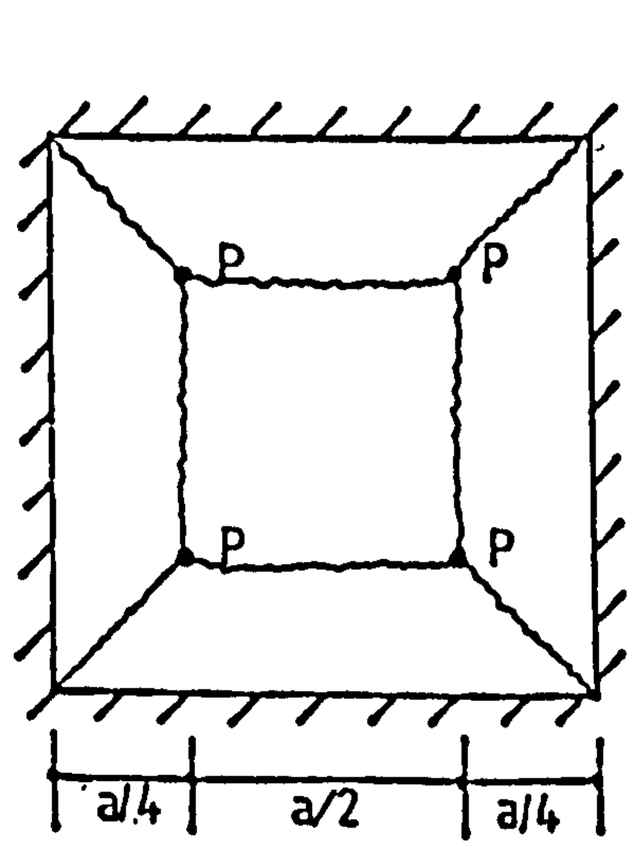

c) Model S3 4P4, Four Point Loads

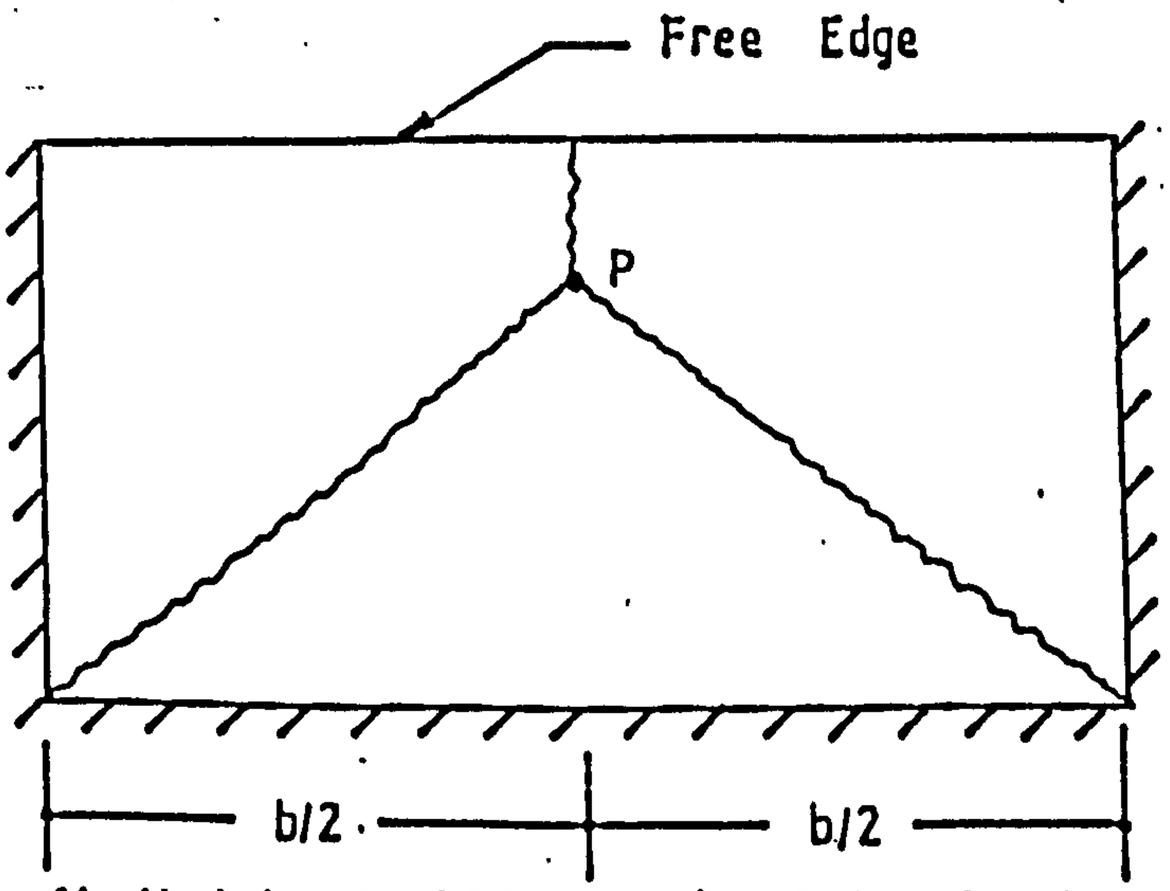

f) Model S6 3P1, Single Point Load

FIG. B.1 Assumed Yield Line Patterns for the Test Slabs

Appendix C
BRIEF ACCOUNT OF DATA INPUT

The sequential card by card input variables along with the format of the respective read statements are given in a following section. A sample data set for an example problem is also attached thereafter. But first, the meaning of the input variable names are briefly described below.

TITLE Any title for user's convenience of identification of the current problem. Up to 60 Alpha-Numeric characters allowed.

LABEL Up to 10 Alpha-Numeric Characters for problem identification. This label is tacked into the graphical outputs.

NSCAL Possible value of 1, 2 or 4 for Full, Half or 1/4th part of the whole slab discretised for analysis.

NALGO Solution Algorithm Selector.

Hint: 1 - Constant Stiffness; 2 or 3 Newton-Raphson method with stiffness updates at 1st or 2nd iteration; 4 - variable stiffness.

NRESI Residual Force Computation Switch.

Hint: 0 - Initial stress method; 1 - Equilibrium check after first iteration, then initial stress scheme; 5 - Equilibrium check allthrough.

NGAUS 2 for 2 x 2 Gaussian Integration Rule.

NTENS Tension Stiffening Scheme Selector.

Hint: 1 to 4 - Four tension stiffening curves respectively; 7 - automatic scheme.

NCOMP Biaxial Compressive Law Selector.

Hint: 2 for Bilinearly elastic model; any other value for Gerstle's formulation.

NCODE (1) - NCODE (10) Output control codes.

NPROB Any nonzero value would permit the programme to run up to specified maxm. displacement if it does not fail due to ill conditioning.

NINCR,NITER

Number of specified Load Increments and Iterations respectively (Possible maximum NINCR is 100).

SCALOD Fraction of Cracking Load by which the subsequent load increments to be applied.

DNTOL,RNTOL

Tolerance specification for iterative displacement and residual force norms.

TOLDP Percentage of minimum element thickness up to which the analysis should be continued.

NDIF, NELP, NLAY, NDFN

Number of different element types (maxm. 6); Total number of elements (maxm. 64); Total number of layers per element (maxm. 12); Number of degrees of freedom per node (5 for ACM element).

PROP(I,J)

Various properties of each element types, (Hint: see following Input sequence section).

STANG(I,J)

Angles of steel layout for each element types (maxm. 2 directions permitted).

LMARK(I,J)

Layer markings for each layers of each element types (1 & 2 for steel layers in two directions; 3 for concrete layer).

PTHC(I,J)

Thickness of each layer in percentage of total thickness of respective element types.

MTYPE(I)

Element types of each of the NELP elements. This is not to be supplied if all the elements are identical types.

IREG Indicator for regular or irregular grid.

Hint: 1 if both discretised lengths in X and Y directions are subdivided into regular grids; Else any other value.

NDX, NDY, XLENG, YLENG

Number of divisions in X and Y directions; X and Y direction discretised lengths.

XSIDE(I), YSIDE(I)

Lengths of each subdivision in X and Y directions respectively; Not necessary if regular grid.

NBOUN Number of Nodes where some boundary restraints are to be applied (maxm. 50).

NODBC (IFX), IDFIX (I), PRESC (IFX,J)

Node Number, Fixity code value and the magnitude of prescribed displacements corresponding to each D.O.F. for each of the NBOUN boundary nodes; Fixity code example:10101 indicates u, w and θ_y restrained.

NCONL Number of Point Loads.

NUDL, NSEL, NUMO

Indicators for existence of distributed load, self weight and point moments.

SFACT(I)

Relative ratio of the subsequent load increments for Applied Point Loads corresponding to each degrees of freedom. Even if there is no point load, SFACT (3) should be specified 1.0 and rest zeros.

UMOM(I)

Applied moments Mx and My per unit length if any, although their equivalents are to be given as point loads (moments) at the appropriate nodes.

LODPT(I), CONLD(I,J)

Node numbers where the point loads are being applied and their magnitudes corresponding to each degrees of freedom.

NOUTP, NPELO, NDISO

Total number of specified Increments, Elements and Nodes respectively for which various output are to be made.

IF (NOUTP.NE.NINCR) then the specified increment numbers are to be supplied.

IF (NPELO.NE.NELP) then the specified element numbers are to be supplied.

IDPNO(I), NPCOD(I)

The specified node number and its code number (similar to fixity code). These will be stored in a separate file during execution which may be used after minimum editing by another plotting programme.

DATA INPUT SEQUENCE
**** ***** ********

```
Card 1+     READ     : TITLE  &  LABEL
            FORMAT   = 10A6/5A2
Card 2      READ     : NSCAL,NALGO,NRESI,NGAUS,NTENS,NCOMP
            FORMAT   = 6I3
Card 3      READ     : NCODE (1-10)
            FORMAT   = 7I3,3I5
Card 4      READ     : NPROB,NINCR,NITER,SCALOD,DNTOL,RNTOL,TOLDP
            FORMAT   = 3I3,4F8.3
Card 5      READ     : NDIF,NELP,NLAY,NDFN
            FORMAT   = 4I3
Comment :   For Each 'NDIF' (i.e. element type)
            Read Material Property set & Relevant Data.
Note ::     For each set, the Different Properties are :-
C           1.ECON,2.ECBI,3.FCU,4.FCA,5.FCT,6.ESTL,7.FSU
C           8.POIS,9.BETA,10.ECRUS,11.ECRIT,12.SELW,13.UDL,
C           14.THICK,15.ZMID
C
Card 6+     READ     : PROP (I,J) J=1,NPROP
            FORMAT   = 8E10.3 (usually in 2 Cards,NPROP=15)
Card 7      READ     : (STANG(I,J),J=1,2)
            FORMAT   = 2F8.3
Card 8      READ     : LMARK (I,J),J=1,NLAY
            FORMAT   = 12I3
Card 9+     READ     : PTHC (I,J),J=1,NLAY
            FORMAT   = 10 F8.3
Note :      If FCA=0, Then FCA=0.45 * FCU
            If ECBI=0,Then ECBI=(FCU-FCA)/(.72*ECRUS-FCA/ECON)
Comment :   Material Sets End. So Next Card.
Card 10+    If (NDIF.NE.1 ,Then only
            READ     : MTYPE(I) , I=1,NELP
            FORMAT   = 24I3
Card 11     READ     : IREG,NDX,NDY,XLENG,YLENG
            FORMAT   = 3I3,2F8.3
Note :      If (IREG.NE.1)
Card 12     READ     : XSIDE(I),I=1,NDX (maxm NDX=9)
Card 13     READ     : YSIDE(I),I=1,NDY (maxm NDY=9)
            FORMAT   = 8F8.3 (for both cases)
Card 14     READ     : NBOUN (Maxm. NBOUN=50)
            FORMAT   = I3
Card 15+    READ     : NODBC(IFX),(IDFIX(I),I=1,NDFN)
                       ,(PRESC(IFX,J),J=1,NDFN)
            FORMAT   = I3,3X,5I1,5F8.4
Note :      Supply Card 15 information 'NBOUN' times i.e
            for EACH Boundary Nodes. IDFIX is the FIXITY
            CODE corresponding to each degrees of freedom.
Card 16     READ     : NCONL,NUDL,NSEL,NUMO
            FORMAT   = 4I3
Card 17     READ     : SFACT(I),I=1,NDFN
            FORMAT   = 6F8.3
Note :      If (NUMO.NE.0) Then only
Card 18     READ     : UMOM(I),I=1,NUMO
            FORMAT   = 3E10.3
Note :      If (NCONL.NE.0) ,Then for each I of NCONL
Card 19+    READ     : LODPT(I),CONLD(I,J), J=1,NDFN
            FORMAT   = Free format
```

```
Comment :   Output Control Data follow Skipping 1 Card.

Card 20     READ     : NOUTP,NPELO,NDISO
            FORMAT   = /3I3
Card 21     If (NOUTP.NE.NINCR)
            READ     : OUTPUT INCREMENTS
            FORMAT   = 20I4
Note :      Output Increment Nos -ve for which Plot asked.

Card 22+    If (NPELO.NE.NELP)
            READ     : SPECIFIED plate Elements
            FORMAT   = 20I4
Card 23+    IF (NDISO.NE.0)
            READ     : IDPNO(I),NPCOD(I)
            FORMAT   = (5(I3,I7))
Note :      Put the Node Number followed by its Plotting code.
     :      Nodal Plotting CODES -ve for Smooth Curve fitting.


            AN EXAMPLE DATA SET
            ***********************


 EFFECT OF NO. OF LAYERS,(HALF) SLAB:S63P1;(8 LAYERS)
S63P1  8LR
  2  3  5  2  7  2
  0  0  0  1  3  3 01   000   100   001
 1 90 12 0.100E 00 0.001E 00 0.001E 00 0.900E 02
 1 16  8  5                                                    0.200E 00
0.160E 05 0.600E 04 0.146E 02 0.730E 01 0.169E 01 0.200E 06 0.240E 03
0.500E 00 0.300E-02 0.000E 00 0.000E 00 0.000E 00 0.380E 02 0.190E 02
 00.000  90.000
 3  1  3  2  3  3  3  3
 18.008  0.824  10.108   0.412  20.648  16.670  16.670  16.660
 1  4  4 760.000 760.000
13
 1    11111  0.0000  0.0000  0.0000  0.0000  0.0000
 2    00101  0.0000  0.0000  0.0000  0.0000  0.0000
 3    00101  0.0000  0.0000  0.0000  0.0000  0.0000
 4    00101  0.0000  0.0000  0.0000  0.0000  0.0000
 5    10101  0.0000  0.0000  0.0000  0.0000  0.0000
 6    00110  0.0000  0.0000  0.0000  0.0000  0.0000
10    10001  0.0000  0.0000  0.0000  0.0000  0.0000
11    00110  0.0000  0.0000  0.0000  0.0000  0.0000
15    10001  0.0000  0.0000  0.0000  0.0000  0.0000
16    00110  0.0000  0.0000  0.0000  0.0000  0.0000
20    10001  0.0000  0.0000  0.0000  0.0000  0.0000
21    00110  0.0000  0.0000  0.0000  0.0000  0.0000
25    10001  0.0000  0.0000  0.0000  0.0000  0.0000
 1  0  0  0,
  0.000  00.000   1.000  00.000  00.000
20  00.000  00.000 100.000  00.000  00.000
COMMENT:: OUTPUT CODE DATA
 8  3  1
  1   2  -4   9  16 -26  30 -36
 12  14  16
25  00100
```

APPENDIX D

ADDITIONAL FIGURES

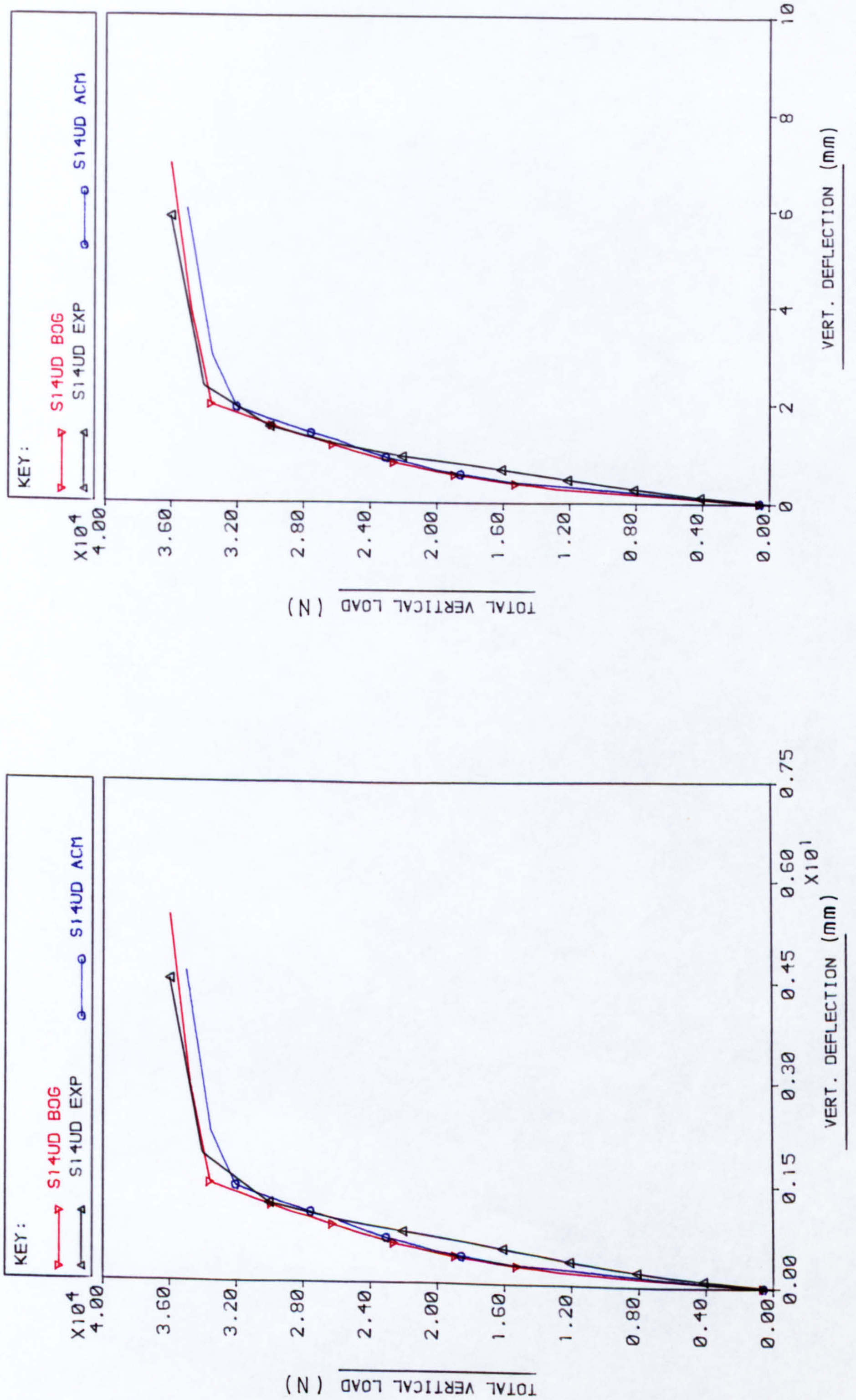
KEY:
S14UD BOG
S14UD EXP
S14UD ACM
X10⁴
4.00
3.60
3.20
2.80
2.40
2.00
1.60
1.20
0.80
0.40
0.00
TOTAL VERTICAL LOAD (N)
0
2
4
6
8
10
VERT. DEFLECTION (mm)
LOAD Vs DISPLACEMENT CURVES
FOR NODE 15
0.00
0.15
0.30
0.45
0.60
0.75
X10¹
VERT. DEFLECTION (mm)
LOAD Vs DISPLACEMENT CURVES
FOR NODE 13

FIG. D.2

FIG. D.1

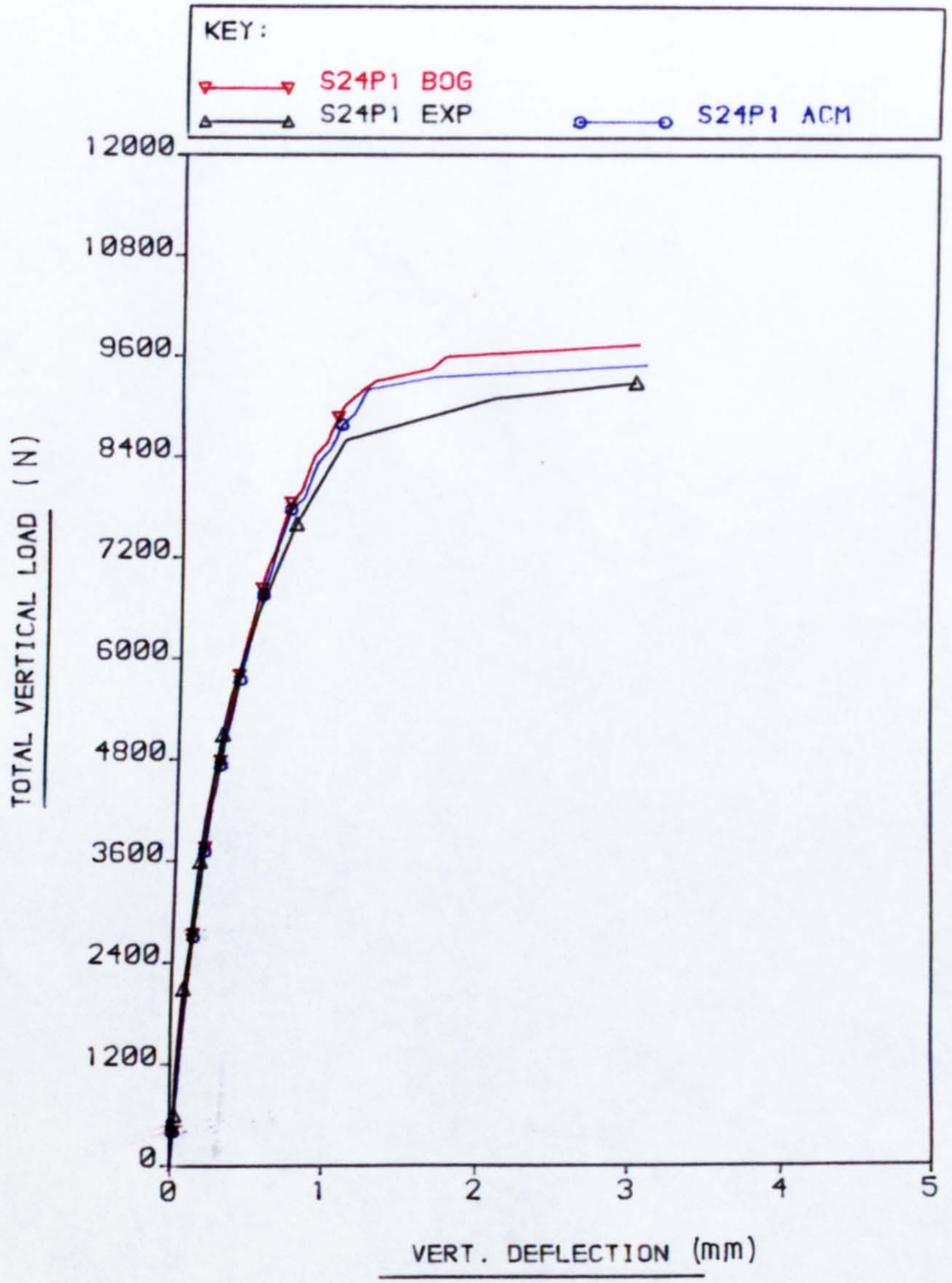

FIG. D.3 LOAD Vs DISPLACEMENT CURVES FOR NODE *13*

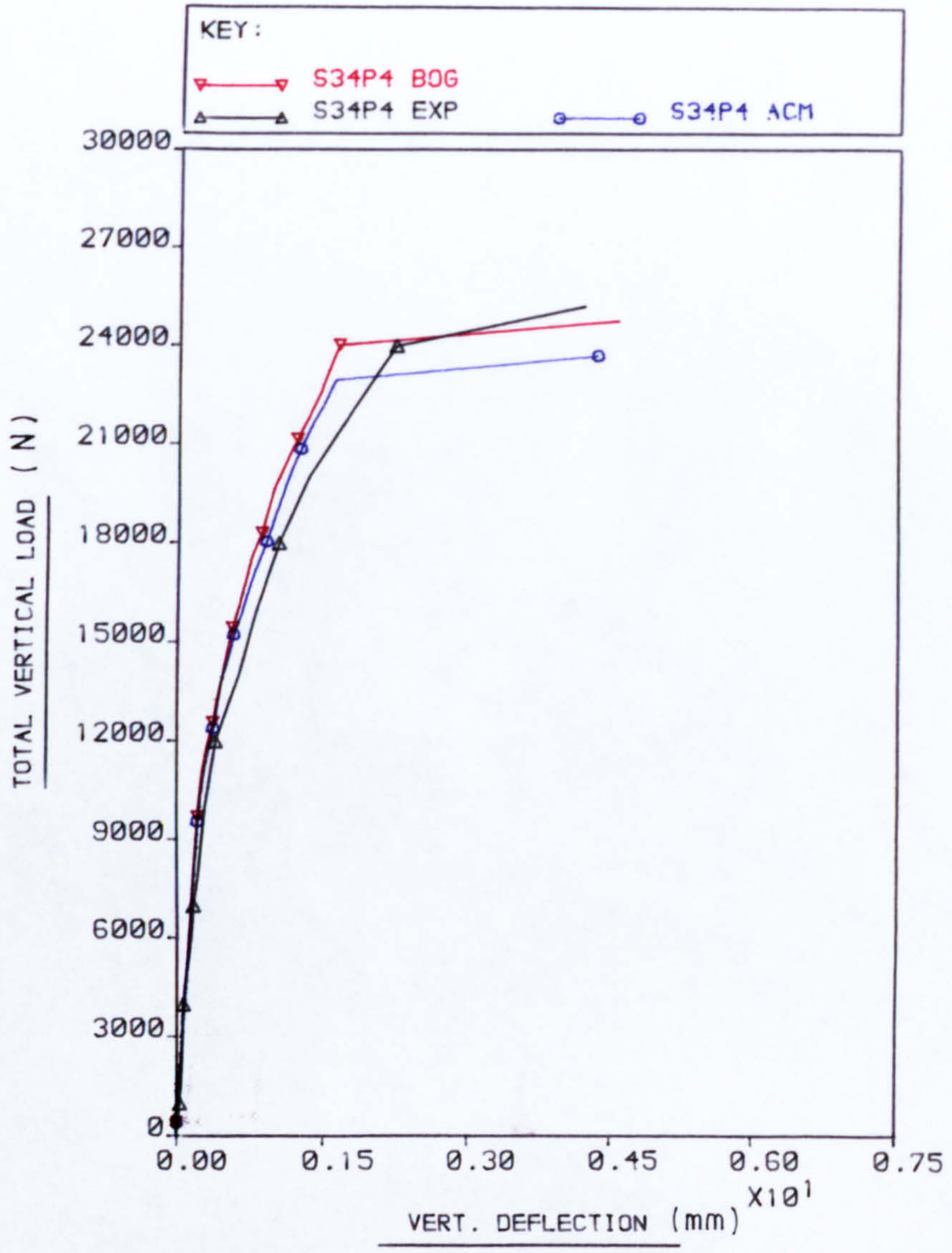

FIG. D.4 LOAD Vs DISPLACEMENT CURVES FOR NODE *13*

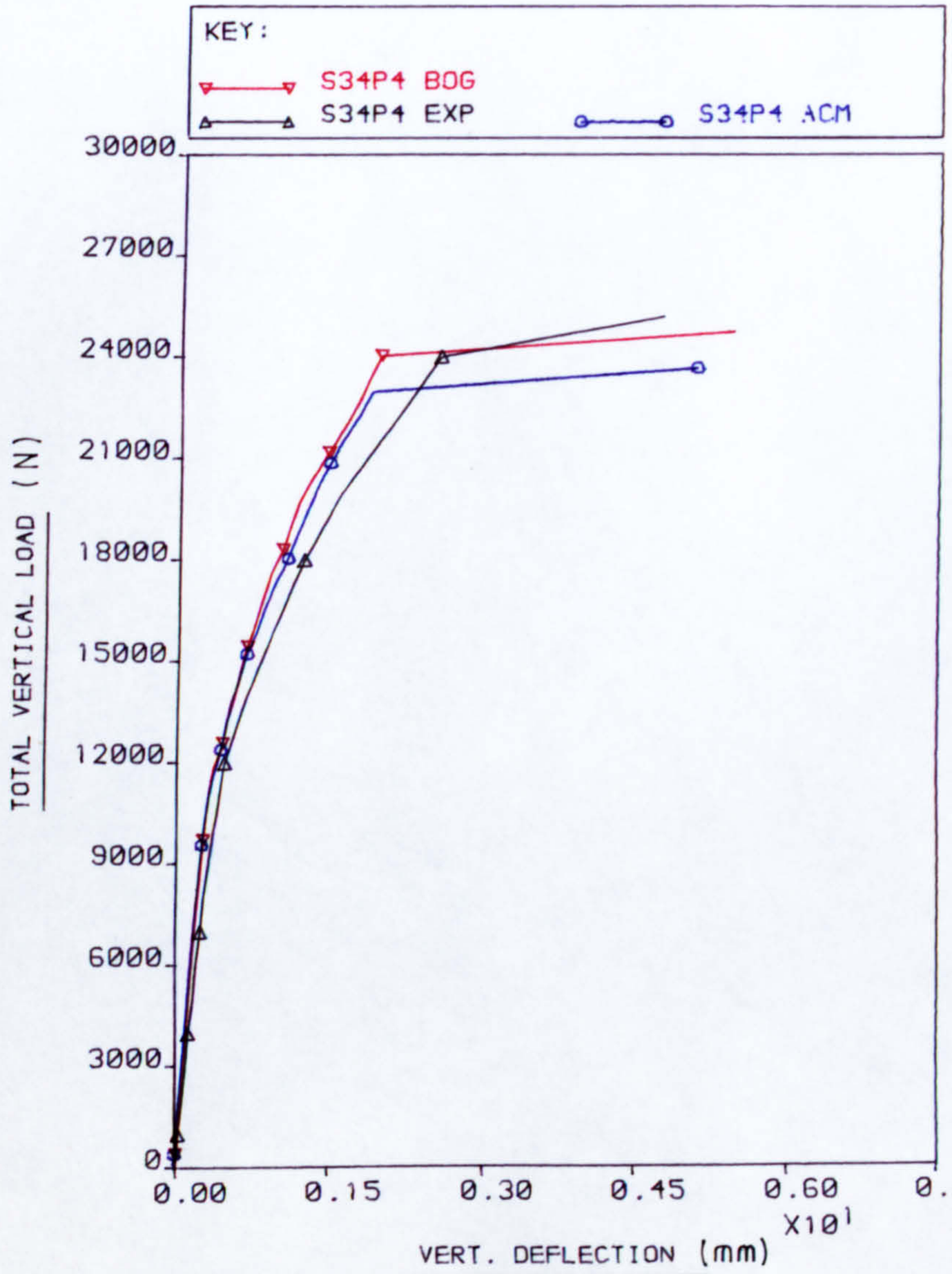

FIG. D.5 LOAD Vs DISPLACEMENT CURVES FOR NODE *15*

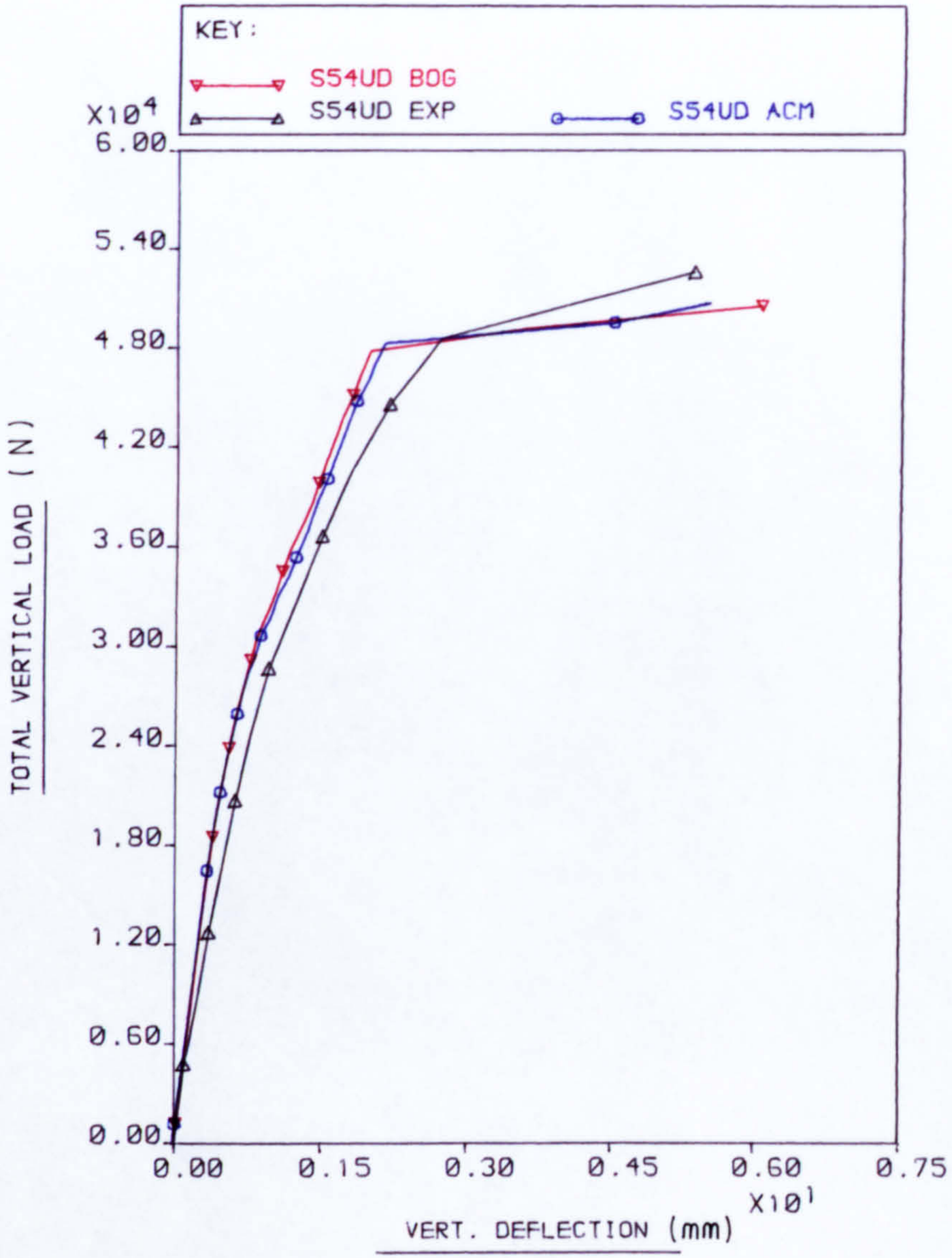

FIG. D.6 LOAD Vs DISPLACEMENT CURVES FOR NODE *13*

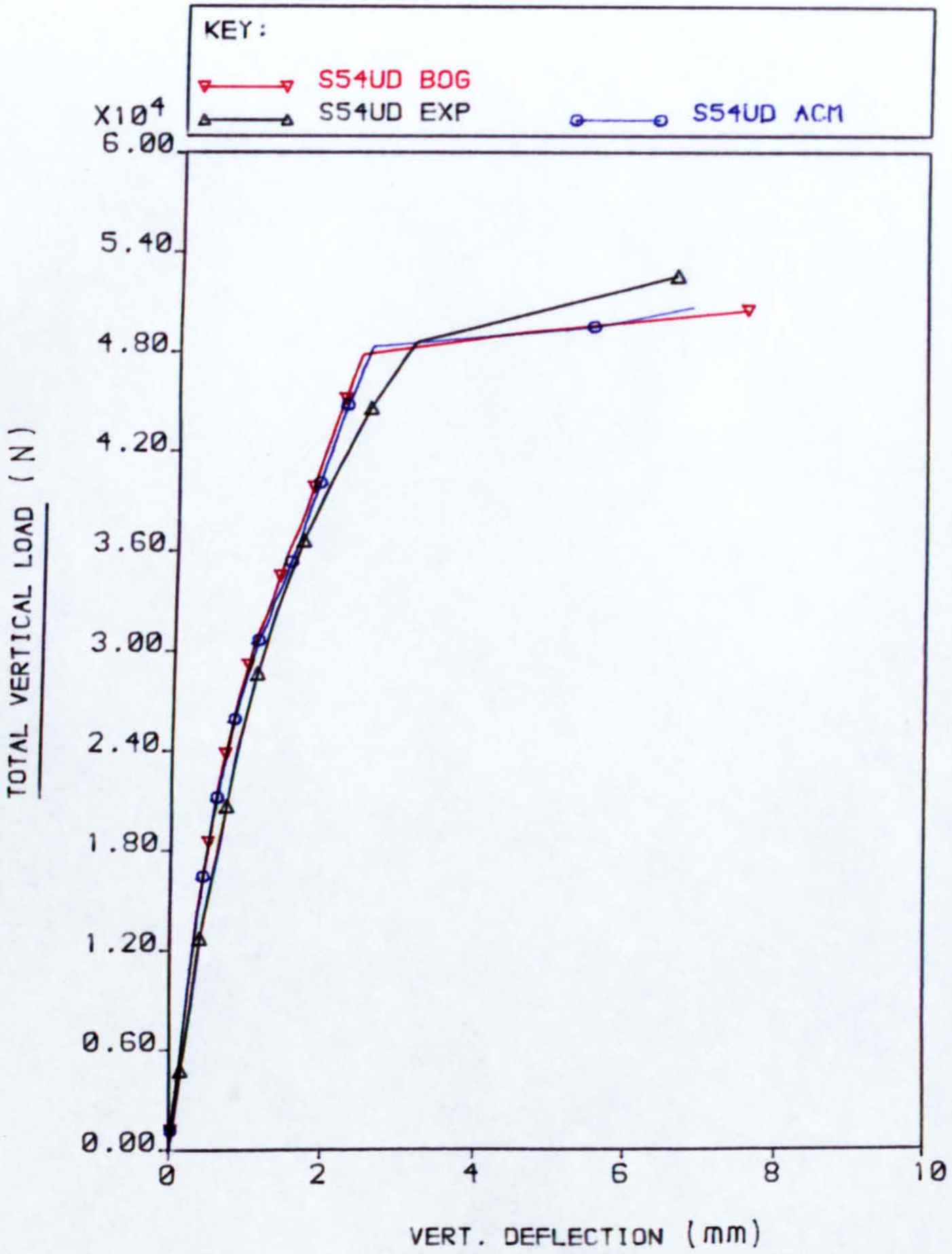

FIG. D.7 LOAD Vs DISPLACEMENT CURVES FOR NODE *15*

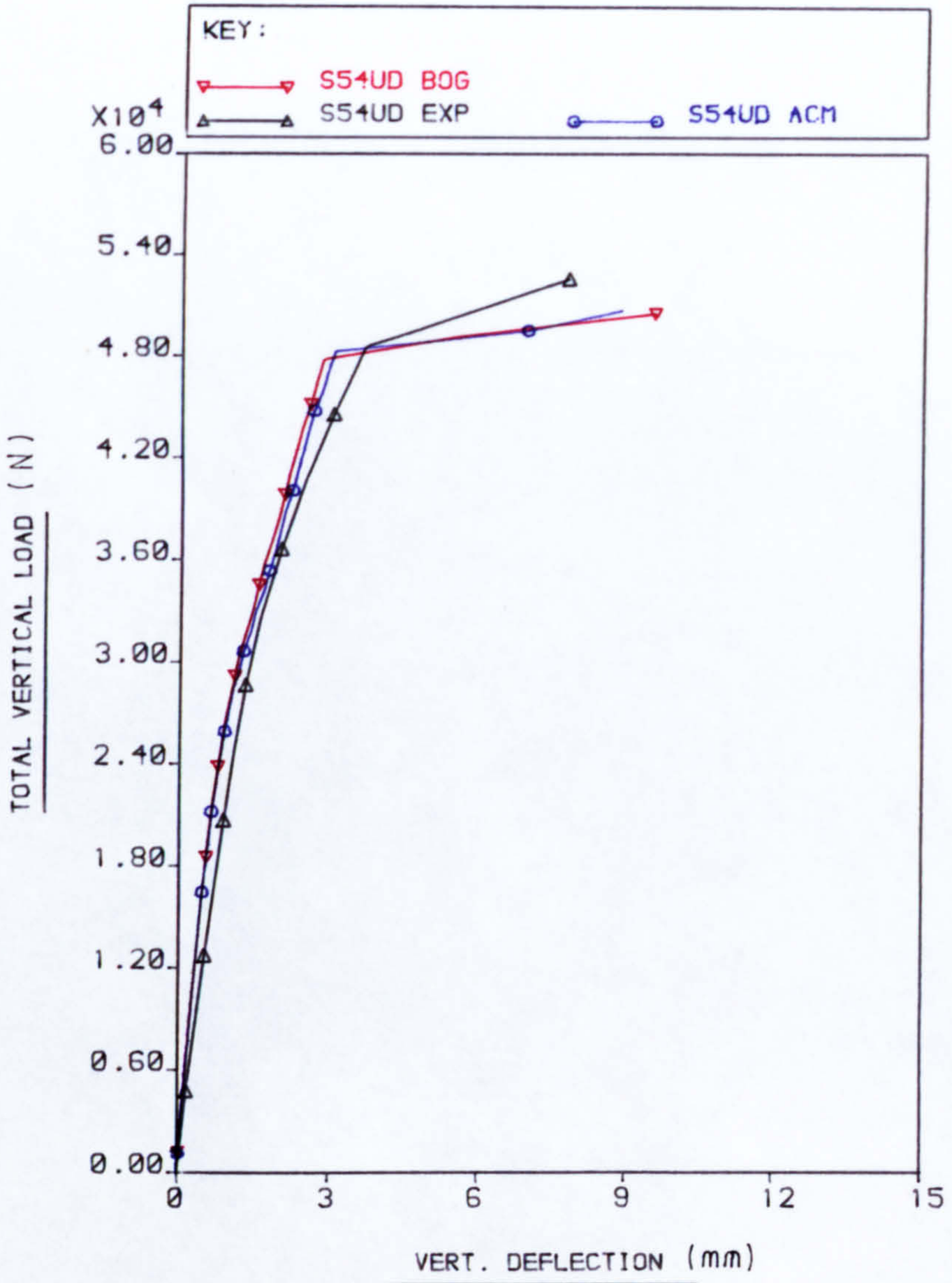

FIG. D.8 LOAD Vs DISPLACEMENT CURVES FOR NODE *23*

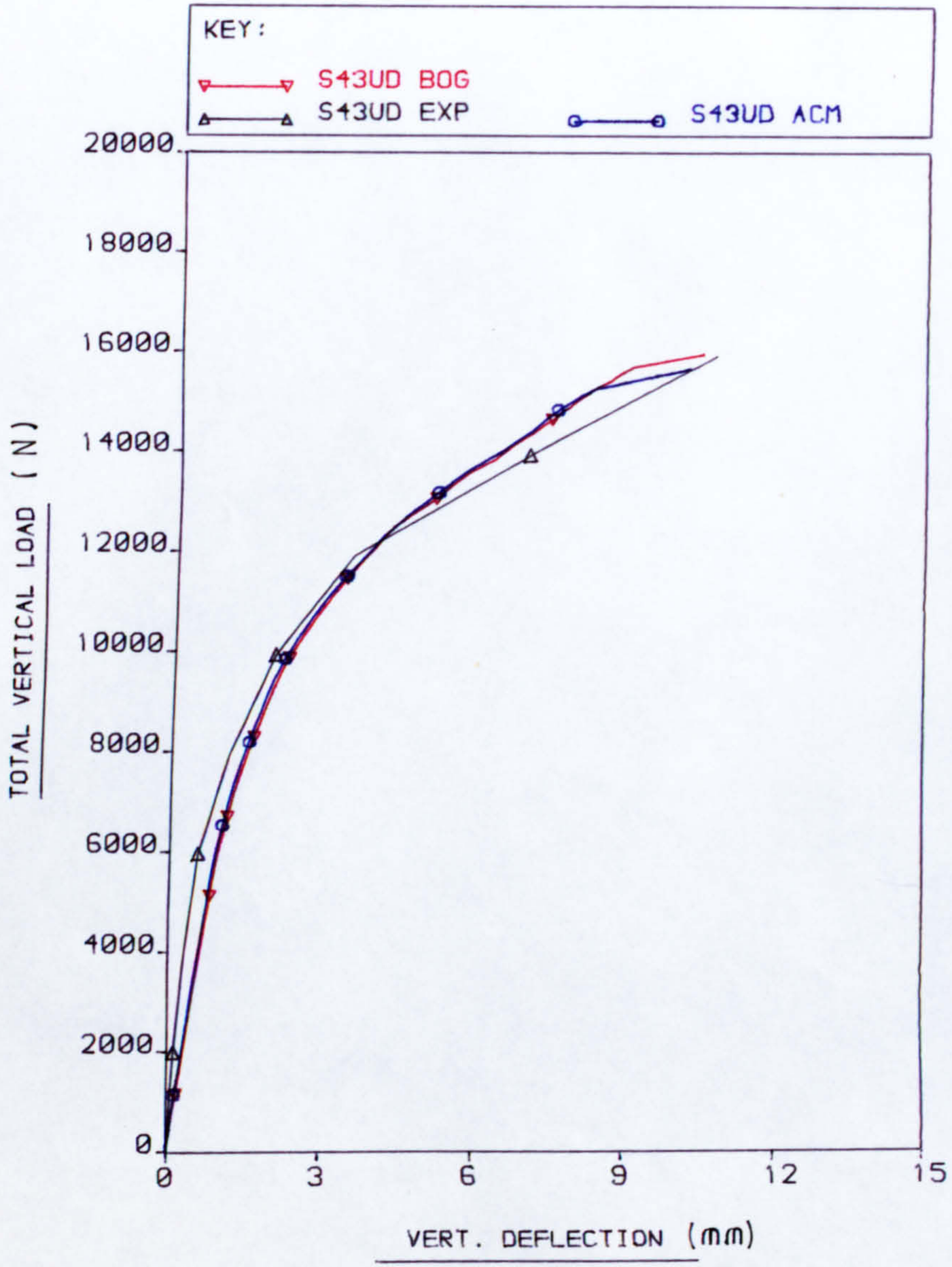

FIG. D.9 LOAD Vs DISPLACEMENT CURVES FOR NODE *13*

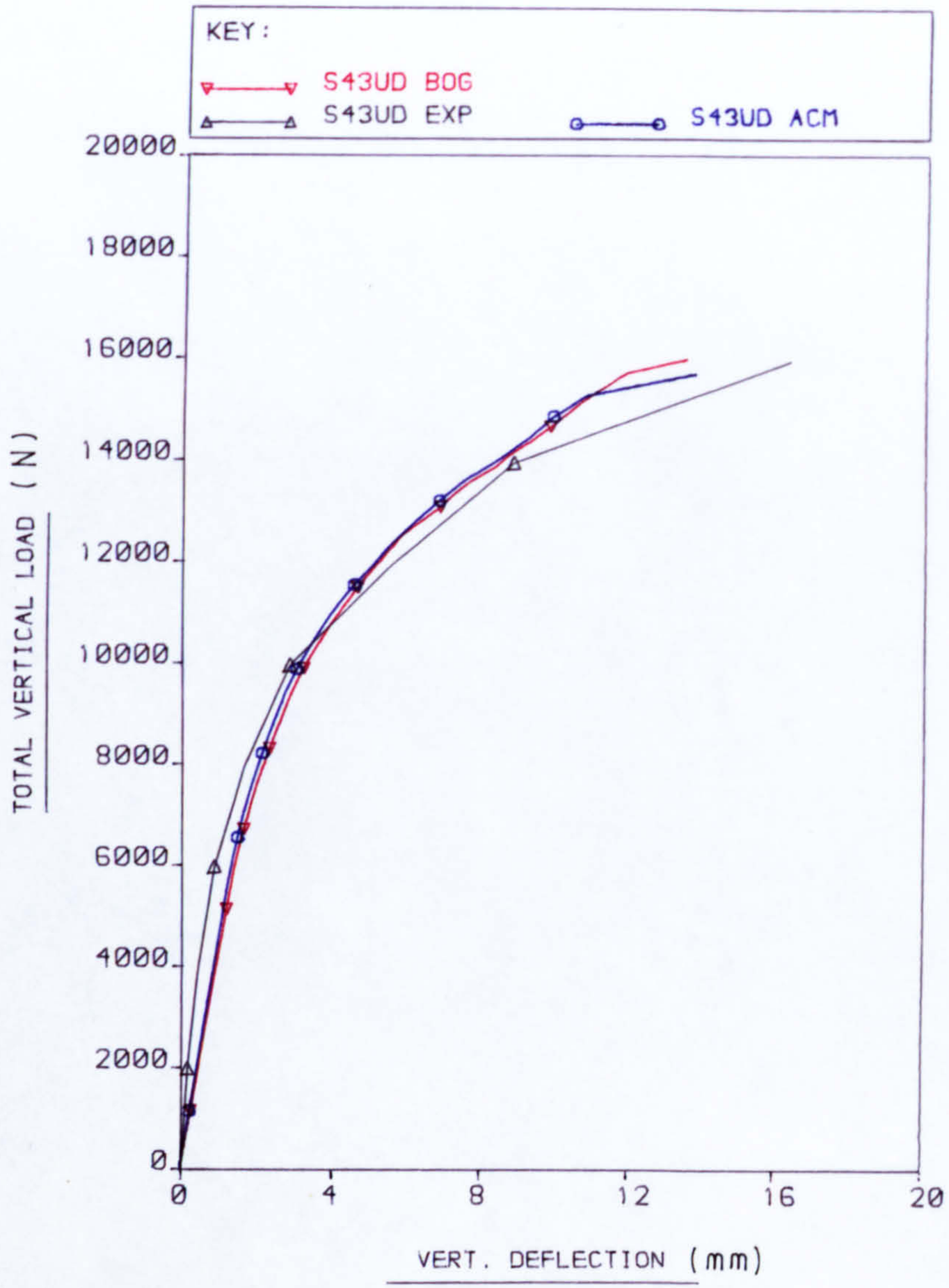

FIG. D.10 LOAD Vs DISPLACEMENT CURVES FOR NODE *15*

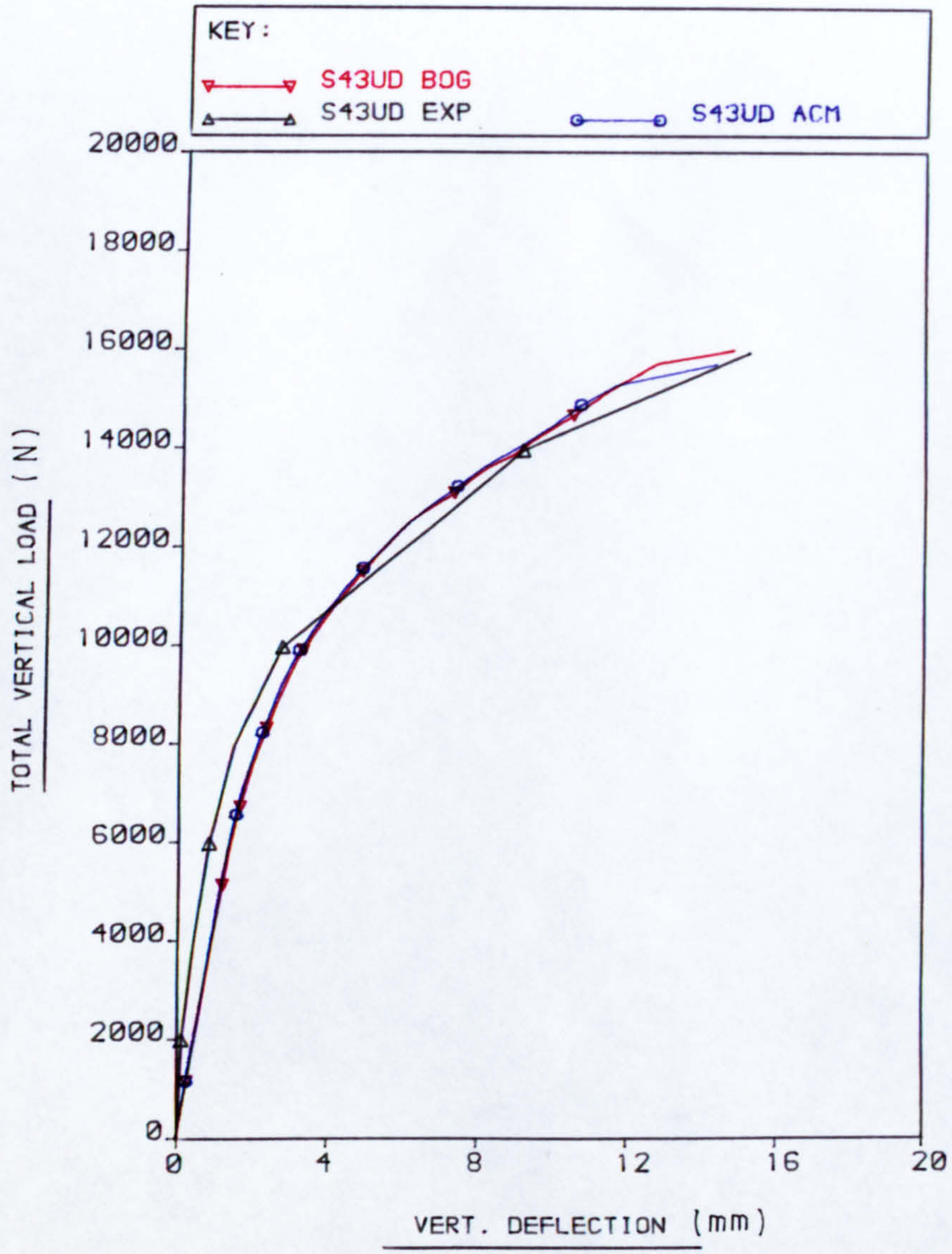

FIG. D.11 LOAD Vs DISPLACEMENT CURVES FOR NODE *18*

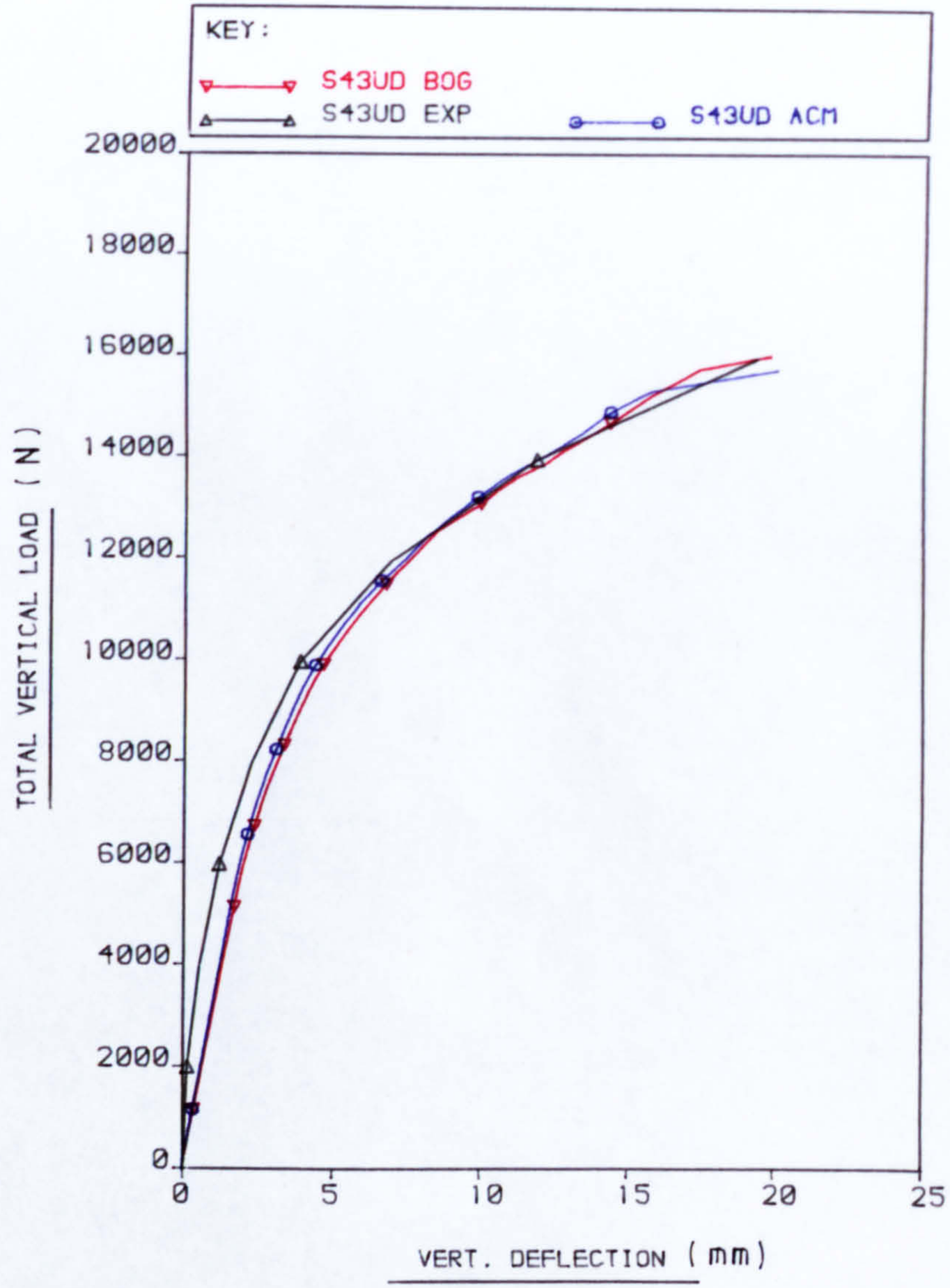

FIG. D.12 LOAD Vs DISPLACEMENT CURVES FOR NODE *20*

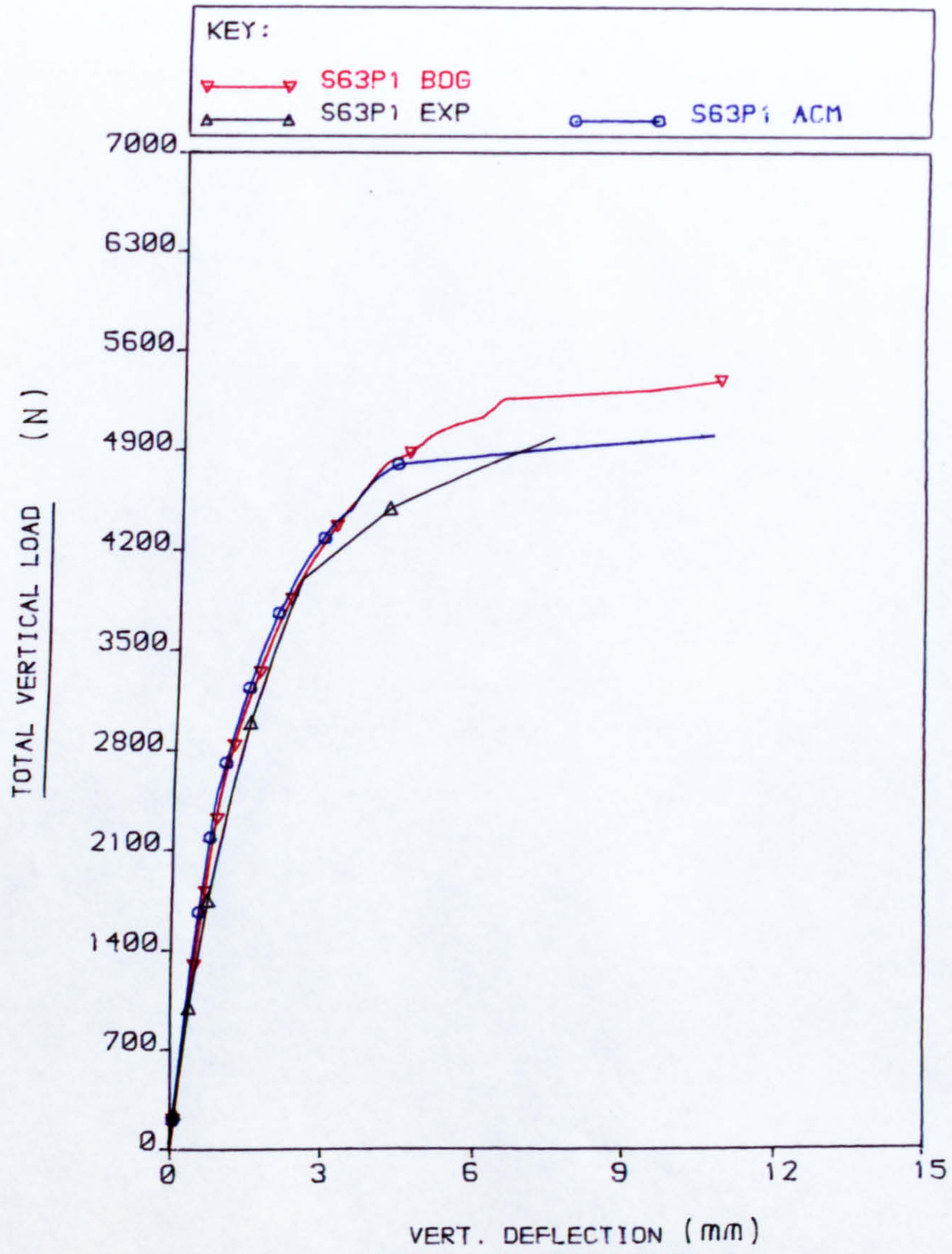

FIG. D.13 LOAD Vs DISPLACEMENT CURVES FOR NODE *13*

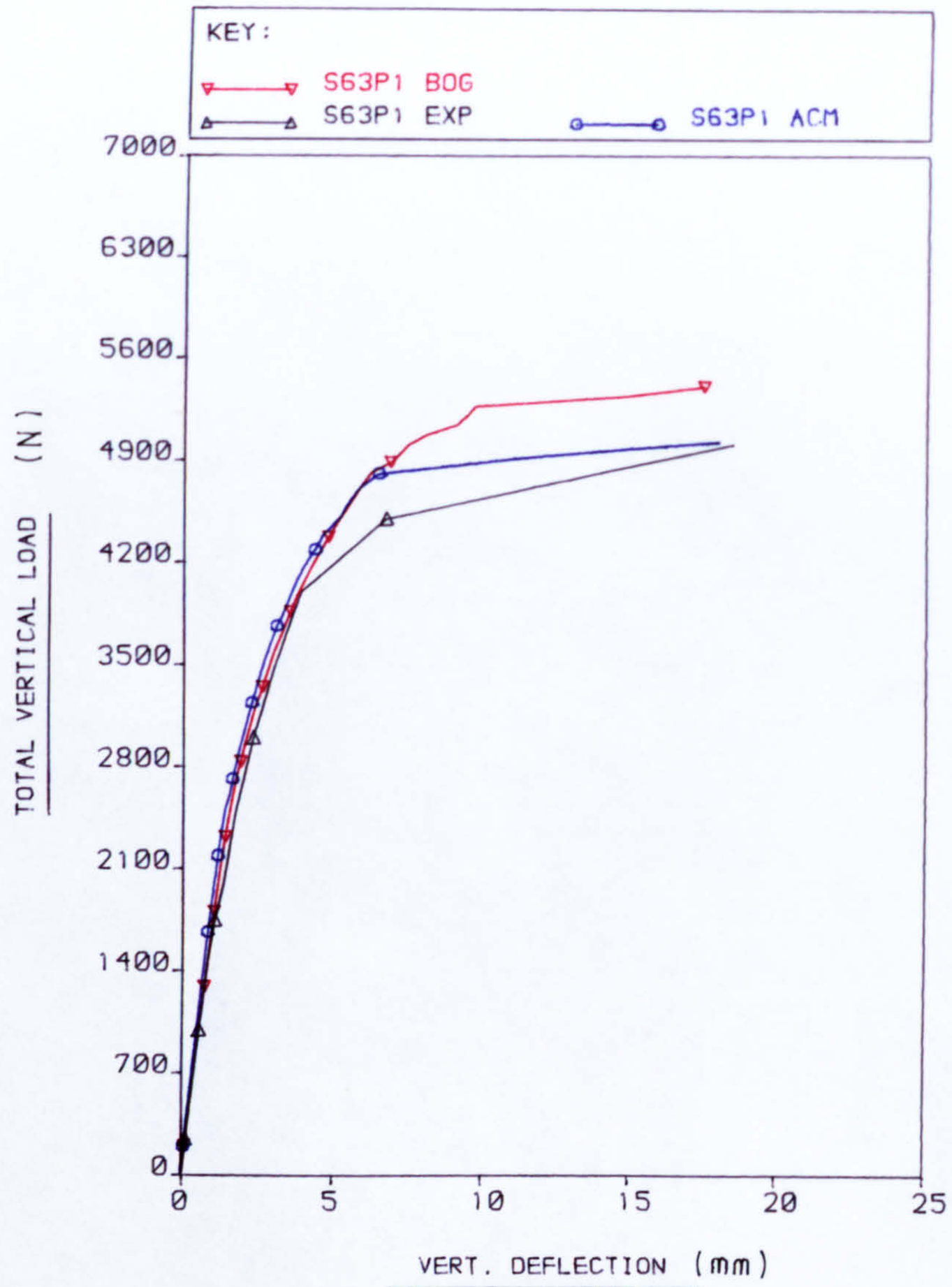

FIG. D.14 LOAD Vs DISPLACEMENT CURVES FOR NODE *15*

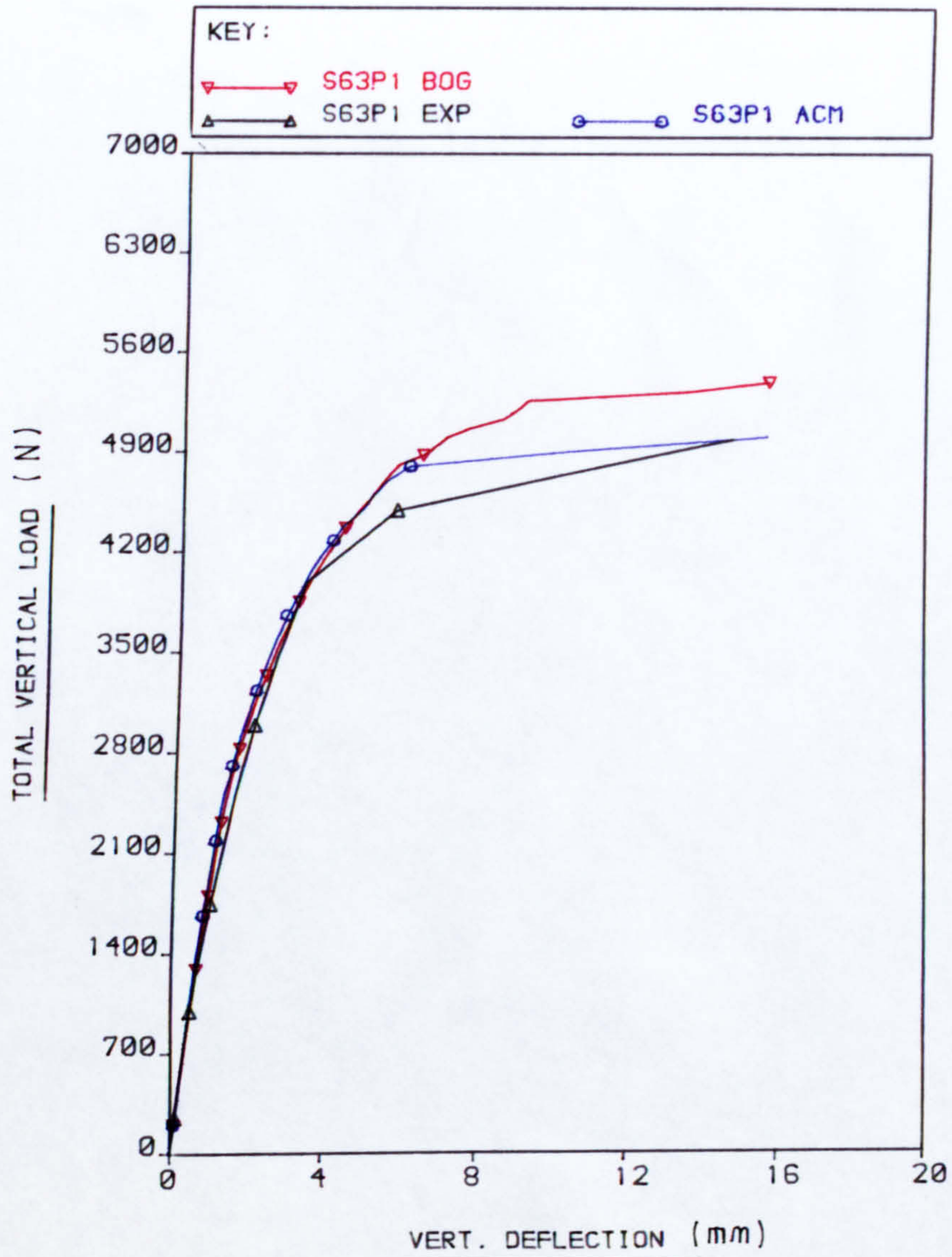

FIG. D.15 LOAD Vs DISPLACEMENT CURVES FOR NODE *18*

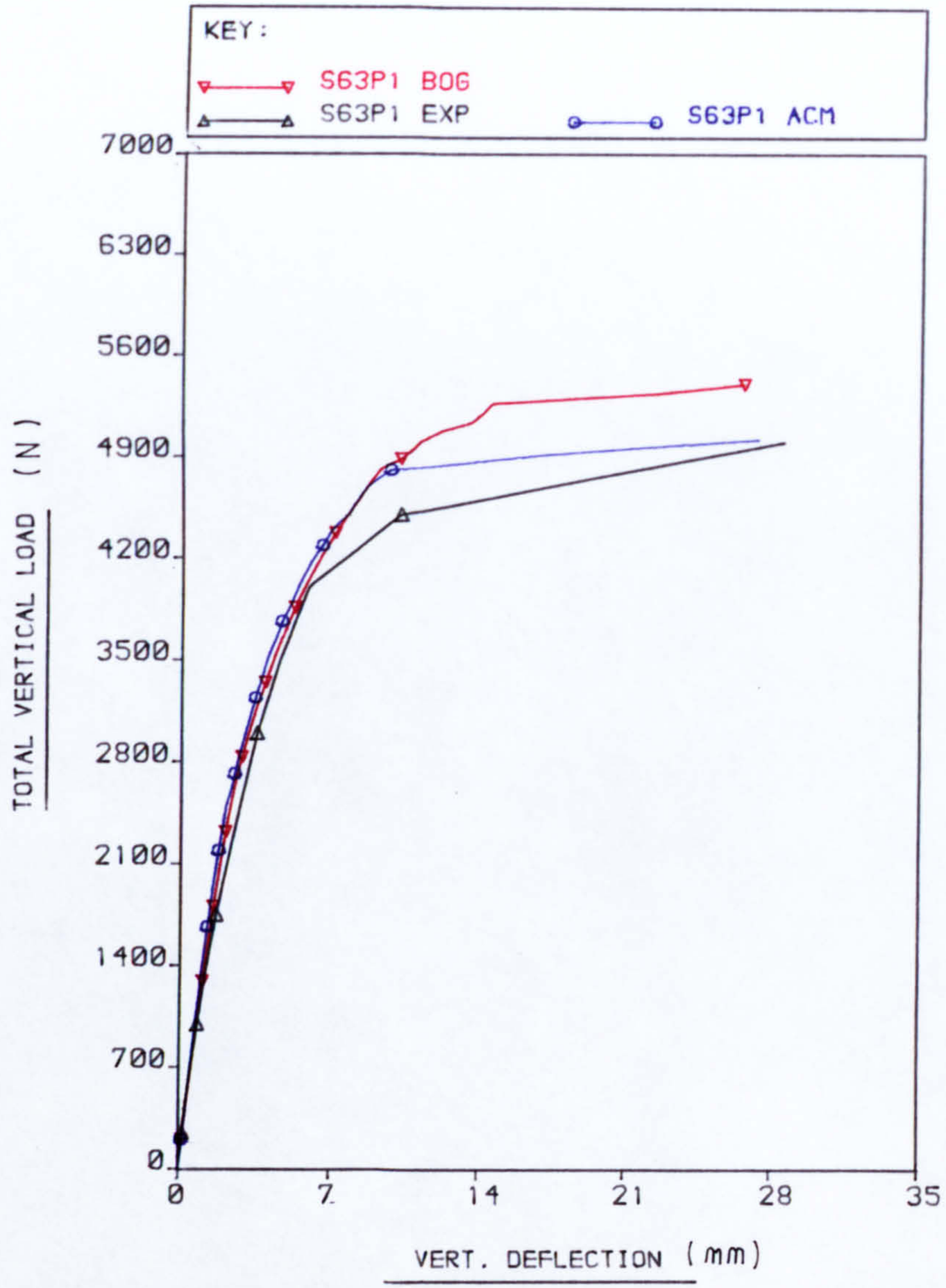

FIG. D.16 LOAD Vs DISPLACEMENT CURVES FOR NODE *20*

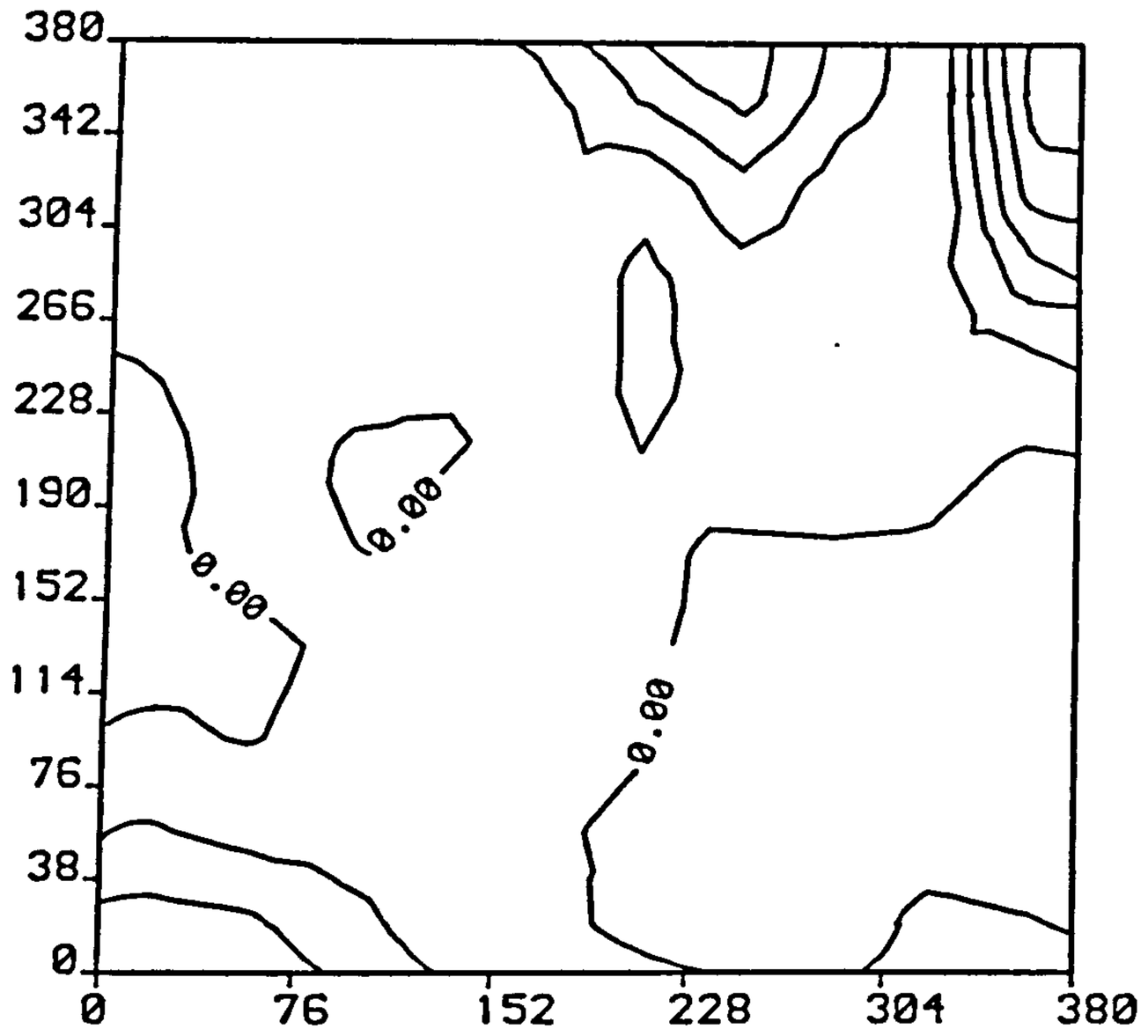

FIG. D.17 CONTOUR OF NX FOR S24P1 ACM
AT TOTAL VERTICAL LOAD= 7042.5 N
(N/mm)

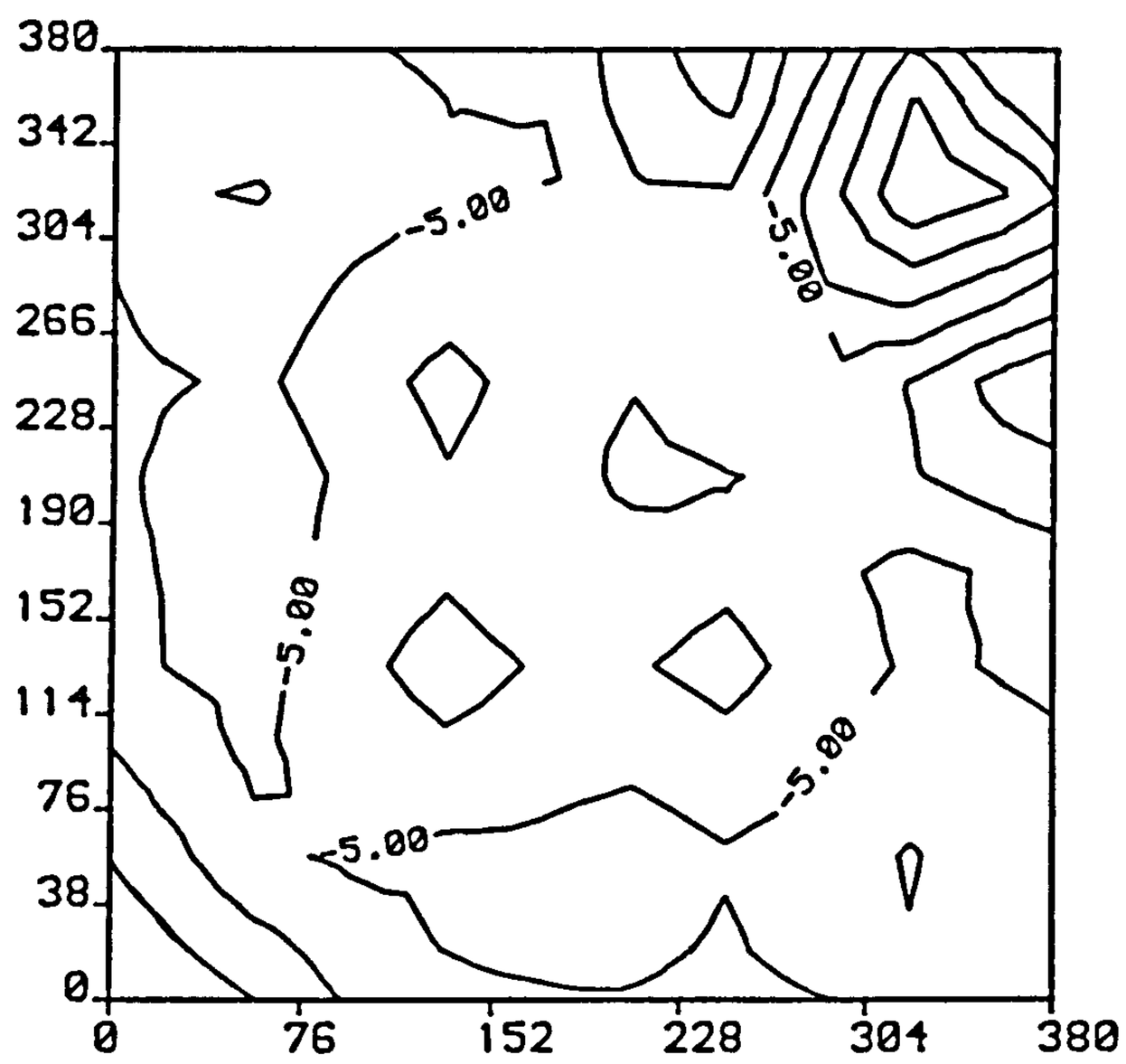

FIG. D.18 CONTOUR OF NXY FOR S24P1 ACM
AT TOTAL VERTICAL LOAD= 7042.5 N
(N/mm)

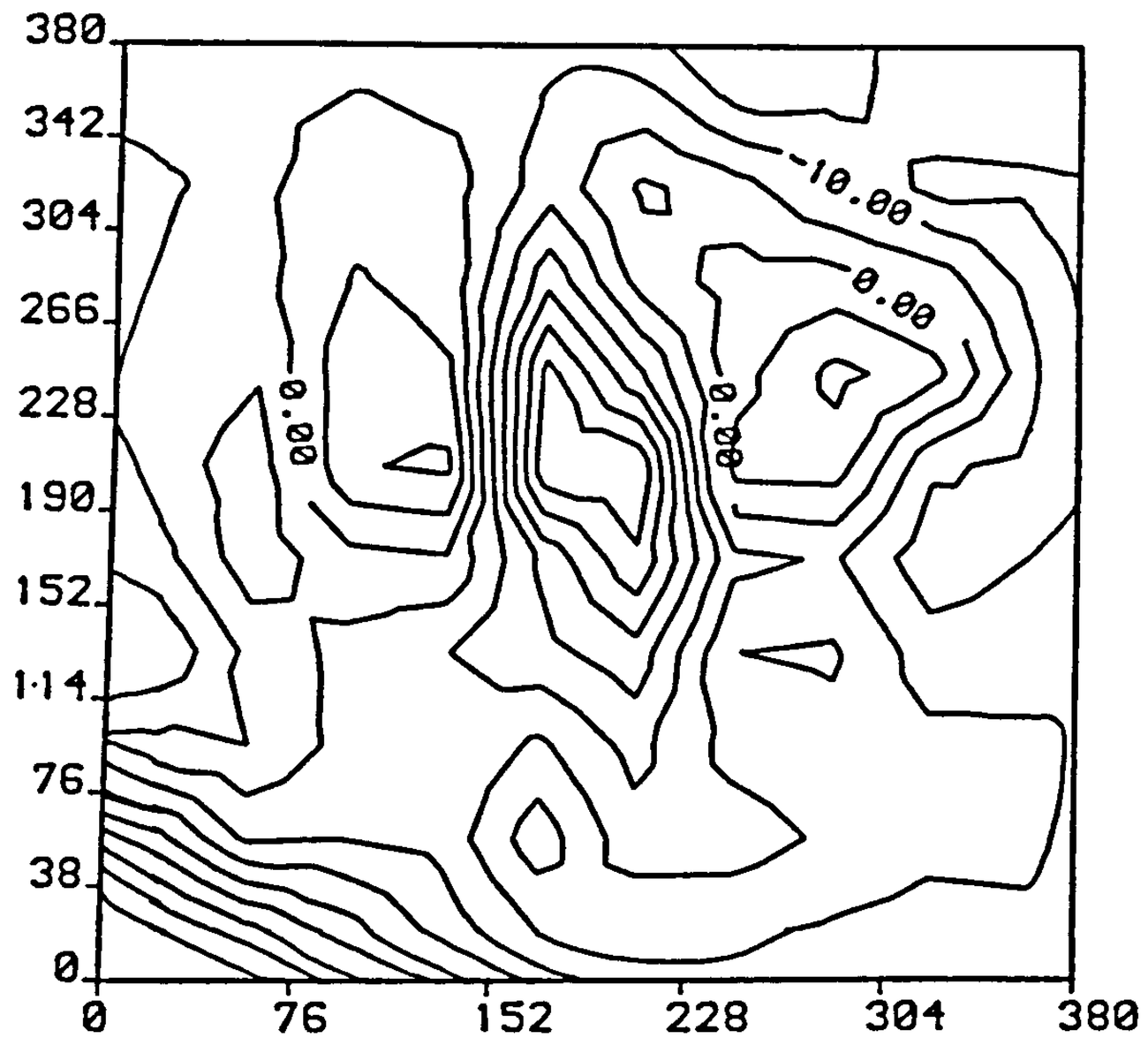

FIG. D.19 CONTOUR OF NX FOR S34P4 ACM
AT TOTAL VERTICAL LOAD= 16620.7 N
(N/mm)

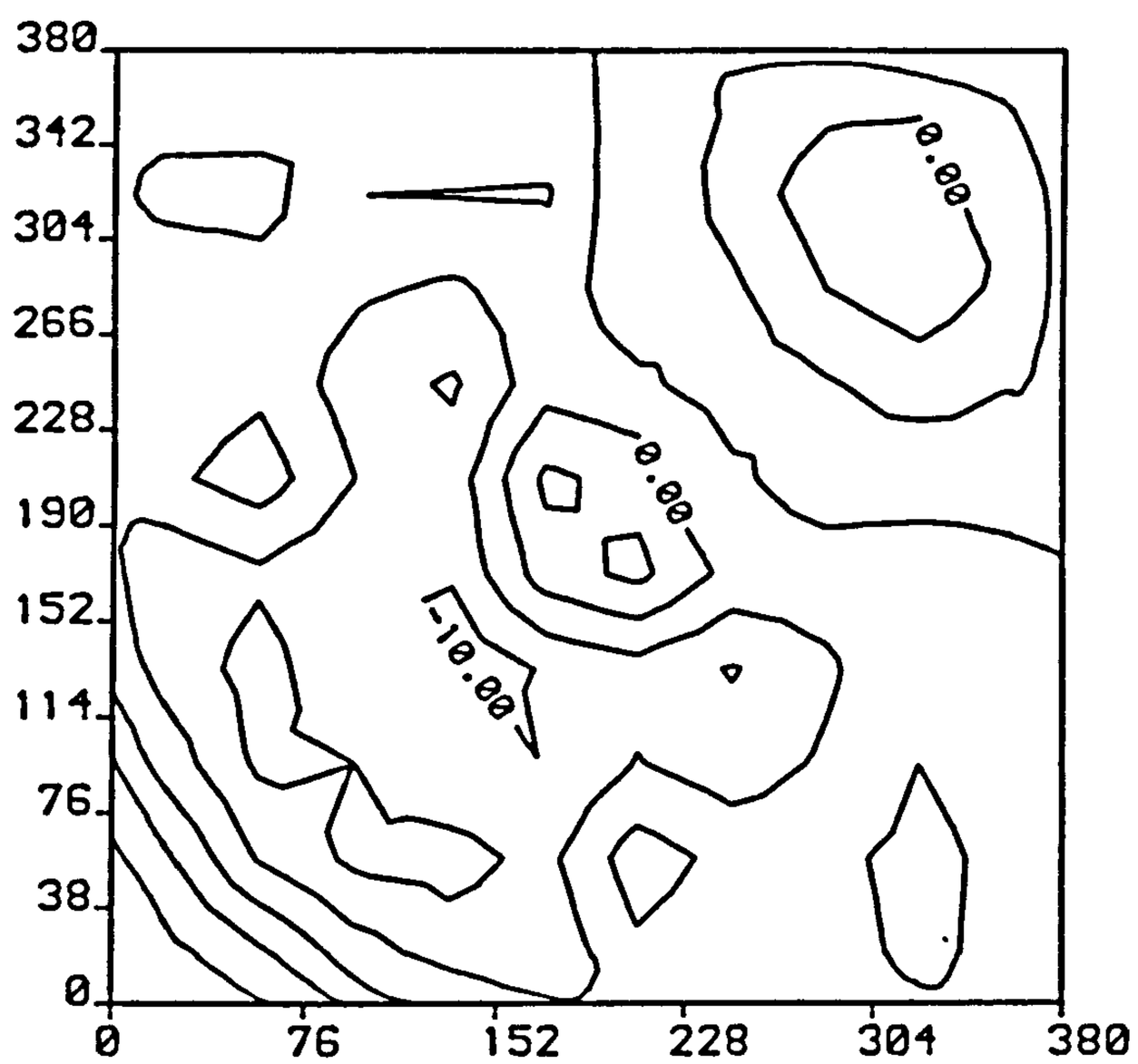

FIG. D.20 CONTOUR OF NXY FOR S34P4 ACM
AT TOTAL VERTICAL LOAD= 16620.7 N
(N/mm)

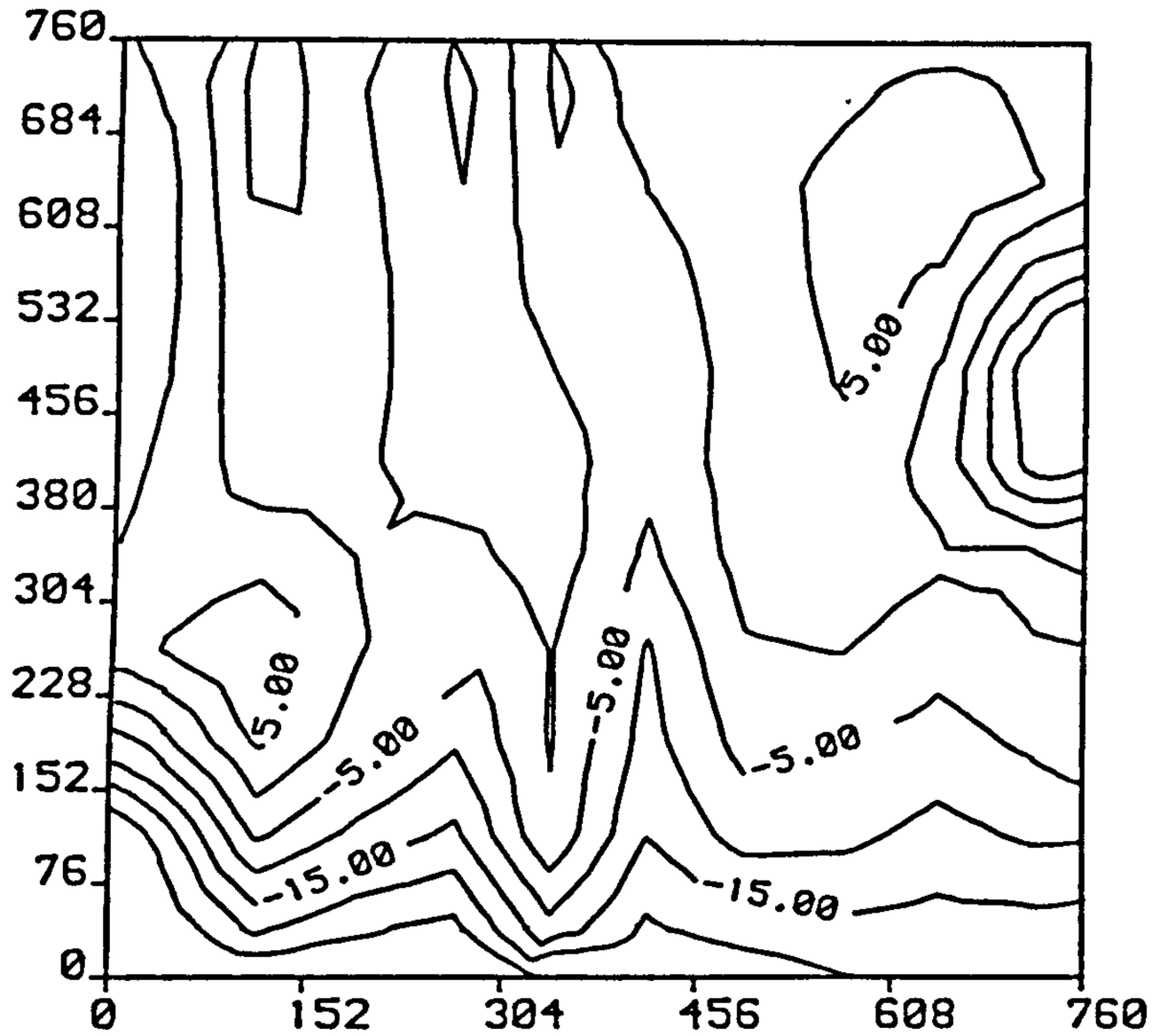

FIG. D.21 CONTOUR OF NX FOR S43UD ACM
AT TOTAL VERTICAL LOAD= 11958.2 N
(N/mm)

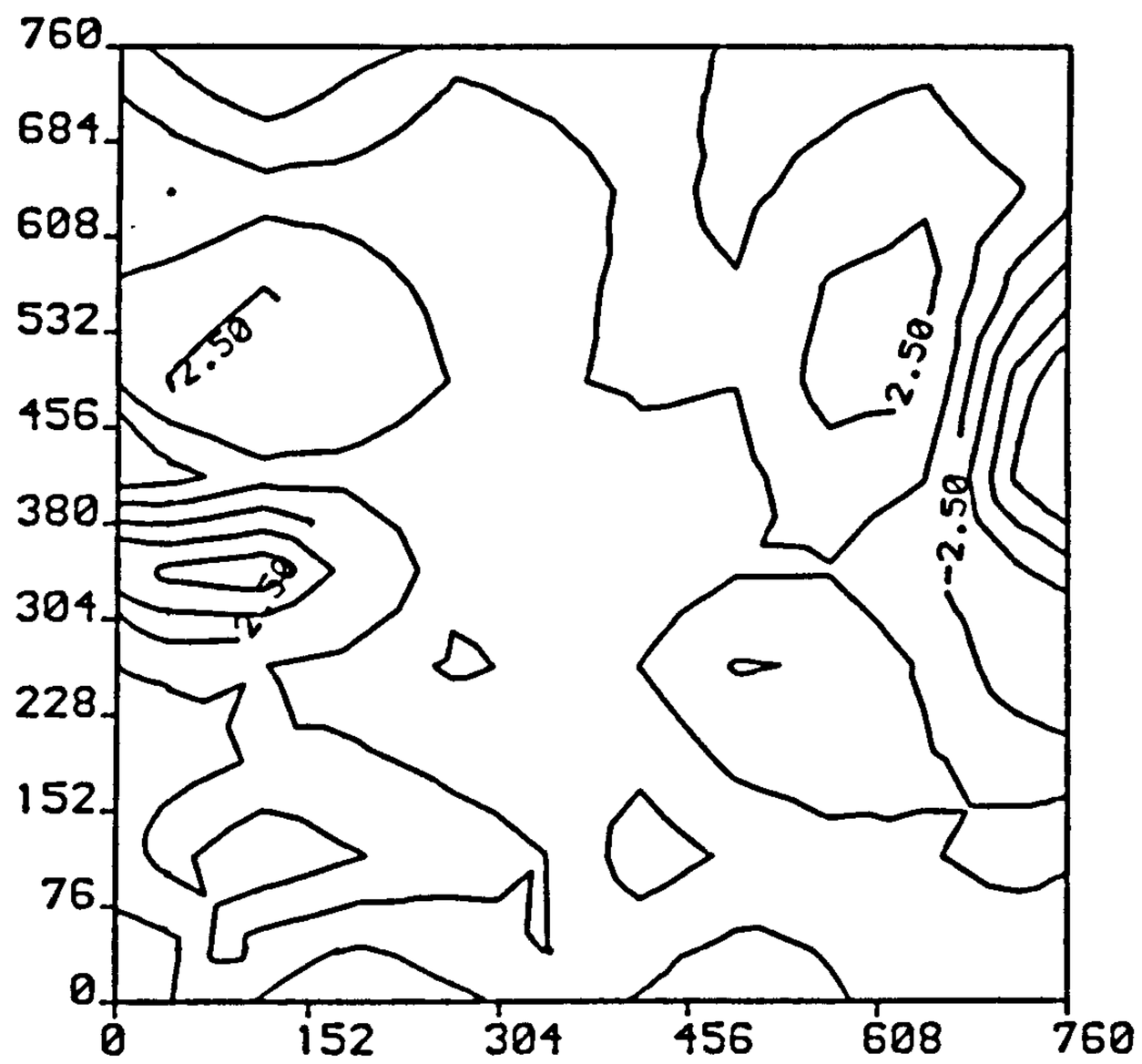

FIG. D.22 CONTOUR OF NY FOR S43UD ACM
AT TOTAL VERTICAL LOAD= 11958.2 N
(N/mm)

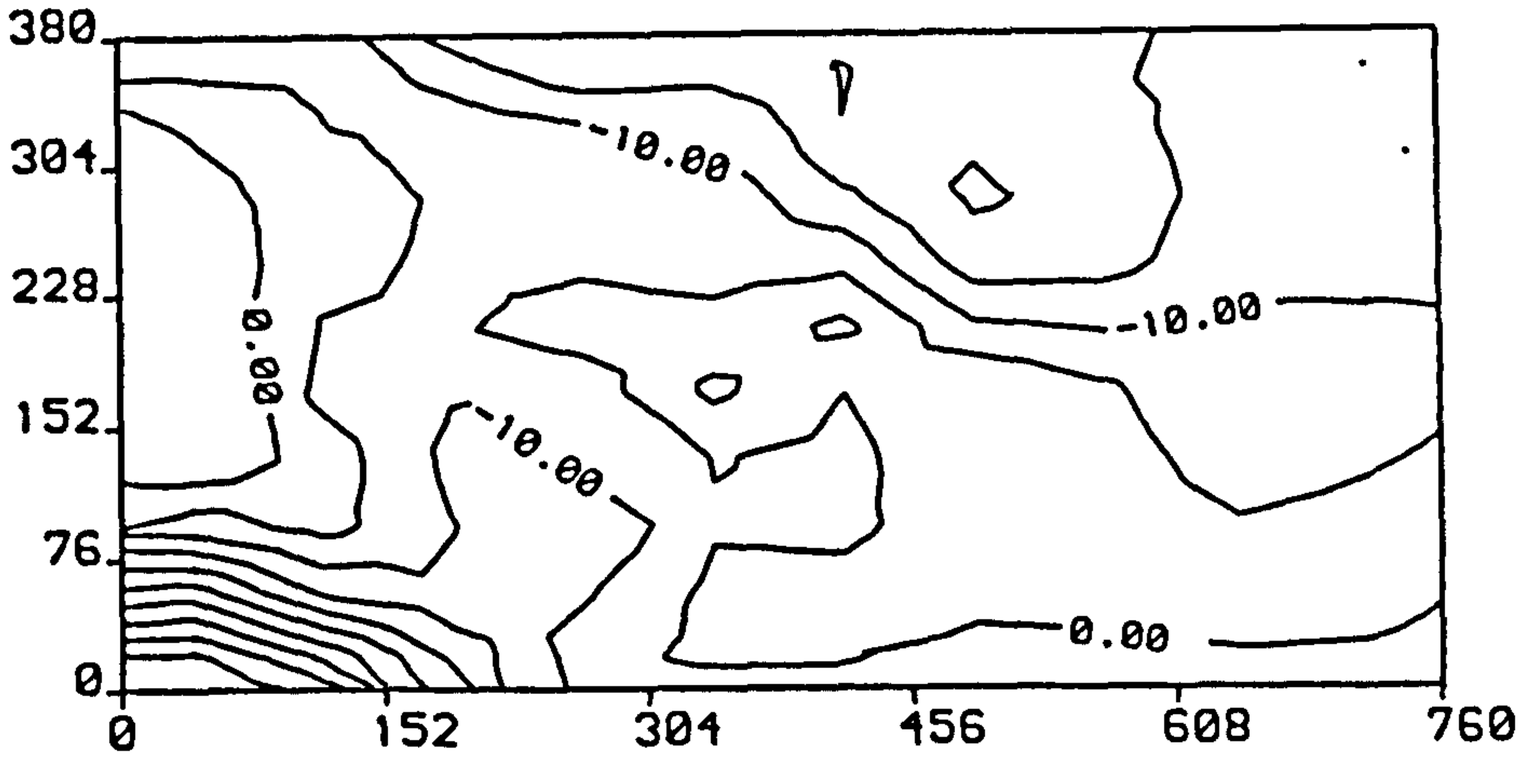

FIG. D.23 CONTOUR OF NX FOR S54UD ACM
AT TOTAL VERTICAL LOAD = 38881.5 N
(N/mm)

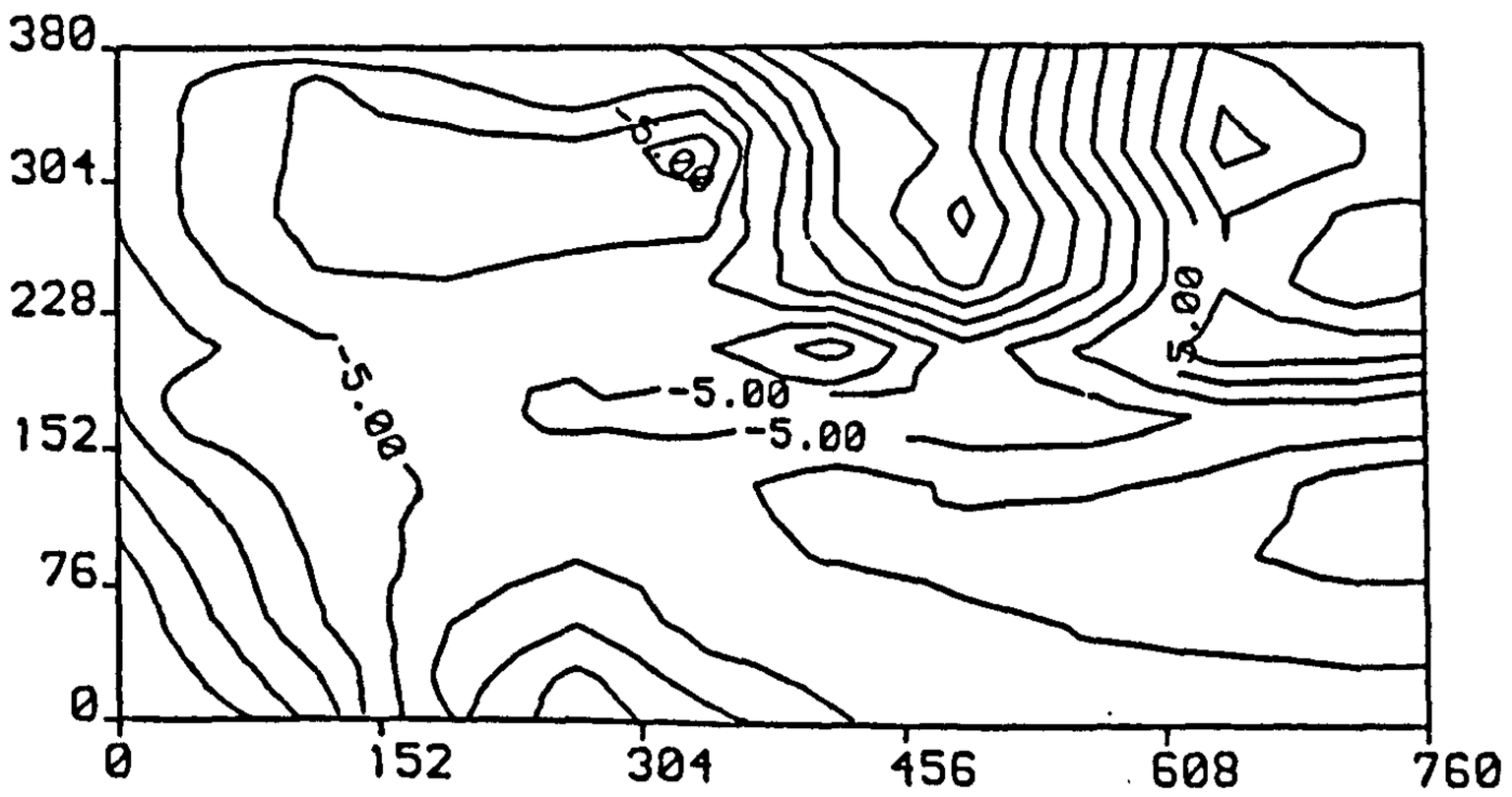

FIG. D.24 CONTOUR OF NY FOR S54UD ACM
AT TOTAL VERTICAL LOAD = 38881.5 N
(N/mm)

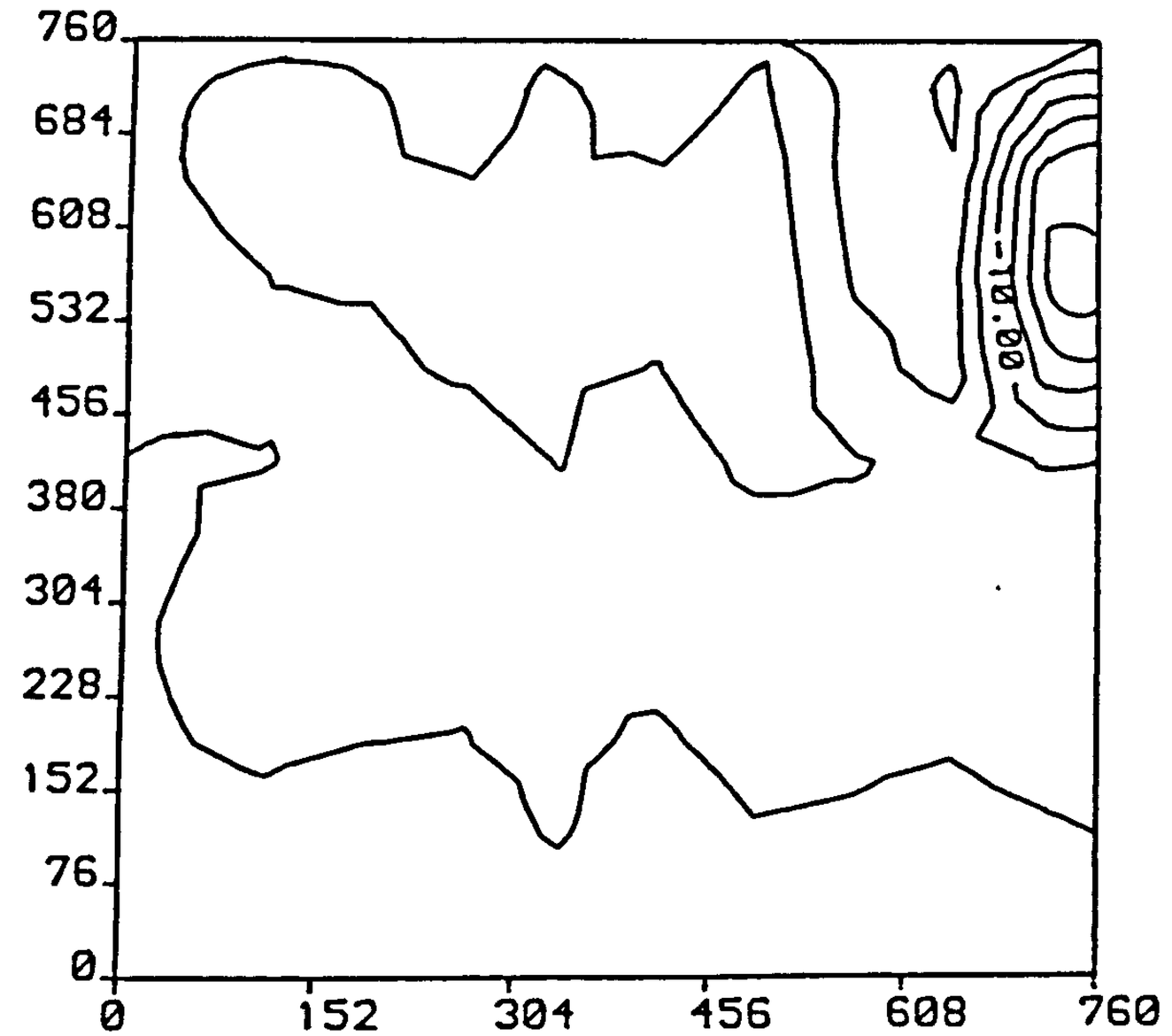

FIG. D.25 CONTOUR OF NX FOR S63P1 ACM
AT TOTAL VERTICAL LOAD= 3763.4 N
(N/mm)

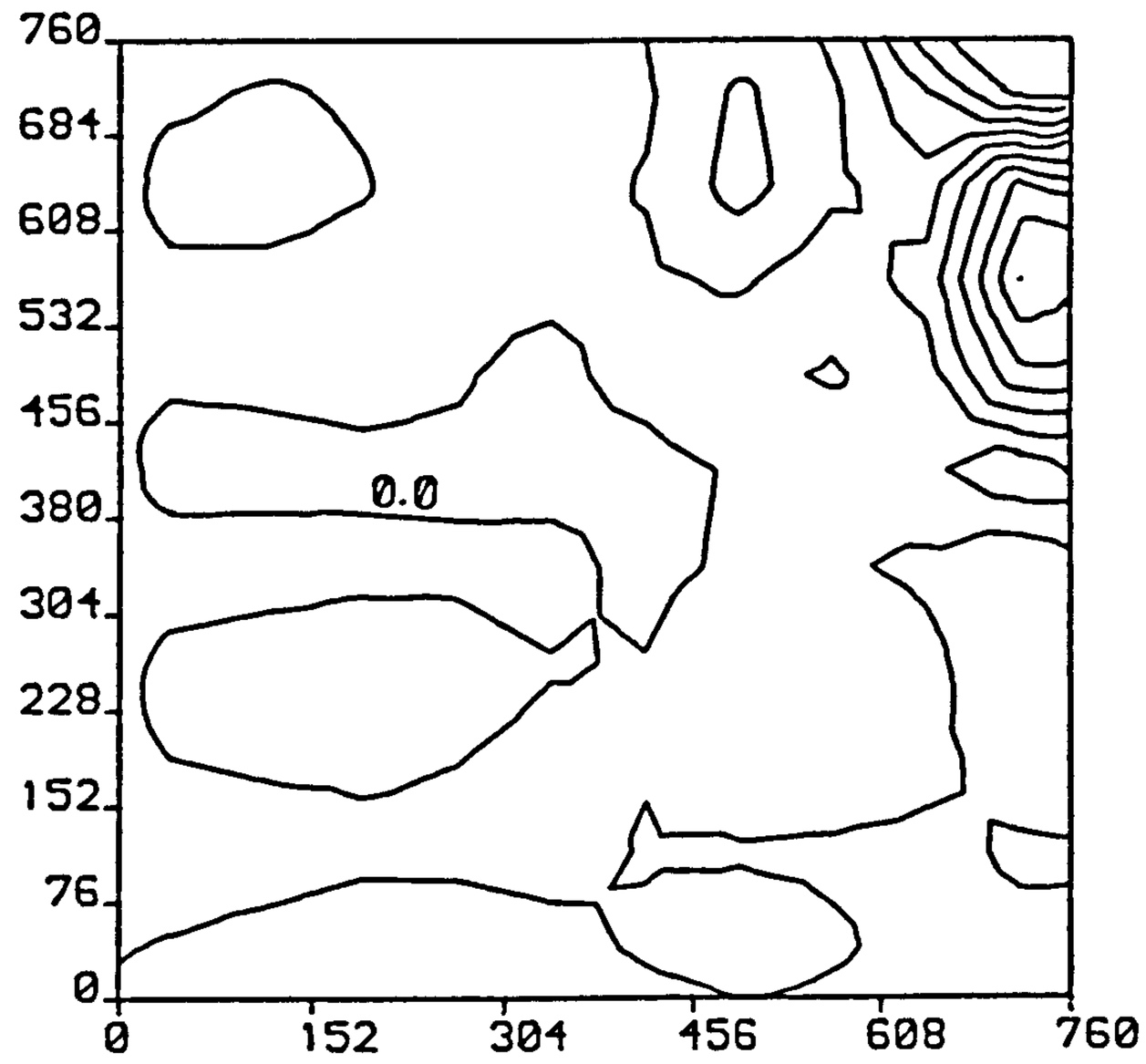

FIG. D.26 CONTOUR OF NY FOR S63P1 ACM
AT TOTAL VERTICAL LOAD= 3763.4 N
(N/mm)

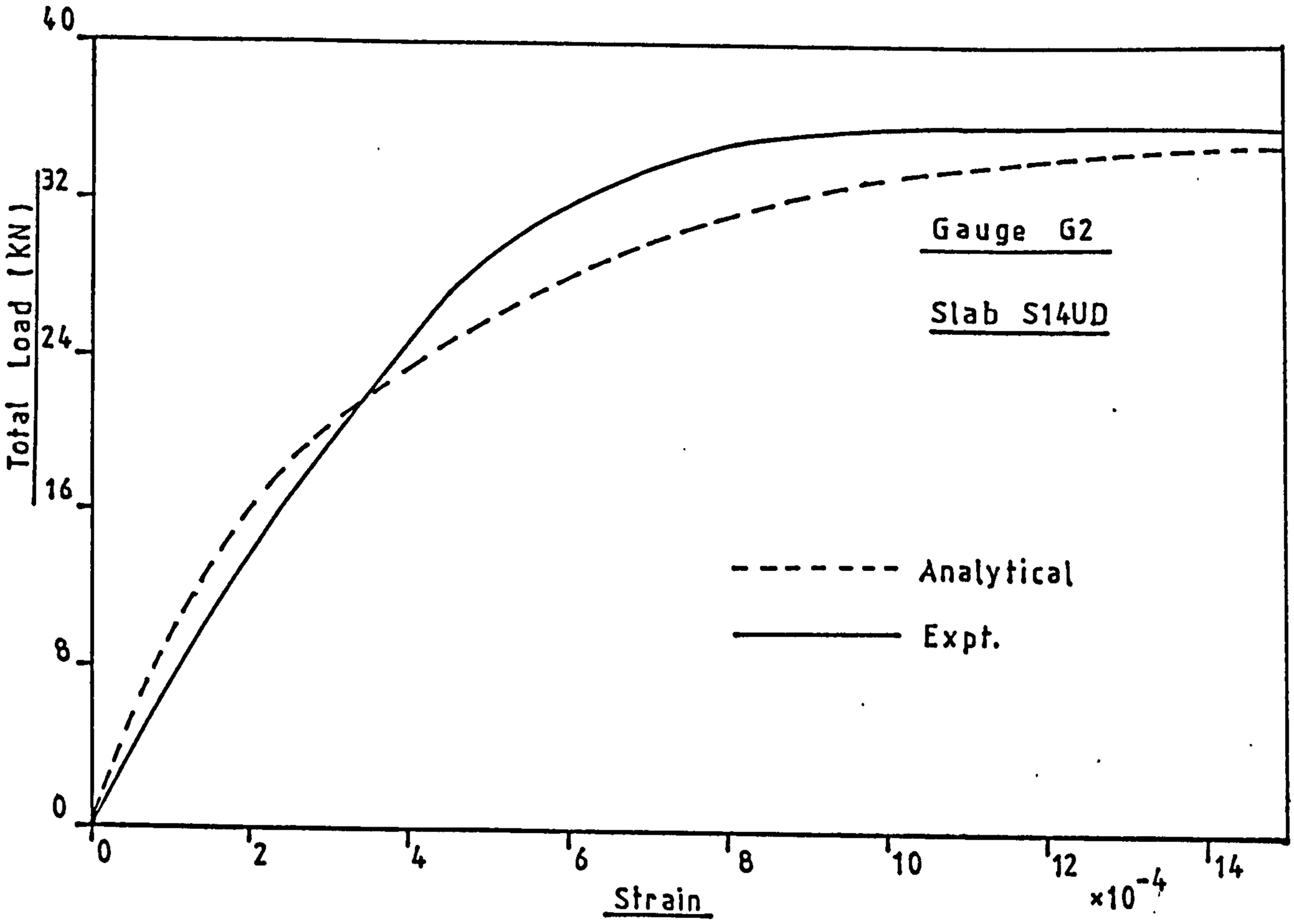

FIG. D.27 Comparison of Load-Steel Strain Responses for Slab S14UD.

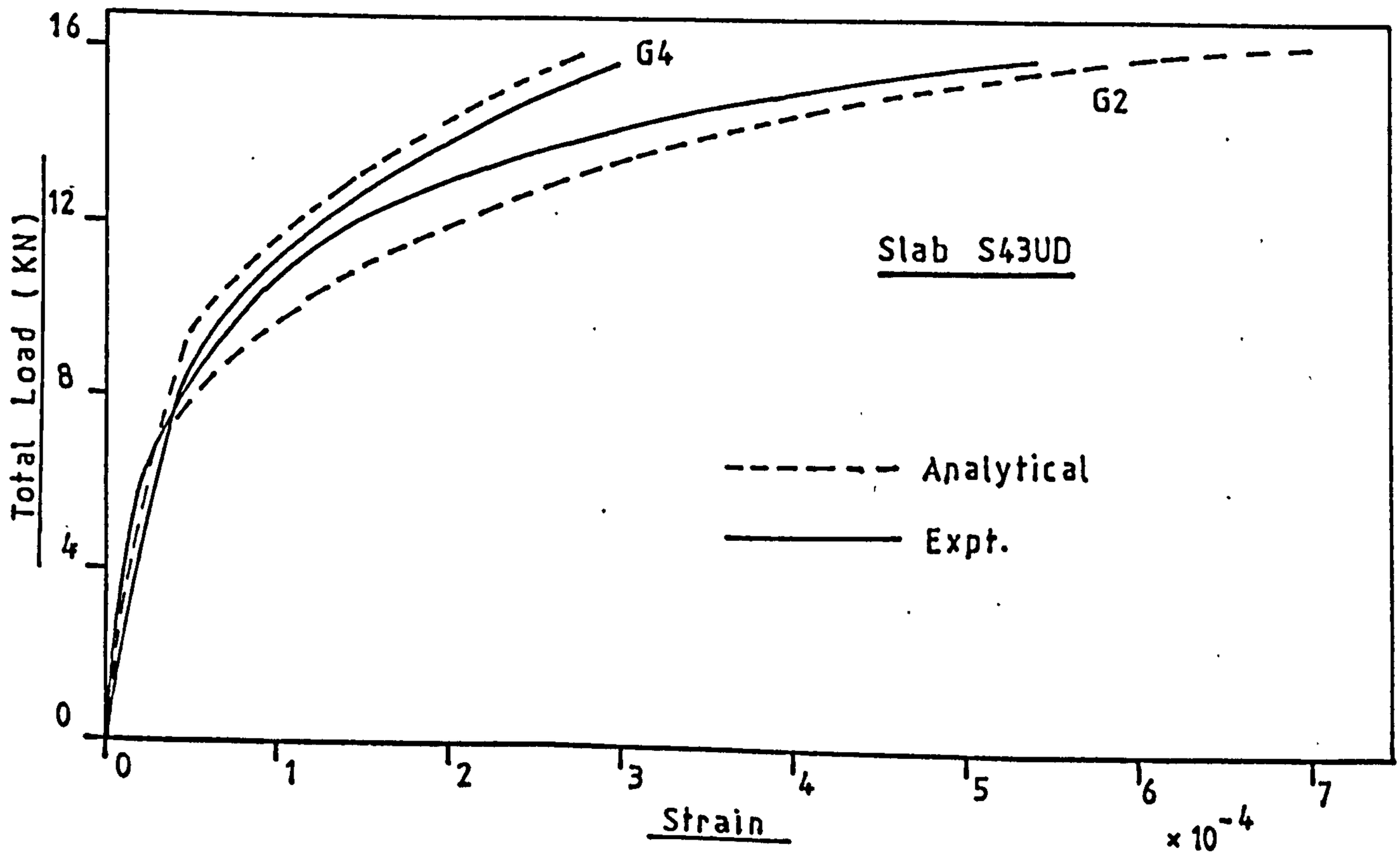

FIG. D.28 Comparison of Load-Steel Strain Responses for Slab S43UD.

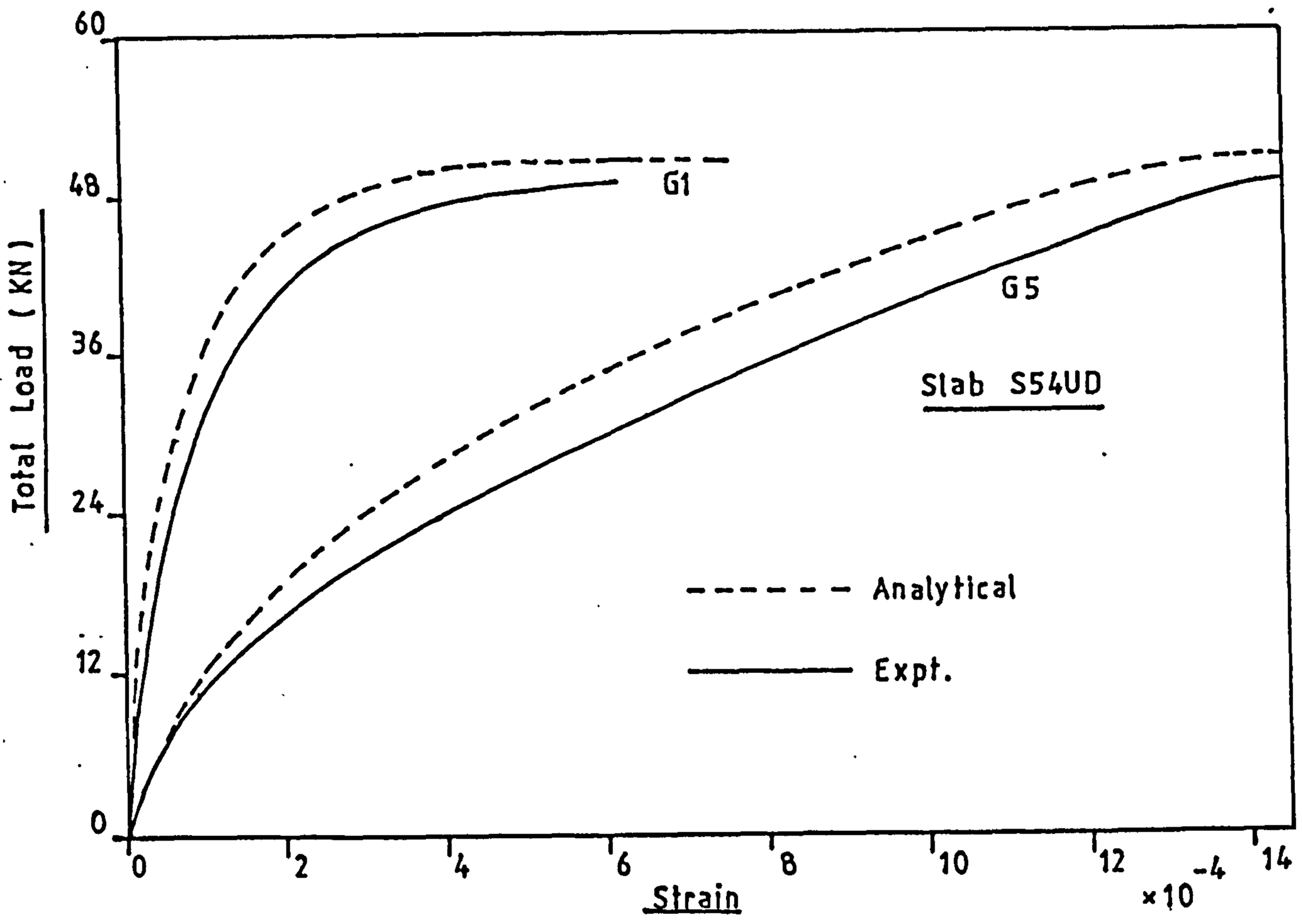

FIG. D.29 Comparison of Load-Steel Strain Responses for Slab S54UD

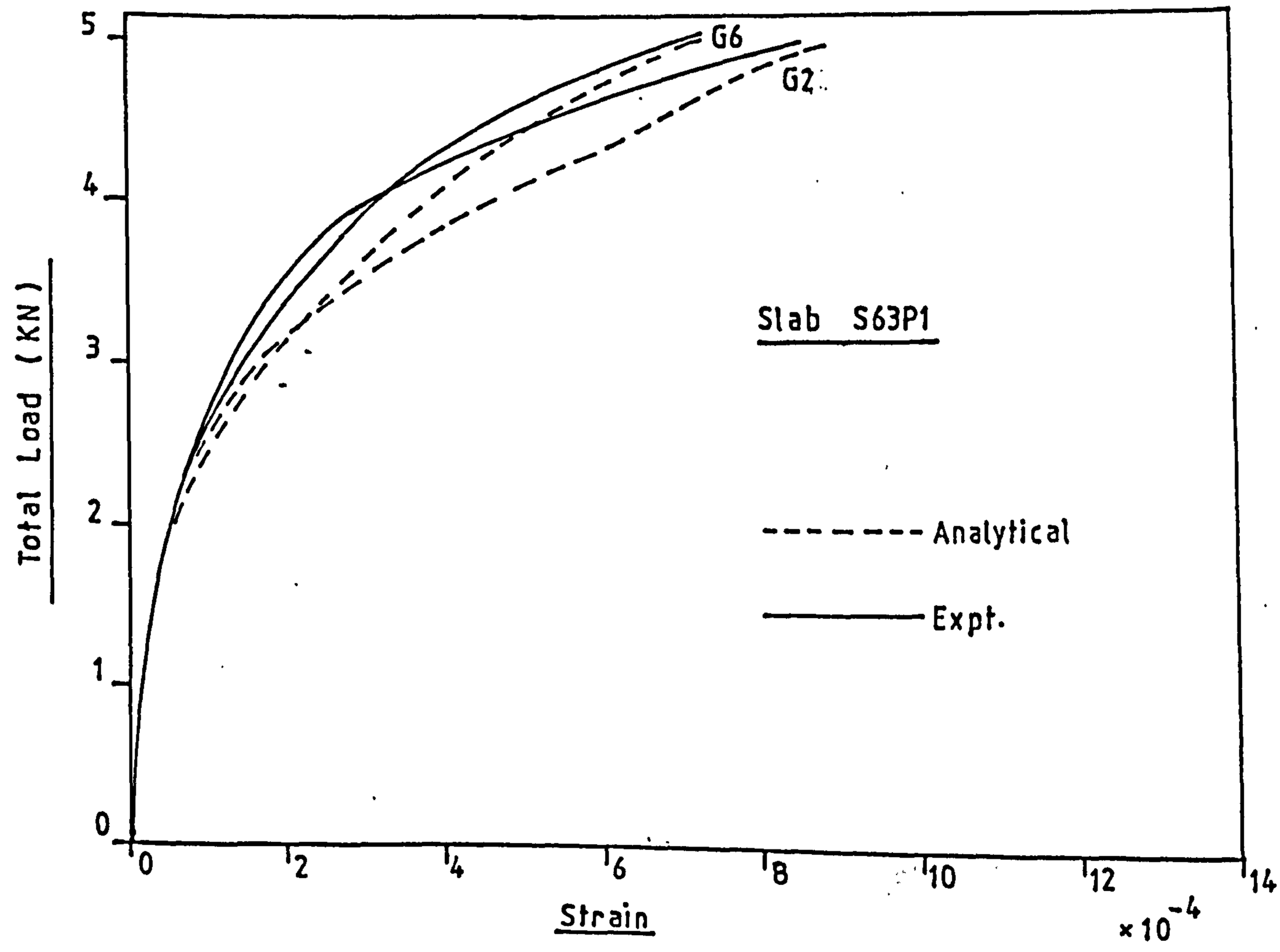

FIG. D.30 Comparison of Load-Steel Strain Responses for Slab S63P1.